Vol. 201, October 15, 1987
Complete in one issue

ISSN 0003-2670

ANALYTICA CHIMICA ACTA

International journal devoted to all branches of analytical chemistry

ELSEVIER

ANALYTICA CHIMICA ACTA

International journal devoted to all branches of analytical chemistry
Revue internationale consacrée à tous les domaines de la chimie analytique
Internationale Zeitschrift für alle Gebiete der analytischen Chemie

PUBLICATION SCHEDULE FOR 1987

	J	F	M	A	M	J	J	A	S	O	N	D
Analytica Chimica Acta	192	193	194	195	196	197	198	199	200/1 200/2	201	202	20 20

Scope. *Analytica Chimica Acta* publishes original papers, short communications, and reviews dealing with e aspect of modern chemical analysis both fundamental and applied.

Submission of Papers. Manuscripts (three copies) should be submitted as designated below for rapid efficient handling:

Papers from the Americas to: Professor Harry L. Pardue, Department of Chemistry, Purdue University, ' Lafayette, IN 47907, U.S.A.

Papers from all other countries to: Dr. A. M. G. Macdonald, Department of Chemistry, The University, P.O. Box Birmingham B15 2TT, England. Papers dealing particularly with computer techniques to: Professor J. T. C Universität Bern, Pharmazeutisches Institut, Baltzerstrasse 5, CH-3012 Bern, Switzerland.

Submission of an article is understood to imply that the article is original and unpublished and is not b considered for publication elsewhere. Papers in English, French and German are published. There are no | charges. Manuscripts should conform in layout and style to the papers published in this Volume. See inside cover for "Information for Authors".

Reprints. Fifty reprints will be supplied free of charge. Additional reprints (minimum 100) can be ordered order form containing price quotations will be sent to the authors together with the proofs of their article.

Publication. *Analytica Chimica Acta* appears in 12 volumes in 1987. The subscription for 1987 (Vols. 192–20 Dfl. 2700.00 plus Dfl. 300.00 (p.p.h.) (total approx. US $1463.40). All earlier volumes (Vols. 1–191) except ' 23 and 28 are available at Dfl. 243.00 (US $118.50), plus Dfl. 18.00 (US $8.80) p.p.h., per volume.

Our p.p.h. (postage, packing and handling) charge includes surface delivery of all issues, except to subscribe the U.S.A., Canada, Australia, New Zealand, P.R. China, India, Israel, South Africa, Malaysia, Thailand, Singa South Korea, Taiwan, Pakistan, Hong Kong, Brazil, Argentina and Mexico, who receive all issues by air del (S.A.L. — Surface Air Lifted) at no extra cost. For Japan, air delivery requires 50% additional charge; for all c countries airmail and S.A.L. charges are available upon request.

Subscription. Subscription should be sent to: Elsevier Science Publishers B.V., Journals Department, P.O. 211, 1000 AE Amsterdam, The Netherlands. Tel: 5803 911, Telex: 18582, to which requests for sample copies also be sent. Claims for issues not received should be made within three months of publication of the issues. I they cannot be honoured free of charge. Readers in the U.S.A. and Canada can contact the following add Elsevier Science Publishing Co. Inc., Journal Information Center, 52 Vanderbilt Avenue, New York, NY 10 U.S.A., Tel: (212) 916-1250, for further information, or a free sample copy of this or any other Elsevier Sci Publishers journal.

Advertisements. Advertisement rates are available from the publisher on request.

0003-2670/87/$

Printed in The Netherlands

ANALYTICA CHIMICA ACTA

International journal devoted to all branches of analytical chemistry

(Abstracted, Indexed in: Anal. Abstr.; Biol. Abstr.; Chem. Abstr.; Curr. Contents Phys. Chem. Earth Sci.; Life Sci.; Index Med.; Mass Spectrom. Bull.; Sci. Citation Index; Excerpta Med.)

L. 201 **CONTENTS** **OCTOBER 15, 1987**

(Continued overleaf)

(*Contents continued*)

ANALYTICA CHIMICA ACTA
VOL. 201 (1987)

ANALYTICA CHIMICA ACTA

International journal devoted to all branches of analytical chemistry

ELSEVIER Amsterdam–Oxford–New York–Tokyo

Analytica Chimica Acta, 201 (1987) 1—9
Elsevier Science Publishers B.V., Amsterdam — Printed in The Netherlands

FLOW POTENTIOMETRIC AND CONSTANT-CURRENT STRIPPING ANALYSIS FOR MERCURY(II) WITH GOLD, PLATINUM AND CARBON FIBRE WORKING ELECTRODES

Application to the Analysis of Tap Water

HUANG HUILIANG[a], DANIEL JAGNER* and LARS RENMAN

Department of Technical Analytical Chemistry, Chemical Center, P.O. Box 124, S-221 00 Lund (Sweden)

(Received 6th April 1987)

SUMMARY

Gold, platinum and carbon fibres with 10-μm diameter were mounted in PVC tubes and used as flow sensors in computerized potentiometric and constant-current stripping analysis for mercury, after electroplating of a gold film onto the fibre surfaces. Compared to gold and glassy carbon disc electrodes, the fibre electrodes gave increased sensitivity and stability and were considerably simpler to handle. The gold-coated carbon fibre electrode gave a higher background than the gold fibre electrode, in both the potentiometric and constant-current stripping modes. Mercury(II) could be determined in presence of a 10^5-fold (molar) amount of copper(II) by constant-current stripping in media with chloride concentrations below 0.05 M. The detection limit for mercury(II) after 10 min of electrolysis was 45 ng l^{-1} at the 3 σ level.

It has recently been shown that mercury-coated carbon fibres can be used as flow sensors in potentiometric stripping analysis [1]. The main advantages of the fibre electrodes compared with thin-layer glassy carbon disc electrodes are enhanced diffusional characteristics, low dead volumes and negligible internal resistance potential drop. In addition, the flow fibre electrodes are virtually free from leakage problems and the material cost is very low.

Mercury has been determined by means of flow potentiometric stripping analysis with either gold disc electrodes or glassy carbon discs electrolytically covered with a film of gold [2, 3]. Owing to the advantages inherent in using fibre electrodes as flow sensors, it was considered interesting to investigate if carbon or metal fibre electrodes could be used for the potentiometric stripping determination of mercury and, at the same time, to compare potentiometric and constant-current stripping in various media, both techniques being based on the rapid monitoring of the potential vs. time stripping transient and thus accessible with the same instrument [4].

---

[a]Permanent address: Scientific Instrumentation Department, Xiamen (Amoy) University, Fujian Province, China.

0003-2670/87/$03.50

EXPERIMENTAL

Instrumentation

The computerized potentiometric and constant-current analyzer described in detail elsewhere [4] was used for all experiments. The instrument incorporated a peristaltic pump by means of which six different solutions could be sucked through the flow cell in random-choice order by computer-controlled opening and closing of magnetic valves. Electrolysis potentials in the range ±2.05 V vs. the reference electrode and with a resolution of 1 mV could be applied to the working electrode. During stripping, the potential vs. time transient was recorded with a real-time sampling rate of 25.6 kHz. In the constant-current stripping mode, the oxidizing current could be varied in the range 0.01–20 μA in steps of 10 nA.

After recording of the stripping curve and subtraction of the background, the analyzer located and integrated the mercury stripping peak and presented the results graphically and digitally on a printer/plotter [4].

Electrodes

Gold fibre electrodes (diameter 10 μm, 99.99% purity) and platinum fibres with the same diameter (99.999% purity) were obtained from Goodfellow (Cambridge, England). These were mounted perpendicularly to the flow direction in a PVC tube (inner diameter 0.8 mm) in the same way as described for carbon fibres [1]. The reference and then the counter electrodes were mounted downstream from the fibre working electrode.

Three different kinds of reference electrode were used, namely a calomel electrode in a thin-layer cell arrangement [5], a silver tube (inner diameter 0.7 mm) lined inside with silver chloride, and a glassy carbon rod electrode (GCE) (diameter 1 mm) mounted perpendicularly to the flow direction in a PVC tube (inner diameter 2 mm). Because of its large dimensions, the calomel electrode (Radiometer K401) exhibited much more noise than the other two reference electrodes and was therefore used only in the calibration of the other electrodes. The Ag/AgCl electrode could not be used in connection with potentiometric stripping media containing gold(III) because of the spontaneous reaction between silver and gold(III). For this reason, all potentials given below are versus the glassy carbon electrode (GCE). The mechanism of this electrode is the same as for the oxygen electrode [6]. In the results reported below, the potential of the glassy carbon electrode was 0.50 ± 0.12 V vs. the saturated calomel electrode.

The 2-mm diameter gold and glassy carbon disc electrodes used for comparison with the fibre electrodes were mounted in the thin-layer arrangement described previously [4]. A platinum tube was used as counter electrode in all experiments [1].

Reagents

All chemicals used were of analytical grade except the mineral acids which were of Suprapur grade (Merck). All dilutions were made with Millipore-Q water.

Lead(II), gold(III), mercury(II) and copper(II) stock solutions (1 g l^{-1}) were made from Titrisol ampoules (Merck) and were diluted prior to use. The gold-plating solution contained 100 mg l^{-1} gold(III) in 1 M hydrochloric acid. The electrode test solution contained 10 $\mu g\, l^{-1}$ mercury(II) and 50 $\mu g\, l^{-1}$ copper(II) in 0.1 M hydrochloric acid.

General procedure

Prior to each electrolysis/stripping cycle, a fresh surface of gold was plated onto the carbon, platinum or gold fibre working electrode. In the initial step of this procedure, the gold-plating solution was allowed into the flow cell for 10 s in the absence of an applied potential. During this step, mercury which might have accumulated on the working electrode during storage was oxidized. A fresh surface of gold was then plated onto the working electrode by means of electrolysis at −0.40 V vs. GCE for 20 s. Prior to entry of the sample solution into the flow cell, the potential was increased to 0.05 V vs. GCE for 2 s in order to oxidize elements which might have been co-deposited during plating of the fresh gold surface. After electrolysis in the sample, the appropriate stripping medium was introduced for 20 s prior to potentiometric or constant-current stripping. Finally, the background was recorded after 2 s of electrolysis in the stripping medium. Subsequent to each electrolysis/stripping cycle, 0.1 M hydrochloric acid in 50% (v/v) ethanol (rinsing solution) was sucked through the cell for 10 s, in the absence of an applied potential, in order to remove microbubbles and organic matter which might have adhered to the electrode surface. All flow rates were 1.2 ml min^{-1}.

Determination of mercury(II) in tap water

Acidify a 100-ml tap-water sample with 5.0 ml of concentrated nitric acid and add 0.50 ml of 0.01 M potassium permanganate in order to oxidize traces of organic matter which might be present in the sample. Treat another 100-ml portion of the tap water solution in the same way and add 1—10 $\mu g\, l^{-1}$ mercury(II). The magnitude of this standard addition should be chosen so that it is approximately four times higher than the expected sample concentration of mercury(II). Place the two solutions at two inlets of the flow analyzer. Place a fresh film of gold onto the working electrode as described above. Electrolyze in the sample according to a pulsed potential procedure; a potential of −0.70 V vs. GCE is applied for 9 s followed by a potential of −0.50 V for 1 s. At this potential, most of the copper deposited at −0.70 V is reoxidized. Repeat this pulse sequence for 1—10 min depending on the detection limit desired. Allow a stripping solution of 0.5 M nitric acid and 0.02 M hydrochloric acid into the cell for 20 s, adjust the potential to −0.35 V vs. GCE for 5 s in order to reoxidize copper, and record the constant-current stripping curve in the potential range −0.35 to 0.20 V vs. GCE, using a current of 50 nA. Record the background after 2 s of electrolysis at −0.35 V vs. GCE.

Repeat the procedure in the sample containing the standard addition of

mercury(II) and let the computer calculate the mercury(II) concentration in the sample from the normal equations for standard addition.

RESULTS AND DISCUSSION

Stripping media for potentiometric and constant-current stripping

In most real samples, the copper(II) concentration is in great excess of the mercury(II) concentration, thus a major problem in the electrochemical stripping analysis for mercury(II) is the potential overlap from copper [7]. The stripping potentials for copper and mercury when gold working electrodes are used are highly dependent on the chloride concentration in the stripping medium. Experiments with constant-current stripping and a gold-fibre electrode showed that the mercury stripping peak is cathodic to the copper stripping peak at chloride concentrations above approximately 3 M but anodic to the copper peak at lower chloride concentrations, i.e., Hg(Au) can be oxidized either before or after Cu(Au), depending on the chloride concentration. Figure 1A shows the potentiometric stripping curve obtained after 60 s of electrolysis at —0.80 V vs. GCE in the test solution and subsequent stripping in 0.10 M hydrochloric acid containing 0.25 mM gold(III) as oxidant. Figure 1B shows the constant-current stripping curve obtained under the same electrolysis conditions and stripping in 0.10 M hydrochloric acid with a current of 50 nA. As can be seen, the stripping potentials for copper and for mercury are independent of the oxidation mode.

The oxidation rates in potentiometric and constant-current stripping analysis were investigated under the same experimental conditions as those in Fig. 1 with the exceptions that the gold(III) concentration was varied in the range 0.01—1 mM and the oxidizing current in the range 0.01—1 μA. It was found that the mercury signal varied linearly with the inverse of the gold(III)

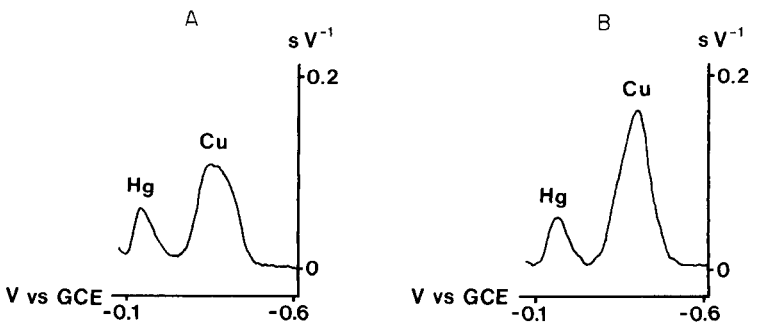

Fig. 1. Background-corrected differentiated stripping curves obtained with a gold-fibre electrode. (A) Potentiometric stripping after electrolysis for 60 s at —0.80 V vs. GCE in 0.1 M hydrochloric acid containing 10 μg l^{-1} mercury(II) and 50 μg l^{-1} copper(II). Potentiometric stripping in 0.10 M hydrochloric acid containing 0.25 mM gold(III); (B) constant-current stripping in 0.10 M hydrochloric acid with a constant current of 50 nA.

concentration and with the inverse of the stripping current. A current of 60 nA yielded the same oxidation rate as 0.25 mM gold(III), in agreement with the mass-transport calculations at fibre electrodes published by Hussam and Coetzee [8].

Comparison between gold-coated carbon fibre electrodes and gold fibre electrodes

The gold, platinum and carbon fibre electrodes were compared by means of consecutive electrolysis/stripping cycles. The experimental conditions were the same as those in Fig. 1B.

In contrast to the gold fibre electrodes, the carbon and platinum fibre electrodes yielded reproducible copper and mercury signals only after five to ten electrolysis/stripping cycles, each cycle being preceded by the gold-plating procedure described above. This was attributed to the slow coverage of the gold film on the carbon and platinum fibre surfaces. Once gold-coated, the carbon and platinum fibre could, however, be used for several hundred electrolysis/stripping cycles. Even after complete coverage with a gold film, the carbon fibres yielded higher backgrounds than the gold fibre electrodes. No significant difference was observed between the backgrounds of the gold-coated platinum fibre electrode and the gold fibre electrode.

Comparison between fibre and disc electrodes

The glassy carbon disc electrode and the gold disc electrode were compared with the carbon and gold fibre electrodes by electrolysis in the electrode test solution and subsequent stripping in the potentiometric and constant-current modes. The same experimental conditions as those in Fig. 1 were used, except that the constant current was 10 μA.

Similarly to the carbon fibre electrode, the glassy carbon disc electrode yielded reproducible stripping signals only after five to ten electrolysis/stripping cycles. The signal-to-background ratio was about twice as good on the gold-coated carbon fibre electrode than on the gold-coated glassy carbon disc electrode, both in the potentiometric and constant-current stripping modes. This is in good agreement with the results previously obtained on mercury-coated carbon fibre and glassy carbon disc electrodes and is attributed to enhanced diffusional characteristics [1].

The improvement in going from gold disc electrodes to gold fibre electrodes varied by factors between two and four. This improvement was partly due to enhanced diffusional conditions and partly due to the higher purity of the gold fibre electrode. In gold disc electrodes (diameter 2 mm, length 15 mm) copper impurities in the gold material diffuse continuously towards the electrode surface from the bulk of the electrode, thus contributing to an increased background. This effect is much less pronounced in gold fibre electrodes because of the higher purity of the gold matrix. Moreover, because the maximum diffusion distance to the electrode surface in the fibre electrode is 5 μm (diameter 10 μm), compared with 15 mm in the disc electrodes, the

fibre electrode is depleted of copper soon after it has been taken into use. This is, of course, an additional advantage of gold fibre electrodes compared to gold disc electrodes.

Copper(II) interference

As mentioned above, interference from copper is the most serious problem in electrochemical stripping analysis for mercury(II). As can be seen from Fig. 1, the copper peak is well separated from the mercury peak in 0.10 M chloride stripping medium. The interference from copper can be reduced further by a two-step stripping procedure in this medium. In the first step, the electrode potential is decreased to —0.35 V vs. GCE in the stripping medium. At this potential, Cu(Au), but not Hg(Au), is oxidized (cf. Fig. 1A and B). In the next stripping step, Hg(Au) is reoxidized.

By increasing the copper(II) concentration in the electrode test solution and by following the same experimental conditions as in Fig. 1B, it was shown that this two-step stripping procedure permitted the determination of mercury(II) in the presence of a 10^4-fold molar amount of copper(II), i.e., an increase in copper(II) concentration in the test solution from 50 $\mu g\ l^{-1}$ to 20 mg l^{-1} did not affect the mercury signal. By applying the pulsed electrolysis potential mode described above for tap water, the possible copper/mercury concentration ratio could be increased by another order of magnitude, i.e., mercury(II) could be determined in a 10^5-fold molar amount of copper(II).

Reproducibility and linear range

The reproducibility of potentiometric and constant-current stripping at gold and carbon fibre electrodes was investigated by 25 consecutive analysis cycles in the electrode test solution. The same experimental conditions as those in Fig. 1 were used and the results are summarized in Table 1. As can be seen, the relative standard deviation is less than 5% for both techniques, irrespective of the electrode used. It is also obvious that constant-current stripping yields slightly better reproducibility than potentiometric stripping and that the gold fibre is more reproducible than the carbon fibre. The better

TABLE 1

Reproducibility in the potentiometric and constant-current stripping procedures for mercury(II) with gold and gold-coated carbon fibre electrodes

Stripping mode	Working electrode	Relative standard deviation[a] (%)
Potentiometric	Gold fibre	4.2
Potentiometric	Carbon fibre	4.8
Constant-current	Gold fibre	2.9
Constant-current	Carbon fibre	3.8

[a] $n = 25$.

precision of the constant-current stripping mode was attributed to the instability of the gold(III) ions in the potentiometric stripping medium where chloride was slowly oxidized.

The linear range in potentiometric and constant-current stripping with gold fibre electrodes was investigated by varying the mercury(II) concentration in the electrode test solution and by using the experimental conditions for procedures in Figs. 1B and 2. Taking the relative standard deviation in the individual measurements (Table 1) into consideration, no significant deviation from linearity was obtained in the 2—100 $\mu g\ l^{-1}$ concentration range investigated.

Analysis of tap water and detection limit

Figure 2A shows the background-corrected constant-current stripping curve obtained on a gold fibre electrode after pulsed potential electrolysis for 10 min in a tap-water sample containing 70 $\mu g\ l^{-1}$ copper(II). In this experiment, the potential in the stripping medium was not increased to —0.35 V vs. GCE prior to stripping in order to show the copper signal. Figure 2B shows the constant-current stripping peak obtained under the same experimental conditions after the standard addition of 1 $\mu g\ l^{-1}$ mercury(II). Five consecutive analyses of this sample yielded an average value for the mercury(II) concentration equal to 0.09 $\mu g\ l^{-1}$ with a standard deviation of 0.0012 $\mu g\ l^{-1}$. From these values, a detection limit of 0.0015 $\mu g\ l^{-1}$ on the 1 σ level can be estimated.

The mercury(II) concentration obtained for the tap water is the sum of sample concentration and any contribution from contamination by reagents and the laboratory environment. The accuracy of the constant-current stripping method was investigated by adding known concentrations of mercury(II)

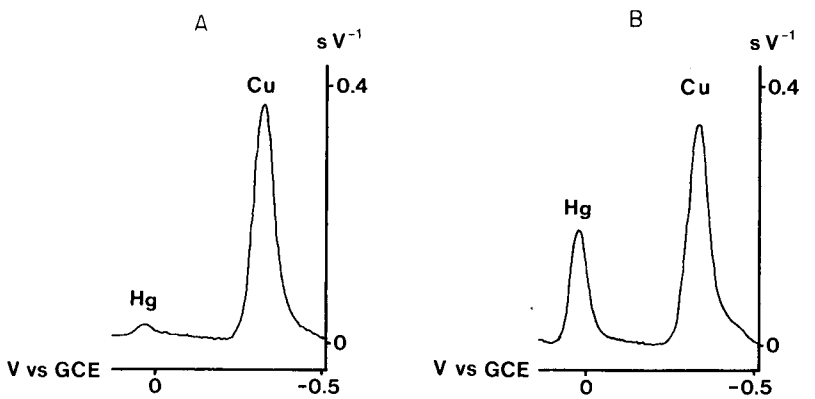

Fig. 2. Background-corrected differentiated constant-current stripping curves obtained on a gold fibre electrode after electrolysis for 10 min in a tap-water solution containing 70 $\mu g\ l^{-1}$ copper: (A) before, and (B) after, the addition of 1 $\mu g\ l^{-1}$ mercury(II). Constant-current stripping (50 nA) in 0.10 M hydrochloric acid.

TABLE 2

Recovery of mercury(II) added to a tap-water sample at different copper(II) concentrations with a gold fibre electrode

Mercury(II) added ($\mu g\ l^{-1}$)	Time of electrolysis (s)	Magnitude of mercury(II) std. add. ($\mu g\ l^{-1}$)	Copper(II) concentration ($mg\ l^{-1}$)	Mercury(II) found[a] ($\mu g\ l^{-1}$)
—	600	1	0.07	0.090 ± 0.012
0.50	300	2	0.07	0.53 ± 0.08
0.50	300	2	70	0.59 ± 0.09
1.50	300	5	0.07	1.45 ± 0.21
1.50	300	5	0.7	1.61 ± 0.19
2.00	300	5	70	2.10 ± 0.30
5.00	180	20	70	5.29 ± 0.63
10.00	60	50	70	10.7 ± 1.3
20.00	60	50	70	21.7 ± 1.8

[a]Mean and standard deviation for $n = 5$.

to a tap-water sample. The results are summarized in Table 2. As can be seen, the recovery of the mercury(II) is satisfactory even at low mercury(II) concentrations and it is independent of copper(II) concentration.

Conclusions

Gold and gold-plated platinum and carbon fibres can be used successfully as flow sensors in potentiometric and constant-current stripping analysis for mercury(II). Compared to disc electrodes in a thin-layer cell arrangement, they give increased sensitivity and long-term stability. From a practical point of view they are, furthermore, much simpler to handle with respect to leakage problems and changing of electrodes. In addition, they are very much simpler to manufacture and considerably less expensive. In order to obtain optimum reproducibility, not only the carbon and platinum but also the gold fibre electrode have to be coated with a fresh gold film prior to each electrolysis/stripping cycle. Because this is more easily achieved on the gold fibre than on the two other fibre types investigated, the gold fibre is best suited for routine work. From the results presented above and from the results obtained in current work on the determination of mercury(II) in urine, fish muscle and flue gases, it can be concluded that the gold fibre electrode is a very useful and reliable flow sensor in both potentiometric and constant-current stripping analysis.

REFERENCES

1 Huang Huiliang, Chi Hua, D. Jagner and L. Renman, Anal. Chim. Acta, 193 (1987) 61.
2 D. Jagner, M. Josefsson and K. Arén, Anal. Chim. Acta, 141 (1982) 147.
3 D. Jagner, Anal. Chim. Acta, 105 (1979) 33.

4 L. Renman, D. Jagner and R. Berglund, Anal. Chim. Acta, 188 (1986) 137.
5 L. Andersson, D. Jagner and M. Josefsson, Anal. Chim. Acta, 83 (1976) 19.
6 D. J. G. Ives and G. J. Janz, Reference Electrodes, Academic, New York, 1961.
7 J. Wang, Stripping Analysis, VCH, Deerfield Beach, FL, 1985.
8 A. Hussam and J. F. Coetzee, Anal. Chem., 57 (1985) 581.

Analytica Chimica Acta, 201 (1987) 11—22
Elsevier Science Publishers B.V., Amsterdam — Printed in The Netherlands

CATHODIC AND ANODIC STRIPPING DETERMINATION OF TRACES OF ADENINE AND ADENOSINE BASED ON ACCUMULATION OF COPPER(I) COMPOUNDS AT MERCURY OR AMALGAM ELECTRODES

STEFAN GŁODOWSKI, RENATA BILEWICZ and ZENON KUBLIK*
Department of Chemistry, University of Warsaw, ul. Pasteura 1, Warsaw 02093 (Poland)
(Received 29th December 1986)

SUMMARY

In the presence of adenine and adenosine, the copper(II)/copper(Hg) couple splits to the copper(II)/copper(I) and copper(I)/copper(Hg) couples. Sparingly soluble complexes of copper(I) with adenine and adenosine can be accumulated on the electrode surface either by reduction of Cu(II) ions or by oxidation of the copper amalgam electrode. The copper(I)/adenine deposit can be stripped either cathodically or anodically with detection limits of 5×10^{-9} and 2×10^{-8} mol dm^{-3}, respectively. The copper(I)/adenosine complex yields only the cathodic stripping peak with a detection limit of 9×10^{-8} mol dm^{-3}. The stripping peaks obtained for the copper(I)/adenine and copper(I)/adenosine complexes are better defined and appear over a wider range of pH than the peaks related to the corresponding mercury compounds. Adenosine cannot be determined in the presence of adenine but adenine can be determined in the presence of moderate amounts of adenosine.

Determination of traces of purines, pyrimidines and their nucleosides is a difficult problem [1]. Among the most sensitive methods proposed for determining traces of these substances, cathodic stripping voltammetry (c.s.v.) at the hanging mercury drop electrode (HMDE) [2—4] seems to be the simplest. Based on earlier work in this laboratory [5—8], it seemed that a further improvement of this general method could be obtained by the use of the hanging copper amalgam drop electrode (HCADE) instead of the HMDE. The cathodic stripping peaks obtained at the HCADE for iodides [5], cysteine and tryptophan [6] were better separated from the anodic limit than the peaks obtained for these substances with the HMDE. Moreover, the HCADE enabled cathodic stripping peaks to be obtained in cases where no such peaks could be seen with the HMDE [7, 8]. Recent cyclic experiments have shown [9] that in the presence of adenine the Cu(II)/Cu(Hg) system split into two systems corresponding to the Cu(II)/Cu(I) and Cu(I)/Cu(Hg) couples. The intermediate product, the Cu(I)/adenine complex, was adsorbed on the electrode surface; therefore it was supposed that this effect could be exploited for the determination of traces of adenine by stripping techniques. Sparingly soluble copper(I) complexes can also be accumulated on the HMDE during electroreduction of copper(II) ions added

0003-2670/87/$03.50

to the bulk solution [5, 7, 10]. The aim of the present work was to evaluate the possibilities of stripping voltammetry at the HCADE and HMDE in the presence of Cu(II) ions for the determination of traces of adenine and adenosine.

Adenine, under polarographic [11—13] and voltammetric [14] conditions, is reduced irreversibly in acidic solutions, yielding a single signal at a potential slightly more negative than —1 V. Tensammetric and electrocapillary studies [14, 15] showed that adenine is adsorbed on the mercury electrode in the region of the electrocapillary maximum. Paleček et al. [4], using d.c. and differential pulse polarography, observed for adenine an anodic signal located quite close to the mercury dissolution current. Florence [16] did not find a cathodic stripping peak for adenine at a mercury pool electrode but Paleček [2, 3] re-investigated the system and reported a stripping peak at the HMDE with a different pre-electrolysis potential.

Adenosine is adsorbed at the mercury electrode and gives an irreversible cathodic signal close to the adenine wave [12—14]. Florence [16] reported that adenosine is inactive under cathodic film-stripping conditions at a mercury pool electrode but Paleček [3] mentioned briefly that nucleosides derived from purine bases yield the cathodic film-stripping peaks at the HMDE.

EXPERIMENTAL

The copper(I)/adenine and copper(I)/adenosine complexes were prepared in situ either by oxidation of the copper amalgam electrode or by reduction of the copper(II) ions added to the bulk solution.

The voltammetric curves were recorded with a Radelkis OH-105 polarograph and the conventional three-electrode cell. Differential-pulse (d.p.) voltammetric curves were obtained with a Unitra PP04 pulse polarograph connected with a Kabid-Press 6801 X—Y recorder. The reference electrode was a saturated calomel electrode and all the potentials given are referred to this electrode. The counter electrode was a platinum foil with surface area 2 cm^2. The indicating electrode was the HMDE [17] or the HCADE. The latter electrode was prepared by filling the container for the HMDE with the copper amalgam. The surface areas of both electrodes were 0.024 cm^2. Copper amalgam was prepared by dissolving copper metal in pure mercury. The concentration of copper in the amalgam was determined on the basis of the Ševčik-Randles equation from the height of the copper dissolution peaks recorded in a solution of 0.1 mol dm^{-3} lithium or sodium perchlorate. The value of the diffusion coefficient of copper in mercury, used to calculate the concentration of copper in mercury, was 1.06×10^{-5} cm^2 s^{-1} [18]. Unless otherwise stated, the concentration of copper in amalgam was 3×10^{-3} mol dm^{-3}. The quantity of electricity passed during recording of the stripping peaks was calculated from the peak areas.

The aqueous stock solutions of adenine and adenosine (both from Sigma Chemical Company) were 1×10^{-3} mol dm^{-3}. In cyclic voltammetric experiments, a small aliquot of the stock solution was added to the deoxygenated supporting electrolyte from a microsyringe. In stripping experiments, the stock solutions were diluted prior to use. Oxygen was removed from the solutions by sparging with argon. All other chemicals used were of reagent grade. Water was distilled thrice. In some experiments, the supporting electrolytes were further purified by electrolysis at a large mercury cathode in order to remove trace metal ions present in the solutions as contaminants.

RESULTS AND DISCUSSION

Preliminary experiments with cyclic voltammetry

Figure 1A shows that, in the presence of adenine, the single reversible system of peaks, corresponding to the Cu(II)/Cu(Hg) couple, diminishes and simultaneously two new systems of peaks, c_1/a_1 and c_3/a_3, appear on the cyclic curve. Thus, the Cu(II)/Cu(Hg) system is affected by adenine in much the same way as by ammonia [19] or purine [8], i.e. the single two-electron process is split into two one-electron processes corresponding to the Cu(II)/Cu(I) adenine and Cu(I) adenine/Cu(Hg) couples. When the potential scan was stopped for ca. 30 s just after passing peak c_1 and the anodic or cathodic curves were then recorded, peaks a_1 and c_3 increased. These results suggest that the Cu(I)/adenine complex is accumulated on the electrode surface. With a rise in the adenine concentration, the heights of peaks c_2/a_2 decrease further and the heights of peaks c_1/a_1 and c_3/a_3 increase.

With a decrease of pH from pH 3, the separation of peaks c_1/a_1 and c_3/a_3 diminishes and at pH 1 the one-electron peaks are overlapped by the main system of peaks. An increase of pH improves the separation of the c_1/a_1 and c_3/a_3 peaks but at pH > 4, peak a_1 forms only a shoulder on the mercury dissolution current and, in addition, a new system of peaks, c_4/a_4 occurs on the cyclic voltammetric curve. This new system appears only in solutions with sufficiently high adenine concentration. The general behaviour suggests that the c_3/a_3 and c_4/a_4 peaks correspond to formation and reduction of a mono- and multi-layer of the Cu(I)/adenine deposit.

The interaction between adenine and the copper species was also studied in neutral, unbuffered solutions containing 0.15 mol dm^{-3} chloride. The presence of chloride has three effects: the anodic oxidation of mercury shifts markedly towards more negative potentials, the Cu(II)/Cu(Hg) couple splits into two one-electron couples and the Cu(II)/Cu(I) couple is completely masked by the mercury dissolution current. Under these conditions, the Cu(II)/Cu(I) adenine couple is also masked by the mercury dissolution current, whereas the peaks of the Cu(I)/adenine/Cu(Hg) couple can still be observed. However, these peaks are ill-defined compared with

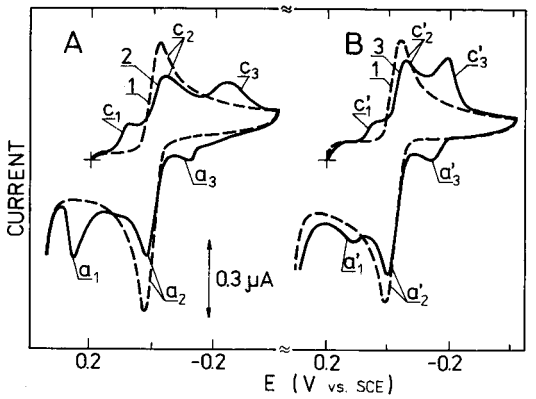

Fig. 1. The influence of adenine and adenosine on the cyclic voltammetric curves obtained for the Cu(II)/Cu(Hg) system at the HMDE. Solutions: (A) 0.3 mol dm^{-3} acetic acid/0.1 mol dm^{-3} $LiClO_4$; (B) acetate buffer, pH 4.8. Curves: (1) 5×10^{-5} mol dm^{-3} Cu(II); (2) as 1 + 1×10^{-5} adenine; (3) as 1 + 1×10^{-5} mol dm^{-3} adenosine. Scan rate, 2 V min^{-1}.

their appearance when acetate buffer is used.

Adenosine in acidic solution (pH 2) does not affect the Cu(II)/Cu(Hg) couple. At pH 3.5, adenosine causes a slight split of this system and at pH 4.8 the split is well defined (Fig. 1B). Here again, stopping the potential scan for a short time just after passing peak c_1' followed by recording the anodic or cathodic curves leads to enhancement of the heights of peaks a_1' and c_3'. Thus, the Cu(I)/adenosine complex is also accumulated on the electrode surface. An increase of the adenosine concentration leads initially to increased peak height but later the height of the a_3/c_3 system becomes constant. A further rise of pH leads to improved separation of the one-electron peaks. However, in neutral and borate buffer solutions containing adenosine and copper(II) ions, a precipitate appears in the bulk solution and the curves obtained under such conditions are severely distorted.

In principle, similar results can be obtained at the HCADE without addition of Cu(II) ions to the solution. The use of each of the electrodes has its advantages and disadvantages. The use of the HMDE, in the presence of Cu(II) ions, enhances the background currents at potentials more negative than peak c_2 because of Cu(II) ion reduction; the study of the cathodic stripping peak thus becomes more difficult. In contrast, use of the HCADE enhances the background currents at potentials more positive than peak c_2 because of oxidation of the copper amalgam; the conditions for studying the anodic stripping peak are then worse.

Figure 2 shows a comparison of cyclic voltammograms obtained for adenine and adenosine at the HMDE and at the HCADE in a solution of pH 5.6. The curve obtained for adenosine at the HMDE does not differ from the background current (curve 1), i.e., adenosine does not react with mercury

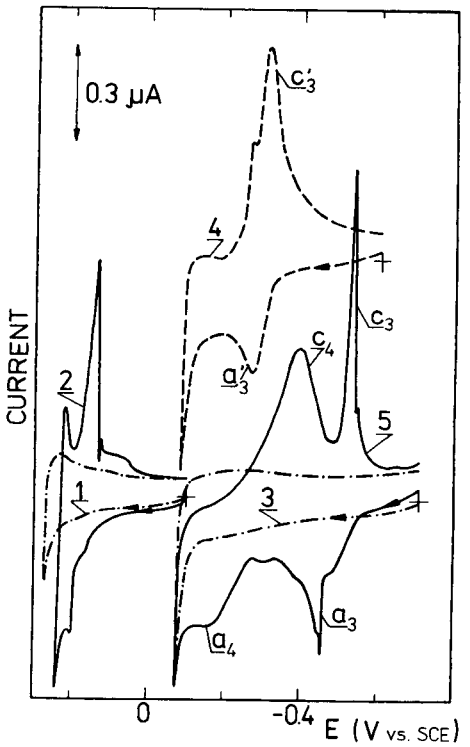

Fig. 2. Comparison of cyclic voltammetric curves obtained with the HMDE (1, 2) and the HCADE (3—5) in acetate buffer solution, pH 5.6. Curves: (1, 3) blank tests; (2, 5) 4×10^{-5} mol dm^{-3} adenine; (4) 4×10^{-5} mol dm^{-3} adenosine. Scan rate 2 V min^{-1}.

prior to the mercury dissolution current, and so no cathodic stripping peak is obtainable. In contrast to such behaviour, curve 4 obtained for adenosine at the HCADE shows the well-defined peaks a'_3 and c'_3 corresponding to the anodic formation and cathodic reduction of the Cu(I)/adenosine complex, respectively. Moreover, the cathodic peak is higher than the anodic one (Fig. 2, curve 4) which means that the Cu(I)/adenosine complex is accumulated on the electrode surface.

Curve 2 obtained for adenine at the HMDE reveals only a shoulder on the mercury dissolution current which can be attributed to the formation of an adenine compound with mercury. Reduction of this compound yields a sharp cathodic peak but it is located too close to the anodic limit for easy use in cathodic stripping voltammetry. Much better separation of the adenine peak from the anodic limit was observed on the voltammogram obtained at the HCADE (curve 5), though under these conditions an additional system of peaks, c_4/a_4, appears. The properties of these peaks were studied more thoroughly in recent work [9] in which their occurrence was explained in terms of separation of peaks of mono- and multi-layers of

the Cu(I)/adenine deposit. The charge involved in the formation and reduction of the monolayer was ca. 60 μC cm^{-2}.

In solutions containing Cu(II) ions, a further rise of pH led to serious distortion of the cyclic voltammograms because of precipitation of copper(II) hydroxide. The use of the HCADE in solutions with the same pH gave much better defined curves on which the peaks c_4/a_4 and c_3/a_3 shifted to markedly more negative potentials.

Anodic film stripping

The experiments described above showed that anodic peaks corresponding to oxidation of the Cu(I)/adenine or Cu(I)/adenosine complexes deposited on the electrode surface can be obtained. Such deposits were also formed for much lower concentrations of adenine. The best conditions for the proper location of peak a_1 with the HMDE were an accumulation potential of 0.0 V and a supporting electrolyte composed of acetic acid, pH 2.7 (0.3 mol dm^{-3}) and lithium or sodium perchlorate (0.1 mol dm^{-3}). When the accumulation potential is too negative or when pH of the solution is too low, then peak a_1 is affected by the copper dissolution current; if the accumulation potential is too positive, peak a_1 decreases in height. At higher pH, the stripping peak shifts to more positive potentials and forms only a shoulder on the mercury dissolution current. Figure 3 presents several curves obtained for adenine under optimum conditions; the anodic film stripping peak, a_1, is very well defined. Its width at half height is only 45 mV. The detection limit attained under these conditions was 2×10^{-8} mol dm^{-3}. For a 2-min accumulation time, the dependence between the peak height and the adenine concentration was linear over the range $0.5—4 \times 10^{-7}$ mol dm^{-3}. For longer accumulation times, the upper limit decreased. Above the upper limit, the stripping peak height became nearly constant, indicating that the peak corresponds to the oxidation of a monolayer only. The charge involved in the formation of peak a_1, when its height was independent of adenine concentration was 50 ± 5 μC cm^{-2}. This value is close to the charge found for reduction of a monolayer of the Cu(I)/adenine complex but is very different from the charge involved (31 ± 2 μC cm^{-2}) in reduction of the Cu(I)/purine monolayer [8].

In similar experiments with 1×10^{-7} mol dm^{-3} adenosine in acetate buffer (pH 4.8 and 5.6), the anodic film stripping peak was significantly smaller than the peak obtained under these conditions for adenine. Moreover, the height of this peak diminished markedly with decreasing pH and reproducibility was poor. Thus, the peak a_1' cannot be exploited for determining traces of adenosine by anodic film stripping.

Cathodic stripping

With the HCADE (Fig. 4), the peaks were well defined for both adenine and adenosine ($9 \times 10^{-8}—1 \times 10^{-6}$ mol dm^{-3}) though their width at half height (ca. 75 mV) was markedly larger than that of the peaks in Fig. 3.

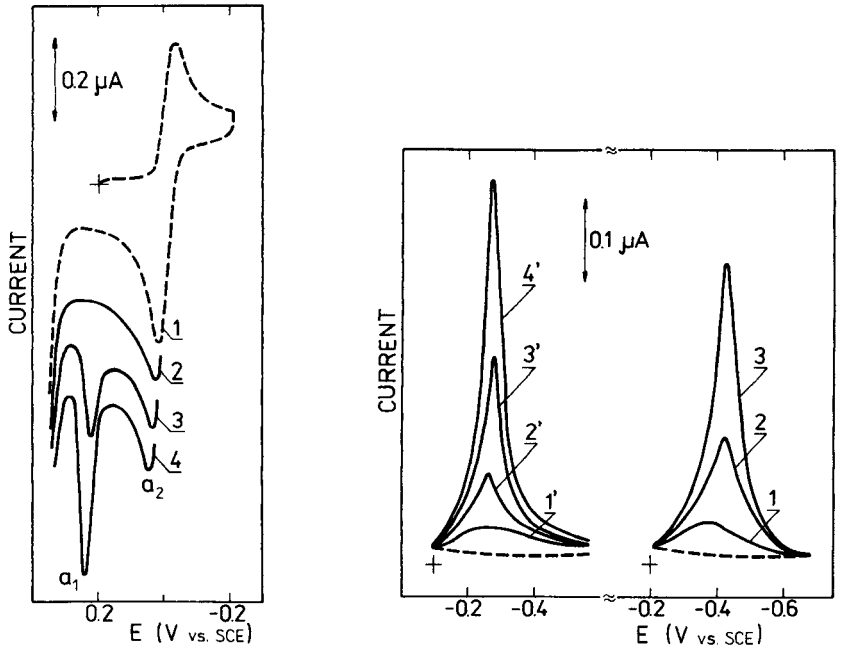

Fig. 3. Cyclic voltammetric curve (1) and anodic stripping curves (2—4) obtained with the HMDE. Solution: 0.3 mol dm^{-3} acetic acid/0.1 mol dm^{-3} lithium perchlorate/4 × 10^{-5} mol dm^{-3} Cu(II) ion. Adenine concentration: (1, 2) 0; (3) 4 × 10^{-8}; (4) 8 × 10^{-8} mol dm^{-3}. Accumulation at 0.0 V for 5 min in stirred solution; scan rate 2 V min^{-1}.

Fig. 4. Cathodic stripping curves obtained with the HCADE: (1—3) adenine; (1'—4') adenosine. Concentration of adenine or adenosine: (1, 1') 9 × 10^{-8}; (2, 2') 2 × 10^{-7}; (3, 3') 5 × 10^{-7}; (4') 1 × 10^{-6} mol dm^{-3}. Acetate buffer, pH 5.6; accumulation time 3 min with stirring at —0.08 V for adenosine and at —0.2 V for adenine; scan rate 1 V min^{-1}. (- - -) Blank tests.

At concentrations exceeding 1 × 10^{-6} mol dm^{-3}, the adenine peaks were distorted whereas the adenosine peak heights became almost constant. In order to find the optimum conditions for very low concentrations of adenine, the influence of many factors on the cathodic stripping peak of the Cu(I)/adenine complex was studied. It was found that the reduction of Cu(II) ions at the HMDE also leads to accumulation of the Cu(I)/adenine complex on the electrode; the cathodic stripping peaks obtained for adenine with 2 × 10^{-6} mol dm^{-3} Cu(II) ion in solution were nearly identical with the peaks in Fig. 4 but higher concentrations of Cu(II) ions distorted the peak shape.

The effects of the accumulation potential and accumulation time (with the HCADE) on the Cu(I)/adenine stripping peak are presented in Fig. 5. The peak height is independent of the accumulation potential over the range —0.1 to —0.2 V (curve A); accumulation at more positive potentials leads to some dissolution of copper from the amalgam and the stripping peak is distorted by the Cu(II) reduction current. It should be noted that the

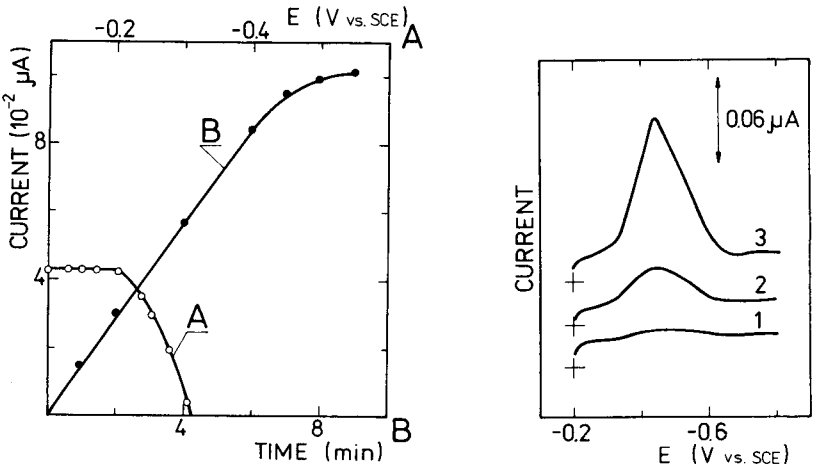

Fig. 5. Dependence of the stripping peak height on accumulation potential (A) and accumulation time (B). Acetate buffer solution, pH 5.6, containing 1×10^{-7} mol dm^{-3} adenine; plot A was obtained for a 3-min accumulation time and plot B for an accumulation potential of —0.2 V.

Fig. 6. Cathodic stripping curves obtained with the HCADE in acetate buffer, pH 4.8. Adenine concentration: (1) 0; (2) 1×10^{-8}; (3) 4×10^{-8} mol dm^{-3}. Accumulation for 5 min at —0.2 V with stirring; scan rate 2 V min^{-1}.

optimum potential range depends on the pH of the solution. The dependence between the stripping peak height and the accumulation time is linear up to 7 min (curve B).

The influence of temperature on the adenine stripping peak was studied over the range 7—40°C. A decrease from 20 to 7°C led to a marked decrease of peak height with simultaneous increase of peak width. An increase in temperature from 20 to 40°C increased the peak height, the temperature coefficient being 1.6%/°C. However, at the higher temperature, the reproducibility of results was worse than at 20°C. The dependence of the peak height on the voltage scan rate was studied for 5×10^{-7} mol dm^{-3} adenine at an accumulation time of 2 min; peak heights increased linearly with scan rate in the range 0.25—4 V. The influence of pH on the cathodic stripping peak was studied for 2×10^{-7} mol dm^{-3} adenine in the following solutions: 0.01 mol dm^{-3} $HClO_4$/0.1 mol dm^{-3} $LiClO_4$; acetate buffer of pH 4.0, 4.8 and 5.6; neutral 0.15 mol dm^{-3} NaCl; and borate buffer, pH 9.2. For a 2-min accumulation time, the cathodic stripping peaks were observed in all these solutions. Not surprisingly, the most distorted stripping peak was observed in the sodium chloride solution; the best was obtained from acetate buffer pH 4.8 or 5.6.

Figure 6 shows the cathodic stripping curves obtained for $1—4 \times 10^{-8}$ mol dm^{-3} adenine. The peaks are less well defined than those shown in

Fig. 4. Their width at half height increased to ca. 150 mV, but they are still sufficiently well defined for quantitative purposes. The height of the stripping peak (pH 5.6, 3-min accumulation time) was related linearly to the adenine concentration (correlation coefficient 0.9998, $n = 12$) over the range 5×10^{-9}—1×10^{-6} mol dm^{-3}. The relative standard deviation ($n = 5$) for 4×10^{-7} mol dm^{-3} adenine was 3%. At concentrations higher than 1×10^{-6} mol dm^{-3}, the plot gradually became level.

The copper(I)/adenine complex deposited on the surface of the HCADE can also be stripped in the differential-pulse mode. Voltammograms obtained for the electroreduction of the deposit with the linear-sweep and differential-pulse (d.p.) modes were compared. The d.p. mode yielded slightly higher analytical signals (for a scan rate of 2 V min^{-1}) but the background currents were definitely worse. Thus, the use of the differential-pulse mode does not provide lower detection limits.

Similar experiments were done for adenosine. The best pH range for adenosine determination was 4.8—5.6. The Cu(I)/adenosine cathodic stripping peak occurs at a slightly more positive potential than the Cu(I)/adenine peak and for the determination of adenosine the optimum accumulation potential was in the range —0.08 to —0.20 V. The plot of peak height vs. accumulation time was linear up to 8 min. The calibration plot was linear, with a correlation coefficient of 0.9996, over the range 9.0×10^{-8}—1.05×10^{-6} mol dm^{-3}. The method based on exploitation of the adenosine stripping peak obtained in borate buffer solutions at pH 8.0—9.0 gave slightly lower detection limit.

Attempts to determine adenine and adenosine in mixtures

The presence of two closely related solid substances on the electrode surface makes stripping analysis very difficult or even impossible. The difficulties may decrease when only one component of the mixture has to be determined. In such a case, it is necessary to search for conditions under which only the required component is deposited on the electrode surface during the accumulation step. In an attempt to find such conditions, the composition of the solution and the deposition potential were varied. As described above, the optimum pH for obtaining the anodic film stripping peak for adenine is 2.7, but this value is highly unfavourable for obtaining the anodic stripping peak of adenosine. Consequently, at pH 2.7, 1×10^{-7} mol dm^{-3} adenine can be determined, on the basis of the anodic film stripping peak, even in the presence of 1×10^{-6} mol dm^{-3} adenosine. Another possibility is to exploit the lack of a cathodic stripping peak for adenosine in solutions at pH < 3.5; in this medium adenine yields a quite well-defined cathodic stripping peak.

Figure 7 presents the cathodic stripping curves obtained for adenine and adenosine at pH 4.8. It is evident that separation of the peak of adenine (curve 4) and adenosine (curve 3) is rather poor. Curve 5 obtained for a

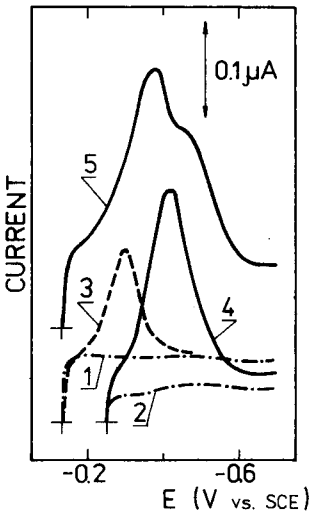

Fig. 7. Cathodic stripping voltammograms for adenine and adenosine in acetate buffer pH 4.8. Curves: (1, 2) blank solutions; (3) 1×10^{-7} mol dm^{-3} adenosine; (4) 1×10^{-7} mol dm^{-3} adenine; (5) 1×10^{-7} mol dm^{-3} each of adenine and adenosine. Accumulation potential (for 5 min in stirred solution): (1, 3, 5) —0.13 V; (2, 4) —0.25 V. Scan rate 2 V min^{-1}.

mixture of adenine and adenosine, after accumulation at —0.13 V (i.e., at the optimum potential for determining adenosine) is very complex and could not be exploited for the determination of either adenine or adenosine unless deconvolution programs were used which take into account not only the change in peak height but also the change in peak potential with the concentrations of the two analytes. More simply, the cathodic stripping curve obtained for a mixture of adenine and adenosine after accumulation at —0.25 V showed only a single, well-defined peak that, in practice, does not differ from the peak obtained for adenine alone (curve 4). Thus, it is evident that accumulation at —0.25 V enables adenine to be determined in the presence of adenosine. Additional experiments showed that even a 5-fold excess of adenosine does not interfere with the determination of adenine.

A thorough evaluation of the data presented in Fig. 7 suggests that a rough simple estimation of adenosine is possible. The difference between the well-defined adenine (curve 4) and the overlapping distorted signals from the mixture (curve 5) should correspond to the signal of adenosine. In such rough estimations the peak areas must be used. This suggestion was verified by analysing mixtures containing 1×10^{-7} mol dm^{-3} each of adenine and adenosine; the concentration of adenosine was estimated with a ±25% error.

Interferences

In principle, the most severe interferences could be caused by the formation of adenine and adenosine complexes with mercury species and by the formation of Cu(I) complexes of substances present in the solution studied. In practice, the peaks of the complexes of mercury with adenine and adenosine either did not occur at all or appeared at such positive potentials that they were easily eliminated by the choice of the correct deposition potential. Interferences involving formation of copper(I) complexes may occur in the presence of purine [8], thiocyanates [7], iodides [5], cysteine [6, 10] and tryptophan [6]. The harmful effect of tryptophan can be eliminated simply by decreasing the pH [6]. The other substances mentioned yield stripping peaks over a wider pH range and therefore their influence cannot be eliminated so easily.

The influence of salts commonly used as supporting electrolytes was studied in acetate buffer, pH 5.6, containing 2×10^{-7} mol dm^{-3} adenine or adenosine. The adenosine and adenine stripping peaks obtained after 2-min accumulation in stirred solution were not affected by perchlorate, sulphate or nitrate at concentrations below 0.2 mol dm^{-3}. In the presence of chloride, the anodic stripping anodic peak of adenine was obscured by chloride-promoted oxidation of copper and mercury, but the cathodic stripping peak of adenine was affected only slightly. Under the same conditions, the cathodic stripping peak of adenosine could be used quantitatively.

Conclusions

The results obtained show that adenine and adenosine form stronger complexes with copper(I) than with copper(II). These compounds are sparingly soluble and are easily accumulated on the surface of mercury or amalgam electrodes. Such properties are convenient for determining traces of adenine and adenosine by stripping techniques. The essential advantage of the use of copper(I) deposits in film stripping voltammetry is that their stripping peaks occur at more negative potentials than those of the corresponding mercury compounds. Thus a stripping peak for adenosine was obtained even in slightly acidic solutions; in such a medium, no stripping peak can be obtained for the appropriate mercury compound. For determination of traces of adenine, Paleček proposed the accumulation of the adenine/mercury compound which yields a well-defined stripping peak only in borate buffer; in the present work with the HCADE, well-defined cathodic stripping peaks were also obtained in neutral and acidic media. This broader possible range of pH offers two essential advantages. First, nearly neutral and acidic solutions (i.e., conditions more similar to those existing in living organisms) can be studied. Secondly, variations in pH can help to eliminate mutual interference between adenine and adenosine.

An essential advantage of the use of the copper(I) deposits is the possibility of obtaining anodic film stripping peaks. In general, when mercury

compounds are accumulated on the HMDE, it may be difficult to obtain good anodic stripping peaks prior to the main oxidation current of mercury. Anodic film-stripping peaks have been obtained for several copper compounds accumulated on the mercury electrode. For example, Berge and Jeroschewski [20] observed such stripping peaks in the presence of cyanides, and Forsman [21] and Tanaka and Yoshida [22] in cysteine-containing solutions. In recent work [8] a similar peak was observed for purine and in the present work for adenine.

This work was done as part of Problem CPBP 01.17.

REFERENCES

1 G. Dryhurst, Electrochemistry of Biological Molecules, Academic, New York, 1977.
2 E. Paleček, Anal. Lett., 13 (1980) 331; Anal. Biochem., 108 (1980) 129; Anal. Chim. Acta, 174 (1985) 103.
3 E. Paleček, F. Jelen, Mac Anh Hung and J. Lasovsky, Bioelectrochem. Bioenerg., 8 (1981) 621.
4 E. Paleček, J. Osteryoung and R. A. Osteryoung, Anal. Chem., 54 (1982) 1389.
5 R. Bilewicz and Z. Kublik, Anal. Chim. Acta, 171 (1985) 205.
6 M. Donten and Z. Kublik, Anal. Chim. Acta, 185 (1986) 209.
7 R. Bilewicz and Z. Kublik, Anal. Chim. Acta, 123 (1981) 201.
8 S. Głodowski, R. Bilewicz and Z. Kublik, Anal. Chim. Acta, 186 (1986) 39.
9 R. Bilewicz, S. Głodowski and Z. Kublik, J. Electroanal. Chem., in preparation.
10 U. Forsman, J. Electroanal. Chem., 111 (1980) 325; 122 (1981) 215; Anal. Chim. Acta, 146 (1983) 71.
11 D. L. Smith and P. J. Elving, J. Am. Chem. Soc., 84 (1962) 1412.
12 B. Janik and P. J. Elving, Chem. Rev., 68 (1968) 295; J. Am. Chem. Soc., 92 (1970) 235.
13 T. E. Cummings, J. R. Frazer and P. J. Elving, Anal. Chem., 52 (1980) 558.
14 G. Dryhurst and P. J. Elving, Talanta, 16 (1969) 855.
15 V. Vetterl, Collect. Czech. Chem. Commun., 31 (1966) 2105.
16 T. M. Florence, J. Electroanal. Chem., 97 (1979) 219.
17 W. Kemula and Z. Kublik, Anal. Chim. Acta, 18 (1958) 104.
18 Z. Galus, Crit. Rev. Anal. Chem., 4 (1975) 396.
19 M. Van Stackelberg and H. Van Freyhold, Z. Electrochem., 46 (1940) 120.
20 H. Berge and P. Jeroschewski, Fresenius' Z. Anal. Chem., 228 (1967) 9.
21 U. Forsman, J. Electroanal. Chem., 152 (1983) 241.
22 S. Tanaka and H. Yoshida, J. Electroanal. Chem., 137 (1982) 261; 149 (1983) 213.

Analytica Chimica Acta, 201 (1987) 23—32
Elsevier Science Publishers B.V., Amsterdam — Printed in The Netherlands

DETERMINATION OF SELENIUM(IV) BY DIFFERENTIAL PULSE VOLTAMMETRY OF THE 3,3'-DIAMINOBENZIDINE PIAZSELENOL

PH. BREYER and B. P. GILBERT*

Laboratory of Analytical Chemistry and Radiochemistry, University of Liège, Sart Tilman, B-4000 Liège (Belgium)

(Received 5th March 1987)

SUMMARY

The determination of selenium(IV) by voltammetry through the formation of a piazselenol with 3,3'-diaminobenzidine (DAB) is described. At pH 1.5 and with a large excess of DAB, the formation of piazselenol is quantitative. In a borate-buffered electrolyte at pH 9, the piazselenol gives reduction peaks at potentials of −0.64 V and −0.82 V vs. SCE. The influence of DAB concentration on the sensitivity of the method is discussed. The calibration graphs are linear over the range 0—200 $\mu g\ l^{-1}$ Se(IV) and the detection limit is 0.10 $\mu g\ l^{-1}$. Copper(II) and lead(II) are tolerated in 500-fold amounts; the method is applicable to the determination of selenium in NBS Oyster Tissue.

Selenium has received much attention from biologists because of its dual role as both a trace nutrient at low concentration and a toxic compound at higher levels. This interest has created a need for reliable analytical methods for the determination of selenium in various biological samples where sub-mg l^{-1} levels are encountered. Such methods should be capable not only of determining the total selenium content but also of distinguishing the different oxidation states encountered in biological samples, because the physiological and toxicological properties of selenium are markedly influenced by the oxidation state and the type of compound formed. Among the techniques which have been proposed, the most extensively used are atomic absorption spectrometry with hydride generation [1—3] and fluorimetry after reaction with an *o*-diamine [4, 5]. These techniques often require a prior chemical separation of the selenium in order to eliminate the interferences which occur when biological samples are analysed. The high sensitivity of neutron activation methods makes them attractive, but the special skills, time and costs related to this technique limit its application in routine analysis [6, 7].

Electrochemical techniques, and especially differential pulse voltammetry, can provide a cheap, simple and highly sensitive way of determining selenium in biological materials. At the mercury electrode, Se(IV) gives two reduction waves corresponding to a two-step reduction to HgSe and then to Se(−II). Both reactions have been used for the determination of selenium in various media, but the method suffers from several interferences [8—10].

The reaction between Se(IV) and aromatic diamines to form piazselenols

0003-2670/87/$03.50

has been used in polarography since the early work of Le Peintre [11]. The reaction is specific to the different oxidation states of selenium [12–15]. The 3,3′-diaminobenzidine (DAB) has been most widely used for the determination of selenium in biological matrices [11–14]. Interferences can be avoided by extraction of the piazselenol into an organic solvent and back-extraction into an aqueous solution suitable for polarography. The extraction procedure involves some preconcentration of the selenium and the detection limit is then lowered to 0.5 $\mu g\ l^{-1}$.

In this work, the use of DAB has been re-investigated for the differential pulse voltammetric determination of Se(IV) in biological media. The voltammetric behaviour of the piazselenol is discussed and a procedure is described which allows the determination of selenium down to 0.5 $\mu g\ l^{-1}$ without any preconcentration.

EXPERIMENTAL

Reagents, solutions and apparatus

As is well known, 3,3′-diaminobenzidine tetrahydrochloride (DAB) solutions are unstable, being oxidized in contact with air. The commercially available reagent is always contaminated by oxidation products and needs preliminary purification by repeated recrystallization from 3 M hydrochloric acid. 3,3′-Diaminobenzidine tetrahydrochloride was then obtained as colourless needles which were dried in vacuo and stored in the dark. Under these conditions, the reagent was stable for several months. Stock solutions (0.1%, w/v) were prepared by dissolving the purified reagent in water. They could be stored in the dark in a refrigerator (4°C) for more than one week.

Selenium(IV) standard solutions (1 mg ml^{-1}) were prepared by dissolving elemental selenium in concentrated nitric acid and diluting with ultrapure water. Standard solutions of piazselenol (1 μg Se l^{-1}) were obtained by mixing a measured volume of stock selenium solution with a large excess of DAB (1 mg ml^{-1}) in 0.02 M HCl. These solutions could be stored in the dark in a refrigerator for a week without degradation. Solutions of lower concentration were prepared by successive dilutions when they were needed.

High-purity water was supplied from a Millipore Milli-Q ion-exchange unit. Acids and salts were of Suprapur grade (Merck).

A Bruker E310 modular polarographic analyzer was used with a three-electrode system. The working, reference and auxiliary electrodes were a hanging mercury drop electrode (HMDE; Metrohm E410), a saturated calomel electrode (SCE) and a platinum wire, respectively. The operating conditions for differential pulse voltammetry were as follows: pulse amplitude 50 mV, pulse period 1 s, scan rate 2 mV s^{-1}.

Procedure

The Se(IV) samples were acidified to approximately pH 1.5, an amount of DAB between 100 and 200 mg l^{-1} was added and the solution was left in the dark for 1 h to ensure complete formation of the piazselenol.

After the pH of the sample has been adjusted to 9 by adding borax up to a concentration of 0.05 M and a few drops of dilute sodium hydroxide solution, the solution was transferred to the electrolytic cell and deaerated with nitrogen for 15 min.

The differential pulse (d.p.) voltammogram was then recorded from −0.35 V to −1.00 V and the two reduction peaks of piazselenol can be used for the determination. The concentration of Se(IV) in the sample was quantified by the method of standard addition.

RESULTS AND DISCUSSION

Formation of piazselenol

The reaction between aromatic *o*-diamines and selenium is specific for selenite. The mechanism of the reaction for 1,2-diaminobenzene has been discussed by Barcza [16] and involves, as rate-determining step, a bimolecular reaction between undissociated selenious acid and the monoprotonated diamine. At suitable reactant ratios, the reaction with DAB can lead to the formation of either a 1:1 or a 2:1 Se/DAB compound [17]:

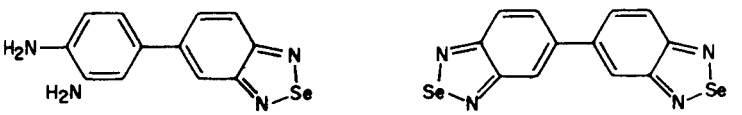

The formation of the dipiazselenol can be avoided by using a large excess of DAB, but the reaction rate is then so high that a spectrophotometric study of the kinetics is no longer possible.

Here, the kinetics of the reaction was investigated by voltammetry at a lower selenium concentration in order to slow down the reaction rate. The reaction was followed by measuring the formation of the piazselenol as a function of time at 25°C. A typical plot of the height of the voltammetric peak of piazselenol versus time at constant pH is shown in Fig. 1. The relative rate of the reaction is obtained by measuring the initial slope of the curve. Pseudo orders for DAB and selenious acid are obtained from the slope of the logarithmic plot of this relative rate versus the logarithm of the concentration of one reagent, while the concentration of the other reagent is kept constant. In this way, it was found that the reaction follows a pseudo-first-order kinetics for both selenious acid and DAB.

The rate constant was derived from the second-order rate plots (Fig. 2), following the integrated second-order rate law

$$\ln [(a-x)/(b-x)] \ln (b-a) + k\,(a-b)t$$

where a is the initial concentration of selenious acid, b the initial concentration of DAB, and x the concentration of piazselenol at time t. The second-order rate constants and the conditions under which they were obtained, are summarized in Table 1.

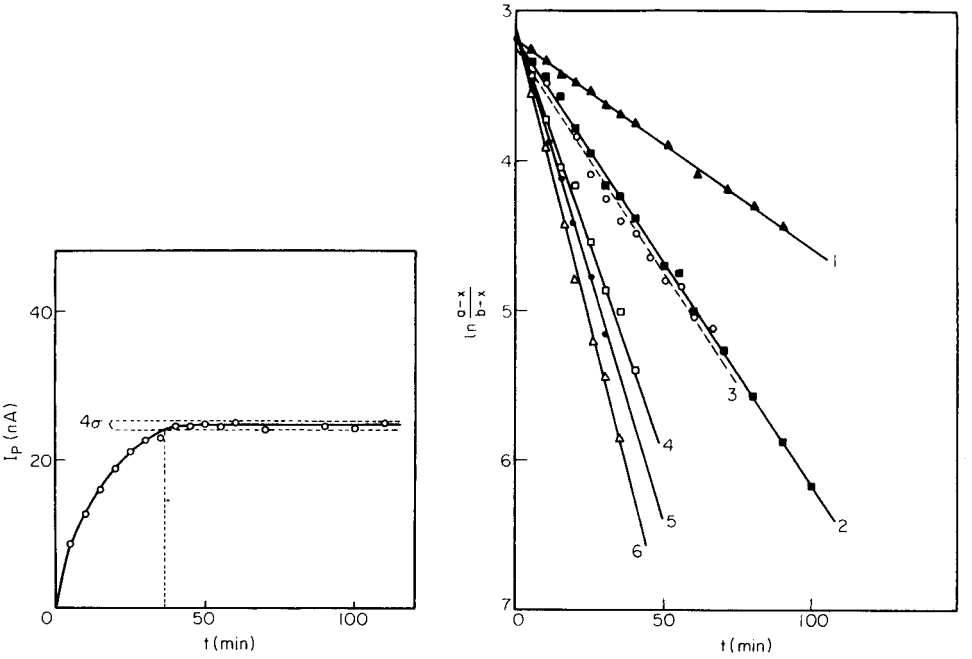

Fig. 1. Height of the voltammetric peak of monopiazselenol vs. time. Conditions: 27 $\mu g\ l^{-1}$ (3.4×10^{-7} M) selenium, 180 mg l^{-1} (5.0×10^{-4} M) DAB, pH 1.5.

Fig. 2. Second-order integrated rate constants (k') at various pH values (1.67×10^{-6} M selenium, 4.06×10^{-4} M DAB). Plots: (1) pH 3.3, $k' = 36$; (2) pH 2.9, $k' = 77$; (3) pH 0.4, $k' = 78$; (4) pH 0.9, $k' = 145$; (5) pH 2.1, $k' = 168$; (6) pH 1.5, $k' = 197$.

TABLE 1

Second-order rate constants

pH	H_2SeO_3 (μmol l^{-1})	DAB (μmol l^{-1})	k' (l mol^{-1} min^{-1})	pH	H_2SeO_3 (μmol l^{-1})	DAB (μmol l^{-1})	k' (l mol^{-1} min^{-1})
2.2	8.4	170	161	1.5	16.7	170	195
2.2	16.7	440	156	1.5	16.7	250	199
2.2	4.15	440	153	1.5	16.7	660	194
2.2	8.2	660	173	1.5	16.7	820	199
2.2	2.1	440	176	1.2	16.7	406	184
2.2	0.33	440	162	0.9	16.7	406	145
2.2	0.17	440	169	0.4	16.7	406	78
1.8	16.7	406	190	3.3	16.7	406	36
1.5	16.7	406	197	2.9	16.7	406	77
1.5	16.7	500	201	2.1	16.7	406	168

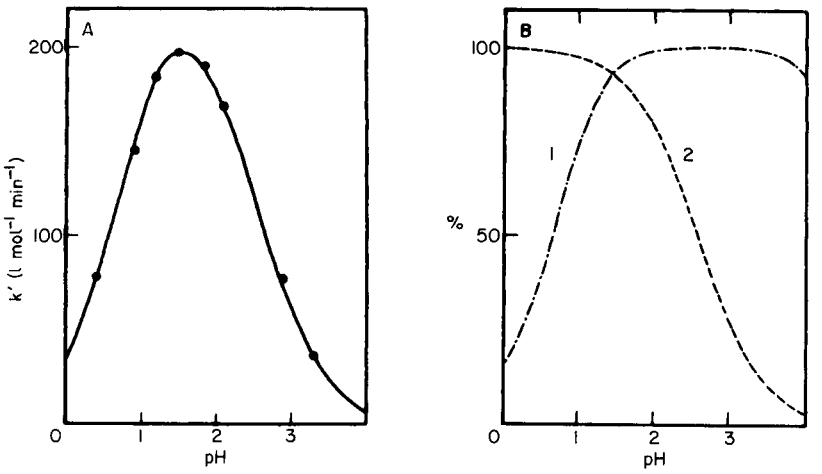

Fig. 3. Influence of pH on the rate of formation of the piazselenol (1.67×10^{-5} M selenium, 4.06×10^{-4} M DAB). (A) Second-order rate constant; the points represent experimental values. (B) Distribution of the reacting species: (1) undissociated selenious acid; (2) monoprotonated amino groups of DAB.

Figure 3A shows the influence of the pH on the second-order rate constant. The curve passes through a maximum at pH 1.5 and its shape corresponds to the distribution of undissociated selenious acid and monoprotonated forms of DAB (Fig. 3B). This behaviour shows that the reaction with DAB follows the same mechanism as described by Barcza for the reaction with 1,2-diaminobenzene, provided that DAB is present in large excess to avoid the formation of the dipiazselenol.

The concentration of DAB was shown to have a great influence on the reaction time (Fig. 4). In order to maintain the reaction time within acceptable limits, the DAB concentration must be fixed between 100 and 200 mg l^{-1}. The use of a higher reagent concentration reduces the reaction time but leads to the formation of spurious peaks in the voltammogram which are believed to be due to oxidation products of DAB. Such observations indicated that the reaction should be at room temperature and in subdued light, because both sunlight and temperature promote reagent decomposition. A concentration range of 100–200 mg l^{-1} DAB represents a large excess with respect to the usual selenium concentration (up to 1 mg l^{-1} Se); the reaction time does not then depend on the selenium concentration. The use of a large excess of DAB ensures also that the reaction is quantitative and leads to the exclusive formation of the monopiazselenol.

Voltammetric behaviour of piazselenol

Le Peintre [11] studied the piazselenol formed by reaction with DAB. At the dropping mercury electrode, the component shows two reduction waves corresponding to a two-step reduction, first to HgSe and then to Se(−II). In

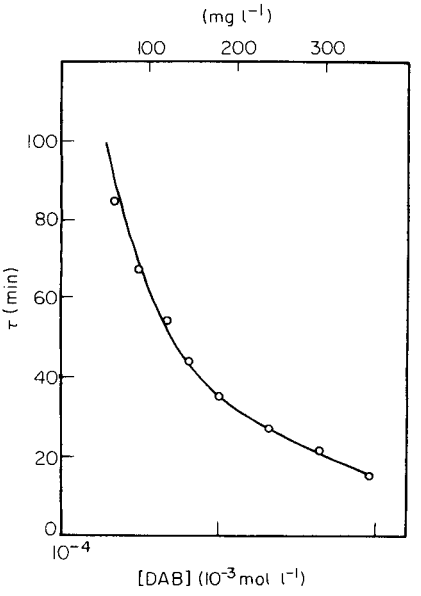

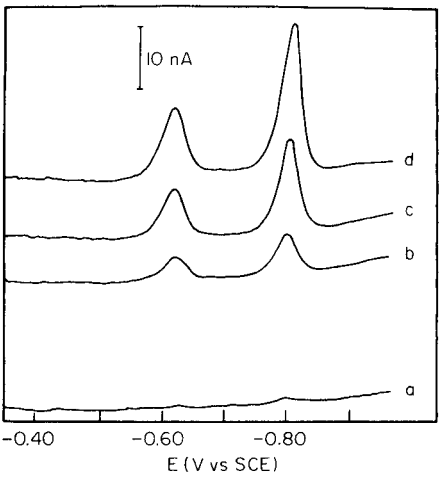

Fig. 4. Effect of DAB concentration on the reaction time for 1.67×10^{-5} M (1.3 μg l^{-1}) selenium at pH 1.5. $\tau = \ln (100/3)/k'$ [DAB].

Fig. 5. D.p. voltammograms for determination of selenium in borate buffer (pH 9) with 100 mg l^{-1} DAB present. Selenium concentration (μg l^{-1}): (a) 0; (b) 2.5; (c) 5; (d) 7.5.

the present work, it was observed that the reduction of piazselenol at the HMDE follows the same mechanism over the whole pH range, but the position and height of the peaks are influenced by the pH value (Table 2). Accordingly, borate buffer at pH 9 was used in order to provide greater sensitivity. Both reduction peaks can be used for quantitative purposes (Fig. 5).

D.c. polarographic experiments on pure piazselenol solutions showed that the sensitivity can be dramatically increased by polarizing the electrode at −0.35 V and stirring the solution (Table 3). This behaviour is due to adsorption of the piazselenol on the mercury electrode, as was confirmed by tensammetric experiments. Figure 6A shows that an increase in piazselenol concentration causes a decrease in the double-layer capacity in the adsorption

TABLE 2

Influence of pH on the position and the intensity of the two reduction peaks of piazselenol in d.p. voltammetry (6 μg l^{-1} selenium)

pH	2	4	8	9
i_{p_1} (nA)	5	5	9	12.5
i_{p_2} (nA)	10	10	26	32
E_{p_1} (V)	−0.075	−0.29	−0.59	−0.64
E_{p_2} (V)	−0.56	−0.645	−0.79	−0.82

TABLE 3

Influence of the deposition time at −0.35 V on the sensitivity of the d.c. voltammetric method for pure piazselenol solutions

Se conc. ($\mu g\ l^{-1}$)	Peak height (nA) after deposition for 0—5 min			
	0	1	2	5
1.1	1.5	12	26.8	42.5
4.6	6	55	123.5	125
9.2	13.5	150	210	200

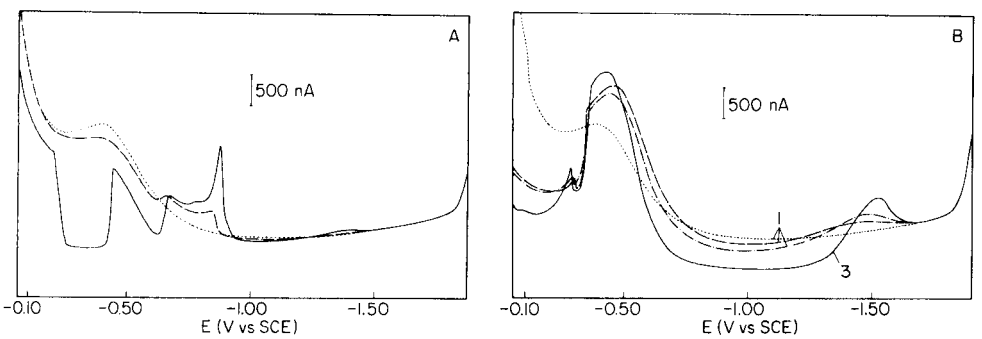

Fig. 6. Tensammetric curves for pure piazselenol (A) and for DAB (B) in 0.5 M NaCl/borax at pH 9, obtained by a.c. voltammetry (ΔE = 5 mV; frequency 510 Hz; phase angle 90°). For A: (···) baseline; (- - -) 115 $\mu g\ l^{-1}$ piazselenol; (—) 1 mg l^{-1} piazselenol. For B: (···) baseline; (- - -) 15 mg l^{-1} DAB; (···) 115 mg l^{-1} DAB; (—) 1150 mg l^{-1} DAB.

potential region. Similar experiments showed that DAB is strongly adsorbed on the electrode surface (Fig. 6B). In practical conditions (i.e., with a large excess of DAB), the adsorption of DAB exceeds that of piazselenol, so that accumulation of the piazselenol by adsorption on the electrode is no longer possible. The DAB concentration has a dramatic influence on the sensitivity of the voltammetric determination of selenium (Fig. 7). Therefore, for the determination of selenium, an excess of DAB larger than 200 mg l^{-1} should not be used although a larger concentration enhances the formation rate of the piazselenol.

Provided that a constant DAB concentration is used in the voltammetric determination the height of either reduction peak of the piazselenol is proportional to the selenium concentration in the range 0—200 μg Se l^{-1}. The detection limit, based on 3 times the standard deviation of the blank, is 0.5 μg Se l^{-1} for the first reduction peak and 0.1 μg Se l^{-1} for the second peak. Replicate analyses of solutions containing 5 and 100 μg Se l^{-1} gave relative standard deviations (2 σ) of 5 and 2%, respectively.

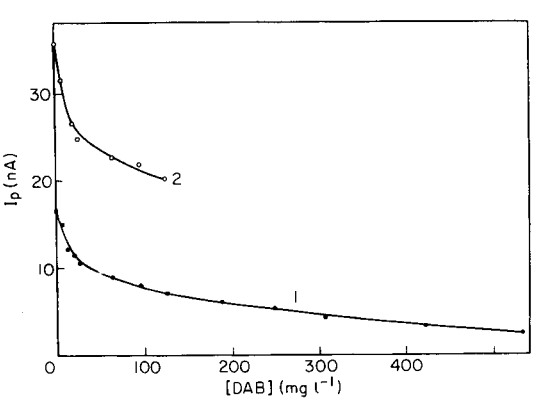

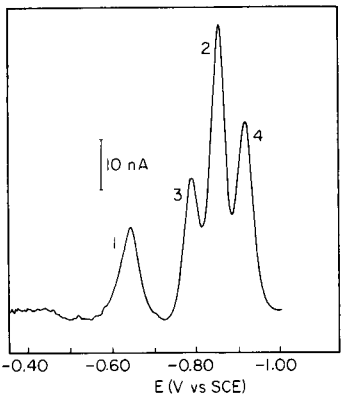

Fig. 7. Influence of DAB concentration on the determination of selenium (5 $\mu g\ l^{-1}$) in borate buffer at pH 9: (1) first reduction peak of piazselenol at −0.62 V; (2) second reduction peak of piazselenol at −0.80 V.

Fig. 8. D.p. voltammetry of a sample contaminated by DAB oxidation. Peaks: (1, 2) reduction peaks of piazselenol; (3, 4) spurious peaks from oxidation products of DAB. Conditions: borate buffer pH 9, 12 $\mu g\ l^{-1}$ selenium, 120 mg l^{-1} DAB.

Interferences

Two types of interferences are encountered. First, oxidizing compounds enhance the DAB degradation. Figure 8 shows that DAB degradation produces spurious peaks which hinder the accurate measurement of the second reduction peak of the piazselenol. However, selenium can still be determined from the first reduction peak. Secondly, various metals interfere. Figure 9 shows the effects of copper(II) and lead(II) on the voltammetry of piazselenol. A slight increase in the metal concentration produces a dramatic modification of the second reduction peak owing to the formation of insoluble selenides on the surface or in the vicinity of the electrode [8]. However, the first reduction peak of piazselenol is not affected by the metal concentration and selenium can be determined in the presence of 500-fold amounts of Cu(II) or Pb(II).

Accuracy and precision

The accuracy of the method was assessed by determining the selenium content of the NBS standard reference material Oyster Tissue (SRM 1566). The procedure was as follows: the dried and weighed sample (ca. 200 mg) was digested in a sealed teflon bomb [18] with 6 ml of a 1:1 nitric acid/hydrogen peroxide mixture at 150°C for 6 h; the residue was digested with 2 ml of 70% perchloric acid for 1 h. Subsequently, Se(VI) was reduced to Se(IV) by boiling the perchloric acid solution with hydrogen peroxide, as described by Nève et al. [19] and the solution was diluted to 100 ml. The procedure for the determination of selenium was then applied.

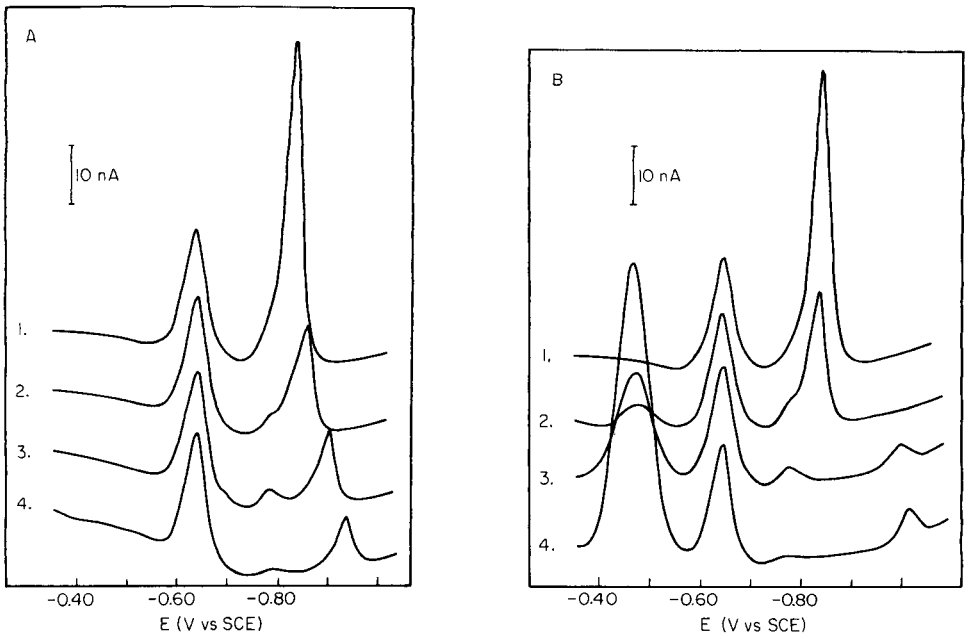

Fig. 9. Effects of copper (A) and lead (B) on the determination of selenium by d.p. voltammetry. Copper concentration (mg l^{-1}): (1) 0; (2) 0.45, (3) 1.75, (4) 5.50. Lead concentration (mg l^{-1}): (1) 0, (2) 0.065, (3) 0.31, (4) 0.93. Conditions: 0.5 M NaCl/borax pH 9, 17 $\mu g\ l^{-1}$ selenium, 100 mg l^{-1} DAB.

The analysis of 10 samples gave a mean content of 1.95 ± 0.4 $\mu g\ g^{-1}$ selenium; the NBS certified content is 2.1 ± 0.5 $\mu g\ g^{-1}$. These results indicate that the method provides accurate and precise values.

Conclusion

The proposed method, based on differential pulse voltammetry of DAB piazselenol at a hanging mercury drop electrode, provides a simple and sensitive approach for the determination of selenium(IV) in biological samples.

At pH 1.5, with a DAB concentration between 100 and 200 mg l^{-1}, the formation of the piazselenol is complete within 60 min. The use of a borate buffer at pH 9 without further treatment allows the voltammetric determination of selenium with a detection limit of 0.10 $\mu g\ l^{-1}$. Even 500-fold amounts of ions such as Cu(II) and Pb(II) can be tolerated. The reproducibility of the method is 5% at the 5 $\mu g\ l^{-1}$ level and the concentrations measured can be regarded as accurate.

This work was supported by the "Institut pour l'Encouragement de la Recherche Scientifique dans l'Industrie et l'Agriculture" (IRSIA, Brussels).

REFERENCES

1 M. McDaniel, A. D. Shendrikar, K. D. Reiszner and P. W. West, Anal. Chem., 48 (1976) 2240.
2 F. D. Pierce and H. R. Brown, Anal. Chem., 49 (1977) 1417.
3 A. D. Meyer, C. Hofer, G. Tölg, S. Raptis and G. Knapp, Frezenius' Z. Anal. Chem., 296 (1979) 337.
4 N. Michie, E. J. Dixon and E. G. Bunton, J. Assoc. Off. Anal. Chem., 61 (1978) 48.
5 A. Azad, G. F. Kirkbright and R. D. Snook, Analyst, 104 (1979) 232.
6 K. Jorstad and B. Salbu, Anal. Chem., 52 (1980) 672.
7 E. Damsgaard, K. Ostergaard and K. Heydorn, J. Radioanal. Chem., 70 (1982) 67.
8 S. Forbes, G. P. Bound and T. S. West, Talanta, 26 (1979) 479.
9 G. Jarzabek and Z. Kublik, Anal. Chim. Acta, 143 (1982) 121.
10 S. B. Adeloju, A. M. Bond and H. C. Hughes, Anal. Chim. Acta, 148 (1983) 59.
11 C. le Peintre, C.R. Acad. Sci., 252 (1961) 1968.
12 M. W. Blades, J. A. Dalziel and C. M. Elson, J. Assoc. Off. Anal. Chem., 59 (1976) 1234.
13 G. D. Christian, E. C. Knoblock and W. C. Purdy, J. Assoc. Off. Agric. Chem., 48 (1966) 877.
14 D. A. Griffin, Anal. Chem., 41 (1969) 462.
15 A. G. Howard, M. R. Gray, A. J. Waters and A. R. Oromiehie, Anal. Chim. Acta, 118 (1980) 87.
16 L. Barcza, Mikrochim. Acta, (1964) 136.
17 L. Barcza, Mikrochim. Acta, (1964) 967.
18 G. Gillain, Talanta, 29 (1982) 651.
19 J. Nève, M. Hanocq and L. Molle, Mikrochim. Acta, Part I, (1980) 259.

Analytica Chimica Acta, 201 (1987) 33—41
Elsevier Science Publishers B.V., Amsterdam — Printed in The Netherlands

DETERMINATION OF VERY LOW LEVELS OF SELENIUM(IV) IN SEA WATER BY DIFFERENTIAL-PULSE CATHODIC STRIPPING VOLTAMMETRY AFTER EXTRACTION OF THE 3,3′-DIAMINOBENZIDINE PIAZSELENOL

PH. BREYER and B. P. GILBERT*

Laboratory of Analytical Chemistry and Radiochemistry, University of Liège, Sart Tilman, B-4000 Liège (Belgium)

(Received 5th March 1987)

SUMMARY

Selenium(IV) is determined by cathodic stripping voltammetry after the formation of a piazselenol with 3,3′-diaminobenzidine. The selenium is then accumulated as HgSe on a mercury electrode by deposition at −0.45 V. The differential-pulse cathodic stripping peak allows a detection limit of 0.01 $\mu g\ l^{-1}$. For the determination of selenium in natural waters, interferences can be avoided by extraction of the piazselenol into toluene followed by a back-extraction into 0.5 M hydrochloric acid. The accuracy of the overall procedure was checked by analyses of a standard reference material. The method was applied to the determination of selenium(IV) in sea-water samples at levels as low as 20 $ng\ l^{-1}$ with a concentration factor of 10 during the extraction procedure.

Selenium is widely distributed in nature and has received much attention from biologists for its dual role as a trace nutrient at low levels and a toxic compound at higher concentration. However, the distribution and role of selenium in natural waters, especially in sea water, are not well known because of the very low concentrations encountered ($<0.1\ \mu g\ l^{-1}$) [1, 2]. As with many other elements, the oxidation state of selenium and the type of compounds formed should govern its biogeochemical role as well as its toxic effects. For these reasons, procedures for the determination of selenium in natural waters must combine high sensitivity and selectivity with respect to the oxidation state. The latter condition is fulfilled by the use of aromatic *o*-diamines which react specifically with selenite to form piazselenols. This reaction is used in fluorimetric [3, 4] and gas chromatographic [5–7] determinations of selenium in water.

Voltammetry, especially the cathodic stripping technique, has been used for the determination of selenium in biological samples [8–10]. The method is very sensitive, providing results down to the 0.01 $\mu g\ l^{-1}$ level, but suffers from several interferences. In the preceding paper [11], a method was described for the determination of selenium by differential pulse voltammetry of 3,3′-diaminobenzidine piazselenol at the $\mu g\ l^{-1}$ level. It was thought therefore that the use of cathodic stripping voltammetry (c.s.v.) in conjunction

0003-2670/87/$03.50

with a piazselenol formation should improve the sensitivity of the voltammetric technique and eliminate the interferences.

EXPERIMENTAL

Reagents, solutions and apparatus

Aqueous 3,3'-diaminobenzidine tetrahydrochloride (DAB) solutions (0.1%, w/v) were prepared from purified material and stored in the dark in a refrigerator, as described previously [11]. Standard solutions of selenium(IV) (1 mg ml^{-1}) and of piazselenol (1 μg ml^{-1} Se) were prepared and used as described [11].

High-purity water was supplied from a Millipore Milli-Q ion-exchange unit. Acids and salts were of Suprapur grade (Merck). Toluene was purified by distillation. The distilled toluene was washed twice with 1 M hydrochloric acid and then rinsed twice with ultrapure water.

A Bruker E310 modular polarographic analyzer was used in conjunction with the conventional three-electrode system comprising a hanging mercury drop electrode (HMDE; Metrohm E410), a saturated calomel reference electrode (SCE) and a platinum wire auxiliary electrode. The SCE was connected to the solution by a salt bridge (0.5 M NaCl).

The procedure was found to be extremely sensitive to the presence of residual oxygen. A hermetically sealed cell made in this laboratory was therefore used and the nitrogen used for deaerating the solution was first purified by bubbling through a vanadium(II) chloride solution.

The operating conditions for differential pulse voltammetry were as follows: pulse amplitude 50 mV, pulse period 1s, scan rate 2 mV s^{-1}.

Procedure

Filtered water samples (200 ml) containing Se(IV) was acidified to ca. pH 1.5, 200 mg l^{-1} DAB was added and the solution was left in the dark for two hours to ensure complete formation of the piazselenol. The pH was adjusted to about 8 and the sample was successively extracted by two 15-ml fractions of toluene. The separated toluene solution was then back-extracted with 20 ml of 0.5 M hydrochloric acid. Finally, this acid solution was transferred to the electrolytic cell and the pH was adjusted to 4.5 with sodium acetate and sodium hydroxide solutions. The final volume was measured by weighing. The solution was then deaerated with nitrogen for 30 min.

The selenium content was determined by differential-pulse cathodic stripping voltammetry after a deposition time of 10 min at a potential of -0.45 V vs. SCE. The concentration of Se(IV) in the sample was quantified by the method of standard addition.

RESULTS AND DISCUSSION

Formation and voltammetric behaviour of the piazselenol

The parameters governing the rate and the yield of the formation of the piazselenol were studied previously [11]. The pH of the solution must be

adjusted between 1.3 and 1.9. Provided that the DAB concentration is maintained between 100 and 200 mg l^{-1}, the formation of the monopiazselenol is complete within 60 min. The reaction is left to proceed in subdued light to hinder reagent decomposition.

At the mercury electrode, the reduction of the piazselenol follows a two-step mechanism: first, reduction produces mercury(II) selenide on the electrode and then this deposit is reduced to soluble Se(—II) in the second step. The direct reduction of the piazselenol was studied thoroughly for the determination of selenium [11], but the sensitivity obtained was not sufficient for its application to the determination of selenium in natural waters. It was found [11], unfortunately, that the strong adsorption of the piazselenol on the mercury surface could not be used to improve the sensitivity of the determination because of the stronger adsorption of DAB itself. The formation of a mercury selenide deposit as a result of the first reduction step, however, allows the use of the cathodic stripping technique in which the HgSe is first accumulated on the electrode and then reduced in a cathodic potential scan.

From preliminary experiments [11], it was known that the oxidation of DAB is responsible for the appearance of spurious peaks in the vicinity of the HgSe stripping peak. The potential difference between spurious and stripping peaks is strongly pH-dependent (Table 1) and the resolution increases at low pH values. Voltammograms were obtained at pH 4.5 (acetate buffer) because at lower pH, the proton reduction wave interferes with the measurement of the stripping peak.

The DAB concentration has no influence on the intensity of the cathodic stripping peaks (Table 2). However, large concentrations of DAB (more than 200 mg l^{-1}) cause an unexpected fall of the mercury drop, especially when long electrolysis times are used. This behaviour is due to the strong adsorption of the DAB on the mercury surface which lowers the interfacial tension at the mercury/solution interface.

Figure 1 shows the influence of the deposition potential on the height of the stripping peak at pH 4.5. Maximal peak height is obtained for potentials between −0.40 and −0.55 V vs. SCE; in practice, the deposition potential was fixed at −0.45 V vs. SCE.

The height of the stripping peak was proportional to the deposition time

TABLE 1

Potentials of the DAB spurious peak and the selenium stripping peak as a function of pH[a]

pH	Peak potential (V vs. SCE)		pH	Peak potential (V vs. SCE)	
	DAB	Se		DAB	Se
9	−0.780	−0.850	4.5	−0.495	−0.695
8	−0.715	−0.820	2	−0.355	−0.590
5	−0.540	−0.720	1	−0.325	−0.545

[a] 4 μg l^{-1} selenium, 60 mg l^{-1} DAB, deposition time 10 min.

TABLE 2

Influence of the DAB concentration on the determination of 1.15 $\mu g\ l^{-1}$ selenium with a deposition time of 10 min

DAB (mg l^{-1})	0	8	16	24	40	5	150	220
Current (nA)	72.5	71.5	74	75	72	71	72	72.5

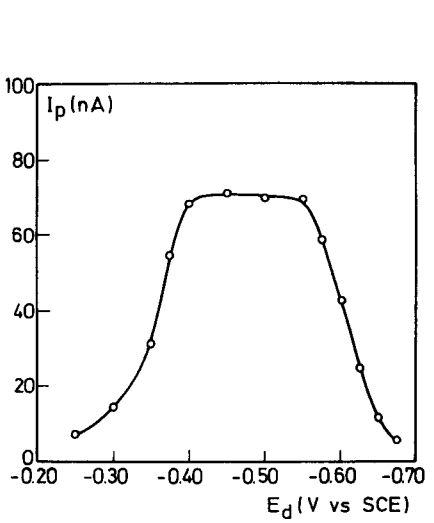

Fig. 1. Influence of deposition potential, E_d, on the sensitivity of the cathodic stripping process. Conditions: 0.9 $\mu g\ l^{-1}$ selenium, 100 mg l^{-1} DAB, pH 4.5, deposition time 10 min.

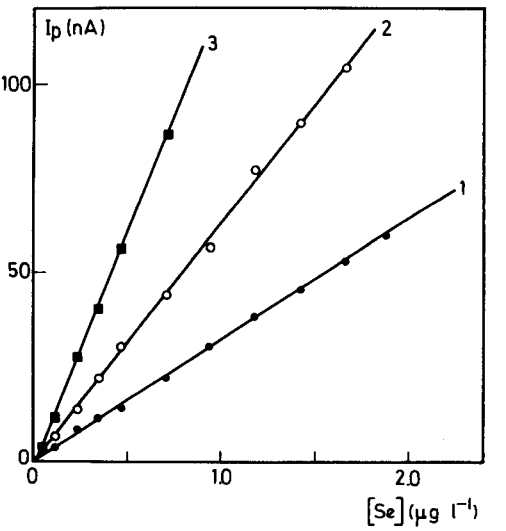

Fig. 2. Calibration graphs obtained for different deposition times: (1) 5 min; (2) 10 min; (3) 20 min. Conditions: 100 mg l^{-1} DAB, pH 4.5, deposition potential −0.45 V vs. SCE.

up to 30 min for selenium concentrations of 0.2 and 2 $\mu g\ l^{-1}$. However, a deviation occurred at higher concentration, accompanied by a shift of the stripping peak to more negative potentials (from −0.68 V vs. SCE for 0.2 μg Se l^{-1} to −0.75 V for 2 $\mu g\ l^{-1}$ for 15 min of electrolysis). Similar behaviour was observed by Jarzabek and Kublik [12] during the cathodic stripping of Se in 0.1 M perchloric acid. The authors explained this behaviour as the deposition of mercury selenide in different polymorphic forms which are reduced at slightly different potentials. A linear relationship between the height of the stripping peak and the deposition time was obtained at various selenium concentrations provided that the product of the selenium concentration ($\mu g\ l^{-1}$) and the electrolysis time (min) was <12 min $\mu g\ l^{-1}$. Under such conditions, the electrolysis time could be adjusted to give the highest sensitivity.

Calibration, detection limit and reproducibility

Calibration plots constructed for various deposition times (t_{dep}) were linear in the range 0–2 $\mu g\ l^{-1}$ selenium (Fig. 2). The detection limit, based on three times the standard deviation of the blank, was 0.005 μg Se l^{-1} for a 30-min deposition time. An experimental lower determination limit can be estimated from the voltammograms shown in Fig. 3. The peak of curve 1 (corresponding to 0.016 $\mu g\ l^{-1}$ Se) can be measured with a precision of about 10% and can be regarded as a practical limit for the determination of selenium.

The reproducibility was evaluated by calculating the relative standard deviations (95% confidence level) on the mean stripping peak heights from five successive voltammograms obtained for various selenium concentrations. The relative standard deviations obtained for 1.5 $\mu g\ l^{-1}$ (t_{dep} = 5 min), 0.5 $\mu g\ l^{-1}$ (t_{dep} = 10 min) and 0.02 $\mu g\ l^{-1}$ (t_{dep} = 20 min) were 5, 8 and 11%, respectively.

Interferences and extraction procedure

Lead(II) and copper(II) were found to interfere seriously with the stripping voltammetric determination of selenium. The presence of 10 $\mu g\ l^{-1}$ Cu(II) and 7 $\mu g\ l^{-1}$ Pb(II) resulted in the disappearance of the stripping peak and in the formation of an additional peak situated at a more negative potential. This peak can be assigned to the reduction of lead or copper selenide formed on the electrode during the deposition step [9, 10]. In such conditions, the height of the HgSe stripping peak is no longer proportional to the selenium concentration.

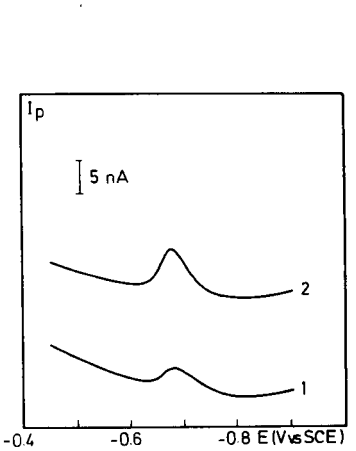

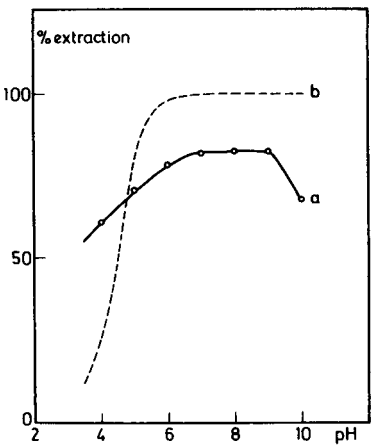

Fig. 3. Cathodic stripping voltammograms for different selenium concentrations: (1) 0.016 $\mu g\ l^{-1}$; (2) 0.032 $\mu g\ l^{-1}$. Deposition time 20 min; other conditions as for Fig. 2.

Fig. 4. Influence of pH on the extraction of piazselenol in toluene: (a) selenium recovery; (b) percentage of the unprotonated form of monopiazselenol. 20-ml sample extracted with 2 ml of toluene.

A severe interference was also caused by the oxidation of the DAB which occurs to some extent during the formation of the piazselenol. A spurious peak was formed close to the selenium stripping peak and hinders the accurate measurement of the stripping peak. Attempts to suppress the DAB oxidation by the use of reducing agents were not successful because those reagents interfered in the electrochemical process. Further, several preliminary investigations of natural waters showed that surface-active substances which coat the mercury electrode, interfere strongly by decreasing the amount of deposited selenium.

These interferences mean that a chemical separation step prior to the voltammetric determination is essential. This separation was accomplished by extraction of the piazselenol into toluene followed by back-extraction into an aqueous solution suitable for the subsequent treatment. Moreover, given the low concentrations encountered in waters, one can benefit from this procedure by using it also to preconcentrate the piazselenol.

The extraction efficiency was investigated in sea-water samples doped with ^{75}Se at the 0.10 $\mu g\ l^{-1}$ selenium level. The extraction yield in toluene was maximal at pH values above 7, according to the distribution of the unprotonated form of the monopiazselenol, as shown in Fig. 4. Above pH 9, hydroxides precipitated, leading to coprecipitation of selenite and consequently to a decrease in the selenium recovery. At pH 8, experiments in which 20-ml samples were extracted with 2 ml of toluene indicated that the recovery was 82%. With two sequential 1.5-ml extractions, an extraction yield of 96 ± 6% was achieved.

The presence of two free amino groups on the monopiazselenol molecule allows back-extraction of the compound into an acidic solution where protonation of the amino groups is possible. For the subsequent voltammetric determination, however, the acidity should be as low as possible. When 4 ml of piazselenol solution in toluene was back-extracted with 4 ml of 2, 1, 0.5 or 0.1 M hydrochloric acid, the recoveries were 102.6, 98.6, 99.6 and 88.6%, respectively. Considering these results, the back-extraction was done with 0.5 M hydrochloric acid.

Figure 5 and Table 3 show that the extraction procedure renders the analysis free of interferences from (a) the oxidation products of the DAB and (b) metal ions at concentrations between 10 and 100 times their normal concentration in water.

Accuracy and precision

The accuracy and precision of the method were first assessed by determining the selenium content of the NBS standard reference material Orchard Leaves (SRM 1571). The dried and weighed samples (ca. 200 mg) were digested in a teflon bomb [13] with 8 ml of a 1:1 HNO_3/H_2O_2 mixture at 150°C for 6 h; after addition of 5 ml of concentrated hydrochloric acid, the solution was heated at 90°C for 5 min to reduce Se(VI) to Se(IV). The resulting solution was diluted to 100 ml and the procedure for the determination of selenium

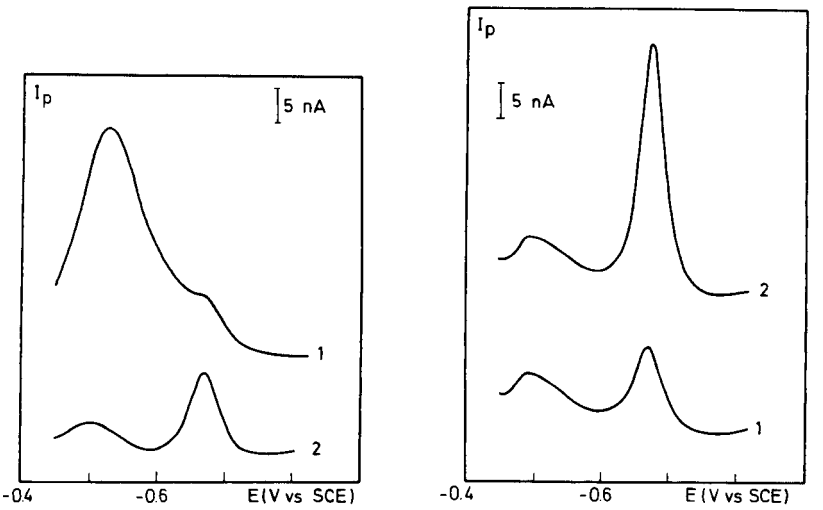

Fig. 5. Cathodic stripping voltammograms of a solution where partial oxidation of DAB had occurred (1) without extraction; (2) after extraction into 0.5 M HCl. Conditions: pH 4.5; deposition time 10 min at −0.45 V.

Fig. 6. Cathodic stripping voltammograms of selenium from a sea-water sample: (1) 0.13 $\mu g\ l^{-1}$ selenium after extraction; (2) after standard addition of 0.30 $\mu g\ l^{-1}$. Conditions: 200 ml of sea water extracted with 2 × 15 ml of toluene; back-extraction into 20 ml of 0.5 M HCl; c.s.v. at pH 4.5 with a deposition time of 10 min at −0.45 V.

TABLE 3

Recovery of selenium (0.07 $\mu g\ l^{-1}$) in presence of diverse ions[a]

Metal	Conc. (mg l^{-1})	Se recovery (%)	Metal	Conc. (mg l^{-1})	Se recovery (%)
Cu^{2+}	1.8	103	Cr^{3+}	0.5	101
	20	98	Cr(VI)	0.5	94
Pb^{2+}	1.3	100		2	89
	12	104		10	—[b]
Cd^{2+}	1.9	102	Fe^{2+}	6.5	91
Zn^{2+}	1.2	108	Fe^{3+}	1.0	109
As^{3+}	0.5	109		11	95
Ni^{2+}	0.65	96		55	—[b]
V(V)	1.1	99			

[a]Deposition time of 10 min at −0.45 V. [b]Severe oxidation of DAB which can be avoided by addition of 1 g l^{-1} hydroxylammonium chloride before DAB.

was then applied. Analyses of 10 samples gave an average selenium concentration of 80 ± 7 ng g^{-1}; the NBS certified content is 80 ± 10 ng g^{-1}.

Determination of Se(IV) in sea water

The sea-water samples were collected from the North Sea (Belgian coast) and were filtered through 0.45-μm filters, as described by Gillain and Brihaye [14]. After collection, the samples were quickly frozen and stored in a freezer until required.

Owing to the very low concentrations encountered in sea water, a concentration factor of 10 was used during the extraction procedure (i.e., 200 ml of sample and 20 ml of hydrochloric acid solution). A detection limit of 1 ng l^{-1} was then obtained for a deposition time of 30 min. A typical stripping voltammogram is shown in Fig. 6.

The accuracy of the determination in sea water was evaluated by measuring the recovery of selenium spikes through the overall procedure; the results are given in Table 4. The precision was evaluated by replicate (n = 10) analyses of water samples; the standard deviation was 4.2% at the 0.02 μg l^{-1} selenium level.

The selenium(IV) content found in various samples from the North Sea varied between 0.09 and 0.110 μg l^{-1}. These results are in good agreement with available data from adjacent zones of the North Sea [15].

Conclusions

Cathodic stripping voltammetry used in conjunction with the formation of a piazselenol provides a very sensitive technique for the determination of Se(IV) in waters. The detection limit is 0.01 μg Se l^{-1} without any pretreatment.

Both inorganic and organic interferences can be avoided by extraction of the piazselenol in toluene followed by back-extraction into an aqueous solution suitable for voltammetry. This extraction can be used to concentrate the selenium in order to lower the detection limit. For the determination in sea water, where the lowest levels are encountered, a detection limit of 1 ng l^{-1} was attainable. Selenium can be determined over a wide range of concentrations (0.001—2 μg Se l^{-1}) by adjusting the electrochemical and extraction parameters. The method is specific for the determination of selenite and could be applied to the study of the speciation of selenium in sea or river water.

TABLE 4

Recovery of selenium from spiked sea water

Selenium concentration (ng l^{-1})		Recovery (%)
Added	Measured	
0	22	—
30	54	106.7
60	80	96.7
90	112	100
150	170	99.3

This work was supported by the "Institut pour l'Encouragement de la Recherche Scientifique dans l'Industrie et l'Agriculture" (IRSIA, Brussels).

REFERENCES

1 C. I. Measures and J. D. Burton, Earth. Planet. Sci. Lett., 46 (1980) 385.
2 C. I. Measures, R. E. McDuff and J. M. Edmond, Earth. Planet. Sci. Lett., 49 (1981) 102.
3 Y. Sugimura, Y. Suzuki and Y. Miyake, J. Oceanogr. Soc. Japan, 32 (1976) 235; 34 (1978) 93.
4 K. Takayanagi and G. T. F. Wong, Anal. Chim. Acta, 148 (1983) 263.
5 C. I. Measures and J. D. Burton, Anal. Chim. Acta, 120 (1980) 177.
6 Y. Shimoishi and K. Toei, Anal. Chim. Acta, 100 (1978) 65.
7 K. Uchida, Y. Shimoishi and K. Toei, Environ. Sci. Technol., 53 (1980) 541.
8 S. B. Adeloju, A. M. Bond and H. C. Hughes, Anal. Chim. Acta, 148 (1983) 59.
9 G. Kenze, P. Monks, G. Tölg, F. Umland and E. Wessling, Frezenius' Z. Anal. Chem., 295 (1979) 1.
10 U. Baltensperger and J. Hertz, Anal. Chim. Acta, 172 (1985) 49.
11 P. Breyer and B. P. Gilbert, Anal. Chim. Acta, 201 (1987) 23.
12 G. Jarzabek and Z. Kublik, J. Electroanal. Chem., 137 (1982) 247; Anal. Chim. Acta, 143 (1982) 121.
13 G. Gillain, Talanta, 29 (1982) 651.
14 G. Gillain and C. Brihaye, Anal. Chim. Acta, 167 (1985) 387.
15 H. Robrerecht, R. Van Grieken, M. Van Sprundel, D. Vanden Berghe and H. Deelstra, Sci. Total. Environ., 26 (1983) 163.

Analytica Chimica Acta, 201 (1987) 43—50
Elsevier Science Publishers B.V., Amsterdam — Printed in The Netherlands

TRACE METAL SPECIATION BY ADSORPTIVE STRIPPING VOLTAMMETRY OF METAL CHELATES OF SOLOCHROME VIOLET RS

JOSEPH WANG*, PENG TUZHI and TEDDY MARTINEZ
Department of Chemistry, New Mexico State University, Las Cruces, NM 88003 (U.S.A.)
(Received 7th April 1987)

SUMMARY

Adsorptive stripping voltammetry has become one of the most sensitive methods for trace metal determinations. The growing application of the method to natural water systems prompted an investigation into the fraction of the metal concentration that contributes to the adsorptive stripping response. Recent procedures for trace measurement of iron, titanium and gallium, based on chelation with solochrome violet RS (SVRS) are coupled to systematic ligand competition experiments. Tannic acid, EDTA, NTA, glycine, cysteine, carbonate and chloride ions are used as model natural ligands. It is shown that adsorptive stripping voltammetry measures the free ion and metal displaced from complexes by the "analytical" ligand. The exact fraction of the metal measured thus depends on the thermodynamic stability of the metal-SVRS chelate (compared to that of natural complexes), and on the relative concentrations of the competing ligands. The method offers possible distinction between metal complexes, based on their thermodynamic stabilities. The use of a large excess of the "analytical" ligand can lead to measurement of the total metal content. Implications of these results relative to the use of this procedure for studying the speciation of trace elements in natural waters are discussed.

The aquatic toxicity of trace metals is critically dependent on the chemical forms of the metals. Therefore, elucidation of the speciation of trace metals constitutes one of the most significant tasks of environmental analytical research. Voltammetric methods, and in particular anodic stripping voltammetry (a.s.v.), are widely used for the study of metal speciation in natural waters [1—3]. The electrochemically labile species measured in a.s.v. represent the fraction of the total dissolved metal that can react at the electrode, under operationally defined conditions and within the time scale of the measurement. This fraction has often been assumed to be similar to the toxic fraction of the dissolved metal. Very useful speciation data can thus be obtained for about 15 elements, commonly measured by conventional a.s.v. Obviously, there is a need to develop electroanalytical speciation schemes for additional elements of environmental concern.

Recently, a variant of stripping voltammetry, adsorptive stripping voltammetry, was developed primarily for extending its scope to numerous metals that cannot be quantified by the conventional version [1—5]. This method

0003-2670/87/$03.50

involves the formation of an appropriate surface-active complex of the metal, its interfacial collection onto the hanging mercury drop electrode, and the voltammetric quantification of the surface-bound complex. The (solution-phase) complexation and interfacial accumulation processes can be described respectively, by

$$M + L_A \rightleftharpoons ML_A; ML_A \rightleftharpoons ML_{A,ads}$$

(where charges are deleted for simplicity). The surface concentration of the complex relates to its solution concentration via the corresponding adsorption isotherm. Hence, subnanomolar levels of about twenty additional elements, including the environmentally important iron, aluminum, uranium, titanium, nickel or vanadium, can easily be determined via a judicious choice of the complexing ligand. The adsorptive stripping method also offers an alternative (and often more effective) scheme for some trace metals measurable by conventional a.s.v. Because of its inherent sensitivity and simplicity, adsorptive stripping voltammetry is less prone to the contamination often encountered with other techniques used for speciation work. The response, however, can be strongly affected by the presence of surface-active materials.

Because the adsorptive stripping procedure is based on fundamentally different detection principles than conventional a.s.v., it is essential to establish which fraction of the metal concentration contributes to the adsorptive stripping response. In view of the fact that adsorptive stripping schemes are becoming increasingly used in marine investigations, including speciation work [1], systematic studies are necessary to elucidate this matter. Without such understanding, the actual analytical efficacies of speciation measurements cannot be reliably assessed, nor can the results obtained be realistically evaluated. Bond and Luscombe [6] have recently stressed these needs, and demonstrated that the adsorptive stripping procedure for nickel and cobalt, in the presence of dimethyglyoxime, provides direct determination of the total content of these metals.

The aim of the work described here was to obtain better understanding of the speciation data obtained by adsorptive stripping voltammetry. The recently introduced stripping procedures for measuring iron [7], titanium [8], and gallium [9], based on chelation with the dihydroxyazo dye, solochrome violet RS (SVRS), are coupled to systematic ligand competition experiments to achieve the desired information. Such ligand-exchange behavior is obtained for a variety of naturally occurring ligands, and at different concentrations of the metal, SVRS, and the competing ligand. The results illustrate that not all the metal is displaced from natural complexes by SVRS. In order to measure the total metal content, the "analytical" ligand must form a highly stable complex with the metal of interest, and be present at substantially higher concentration than the natural complexing agents.

EXPERIMENTAL

The instrumentation used, including the EG & G PAR Model 264A voltammetric analyzer and the EG & G PAR Model 303 static mercury drop electrode, has been described previously [7—9]. Voltammograms were displayed on an EG & G PAR Model 0073 X—Y recorder. All solutions were prepared from double-distilled water. Nitrilotriacetic acid (NTA), SVRS, as well as stock solutions (1000 mg l^{-1}) of iron, titanium and gallium, were purchased from Aldrich. Glycine and cysteine were obtained from Fisher, EDTA from Matheson Coleman & Bell, and tannic acid and sodium carbonate from Baker. The supporting electrolyte was 0.1 M acetate buffer (pH 5.1).

The absorptive stripping procedure used for trace measurements and speciation studies of the model analytes was as described previously [7—9].

RESULTS AND DISCUSSION

Figures 1—3 show calibration plots for iron, titanium, and gallium, respectively, obtained in the absence (b) and presence (a) of EDTA (A), NTA (B) and tannic acid (C), in solutions containing 1.5×10^{-6} M SVRS, which has been shown to yield optimum response for these metals [7—9]. Different profiles are observed for the different metal/ligand systems. For example, substantially lower response peaks are observed for the three metals in the presence of EDTA compared to analogous measurements without EDTA (compare A, a, and b). Tannic acid, in contrast, does not affect the iron response, but causes severe depression of the titanium and gallium peaks (C). This behavior is attributed to competition between the "analytical" ligand (SVRS) and EDTA, NTA or tannic acid.

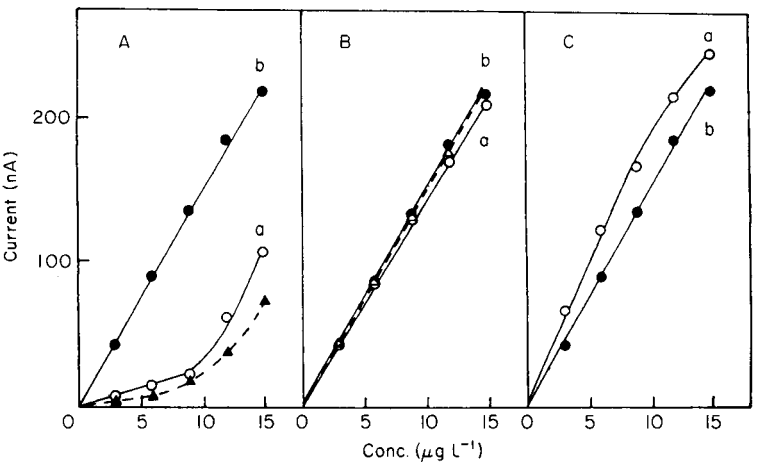

Fig. 1. Dependence of the stripping peak current on the iron concentration, in the absence (b) and presence (a) of 0.2×10^{-6} M EDTA (A), NTA (B), and 0.4×10^{-6} M tannic acid (C). Preconcentration for 30 s at —0.40 V. Scan rate, 50 mV s^{-1}; acetate buffer (pH 5.1) containing 1.5×10^{-6} M SVRS. Dotted lines represent the theoretical response, calculated from Eqns. 1 and 2.

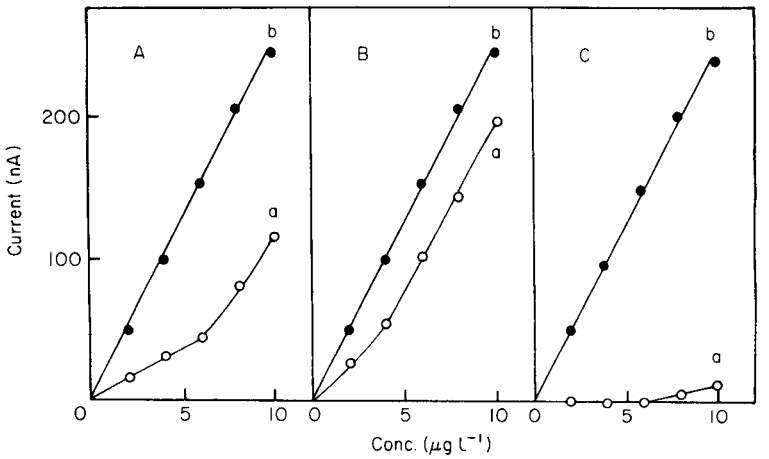

Fig. 2. Dependence of the stripping peak current on the titanium concentration, in the absence (b) and presence (a) of EDTA (A), NTA (B), and tannic acid (C). Preconcentration for 20 s at −0.38 V. Other conditions as in Fig. 1.

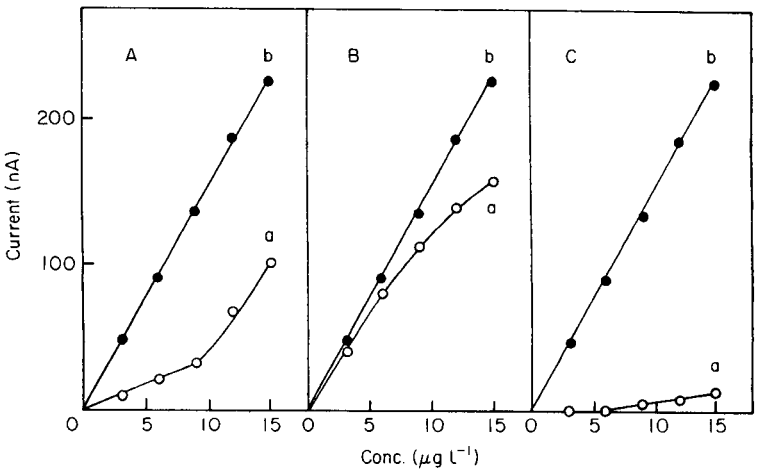

Fig. 3. Dependence of the stripping peak current on the gallium concentration, in the absence (b) and presence (a) of EDTA (A), NTA (B), and tannic acid (C). Preconcentration for 30 s at −0.37 V. Other conditions as in Fig. 1.

The competing effects can be quantified by using the effective stability constants of the various complexes in the presence of both "analytical" and "natural" ligands (L_A and L_N, respectively). The conditional formation constant for ML_A is given by

$$K'_{ML_A} = K_{ML_A} \alpha_{L(A)} / (1 + K_{ML_N}[L_N]) \quad (1)$$

where K_{ML_A} and K_{ML_N} are the thermodynamic formation constants of ML_A

and ML_N, respectively, and $\alpha_{L(A)}$ is the fraction of L_A that is not protonated. The analogous conditional formation constant for ML_N is

$$K'_{ML_N} = K_{ML_N} \alpha_{L(N)}/(1 + K_{ML_A}[L_A]) \quad (2)$$

When the conditional formation constants and total concentrations of "natural" ligands are sufficiently low that the "analytical" ligand displaces all the metal ion(s) from the "natural" complexes, then the total metal will be detected because it is expected that the fraction of metal contributing to the adsorptive stripping response will be comprised of the free (hydrated) ion and metal displaced by (L_A) from the "natural" complexes. Obviously the adsorptive stripping measurements will not necessarily yield the total metal content, unless ML_A is stable and a large excess of L_A is used.

To evaluate the fraction of the metal contributing to the response when SVRS is used as "analytical" ligand, iron, titanium, and gallium were measured in the presence of other complexing agents commonly present in natural water systems. Average calibration slopes for iron in the absence and presence of 4×10^{-4} M chloride were essentially the same (16.1 nA l μg^{-1}) for the conditions outlined as in Fig. 1. Similarly, 0.2×10^{-6} M glycine or 0.4×10^{-6} M cysteine had negligible effects on the calibration slopes for titanium (e.g., 26.7 and 25.0 nA l μg^{-1}, respectively, with ligands, vs. 24.9 nA l μg^{-1} without ligands). For the seven ligands tested, only EDTA (because of the large formation constants [10]) strongly affects the adsorptive stripping response of the three metals; NTA and tannic acid had smaller effects because of the smaller formation constants relative to SVRS complexes [11, 12]. Figure 1 includes a comparison of experimental and theoretical plots calculated (with the formation constants) for the iron complexes of EDTA, NTA and SVRS. Relatively good agreement is observed between the experimental and computed results.

The study was extended to include effects of different concentrations of the "analytical" and "natural" ligands. Figure 4 shows calibration plots for titanium in the presence of different levels of NTA ($0—1 \times 10^{-6}$ M). As expected, the Ti-SVRS response decreases with increasing NTA concentration. NTA levels of 1, 0.5, and 0.2×10^{-6} M result in measurement of only 33, 48 and 60%, respectively, of the total titanium content at 10 $\mu g\ l^{-1}$ (see Fig. 4). It should also be noted that the fraction of the metal measured at each NTA level depends on the metal concentration. For example, at 4 $\mu g\ l^{-1}$ titanium, only 22%, 29% and 46% of the metal contribute to the response at 1, 0.5, and 0.2×10^{-6} M NTA, respectively. Such changes are expected from the nonlinear calibrations in presence of complexing agents. Responses similar to those in Fig. 4 were obtained also for iron in the presence of different levels of EDTA; the resulting changes in the fraction of iron measured are summarized in Table 1 along with theoretical values calculated with the aid of the conditional formation constants. The reasons for the discrepancies between the experimental and theoretical values are not clear.

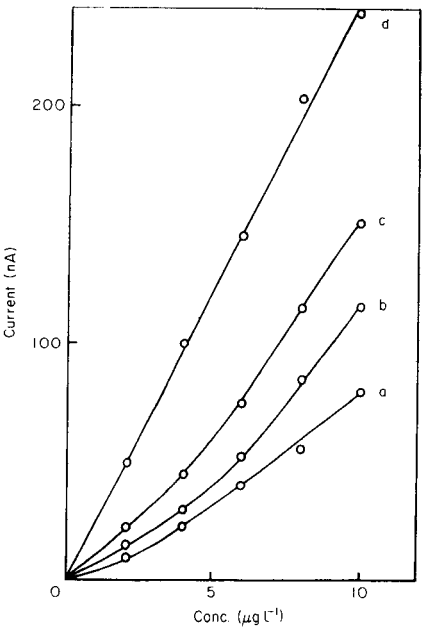

Fig. 4. Dependence of the stripping peak current on the titanium concentration at different levels of NTA: (a) 1×10^{-6} M; (b) 0.5×10^{-6} M; (c) 0.2×10^{-6} M; (d) 0. Other conditions as in Fig. 2.

TABLE 1

Fraction of iron measured in the presence of different EDTA concentrations[a]

Fe^{3+} conc. ($\mu g\ l^{-1}$)	Fraction measured in presence of EDTA		
	0.1×10^{-6} M	0.2×10^{-6} M	0.4×10^{-6} M
3	0.41 (0.18)	0.16 (0.08)	0.05 (0.03)
6	0.47 (0.31)	0.16 (0.11)	0.07 (0.04)
9	0.63 (0.46)	0.17 (0.15)	0.09 (0.05)
12	0.67 (0.58)	0.32 (0.24)	0.11 (0.06)
15	0.77 (0.66)	0.49 (0.35)	0.14 (0.08)

[a]Conditions: as in Fig. 1. The numbers in parentheses correspond to the theoretical values calculated from the conditional formation constants.

The effect of changing the SVRS concentration on the titanium response, at a fixed NTA level, is shown in Fig. 5. As expected, the fraction of titanium contributing to the peak signal increases with increasing SVRS concentration; when SVRS is present at large excess over L_N, the total metal concentration is determined (see frame C). It should be noted, however, that such measurement of the total metal content is accompanied by a substantial diminution

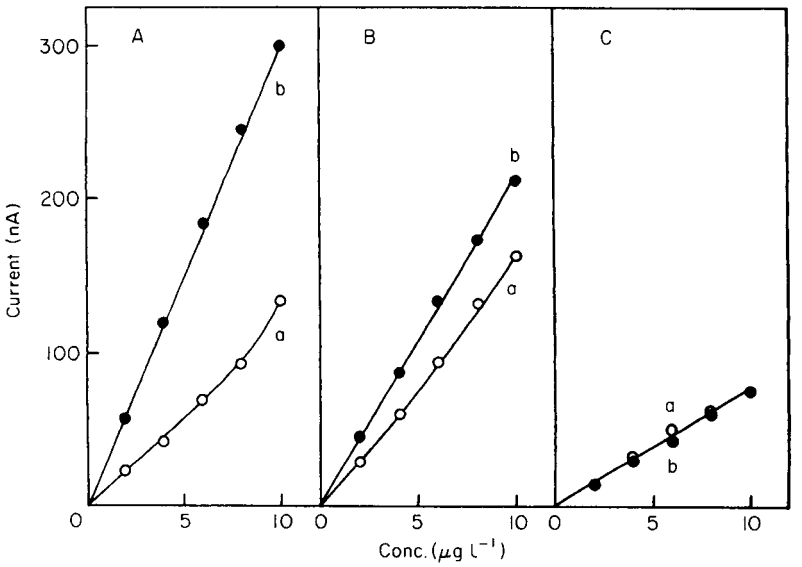

Fig. 5. Dependence of the stripping peak current on the titanium concentration, in the presence of 0.5×10^{-6} M NTA (a) and without NTA (b), for different levels of SVRS: (A) 1.5×10^{-6} M; (B) 30×10^{-6} M; (C) 100×10^{-6} M. Other conditions as in Fig. 2.

of the current response (slopes of 31.3, 21.8 and 7.4 nA l μg^{-1} at 1.5, 30 and 100×10^{-6} M SVRS, respectively, as shown by curves b in Fig. 5). Such behavior is attributed to co-adsorption of the free ligand, which competes with the metal chelate for surface sites. This is illustrated in Fig. 6 which shows the dependence of the Ti-SVRS response upon the ligand concentration. The decrease in the response is accompanied also by increased background current preceding the chelate peak and hence inferior signal-to-background characteristics. In contrast, measurements of iron were not affected by the concentration of the free dye. For example, by using 5×10^{-4} M SVRS, essentially the total iron content was measured in the presence of 0.2×10^{-6} M EDTA (other conditions as in Fig. 1A).

The strong effect that ligand concentrations have on the fraction of the metal measured (Fig. 5) indicates that speciation results obtained by the metal-chelate adsorption approach are operationally-defined, analogously to those obtained by conventional a.s.v. [13]. Other experimental parameters such as the buffer anion and other cations, including the supporting electrolyte, may affect the metal distribution. Further complication may be due to co-adsorption of the free "analytical" ligand on the electrode surface and complexation of metals by the sorbed ligand. On the more positive side, unlike some a.s.v. speciation schemes that are implemented at a thin mercury film electrode (formed in-situ by simultaneous deposition of mercury and trace metals), metal-chelate adsorption measurements are usually done at the hanging mercury drop electrode so that no Hg(II) is present to affect speciation results.

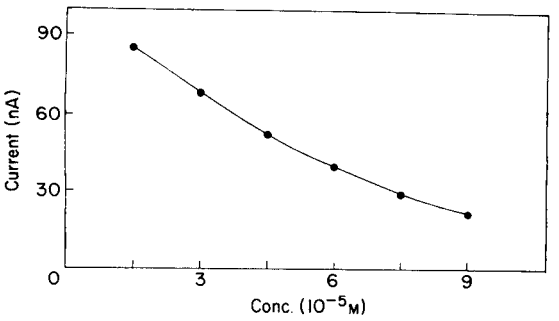

Fig. 6. Effect of SVRS concentration on the stripping peak for 5 μg l^{-1} titanium. Other conditions as in Fig. 2.

Future work will involve the use of different "analytical" ligands for each metal ion to displace it more effectively from different natural complexes. It will involve an evaluation of the correlation (if any) between the fraction of the metal measured by adsorptive stripping voltammetry and the toxicity of the metal.

This work was supported by the National Institutes of Health (Grant No. GM 30913-04), and the New Mexico Water Resources Research Institute.

REFERENCES

1 T. M. Florence, Analyst., 111 (1986) 489.
2 J. Wang, Stripping Analysis: Principles, Instrumentation and Applications, VCH, Deerfield Beach, FL, 1985.
3 H. W. Nürnberg, Anal. Chim. Acta, 164 (1984) 1.
4 J. Wang, Am. Lab., 17 (5) (1985) 41.
5 R. Kalvoda, Anal. Chim. Acta, 138 (1982) 11.
6 A. M. Bond and D. L. Luscombe, J. Electroanal. Chem., 214 (1986) 21.
7 J. Wang and J. S. Mahmoud, Fresenius' Z. Anal. Chem., 327 (1987) 789.
8 J. Wang and J. S. Mahmoud, J. Electroanal. Chem., 208 (1986) 383.
9 J. Wang and J. M. Zadeii, Anal. Chim. Acta, 185 (1986) 229.
10 D. G. Peters, J. M. Hayes and G. M. Hieftje, Chemical Separations and Measurements, W. B. Saunders, Philadelphia, PA, 1974, p. 173.
11 L. G. Sillen, E. Hogfeldt, A. E. Martell and R. M. Smith, Stability Constants, Suppl. No. 1, The Chemical Society, London, 1971.
12 T. M. Florence and W. I. Belew, J. Electroanal. Chem., 21 (1969) 157.
13 T. M. Florence and G. E. Batley, Anal. Chem., 52 (1980) 1962.

Analytica Chimica Acta, 201 (1987) 51—58
Elsevier Science Publishers B.V., Amsterdam — Printed in The Netherlands

ELECTRICAL PROPERTIES OF BILAYER LIPID MEMBRANES CONTAINING IODINE AND IODIDE, INVESTIGATED BY CYCLIC VOLTAMMETRY

CHRISTOPHER J. BENDER and H. T. TIEN*

Membrane Biophysics Laboratory (Giltner Hall), Department of Physiology, Michigan State University, East Lansing, MI 48824 (U.S.A.)

(Received 6th March 1987)

SUMMARY

The conduction properties of lecithin bilayer membranes in iodine-containing solutions are examined from a potentiodynamic experimental approach. Voltammetric data obtained by using a variety of forms (derived from charge-transfer type interactions) of iodide implicate the triiodide ion as the charge carrier accounting for the diffusion-limited voltammetric response whereas the charge transport of iodide seems to be limited by transmembrane diffusion. The data are used to support one of the many proposed mechanisms for conductance of iodide in membranes.

Iodine and its electrochemical behavior in membrane-containing cells is complicated by the diverse interplay between the various redox states of the element. Elemental iodine may be reduced or oxidized to give any number of ionic forms which in addition to elemental iodine may also form complexes of the charge-transfer type. In electrochemical cells partitioned by a bilayer lipid membrane (BLM), the effect of adding iodide to the aqueous solution bathing the membrane (usually a buffered KCl solution) is a marked decrease in electrical resistance [1—3]. The resistance is further lowered by the addition of iodine to the aqueous bathing solution [2]. This finding led to a spate of experiments and associated theories explaining the nature of the enhanced conductance; a review is available [3].

What was proposed to account for the conductance enhancement consisted of a combination of ionic, electronic, and redox processes, each making a contribution to the total conductance of charge across the membrane [3]. These additional mechanisms made available by the presence of iodine open up new pathways for current flux and it is this idea which many authors use to account for the enhanced conductivity. In addition to the membrane-resistance measurements cited above, Tafel plots of membrane cells containing I_2/I^- have been interpreted in terms of an electron-transfer mechanism [4].

The iodine-containing BLM cell is also amenable to investigation by polarographic and therefore voltammetric means. The I_2/I^- BLM was among the first reported [5] to yield a peak in current/voltage curves obtained by cyclic

0003-2670/87/$03.50

voltammetry. This form of voltammetry has the added advantage over classical polarography that it can be correlated with time to provide kinetic information [6].

Previously, we have studied the membrane cell containing 7,7,8,8-tetracyanoquinodimethane (TCNQ) or tetracyanoethylene (TCNE) and their adducts in order to determine the nature of the charge carrier and the mechanism responsible for an observed voltammetric response [7]. As explained there, part of the rationale for using these particular compounds is their propensity to form complexes of the charge-transfer type and the hope that this property might aid in the elucidation of a mechanism for the charge transport which occurs in these electrochemical cells. In a similar vein, there is a rich literature of the electrical response of membranes containing the manifold forms of iodine, and an equally voluminous literature of the molecular interactions of iodine. As was done previously, the BLM system will be examined in detail by exploiting some of the reactive properties of iodine and its redox states. Complexes of iodine with various electron donors and acceptors yield specific forms of iodine which can be used to assess the nature of the charge carrier. Additionally, various aspects of the solution behavior of iodine partitioning between immiscible solvents will be examined as an aid in determining the mechanistic aspects of the voltammetric response.

EXPERIMENTAL

A two-electrode electrochemical BLM cell was used as a means of obtaining voltammetric data and making static electrical measurements. Details of the instrumental arrangement and experimental consideration regarding grounding/shielding are described elsewhere [3]. In this investigation, the use of saturated calomel electrodes (SCE) was retained, care being taken to moderate concentrations of the charge carrier in order to avoid polarization of the SCE.

Membrane preparations were composed of lecithin solutions in dodecane/butanol (3:1). The optimal lecithin concentration for BLM formation was 24 mg ml^{-1}. Modifiers were added directly to this membrane-forming solution, and the solution centrifuged briefly in a tabletop microfuge (Beckman) to remove suspended particulate matter which may not have dissolved. The BLMs were formed from these solutions by injection of 50-μl aliquots onto a 1.5-mm diameter circular orifice in a teflon beaker.

The supporting electrolyte bath was prepared in such a manner as to optimize BLM stability, and to ensure a high conductance in the aqueous phase. The latter criterion is a feature necessary to establish the relationship, $R_m \gg R_{el}$ (where R_m and R_{el} are the membrane and electrolyte resistances, respectively) and minimize error from the iR drop; i.e., ensure that the measured voltage corresponds to the transmembrane potential. The electrolyte consisted of 0.1 M KCl and 20 mM 4-morpholineethanesulfonic acid (MES) buffer adjusted to pH 5.5. Stirring of solutions in each BLM chamber (designated inner and outer) was interrupted only during the time necessary to obtain a voltammogram.

In describing the electrochemical behavior of this system, the notion of membrane overpotential already defined [7] is retained and all voltages are expressed as an overpotential.

RESULTS AND DISCUSSION

Membrane-partitioned electrochemical cells containing various forms of iodine yielded different voltammetric responses. Unmodified membranes situated in a bathing solution containing 10^{-6} M potassium iodide possessed the characteristically low electrical resistance and exhibited a voltammetric response which was suggestive of Butler-Volmer kinetics (Fig. 1A). Interestingly, variation of the iodide concentration did not alter the qualitative shape of the current/voltage curve; nor did a change in polarization rate affect the kinetic nature of the voltammetric response. What makes this data curious is that LeBlanc [8] noted the concentration dependence of the current/voltage curves of ion transport across membranes (iodide was omitted from his discussion). According to LeBlanc [8], at low concentrations of ion, the limiting step is mass transport in the layers adjacent to the membrane (hence a diffusion-limited current/voltage curve), whereas at high concentration, ionic flux within the membrane becomes rate-limiting, and there is observed Butler-Volmer (LeBlanc terms this space-charge-limiting) kinetics.

A further increase in conductance is observed when iodine is dissolved in the lipid solution prior to membrane formation; however, there is no appreciable change in the nature of the voltammetric response. If iodine is added to the aqueous solution of iodide, however, a change in the voltammetric profile is observed, from that of Butler-Volmer kinetics to one indicative of diffusion limitation (Fig. 1B). The occurrence of the apparent change in the kinetics

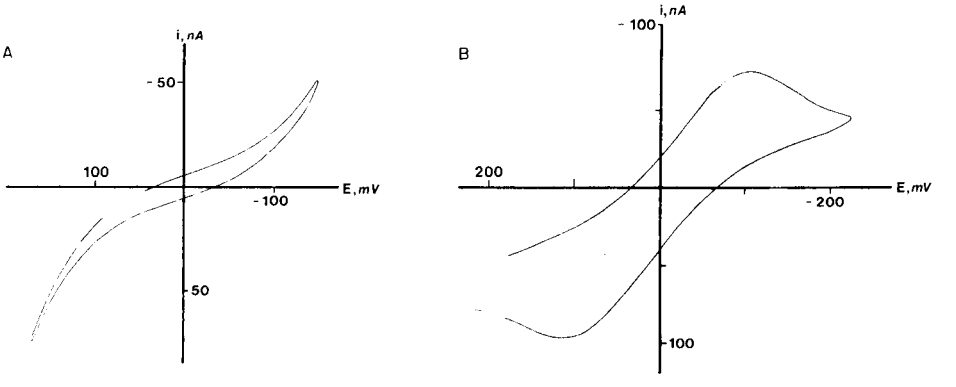

Fig. 1. Cyclic voltammograms of lecithin BLM-partitioned cell containing 1 M KI (A) and after the formation of I_3^- (B) in the aqueous phase. For B, the response was obtained either by the addition of I_2 to the cell described in Fig. 1 or by direct addition of I_3^- to the supporting electrolyte bathing solution. Polarization rate: (A) 100 mV s^{-1}; (B) 200 mV s^{-1}. Supporting electrolyte 0.1 M KCl, 20 mM MES buffer (pH 5.5).

of charge transport is concurrent with the appearance of a brownish tint to the solution (and presumably the formation of triiodide). It seems plausible to attribute this apparent kinetic change to the onset of voltage-induced charge transport of I_3^-. This statement was verified by separately preparing a solution of I_3^- and adding aliquots of this solution to a cell containing an unmodified membrane and supporting electrolyte solution. Doing so resulted in identical voltammetric peaks the heights of which were in direct proportion to the amount of I_3^- added. Furthermore, in a manner similar to that demonstrated in other systems [7, 8], the voltammetric peaks may be individually varied by the addition of I_3^- solution to one side of the membrane or the other. This implies that diffusion limitation occurs at the aqueous layer directly adjacent to the surface of the membrane because limitation of the current by the membrane should not be dependent on the polarity (because the membrane is the central plane of symmetry in the system).

Concerning the nature of these dynamically obtained current/voltage curves, the response of the cell containing I_2/I^- (i.e., I_3^-) accords with polarographic results reported by Liberman and Topaly [5] who obtained a peak at ca. 150 mV vs. SCE. These data agree with our results of approximately 100 mV obtained voltammetrically. A direct comparison of the data obtained by the two methods is not valid because it was found that the voltammetric and polarographic peaks shift with changes in the polarization rate, suggestive of voltammetry of irreversible charge transfer in electrodic systems. If an analogy between the membrane-partitioned cell and those charge-transfer processes occurring at liquid/liquid interfaces [7, 9] is valid, then it might be suggested that charge transfer of triiodide across membranes is purely irreversible.

The kinetics of the I_2/I^- cell demonstrates the concentration dependence discussed above and exhibits those trends outlined by LeBlanc [8] in his theoretical discussion of empirical results. That the cell containing iodide alone does not behave in this manner implies that the transport of iodide across the membrane is rate-limiting throughout the concentration range, i.e., at no concentration does diffusion in the aqueous layers adjacent to the membrane surface become rate-limiting. The dramatic change in membrane conductance following the addition of potassium iodide implies a fairly high mobility of iodide in the membrane, because the conductance $\sigma = z\,\eta_{ion} e\,\mu_{ion}$ where z, η, μ, are charge, concentration, and mobility of a given ion, respectively. It seems that if the BLM were to be rate-limiting at all concentrations, then the conductance of the ion in the BLM, σ_m, would always have to be much less than the conductance, in solution σ_{aq}. Therefore

$$\sigma_m = z\,e\,\eta_{ion,m}\,\mu_{ion,m} \ll z\,e\,\eta_{ion,aq}\,\mu_{ion,aq} = \sigma_{aq} \qquad (1)$$

or, assuming that association of the ion with lipid components does not occur to the extent that z and e are altered: $\eta_{ion,m}\,\mu_{ion,m} \ll \eta_{ion,aq}\,\mu_{ion,aq}$. It would therefore seem that either a low partition coefficient $K = \eta_{ion,m}/\eta_{ion,aq}$ or an imbalance of mobility could account for the observed kinetics. If the

conclusions drawn from the resistance data are valid, the partition coefficient is implicated as the rate-determining factor.

The fact that iodide is an unshielded (naked) anion lends some credence to the above statement. An attempt was made to measure a partition coefficient between the supporting electrolyte and a layer of BLM-forming solution but a reliable assay was not attained. An indirect test was made by replacing iodide with tetrabutylammonium ions which have their charge shielded. These ions would presumably have a better partition coefficient, yet the voltammograms possessed the same characteristic shape. Tetraphenylboron solution, however, yields voltammograms with diffusion-limiting kinetics [7]. Noteworthy is the fact that picrate ions also yield a Butler-Volmer-like response.

Iodine forms a variety of solutions, the colors of which depend on the solvent used, and specifically, on the extent to which the solvent coordinates the iodine [10]. Non-polar solvents such as chloroform yield violet solutions of iodine whereas polar solvents such as ethanol give a corresponding solution which is brown. Upon addition of iodine to dodecane/butanol/lecithin membrane-forming solutions, a brownish solution is formed, and the unmodified membrane-formation solution will become brown if left in contact with an aqueous solution of triiodide. Because organic solvents can extract iodine from aqueous solutions of triiodide, it is not immediately apparent whether the I_3^- or I_2 is diffusing into the BLM-forming solution. The conditions in the organic phase are suitable for both possibilities owing to the charged phospholipids present. Lauger et al. [1] have proposed that lecithin does form an adduct of membrane-bound lecithin– I^+ and mobile iodide based on spectroscopic data [3]. However, any I_2 solvated within the membrane phase would be expected to be brown because of the interaction with the lipids which have phosphate groups that might coordinate the iodine. Clearly, which model of solvation is valid depends on the strength of the interaction between the lipid and iodine. The interaction of the I_2 with lipid and consequent formation of iodide is perhaps the most appealing mechanism based on spectroscopic data [3, 5] and suggests a simple phase-transfer experiment. In these latter experiments, the intensity of the brown color attained when unmodified lipid solution contacts aqueous triiodide solution does not saturate if the concentration of lipid is decreased, and retains the ability to extract triiodide again if an aliquot of the organic phase is mixed with fresh distilled water.

Charge-transfer complexes

In order to test further the hypothesis that triiodide was the charge carrier resulting in the change in the observed voltammetric kinetics, several charge-transfer complexes of I_2 were synthesized in the BLM-forming solution. Two types of complexes were selected; namely a d-π complex such as that formed between iodine and an aromatic ring compound (here perylene was used); and a second class of charge-transfer interaction in which triiodide is produced.

This latter class of interaction is represented by the pyridine—I_2 or carotene—I_2 or complex formation (see below).

Voltammograms of perylene (Fig. 2), anthracene, or tetracene complexes with iodine showed no change from the voltammogram of the unmodified BLM. When potassium iodide was added to the bathing solution, the same Butler-Volmer-type voltammogram was observed for an unmodified membrane as well. Nor was there any response to the presence of exogenous redox agents in the bathing solution. In contrast, immediately upon formation (and during its progression towards the black bilayer state) the carotene—I_2 membrane yields a diffusion-limited voltammetric response. Furthermore, the voltammetric profile is time-dependent, i.e., the peak height steadily decreases with time (Fig. 3). This time-dependence can be interpreted as the loss of triiodide at the interface layers adjacent to the BLM as the ion diffuses into the bulk solution. Peaks can be restored by the addition of aliquots of triiodide.

Lastly, although series of redox couples failed to alter the voltammetric curves of I_2-containing membranes, the addition of the dye 2,6-dichloroindophenol (DCIP) to the aqueous bathing solution/electrolyte did yield a

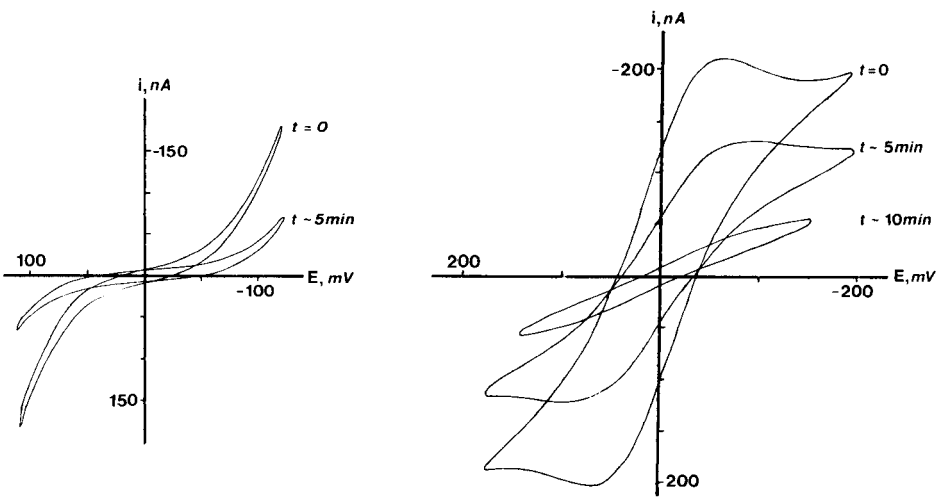

Fig. 2. Cyclic voltammograms of cell partitioned by a BLM into which is incorporated the charge-transfer complex perylene—I_2 (perylene—I^+ + I^-). The characteristic "fatigue effect" indicates a diminishing conductance of the cell as the mobile charge-carrier (I^-) diffuses into the bulk media. Formation of membrane is from a lecithin solution saturated with perylene—I_2; supporting electrolyte 0.1 M KCl, 20 mM MES (pH 5.5); polarization rate 100 mV s^{-1}.

Fig. 3. Cyclic voltammograms of cell partitioned by a BLM into which is incorporated the complex carotene—I_2 (carotene—I^+ + I_3^-). In this system, the aqueous I_3^- permits direct observation of the gradual coloration of the aqueous solution as the voltammetric response decays.

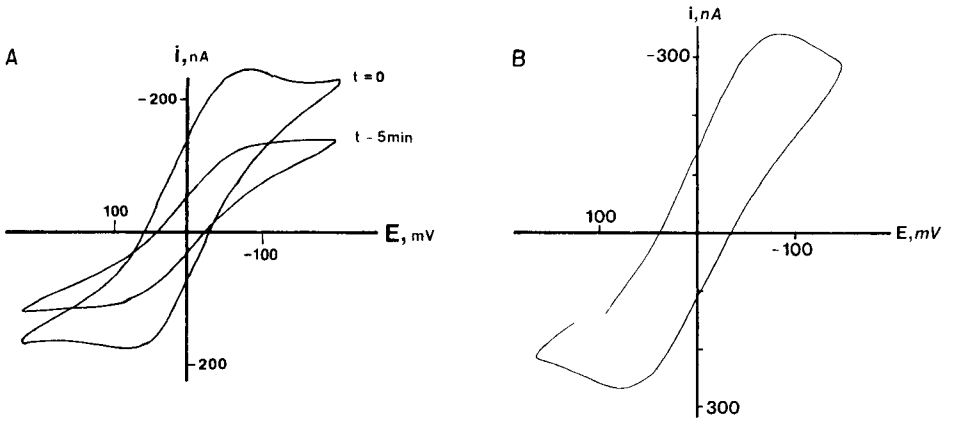

Fig. 4. Cyclic voltammograms for different cells. (A) Cell partitioned by an I_2-containing BLM after phase-transfer-catalyzed oxidation by DCIP; spectroscopic analysis verified the formation of I_3^- as a product of the reaction. (B) Cell partitioned by unmodified BLM after the addition of an aliquot of an aqueous extract of a phase-transfer-catalyzed oxidation of I_2 in chloroform by DCIP in water. Polarization rate 200 mV s^{-1}; supporting electrolyte 0.1 M KCl, 20 mM MES buffer (pH 5.5).

diffusion-controlled voltammogram. Symmetric traces were obtained regardless of whether the dye was added to one or both chambers, and again the voltammetric response diminished with time following the addition of dye (Fig. 4).

This reaction between dye and membrane is easily mimicked by preparing immiscible layers of chloroform and water. If one dissolves iodine in the chloroform and DCIP in the water prior to mixing the two solutions, a brownish color appears in the aqueous phase, a color which does not appear when one omits the DCIP. The dye is bleached when reduced, therefore iodide may be oxidized by DCIP with the formation of triiodide. A solution containing the leuco dye (reduced with ascorbate) did not elicit a voltammetric response, although an aliquot obtained from the aqueous layer of the model reaction did yield the observed voltammetric behavior, and behaved similarly when aqueous triiodide was added. Finally, it is worth noting that the reaction between iodine and DCIP is phase-catalyzed because direct combination of the pair in any solvent failed to yield any component capable of eliciting a voltammetric response. Only when separated by an interfacial boundary does a reaction occur.

Conclusion

Aqueous iodide and triiodide both enhance the conductivity of a phospholipid BLM. The data imply that the passage of charge across the membrane is ionic and occurs via voltage-induced diffusion current/voltage profiles. This implies that the charge movement is governed by more than one kinetic factor; that of triiodide movement seems to be diffusion-limited.

The ionic mechanism is supported by data which implicates triiodide in connection with the appearance of diffusion-controlled voltammograms. The behavior of the current/voltage response obtained can be correlated with expectations based on a kinetic model (i.e., diffusion away from a centralized point of reaction.) Only complexes and reactions which yield I_3^-, i.e.

β-carotene + $2I_2 \rightleftharpoons \beta$-carotene$-I^+ + I_3^-$

$I_2 + I^-_{aq} \rightleftharpoons I_3^-$

DCIP + $2I_2 \rightleftharpoons$ DCIP$-I^+ + I_3^-$

are readily correlated to a diffusion-controlled voltammogram.

In suggesting the above ionic mechanism, the role of triiodide functioning as an oxidant is rejected. Under polarizing conditions, the only source of reducing equivalents is the BLM and any incorporated I_2 or I_3^-. The iodine and triiodide are all oxidants as is any iodate which may be present. Conceivably, the reduction sequence $IO_3^- \xrightarrow{e^-} I_2 \xrightarrow{e^-} I^-$ could be involved if there existed small amounts of iodate present on both sides of the membrane; however, the oxidation of iodine to iodate in such circumstance would be very slow and ordinarily requires alkaline conditions. Furthermore, the magnitudes of the currents obtained are greater than what would be expected for a small amount of iodate and the peak current responds proportionately to the amount of triiodide added.

This work was supported by an ONR grant (N00014-85-K-0394). Thanks are due to Theresa Hubbard for her secretarial service.

REFERENCES

1 P. Lauger, W. Lesslauer, E. Marti and J. Richter, Biochem. Biophys. Acta, 135 (1967) 20.
2 A. Finkelstein and A. Cass, J. Gen. Physiol., 52 (1968) 145s.
3 H. T. Tien, Bilayer Lipid Membranes: Theory and Practice, M. Dekker, New York, 1974.
4 F. A. Siddiqi and H. T. Tien, in G. Milazzo (Ed.), Topics in Bioelectrochemistry and Bioenergetics, Vol. 5, Wiley, New York, 1983, pp. 157—224.
5 H. T. Tien, Bioelectrochem. Bioenerg., 13 (1984) 299.
6 H. T. Tien, in S. G. Davison (Ed.), Progress in Surface Science, Vol. 19, Pergamon, New York, 1985, Chap. 3.
7 C. Bender and H. T. Tien, Anal. Chim. Acta, 198 (1987) 259.
8 O. H. LeBlanc, Biochim. Biophys. Acta, 193 (1969) 350.
9 J. Koryta, Ions, Electrodes and Membranes, Wiley, New York, 1982.
10 J. Kleinberg and A. W. Davidson, Chem. Rev., 42 (1948) 601.

Analytica Chimica Acta, 201 (1987) 59—65
Elsevier Science Publishers B.V., Amsterdam — Printed in The Netherlands

DETERMINATION OF SULPHUR IN FUEL OILS BY ABSORPTION SPECTROMETRY OF ELECTROTHERMALLY GENERATED CARBON SULPHIDE MOLECULES

PAOLO TITTARELLI* and GIOVANNA LAVORATO

Stazione sperimentale per i Combustibili, Viale A. De Gasperi 3, 20097 San Donato Milanese, Milan (Italy)

(Received 30th December 1986)

SUMMARY

Molecular absorption spectra of CS are observed during the vaporization of crude and fuel oils in an electrothermal atomizer. The CS absorbance at 257.6 nm is used to determine the sulphur content of the oil, based on measurements in a conventional electrothermal atomic absorption spectrometer. The results for various fuel oils generally agree with those obtained by x-ray fluorescence spectrometry (ASTM D2622). The detection limit referred to the undiluted oil is 50 mg kg^{-1}, and the repeatability is 3% at the 250 mg kg^{-1} level. Some oils exhibit uneven vaporization of sulphur species.

The determination of nonmetals by atomic absorption spectrometry encounters instrumental problems whenever the resonance lines of the analyte element fall in the far-ultraviolet region [1—4]. In this case, conventional atomic absorption spectrometers must be modified because purged or vacuum optics are required. To overcome this drawback, ultraviolet or visible molecular absorption and emission bands originating from non-metals in flame and electrothermal devices have been used [5]. The flame emission of HPO at 526 nm and S_2 at 394 nm [6] has been proposed for phosphorus and sulphur determinations, respectively, and the molecular absorption of some sulphides [7—9] and halides [9, 10] produced by electrothermal vaporization has been used for determinations of sulphur and halogens.

During a previous investigation [11] concerned with the vapour-phase behaviour of organic and organometallic samples, molecular absorption bands attributable to sulphur species were recorded in the ultraviolet region. These bands were particularly evident during the vaporization of pigments, crude oils and fuel oils, and this stimulated their application to sulphur determination by electrothermal molecular absorption spectrometry, as is described in this paper.

The study is focused on fuel oils; the vapour-phase properties were examined with a diode-array spectrometer, but a conventional atomic absorption spectrometer was used in the final procedure.

0003-2670/87/$03.50

EXPERIMENTAL

Apparatus

The diode-array spectrometer used in this investigation, consisting of a deuterium lamp, electrothermal atomizer and polychromator, was described previously [11]. The atomic absorption spectrometer was a Perkin-Elmer 5000 equipped with a HGA-500 atomizer and AS-40 autosampler. A deuterium lamp and hollow-cathode lamps for manganese, iron and aluminium were used as radiation sources. The x-ray fluorescence spectrometer used to check the sulphur content in oils was a Philips PW-1400 equipped with a chromium x-ray tube, pentaerythritol crystal and proportional flow counter.

Reagents

Organic and inorganic analytical-grade reagents were used. The fuel oils were obtained by distillation up to 340°C of crude oils of various origins following the ASTM D285 method. The residual oils, after distillation of the low-boiling fraction, can be regarded as fuel oils of known sources. Fuel oils from the National Bureau of Standards (Washington, DC) with certified sulphur content (SRM 1634a, 1621b, 1622b) were used to set up the instrumental conditions and for calibration. Calcium and sodium benzenesulphonates were obtained by treating benzenesulphonic acid with a stoichiometric quantity of calcium or sodium carbonate. Standard compounds and fuel oils were diluted to an appropriate sulphur concentration, ranging from 10 to 1000 mg kg^{-1}, depending on the purpose of the measurement.

Procedure

The organic or aqueous solution (20 μl) was introduced in the graphite furnace (HGA 76-B when the diode-array spectrometer was used, HGA 500 for the atomic absorption spectrometer) and vaporized by a four-step thermal cycle: dry, ash, atomize and clean. The drying and cleaning temperatures were maintained throughout the study at 120°C and 2650°C, while the ashing and atomizing temperatures, as well as their respective ramps, were modified according to the desired information. Ultraviolet spectra in the range 200—350 nm were acquired by the diode-array spectrometer with 0.2-s collection time during the "atomization" step only; therefore the vaporization of both atomic and molecular species could be followed simultaneously, thus giving an overall picture of the sample characteristics. The atomic absorption spectrometer was operated at 257.6 nm (0.7-nm slit width) with a deuterium lamp. Vaporization peaks were recorded during the third stage; peak-area measurements were employed for calibration. The sulphur content of fuel oils was determined by using the thermal program reported in Table 1.

RESULTS AND DISCUSSION

A common feature of the vapour-phase spectra of oils collected with the diode-array spectrometer is the appearance of structured bands at high

TABLE 1

Thermal program for the determination of sulphur in fuel oils

Step	Temp. (°C)	Ramp (s)	Hold (s)	Argon flow (ml min^{-1})
1	130	15	25	300
2	900	60	5	120
3	2500	1	9	50
4	2650	1	5	300

temperature during the "atomization" step. Figure 1 shows absorption spectra produced during a typical vaporization of a fuel oil, recorded during the third stage of a thermal program similar to that reported in Table 1, except that the temperature of the third stage was increased to 2650°C. The bands, observed when an uncoated graphite tube was used, exhibit a maximum at 257.6 nm and are always found during the treatment of crude or fuel oils of any origin. Their intensity is related to the sulphur concentration in the oils. The temperatures reported in the Figures are those obtained from the furnace programmers and are not necessarily the true vapour temperature.

The bands cannot be attributed to atomic absorption of any element in the oils because of their width and wavelength. Nevertheless, the fact that they are formed at high temperatures suggests an attribution to simple molecules. When pyrolytically coated tubes are used, the bands are no longer detected (Fig. 1), thus the tube surface is involved in the formation of the vapour-phase species responsible for the structured absorption bands. A comparison of the spectra with those reported in the literature for diatomic molecules allows attribution to the transition $A\,^1\Pi \rightarrow X\,^1\Sigma^+$ of CS [12].

The reaction between the graphite surface and samples to form CS vapour is supported by the spectra in Fig. 2; in this case, only the two most distinctive spectra are reported, for simplicity. The two spectra, acquired during the atomization step, show the initial decomposition of the sample with evolution of SO_2 (spectrum at 2200°C) and the subsequent reaction between decomposition products and graphite with formation of CS (spectrum at 2650°C). Hence CS species in oils do not derive from the simple decomposition of organosulphur molecules, but by reaction with the tube graphite. No SO_2 spectra are seen in Fig. 1 because sulphur in fuel oils is bound mainly in heterocyclic compounds.

These bands are hardly observed during the heating of oils which distil below 300°C (kerosene, gas oil and diesel oil); the low-boiling sulphur species are lost to the vapour-phase before reaction with the graphite can occur. Hence, CS formation occurs at high temperatures. In fuel oils, sulphur species pyrolyze during the ashing step; some sulphur could be lost as hydrogen sulphide [13], the remainder reacting to form CS during the atomization step. Therefore the vaporization of sulphur as CS cannot be considered

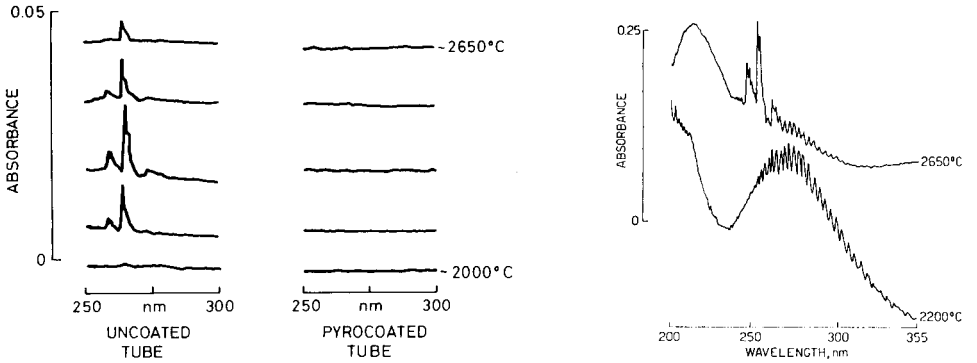

Fig. 1. Absorption spectra of Iranian heavy fuel oil (400 mg kg^{-1} in xylene) recorded at 0.2-s intervals during the atomization step.

Fig. 2. Absorption spectra recorded during the atomization of 1 mg of calcium sulphate under the same conditions as in Fig. 1, with an uncoated tube.

truly quantitative, because of the different behaviours of the various sulphur species.

Different purge gases were used during the ashing step to modify the spectra or to improve the intensity of the CS absorption bands. Oxidizing (air) or reducing (10% methane in argon) gases greatly decreased the band intensities. Air decreased the CS formation by oxidizing the sulphur compounds with subsequent loss as sulphur dioxide, while methane forms pyrolytic graphite which inhibits the reaction between sulphur compounds and the graphite surface.

The diode-array spectrometer enables the formation of CS to be studied spectrally. An analytical method based on CS absorbance measurements at fixed wavelength was developed based on the electrothermal atomic absorption spectrometer. In this case, the deuterium lamp, used for background correction, offers some advantages in comparison with hollow-cathode lamps of elements with lines around 257.6 nm (Al, Fe, Mn). Iron is present in oils at 1—50 mg kg^{-1} and therefore interferes with the sulphur determination when an iron lamp is used, whereas the atomic absorption of iron in diluted oils is almost undetected when a deuterium lamp is employed. The use of manganese and aluminium radiation at 257.61 and 257.51 nm, respectively, produces signal-to-noise ratios for sulphur worse than that obtained with the deuterium lamp. Measurements at 255 and 259 nm indicate that, during "atomization", absorption other than that from CS is negligible, so that the absorbance measured at 257.6 nm is essentially that of CS.

The thermal parameters of the HGA-500 furnace were optimized by using a 200 mg kg^{-1} solution of SRM 1634a fuel oil in xylene. The ashing temperature at 900°C enables the complete charring of the oil sample without

appreciable loss of sulphur and without subsequent appearance of background absorption. Higher ashing temperatures led to decreased molecular absorption, and lower temperatures to non-specific absorption and light scattering during the measurement stage. A slow heating rate up to 900°C (13°C s^{-1}) was applied, together with a decreased gas flow to limit the sulphur loss into the gas phase as hydrogen sulphide [13]. At an atomization temperature of 2500°C, the absorption/time profiles were very close to those of trace elements at the same temperature.

Under the conditions listed in Table 1, a calibration graph for SRM 1634a was linear up to 400 mg kg^{-1} sulphur; this was also valid for the other oils examined. The 3σ detection limit obtained with 20-μl injections was 10 mg kg^{-1}, while the repeatability was 3% at the 50 mg kg^{-1} level. These values convert to 50 mg kg^{-1} and 250 mg kg^{-1}, respectively, for undiluted oils.

Various sulphur compounds were tested for use as aqueous standards for routine calibration. The molecular absorption/time profiles depended strongly on the thermal properties of the compounds (Fig. 3). The sulphates investigated did not exhibit the CS absorption band, except for manganese(II) sulphate. However, sodium and calcium benzenesulphonates gave significant CS peaks by decomposition and reaction with graphite. Comparison at various concentrations of SRM 1634a and calcium benzenesulphonate solutions indicated that the latter can be suitable as a standard for routine analysis (Fig. 4).

The addition of vanadium, nickel and iron up to 20, 10 and 1 mg kg^{-1}, respectively, did not cause interferences in the response of either calcium benzenesulphonate standards or fuel oil solutions having a 500 mg kg^{-1} sulphur concentration, which corresponds to sulphur/element ratios typical of heavy crude oils.

Triplicate results, achieved with use of aqueous standards of calcium benzenesulphonate under the conditions listed in Table 1, for the determination of sulphur in residual oils, are shown in Table 2, and are compared with those obtained by x-ray fluorescence spectrometry (ASTM D-2622 method). Good agreement between the results of these procedures is generally obtained, although the molecular absorption result for the residual oil from Kirkuk

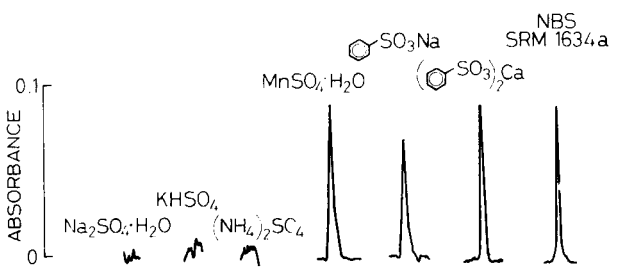

Fig. 3. Absorbance/time peaks of various sulphates and sulphonates at 257.6 nm (aqueous 200 mg kg^{-1} solutions).

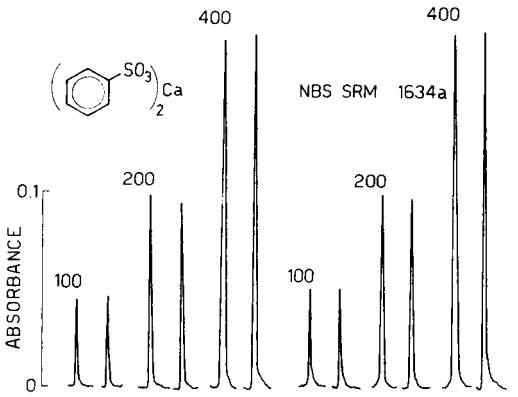

Fig. 4. Comparison of calibration peaks for calcium benzenesulphonate and SRM 1634a fuel oil. The numbers relate to mg kg^{-1} sulphur in the compound or oil.

TABLE 2

Results of sulphur determination in oils by x-ray fluorescence (ASTM D2622) and proposed method

Oil	Sulphur found (%)	
	X-ray fluorescence	Molecular absorption
NBS SRM 1634a	2.85 ± 0.02	2.90 ± 0.05
Belaym	3.27 ± 0.03	3.11 ± 0.08
Es Sider	0.68 ± 0.01	0.60 ± 0.03
Forties	0.67 ± 0.02	0.66 ± 0.03
Iranian Heavy	2.79 ± 0.03	2.63 ± 0.07
Kirkuk	4.50 ± 0.07	3.96 ± 0.10

crude is 15% lower than that obtained by x-ray fluorescence. This behaviour can be attributed to the presence in that oil of thermally-unstable sulphur species that lead to sulphur loss before reaction with the graphite.

Conclusions

The use of a diode-array detector for investigation of vapour-phase phenomena can show the evolution of molecular species suitable for the determination of non-metallic elements. This information can be exploited to set up analytical procedures based on an electrothermal atomic absorption spectrometer so that the use of such spectrometers can be extended to the determination of "unusual" elements. In this case, the formation of CS at high temperatures is dependent on the properties of the sulphur compounds. This can be a drawback to the method, because some fuel oils from particular crude oils can exhibit uneven CS evolution, leading to significant errors in

estimating the sulphur content. Low concentrations of sulphur can be determined, or microsamples, such as those obtained from oil spill incidents, could be analyzed.

The appearance of CS bands during the vaporization of a variety of samples (coals, pigments, polymers) indicates potential development of the technique to these products.

This work was presented in part at the 13th FACSS Meeting, St. Louis, in 1986.

REFERENCES

1 G. F. Kirkbright and M. Marshall, Anal. Chem., 44 (1972) 1288.
2 G. F. Kirkbright, M. Marshall and T. S. West, Anal. Chem., 44 (1972) 2379.
3 G. F. Kirkbright and P. J. Wilson, Anal. Chem., 46 (1974) 1414.
4 G. F. Kirkbright and M. J. Adams, Can. J. Spectrosc., 21 (1976) 127.
5 H. Haraguchi and K. Fuwa, Anal. Chem., 48 (1976) 784.
6 G. L. Everett, T. S. West and R. W. Williams, Anal. Chim. Acta, 68 (1974) 387.
7 K. Tsunoda, K. Chiba, H. Haraguchi, C. L. Chakrabarti and K. Fuwa, Can. J. Spectrosc., 27 (1982) 69.
8 A. Syty, Anal. Chem., 51 (1979) 911.
9 K. Dittrich, B. Vorberg, J. Funk and V. Beyer, Spectrochim. Acta, Part B, 39 (1984) 349.
10 K. Tsunoda, K. Fujiwara and K. Fuwa, Anal. Chem., 50 (1978) 861.
11 P. Tittarelli, R. Lancia and T. Zerlia, Anal. Chem., 57 (1985) 2002.
12 R. W. B. Pearse and A. G. Gaydon, The Identification of Molecular Spectra, 3rd edn., Chapman & Hall, London, 1963.
13 P. E. Savage, M. T. Klein and S. G. Kukes, Ind. Eng. Chem. Process Des. Dev., 24 (1985) 1169.

Analytica Chimica Acta, 201 (1987) 67—76
Elsevier Science Publishers B.V., Amsterdam — Printed in The Netherlands

MICELLAR-CATALYZED REACTIONS FOR FLOW-INJECTION SYSTEMS
Determination of Pyridoxal

MARIA A. HERNÁNDEZ TORRES, MORTEZA G. KHALEDI[a] and JOHN G. DORSEY*
Department of Chemistry, University of Florida, Gainesville, FL 32611 (U.S.A.)
(Received 26th January 1987)

SUMMARY

The advantages of applying the solubilization and catalytic properties of aqueous micelle solutions to reactions taking place in flow-injection systems are demonstrated. The reaction of pyridoxal (a B_6 vitamin) with cyanide was investigated in both aqueous and micellar cetyltrimethylammonium bromide (CTAB) solution. Higher sensitivities and lower limits of detection were obtained for the micellar carrier, with the pseudo-first-order reaction rate increasing by a factor of two in 0.05 M CTAB relative to water carrier. Because the micellar aggregates also increase fluorescence quantum yields, use of fluorescence detection gave further signal enhancement, with the limit of detection lowered by a factor of three. Measurement of dispersion in the two systems was also investigated and compared. A new method of characterizing dispersion in flow-injection systems, based on moment analysis of exponentially modified Gaussian peak shapes, is described.

Aggregation of surfactants in aqueous solution is the result of opposing forces, with the driving force being the hydrophobic effect. Above a certain concentration, termed the critical micelle concentration (c.m.c.), which is unique for every surfactant, the surfactant molecules self-aggregate such that the hydrocarbon tails are oriented toward the center of the aggregate and the polar head groups point outwards. This self-aggregation serves largely to eliminate the hydrocarbon/water interface and is thus very energetically favorable.

Perhaps the most unusual aspect of aqueous micelle solutions is their ability to solubilize hydrophobic compounds that are otherwise insoluble in water. This is likely the feature that makes the study of micelle solutions most interesting for analytical chemists. Along with the increase in solubility comes a change in micro-environment, and then a change in analytical properties. The increase in solubility can result from hydrophobic interaction with the exposed hydrocarbon chains of the micelle, from electrostatic interaction with the head-groups, or a combination of both. Solute partitioning to micelles is then characterized by a partition coefficient just as is any two-phase equilibrium.

---

[a]Present address: Department of Chemistry, University of New Orleans, New Orleans, LA 70148.

0003-2670/87/$03.50

Aqueous micelle solutions have been advantageously applied in many areas of analytical chemistry. They have been shown to increase fluorescence quantum yields, to allow room-temperature liquid-phase phosphorescence, to stabilize electrochemical intermediates and to be useful as chromatographic mobile phases. Both a tutorial on the analytical applications of micelle solutions [1] as well as a comprehensive review of their uses [2] have recently appeared.

Flow-injection analysis (FIA) is firmly established as a fast, precise, accurate, efficient and extremely versatile analytical technique [3]. These systems involve controlled-dispersion, kinetic-based processes in which either formation of a detectable product or depletion of reagent or analyte is measured in an unsegmented flowing system. Two of the most important considerations in FIA are dispersion of the sample zone, and the kinetics of the pertinent reaction. Dispersion has a two-fold effect, as it governs the peak height (and detectability) of a given amount of sample, and also affects sampling rate by controlling the time required for the detector signal to return to baseline. Not only do the kinetics affect the detectability, but also the sampling rate, as slow kinetics requires longer reaction coils and lower sample throughput. A flow-injection system with low dispersion and fast reaction rates should provide low limits of detection and a high sampling rate.

The use of aqueous micelle solutions as the carrier in flow-injection systems offers potential advantages, but has been little utilized. The first report was by Yamada and Suzuki [4], who used a cationic micelle solution to enhance the sensitivity of chemiluminescence detection of copper(II). Aihara et al. [5] further reported the use of micelle solutions to solubilize the ternary complex of europium(III) with thenoyltrifluoroacetone and trioctylphosphine oxide. The use of the micelle carrier allowed this reaction to be done in a flow-injection system rather than as a labor-intensive liquid/liquid extraction. Memon and Worsfold [6] applied micro-emulsions as a carrier for the spectrofluorimetric determination of primary amines, and showed that reactions involving a nonaqueous sample and an aqueous reagent can be quantitatively investigated by the use of organized media. Aihara et al. [7] have reported the use of micelle solutions to solubilize the ternary complex of terbium(III) with pivaloyltrifluoroacetone and trioctylphosphine. Their methods also represent one of the few available flow-injection methods for the determination of the rare earth ions.

This paper reports the applicability of aqueous micelle carrier streams for the catalysis of reactions in FIA. The principal reaction studied is the oxidation of pyridoxal (a B_6 vitamin) in the presence of cyanide [8]. Improvements in sensitivities and limits of detection arise both from faster reaction rates in the micelle system and from enhanced quantum yields when fluorescence detection is used. The quantitative figures of merit for both aqueous and micellar carriers are compared. Dispersion in both systems was also measured and compared, and a new method of defining dispersion in FIA is proposed, based on the exponentially modified Gaussian peak shape and calculation of the resulting second central moment.

EXPERIMENTAL

The flow-injection manifold is shown in Fig. 1. The reagent streams were pumped by an Isco (Lincoln, NE) Tris model peristaltic pump. Samples were introduced with a Rheodyne 7125 sample-injection valve with a 10-μl loop. All tubing was teflon with 0.5-mm i.d. The reaction coil, 200-cm long, was thermostated by immersion in a water bath with a Techne (Princeton, NJ) TE-7 circulator. Both a Varian Fluorichrom fluorescence detector with a 25-μl flow cell, 355-nm excitation and 435-nm emission filters, and a Kratos Spectroflow 757 absorbance detector set at 355 nm with a 12-μl flow cell were used. The output signals were recorded on an OmniScribe strip chart recorder.

For kinetic measurements, the reaction was followed spectrophotometrically by measuring the rate of change in the absorbance of 4-pyridoxolactone, the oxidation product, at 355 nm using a Hewlett-Packard 8450A diode-array spectrophotometer connected to a Hewlett-Packard 7470A plotter.

All reagents were used as received and prepared either in deionized water or in surfactant solutions. The cationic surfactant was cetyltrimethylammonium bromide (CTAB; hexadecyltrimethylammonium bromide, purum grade, Fluka). Standard solutions of pyridoxal (Sigma Chemical Co.) and solutions of potassium cyanide (certified ACS, Fisher Scientific) were used. Phosphate buffer solutions (0.6 M) were pH-adjusted with concentrated hydrochloric acid.

The appropriate weight of surfactant was dissolved in distilled water and the solution then filtered through a 0.45-μm Nylon-66 membrane filter (Rainin Instruments, Woburn, MA). Appropriate amounts of pyridoxal and cyanide were dissolved either in distilled water or micelle solution. All reported values are averages from at least four sample injections. The recommended conditions are summarized in Table 2.

RESULTS AND DISCUSSION

Two excellent treatises on micellar catalysis have appeared [9, 10]. The proper choice of surfactant can substantially enhance the rate of a chemical

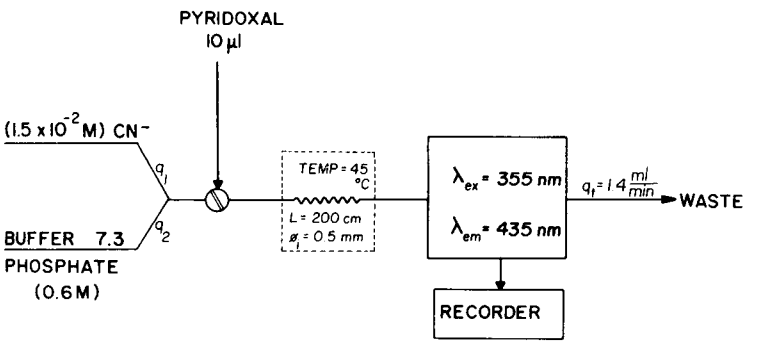

Fig. 1. Flow-injection manifold.

reaction relative to that in the corresponding aqueous system, and it has been shown that it is the micelle structure, not the individual surfactant molecules, that is responsible for the catalysis of organic reactions. The kinetics of organic reactions occurring in micellar systems are a function of electrostatic and hydrophobic interactions between the micelle structures and reactants, transition states and products. The two primary physicochemical factors responsible for the change in kinetics are the change in the reactivity of reagents on transfer from water to the micellar phase and the concentration of reactants into the micellar phase. Then for catalysis to occur, it is necessary that the substrate be solubilized by the micelle and the site of solubilization be such that the reactive site of the substrate is accessible to the attacking reagent. A hydrophobic reactant is bound to a micelle by hydrophobic interactions, independent of the charge on the micelle. If the second reactant is oppositely charged to the micelle, it will be bound to the micelle by electrostatic interactions and the reaction is usually accelerated. When micelles and reactants bear the same charges, the reaction is often inhibited owing to the repulsion forces between the ions and the micelle surface. This repulsion can actually be used advantageously to repel interferents of opposite charge to the analyte.

These catalytic effects should have great significance for the field of flow injection, especially for those reactions that are kinetically slow, where now either long reaction coils are used to allow sufficient time for the reaction to proceed, or a stopped-flow method is used. One such reaction is the determination of pyridoxal, a B_6 vitamin, which is oxidized in the presence of cyanide to form 4-pyridoxolactone.

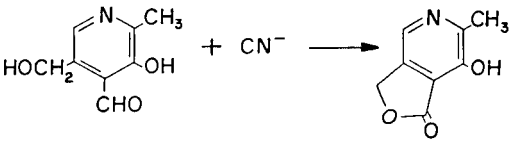

Linares et al. [8] utilized this reaction in a flow-injection method for the determination of pyridoxal and pyridoxal-5-phosphate which required a 6.0-m reaction coil and temperatures of 45°C for maximum efficiency. This is a good example of the type of reaction that is a good candidate for micellar catalysis. One of the reactants is somewhat hydrophobic and the other is anionic, so both should partition to a cationic micelle.

Kinetics

The kinetics of this reaction were studied in both aqueous and 0.05 M CTAB solution by monitoring the change in absorbance with time as the reaction proceeded. The wavelength of maximum absorbance for the reaction product was found to be 355 nm in both solutions, and the concentration of CTAB was chosen to be safely above the critical micelle concentration (c.m.c.), reported as 1.3×10^{-3} M at 25°C [1]. The pseudo-first-order rate constants were calculated from the equation

$$\log (A_\infty - A_t) = (-kt/2.303) + \log (A_\infty - A_0) \quad (1)$$

where A_∞, A_0 and A_t are the absorbances at infinite, initial and time t, respectively; t is time in minutes and k is the rate constant (min^{-1}). Plots of $\log (A_\infty - A_t)$ vs. time were linear and yielded rate constants of 0.0490 and 0.0971 min^{-1} in water and 0.05 M CTAB solutions, respectively. The ratio of these rate constants ($k_{0.05\,M\ CTAB}/k_{water}$) is 1.98, which shows that the reaction is taking place at approximately double the velocity in micellar CTAB compared to water.

To demonstrate the advantages of combining the flow-injection technique with micellar catalysis, measurements of the pyridoxal/cyanide reaction product were made over a range of pyridoxal concentrations. The ratio of the sensitivities (slopes of the calibration curves) of the aqueous and micellar system was 1.3, showing that catalysis was indeed occurring in the flow-injection system; however, the enhancement was substantially less than sug-

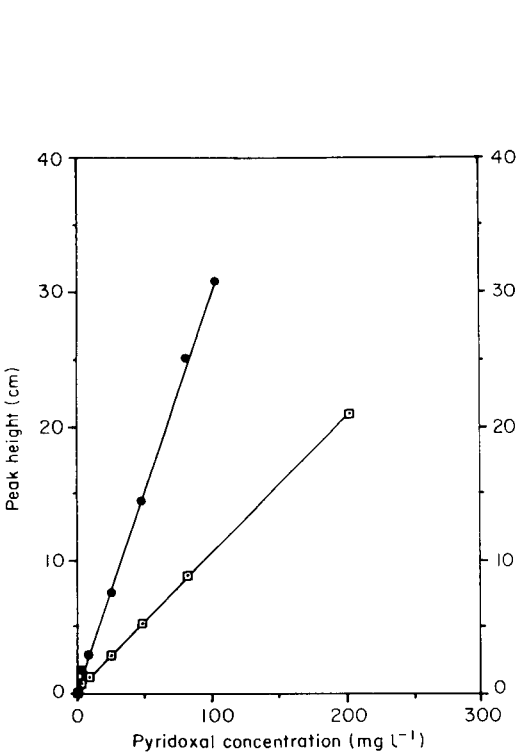

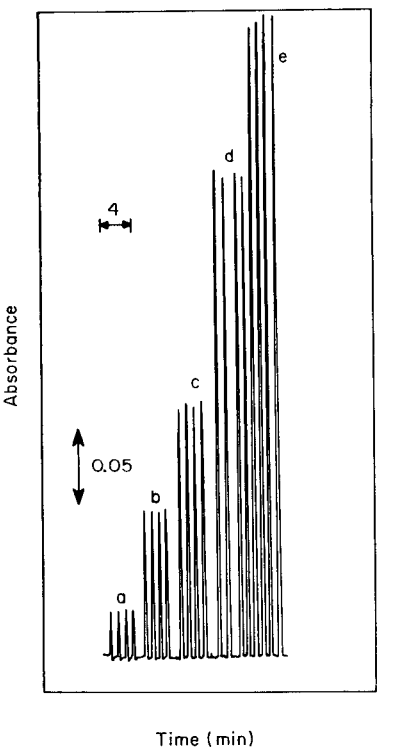

Fig. 2. Calibration plots for pyridoxal determination in aqueous (⊡) and 0.05 M CTAB (•) systems. Flow rate 1.4 ml min^{-1}; temperature 45°C; 0.6 M phosphate buffer, pH 7.3; 1.5 × 10^{-2} M cyanide; 355-nm excitation, 435-nm emission.

Fig. 3. Output for pyridoxal standards in 0.09 M CTAB media. Pyridoxal concentration (mg l^{-1}); (a) 8.10; (b) 24.31; (c) 40.52; (d) 81.04; (e) 105.4. Conditions are final simplex conditions (Table 2).

gested by the ratio of the rate constants. This may be explained by the fact that the kinetics throughout the entire sample plug are not constant. Painton and Mottola [11] have shown that the rate constant can vary throughout the sample plug and that correction factors are needed for the bulk rate constant to match the constant measured in a flow-injection system.

The use of micelle carrier solutions can enhance not only the reaction kinetics, but detection capabilities as well. Calibration graphs for aqueous and micellar systems with a fluorescence detector were linear (Fig. 2); the sensitivity for the micellar system is 2.9 times that of the aqueous system. Here, not only is micellar catalysis taking place, but there is enhancement of the fluorescence quantum yield as well. This fluorescence enhancement comes from a decrease in the collisional deactivation of the excited state brought about by shielding of the analyte in the micelle structure.

Table 1 summarizes the analytical figures of merit for both aqueous and micellar systems. Excellent correlation coefficients were obtained for the four curves, and all were found to be linear over a wide range of concentrations. The linear ranges for the aqueous system were found to be 0.42–2000 ng of pyridoxal for fluorescence detection and 94–2000 ng for absorbance measurement. In 0.05 M CTAB micellar media, the linear dynamic ranges were 0.17–1100 ng of pyridoxal for fluorescence detection and 77–2000 ng for absorbance measurement. Because the limit of detection of flow-injection systems is a function of not only the detection system but also the injection volume and the dispersion of the system [12], limits of detection are better reported as amounts rather than concentrations. The reproducibility of the system was measured by manual injection of 11 replicates of 25.5 mg l^{-1} pyridoxal solution. The relative standard deviation of peak height was found to vary between 0.97 and 3.25%.

TABLE 1

Figures of merit for pyridoxal determination.
(Fluorescence detector: excitation, 355 nm; emission, 435 nm. Ultraviolet absorption detector at 355 nm. 1.5 × 10^{-2} M cyanide, 0.6 M phosphate buffer, pH 7.3. Flow rate 1.4 ml min^{-1}, temperature 30°C. Other conditions as in experimental section)

	Fluorescence		Absorbance	
	Aqueous	0.05 M CTAB	Aqueous	0.05 M CTAB
Sensitivity[a]	0.102	0.294	2.54 × 10^{-3}	3.26 × 10^{-3}
Correlation coefficient	0.9996	0.9992	0.9999	0.9999
Limit of detection[b] (ng)	0.42	0.17	94	77
RSD[c] (%)	2.06	3.25	0.97	1.76

[a]Slope of calibration plot: relative intensity per mg l^{-1} pyridoxal for fluorescence; absorbance per mg l^{-1} for absorption. [b]Amount of material giving signal three times standard deviation of baseline noise. [c]Relative standard deviation for 11 injections at 25.5 mg l^{-1} pyridoxal.

Optimization

Linares et al. [8] used a modified simplex method to optimize the reaction conditions, and their conditions were chosen for initial experiments here. However, optimum conditions for aqueous and micellar systems may be quite different, as micelles change the micro-environment of solubilized molecules [1]. A modified variable-size simplex method [13] was used for optimization of reaction conditions in the micellar carrier with absorbance detection, with peak height serving as the response function. This simplex method has been previously used in flow-injection methods [14, 15]. The four variables optimized were: pH, temperature, flow rate and surfactant concentration. It is necessary to include pH as one of the parameters as it is known that micelles can affect acidity constants [16]. Surfactant concentration was also included, as this controls the concentration of micelle aggregates. Increasing the number of micelle structures increases the sites available for solute solubilization and reaction, but too high a concentration will 'dilute' the reactants by causing them to be associated with different micelles. Table 2 shows the initial and final conditions which were found after 18 experiments (one reflection, two expansions and four contractions). It is likely that optimum conditions for fluorescence detection would be somewhat different, as temperature and ionic strength can affect quenching rates as well.

A calibration graph was then prepared by using the optimized conditions and compared with the calibration plot for the aqueous system run with the previous conditions. The slopes of the two curves absorbance vs. concentration (mg l^{-1}) were 3.84×10^{-3} for the new conditions and 2.09×10^{-3} for the previous aqueous conditions, giving a ratio of 1.8. The simplex then significantly improved the sensitivity of the reaction, and shows that for micellar catalysis to be most effective, conditions must be optimized in the presence of the surfactant. Figure 3 shows a series of standards run under the optimized conditions.

Dispersion

In flow-injection systems, both sample throughput and sample dilution are directly related to dispersion. The dispersion process which takes place during the transport of the sample from the injection device toward the detector

TABLE 2

Initial and final conditions for the modified simplex optimization

Parameter	Initial value	Final value
pH	7.3	6.74
Flow rate[a] (ml min^{-1})	1.4	1.3
Temperature (°C)	45	49
CTAB concentration (M)	0.05	0.09

[a]Total flow rate, q_t, with $q_1 = q_2$ (see Fig. 1).

is one of the less-understood aspects of FIA. The tanks-in-series model is frequently used to describe the dispersion process. According to this model, the flow reactor can be considered as a series of N ideal mixers. If the number of mixing stages, N, is high enough, the resulting curve has a Gaussian shape. However, peaks mostly show a tailing character. In 1981, Reijn et al. [17] described the distribution curve for a flow-injection peak as a modified Gaussian function. However, only the physical aspects of dispersion were taken into consideration, and they assumed that there was no contribution to dispersion from the chemical reaction in the system. This assumption is known to be invalid [11, 18].

The most often used measure of reporting dispersion is the D value, or practical dispersion, proposed by Růžička and Hansen [19]: $D = C^0/C^{max}$, where C^0 is the original concentration and C^{max} is the concentration at peak maximum (after dispersion). It has been argued that this measure loses physical significance when chemical reactions add to the dispersion process [18, 20]: however, it is still widely applied because of the ease of calculation. Reijn et al. [18] proposed the use of the statistical moments of the residence-time distribution function, which certainly offers more fundamental information about the dispersion process, but this has not been easily calculable without digital data acquisition and subsequent computer processing.

While almost never Gaussian, the peaks in FIA have been previously described by a modified Gaussian function [17]. The exponentially modified Gaussian function fits many peaks of analytical interest and this model has been recently reviewed [21]. Foley and Dorsey [22] have recently derived equations for the calculation of chromatographic figures of merit based on statistical moments of Gaussian and exponentially modified Gaussian peaks. These equations then give the ability for manual calculation of statistical moments which will hopefully extend the use of these more relevant peak descriptors to those peaks which are fitted by either of these models. Reporting dispersion as variance rather than the empirical dispersion parameter, D, should offer more fundamental information about the system, as the peak width is immediately understandable from the variance. Furthermore, two systems can be readily compared from their variance values, and the difference in peak widths is easily calculated. Individual contributions to the dispersion process, such as those occurring from pure physical mass transfer and from the kinetics of the chemical reaction should also be easily ascertained through the principle of additivity of variances. Further work on the deconvolution of individual contributions to dispersion is underway.

Assignment of peak shape can be made by comparison of peak descriptors calculated from equations derived from peak width at three different peak heights [21]. If the peak is Gaussian, the peak-width ratio $W_{0.5}$: $W_{0.3}$: $W_{0.1}$ will be 0.5487: 0.7231: 1, where $W_{0.5}$: $W_{0.3}$: $W_{0.1}$ represent total peak width at 50%, 30% and 10%, respectively, of total peak height. Skewed peaks are conveniently described by an asymmetry factor, B/A, measured at 10% peak height, where B is the distance from the center of the peak to the trailing

edge, and A is the corresponding distance from the center of the peak to the leading edge [21]. Gaussian peaks then, by definition, have a B/A value of 1.00. For B/A values of $\geqslant 1.09$, the validity of the modified-Gaussian model can be judged by the agreement of values of σ_G, the standard deviation of the parent Gaussian component, or M_2, the second central moment (variance) evaluated from measurements at 10, 30 and 50% peak height and calculations using equations developed explicitly for this purpose [21].

The peaks generated in the present flow-injection system were well modelled by the modified Gaussian, and this model was then used to compare dispersion between the aqueous and micellar system. Pyridoxal was injected into the flowing system with no cyanide ion present, so dispersion values reported are only for physical processes; no chemical reaction was occurring. By means of variance calculations based on peak measurements at 10% peak height [21]:

$$M_2 = W_{0.1}^2 / [1.764\,(B/A)_{0.1}^2 - 11.15\,(B/A)_{0.1} + 28]$$

the values found were 9300 and 11 000 μl^2 for aqueous and 0.05 M CTAB media, respectively. The dispersion parameter, D, was also calculated for the two dispersion systems and was found to be 17.62 for the aqueous system and 19.14 for the micellar system.

Switching from aqueous to micellar carriers then does increase the dispersion, but the increase in reaction rates is still sufficiently large to lower the limits of detection. The increase in dispersion is likely from the difference in viscosity between the two solutions. It is well known that micellar media are more viscous than aqueous media and that micelle aggregates have small diffusion coefficients. As the pyridoxal molecules are solubilized by the micelle aggregates, their diffusion is restricted and mass transfer in the radial direction decreases. An increase in peak dispersion results because a decrease in mixing across the stream tends to increase dilution of the solute by longitudinal dispersion [20]. Further study of dispersion phenomena in micellar carriers is ongoing in this laboratory.

The authors are grateful to Pfizer Inc., and NSF CHE-8704403 for partial support of this work.

REFERENCES

1 L. J. Cline Love, J. G. Habarta and J. G. Dorsey, Anal. Chem., 56 (1984) 1132A.
2 E. Pelizzetti and E. Pramauro, Anal. Chim. Acta, 169 (1985) 1.
3 J. Růžička and E. H. Hansen, Anal. Chim. Acta, 179 (1986) 1.
4 M. Yamada and S. Suzuki, Anal. Lett., 17 (1984) 251.
5 M. Aihara, M. Arai and T. Taketatsu, Analyst, 111 (1986) 641.
6 M. H. Memon and P. J. Worsfold, Anal. Chim. Acta, 183 (1986) 179.
7 M. Aihara, M. Arai and T. Tomitsugu, Anal. Lett., 19 (1986) 1907.
8 P. Linares, M. D. Luque de Castro and M. Valcárcel, Anal. Lett., 18 (1985) 67.
9 E. Cordes (Ed.), Reaction Kinetics in Micelles, Plenum, New York, 1973.
10 J. H. Fendler and E. J. Fendler, Catalysis in Micellar and Micromolecular Systems, Academic, New York, 1975.

11 C. C. Painton and H. A. Mottola, Anal. Chim. Acta, 158 (1984) 67.
12 J. P. Foley and J. G. Dorsey, Chromatographia, 18 (1984) 503.
13 D. J. Legett, J. Chem. Educ., 60 (1983) 707.
14 D. Betteridge, T. J. Sly and A. P. Wade, Anal. Chem., 55 (1983) 1292.
15 A. Fernández, M. D. Luque de Castro and M. Valcárcel, Anal. Chem., 56 (1984) 1146.
16 A. L. Underwood, Anal. Chim. Acta, 140 (1982) 89.
17 J. M. Reijn, W. E. Van der Linden and H. Poppe, Anal. Chim. Acta, 126 (1981) 1.
18 J. M. Reijn, H. Poppe and W. E. Van der Linden, Anal. Chem., 56 (1984) 943.
19 J. Růžička and E. H. Hansen, Anal. Chim. Acta, 99 (1978) 37.
20 C. C. Painton and H. A. Mottola, Anal. Chem., 53 (1981) 1713.
21 J. P. Foley and J. G. Dorsey, J. Chromatogr. Sci., 22 (1984) 40.
22 J. P. Foley and J. G. Dorsey, Anal. Chem., 55 (1983) 730.

Analytica Chimica Acta, 201 (1987) 77—82
Elsevier Science Publishers B.V., Amsterdam — Printed in The Netherlands

SPECTROFLUORIMETRIC DETERMINATION OF TRIETHYLENETHIOPHOSPHORAMIDE IN BLOOD

AKIRA SANO* and SHOJI TAKITANI

Faculty of Pharmaceutical Sciences, Science University of Tokyo, 12 Ichigaya-funagawara-machi, Shinjuku-ku, Tokyo 162 (Japan)

(Received 20th February 1987)

SUMMARY

The method is based on a reaction of the ethyleneimine group with sodium sulfide, taurine and *o*-phthalaldehyde to give a fluorescent product. Triethylenethiophosphoramide (thioTEPA) can be determined in the range 9.4—945 ng in 100 μl of 1-propanol with a relative standard deviation of 2.3—4.7%. The method is applied to the determination of thioTEPA in rabbit blood plasma. The use of Extrelut 3 proved to be efficient for the clean-up of thioTEPA in plasma samples.

Triethylenethiophosphoramide (thioTEPA, I) is a potent alkylating

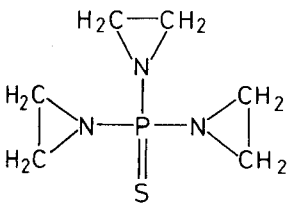

(I)

antitumour agent. It has been shown to be clinically useful and has been applied for about 30 years in cancer treatment. Development of the methodology for monitoring of thioTEPA levels in biological fluids is highly desirable, because of its serious side-effects [1]. Although a recently reported gas chromatographic method with a nitrogen/phosphorus detector [2—4] is very sensitive and permits the determination of both thioTEPA and its metabolite, triethylenephosphoramide (TEPA) [2, 3], a spectrophotometric method with 4-(*p*-nitrobenzyl)pyridine [5—7] and a fluorimetric method with 2-naphthol [8] have also been utilized. However, the application of these spectrometric methods is often limited because they are tedious, insensitive, or of poor color stability or require a large sample volume.

The *o*-phthalaldehyde (OPA) reaction for thiols in the presence of primary amines [9, 10] has been applied to the fluorimetric determination of some epoxides at sub-nanomolar levels [11]. This method is considered to involve

0003-2670/87/$03.50

the S-alkylation reaction of sodium sulfide with the epoxy group and the subsequent condensation reaction with OPA and taurine in borate buffer to form isoindole fluorophores. It seems that thioTEPA can also be determined by its alkylation of the ethyleneimine group. The present work was aimed at establishing a fluorimetric method for determining thioTEPA by utilizing this reaction. A suitable clean-up procedure for the determination of thioTEPA in plasma samples was also examined.

EXPERIMENTAL

Materials and apparatus

ThioTEPA was supplied by Sumitomo Pharmaceuticals Co. (Osaka). A standard solution was prepared in 1-propanol. ThioTEPA injection solutions were purchased from Sumitomo Pharmaceuticals Co. Sodium sulfide nonahydrate, OPA, taurine and ethylenediaminetetraacetic acid, tetrasodium salt (EDTA · 4Na) were obtained from Nakarai Chemicals Co. (Kyoto). The water used was purified on a Milli-RO/Milli-Q system (Millipore). An Extrelut 3 column (Merck) was used for extraction of thioTEPA from blood plasma samples.

Human plasma and albino rabbits (female) were obtained from Nippon Bio-supply Center (Tokyo). All chemicals used were of analytical-reagent grade.

A Shimadzu RF-502 spectrofluorimeter equipped with a xenon lamp was used with a 4 × 10 mm quartz cell at room temperature; the spectral bandwidths were 5 nm for excitation and emission. All fluorescence excitation and emission spectra were uncorrected.

Procedures

Fluorimetric determination of thioTEPA. To 100 μl of sample solution in a 1.5-ml glass-stoppered test tube was added 10 μl of aqueous 40 mM sodium sulfide/50 mM EDTA · 4Na solution. The tube was heated in a water bath at 80°C for 30 min and then cooled to room temperature in a water bath. To the mixture were added 400 μl each of 0.2 mM taurine and 0.3 mM OPA solutions in 0.05 M borate/0.1 M phosphate buffer (pH 8.0). The fluorescence intensity was measured with excitation at 350 nm and emission at 450 nm.

Extraction of thioTEPA from plasma samples. A plasma sample (1 ml) was diluted with water (2.2 ml) and 3 ml of the solution was applied to the Extrelut 3 column. After 15 min, chloroform was passed through the column. The first 4 ml of effluent was collected and evaporated to dryness in an evaporator at a water bath temperature of 20°C. The residue obtained was dissolved in 500 μl of 1-propanol. A 100-μl aliquot of the solution was then examined by the above method.

RESULTS AND DISCUSSION

Fluorimetric determination of thioTEPA

When thioTEPA was treated by the fluorimetric method for the determination of epoxides [11], a blue fluorescence was observed. The intensity, however, was about 30% of the value obtained from 1,2-epoxy-3-phenoxypropane. Thus the effects of various reaction conditions were examined.

1-Propanol was selected as the sample solvent because it gave the highest fluorescence intensity compared to water and other organic solvents such as ethanol, 2-propanol and acetonitrile. Changes in the concentration of sodium sulfide solution from 40 to 100 mM had no effect on the fluorescence intensity. The optimal concentration of sodium sulfide was found to be 40 mM, because the fluorescence of the reagent blank increased with an increase in its concentration. Tetrasodium EDTA increased the fluorescence intensity of thioTEPA as well as lowering the blank fluorescence intensity. The effect was constant in the concentration range 10—100 mM thus 50 mM EDTA · 4Na was used. Addition of disodium or trisodium EDTA was not effective, probably because of the decreasing pH of the reaction mixture. Sodium sulfide and tetrasodium EDTA could be used conveniently as a mixture. The EDTA is used to mask metals to prevent metal-catalyzed oxidation of the thiol.

The effects of reaction temperature and time were also studied (Fig. 1). The reaction of thioTEPA was almost complete at 80°C after 30—40 min; below 70°C, longer times were necessary and above 90°C, fluorescence decay was accelerated. Thus reaction at 80°C for 30 min was selected.

The effects of amine species, pH and reagent concentrations on the subsequent OPA reaction were next examined. The results obtained were similar to those described previously with regard to the determination of epoxides [11] except that slightly lower concentrations of taurine and OPA gave the best results. Thus the use of 0.2 mM taurine and 0.3 mM OPA prepared in

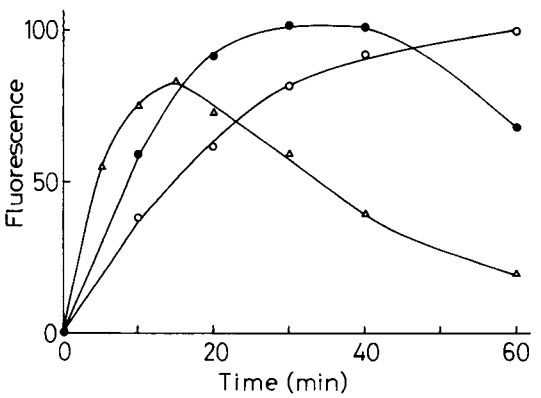

Fig. 1. Effect of reaction temperature and time on the alkylation reaction of thioTEPA (1890 ng ml^{-1}): (○) 70°C; (●) 80°C; (▲) 90°C.

borate/phosphate buffer (pH 8.0) is recommended. On addition of the OPA reagent as the final step on the procedure, the fluorescence reaction was immediately complete at room temperature. The fluorescence was stable for 20 min at this temperature.

The fluorescence maxima of thioTEPA were found to be excitation at 340 nm and emission at 440 nm. But to avoid the influence of the weak fluorescence of the reagent blank, the wavelengths for quantitation were set at 350 nm and 450 nm for excitation and emission, respectively. The fluorescence intensities were proportional to the thioTEPA concentration in the range 94.5—9450 ng ml^{-1} (0.5—50 nmol ml^{-1}). The relative standard deviations (n = 10) were 4.7% (189 ng ml^{-1}) and 2.3% (at 1890 ng ml^{-1}).

Clean-up of thioTEPA in plasma

For the recovery tests, commercial human plasma was spiked with known amounts of thioTEPA. For the separation of thioTEPA from biological fluids, extraction with organic solvents such as chloroform [3] and ethyl acetate [4] is widely used. Such a procedure, however, proved to be inapplicable here, because recovery and reproducibility were unsatisfactory and also a problem arose from the presence of colloidal protein in the plasma. The utility of a Sep-Pak C_{18} cartridge for the clean-up of thioTEPA, in which ethanol was used as an eluent, has been demonstrated [2]. However this was also not acceptable for the present purpose because thioTEPA disappeared on evaporation of its ethanolic solution. Therefore, an Extrelut 3 column (which is generally used for extraction of lipophilic compounds) was examined for the purification of plasma thioTEPA. When plasma (1 ml) to which

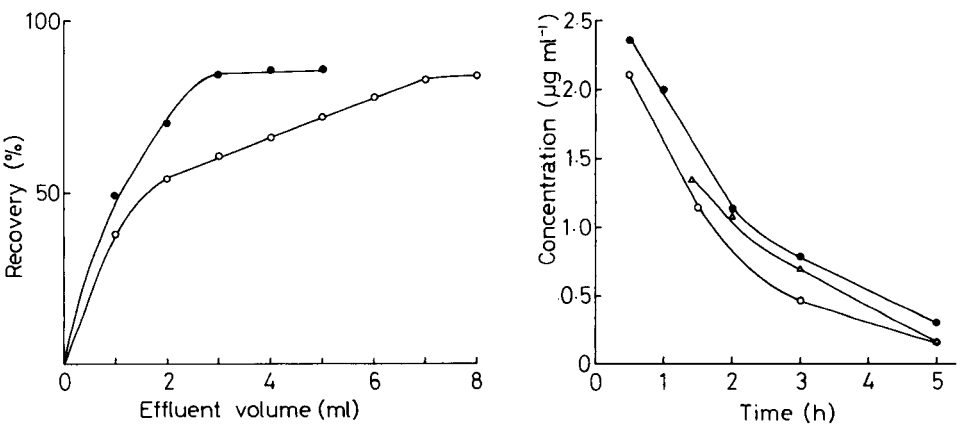

Fig. 2. Elution profiles of thioTEPA (945 ng ml^{-1} plasma) from Extrelut 3: (•) chloroform; (○) ethyl acetate.

Fig. 3. Variation of plasma concentrations of thioTEPA in three rabbits with time following a single intravenous injection (5 mg kg^{-1}): (•) rabbit No. 1; (○) rabbit No. 2; (△) rabbit No. 3.

945 ng of thioTEPA had been added was diluted with water (2.2 ml) and applied to the column, ca. 80% of the thioTEPA was recovered by elution with 3 ml of chloroform or 7 ml of ethyl acetate (Fig. 2). Chloroform (4 ml) was used in the present study because of the necessity to use smaller amounts of solvent. Losses of ca. 20% would be expected because of the volatility of thioTEPA; a similar loss was observed when standard thioTEPA solution in chloroform was evaporated to dryness and assayed. After the clean-up, the fluorescence intensity resulting from blank plasma was only about 2.5 times that from the reagent blank, and the fluorescence intensities of thioTEPA were linear from 76 to 4725 ng ml^{-1} in plasma. As shown in Table 1, the recovery of thioTEPA was 70—80%, with a standard deviation of 2.8—10.4%.

Determination of thioTEPA in rabbit plasma

The proposed method was applied to the determination of thioTEPA in rabbit plasma after a thioTEPA preparation (5 mg/ampoule) had been administered to three female rabbits (No. 1, 1.35 kg; No. 2, 1.6 kg; No. 3, 4 kg) by intravenous injection (5 mg kg^{-1}). Blood specimens were taken by venipuncture into heparinized tubes just before and up to 5 h after drug administration. Because of the lesser volumes of blood obtainable from rabbits No. 1 and No. 2, 0.5 ml of plasma was used for the rabbits. The results obtained are shown in Fig. 3. These profiles are similar to those reported for mice [3, 12], although there is some possibility that TEPA is eluted from the Extrelut 3 column.

Comparison of methods for determination of thioTEPA in blood specimens

The lower limit of determination of thioTEPA in plasma obtained by spectrophotometry with 4-(*p*-nitrobenzyl)pyridine was usually ca. 1 μg ml^{-1} [6, 7]. Although 80 ng ml^{-1} thioTEPA in plasma can be determined by the method of Tan and Cole [5], extraction of the colored material into small volumes of ethyl acetate is required and the color stability is poor. A fluorimetric method based on 2-naphthol [8] is capable of determining 50 ng ml^{-1} thioTEPA in plasma but the method requires 3 ml of plasma and the procedure is time-consuming. The lower limit of determination of plasma thioTEPA obtained by the present method is 76 ng ml^{-1}. However, if all of the residue resulting from the chloroform effluent was used for the fluorescence reaction after redissolving it in 100 μl of 1-propanol, the value may be

TABLE 1

Recovery of thioTEPA added to human plasma

ThioTEPA added (ng ml^{-1})	75.6	189	945	945	4725
Recovery[a] (%)	70.1 ± 10.4	74.6 ± 4.4	80.2 ± 6.0	82.5 ± 2.8[b]	77.5 ± 3.6

[a]Mean and standard deviation (n = 5) for batch assays, unless otherwise stated. [b]Day-to-day variation.

reduced to 15 ng ml^{-1}. In addition, the clean-up method with Extrelut 3 has some excellent features with regard to simplicity and reproducibility compared to many conventional extraction procedures. Therefore, the present method seems to be useful for monitoring thioTEPA in plasma.

Gas chromatography with a nitrogen/phosphorus detector is highly sensitive. ThioTEPA and TEPA can be determined simultaneously with a lower limit of determination of 1—5 ng ml^{-1} [2] or 10—100 ng ml^{-1} [3]. However, high-performance liquid chromatography is preferable to gas chromatography because of the thermal instability of the drug and its metabolite. The fluorogenic reaction described here also seems to be suitable as a detection system in the liquid chromatographic determination of thioTEPA as well as TEPA because of its high sensitivity and simplicity.

The authors are grateful to Sumitomo Pharmaceuticals Co. for supplying the standard thioTEPA, and thank Miss Y. Aoki and Miss Y. Ishiwata for their technical assistance.

REFERENCES

1 S. Eksborg and H. Ehrsson, J. Chromatogr., 340 (1985) 31.
2 B. J. McDermott, J. A. Double, M. C. Bibby, D. E. V. Wilman, P. M. Loadman and R. L. Turner, J. Chromatogr., 338 (1985) 335.
3 M. J. Egorin, B. E. Cohen, E. A. Kohlhepp and P. L. Gutierrez, J. Chromatogr., 343 (1985) 196.
4 B. Hagen, F. Walseth, R. A. Walstad and T. Iversen, J. Chromatogr., 345 (1985) 173.
5 Y. L. Tan and D. R. Cole, Clin. Chem., 11 (1965) 58.
6 C. G. Butler, D. S. Kaushik, J. Maxwell and J. G. P. Stell, J. Mond. Pharm., 10 (1967) 359.
7 G. Lunglmayr and K. Czech, J. Urol., 106 (1971) 72.
8 L. B. Mellett and L. A. Woods, Cancer Res., 20 (1960) 524.
9 H. Nakamura and Z. Tamura, Anal. Chem., 53 (1981) 2190.
10 K. Mopper and D. Delmas, Anal. Chem., 56 (1984) 2557.
11 A. Sano and S. Takitani, Anal. Chem., 57 (1985) 1687.
12 M. J. Egorin, S. R. Akman and P. L. Gutierrez, Cancer Treat. Rep., 68 (1984) 1265.

Analytica Chimica Acta, 201 (1987) 83—94
Elsevier Science Publishers B.V., Amsterdam — Printed in The Netherlands

REAGENT-INJECTION FLOW ANALYSIS: APPLICATION TO THE DETERMINATION OF NANOMOLAR LEVELS OF HYDROGEN PEROXIDE IN SEAWATER

KENNETH S. JOHNSON*, CAROLE M. SAKAMOTO-ARNOLD, STEWART W. WILLASON and CARL L. BEEHLER

Marine Science Institute, University of California, Santa Barbara, CA 93106 (U.S.A.)

(Received 11th March 1987)

SUMMARY

A reagent-injection flow technique, which allows automatic control of the volume of reagent to be injected, is described. The sensitivity of the measurements can be adjusted over a wide range by changing the injection volume. This technique also eliminates problems in photometric determinations arising from refractive index effects and from light scattering by suspended particles in the sample. Consequently, absorbances as small as 0.00004 can be measured. The capabilities of this reagent-injection flow technique were tested by using it to determine hydrogen peroxide in seawater at nanomolar levels with photometric detection. The concentration of hydrogen peroxide was determined as the colored condensation product of *N*-ethyl-*N*-(sulfopropyl)aniline and 4-aminoantipyrene; the detection limit was 12 nM.

Flow injection with spectrophotometric detection is well suited for the determination of chemical concentrations over a fairly broad concentration range and the robustness of such systems makes them well suited for field operations [1]. However, it can be difficult to determine concentrations at nanomolar levels with these systems [2]. In particular, refractive index gradients in the sample slug, detector baseline noise, and light scattering caused by particles in the sample make it difficult to measure absorbance changes smaller than 0.001 related to the chromophore [3, 4]. This restricts detection limits to approximately 100 nM for chromophoric species with molar absorptivities near 10 000 l mol^{-1} cm^{-1}. A significant change in the detector geometry [2] or a significant rearrangement of the reaction manifold [5] is necessary to enable very low concentrations to be determined spectrophotometrically.

In this paper, a flow-injection technique is described that allows nanomolar concentrations to be quantified with photometric detection. The new injection technique permits the user to control the dispersion of the chromophore and, thus, the sensitivity of the determination. The configuration of the reaction manifold reduces problems caused by variations in refractive index or the particulate content of the samples.

0003-2670/87/$03.50

This technique was tested by using it for the determination of hydrogen peroxide in seawater. The chemistry of hydrogen peroxide in natural waters is of considerable interest. It is produced in oceanic and fresh waters by photochemical reactions, which may involve dissolved organic compounds [6—9], and in the atmosphere by gas-phase photochemical reactions which contribute to the peroxide content of rainwater [10—13]. The concentration of hydrogen peroxide ranges from less than 5 nM in deep seawater and groundwater to 300 nM in surface seawater and to 112 000 nM in rainwater [6—13]. Obviously, the samples must be analyzed immediately after collection. A sensitive technique capable of rapidly analyzing many samples in the field with hydrogen peroxide concentrations ranging from nanomolar to micromolar is therefore needed. Previous methods have involved fluorimetric measurements based on the decay of scopoletin fluorescence to achieve sufficient sensitivity [6—9].

In this paper, a modification of the photometric flow-injection method of Madsen and Kromis [14] is described. The method, which has a detection limit of 12 nM hydrogen peroxide in seawater, is based on formation of a colored condensation product of *N*-ethyl-*N*-(sulfopropyl)aniline (ALPS) and 4-aminoantipyrene (AAP) [15]. This reaction has previously been used in a flow-injection system for analyses of rainwater [14]. Representative analyses of seawater which demonstrate the versatility of the new flow-injection configuration are reported here.

EXPERIMENTAL

Apparatus

The reaction manifold (Fig. 1) was configured as a reagent-injection flow system [16]. The reagent rather than the sample is injected in this configuration. Reagent R1 was injected at valve V1 (Fig. 1), which was a solenoid-operated, 3-port stream-switching valve (Neptune Research, 225T031). Valve V2 was a manually-operated, 3-port stream-switching valve (Rheodyne, 5301) used to select between the sample stream or a standard solution. A Gilson Minipuls peristaltic pump was used to propel the sample and reagents. The manifold was contructed from 0.8-mm i.d. PTFE tubing, except for the pump tubes, which were poly(vinyl chloride). Connections were made by flaring the PTFE tubing and using threaded plastic tees and unions.

A light-emitting diode (LED) photometer [14] was used to measure changes in light transmission. Special care was taken to optimize the signal-to-noise ratio because the expected absorbances were low. The signal was maximized by using a Hewlett-Packard ultra-bright LED (HLMP 3950) with a maximum emission at 569 nm (28-nm bandwidth) as the light source and a Hamamatsu PIN photodiode (G1738) as the light detector. A large-diameter flow cell (2.2-mm i.d., 1-cm path length, 40-μl capacity) increased the signal by exposing more active area of the photodiode. Noise was minimized by careful layout of the detector circuit board [17]. A high-impedance, operational amplifier (Precision Monolithics, OP-15) was used in the first stage of

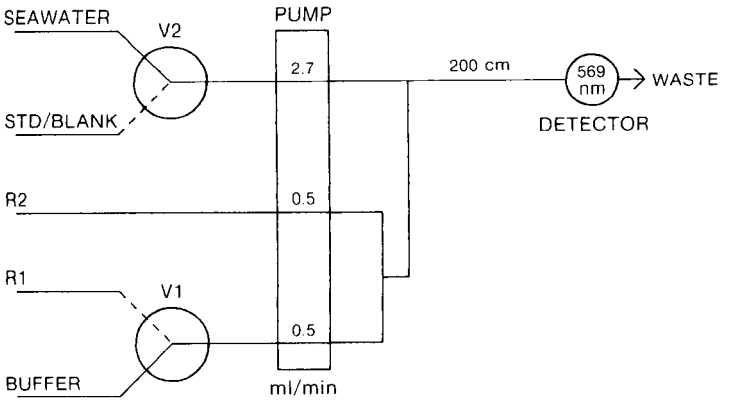

Fig. 1. Manifold for the determination of hydrogen peroxide. R1 is the ALPS reagent and R2 is the 4-AAP/peroxidase reagent.

the circuit to provide a gain of 10^7 with minimal current leakage. A 0.16-Hz low-pass filter was used to reduce high-frequency noise. Because the light output of the LED had a large temperature coefficient, the flow cell was placed in an insulated box to reduce the frequency of the temperature fluctuations to which it was exposed in the shipboard tests. Detector noise and drift caused by static electricity from the peristaltic pump were reduced by grounding the liquid-waste stream flowing from the detector. A Hewlett-Packard 87XM microcomputer and a Quasitronics analog-to-digital and digital output interface (12-bit resolution, −5 to +5 V) were used to monitor the detector output voltage and to control the 3-way valve, V1.

A submersible pumping system with a maximum depth capability of 105 m was used to sample the water column in the field work. The sample inlet of the flow-injection system was connected directly to the outlet of the pumping system. The residence time of water in the pumping system was 2 min. A Neil Brown Mark III CTD probe was used to determine conductivity, temperature and depth at the pump inlet.

Reagents and standards

It was found that a single combined reagent such as that used by Madsen and Kromis [14] acted as a sink for hydrogen peroxide. This rapidly increased the blank in work with nanomolar concentrations. Therefore two separate reagents which gave final concentrations similar to those used earlier [14] were used in this study. The reagent solutions were prepared in water deionized in a Millipore Milli-Q system.

ALPS. Dissolve 0.265 g of *N*-ethyl-*N*-(sulfopropyl)aniline sodium salt in 250 ml of buffer. Keep out of direct sunlight. The ALPS was synthesized as described by Tamaoku et al. [15]. It proved difficult to recrystallize the ALPS from ethanol and acetone mixtures so the final recrystallization was done from water and acetone mixtures.

4-AAP. Dilute 0.203 g of 4-aminoantipyrene (Aldrich) and 25 ml of peroxidase stock solution to 250 ml with buffer and store out of direct sunlight.

Buffer pH 5.3. Dissolve 10.21 g of potassium hydrogenphthalate and 1.2 g of sodium hydroxide in 1 l of water and store out of direct sunlight.

Peroxidase stock. Dissolve 0.040 g of Sigma Type I peroxidase (80 activity units mg^{-1}) in 100 ml of buffer and store in a refrigerator.

Standards. A 1 mM hydrogen peroxide standard was prepared by diluting a 3% (v/v) solution (Mallinckrodt) with water. This solution was standardized by reducing the hydrogen peroxide with iodide in the presence of molybate [18] and determining the triiodide ion produced spectrophotometrically. Standard triiodide solutions prepared from acidified potassium iodate and potassium iodide were used to calibrate the spectrophotometer. Working standards were prepared by spiking the calibrated 1 mM hydrogen peroxide solution into seawater collected with a 30-l Niskin bottle at depths greater than 200 m. Seawater from depths below 200 m has less than 5 nM hydrogen peroxide [8, 9] and the levels remain low if it is stored in the dark. Hydrogen peroxide standards in deep seawater should be used within 10 min of preparation and standards with concentrations less than 500 nM should not be prepared. This problem is discussed further below.

RESULTS AND DISCUSSION

Variable volume injection

The very low concentrations of hydrogen peroxide (<200 nM) found in much of the ocean require the maximum sensitivity available from a photometric detection, i.e., minimal dispersion of the chromophore in the flow-injection system [19]. The injection procedure used here allowed the dispersion coefficient [19] to be varied from nearly 1 (no dilution) to values of 10 or more (high dilution) by controlling the injection volume. The appropriate volume could be selected automatically during the determination to give the required sensitivity. Minimal dispersion did not affect the color formation because the sample and reagents were mixed at confluence points downstream of the injection valve.

The injection volume was adjusted by using a stream selection valve, V1, as the injector (Fig. 1). The ALPS reagent solution (R1) and a buffer solution were connected to the two inlet ports of V1. An alternating stream of ALPS solution and buffer could be drawn into the manifold by switching between the two inlet ports. Operation of the valve during a determination proceeded as follows. The injection valve, V1, in Fig. 1 was normally in the position shown by the solid line, providing the baseline read-out from the sample and buffer. The valve was then switched to the dashed line position, which allowed the ALPS reagent to be injected into the manifold. As the zone containing the ALPS flowed into the detector, a response was obtained which was proportional to the amount of hydrogen peroxide in the sample. The

volume of ALPS reagent that was injected could be controlled by regulating the amount of time that the valve was drawing the reagent. Only a small injection was needed if hydrogen peroxide concentrations were high. Analyses could be completed rapidly, in this case, because <1 min was required for injection and for the injected solution to pass through the detector. Dispersion was high and sensitivity low because the small injected volume was diluted by the carrier solution at each end of the injected plug.

If concentrations were low, then larger volumes of reagent were injected into the manifold by allowing valve V1 to draw reagent for a longer time. The core of the reagent slug, and the chromophore formed by reaction between the sample and reagents, were undiluted by the buffer carrier stream when the volume was large enough and the dispersion was nearly unity. This gave maximum sensitivity but sampling rates were reduced because of the increased time required for injection and for the colored solution to pass through the detector (>4 min).

The injection procedure described above allows a large range of reagent volumes to be injected by changing the time period during which valve, V1, draws reagent. Corresponding changes in the sensitivity are also obtained. A separate standard curve would have to be prepared for each different injection volume unless the hydrodynamic characteristics of the system were very well known, however. This requirement meant that, in practice, only two discrete injection volumes were used, one each for high and low sensitivity.

Figure 2 shows hydrogen peroxide standards in seawater pumped through the same flow-injection manifold operated in the high- and low-sensitivity modes. A 4-min valve cycle was used in the high-sensitivity mode with the valve in each position for 2 min. This corresponded to an injection volume of 840 μl. The plateau on each peak indicates that the dispersion was near unity. Although a shorter valve cycle could have been used to obtain this dispersion, the statistical confidence limits on the peak height were improved by increasing the number of detector readings on the plateau. The signal from the ambient hydrogen peroxide concentration of 40 nM in the unspiked sample is clearly visible. A sample volume of 16 ml is required for a full analysis cycle (baseline, sample, baseline) in this mode.

A 1-min valve cycle was used in the low-sensitivity mode with a 3.00-s injection period, corresponding to a 21-μl injection volume. The peak heights for the standards run in the low-sensitivity mode were reduced by a factor of 4.0. The small injection volume increased dispersion of the chromophore, reducing the peak heights. The detection limit deteriorated to 105 nM (3× the standard deviation of the 200-nM peaks) and the signal from hydrogen peroxide in the ambient seawater was no longer visible. The low-sensitivity mode was suitable for samples with concentrations greater than 500 nM. Samples could be processed rapidly (one per minute) with precision of 5% at 1000 nM. The precision of the analyses in the low-sensitivity mode is much worse than that normally obtained with flow-injection systems. The increased variability is probably due to differences in the volumes of reagent

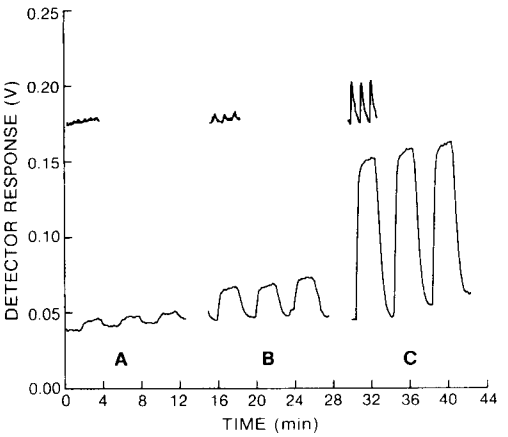

Fig. 2. Detector responses for the determination of hydrogen peroxide in seawater: (A) surface seawater; (B) surface seawater spiked 30 min before analyses began with 200 nM hydrogen peroxide, which was reduced to an actual concentration of 120 nM at the time of analysis; (C) surface seawater spiked with 1000 nM hydrogen peroxide. Upper traces are the recordings for three injections of reagent with the manifold operated in the low-sensitivity mode (ALPS reagent for 0.05 min, buffer for 0.95 min). Lower traces are the recordings for three injections of reagent with the manifold operated in the high-sensitivity mode (ALPS reagent for 2 min, buffer for 2 min).

that are injected in each analysis. Pulsations in the flow rate produced by the peristaltic pump during the 3-s injection period will change the reagent volume that enters the carrier stream. One should not, therefore, expect as high a precision with the injection technique used here as compared to conventional flow-injection systems. However, if the volume can be fixed, then a rotary injection valve can be used to control precisely the injection volume and improve the precision.

Interferences

A large interference effect is produced if there is a difference in refractive index between the carrier stream and the injected solution. Light passing along the axis of the flow cell will be deflected away from the detector in a refractive index gradient, resulting in a signal change even if the chromophore is absent [3]. Therefore, it is necessary to match the refractive indices of the carrier and injected solution closely if small absorbances are to be measured. It is usually possible in flow-injection systems to match the refractive index of the carrier stream to that of the injected sample to minimize this effect. However, the carrier stream must be changed whenever samples of widely different refractive indices are injected in conventional flow-injection systems. This problem was circumvented in the system described here by injecting the reagent into an inert carrier stream with the same refractive index as the injected reagent solution, and then merging the carrier with the

sample stream. Because the composition of the injected reagent and carrier solutions did not change during a series of analyses, no variations in refractive index occurred in the reaction manifold. The same batch of buffer solution was always used to prepare the reagent and the carrier solutions to ensure that the refractive indices of the carrier and reagent were equal. The only difference between the two solutions was the addition of 4 mM ALPS to the reagent, which had a negligible effect on the refractive index. A refractive index signal was generated within the mixing zone between samples of different salinities. However, this zone was of no analytical interest. No further variations in refractive index occurred once the pure sample was flowing through the system. The resulting detection limit corresponded to an absorbance change of 0.00004.

There was no significant difference (*t*-test, 95% confidence limit) in the slopes of standard curves measured in deionized water and seawater, suggesting that the enzyme was not inhibited in the seawater matrix. Possible interferences by organic peroxides were tested by analyzing a 1000 nM solution of t-butyl hydroperoxide; no detectable signal was obtained.

Recovery experiments in spiked seawater samples and deionized water were done to test for interferences at low concentrations. Recovery was always less than 100% and the fraction of hydrogen peroxide that was lost was greatest at the lowest concentrations (Table 1). The low recovery is due to reaction of the hydrogen peroxide in the time period between sample preparation and measurement rather than a real interference. The hydrogen peroxide concentration in standards prepared with deionized water decreased with each subsequent measurement (Fig. 3). The decay rate was about 300 nM h^{-1}. Standards prepared in deep seawater decayed at rates from 10 to 100 nM h^{-1}. Complete recovery of hydrogen peroxide spikes in seawater or deionized water were obtained when the concentrations of hydrogen peroxide found were extrapolated back to the time of sample preparation (Fig. 3). The ambient hydrogen peroxide concentrations in surface seawater samples decreased at a rate of about 10 nM h^{-1} when the water was placed in the dark. Lazrus et al. [12] found that hydrogen peroxide decayed in rainwater samples at a mean rate of 500 nM h^{-1}. Kieber and Helz [20], however, found that hydrogen peroxide decayed more rapidly in saline samples than in fresh water samples. The differences in the decay rates of hydrogen peroxide in these various samples are probably due to the presence of a redox buffering system that is controlled by the history of light exposure and the chemical composition of the sample.

The rate of loss of hydrogen peroxide in standards was nearly independent of the hydrogen peroxide concentration (Fig. 3). The fractional rate of change in hydrogen peroxide concentrations was therefore very high at low concentrations, and it was necessary to avoid using standards with concentrations less than 500 nM. The complete recovery of spikes, after correction for decomposition of hydrogen peroxide, indicates that the calibration line is linear down to the limits of detection, so that there should be no problem

TABLE 1

Summary of hydrogen peroxide recovery experiments from deionized water and natural seawater collected off the central California coast. Analyses were begun immediately following the spike addition

Sample	Collection date[a]	Depth (m)	Spike (nm)	Amount found[b] (nm)	*N*	Recovery (%)
Seawater	7/28	1	0	5 (4)	4	—
			40	36 (8)	2	78
			80	76 (5)	4	89
Seawater	7/29	1	0	20 (8)	3	—
			40	46 (2)	3	77
Seawater	7/29	100	0	13 (7)	4	—
			40	43 (9)	4	81
			80	82 (0)	2	88
Deionized water[c]	—	—	0	0 (5)	4	—
			210	131 (13)	6	62
			850	756 (46)	5	89
			1060	981 (34)	5	93

[a]All in 1986. [b]One standard deviation is shown in parentheses unless $n = 2$ and then the range is shown. [c]Deionized water analyses are based on the data in Fig. 3.

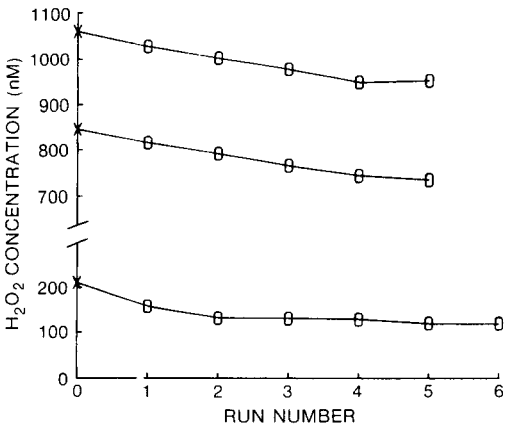

Fig. 3. Measured concentrations of hydrogen peroxide in standards prepared in deionized water as a function of sequential run number. Each analysis required 4 min. The *y* intercept of each line is the nominal concentration of hydrogen peroxide that was calculated from the amount added.

in using standards with high concentrations to calibrate the system. Injection of all standards began within 2 min of their preparation to avoid the necessity of making any corrections to the standard curves.

Field measurements

Hydrogen peroxide was determined in seawater with the manifold shown in Fig. 1 on a research cruise in the western Mediterranean Sea. The high-sensitivity mode had to be used for all these analyses because of the very low concentrations involved. Errors arising from decomposition of hydrogen peroxide were minimized by using a pumping system to collect the water and by interfacing the manifold directly to the pump effluent. It was verified that the pumping system did not affect the hydrogen peroxide concentration by comparing concentrations in the pump effluent (ca. 100 nM) with concentrations in bucket samples collected at the surface next to the pump intake. No significant difference was found in three trials between the means of 4 or 5 replicate determinations of hydrogen peroxide in samples collected by each method.

A profile of hydrogen peroxide measured in the Mediterranean Sea at Station 33 is shown in Fig. 4A. Concentration profiles were similar to that measured by using the scopoletin fluorescence-decay technique of Zika et al. [8] in oligotrophic waters of the Gulf of Mexico (Fig. 4A). The average precision (1 SD) found during the 3-week cruise was ±7 nM for 23 sets of 3—6 replicate measurements made while the sampling pump was held at a constant depth. This is a conservative estimate of the precision that can be obtained under field conditions because there were probably real differences in the hydrogen peroxide concentrations of the replicate samples caused by vertical motions of the ship, pump and water during each sampling interval. Replicate analyses of deep seawater blanks at sea had a precision (1 SD) of ±4 nM, which seems a more reasonable estimate. The detection limit obtained at sea was 12 nM (3 SD).

Light scattering

If samples containing particulate matter are injected into a particle-free carrier stream, then light will be scattered in the detector cell as the sample passes through; this scattering effect is not distinguishable from the required light absorbance. For example, hydrogen peroxide was determined at some stations by using a manifold configured as a flow-injection system, rather than the reagent-injection flow system. This was done simply by switching the positions of valves V1 and V2. Seawater samples were injected into the blank by drawing the sample and blank solutions for 2-min periods each. Valve V2 was set to draw the ALPS reagent (R1) continuously.

A concentration profile obtained with this flow-injection manifold at Station 32 is shown in Fig. 4B. These apparent hydrogen peroxide concentrations were similar to those measured by the reagent-injection method at nearby Station 33 (Fig. 4A), except for the large subsurface maximum at a depth around 70 m at Station 32. This subsurface peak coincided exactly with the deep chlorophyll maximum. Apparently, phytoplankton cells present in samples collected within this maximum had scattered more light than samples from the rest of the water column. The actual amount of light

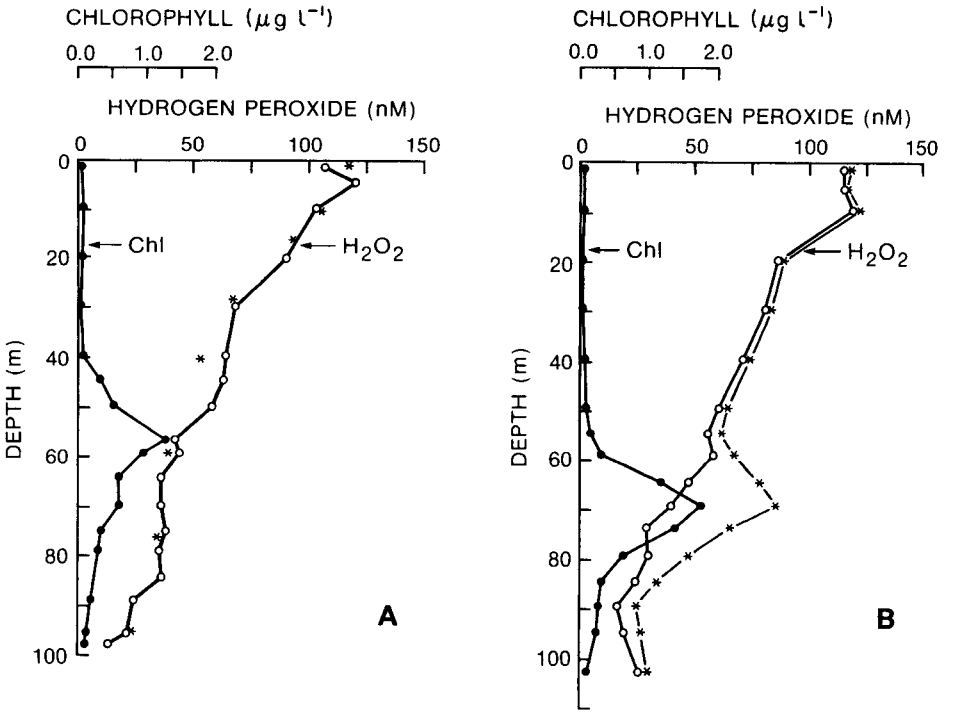

Fig. 4. (A) Concentration profile for hydrogen peroxide in the Mediterranean Sea at Station 33 (37° 32.1 N, 000° 58.8 E) obtained with the reagent-injection method: (○) H_2O_2 concentration in nM; (*) measurements from oligotrophic waters in the Gulf of Mexico (24° 32 N, 85° 46 W; ref. 4) are shown for comparison; (•) particulate chlorophyll concentration. (B) Concentration profile for hydrogen peroxide obtained with the sample-injection method at Station 32 (37°35.4 N, 003°00.8 E): (*) apparent concentration; (○) concentration after correction for light scattering; (•) particulate chlorophyll concentration.

scattering was measured by substituting buffer for the reagents in the flow-injection manifold, so that there was no color formation. When the samples collected at Station 32 were injected into this system, light scattering was at a maximum at 70-m depth and was equivalent to the apparent concentration increase in the deep maximum. The hydrogen peroxide profile at Station 32, corrected for light scattering, is also shown in Fig. 4.

Light scattering was not a problem when samples were analyzed in the reagent-injection manifold (Fig. 1). Particles present in the sample scattered the same amount of light regardless of whether the reagent or buffer was flowing. The net effect of particles was a small offset in the baseline, but no change in peak heights. No subsurface concentration maximum appeared in the hydrogen peroxide profile at Station 33 (or other stations where the reagent-injection manifold was used), although a deep chlorophyll maximum was still present.

Reagent blank

Hydrogen peroxide dissolved in the reagent solutions will cause a blank signal when R1 is injected into R2. Hydrogen peroxide contamination is common in deionized water [21] and a significant reagent blank must be expected. Analyses of deep-seawater samples always gave a signal equivalent to 10—20 nM hydrogen peroxide. This signal was shown to be due to hydrogen peroxide in the reagents by analyzing the deionized water used to prepare the reagents; a signal equivalent to 60 nM hydrogen peroxide was obtained after correction for the blank. If this amount of hydrogen peroxide were present in the reagents, then there should be a blank signal of 16 nM after the reagents were diluted by the sample stream, which accounts for the entire blank signal that was observed in deep seawater.

Conclusions

The reagent-injection technique could be extended to the determination of a variety of other trace species. The determination of the micronutrient elements, phosphate, nitrate and silicate, would be particularly well suited to this arrangement. Deep-water nutrient samples with high concentrations could be rapidly analyzed with the low-sensitivity manifold. Surface nutrient samples, which often have concentrations less than 100 nM, could be processed in the same manifold operated in the high-sensitivity mode. Automatic selection of the appropriate sensitivity could easily be incorporated into the control program of the microcomputer. Drawbacks to the method are that large sample volumes are required to achieve high sensitivity and the precision is decreased, relative to that obtained with conventional injection techniques.

This work was supported by Office of Naval Research Contract N00014-82-K-0740. We thank the officers and crew of the USNS Lynch for their assistance at sea. Ship time aboard the USNS Lynch was provided by D. Wiesenburg, who also provided the CTD data and the sampling system.

REFERENCES

1 K. S. Johnson, R. L. Petty and J. Thomsen, in A. Zirino (Ed.), Mapping Strategies in Chemical Oceanography, Advances in Chemistry Series 209, American Chemical Society, Washington, DC, 1985, p. 7.
2 R. A. Leach, J. Růžička and J. M. Harris, Anal. Chem., 55 (1983) 1669.
3 D. Betteridge, E. L. Dagless, B. Fields and N. F. Graves, Analyst, 103 (1978) 897.
4 W. Kaye, Anal. Chem., 53 (1981) 369.
5 C. M. Sakamoto-Arnold, K. S. Johnson and C. L. Beehler, Limnol. Oceanogr., 31 (1986) 894.
6 C. Van Balen and J. E. Marler, Nature, 211 (1966) 951.
7 W. J. Cooper and R. G. Zika, Science, 220 (1983) 711.
8 R. G. Zika, J. W. Moffett, R. G. Petasne, W. J. Cooper and E. S. Saltzman, Geochim. Cosmochim. Acta, 49 (1985) 1173.
9 R. G. Zika, E. S. Saltzman and W. J. Cooper, Mar. Chem., 17 (1985) 265.
10 G. L. Kok, Environ. Sci. Technol., 9 (1978) 1077.
11 R. G. Zika, E. S. Saltzman, W. L. Chameides and D. Davis, J. Geophys. Res., 87 (1982) 5015.

12 A. L. Lazrus, G. L. Kok, S. N. Gitlin, J. A. Lind and S. E. McLaren, Anal. Chem., 57 (1985) 917.
13 G. L. Kok, Atmos. Environ., 14 (1980) 653.
14 B. C. Madsen and M. S. Kromis, Anal. Chem., 56 (1984) 2849.
15 K. Tamaoku, Y. Murao and K. Akiura, Anal. Chim. Acta, 136 (1982) 121.
16 K. S. Johnson and R. L. Petty, Anal. Chem., 54 (1982) 1185.
17 A. P. Brokaw, An I. C. Amplifier Users' Guide to Decoupling, Grounding, and Making Things go Right for a Change, Analog Devices Data-Acquisition Databook, Vol. I, Analog Devices, Norwood, MA, 1982.
18 W. A. Patrick and H. B. Wagner, Anal. Chem., 21 (1949) 1279.
19 J. Růžička and E. H. Hansen, Flow Injection Analysis, Wiley-Interscience, New York, 1981.
20 R. J. Kieber and G. R. Helz, Anal. Chem., 58 (1986) 2312.
21 H. Hwang and P. K. Dasgupta, Anal. Chem., 58 (1986) 1521.

Analytica Chimica Acta, 201 (1987) 95—107
Elsevier Science Publishers B.V., Amsterdam — Printed in The Netherlands

ION-EXCHANGE RESINS CONTAINING S-BONDED DITHIZONE AND DEHYDRODITHIZONE AS FUNCTIONAL GROUPS

Part 3. Determination of Gold, Platinum and Palladium in Geological Samples by means of a Dehydrodithizone Resin and Plasma Emission Spectrometry

M. GROTE and A. KETTRUP*

University of Paderborn, Dept. Applied Chemistry, P.O. Box 1621, D-4790 Paderborn (Federal Republic of Germany)

(Received 16 March 1987)

SUMMARY

A procedure is described for the determination of gold, platinum and palladium in sulphide ores, concentrates and mattes. The method is based on chromatographic separation and selective elution of precious metals on small resin beds (0.7 × 2.5 cm) of the sorbent P-TD. After roasting, the samples were digested with aqua regia, and the residues fused with sodium peroxide. The acid leaching solutions obtained from both procedures were separately passed through an ion-exchange column. The metals were quantitatively retained after one loading step and eluted by a sequence of 2 M perchloric acid and 5% (w/v) thiourea solution. Preconcentrated Au, Pt and Pd were finally quantified with a d.c. plasma emission spectrometer. The effect of roasting temperature on the recovery of precious metals as well as the efficiency of the aqua regia leaching from the different materials were investigated in detail. Repeated analyses of standard reference samples proved the proposed method to be reliable.

Platinum metals and gold are present in most ores, flotation concentrates and furnace mattes at very low values. The detection limits of atomic absorption or emission spectrometry are not low enough for direct determination of precious metals in solutions of geological samples. Furthermore, the multi-element capability of plasma emission spectrometry is affected by interelement interferences because of the complexity of the sample matrix [1]. Specifically, the direct current (d.c.) plasma spectrometric determination of platinum group metals in presence of major matrix constituents such as Al, Mg, Cu, Fe, Ni and Cr shows significant enhancement of analyte values, which is not eliminated by addition of spectroscopic buffers [2, 3].

To minimize such problems, the analysis must incorporate pre-concentration and separation steps to free the precious metals from base metals. The conventional procedure for the concentration of precious metals is based on fire-assay techniques which require not only special equipment but a thoroughly experienced assayer [4—6]. The collector obtained (buttons of lead or nickel sulfide, etc.) usually results in a simplified matrix compared to the starting material, hence the matching of standards for emission

0003-2670/87/$03.50

spectrometry may become easier. However, the high salt content of solutions derived from fusion procedures can cause nebulizer blockage at the spray chamber of plasma emission spectrometers [1] and interference effects such as those described above.

The application of special hydrometallurgical treatments by means of selective ion-exchangers or liquid extractants can eliminate some of the problems outlined. The separation of platinum and palladium from base metals originating from acid leaching solutions of geological samples, can be achieved by eluting the chloro-complex anions through a cation-exchange resin [7]; the platinum metals were subsequently quantified by inductively-coupled plasma atomic emission spectrometry (ICP/AES). However, deep column beds and large elution volumes were necessary to obtain quantitative recoveries of the elements, just as with the anion-exchanger Dowex 1-X8, which was used for the separation of gold [8].

The application of selective ion-exchange resins, such as polymeric thioethers [9], or the commercially available isothiouronium resin Srafion NMRR, leads to a more straightforward and effective separation procedure. In combination with neutron activation analysis (NAA), the latter sorbent was used successfully for the analysis of standard rocks [10—12]. An elution chromatographic separation of precious metals on Srafion NMRR was reported by Kritsotakis and Tobschall [13]. The elements were determined in the thiourea eluates by electrothermal atomic absorption spectrometry.

In the investigation reported here, a chromatographic procedure was developed for the isolation and subsequent d.c. plasma emission spectrometric determination of aqua regia-soluble Au, Pt and Pd in geological materials. The key aspect of this method is the use of the ion-exchange resin P-TD, which contains sulphur-bonded dehydrodithizone as functional groups [14, 15]. The resin was found to be selective for platinum group metals and gold and it can be regenerated by special sequences of eluents. The utility of the P-TD resin in the analysis of real samples will be demonstrated in this study.

EXPERIMENTAL

Instrumentation

A d.c. argon-plasma emission spectrometer (Spectraspan IIIB, Beckman/ARL) was used as described earlier [15]. The precious metals were determined simultaneously by use of three channels of the multi-element cassette I. The wavelengths selected are listed in Table 1. By means of cassette II, Fe, Cu, Ni and Cr could also be quantified. For these determinations, the solutions contained 2 M $HClO_4$ or 5% (w/v) thiourea in 0.1 M HCl; these solutions were used also as blanks (low standard). For preparation of high standards ranging from 2 to 10 $\mu g\ ml^{-1}$, aliquots of single-element stock solutions (1000 $\mu g\ ml^{-1}$) were made up to volume with the dilute perchloric acid or thiourea solution. The linearity of each channel was confirmed with

TABLE 1

Detection limits c_L of the d.c. plasma multi-element equipment for different matrices

Element	λ(nm)	Order No.	c_L(ng ml^{-1})[a]	
			2 M $HClO_4$	5% thiourea/ 0.1 M HCl
Au	242.795	93	30	45
Pt	265.945	85	50	60
Pd	340.458	66	3	4
Fe	259.940	86	12	25
Cu	324.754	69	2	3
Ni	305.082	74	25	22
Cr	284.984	79	25	35

[a]The c_L were taken as three times the standard deviation of the blank.

serial dilutions of the high standards in the appropriate medium. Limits of detection (Table 1) were calculated on the basis of three times the standard deviation of the background noise using a series of ten 10-s measurements of the blank solutions in the multi-element mode.

The P-TD ion-exchange resin

The preparation of the resin has been already described [15]. Chloromethylated polystyrene (1.3 mmol g^{-1} chlorine, 200—400 mesh, Bio-Rad) was used as starting material. The practical specific capacity of P-TD is 1.0 mmol Au per gram of dry resin.

For the ion-exchange procedure, a 700-mg portion of resin equilibrated with 0.1 M HCl was slurried in the acid and packed in a 0.7 × 10-cm glass column containing a glass frit at the bottom and a socket at the top. A bed height of about 2.5 cm was obtained. The outlet of the column was connected to a peristaltic pump (Ismatec ip4) via capillary tubing (tygon) so that suitable flow rates from 0.2 to 2 ml min^{-1} could be obtained. Solutions were introduced to the ion-exchanger by means of a capillary teflon tube, which was connected to a detachable ground-glass joint and prevented air from being forced into the column. The teflon tube was placed above the resin bed in such a way that a liquid level of about 0.5 cm atop the bed was maintained throughout the ion-exchange procedures.

Reagents

All reagents used were of analytical grade. Synthetic mixtures of solutions of Au, Pt and Pd were prepared from the sodium salts of the individual chloro complexes. Commercially available standards (SPEX Industries) were used for calibration of the d.c. plasma spectrometer. The samples analysed include the certified reference material SARM-7 (MINTEK) and the Canadian standards SU-1a, PTC1-1 and PTM-1.

TABLE 2

Recoveries of precious metals from geological samples by acid leaching and peroxide fusion of residues

Sample	Certified values ($\mu g\ g^{-1}$)			Recovery (%)[a]			
	Au	Pt	Pd		Au	Pt	Pd
SARM-7[b]	0.31	3.74	1.53	Acid leach	87.3	84.1	74.5
				Fusion	15.9	11.3	24.9
				Total	103.2	95.4	99.4
PTC-1[c]	0.65	3.0	12.7	Acid leach	69.8	73.5	84.2
				Fusion	13.3	7.8	7.9
				Total	83.1	81.3	92.1
PTM-1[d]	1.8	5.8	8.1	Acid leach[e]	88.9	87.8	96.2
SU-1a[f]	0.15[g]	0.41	0.37	Acid leach[e]	33.3	78.1	64.9

[a]Recoveries are mean values of four or eight (PTM-1) separate analyses, calculated by taking the certified value as 100%. [b]Pt ore, roasting temperature 700°C. [c]Flotation concentrate, roasting temperature 600°C. [d]Matte, roasting temperature 800°C. [e]No additional amounts of precious metals found in the residues by fusion. [f]Ni/Cu/Co ore, roasting temperature 700°C. [g]Uncertified value.

Procedures

Roasting and acid leaching. Weigh 2.5 g of the sample into a flat roasting dish (ALSINT, 3.5 × 4.5 cm), place it in a preheated muffle furnace for 30 min at 300°C, raise the temperature to the appropriate value (see Table 2) and roast for 60 min. Cool to room temperature and transfer the roasted sample to a 400-ml beaker. Add 12 ml of 6 M HCl and place on a sand-bath under cover at 90°C for 1 h. Then carefully add 3 ml of concentrated nitric acid (65%) and cover the sample with a watchglass until the reaction subsides. Remove the watchglass and evaporate the solution until a small volume of solution remains. Add 0.1 g of sodium chloride and continue the evaporation to incipient dryness. Treat the residue with 5 ml of concentrated hydrochloric acid (25%) twice. Evaporate to dryness after each addition. Add 5 ml of concentrated hydrochloric acid, and 0.5 ml of potassium chlorate solution (2% w/w) and evaporate again to incipient dryness. Suspend the residue in 1 ml of concentrated hydrochloric acid and 15 ml of boiling water and heat on the sand-bath for 30 min.

Filter the solution under vacuum through a Sartorius glass filter holder containing a Blue Ribbon filter paper (4.7-cm diameter; Schleicher & Schüll 589/3), passing the filtrate directly into a 100-ml beaker. Transfer all the residue to the filter and wash it with at least 15 ml of boiling water. Combine the filtrate and wash solution. The final volume should be 40—50 ml. The acidity of the combined solution corresponds to 0.2 M HCl.

Ion-exchange separation. Adjust the liquid level of the 0.1 M HCl to just above the resin bed of P-TD. From micropipette, layer 1 ml of the sample

atop the resin without significant disturbance to the polymeric particles. Connect the top of the column to the feed solution with teflon tubing and start the peristaltic pump. Pass the liquid sample through the ion-exchanger at 1 ml min^{-1} continuously. Transfer the sample completely to the column by washing the walls of the beaker with 0.1 M HCl. Then wash the column with 10—15 ml of 0.1 M HCl. As the liquid level approaches the resin bed, add carefully 5.5 ml of 2 M $HClO_4$ into the column from a disposable pipette. Disconnect the tube from the outlet of the column and pump it empty. Collect the first 0.5-ml fraction which comes dropwise from the column in a precalibrated vessel and disregard it. Then couple the pump immediately to the column by the tubing and collect the eluate at a flow rate of 0.5 ml min^{-1} in a 5-ml calibrated flask. Collect a second 5-ml fraction to ensure quantitative recovery of platinum. Then wash the column with 10 ml of 0.1 M HCl (1 ml min^{-1}) and elute gold and palladium with a solution of 5% (w/v) thiourea in 0.1 M HCl. Apply the same technique as described above.

Determination of Au, Pt, and Pd. Determine the concentrations of the precious metals simultaneously in the diverse 5-ml eluates by emission spectrometer as outlined above. The sample volume of 5 ml suffices for running six determinations of each element. Use an integration time of 10 s.

Analysis of the residues. The residue obtained from the acid leaching, and dried at 130°C together with the filter paper, is placed in a nickel crucible and ignited. Then add a five-fold excess of sodium peroxide, mix and fuse in a muffle furnace at 680°C until a clear melt is obtained. Allow the crucible to cool for 15 min and transfer to a 400-ml beaker containing about 40 ml of water. Add concentrated hydrochloric acid until a clear green solution is obtained. Remove the crucible, rinse it with 1 M HCl and transfer all washings to the beaker.

Evaporate the total solution to incipient dryness, add 5 ml of concentrated hydrochloric acid and repeat the evaporation. Add a further 5 ml of the acid; evaporate again. Finally, add 5 ml of the hydrochloric acid and sodium chlorate solution, and treat the mixture as described above. Apply ion-exchange separation and emission spectroscopy as specified above.

Choice of contact materials

The vessels used for evaporation and storage of solutions obtained from the geological samples were made of teflon or Sigradur glassy carbon (Sigri Elektrographit, Meitingen). For comparison, use of the latter material resulted in a much faster procedure. No differences in results, caused by losses of Au, Pt or Pd either by reduction or adsorption onto the different surfaces, could be observed. However, very careful pretreatment of all vessels and glass columns with hot aqua regia or concentrated acids was necessary in all cases to avoid contamination of the sample solutions [10, 13, 16].

RESULTS AND DISCUSSION

Development of the ion-exchange procedure

The results of the earlier experiments with synthetic mixtures of precious metals, base metals and alkali chlorides [14] were utilized and conditions were adapted to the present analytical procedure. For this purpose, model solutions containing a total amount of precious metals such as would be obtained from acidic leach liquors of the geological samples were prepared. Thus, 5 μg of Au, 20 μg of Pt and 50 μg of Pd present as their common chloroanions ($AuCl_4^-$, $PtCl_6^{2-}$, $PdCl_4^{2-}$) were added to 50 ml of 1 M HCl and passed once only through a P-TD ion exchange column at a flow rate of 2 ml min^{-1}. Analysis of the effluent showed that the retention of palladium was incomplete (ca. 80%), whereas Au and Pt were retained completely. Lowering the flow rate (1 ml min^{-1}) and decreasing the hydrochloric acid molarity (0.2 M) resulted in a quantitative sorption of the precious metals by the ion exchanger.

As described previously, elution of Pd, Pt and Au can be achieved by an acidified solution of thiourea (5% w/v in 0.1 M HCl) [14]. This solution releases Au and Pd immediately from the resin in a sharp elution band; 5 ml of the thiourea solution is sufficient to recover >95% of each metal. However, the elution of platinum shows marked tailing, because of the slower rates of ligand exchange during the formation of cationic Pt(II, IV)/thiourea complexes. As expected, the tailing observed depends strongly on the flow of the eluting agent. Figure 1 demonstrates that the recovery of platinum in the first 5-ml fraction increases from 45% at 1 ml min^{-1} to

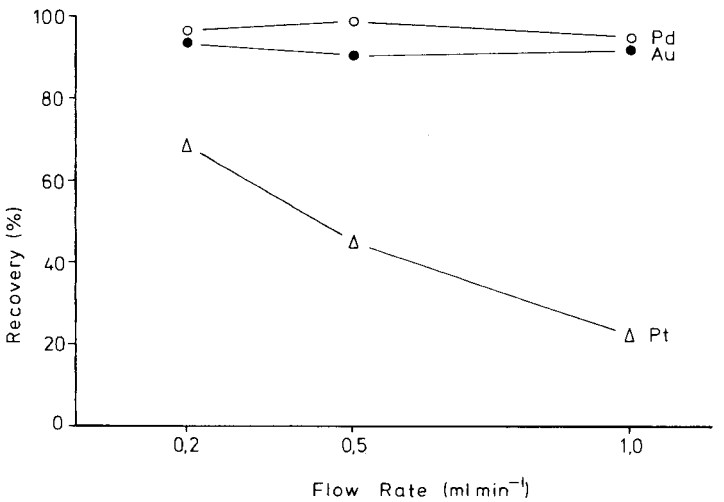

Fig. 1. Recovery of precious metals from P-TD resin as function of flow rate of the eluent (5 ml of 5% thiourea in 0.1 M HCl). Loading conditions: 50 ml of 0.2 M HCl containing 5 μg Au, 20 μg Pt, 50 μg Pd.

68% at 0.2 ml min^{-1}. Considerable amounts of platinum were still detectable in the eluate after passage of 20 ml of thiourea solution through the column. Such an elution procedure with thiourea will suffice for the simultaneous separation and enrichment of palladium and gold from acidic extracts of geological samples. However, the limits of determination would deteriorate markedly owing to poor preconcentration factors if the analysis includes platinum, which is eluted only inefficiently by thiourea.

The application of a sequence of 2 M perchloric acid and thiourea solution improves the preconcentration of platinum. With this procedure, perchloric acid first desorbs platinum (ca. 90%) and some palladium (1—10%). After a wash with 0.1 M HCl, the column is treated with thiourea to elute gold and the bulk of palladium. The individual fractions are collected separately in two 5-ml volumetric flasks and analyzed by emission spectrometry (see Experimental).

A comparison of the results obtained by the different elution techniques (thiourea with and without perchloric acid) showed a slight decrease (2—3%) of Au and Pd recoveries for the sequential perchloric acid/thiourea procedure. It is assumed that the conversion of the metal-loaded P-TD resin from the chloride to perchlorate form causes dehydration and thus shrinkage of the polymer network similar to other anion-exchange resins [17] so that the subsequent action of thiourea is affected. Nevertheless, the average recoveries for Au (94.7%, with standard deviation s = 3.2%), Pd (96.8%, s = 1.7%) and Pt (95.8%, s = 3.3%) obtained from eight individual loadings of synthetic mixtures were always >90%, which was considered adequate for preconcentration in the analysis of geological samples.

Analysis of geological samples

The certified reference materials investigated were the platinum ore SARM-7, the Ni/Cu/Co ore SU-1a, the Ni/Cu matte PTM-1 and the flotation concentrate PTC-1. The individual recommended values for Au, Pt and Pd cover the range from 0.3 to 12.7 $\mu g\ g^{-1}$ (see Table 2).

The digestion of the samples is based on a method proposed by several investigators [18—22], who suggested that the aqua regia-soluble Pd, Pt and Au represented the total amount of these metals in rocks. Thus, the samples were roasted to remove sulphur and any organic matter, and then simply attacked with concentrated hydrochloric acid and aqua regia. The solubles converted to chlorides were extracted with dilute acid (0.2 M HCl), the residues were filtered off and the filtrate was passed through a PT-D ion-exchange column. The precious metals extracted were eluted from the resin, and so preconcentrated, by the sequential procedure described above. Finally, the metals were determined in the fractions by the d.c. plasma method. The unattacked precious metals in the acid leach residues were also determined in order to ascertain the efficiency of the leaching procedure. Complete decomposition of the residues was obtained by peroxide fusion [11, 12, 23, 24], hydrochloric acid leaching of the melt and the preconcentration steps outlined before.

TABLE 3

Analytical data for certified reference materials
(Values are given in $\mu g\ g^{-1}$, except for s_r.)

Metal	Certified value[a]	This work[b]				Literature values					
		Mean	s	s_r(ac)	s_r(fu)	Mean	s	Mean	s	Mean	s
SARM-7		(n = 4)									
Au	0.31 ± 0.015	0.32	0.10	0.13	1.73	0.299[c]	0.073	0.322[d]	0.041		
Pt	3.74 ± 0.045	3.57	0.17	0.11	0.86	3.763	0.03	—	—		
Pd	1.53 ± 0.032	1.52	0.06	0.07	0.09	1.455	0.14	1.542	0.026	1.59[b]	0.05
PTC-1		(n = 4)									
Au	0.65 ± 0.1	0.54	0.19	0.39	0.85	0.609[c]	0.08	0.39[e]	0.23	0.636[d]	0.07
Pt	3.0 ± 0.2	2.44	0.38	0.19	0.55	3.3	0.07	1.8	1.1		
Pd	12.7 ± 0.7	11.70	0.62	0.04	0.41	12.75	0.09	11.8	1.8		
PTM-1		(n = 8)									
Au	1.8 ± 0.2	1.60	0.06	0.04		1.812[c]	0.06	1.78[e]	0.32	1.72[f]	0.05
Pt	5.8 ± 0.4	5.09	0.24	0.05		4.413	0.62	5.97	0.53		
Pd	8.1 ± 0.7	7.79	0.19	0.02		7.633	0.49	8.81	1.56		
SU-1a		(n = 4)									
Au	(0.15)	0.05	0.02	0.36							
Pt	0.41 ± 0.06	0.32	0.05	0.15							
Pd	0.37 ± 0.03	0.24	0.02	0.07		0.31[g]	0.03				

[a]With standard deviation at the 95% confidence level. [b]Mean of total values found by combination of acid leaching and peroxide fusion of the residue; s, standard deviation of total values; s_r(ac), relative standard deviation based on the acid procedure; s_r(fu), relative standard deviation based on the peroxide fusion. [c–g]Methods used in the literature: [c]pressure digestion, ion exchange (Srafion NMRR), AAS [13]; [d]acid leaching, solvent extraction, AAS [21]; [e]peroxide fusion, ion exchange (Srafion NMRR), NAA [10, 11]; [f]acid leaching, solvent extraction, AAS (0.52 ± 0.08 $\mu g\ g^{-1}$ Au for PTC-1 also reported by this method) [22]; [g]acid leaching, coprecipitation (α-benzildioxime), NAA [25].

Palladium, platinum and gold were determined in the extracts and residues separately. For final statistical evaluation, the analytical data for a sample obtained by the two decomposition procedures were treated both individually and combined (Tables 2 and 3).

Effect of roasting temperature

It is usually recommended to roast sulphide minerals prior to the acid decomposition and dissolution steps. The absorption of precious metal ions by elemental sulphur can thus be avoided during the leaching step [21, 22, 24]. Heating at 700–800°C is often used [23, 24], but some investigators [20–22] found 600°C to be the optimum temperature before dissolution of Au and Pd from sulphide ores and concentrates by acid attack. It has been stated that roasting temperatures above 650°C may cause losses of gold by volatilization if arsenic is present in the material [22].

To find the optimum roasting conditions for the certified materials, temperatures from 600°C to 900°C were tested. At least two portions (2.5 g) of each sample were slowly heated to 300°C, and then the temperature was raised to the appropriate value and maintained for one hour. After the roasting step, the samples were processed as described in the Experimental section. The recoveries of Au, Pd and Pt as a function of roasting temperature are illustrated in Fig. 2, representing the results for a Ni/Cu matte (PTM-1) and a flotation concentrate (PTC-1) which contains similar values of precious metals. Both materials are characterized by high contents of sulphur (>20%) but differ in their composition of base metals.

Obviously, the preliminary roast affects the various materials in different ways and causes high or low recoveries of the individual precious metals. For example, the Cu/Ni matte yields gold and palladium nearly quantitatively to aqua regia without marked influence of the roasting temperature

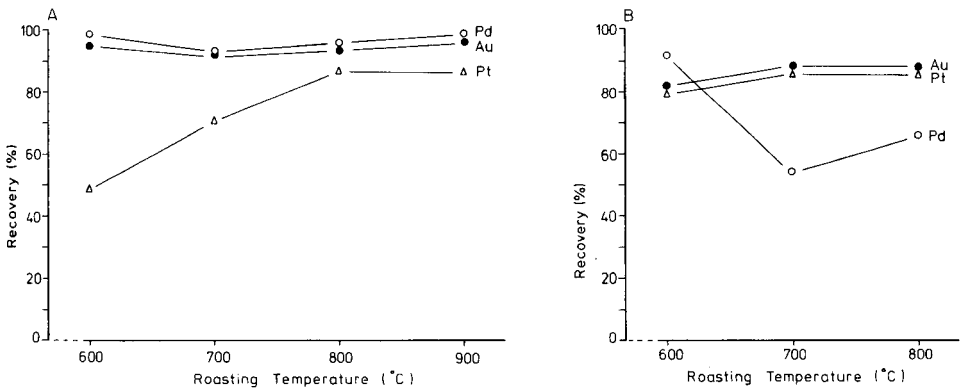

Fig. 2. Recovery of precious metals as a function of roasting temperature: (A) from Cu/Ni matte PTM-1 (acid leaching, ion-exchange separation by means of P-TD); (B) from flotation concentrate PTC-1 (acid leaching, peroxide fusion of residue, ion-exchange separation by means of P-TD).

within the range used (Fig. 2A), whereas in the case of platinum preliminary heating at 800°C is necessary to reach maximum recovery. In contrast, the effectiveness of the separation of palladium from the flotation concentrate PTC-1 is very sensitive to roasting conditions. Heating at $\geqslant$700°C drastically lowers the recovery of palladium but slightly improves the release of platinum and gold (Fig. 2B). It must be emphasized that the acid extraction from PTC-1 is relatively incomplete and considerable amounts of gold, palladium and platinum (7—13%) were still found in the residues (see Table 2). To increase the low recoveries of palladium, which could be due to the presence of acid-resistant minerals [18], complete decomposition of some residues was achieved by treatment with a mixture of aqua regia and hydrofluoric acid [9, 24, 25]. This method did not improve the results compared to those obtained by the fusion method.

Low palladium values caused by the action of high temperatures have also been reported by Grimaldi and Schnepfe [18], who coprecipitated dissolved palladium with tellurium. The subsequent ignition of the precipitate was found to be critical, as temperatures of 700°C caused losses of palladium when the residue was treated with aqua regia. Volatilization of palladium compounds and the formation of insoluble, inert palladium species were assumed to cause low recoveries. Such reactions may also affect the recovery of palladium from the flotation concentrate PTC-1. The optimum roasting temperatures found for each sample and used for further work are mentioned in Table 2.

Efficiency of the acid extraction

The acid leach liquors and the sample residues were examined separately to estimate the effectiveness of the extraction. The data obtained were evaluated as mean percentage recoveries (Table 2). The results show that high recoveries of these three precious metals can be achieved only by acid extraction from the Ni/Cu matte (PTM-1). Analysis of the residues yielded no detectable amounts of palladium, platinum and gold. Similar results were obtained in the investigation of the Ni/Cu/Co ore (SU-1a), although the percentage recovery of palladium was less satisfactory (64.8%). Nevertheless, it should be noted that the palladium content in this ore is low (0.37 μg Pd g^{-1}) compared to that in the matte (8.1 $\mu g\ g^{-1}$).

As already mentioned, acid leaching of the flotation concentrate PTC-1 did not yield the precious metals quantitatively (ca. 70% Au, Pt; ca. 85% Pd). The additional amounts of gold and platinum found in the residues did not give a total recovery exceeding 83%, whereas >90% of the palladium was separated. Similarly, the acid extraction of precious metals from the certified platinum ore SARM-7 was incomplete (ca. 75—87%). This result is consistent with the fact that generally some mineral constituents of the ore, such as chromite, cooperite and sperrylite, are very resistant to attack by aqua regia [18, 20]. Nevertheless, subsequent fusion of the residue with sodium peroxide gave quantitative total recoveries of all three metals.

Depending on the actual analytical problem, acid extraction of Au, Pd and Pt from ores and concentrates may be sufficient. However, if the total of these metals in the sample is to be determined, the insoluble residues must also be analyzed. With regard to the efficiencies of acid extraction in connection with the effect of roasting procedures as described above, the quite different behaviour of the geological samples is obvious. Hence, the manner of occurrence of the individual precious metals in their ores and concentrates affects their recovery in analytical procedures as well as metallurgical processes [26].

Efficiency and selectivity of P-TD resin

Based on the earlier investigations [14], the anion-exchange resin P-TD would be expected to separate Au, Pd and Pt from the bulk of accompanying elements effectively. In fact, when a small bed of P-TD resin (2.5-cm bed height, 0.7-cm diameter) was used, only one loading step at 1 ml min^{-1} was needed to provide quantitative sorption of the precious metals from 40—50 ml of weakly acidic leach liquors. Hence, this dehydrodithizone resin seems to separate the precious metals in question more efficiently than the isothiouronium-functionalized Srafion NMRR polymer [12, 13, 27]. As reported, use of the commercially available Srafion NMRR requires larger columns (bed heights 10—15 cm) and repeated loading steps. The elution of the metals from P-TD by perchloric acid followed by thiourea is advantageous in comparison to elution with thiourea solution only, which affords larger elution volumes. The latter method necessitates final evaporation of the eluate to achieve preconcentration of the metals [13].

In the present study, 5 ml of each eluting agent was usually sufficient for complete recovery of the metals retained, if their total amount per portion of sample did not exceed 40 μg Pd, 20 μg Pt and 5 μg Au. But it is advisable to pass a second 5-ml fraction of 2 M perchloric acid and 5% thiourea solution to ascertain the completeness of the first elution step.

The selectivity of the ion-exchange procedure was confirmed by determining some major base metals in the eluates. For this purpose, a 5-g portion of the matte PTM-1, containing 44.8% Ni, 30.2% Cu and 1.58% Fe, was investigated. The recommended procedure was followed and a 10-ml fraction of each effluent was examined. Only traces of copper and iron were found (0.13—0.25 μg ml^{-1}). Nickel was not detected in the thiourea solution (<0.025 μg ml^{-1}) whereas the perchloric acid contained very minute amounts (0.05 μg ml^{-1}). The concentration of chromium was always below the detection limit (0.03 μg ml^{-1}). In these solutions, the values for Au, Pd and Pt lie in the range between 0.9 μg ml^{-1} (Au) and 3.5 μg ml^{-1} (Pd). A comparison of the ratio of base metals and precious metals in the eluates suggests negligible interelement interferences in the emission spectrometry [3].

It should be realized that, after the eluent had passed through the ion-exchange bed, only 10 ml of wash solution (0.1 M HCl) was applied, so that the precious metals are freed from the bulk of base metals very effectively.

The complexity of the original sample matrix is thus dramatically reduced and the preparation of multi-element standard solutions for calibration of the plasma emission spectrometer then becomes simple. Aliquots of stock solutions of the precious metals were simply diluted serially with 2 M perchloric acid or thiourea solution as appropriate. The standards were then in a form quite similar to that encountered in the two different eluates.

Accuracy and precision

The accuracy and precision data are presented in Table 3, where they are compared with literature values based on a wide variety of methods. Generally, the agreement of the values found by the proposed method to the certified values is satisfactory and even excellent in the case of SARM-7. With regard to the concentrate PTC-1, the results for palladium and platinum lie significantly outside the 95% confidence interval of the recommended values. However, these data are similar to those reported for a method based on peroxide fusion, sorption onto Srafion NMRR and neutron activation analysis (NAA) [8, 11]. Better results were achieved by using the same type of resin and pressure digestion of the sample [13]. Application of the same procedure to the matte PTM-1 produced less accurate values.

It is evident that the procedure chosen for dissolution of diverse geological materials can have a great influence on the accuracy as well as the precision of the analysis. For illustration, the overall precision of the present results, expressed as standard deviation of the total values, varies from 0.02 to 0.62 $\mu g\ g^{-1}$ for palladium. As the metal content was determined by separate techniques (acid leaching, fusion), their individual relative standard deviations could be calculated and compared. It is striking that in most cases the reproducibility after the acid leaching procedure is clearly better than that based on peroxide fusion. This result agrees with the poor precision of the data which were obtained after fusion of the roasted samples (PTC-1) without prior aqua-regia treatment (not listed). Furthermore, combination of aqua regia leachate and the leached melt of the residue, which has been recommended [24], did not yield improved reproducibility. Based on earlier studies [14] on ion exchange with synthetic mixtures of alkali chlorides and precious metals, it appears that varying high salt contents in the leachates of the melts can produce significant deterioration of the sorption efficiency. The relatively high standard deviations of the literature values for PTC-1 and PTM-1, obtained by using only peroxide fusion and ion-exchange, can be explained similarly, although sample inhomogeneity may also play a role [10, 11].

It can be concluded that the proposed method for the determination of Au, Pt and Pd in geological materials, combining simple techniques of acid extraction, peroxide fusion, and selective and reversible sorption on P-TD resin, provides useful analytical data. The detection limits for the d.c. plasma emission (see Table 1) are equivalent to 0.09 $\mu g\ g^{-1}$ Au, 0.10 $\mu g\ g^{-1}$ Pt and 0.008 $\mu g\ g^{-1}$ Pd in an original 2.5-g sample, so that the method provides sufficient sensitivity.

Further analytical applications of polymers and liquid extractants based on derivatives of dehydrodithizone, involving iridium and rhodium are in progress.

The authors thank the Deutsche Forschungsgemeinschaft for financial support and Degussa A. G., Hanau, for donating the precious metal salts. The contribution of Mrs. R. Knaup in helpful technical assistance is also acknowledged.

REFERENCES

1 R. B. Wemyss and R. H. Scott, Anal. Chem., 50 (1978) 1694.
2 R. Fox, Appl. Spectrosc., 38 (1984) 644.
3 R. Fox, Spectrochim. Acta Part B, 40 (1985) 287.
4 J. C. van Loon, Pure Appl. Chem., 49 (1977) 1495.
5 F. E. Beamish and J. C. van Loon, Analysis of Noble Metals, Academic, New York, 1977.
6 Chemikerausschuß der Gesellschaft Deutscher Metallhütten (Eds.), Edelmetall-Analyse, Springer, Berlin, 1964.
7 R. J. Brown and W. R. Biggs, Anal. Chem., 56 (1984) 56.
8 F. Bea Barredo, C. Polo Polo and L. Polo Diez, Anal. Chim. Acta, 94 (1977) 283.
9 Y. A. Zolotov, O. M. Petrukhin, G. I. Malofeeva, O. A. Shiryaeva, V. A. Shestakov, V. G. Miskaryants, V. I. Nefedov, Y. I. Murinov and Y. E. Nikitin, Anal. Chim. Acta, 148 (1983) 135.
10 S. J. Parry, Analyst, 105 (1980) 816.
11 S. J. Parry, Analyst, 105 (1980) 1157.
12 R. A. Nadkarni and G. H. Morrison, Anal. Chem., 46 (1974) 232.
13 K. Kritsotakis and H. J. Tobschall, Fresenius' Z. Anal. Chem., 320 (1985) 15.
14 M. Grote and A. Kettrup, Anal. Chim. Acta, 175 (1985) 239 (Part 2).
15 M. Grote and A. Kettrup, Anal. Chim. Acta, 172 (1985) 223 (Part 1).
16 G. Tölg, Pure Appl. Chem., 55 (1983) 1989.
17 R. K. Petrie and J. W. Morgan, J. Radioanal. Chem., 74 (1982) 15.
18 F. S. Grimaldi and M. M. Schnepfe, U.S. Geol. Survey Prof. Paper, 575-C (1967) C141.
19 F. S. Grimaldi and M. M. Schnepfe, U.S. Geol. Survey Prof. Paper, 600-B (1968) B99.
20 I. Palmer, G. Streichert and A. Wilson, Natl. Inst. Metall. Repub. S. Afr., Rep. No. 1218, Johannesburg, 1971.
21 A. Parkes and R. Murray-Smith, At. Absorbt. Newsl., 18 (1979) 57.
22 B. Strong and R. Murray-Smith, Talanta, 21 (1974) 1253.
23 C. Pohlandt and M. Hegetschweiler, Natl. Inst. Metall. Repub. S. Afr., Rep. No. 1940, Johannesburg, 1978.
24 V. P. Khostova and S. V. Golovnya, Ind. Lab. (USSR), 48 (1982) 631.
25 H. Bem and D. E. Ryan, Anal. Chim. Acta, 169 (1985) 79.
26 C. Gasparrini, Precious Metal: Min., Extr., Process. Proc., Int. Symp., Los Angeles, CA, (1984) 101.
27 L. C. Sundberg, Anal. Chem., 47 (1975) 2037.

Analytica Chimica Acta, 201 (1987) 109—116
Elsevier Science Publishers B.V., Amsterdam — Printed in The Netherlands

UNSTEADY MOTION IN SINGLE-LINE FLOW-INJECTION SYSTEMS

ŠPAS D. KOLEV and ERNŐ PUNGOR*

Institute of General and Analytical Chemistry, Technical University of Budapest, Gellért tér 4, H-1502 Budapest XI (Hungary)

(Received 14th February 1987)

SUMMARY

Unsteady motion in single-line flow-injection systems consisting of n tubular elements with valve or hydrodynamic injection is studied theoretically. A formula for the duration of the initial period of unsteady flow is derived. This initial period is much shorter than the mean residence time of the analyte in practical systems. It can therefore be neglected in mathematical modelling of such systems. Experimental data obtained with single-line systems with valve and hydrodynamic injection confirmed the validity of the theoretical equations.

All mathematical models for flow-injection analysis (FIA) assume that the fluid motion in the system is steady, i.e., at a fixed point in the flow field there are no changes of velocity with time. Such a situation is found in practice to some extent, only when the sample is introduced by syringe at very low velocity so that the total volumetric flow rate in the system remains practically unchanged. In the general case, when different types of valves are used or when the sample is introduced by hydrodynamic injection, fluid motion in the system is unsteady for some initial period of time. During this time, the flow is accelerated from the condition of rest to condition of steady motion characterized by a volumetric flow rate corresponding to the pressure drop applied at the ends of the system and the energy dissipation in it. Obviously, if the duration of this initial period is much smaller than the mean residence time of the sample in the modelled system, then the assumption of permanent steady motion could be accepted as correct. For that reason, there is a need to be able to predict this duration on the basis of the system parameters (e.g., geometrical dimensions and flow rate).

THEORY

A single-line flow-injection system with straight tube reactor is considered here. Because very often such systems are composed mainly of tubular elements, it will be assumed that the system considered consists of n tubes connected in series. For each of these, the basic equation for flow in a cylindrical tube can be applied [1]:

0003-2670/87/$03.50

$$[(P_1 - P_2)/\rho g] + z_1 - z_2 = \lambda(L/d)(u^2/2g) + (L/g)K_m(du/dt) \quad (1)$$

(Symbols are defined in Table 1). In Eqn. 1, the friction factor λ and the momentum-flux coefficient K_m are functions of the flow regime, which is determined by the Reynolds number (Re). In flow-injection systems, laminar flow exists (i.e., $Re < 2000$ [1]) so that λ and K_m are defined by the following equations, respectively [2]:

$$\lambda = 64/Re = 64\nu/ud \quad (2)$$

$$K_m = \int_0^{d/2} q^2 \rho \mathrm{d}(\pi r^2)/(u^2 \rho \pi d^2/4) = 4 \int_0^{d/2} (1 - 4r^2/d^2)^2 \mathrm{d}(4r^2/d^2) = 4/3 \quad (3)$$

For a system of n pipes connected in series, the following set of equations

TABLE 1

Symbols and definitions[a]

A	Quantity defined by Eqn. 15 (s^{-1})
d	Diameter of tube (m)
D	Quantity defined in Eqn. 7 (m)
g	Gravitational acceleration (m s^{-2})
h	Expansion or contraction head loss (m)
H	Sum of head losses caused by local nonuniformities of flow (m)
K_e	Kinetic-energy flux correction
K_m	Momentum-flux correction
L	Length of tube (m)
n	Number of tubes in the system
P	Pressure (Pa, N m^{-2})
q	Linear flow rate (m s^{-1})[b]
Q	Volume of fluid passed through the system over a time interval θ (m^3)
r	Radial coordinate (m)
Re	= ud/ν. Reynolds number
s	Standard deviation of ΔQ_{exp} (μl)
t	Time (s)
T	Duration of the transition period (s)
u	Average linear flow rate (m s^{-1})[b]
v	Volumetric flow rate (m^3 s^{-1})[b]
z	Elevation (m)
θ	Time interval during which the effluent from the system is collected (s)
λ	Friction factor
ν	Kinematic viscosity (m^2 s^{-1})
ρ	Density (kg m^{-3})
ΔQ	Quantity defined by Eqn. 17 (m^3)

[a]Subscripts a and b refer to cross-sections a and b, respectively (Fig. 1); subscripts calc and exp refer to theoretically calculated and experimentally determined value, respectively; subscript i refers to the ith section of the system (Fig. 1); subscript st refers to steady flow. [b]In the general case, the flow rate is time-dependent.

will describe the laminar flow in them:

$$(P_1/\rho g) + z_1 = (P_2/\rho g) + z_2 + 32\,(L_1\nu/gd_1^2)\,u_1 + (L_1/g)K_m\,(du_1/dt)$$

$$(P_i/\rho g) + z_i = (P_{i+1}/\rho g) + z_{i+1} + 32\,(L_i\nu/gd_i^2)u_i + (L_i/g)K_m(du_i/dt) \qquad (4)$$

$$(P_{n-1}/\rho g) + z_{n-1} = (P_n/\rho g) + z_n + 32\,(L_n\nu/gd_n^2)u_n + (L_n/g)\,K_m(du_n/dt)$$

The initial conditions are: $u_i(0) = 0$ for $i = 1,2,\ldots,n$.

If Eqns. 4 are summed and the average linear flow rate (u) is replaced by the volumetric flow rate (v), the following nonhomogeneous ordinary differential equation of first order is obtained:

$$[(4K_m/\pi g)\sum_{i=1}^{n}(L_i/d_i^2)](dv/dt) + [(128\nu/\pi g)\sum_{i=1}^{n}(L_i/d_i^4)]\,v$$

$$= [(P_1 - P_n)/\rho g] + z_1 - z_n \qquad (5)$$

with the initial condition: $v(0) = 0$.

In Eqn. 5, only energy dissipation caused by friction is taken into account. In addition to this, mechanical energy is lost by other phenomena causing nonuniform flow such as change in flow direction, abrupt enlargements and contractions [2]. A bend in a uniform conduit generates secondary spiral motions and separation within and downstream of it. The magnitude of the energy dissipation caused by the bend depends on the extent to which secondary spiral flow and separation occur. The intensity of these phenomena are related to the curvature in the bend [2]. As far as flow-injection systems with a straight-tube reactor are concerned, it can be assumed that everywhere in the system the ratios between the radii of the bends and the corresponding radii of the tubes are very large and that both secondary flow and separation can be neglected [3]. Most of the work on expansion and contraction losses in laminar flow is highly empirical and the findings of the various workers are usually at variance [4]. The main reason for this situation is that in laminar flow viscous forces are considerable and cannot be neglected as is done for turbulent flow. For very small Reynolds numbers ($Re < 10$) the head losses caused by expansion and contraction are calculated from the following equation [5]:

$$h = 25.2\,u^2/(Re \times 2g) \qquad (6)$$

For large Reynolds numbers, the friction factor ($\lambda = 25.2/Re$) begins to depend also on the diameters of the adjacent tubes. For a given ratio of diameters, this dependence is no longer linear with respect to $1/Re$; with decrease of $1/Re$, the friction factor decreases asymptotically, approaching a constant value in the turbulent region which is independent of the viscous forces. There are theoretical equations for calculation of this value [1, 2, 4, 5].

In flow-injection systems, the Reynolds number usually varies from 5 to

100. In a first approximation, it will be assumed that Eqn. 6 holds for this whole range of Re values so that Eqn. 5 becomes

$$[(4K_m/\pi g)\sum_{i=1}^{n}(L_i/d_i^2)]\,(dv/dt) + (\nu/\pi g)[128\sum_{i=1}^{n}(L_i/d_i^4) + 50.4\sum_{i=1}^{n-1}(1/D_i^3)]v = [(P_1 - P_n)/\rho g] + z_1 - z_n \tag{7}$$

where $v(0) = 0$ and $D_i = \begin{cases} d_i & d_i < d_{i+1} \\ d_{i+1} & d_i > d_{i+1} \\ \infty & d_i = d_{i+1} \end{cases}$

Equation 7 can be solved by the method of variation of the coefficients [6] and the corresponding solution is:

$$v = \frac{[(P_1 - P_n)/\rho g] + z_1 - z_n}{(\nu/\pi g)\,[128\sum_{i=1}^{n}(L_i/d_i^4) + 50.4\sum_{i=1}^{n-1}(1/D_i^3)]}\left\{1 - \exp\left[-\frac{\nu}{K_m}\left(32\,\frac{\sum_{i=1}^{n}(L_i/d_i^4)}{\sum_{i=1}^{n}(L_i/d_i^2)} + 12.6\,\frac{\sum_{i=1}^{n-1}(1/D_i^3)}{\sum_{i=1}^{n}(L_i/d_i^2)}\right)t\right]\right\} \tag{8}$$

For steady flow, i.e., $t \to \infty$, the following equation is valid:

$$v_{st} = [(P_1 - P_n)/(\rho g) + z_1 - z_n]\,/\,\{(\nu/\pi g)\,[128\sum_{i=1}^{n}(L_i/d_i^4) + 50.4\sum_{i=1}^{n-1}(1/D_i^3)]\} \tag{9}$$

and Eqn. 8 becomes

$$v = v_{st}\left\{1 - \exp\left[-\frac{\nu}{K_m}\left(32\,\frac{\sum_{i=1}^{n}(L_i/d_i^4)}{\sum_{i=1}^{n}(L_i/d_i^2)} + 12.6\,\frac{\sum_{i=1}^{n-1}(1/D_i^3)}{\sum_{i=1}^{n}(L_i/d_i^2)}\right)t\right]\right\} \tag{10}$$

On the basis of the solution obtained (Eqn. 10), it can be concluded that energy dissipation caused by abrupt enlargements and contractions decreases the time interval during which the flow is accelerated from condition of rest to that of steady motion. This means that if expansion, contraction and other types of loss (e.g., from bends) are neglected, i.e., $D_i \to \infty$, the time interval calculated by Eqn. 10 will be the upper limit for the duration of the initial period during which steady motion is established.

In a similar way, it can be concluded that this time interval is also the

upper limit for single-line flow-injection systems with different types of reactors (e.g., coiled tube, packed bed, single-bead-string, etc.) because among these the straight-tube reactor is characterized by the smallest hydraulic resistance and so by the smallest energy dissipation.

If it is assumed that, when $v/v_{st} = 0.999$, steady motion exists, then the time necessary for its establishment is defined by

$$T = 0.288/v \left[\sum_{i=1}^{n} (L_i/d_i^2) \Big/ \sum_{i=1}^{n} (L_i/d_i^4) \right] \quad (11)$$

By inserting the geometrical characteristics of a given single-line flow-injection system in Eqn. 11, then for a known mean residence time, the assumption of permanent steady motion from the injection to the detection of the analyte could be tested.

EXPERIMENTAL

The experiments were done with a single-line manifold with valve or hydrodynamic injection (Fig. 1). The main geometrical dimensions are presented in Table 2. The injection valve (Labor MIM, Hungary) was of rotary type. Conductimetric measurement cells of tubular type with two platinum disc electrodes and volumes of 0.45 μl, similar to the cell proposed by Stankoviansky et al. [7], were incorporated in the manifolds. The value of the volumetric flow rate in the systems was governed by the pressure head of the fluid in the source bottle (a, Fig. 1). The gauge pressure in this bottle was measured with a mercury manometer. The flow rate was measured by collecting and weighing the effluent over intervals of 3 min. The tube diameters were calculated from the volume of twice-distilled water with which they could be filled. The hydrodynamic injection section was connected with the other tubes by two T-pieces each of which had a volume of 0.2 μl.

Two groups of experiments were done. In the first group, the significance of the local resistances arising from nonuniform flow (e.g., abrupt expansions and contractions of the flow, bends, etc.) were studied. For that purpose, the gauge pressures necessary for the flow to reach four different flow rates were measured. For the manifold with hydrodynamic injection, the flow rates were 0.5011, 1.0050, 1.4926 and 2.0055 ml min^{-1}; for the manifold with valve injection, the flow rates were 0.4980, 1.0100, 1.5110 and 2.0021 ml min^{-1}.

In the second group, Eqn. 11 was checked. For that purpose, the effluent of the system with valve injection was collected and weighed over intervals of 3 min in two different ways. In the first, the flow was stopped every 10 s by slight revolution of the valve rotor; the flow was thus stopped 18 times during each experiment. This was done because the effect of the initial period of unsteady motion on the weight of the effluent collected at the exit of the system (b, Fig. 1) was very small (<0.3 mg) and multiplication of this

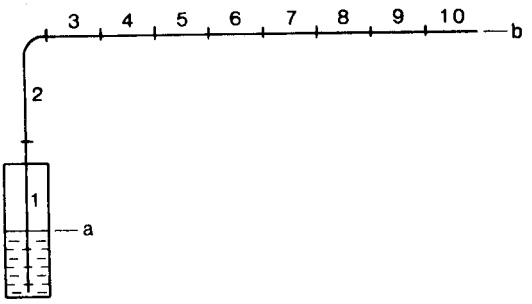

Fig. 1. Diagram of the experimental single-line manifold. For hydrodynamic injection: (1, 2, 3, 4, 10) connecting tubes; (5, 7) T-pieces; (6) injection section; (8) straight-tube reactor; (9) measurement cell. For valve injection: (1, 2, 10) connecting tubes; (3, 4, 6, 7) valve conduits; (5) external loop; (8) straight-tube reactor; (9) measurement cell. For a and b, see text.

TABLE 2

Dimensions of the manifolds (Fig. 1) with hydrodynamic or valve injection

Section	Hydrodynamic injection			Valve injection		
	L (m)	d (10^{-4} m)	Material	L (m)	d (10^{-4} m)	Material
1	0.5310	3.296	Teflon	0.5310	3.296	Teflon
2	1.2631	6.088	Teflon	1.2631	6.088	Teflon
3	0.0010	5.000	Teflon	0.0065	8.011	SS[a]
4	0.2582	5.353	SS[a]	0.0050	3.192	Teflon
5	0.0010	5.000	Perspex	0.1751	6.091	Teflon
6	0.1995	5.364	SS[a]	0.0050	3.192	Teflon
7	0.0010	5.000	Perspex	0.0065	8.011	SS[a]
8	0.5520	5.353	SS[a]	1.2550	6.067	Teflon
9	0.0023	5.011	Platinum	0.0023	5.011	Platinum
10	0.5221	8.212	Teflon	0.3400	6.067	Teflon

[a]Stainless steel.

effect was necessary to obtain more accurate measurements. In the second case, the collection of the fluid was started after the initial period of unsteady flow (i.e., at $t > T$) and the flow was not stopped during the 3-min period. Six sets of such pairs of measurements were obtained for each of the flow rates mentioned above.

RESULTS AND DISCUSSION

For the calculation of the sum of energy losses caused by local nonuniformities of the flow (H), the Bernoulli equation [1] written for cross-sections a and b (Fig. 1) could be used:

$$H = z_a - z_b + [(P_a - P_b)/\rho g] + [K_e(u_a^2 - u_b^2)/2g]$$

$$- \sum_{i=1}^{n} [(64L_i/Re_i d_i)(u_i^2/2g)] \quad (12)$$

where the kinetic-energy flux correction (K_e) is defined [2] by

$$K_e = \int_0^{d/2} q^3 \rho \, d(\pi r^2)/(u^3 \rho \pi d^2/4) = 2 \quad (13)$$

The kinetic-energy term in Eqn. 12 is very small and can be neglected. The measured gauge pressure in the source bottle is ($P_a - P_b$) and the difference in the elevation between cross-sections a and b was found to be 0.805 m for the manifold with hydrodynamic injection and 0.640 m for the manifold with valve injection. The results presented in Tables 3 and 4 show that H is less than 1.0% of the applied gauge pressure and can be regarded as insignificant in comparison with the energy losses caused by friction. This result agrees with the magnitude of the values predicted by Eqn. 6. For these reasons, the single-line flow-injection systems investigated can be regarded as "long pipe systems" [1], where mechanical energy is dissipated almost entirely by friction.

The volume of fluid passed through the system over an interval including the transition period of unsteady flow can be calculated by the following equation:

$$Q = \int_0^{\theta} v \, dt = v_{st} \{\theta - [1 - \exp(-A\theta)]/A\} \quad (14)$$

where

$$A = 32\nu \sum_{i=1}^{n} (L_i/d_i^4)/(K_m \sum_{i=1}^{n} L_i/d_i^2) \quad (15)$$

If the interval mentioned above starts from $t > T$, then Eqn. 14 can be reduced to

$$Q = v_{st}\theta \quad (16)$$

The difference between the volumes defined by Eqns. 16 and 14 which is the result of the unsteady motion is

$$\Delta Q = v_{st}[1 - \exp(-A\theta)]/A \quad (17)$$

Even for very small values of θ, the inequality $\exp(-A\theta) \ll 1$ is valid so that Eqn. 17 is reduced to

$$\Delta Q = v_{st}/A \quad (18)$$

TABLE 3

Experimental results for the flow-injection system with hydrodynamic injection

v (ml min^{-1})	0.5011	1.0050	1.4926	2.0055
$P_a - P_b$ (10^4 Pa)	3.057	5.308	7.494	10.014
H (10^4 Pa)	0.039	0.049	0.065	0.083

TABLE 4

Experimental results for the flow-injection manifold with valve injection

v (ml min^{-1})	$P_a - P_b$ (10^4 Pa)	H (10^4 Pa)	ΔQ_{exp} (μl)	s (μl)	ΔQ_{calc} (μl)
0.4980	2.8494	0.0142	2.0	1.5	1.26
1.0100	5.1418	0.0357	1.8	1.4	2.55
1.5110	7.3860	0.0586	5.0	3.8	3.82
2.0021	9.5915	0.0852	6.6	4.5	5.06

The experimental results presented in Table 4 are in moderately good agreement with the theoretical predictions made by Eqn. 18. It should be taken into consideration that $\Delta Q_{calc} = 18\Delta Q$ (see Experimental).

On the basis of both the theoretical predictions and the experimental results obtained in this study, it can be concluded that the time necessary for acceleration of the flow from the condition of rest to that of steady motion is much shorter than the mean residence time of the analyte in the section of the manifold between the points of sample introduction and detection. Insofar as the mean residence time is the time-scale unit of the processes occurring in flow-injection systems which are responsible for the shape and magnitude of the output signal, then the initial transition period discussed above can be neglected when mathematical models are developed.

REFERENCES

1 R. R. Chugaev, Hydraulics, Energia, Leningrad, 1970 (in Russian).
2 J. W. Daily and D. R. F. Harleman, Fluid Dynamics, Addison-Wesley, Reading, MA, 1966.
3 J. M. Reijn, W. E. van der Linden and H. Poppe, Anal. Chim. Acta, 126 (1981) 1.
4 W. L. Wilkinson, Non-Newtonian Fluids, Pergamon, London, 1960.
5 A. D. Altshul, Hydraulic Resistances, Nedra, Moscow, 1982 (in Russian).
6 W. Kaplan, Ordinary Differential Equations, Addison-Wesley, Reading, MA, 1962.
7 S. Stankoviansky, P. Čičmanec and D. Kamiansky, J. Chromatogr., 106 (1975) 131.

Analytica Chimica Acta, 201 (1987) 117—125
Elsevier Science Publishers B.V., Amsterdam — Printed in The Netherlands

STABILITY CONSTANTS FOR SOME DIVALENT METAL ION/ CROWN ETHER COMPLEXES IN METHANOL DETERMINED BY POLAROGRAPHY AND CONDUCTOMETRY

L. CHEN[a], M. BOS*, P. D. J. GROOTENHUIS[b], A. CHRISTENHUSZ, E. HOOGENDAM, D. N. REINHOUDT[b] and W. E. VAN DER LINDEN

Laboratory of Analytical Chemistry, Department of Chemical Technology, Twente University of Technology, P.O. Box 217, 7500 AE Enschede (The Netherlands)

(Received 26th May 1987)

SUMMARY

Stability constants in methanol at 25.0°C were evaluated for the complexes of the divalent cations Ca^{2+}, Ni^{2+}, Zn^{2+}, Pb^{2+}, Mg^{2+}, Co^{2+} and Cu^{2+} with the macrocyclic polyethers 15-crown-5 (15C5), 18-crown-6 (18C6), dicyclohexyl-18-crown-6 (DC18C6) and dibenzo-24-crown-8 (DB24C8). The log K values of the 1:1 complexes were generally in the range 2.1—4.2, which is low in comparison to the values of the corresponding crown ether/alkali metal ion complexes. M_2L complexes were observed for the systems Pb^{2+}/18C6, Pb^{2+}/DC18C6, Ca^{2+}/DC18C6 and Cu^{2+}/D18C6, whereas ML_2 complexes were found for Ca^{2+}/18C6 and Cu^{2+}/18C6. Within the series of complexes studied, there was no clear relationship between cation diameter and hole size.

Interest in the complexation of divalent cations by macrocyclic polyethers originates from work in this department on the complexation of neutral molecules like urea [1], alcohols [2] and related polyfunctional molecules. It was shown that the thermodynamic stability of complexes of crown ethers with neutral guest molecules is low in comparison to the stabilities of the corresponding complexes with cationic guests [3, 4]. Therefore, attempts were made to increase the interactions between host and neutral guest by using a co-complexed electrophilic cation (Li^+) capable of polarizing the guest. This concept has resulted in the construction of macrocyclic polyethers that complex both an electrophilic cation and a neutral guest molecule. Recently, the crystal structure of a complex of a 2,6-pyridyl crown ether with Li^+ and two molecules of urea [5] was reported. Such systems can serve as models for complicated biological systems, such as metalloproteins.

Divalent (transition) metal cations are known to coordinate various types of ions and neutral molecules [6] and are therefore potentially interesting electrophiles. In order to design host molecules that co-complex a divalent

[a]Present address: Department of Chemistry, Anhui University, Hefei, Anhui, People's Republic of China.
[b]Present address: Laboratory of Organic Chemistry, Twente University of Technology.

0003-2670/87/$03.50

cation together with a neutral molecule, it is important to know more about the thermodynamics of complexation of macrocyclic polyethers with divalent cations. This binding of divalent cations by macrocyclic polyethers has received little attention in comparison to the complexes of such polyethers with alkali metal ions, as can be seen from the review of Izatt et al. [7]. Thermodynamic data on the complex formation for divalent cations were obtained calorimetrically [8—11]. For some of the transition metal ions, no significant heat effect was observed, which means either that no complexes are formed or that the enthalpy of complexation is very small. In this work, conductivity [12] and polarographic [13, 14] methods were used to study the effects of ring size and substituents on the ring on the strength of the complexation of divalent transition metals (Co^{2+}, Ni^{2+}, Cu^{2+}) and main-group metals (Ca^{2+}, Mg^{2+}, Zn^{2+}, Pb^{2+}). These methods are particularly suitable for these types of metal ion; they are not restricted to complex-formation reactions with a significant heat effect, but are also applicable to complex formations driven by entropy effects.

EXPERIMENTAL

Chemicals

The crown ethers dicyclohexyl-18-crown-6 (DC18C6) and dibenzo-24-crown-8 (DB24C8) were used as received (Merck). 15-Crown-5 (15C5) and 18-crown-6 (18C6), also from Merck, were purified before use to remove acidic impurities: 15C5 was distilled under vacuum and 18C6 was purified by preparing its acetonitrile complex and then removing the acetonitrile under vacuum [15].

The supporting electrolytes used in the polarographic studies were tetraethylammonium iodide (TEAI; Janssen Chimica) and tetrabutylammonium perchlorate (TBAP; Eastman), used as received. Reagent-grade methanol (Merck) was used as the solvent in all experiments; it contained no more than 0.01% (w/w) of water, as checked by Karl Fischer titration.

The metal salts for the complexation experiments were all of analytical-reagent grade. Calcium chloride, zinc sulphate, lead nitrate, magnesium sulphate, cobalt chloride hexahydrate (all Merck), nickel nitrate (Baker) and copper sulphate (Fluka) were used in the conductometric experiments; in the polarographic experiments, another anion was chosen for some of these metals, i.e., zinc acetate dihydrate (BDH), magnesium chloride (Baker) or lead acetate trihydrate (UCB).

Equipment

The polarographic equipment consisted of a Metrohm E506 Polarecord with a E505 polarographic stand and was operated in the 3-electrode mode. The counter electrode was a platinum wire. The silver/silver chloride reference electrode (Metrohm EA441/5) was filled with 0.1 M tetraethylammonium chloride in methanol. Glass capillaries from Metrohm (Type EA1019/2)

were used for the dropping mercury electrode. The natural drop-time of these capillaries at a mercury column height of 40—50 cm at open circuit was 6—7 s and the mercury flow was ca. 1 mg s^{-1} in 0.1 M TBAP in methanol. This equipment was computerized by means of a Apple IIE computer, a Digiloc (type ADC16-12/3) 12-bit A/D converter and a Kronemuis 12-bit D/A converter as described earlier [14].

For the conductivity measurements, a Philips PW9509 conductivity meter was used (accuracy, 0.15% of full-scale reading) with a Philips PW9510/60 measuring cell; the cell constant (0.77 cm^{-1}) was determined with aqueous potassium chloride solutions. For the addition of titrant, a Radiometer autoburette ABU12a (total volume, 2.5 or 25.0 ml) was used. Additions were computer-controlled, fixed-volume increments of 0.01 or 0.100 ml. The accuracy of the burette is 0.1%. The titration vessel with the conductivity cell was kept at 25.0 ± 0.1°C by a Tamson thermostat. The recorder output of the conductivity meter was used for data acquisition by a Basis-108 microcomputer equipped with a 12-bit A/D converter with a 1.000-V range (Digiloc, type ADC16-12/3).

Procedures

Conductivity measurements. The vessel was filled with a known volume of a standardized solution of a salt of the cation to be investigated. The titrant solutions were prepared by dissolving the ligands in the same salt solution as used for the starting solution in the titration vessel in order to maintain constant ionic strength. For a given system, the titrations were continued to various final metal ion/ligand concentration ratios to establish the most favourable change in conductivity to be used in the calculations. The solution was stirred magnetically.

The results were calculated with a simplex curve-fitting procedure [12] based on a 1:1 metal/ligand complex formation model and on a model also containing the ML_2 complex. The second model was adopted if the first showed a characteristic "deviation plot" and a significant improvement in the fit was observed. An example of this situation is given in Fig. 1.

Sampled d.c. polarography. The polarographic cell was thermostated to 25.0 ± 0.1°C. Nitrogen, presaturated with methanol at this temperature, was passed for 25 min through the solution (5 ml of 5×10^{-4} M metal ion in the relevant electrolyte) to expel oxygen. During the recording of the polarograms, the solution was blanketed with nitrogen. The polarographic half-wave potential and limiting current of the simple metal ion were measured. Complex formation was studied by stepwise addition of a concentrated solution of the crown ether ligand into the starting solution (8—10 steps) until the final concentration ratio of the ligand and metal ion reached 10:1. After each addition of ligand solution, nitrogen was bubbled through the solution for 3 min before the polarogram was recorded. The polarograph was operated in the d.c. Tast mode, with the drop-time set at 0.8 or 1 s. The scan speed was 2.5, 3 or 4 mV s^{-1}, depending on the polarographic

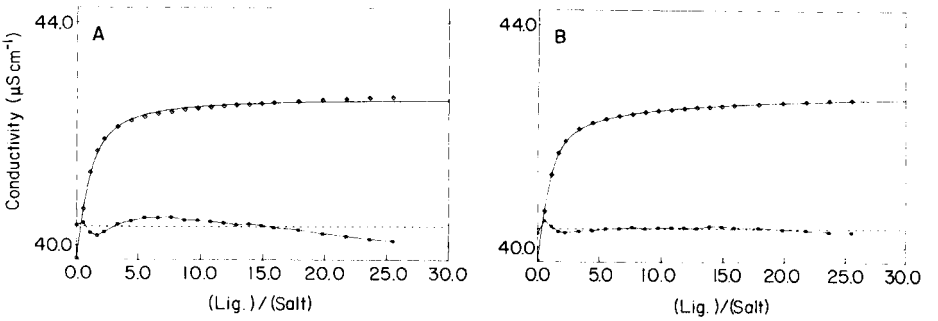

Fig. 1. Conductivity plots for Ca^{2+} (5×10^{-4} M)/18C6/methanol systems: (A) with ML formation only; (B) with the ML/ML_2 model. (◇) Measurements; (——) calculated curve; (○) deviation plot; (— — —) zero line.

behaviour. At each step, the shift of the half-wave potential and the limiting current were measured from the polarogram.

Both the crown ether and the metal ion were dissolved in methanol containing 0.1 M supporting electrolyte, TEAI for Ca^{2+}, Mg^{2+}, Ni^{2+} and Zn^{2+}, and TBAP for Pb^{2+}, Co^{2+} and Cu^{2+}.

Half-wave potentials and limiting currents were calculated from the polarograms by the FORTH computer program described earlier [14]. Stability constants were calculated with the use of the POLAG computer program, kindly made available by Leggett [16], which was adapted for changing total metal-ion concentration.

RESULTS AND DISCUSSION

Complexation behaviour of divalent cations and crown ethers

In Table 1, the formation constants of the complexes of four crown ethers with various divalent cations are given. Generally, the data obtained from the polarographic and conductometric method agree quite well. The log K values corresponding to the complexes with a 1:1 stoichiometry fall in the range 2.1—4.2 if the extremely high values for the complexes of Pb^{2+} with 18C6 and DC18C6 are ignored. This means that the thermodynamic stabilities of the complexes with divalent cations are low in comparison to complexes with the monovalent (alkali metal) cations. For instance, 18C6 forms 1:1 complexes with the alkali cations Na^+, K^+, Rb^+ and Cs^+ in methanol, with log K values in the range 4.3—6.2 [7]. This may be caused by the fact that the divalent cations are solvated much better than the monovalent cations [17]. On complex formation with the divalent cations, the crown ether ligand has to replace the tightly bound methanol molecules, which makes the driving force for the complexation much more entropic in nature than in the case of complex formation of monovalent cations. The delicate balance between the effects of enthalpy and entropy apparently favours the

TABLE 1

Formation constants (log β) for complexation of divalent metal ions by crown ethers in methanol at 25° C. The metal ions are listed in order of increasing ionic radius

Metal ion	15C5		18C6		DC18C6	DB24C8	
	Conduc.	Polar.[a]	Conduc.	Polar.[a]	Polar.[a]	Conduc.	Polar.[a]
Mg^{2+}	—[b]	2.30 ± 0.10	—[b]	2.26 ± 0.08	2.10 ± 0.22	2.71 ± 0.05	2.37 ± 0.06
Ni^{2+}	2.32 ± 0.05	2.59 ± 0.12	2.51 ± 0.05	2.47 ± 0.03	2.34 ± 0.12	—[b]	2.68 ± 0.06
Co^{2+}	—[b]	3.62 ± 0.25	—[b]	3.41 ± 0.07	3.60 ± 0.15	2.71 ± 0.05	2.79 ± 0.04
Cu^{2+}	—[b]	2.20 ± 0.05	ML 2.68 ± 0.12	2.47 ± 0.05	ML 2.90 ± 0.04		
			ML_2 3.85 ± 0.20		M_2L 5.54 ± 0.4	2.02 ± 0.05	1.75 ± 0.02
Zn^{2+}	—[b]	2.29 ± 0.08	—[b]	2.22 ± 0.04	2.39 ± 0.04	—[b]	2.63 ± 0.02
Ca^{2+}	2.42 ± 0.05[c]	—	ML 3.96 ± 0.05[d]	4.40 ± 0.03	ML 3.52 ± 0.01[e]		
			ML_2 6.0 ± 0.3		M_2L 5.98 ± 0.27	2.40 ± 0.05	2.53 ± 0.03
Pb^{2+}	—[f]	3.36 ± 0.01	—[f]	ML 7.52 ± 0.06	ML 7.47 ± 0.01		
				M_2L 14.78 ± 0.38	M_2L 14.04 ± 0.07	2.33 ± 0.05	2.33 ± 0.02

[a]Measured at ionic strength of 0.1 M. [b]No or very small change in specific conductance. [c]Lit. value, 2.0 [11]. [d]Lit. value, 3.87 [11]. [e]Lit. value, 3.54 [11]. [f]Change of pH during complexation.

complexation of macrocyclic polyethers with monovalent cations. Unfortunately, the methods described here yield information only on the free energy of complexation.

The diameters of the Ni^{2+}, Co^{2+}, Mg^{2+}, Zn^{2+} and Cu^{2+} ions are small (0.6–0.8 Å) compared to the hole size of the smallest ligand in this study, 15C5 (0.8–0.9 Å) [7]. The diameters of Cu^{2+} (1.00 Å) and Pb^{2+} (1.19 Å) are somewhat larger, and these cations form stronger complexes with 18C6 (1.3–1.4 Å) than with 15C5 [7]. However, a clear relationship between cation diameter and hole size [18–20] is not observed, which is in agreement with the above comments on the role of entropy.

Complexes with a host/guest ratio of 2:1 were observed (in solution) for 18C6 with Cu^{2+} and Ca^{2+}. Such complexes have been observed in the solid state for crown ethers with smaller ring sizes [7], but different stoichiometries may be found in solid state and in solution. For instance, B15C5 forms a 1:2 sandwich-type complex with potassium iodide in the solid state [21] whereas in methanol/water mixtures a 1:1 stoichiometry was indicated [22].

Complexes comprising a ligand with two metal cations [23] were observed in some cases (Table 1). Although many such complexes have been reported, the ligands mostly possess nitrogen, sulphur or phosphorus hetero-atoms [23]. To our knowledge, the only x-ray study of a 1:2 complex of a macrocyclic polyether having only oxygen hetero-atoms is concerned with the 1:2 DB24C8/potassium thiocyanate complex reported by Mercer and Truter [24].

Comparison of the polarographic and conductometric methods

The polarographic method was more generally applicable than the conductometric method. This is due to the fact that it is based on the measurements of two separate effects caused by complexation, the change of the half-wave potential and the change in the diffusion current. It is sufficient that only one of the two effects is present to be able to follow complexation by this technique. The polarographic method failed only for one of the systems investigated; in the calcium chloride/15C5/0.1 M TEAI system in methanol, a polarographic maximum developed on addition of the 15C5 ligand. A second advantage of the polarographic method in comparison to the conductivity method is that it is insensitive to the presence of small amounts of ionic impurities in the crown ethers. A third advantage is its ability to deal with the occurrence of species other than ML and ML_2. The conductometric method in its present form cannot easily be extended to include species like M_2L because the ionic strength changes if this type of complex is formed. A curve-fitting procedure for this situation should include the two constants from the Onsager equation for each ionic species, which makes the total number of parameters to be fitted too large for practical use.

In a significant number of cases, evaluation of the polarographic data with the Leggett [16] program showed a better fit if the M_2L species was included in the model. However, results were accepted only if the sum of the squared

errors improved significantly on the inclusion of the M_2L species without impairing the error in the log K value. An example of a data set illustrating such a situation is given in Table 2.

With regard to the missing entries under the conductometric method in Table 1, either there was no change in the specific conductance on addition of the ligand or the polarographic experiments indicated M_2L formation. Observations of the first category are in agreement with those from polarography in as much as no change in the diffusion current constant was observed when ligand was added. For the second category, the evaluation of the conductometric experiments, based on the ML or ML/ML_2 model only, was obviously incorrect and produced log K values that deviated significantly from those obtained by polarography. Generally, this situation can be recognized early by the larger values of the sum of the squared errors that are obtained in the curve-fitting procedure for these cases. For DC18C6, no reliable conductometric results could be obtained, because of the presence of a minor acidic impurity.

The systems $15C5/Pb^{2+}$, $18C6/Pb^{2+}$ and $DC18C6/Pb^{2+}$ behaved differently from the other systems investigated. In the polarographic experiments, the diffusion current constant of the waves did not change significantly, which means that the diffusion constants of the free lead ion and its complexes have about the same magnitude. During the conductometric titrations, however, the conductance changed considerably on addition of the ligands. As this cannot be attributed to a difference in the equivalent conductances of the free metal ion and its complexes, a possible explanation was sought in the occurrence of acid/base reactions accompanying the complexation reaction. Indeed, an increase of pH was found during the titration of lead(II) ion with 18-crown-6, which completely invalidates the evaluation method for the conductivity measurements of these systems. To test the influence of pH on the complexation of lead(II) in the polarographic method, the system lead(II)/18-crown-6 was rerun with 0.01 M perchloric acid added to the supporting

TABLE 2

Polarographic data for the system Pb^{2+}/dicyclohexyl-18-crown-6/0.1 M TBAP/methanol

Ligand conc. (10^{-3} M)	Lead(II) conc. (10^{-3} M)	$E_{1/2}$ (V)	Limiting current (μA)	Ligand conc. (10^{-3} M)	Lead(II) conc. (10^{-3} M)	$E_{1/2}$ (V)	Limiting current (μA)
—	0.500	−0.3038	1.290	2.830	0.472	−0.4470	1.201
0.980	0.490	−0.4300	1.211	3.704	0.463	−0.4511	1.181
1.456	0.485	−0.4377	1.217	4.128	0.459	−0.4532	1.181
1.923	0.480	−0.4412	1.211	4.546	0.455	−0.4551	1.178
2.381	0.476	−0.4442	1.202				

Model: M + L = ML and 2 M + L = M_2L. Log K_{ML} = 7.46 ± 0.01, Log β_{M_2L} = 14.2 ± 0.1, sum of square errors = 1.9×10^{-6}.

Model: M + L = ML. Log K = 7.50 ± 0.02, sum of square errors = 1.2×10^{-5}.

electrolyte. The results were not significantly different from the values obtained in the neutral supporting electrolyte: $\log K_{ML} = 7.91$ and $\log \beta_{M_2L} = 16.00$.

For the system $15C5/Cu^{2+}$, the conductometric method indicated ML_2 formation. This was not confirmed by the polarographic results. Apparently, the conductometric method is more sensitive in distinguishing the occurrence of ML_2 formation.

Conclusions

The results described show that macrocyclic polyethers form complexes with divalent cations in polar media. The combination of polarographic and conductometric methods for the determination of stability constants gives an accurate indication of the thermodynamic stabilities of the complexes formed. For the proposed application, i.e., using ligands with a co-complexed electrophile for the complexation of neutral molecules, the stabilities of the complexes are too low. Clearly, for the formation of more stable complexes, functionalized macrocyclic polyethers are required; these will be described elsewhere.

REFERENCES

1 V. M. L. J. Aarts, J. Geevers, D. N. Reinhoudt, W. Lengton, M. Bos, J. W. H. M. Uiterwijk and S. Harkema, Tetrahedron, 43 (1987) 617.
2 P. D. J. Grootenhuis, J. W. H. M. Uiterwijk, D. N. Reinhoudt, C. J. van Staveren, E. J. R. Sudhölter, M. Bos, J. van Eerden, W. T. Klooster, L. Kruise and S. Harkema, J. Am. Chem. Soc., 108 (1986) 780.
3 J. A. A. de Boer, D. N. Reinhoudt, S. Harkema, G. J. van Hummel and F. de Jong, J. Am. Chem. Soc., 104 (1982) 4073.
4 C. J. van Staveren, V. M. L. J. Aarts, P. D. J. Grootenhuis, J. van Eerden, S. Harkema and D. N. Reinhoudt, J. Am. Chem. Soc., 108 (1986) 5271.
5 V. M. L. J. Aarts, C. J. van Staveren, P. D. J. Grootenhuis, J. van Eerden, L. Kruise, S. Harkema and D. N. Reinhoudt, J. Am. Chem. Soc., 108 (1986) 5035.
6 F. A. Cotton and A. Wilkinson, Advanced Inorganic Chemistry, 4th edn., Wiley, New York, 1980.
7 R. M. Izatt, J. S. Bradshaw, S. A. Nielsen, J. D. Lamb and J. J. Christensen, Chem. Rev., 85 (1985) 271.
8 R. M. Izatt, D. P. Nelson, J. H. Rytting, B. L. Haymore and J. J. Christensen, J. Am. Chem. Soc., 93 (1971) 1619.
9 R. M. Izatt, R. E. Terry, B. L. Haymore, L. D. Hansen, N. K. Dalley, A. G. Avondet and J. J. Christensen, J. Am. Chem. Soc., 98 (1976) 7620.
10 R. M. Izatt, R. E. Terry, D. P. Nelson, Y. Chan, D. J. Eatough, J. S. Bradshaw, L. D. Hansen and J. J. Christensen, J. Am. Chem. Soc., 98 (1976) 7626.
11 H. H. Buschmann, Chem. Ber., 118 (1985) 2746.
12 D. Ph. Zollinger, Ph.D. Thesis, Twente University of Technology, 1986.
13 D. Ph. Zollinger, M. Bos, A. M. W. van Veen-Blaauw and W. E. van der Linden, Anal. Chim. Acta, 161 (1984) 83.
14 D. Ph. Zollinger, M. Bos, A. M. W. van Veen-Blaauw and W. E. van der Linden, Anal. Chim. Acta, 167 (1985) 89.
15 H. S. Gold and M. R. Rice, Talanta, 29 (1980) 637.
16 D. J. Leggett, Talanta, 27 (1980) 787.

17 Y. Marcus, Ion Solvation, Wiley, Chichester, 1985.
18 G. W. Gokel, D. M. Goli, C. Miganti and L. Echegoyen, J. Am. Chem. Soc., 105 (1983) 6786.
19 P. D. J. Grootenhuis, P. D. van der Wal and D. N. Reinhoudt, Tetrahedron, 43 (1987) 397.
20 F. de Jong and D. N. Reinhoudt, Adv. Phys. Org. Chem., 17 (1980) 279.
21 P. R. Mallinson and M. R. Truter, J. Chem. Soc., Perkin Trans. 2, (1972) 1818.
22 J. D. Lamb, R. M. Izatt, C. S. Swain, J. S. Bradshaw and J. J. Christensen, J. Am. Chem. Soc., 102 (1980) 479.
23 C. J. van Staveren, D. N. Reinhoudt, J. van Eerden and S. Harkema, J. Chem. Commun., (1987) 974, and references cited therein.
24 M. Mercer and M. R. Truter, J. Chem. Soc., Dalton Trans., (1973) 2469.

Analytica Chimica Acta, 201 (1987) 127—133
Elsevier Science Publishers B.V., Amsterdam — Printed in The Netherlands

DETERMINATION OF PICOMOLAR LEVELS OF FLAVINS IN NATURAL WATERS BY SOLID-PHASE ION-PAIR EXTRACTION AND LIQUID CHROMATOGRAPHY

SUSAN E. VASTANO*, PETER J. MILNE, WILLIAM L. STAHOVEC and KENNETH MOPPER

Rosenstiel School of Marine and Atmospheric Science, Division of Marine and Atmospheric Chemistry, University of Miami, 4600 Rickenbacker Causeway, Miami, FL 33149-1098 (U.S.A.)

(Received 6th May 1987)

SUMMARY

A method is described for the rapid determination of flavins in sea water, based on solid-phase extraction followed by ion-pair high-performance liquid chromatography (HPLC) with fluorescence detection. Riboflavin, flavin mononucleotide (FMN), and flavin adenine dinucleotide (FAD) and their photochemical breakdown products, lumiflavin, formylmethylflavin, and lumichrome can be determined with subpicomolar detection limits. The method was used at sea in the analysis of coastal and open ocean waters. In both environments, riboflavin, lumiflavin and lumichrome were routinely observed at concentrations in the picomolar range; lumiflavin and lumichrome were generally confined to the photic zone while riboflavin was present throughout the water column. Formylmethylflavin, FMN, and FAD were only occasionally observed; when present, these flavins were observed at consistently higher concentrations than riboflavin, lumiflavin and lumichrome.

Flavins are biologically and chemically important trace components of sea water. Riboflavin, flavin adenine dinucleotide (FAD), and flavin mononucleotide (FMN) play critical roles in biochemical cycles of most organisms [1]. Additionally, flavins are highly reactive photochemically and may influence the composition of sea water through photosensitized reactions involving riboflavin, FAD, and FMN and their photochemical degradation products lumiflavin, formylmethylflavin and lumichrome [2].

Owing to the biochemical importance of riboflavin, FMN, and FAD, numerous studies of these flavins in foods and beverages have been reported [3—5]. However, in the marine environment, the lack of a practical analytical method with sufficient sensitivity for quantitative studies has inhibited the study of flavins. Momzikoff [6] first reported riboflavin in sea water. This determination involved extraction of large volumes of sea water (on the order of 20 000 l), which would be impractical for routine application. More recently, Dunlap and Susic [7] reported a method for flavin analysis in sea water using HPLC. The method is sensitive and reliable, but sample prepara-

0003-2670/87/$03.50

tion is lengthy and complicated. As a result, this method is unsuitable for shipboard applications or routine work.

In this paper, a rapid, simple but sensitive method is reported for the determination of flavins in sea water, based on solid-phase extraction followed by ion-pair high-performance liquid chromatography (HPLC) with fluorescence detection. The method has been used successfully at sea on several occasions to investigate flavin distributions and photodynamic processes in the water column.

EXPERIMENTAL

Apparatus and chromatographic conditions

The liquid chromatograph used in this method consisted of an Eldex Model Chromat-A-Trol gradient controller and an Eldex Model 100A single piston pump (Eldex Laboratories, Menlo Park, CA), a Valco Model CV-6-UHPa-N60 injection valve (Valco Instrument Co., Houston, TX), and a Hewlett-Packard 100 × 4.6 Hypersil C-18 reversed-phase column with 5-μm packing. The fluorimeter was a Gilson Model 121 filter fluorimeter (Gilson Instruments, Middleton, WI) with excitation and emission wavelengths set at 305—395 nm and 435—650 nm, respectively. Results were reported on a Hewlett-Packard Model 3390A reporting integrator.

The mobile phase consisted of 4.5 mM tetrabutylammonium acetate (TBAA) in 30/70 (v/v) methanol/10 mM sodium acetate buffer, with pH adjusted to 5.80 with acetic acid. The mobile phase flow rate was 1.8 ml min^{-1} with isocratic elution. The injection loop was 200 μl.

Reagents and standards

Riboflavin, lumiflavin, lumichrome, FMN, and FAD were obtained from Sigma Chemical Company. Formylmethylflavin was prepared by periodic acid cleavage of riboflavin using the method of Fall and Petering [8]. Concentrated standards (approximately 1×10^{-4} M) were prepared in 50/50 (v/v) acetonitrile/methanol or 50/50 (v/v) water/methanol, depending on solubility. The stock solutions were diluted to 1.0 μM in 10/90 (v/v) methanol/water and stored in the dark at 4°C.

Chromatographic-grade methanol and acetonitrile were obtained from Burdick and Jackson (Muskegon, MI), chromatographic-grade sodium acetate from Baker Chemical Co., and tetrabutylammonium acetate from Fluka Chemical Co.

Sample preparation

After collection, sea water samples were stored immediately in amber or opaque bottles. Samples were concentrated by pumping 500 ml in succession through an in-line Whatman GF/C filter and a Sep-Pak C_{18} cartridge (Waters Chromatography Division) which had been pre-conditioned with 2 ml of methanol followed by 3 ml of 4.5 mM TBAA. The pump flow rate was 18 ml min^{-1} (Ismatec IPS peristaltic pump).

The concentrated sample retained on the Sep-Pak was washed with 3 ml of water to remove residual sea salts. Flavins were eluted with 1.0 ml of methanol followed by 3.0 ml of water. This procedure resulted in a concentration factor of 125. If a greater concentration factor was required, a larger initial sea water sample was used. The sample extract was stored in the dark at 4°C until injection. If the extract was to be stored for more than 48 h before injection, the 100% methanol eluate was stored with dilution to 25% methanol prior to injection.

At all stages of sample preparation, storage, and processing, care was taken to prevent exposure to light, because of the photosensitivity of some flavins.

RESULTS AND DISCUSSION

Extraction efficiency, precision and detection limits

Extraction efficiency was tested by using sea water samples spiked with flavin standards to levels allowing direct injection (0.1—1.0 nM). The average percent recovery calculated for all flavins was 104 ± 3% (Table 1). Additionally, recoveries at various pump flow rates were examined to determine the maximum feasible extraction flow rate. A noticeable drop in percent recovery was observed at flow rates above 18 ml min^{-1} (Table 2).

In order to evaluate the extraction precision, a large volume of spiked sea water was split into eight aliquots which were simultaneously extracted and processed. For all flavins except FAD, the relative standard deviation was less than 10% (Table 1). The lower precision in the determination of FAD can be attributed to difficulties in quantifying the broader FAD peak (see Fig. 1b).

The detection limits shown in Table 1 were evaluated for a signal-to-noise ratio of 3. It should be noted that these detection limits were the limits for direct injection of unconcentrated sea water. The detection limit for a concentrated sea-water sample depended on the volume of sea water extracted and the concentration of interfering fluorescent compounds (such as humic substances) in the sample.

TABLE 1

Method efficiency and precision

Flavin	Recovery (%)	Relative standard deviation (%)	Standard deviation	Detection limit (nM)
Riboflavin	100	6.47	0.65	0.32
Lumiflavin	109	2.59	0.08	0.38
Formylmethylflavin	113	5.85	0.16	2.06
FMN	100	7.27	0.23	4.50
Lumichrome	112	7.34	0.16	3.75
FAD	102	13.34	0.15	28.56

TABLE 2

Recovery as a function of extraction flow rate (6—24 ml min^{-1})

Extracted flavin[a]	Average recovery[b] (%) at different flow rates (ml min^{-1})				
	6	9	12	18	24
Riboflavin	96.7 ± 9.6	100.0 ± 14.0	102.5 ± 9.0	100.0 ± 18.6	82.5 ± 2.5
Lumiflavin	102.3 ± 8.4	115.0 ± 3.0	97.2 ± 10.3	108.8 ± 12.4	72.0 ± 4.0
Formylmethylflavin	114.7 ± 1.1	106.0 ± 10.0	102.8 ± 16.3	113.1 ± 15.2	66.0 ± 11.0
Lumichrome	102.0 ± 7.3	104.5 ± 11.5	102.0 ± 11.5	111.5 ± 7.5	74.0 ± 30.0
FMN				101.0 ± 4.5	
FAD				102.3 ± 6.1	

[a]200 ml of sea water was extracted. Samples were spiked with 0.1 nM riboflavin, lumiflavin and formylmethylflavin, and 0.3 nM lumichrome, and (in the 18 ml min^{-1} sample) with 0.4 nM FMN and 0.8 nM FAD. 200 ml of unspiked sea water was extracted at each flow rate. [b]$n = 3$.

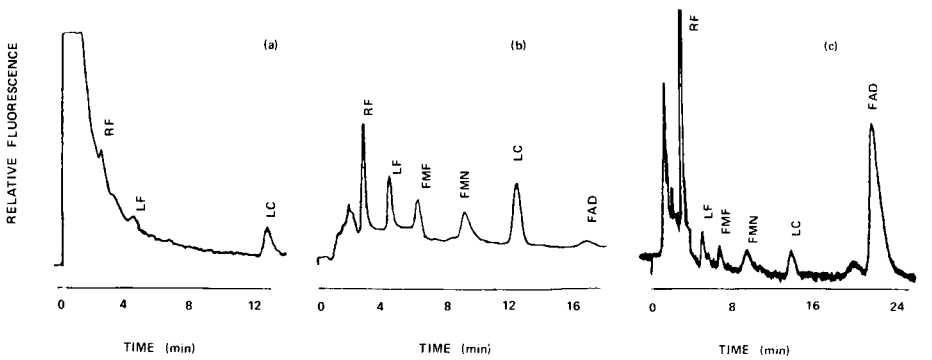

Fig. 1. The effect of the addition of the ion-pairing agent to the mobile phase, and application in the analysis of natural samples: (a) Biscayne Bay water extracted and processed without ion-pairing; (b) Biscayne Bay water spiked with flavin standards, extracted and processed with ion-pairing; (c) Sargasso Sea water (150 m) processed with ion-pairing. Peaks: RF, riboflavin; LF, lumiflavin; LC, lumichrome; FMF, formylmethylflavin.

Optimization of the ion-pairing agent

The addition of an ion-pairing agent to the mobile phase had two important effects: a flattening of a large interference peak (presumably humic substances) that eluted at the beginning of the run, and an increase in the retention times of the ionic species FMN and FAD. Without this increase in retention time, FMN and FAD eluted near the system dead volume and were not quantifiable. Additionally, without flattening of the early eluting interference peak, flavins eluting near the beginning of the run could not be accurately quantified (see Fig. 1a).

Several quaternary ammonium salts were tested as ion-pairing agents. Addition of tetrabutylammonium acetate (TBAA) at concentrations of 2.0

mM to 5.0 mM provided the desired increase in retention times and flattening of the interference peak (Fig. 1b). It should be noted that the optimum concentration of TBAA, i.e., the concentration that gave the best separation with an acceptable run time, varied with the make of reversed-phase column used. It is important, therefore, to optimize the concentration of TBAA for each system.

Comparison of filtered and unfiltered samples

Tests were done to establish the effect of filtration on the extraction procedure. Samples of sea water enriched with a variety of marine bacteria and phytoplankton were split into two aliquots, one of the aliquots was filtered, and both were analyzed (Table 3). While lumiflavin and lumichrome appeared to be unaffected by filtration, a slight decrease in the concentration of riboflavin was consistently observed in filtered samples. The magnitude of this effect increased slightly with decreasing filter pore size, suggesting that the decrease in flavin concentration was due to removal of particles from the water sample (Table 4). However, even for the smallest filter pore-size, this effect was small; thus, it may be inferred that flavins in sea water are predominantly in the dissolved form.

Pteridines

Pteridines are a class of compounds closely related to the flavins. To establish if the pteridines interfere with the flavin chromatography (e.g.,

TABLE 3

Effect of filtration on determination of flavins in sea water[a]

Run	Filter pore size (μm)	Flavin	Concentration (pM)		Difference (%)
			Unfiltered	Filtered	
1	0.2	RF	440	390	−13
		LF	20	21	+5
		LC	85	94	+9
2	0.2	RF	52	42	−19
		LF	29	32	+9
		LC	79	78	−1
3	0.7	RF	780	720	−8
		LF	16	15	−6
		LC	77	80	+4
4	0.7	RF	780	670	−13
		LF	9	8	−9
		LC	83	78	−7

[a]Sea water enriched with marine bacteria; water held in dark cabinet for 1 week, then irradiated for 90—120 s to photodegrade riboflavin (RF) partially to lumiflavin (LF) and lumichrome (LC).

TABLE 4

Effect of filtration on observed flavin concentrations: extraction of particulates collected through filtration of sea-water[a] samples

Run	Filter pore size (μm)	Observed concentration (pM)				Difference[b] (%)
		Unfiltered water	Filtered water	Extracted particles	Filtered + particulate	
1	0.2	440	390	89	479	+8
2	0.2	52	42	18	60	+13
3	0.7	780	720	200	920	+15
4	0.7	780	670	180	850	+8

[a]See footnote to Table 3. [b]Percent difference between riboflavin concentration in unfiltered water and in filtered water plus extracted particulates.

through co-elution) or if any of a number of unknown compounds found in natural samples were pteridines, standards of several common pteridines were run under the same chromatographic conditions used for flavins. The standards run included pterin, pterin-6-carboxylic acid, xanthopterin, isoxanthopterin, and lumazine. In all cases, the pteridines eluted near the system dead volume.

Analysis of natural samples

Samples were collected at coastal and open ocean sites. A chromatogram of a natural water sample is shown in Fig. 1c. Riboflavin, lumiflavin, and lumichrome were found at all sampling areas although lumiflavin and lumichrome were generally confined to the photic zone. Riboflavin and lumiflavin were generally found at concentrations ranging from 2 to 20 pM while lumichrome was generally found at 20—200 pM. These values are similar to the values reported by Momzikoff [6] and Dunlap and Susic [7]. Formylmethylflavin, flavin mononucleotide, and flavin adenine dinucleotide were observed at few locations. When observed, however, their concentrations were usually somewhat higher than those of other flavins (on the order of 100—1000 pM).

Our field studies have demonstrated that flavins generally follow several major trends which can be explained in terms of their biological and photochemical activities. As would be expected, flavins were found at higher concentrations in more biologically active areas such as coastal areas or biologically active depths in the water column in the open ocean. Additionally, flavins display a distinct diurnal variation, with concentrations highest during dark hours (as would be predicted by their photochemical behavior [2]). However, these were general trends only, and several deviations were observed. Details of field studies will be presented in separate publications.

This work was supported by a grant from the National Science Foundation (Grant No. OCE-8517041), with some ship time supported by National

Science Foundation Grant No. OCE-8411781 and Office of Naval Research Grant No. N0014-85-C-0020.

REFERENCES

1 A. L. Lehninger, Biochemistry, Worth Publishers, New York, 1975.
2 R. G. Zika and W. J. Cooper (Eds.), Photochemistry of Environmental Aquatic Systems, American Chemical Society, Washington, DC, 1987, p. 174.
3 A. E. Watada and T. T. Tran, J. Liquid Chromatogr., 8 (1985) 1651.
4 J. Augustin, J. Assoc. Off. Anal. Chem., 67 (1984) 1012.
5 J. F. Kamman, T. P. Labuza and J. J. Warthesen, J. Food Sci., 45 (1980) 1497.
6 A. Momzikoff, Cah. Biol. Mar., 10 (1969) 221.
7 W. C. Dunlap and M. Susic, Mar. Chem., 17 (1985) 185.
8 H. H. Fall and H. G. Petering, J. Am. Chem. Soc., 78 (1956) 377.

Analytica Chimica Acta, 201 (1987) 135—144
Elsevier Science Publishers B.V., Amsterdam — Printed in The Netherlands

TRANSPORT BEHAVIOUR OF WATER AND NITRIC ACID IN TRIBUTYL PHOSPHATE/n-DODECANE MIXTURES

V. FRIEHMELT*, A. HE[a], Z. YANG[a] and G. MARX

Institut für Anorganische und Analytische Chemie, Forschungsgruppe Radiochemie, Freie Universität Berlin, Fabeckstrasse 34—36, 1000 Berlin 33 (Federal Republic of Germany)

(Received 30th April 1987)

SUMMARY

The diffusion coefficients of water and nitric acid in different mixtures of tributyl phosphate (TBP)/n-dodecane were measured with the aid of an analytical ultracentrifuge, in order to elucidate the transport behaviour in the organic phase of the PUREX process. Measurements were made at 298 K for different solute concentrations, the TBP content of the organic solutions being varied from pure TBP to a 30/70 (v/v) TBP/n-dodecane mixture. The Stokes' radii and the molecular volumes of the solute particles were evaluated for each system from diffusion coefficients and viscosity by an approximate method based on Stokes' law. Comparisons of the molecular volumes obtained from diffusion with those from density measurements showed that, in the presence of n-dodecane, aggregates of the particles are formed, which consist of water and nitric acid bound to TBP molecules. In pure TBP, however, the diffusion of water was faster, indicating that the molecules then move separately by a slipping mechanism.

In the industrial application of extraction processes, significant effort is dedicated to mathematical modelling of the mass transfer in order to achieve improvement of quality, safety and economy by process control [1]. Separation techniques have been widely applied to the recovery and purification of valuable heavy metals. Special emphasis has been placed on tributyl phosphate (TBP) acting as extractant, for example, in the PUREX process. Quite a lot of distribution data are available, which are taken into account for modelling such systems, but when the calculations are considered in detail, additional complications may arise from the different species present in the organic phase. The nature and transport behaviour of these species, significantly influencing the chemical kinetics, have to be characterized to predict accurately the mass transport from a thermodynamic point of view [2, 3].

The extraction of nitrates from aqueous nitric acid solutions is based on the formation of complexes with TBP, but a considerable affinity of the organic phase for water and nitric acid itself must also be considered. Because the complexes are undissociated in the organic solutions, solubility

[a]Permanent address: Fudan University, Shanghai, People's Republic of China.

0003-2670/87/$03.50

experiments give evidence for a monohydrate TBP·H_2O and a similar complex with nitric acid, TBP·HNO_3 [4, 5]. In the saturated systems, the introduction of nitric acid into the receiving phase is accompanied by replacement of an equivalent of water initially bound to TBP, indicating stronger hydrogen bonding of the nitric acid to the polar P=O group of the extractant [6, 7]. In addition to the competition between water and nitric acid for the available TBP molecules, there has been considerable interest, and even controversy, as to whether or not separate species or hydrated complexes actually exist. In the interpretation of the experimental data from H-NMR and infrared spectroscopy, discrepancies have appeared favouring an explanation of the results in terms either of linear and ring polymers of varying complexity or of monomer species with quite weak or even repulsive interactions [8, 9].

The present investigations of density and viscosity were initiated in order to provide information about the interactions between the solvent and the solute. Because the measurements were made at different concentrations, the manner in which the viscosity of the organic solutions varied was described by the viscosity *B*-coefficient of the Jones—Dole equation [10]. From the change in density, the molar volumes could be obtained by extrapolation. The empirical equations obtained will facilitate accurate determination of the composition of the organic solutions if either the water content or the nitric acid concentration is known. Because the TBP extractant in technological applications is diluted with hydrocarbons, the influence of n-dodecane added in different quantities was examined. In these mixtures, however, the reduced solubility of water and nitric acid implies a narrower concentration range, because a deviation from ideal behaviour in the saturated solutions has commonly been accepted [11]. From the transport behaviour, monitored by use of the optical systems of the analytical ultracentrifuge, both the tendency of the solute species to form complexes and the size of the moving particles were estimated. Thus, by interpretation of the diffusion coefficients in terms of the Stokes' radius, an attempt was made to elucidate the underlying chemical mechanism of transport in the organic systems.

EXPERIMENTAL

Preparation of mixtures

The organic mixtures were prepared gravimetrically by weighing definite quantities of TBP, n-dodecane, and water or aqueous nitric acid. The chemicals used were of analytical-reagent grade. Because the preparation of water-free organic solutions of nitric acid was found to be impossible, the concentration of the nitric acid in the aqueous standard solutions was varied to allow investigation of the individual behaviour of water and nitric acid by extrapolation. The amount of aqueous solution added was kept below saturation, so that titration of the organic solutions was not necessary. The water content in the organic mixtures was monitored by H-NMR spectrometry with a Jeol FX-90-Q spectrometer [12].

The concentrations were also determined precisely by density measurements, which were made with a digital densitometer (Paar KG, type DMA). The data were accurate to the fifth decimal place; air and twice-distilled water were used for calibration. This procedure was checked by comparing the data of the pure solvents with literature values [1]. The organic solutions were measured directly after finishing the preparation in order to avoid degradation of TBP by reaction with nitric acid.

Viscosities were measured with a Schott AVS instrument and a calibrated Ubbelohde-type viscometer. The values of the viscosity η were calculated from the flow times and densities.

Methods

A Beckman Model E analytical ultracentrifuge was used. The transport behaviour of the solute molecules was recorded by means of the optical systems. All measurements were made in a cell containing a capillary-type centrepiece. The two compartments of the centrepiece could be filled separately. For the diffusion measurements, one sector was filled with 0.12 ml of the organic solution, and the other sector with 0.36 ml of the organic solvent. The cell was fitted carefully into a titanium rotor and accelerated to a final measurement velocity of 5.200 rpm. The temperature of the rotor was detected and controlled at (25.00 ± 0.01)°C by a thermistor unit. At a velocity of 1000 rpm, the solvent was pressed through the capillary into the solute sector, creating a sharp boundary.

The light beam passing through the cell was deflected by refraction at the boundary. Because it was shown that the refractive index is a linear function of the water concentration, the Schlieren optical system provided a plot of the actual change in concentration between the solvent and the solution [1]. The photographic images obtained at preselected intervals were transmitted by an electronic camera to a bit-plane processor. The values of the height and the area of the Schlieren peaks were evaluated by a Pattern Considering System and stored in a command-protocol data set [13]. By means of the ultraviolet optics, the concentration profiles of the nitric acid were obtained by plotting the absorbances at 350 nm versus the distance from the axis of rotation. The diffusion coefficients were calculated in the usual way from the height and the area of the Schlieren peaks, and the patterns were recorded by the ultraviolet system at different times during the run [14, 15]. Because both optical systems were used simultaneously, the absorption optics showed the transport of the nitric acid, while the Schlieren optical system presented the sum of the diffusion of nitric acid and water. The error of the results was ±3%, or less for high concentrations.

RESULTS AND DISCUSSION

Density

Quantitative description of the organic solutions by analytical methods is needed to predict the composition and behaviour as a function of the degree

of saturation with water and nitric acid [16]. Previous results have already led to applications of density measurements by in-line instrumentation to achieve effective quality control during the extraction process. Sets of data were obtained for various solutions of water and nitric acid in pure TBP (Table 1). The accuracy of this method is quite satisfactory and in agreement with other techniques, yielding a linear relation between the concentration, c, of the solute and the density, ρ_3, of the solution:

$$\rho_3 = \rho_1 + m\,c$$

where the value ρ_1 is attributed to the density of the organic solvent mixture at zero solute concentration. In order to characterize the different organic mixtures, the density coefficients (m) are given in Tables 2 and 3. Because of the linear increase, the density of any solution can be calculated up to rather high concentrations. The density coefficients given in the tables are valid when considering either water or aqueous nitric acid as the solute, and can be converted by the relevant molecular weights if other species (e.g., $H_2O \cdot TBP$) are assumed to be present in the solutions.

The density measurements are also an effective means of gaining insight into the structure of the solutions, because the density coefficient, m, can be related to the partial specific volume, V^*, of the solute species: $m = 1 - V^* \rho_0$. In the mixed organic solvents, the density ρ_0 of pure TBP (the extractant) has to be taken into account, because the n-dodecane (diluent) has a negligible tendency to dissolve in water. From the specific volume, V^*, the density of the dissolved species, $\rho^* = 1/V^*$, can be calculated. If the volume of the TBP molecules is assumed to be constant, the hypothetical densities obtained for water and nitric acid in TBP will be higher than the densities, ρ_2, of water and of the pure aqueous nitric acid stock solutions given in Table 2. A similar volume contraction was also observed in saturated solutions. This feature seems to support the existence of a $H_2O \cdot TBP$ compound or at least interactions that cannot be neglected. The values of the density coefficient increase systematically as the content of dodecane in the

TABLE 1

Viscosity and density of solutions with varying contents of water and 10.0 M nitric acid in TBP

Solute: H_2O					
$c \times 10^2$ (g cm^{-3})	0.482	0.986	1.565	2.635	5.026
ρ (g cm^{-3})	0.97285	0.97307	0.97335	0.97389	0.97500
η (mPa s)	3.360	3.400	3.450	3.551	3.817
η_{sp}/c (g^{-1} cm^3)	1.93	2.16	2.32	2.53	2.91
Solute: 10.0 M HNO_3					
$c \times 10^2$ (g cm^{-3})	0	0.505	0.991	1.434	1.886
ρ (g cm^{-3})	0.97268	0.97375	0.97464	0.97556	0.97644
η (mPa s)	3.329	3.357	3.405	3.468	3.516
η_{sp}/c (g^{-1} cm^3)	—	1.66	2.30	2.91	2.97

TABLE 2

Viscosity coefficients (A and B) and density coefficient (m) of water and nitric acid in TBP, and density (ρ) of the stock solutions

Solute	ρ_2 (g cm^{-3})	B (cm^3 g^{-1})	A	m
H_2O	0.99708	3.44	−0.13	0.047
3.0 M HNO_3	1.09545	4.08	−0.17	0.102
5.0 M HNO_3	1.15764	4.35	−0.18	0.130
10.0 M HNO_3	1.29325	4.31	−0.21	0.199
14.6 M HNO_3	1.38738	4.39	−0.21	0.250

TABLE 3

Viscosity coefficients (A and B) and density coefficient (m) of water and 10.0 M nitric acid in the solvent systems

TBP/$C_{12}H_{26}$	Water			10.0 M HNO_3		
	B (cm^3 g^{-1})	A	m	B (cm^3 g^{-1})	A	m
90/10	3.59	−0.15	0.054	5.25	−0.28	0.249
80/20	4.31	−0.11	0.066	5.45	−0.27	0.265
70/30	4.84	−0.08	0.107	5.65	−0.24	0.272
60/40	5.39	−0.14	0.132	5.93	−0.22	0.287
50/50	6.25	−0.10	0.161	6.62	−0.28	0.298
30/70	7.11	−0.12	0.135	7.67	−0.26	0.307

organic mixtures is increased. In the same way, the density of the solute particles will increase, while the partial specific volume decreases. This behaviour shows that the interactions between TBP and water are even stronger in the presence of the diluent.

In order to elucidate the mechanism, the volume of a single molecule, V_2, can be expressed in terms of the partial specific volume, V^*, and Avogadro's constant, N_A, if the molecular weight, M, of the relevant species is known: $V_2 = M\,V^*/N_A$. Because species in solution cannot be distinguished by density measurements alone, different volumes will be obtained depending on the molecular weight of the assumed particle. For a single water molecule, the volume derived is 0.029 nm^3, whereas the volume of the $H_2O{\cdot}$TPB complex is 0.484 nm^3, or 0.968 nm^3 for the dimer $(H_2O{\cdot}TPB)_2$. In order to decide which species predominates, other analytical methods are needed, e.g., diffusion measurements.

H-NMR spectrometry

Proton magnetic resonance provides a very fast and precise method for determining the water content of organic solutions. The chemical shift of

the water proton resonance depends linearly on the concentration. In the presence of nitric acid, however, the peak is shifted to a much lower field and only one signal is obtained for the protons of water and nitric acid; this method is thus limited to the detection of water in acid-free solutions. The appearance of a single, sharp resonance for the water protons indicates a rapid exchange of any co-existing species. Interpretation of the chemical shift in terms of strong bonding, combined with polymerization in pure TBP and the tendency of diluents to break up the bonds assumed by Bullock and Tuck [8], is contradicted by the density measurements. Quite a different mechanism was confirmed by solubility experiments. As the content of diluent increases, water is expelled from the organic phase, but the interactions between water and the TBP molecules increase. In the presence of some inorganic salts, however, the diluent may even be expelled from the organic solution to form a third phase, while water remains in the TBP layer.

Viscosity

Viscosity measurements are another means of gaining insight into the structure and transport properties of the solutions. When water or nitric acid is added to the organic solutions, there is a significant increase in the viscosity, which may even produce a large increase in the specific viscosity η_{sp}/c. The viscosities, η, calculated from the experimental flow times and densities, are shown in Table 1 as a function of the water or nitric acid concentration. The relative change in viscosity can be fitted by the Jones–Dole equation [10]:

$$\eta/\eta_0 = 1 + A^{1/2} c + Bc$$

The coefficient, A, of this semi-empirical equation is the contribution from forces between the species that tend to interfere with the flow of solution. The B-coefficient is related to the size of the particles and their effects on the structure of the solvent. The viscosity values obtained for each solvent system showed that the solutions can be characterized by the coefficients A and B given in Tables 2 and 3. The solvent viscosities, η_0, are presented in Table 4.

Similar behaviour was observed for all the TBP/n-dodecane solutions, and by use of the empirical equations the viscosity of any solution can be approximated. The positive B-coefficients indicate that the behaviour of water and nitric acid in the solutions has to be described as that of a "structure maker" [17]. This influence is quite strong in pure TBP and even increases if n-dodecane is present. In these organic systems, interpretation of the B-values does not suffice to obtain the effective volume of the solute molecules, because it is difficult to separate the size effect from the structural effect of the different species in the solvent mixtures. A similar structure-making effect was found for uranyl nitrate in trialkyl phosphate solutions [18]. The viscosity A-coefficients in those systems, however, were quite close to zero, because interactions between the complex particles were negligibly weak.

TABLE 4

Diffusion coefficient (D_0) and Stokes' radius (r) of 10.0 M nitric acid, and viscosity and density of the solvent mixtures

TBP/$C_{12}H_{26}$	η_0 (mPa s)	ρ (g cm^{-3})	$D_0 \times 10^6$ (cm^2 s^{-1})	r (nm)
100/0	3.329	0.97268	1.94	0.338
90/10	2.861	0.94211	1.69	0.452
80/20	2.498	0.91465	1.30	0.672
70/30	2.208	0.88875	1.26	0.785
60/40	1.993	0.86276	1.19	0.921
50/50	1.825	0.84081	0.95	1.259
30/70	1.564	0.79871	0.89	1.568

Diffusion

The incorporated equipment and standard assembly of the cells of an analytical ultracentrifuge permit a precise determination of the diffusion coefficients. The application of this technique is restricted, however, by the difficult and time-consuming procedure. The centrifugal force provides overlaying of two solutions of different solute concentration, avoiding turbulence at the boundary. The movement of the particles caused by the concentration gradient is monitored by the optical systems. The optical patterns showed that no sedimentation effects were interfering with the transport phenomena, because a low rotor speed was used. The evaluation of the optical patterns and the validity of Fick's law in obtaining the diffusion coefficients has been discussed in detail [16].

With respect to the distribution of the solute particles, the concentration, c, in the boundary remained constant during the measurement. Therefore, the diffusion coefficients, D, were evaluated as a function of this concentration, which was calculated from $(c_1 + c_0)/2$, where c_1 and c_0 are the concentrations of the water or nitric acid in the top and bottom organic solutions, respectively. The diffusion coefficients of water in pure TBP obtained with the Schlieren optical system are given in Table 5. The values at high concentrations of water are in accord with the value $D = 4.51$ cm^2 s^{-1} obtained by Michaeli and Kedem [19], who used tracer techniques in water-saturated TBP. The results show that the diffusion coefficients of water depend only slightly on the concentration of water.

The diffusion coefficients of aqueous nitric acid in TBP are presented in Fig. 1. In these systems, the difficulty of the determination increases with the number of components. The simultaneous use of two optical systems, however, facilitated the study of the transport behaviour. The absorption measurements provided the diffusion coefficient of the species containing the nitric acid. The D values of nitric acid appeared to be independent of the concentration. With the Schlieren optics, a sum of diffusion coefficients was evaluated, which is attributed to all species of water and nitric acid present

TABLE 5

Diffusion coefficients (D) of water in TBP

$c \times 10^2$ (g cm^{-3})	0.25	0.37	0.80	1.04	1.19	1.35
$D \times 10^6$ (cm^2 s^{-1})	4.72	4.70	4.68	4.66	4.69	4.62

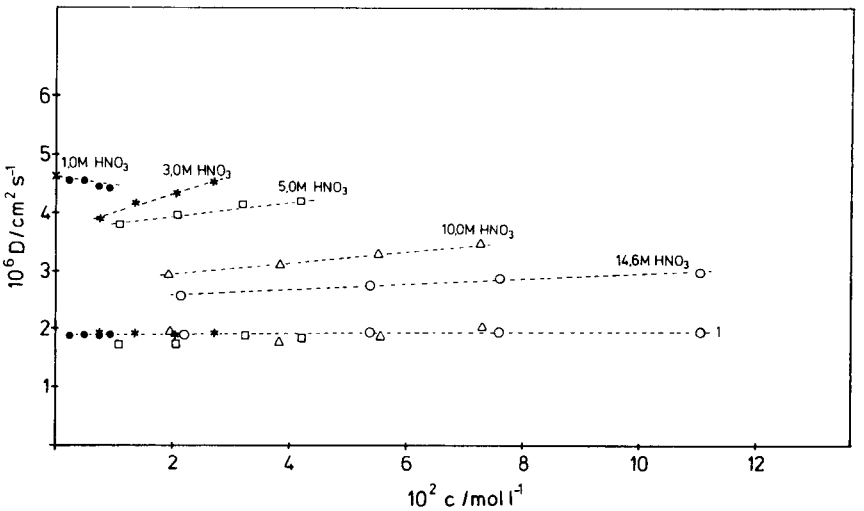

Fig. 1. Diffusion coefficient of H_2O/HNO_3 in TBP measured with both optical systems. Line 1 was obtained for HNO_3 with the absorption optical system; all other points were obtained with the Schlieren optical system.

in the organic mixture. Those values decreased as the H_2O/HNO_3 ratio decreased, but they were always higher than the diffusion coefficients obtained with the absorption optics. The interpretation of the Schlieren optical results is difficult in a multicomponent system; it requires knowledge of the contribution of the nitric acid species to the refractive index in order to determine accurately the diffusion coefficient of water. Nevertheless, it can be estimated that the diffusion coefficient of water is about twice that of nitric acid. In spite of the faster diffusion of water, no interference with that of the nitric acid is apparent from Fig. 1, which indicates separate transport of the different species.

The measurements were made at different concentrations to allow extrapolation of the diffusion coefficients obtained at finite concentrations to those valid at infinite dilution. Because the data were only slightly dependent on the concentration, or even independent of it, activity coefficients were not taken into consideration. It was implicitly assumed that the laws of dilute solutions are obeyed, thus obtaining the D_0 value, which depends only on the absolute temperature, T, of the system and the frictional coefficient,

f, of the solute molecule in the pure solvent [20]: $D_0 = kT/f$. In the usual derivations of Stokes' law, the frictional coefficient is related to the radius, of a sphere, moving through a medium of viscosity, η_0 [21]: $f = 6\pi\eta_0 r$. For experiments at the same temperature, T, the values of the diffusion coefficients in different systems are commonly compared by taking the solvent viscosity, η_0, into consideration. The validity of the equation has been proved for many different systems, and Stokes' law has often been used to describe the diffusion of molecules having dimensions comparable to those of the solvent molecules [18, 21]. The values of the diffusion coefficients, D_0, extrapolated to infinite dilution are listed in Tables 4 and 6. As can be seen from Table 4, the viscosity of the organic mixtures varies by a factor of 2. The values of the diffusion coefficients, however, decrease if dodecane is present in the solutions, and the viscosity becomes less.

Molecules offer a considerable resistance to transport. Therefore, from the frictional coefficient of the solute, a correlation is available for describing behaviour in solutions by use of the Stokes' radius. For the calculation of this parameter, it is assumed that the particles are spherical, in order to provide a kind of submicroscopic picture of the solution. The Stokes' radius, of course, is not the best representation of molecular dimensions, but it serves for comparing similar species, because the physical behaviour and chemical properties of the organic solutions depend predominantly on the characteristics of individual solute molecules. A systematic increase of the r values can be seen in Tables 4 and 6, as the content of n-dodecane is increased in the organic mixtures. Therefore, it is reasonable to regard a change to larger units of the species in such solutions.

The diffusion measurements for water with the Schlieren optical system permit evaluation of Stokes' radius and so calculation of the volume, V, of the sphere. The volumes given in Table 6 for each organic mixture should correspond to the volume of the solute particle obtained by the density measurements. Although the diffusion experiments were done at low rotor speeds, the effect of pressure must be taken into account in the organic

TABLE 6

Diffusion coefficient (D_0), Stokes' radius (r) and volume (V) of water in TBP/dodecane mixtures

TBP/$C_{12}H_{26}$	$D_0 \times 10^6$ ($cm^2\ s^{-1}$)	r (nm)	V (nm^3)
100/0	4.74	0.138	0.011
90/10	1.90	0.402	0.271
80/20	1.62	0.539	0.658
70/30	1.45	0.682	1.328
60/40	1.30	0.843	2.506
50/50	1.26	0.949	3.585
30/70	1.16	1.203	7.299

solutions, causing lower values of the volumes. Furthermore, accurate values for the particle volumes cannot be expected by this procedure, because the molecules are not ideal spheres. Despite that fact, a significant change of the water species as a function of the solvent composition is evident from the results. The small volume in pure TBP indicates that free water molecules are the predominant species in that solvent, the particles moving by a slipping mechanism. For the nitric acid species, however, the larger Stokes' radius indicates an increased tendency to form the 1:1 complex with TBP, which complex moves separately from the water. This phenomenon also proves the mechanism based on the assumption that the species are unsolvated particles.

In the presence of dodecane, the interpretation becomes more difficult because there is no uniquely defined species to be detected, but a mixture of the 1:1 complex, the 1:2 complex ($H_2O \cdot 2TBP$) and the aggregates. The fraction of uncomplexed water can be neglected if the content of dodecane is raised to 40%, whereas the amount of the dimeric species is increased. It should be mentioned, however, that such complexes are less stable than complexes of inorganic salts, e.g., $UO_2(NO_3)_2 \cdot 2TBP$. In the presence of higher concentrations of dodecane, the data refer to larger aggregates or even polymeric structures as can be seen from Table 6. For the nitric acid species, similar behaviour becomes obvious from Table 4. These results confirm the information, obtained from the density and viscosity measurements, that the interactions between water or nitric acid and the extractant TBP become stronger in the presence of diluent.

We thank the Bundesministerium für Forschung und Technologie, Bonn for financial support.

REFERENCES

1 W. Davis, Jr., J. Mrochek and C. J. Hardy, J. Inorg. Nucl. Chem., 28 (1966) 2001.
2 W. H. Baldwin, C. E. Higgins and B. A. Soldano, J. Phys. Chem., 63 (1959) 118.
3 K. Alcock, S. S. Grimley, T. V. Healy, J. Kennedy and H. A. McKay, Trans. Faraday Soc., 52 (1956) 39.
4 E. Hesford and H. A. C. McKay, J. Inorg. Nucl. Chem., 13 (1960) 156.
5 T. V. Healy and H. A. C. McKay, Trans. Faraday Soc., 52 (1956) 633.
6 J. W. Roddy, J. Inorg. Nucl. Chem., 40 (1978) 1787.
7 A. Apelblat and A. Hornig, Trans. Faraday Soc., 63 (1967) 185.
8 E. Bullock and D. G. Tuck, Trans. Faraday Soc., 59 (1963) 1293.
9 A. L. Mills and W. R. Logan, J. Inorg. Nucl. Chem., 26 (1964) 2191.
10 G. Jones and M. Dole, J. Am. Chem. Soc., 51 (1929) 2950.
11 J. W. Roddy and J. Mrochek, J. Inorg. Nucl. Chem., 28 (1966) 3019.
12 B. B. Murray and R. C. Axtmann, Anal. Chem., 31 (1959) 450.
13 D. Vollath, R. Friehmelt, A. Nasraoui, J. Pecht and P. Stiller, Umschau, 86 (1986) 90.
14 L. J. Gosting, Adv. Protein Chem., 11 (1956) 429.
15 H. K. Schachman and S. J. Edelstein, Biochemistry, 5 (1966) 2681.
16 D. G. Tuck, J. Chem. Soc., (1958) 2783.
17 D. G. Tuck, Trans. Faraday Soc., 57 (1961) 1297.
18 V. Friehmelt, A. He, Z. Yang and G. Marx, Inorg. Chim. Acta, 111 (1986) 89.
19 G. Michaeli and O. Kedem, Desalination, 8 (1970) 359.
20 A. Polson, Kolloid-Z., 88 (1939) 51.
21 R. H. Stokes, P. J. Dunlop and J. R. Hall, Trans. Faraday Soc., 49 (1953) 886.

Analytica Chimica Acta, 201 (1987) 145—151
Elsevier Science Publishers B.V., Amsterdam — Printed in The Netherlands

ESSAIS EN AUTOCLAVE DE FLACONS DE VERRE A USAGE PHARMACEUTIQUE

Comparaison des analyses des ions passés en solution et des profils de concentration des surfaces de verre testées

P. LEHUEDE et J. L. ROUSSEAU

Saint-Gobain Recherche, 39 Quai Lucien Lefranc, 93304 Aubervilliers (France)

V. BISSERY, D. BAYLOCQ et F. PELLERIN*

Laboratoire de Chimie Analytique, Faculte de Pharmacie, Université de Paris XI, Rue Jean-Baptiste Clément, 92290 Chatenay Malabry (France)

(Reçu le 22 avril 1986)

SUMMARY

(*Autoclave testing of glass bottles for pharmaceutical use. Comparison of the amounts of leached ions and the depth profiles of glass surfaces.*)

The behaviour in autoclave testing (French Pharmacopoeia) of bottles made from borosilicate glass (class I), surface-treated soda-lime glass (class II) and untreated soda-lime glass (class III) is compared. Several (6—10) elements were determined by wet-chemical methods in the autoclave solutions. The results are compared with surface data obtained by secondary-ion mass spectrometry (SIMS) before and after the autoclaving. The SIMS profiles show that autoclaving of class I and II glasses scarcely modifies the surfaces of these glasses whereas class III glass is attacked to a depth of ca. 40 nm. The surface treatment with ammonium sulphate is shown to be efficient in reducing the diffusion of ions from the glass surface to the leaching solution. The validity of the hydrolytic resistance test given in the French Pharmacopoeia is confirmed.

RESUME

Les analyses chimiques effectuées sur les autoclavats et les études de surface réalisées par la méthode SIMS sur des verres des différentes classes de la Pharmacopée Française permettent de confirmer la résistance hydrolytique élevée des verres de types I et II et de montrer l'efficacité du traitement de désalcalinisation pratiqué industriellement pour les verres de type II. Les profils SIMS mettent en évidence que la surface interne du verre n'est pratiquement pas modifiée pour les verres de classes I et II alors que dans le cas des verres III (sodocalciques ordinaires) la désalcalinisation est observée sur une profondeur de 40 nm environ.

Une propriété très importante pour les flacons en verre, spécialement ceux à usage pharmaceutique, est leur aptitude à résister à l'attaque lors d'un contact prolongé avec un liquide. Ainsi une normalisation selon l'essai Codex de résistance hydrolytique (Pharmacopée Française, 10ème édition, 1983) permet de distinguer les flacons de classe I (qui intrinsèquement ne relarguent pratiquement pas d'ions après contact d'une heure avec de l'eau à 121°C),

0003-2670/87/$03.50

des flacons de classe II (qui parviennent à un résultat voisin grâce à un traitement de surface ayant généralement pour but de désalcaliniser la surface) et des flacons de classe III (qui au contraire relarguent une quantité mesurable d'ions lors du même test, ce qui est le cas par exemple pour les compositions sodocalciques classiques).

L'essai qui permet de classer les verres consiste à porter, dans un autoclave, le flacon à tester, rempli aux 9/10èmes d'eau distillée, pendant 1 h à 121°C avec une montée de 100 à 121°C de 20 min et une descente de 121 à 100°C de 40 min. Après refroidissement on dose l'alcalinité par ajout d'acide chlorhydrique 0,01 M jusqu'au virage du rouge de méthyle, et c'est cette valeur qui est prise en compte pour le classement, suivant la capacité du flacon. Toutefois, pour une meilleure compréhension des phénomènes intervenant lors de l'attaque hydrolytique du verre, il peut être intéressant d'étudier la nature et la quantité des ions qui passent en solution, et également la composition de la surface du verre après attaque par l'eau.

COMPARAISON DES DIFFERENTES METHODES D'ANALYSE DE LA COMPOSITION SUPERFICIELLE DU VERRE

Il existe plusieurs techniques analytiques permettant d'établir un profil de concentration en profondeur à partir de la surface du verre. L'attaque chimique partielle à l'acide fluorhydrique et analyse chimique des ions ainsi extraits du verre est toutefois longue et délicate à mettre en oeuvre à cause de la faible quantité d'ions à doser; de plus on maîtrise souvent mal l'épaisseur analysée. On peut, par XPS (x-ray photoelectron spectroscopy) obtenir la composition d'une couche superficielle de quelques nanomètres. En associant un décapage ionique, on peut donc tracer des profils en profondeur. L'étalonnage en profondeur est parfois difficile à établir et les manipulations sont un peu longues. L'analyse spectroscopique Auger offre des similitudes avec le XPS, mais l'utilisation d'un faisceau d'électrons comme source excitatrice apporte une difficulté supplémentaire dans le cas des isolants: l'accumulation de charges en surface. En utilisant les réactions nucléaires résonantes, en suivant le produit d'une réaction nucléaire entre un ion de l'échantillon et une particule incidente de haute énergie, on peut remonter à la concentration de cet ion; si on fait varier l'énergie de la particule incidente, on peut obtenir une variation de la concentration de l'ion avec la profondeur. Cette technique, très intéressante en particulier dans le cas de l'hydrogène, est très lourde à mettre en oeuvre: il faut utiliser un accélérateur d'ions de haute énergie.

Dans la méthode SIMS (secondary-ion mass spectrometry), on bombarde la surface de l'échantillon avec des ions d'énergie faible (quelques keV); ces ions pulvérisent les couches les plus superficielles de l'échantillon et les ions ainsi extraits sont analysés à l'aide d'un spectromètre de masse. On peut donc obtenir, en fonction du temps, donc de la profondeur, un signal qui est fonction de la concentration de l'ion étudié. Cette technique est donc bien

adaptée à l'obtention des profils en profondeur. Tous les ions peuvent être analysés, ainsi que les isotopes; la sensibilité est très variable d'un élément à l'autre, mais elle est généralement grande (la limite de détection est souvent meilleure que la partie par million). C'est cette technique qui a été employée.

PARTIE EXPERIMENTALE

Nous avons utilisé des flacons de 125 ml dont la composition du verre de masse est donnée dans le Tableau 1. Les verres de classes II et III sont très proches: les flacons de classe II sont obtenus, à partir de flacons de classe III, par un traitement de désalcalinisation au sulfate d'ammonium dans l'arche de recuisson.

Ces flacons ont été soumis au test Codex de résistance hydrolytique. Sur les autoclavats nous avons déterminé l'alcalinité et nous avons dosé un certain nombre d'ions passés en solution: Na, K, Ca, Si par absorption atomique de flamme, Al par colorimétrie avec le chromazurol S, B par potentiométrie de l'acide mannitoborique, et F par chromatographie ionique liquide (appareil Dionex).

Enfin, nous avons prélevé un fragment de fût de chaque flacon pour effectuer des profils SIMS sur la face interne (appareil IMS-3F de Cameca). Pour ces analyses, les échantillons ont été recouverts d'une couche d'or pour assurer la conduction électrique en surface. Nous avons utilisé un faisceau d'ions primaires O_2^+ de 5,5 keV et simultanément un faisceau d'électrons pour s'affranchir des problèmes de charge, suivant une procédure déja décrite [1]. L'interprétation des variations d'intensité en fonction de la profondeur est parfois délicate [2]: l'intensité des signaux ioniques secondaires est souvent perturbée au niveau des interfaces, et en particulier de la surface, sur quelques dizaines de nanomètres à cause des effets de pulvérisation. Par contre, la comparaison du profil obtenu pour un échantillon et pour un témoin permet de mettre en évidence des écarts de composition de façon

TABLEAU 1

Composition des verres utilisés (en pourcentage en poids d'oxyde)

	Classe I	Classe II	Classe III
SiO_2	66,5	73,0	71,8
SO_3	—	0,2	0,2
Al_2O_3	5,8	2,0	2,0
CaO	1,2	11,1	10,1
MgO	—	0,1	2,2
Na_2O	7,9	12,8	12,8
K_2O	2,0	0,6	0,6
BaO	2,8	—	—
B_2O_3	12,0	—	—
F	0,5	—	—
ZnO	1,1	—	—

rigoureusement reproductible. La vitesse de pulvérisation a été mesurée sur un échantillon de verre de même composition, mais en section polie, par détermination de la profondeur du cratère à l'aide d'un micropalpeur et en supposant la vitesse de pulvérisation constante. Les ions positives étudiés ont été ^{11}B, ^{23}Na, ^{24}Mg, ^{27}Al, ^{28}Si, ^{39}K et ^{40}Ca.

RESULTATS ET INTERPRETATION

Les valeurs de l'alcalinité observée ainsi que les concentrations en différents ions dans les autoclavats sont données dans le Tableau 2.

Les valeurs obtenues pour les alcalinités sont inférieures aux limites de la classe correspondante. Les résultats des analyses chimiques montrent que très peu d'éléments passent en solution pour les verres de classes I et II: on trouve seulement un peu de sodium et des traces de potassium et de calcium. Par contre, pour le verre de classe III les quantités d'ions sont plus importantes. Si l'on admet qu'une partie du verre passe en solution par une simple dissolution congruente, à partir de la concentration en silicium de la solution et connaissant la composition du verre de départ, on peut calculer la quantité théorique des autres ions que l'on devrait trouver en solution (voir Tableau 3). On observe un bon accord entre ces valeurs, aux incertitudes d'analyse près, sauf pour le sodium: la quantité obtenue expérimentalement est nettement supérieure à la valeur calculée. Il faut donc admettre que la dissolution n'est pas congruente, ce qui n'est pas étonnant pour les premiers stades de l'attaque qui correspondent à des pH moyens.

Les profils SIMS des échantillons de classe I avant et après test Codex sont

TABLEAU 2

Analyse des solutions d'attaque après test d'autoclavage (en ml HCl 0,01 M pour 100 ml de solution pour l'alcalinité et en mg l^{-1} pour les oxydes)

	Verre de classe I	Verre de classe II	Verre de classe III
Alcalinité observée	0,1	0,1	2,4
Alcalinité max. théorique[a]	0,4	0,4	3,8
SiO_2	$\leqslant 1$	$\leqslant 1$	20,5
Al_2O_3	0,03	$\leqslant 0,03$	0,65
CaO	0,15	0,15	2,85
MgO	0,10	0,10	0,60
Na_2O	0,55	0,40	4,60
K_2O	0,10	0,05	0,20
BaO	0,3	—	—
B_2O_3	0,5	0,5	—
ZnO	0,1	—	—
F	0,02	—	—

[a]Flacons de 125 ml.

TABLEAU 3

Comparaison entre la quantité d'ions passés en solution, obtenue expérimentalement, et celle calculée à partir de la composition du verre de départ et de la teneur en SiO_2 observée en solution (flacon de classe III)

	Verre de départ (% en poids)	Concentrations expér. en solution ($mg\ l^{-1}$)	Concentrations théoriques ($mg\ l^{-1}$)
SiO_2	71,8	20,5	—
Al_2O_3	2,0	0,65	0,59
CaO	10,1	2,85	2,9
MgO	2,2	0,60	0,63
Na_2O	12,8	4,60	3,6
K_2O	0,65	0,20	0,19

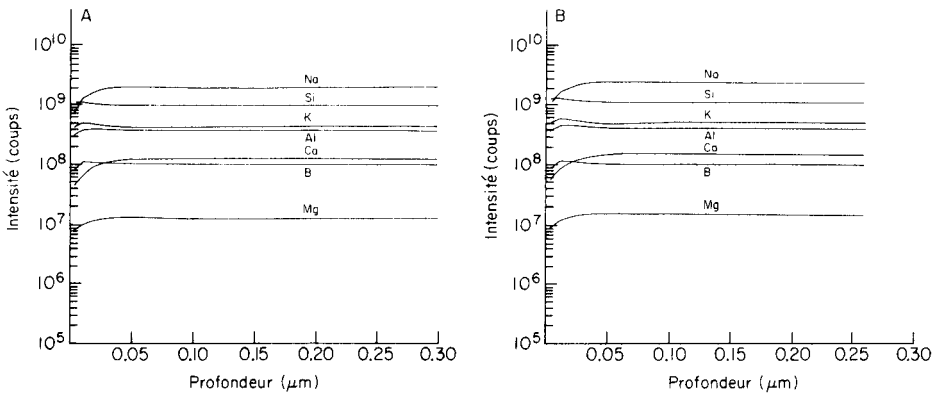

Fig. 1. Profil en profondeur SIMS des flacons de classe I avant (A) et après test d'autoclavage (B); variation de l'intensité des signaux ioniques secondaires en fonction de la profondeur.

extrêmement voisins, ce qui est en accord avec les analyses des ions passés en solution: ces surfaces sont considérées comme inertes (Fig. 1). Il en est de même pour les profils des échantillons de classe II (Fig. 2) examinés dans cette étude, mais dans ce cas on voit parfaitement l'effet du traitement de désalcalinisation: l'appauvrissement en sodium est sensible sur plus de 0,3 μm, ce qui est à comparer à la désalcalinisation sur 0,18 μm observée par Ryder et al. [3] pour des traitements SO_3 avec vapeur d'eau. On remarque également un léger recul du calcium, sur 20 nm environ. Ce recul avait déjà été observé par Harris [4] lors de traitements par SO_2.

Par contre, les profils obtenus pour les échantillons de classe III sont assez nettement différents (Fig. 3): après test Codex on observe un recul du sodium qui est de l'ordre de 40 nm tandis que les autres éléments, en particulier le calcium, ne varient pratiquement pas. Ce résultat est en accord avec les

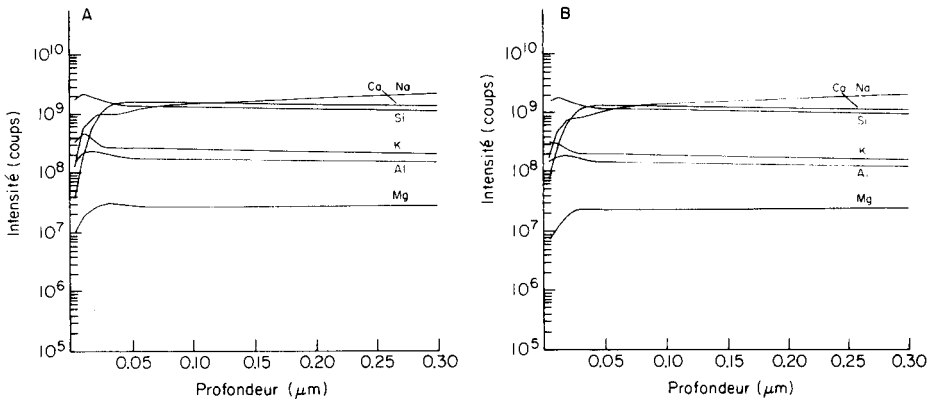

Fig. 2. Profil en profondeur SIMS des flacons de classe II avant (A) et après test d'autoclavage (B); variation de l'intensité des signaux ioniques secondaires en fonction de la profondeur.

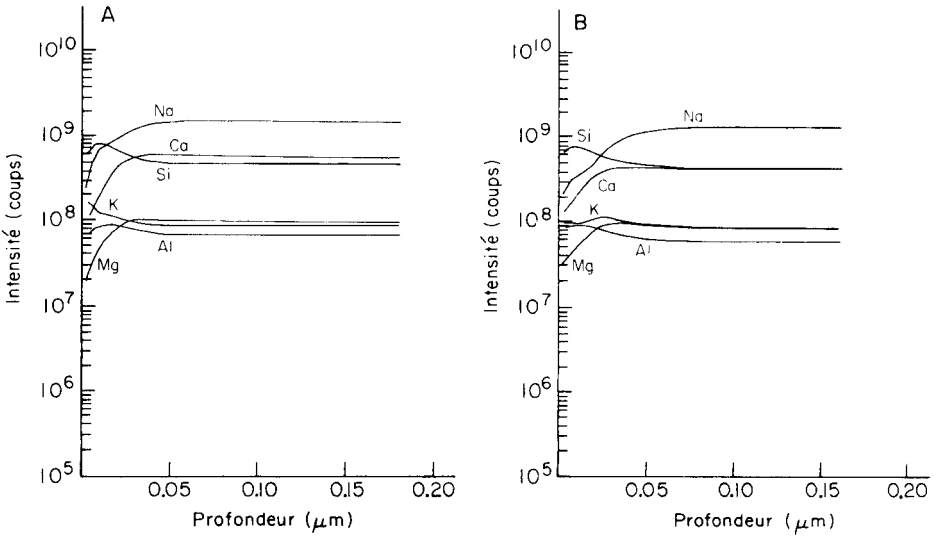

Fig. 3. Profil en profondeur SIMS des flacons de classe III avant (A) et après test d'autoclavage (B); variation de l'intensité des signaux ioniques secondaires en fonction de la profondeur (en microns).

analyses chimiques des ions passés en solution qui montraient que le rapport Na_2O/SiO_2 dans la solution d'attaque était plus fort que celui du verre de départ: c'est donc que la surface du verre s'est appauvrie en sodium préférentiellement. On peut du reste faire le calcul de l'épaisseur désalcalinisée en admettant que l'excès de sodium exprimé en poids de Na_2O dans la solution d'attaque est de 1 mg l^{-1}, sachant que la surface de contact avec l'eau est de l'ordre de 120 cm^2 et que les bouteilles sont remplies à 110 ml: on obtient 30 nm, en supposant un profil en marche d'escalier, ce qui n'est pas très

différent des 40 nm observés au SIMS. Les autres éléments ne sont pas affectés par le traitement en autoclave, sauf peut-être le potassium, mais la faible concentration de cet élément dans le verre incite à une certaine prudence.

L'attaque d'un verre sodocalcique par l'eau a déjà fait l'objet d'une abondante littérature [5—7].

Les premiers stades de la réaction correspondent à des pH moyens; mais si l'attaque se poursuit, le pH augmente, et la dissolution du verre commence, ce que montrent parfaitement les analyses des ions passés en solution pour le verre de classe III. Néanmoins on observe un excès de sodium dans les analyses chimiques, parfaitement corrélé au recul de sodium dans les profils SIMS. Il semble donc que même quand le réseau de la silice s'attaque, le sodium passe préférentiellement en solution probablement suivant un mécanisme diffusionnel:

$$Na^+ \text{ (verre)} + H_3O^+ \text{ (solution)} \rightleftharpoons Na^+ \text{ (solution)} + H_3O^+ \text{ (verre)}$$

Conclusion

Les analyses chimiques effectuées sur les autoclavats et les études de surface réalisées par la méthode SIMS sur des verres des différentes classes de la Pharmacopée permettent de confirmer la résistance hydrolytique élevée des verres de types I et II et de montrer l'efficacité du traitement de désalcalinisation pratiqué industriellement pour les verres de type II. Dans le cas des flacons en verre de type II, les surfaces internes sont appauvries en sodium, après le traitement de désalcalinisation, sur une profondeur supérieure à 0,3 μm; un léger appauvrissement en calcium est également observé sur une profondeur de 0,02 μm per rapport à un échantillon non traité.

Dans le cas d'échantillons ayant subi le test de résistance hydrolytique de la Pharmacopée Française, les profils SIMS sont en accord avec le résultat des analyses effectuées par voie chimique: la surface interne du verre n'est pratiquement pas modifiée pour les verres de classes I et II alors que dans le cas des verres III (sodocalciques ordinaires) la désalcalinisation est observée sur une profondeur de 40 nm environ. Il faut toutefois noter que même dans ce cas après le test d'autoclavage les quantités d'ions relarguées restent très faibles vis-à-vis des teneurs de liquides tels que les eaux minérales naturelles.

D'une façon générale, il est possible de conclure que les méthodes analytiques utilisées dans cette étude, qui ne sont pas d'un usage courant dans le contrôle des emballages en verre pratiqué par l'industrie pharmaceutique, vérifient et confirment la validité des tests de résistance hydrolytique prévus par la Pharmacopée.

BIBLIOGRAPHIE

1 P. Lehuede, J. Microsc. Spectrosc. Electron., 9 (1984) 507.
2 J. P. Lacharme et P. Lehuede, J. Am. Ceram. Soc., 68 (1985) C134.
3 R. J. Ryder, W. J. Poad et C. G. Pantano, J. Can. Ceram. Soc., 51 (1982) 21.
4 N. M. Harris, Riv. Staz. Sper. Vetro, 14 (1984) 91.
5 D. E. Clark, C. G. Pantano et L. L. Hench, Corrosion of Glass, Books for Industry, New York, 1979.
6 B. M. Smets et T. P. A. Lommen, Phys. Chem. Glasses, 24 (1983) 35.
7 R. H. Doremus, Y. Mehrotra, W. A. Lanford et C. Burman, J. Mater. Sci., 18 (1983) 612.

Analytica Chimica Acta, 201 (1987) 153—170
Elsevier Science Publishers B.V., Amsterdam — Printed in The Netherlands

RECOGNIZING CHROMATOGRAPHIC PEAKS WITH PATTERN RECOGNITION METHODS
Part 1. Development of a *k*-Nearest-Neighbour Technique

GREGOR REICH

Institute for Analytical Chemistry, University of Vienna, Waehringerstr. 38, A-1090 Vienna (Austria)

(Received 21st May 1987)

SUMMARY

Problems in automated peak recognition in chromatography are discussed. An algorithm based on the *k*-nearest neighbour technique is proposed. Recognition of a peak is done by comparing it with a predefined profile function (normally a Gaussian peak profile). The profile and a part of the chromatogram are both interpreted as points in a multi-dimensional pattern space. The distance between the two points gives the value of the peak recognition function. The effects of different properties of chromatographic peaks (i.e., peak width, peak height and noise) and of the profile parameter (i.e., dimension of the pattern space, shape and width of the function, and characteristics of the distance measure) are evaluated. The method has excellent properties for recognizing peaks with low signal/noise (*S/N*) ratios; an example with $S/N = 1$ is shown. Changing peak widths and drifting baselines have little effect on the recognition ability. Difficulties with changing peak heights can be compensated by range scaling. Problems occur when two peaks are not sufficiently separated.

The automatic evaluation of chromatograms is now routine practice in many laboratories. The computing devices used range from simple fixed programmed integrators to powerful laboratory data systems. The power of the small integrators has been increased in recent years, primarily because of the availability of cheaper memory devices and more powerful processing units. The algorithms used in this variety of data-processing systems are basically the same, but it is surprising to realize that these algorithms have been used virtually unchanged since the introduction of data-processing techniques in chromatography [1—8]. Some work has been done on more accurate evaluation of peak areas by integration of the whole chromatograms [9, 10]. The properties of the noise and its influence on the processing of chromatograms have been discussed [11, 12]. Correlation chromatography is one way to increase the detection sensitivity [13—15]; another way is to fit whole chromatograms with orthogonal functions [16—18]. In recent years, some work has been done on peak recognition for the "hyphenated" methods [19],

0003-2670/87/$03.50

especially gas chromatography/mass spectrometry [20], gas chromatography/Fourier-transform infrared spectroscopy [21, 22] and liquid chromatography/diode-array detectors [23, 24]. It is interesting to note that descriptions of complete software systems for automated chromatographs are given without even mentioning the step of recognizing the peak, but with a lengthy discussion on the best integration formula [25]. But there are also descriptions of microcomputer data systems which include the peak-finding algorithm [26, 27].

An ever-increasing area of application for chromatography is in monitoring and characterization of the environment. In this area, the most important information is mostly contained in the smallest peaks. Automatic recognition and evaluation of these peaks are therefore essential. Commercially available data systems have great difficulties with such peaks. A possibility for evaluating these peaks correctly is to use more advanced and more powerful algorithms. The starting point for the selection of better algorithms is consideration of the peak as a whole rather than as a series of digitized points. There are several algorithms (pattern recognition methods) which have been designed for processing multidimensional data. Of these methods, the *k*-nearest neighbour method (KNN) [28, 29] is selected here because of its easy applicability to this problem. In this paper, the properties of the KNN algorithm for recognizing chromatographic peaks are evaluated.

EXPERIMENTAL

Instrumentation

The calculations were done with an IBM 3083 at the computing center of the University of Vienna. The graphic output was plotted on a Hewlett-Packard 7550 plotter with the ERLGRAPH graphics package. All programs were written in FORTRAN 77. The use of the mainframe computer is not essential for these calculations, but was used for easier handling of the large number of processing steps involved in the simulation of the characteristics of this algorithm. The algorithm will now be implemented on an industrial standard microcomputer (IBM-PC-compatible system). The processing time of the algorithm is not much longer than that of the commonly used algorithms.

Description of the algorithm

One of the most crucial steps in the processing of a chromatogram is the recognition of the peaks because these peaks are the information carrier. The standard means for recognition is based on the first or second derivative of the detector signal. Unfortunately, the calculation of the derivative has a bad effect on the signal-to-noise ratio (*S/N*). The derivation is a frequency-dependent transformation of the signal, and the parts of the signal with higher frequency are more increased than the parts at lower frequency. Therefore the amplitude of the lower frequencies (i.e., the useful signal) is decreased in comparison with the amplitude of the higher frequencies

(i.e., noise), and the *S/N* ratio is decreased. This effect is demonstrated in Fig. 1, which shows a Gaussian peak and its first and second derivatives, without noise and with different *S/N* ratios. It can be seen that with a *S/N* ratio of 10, the peak cannot be found by using the first derivative. The limit of the *S/N* ratio for recognizing peaks can and will be decreased with smoothing algorithms. But such smoothing algorithms tend to produce deformation of peak shapes [30, 31]. This affects the resolution, and therefore the accuracy of the evaluation of peaks and of the analytical results.

The KNN technique is a classification algorithm for discrete categories. To process a chromatogram with this technique, a model of a chromatographic peak has to be developed. The model consists of a given peak profile which is represented by a number of values corresponding to the amplitudes of the peak at consecutive positions. For example, if twenty different positions are selected (Fig. 2a), then the peak can be described by a point in a 20-dimensional pattern space (the "profile point"), where the twenty different values, x_i, are the coordinates of this point in the pattern space. If there are different peak shapes, then these peaks are represented by different points (Fig. 2b). It is also possible to use a combination of peaks as a peak-profile model. Two peaks with different separations and different height ratios give also different points in the pattern space (Fig. 2c and d).

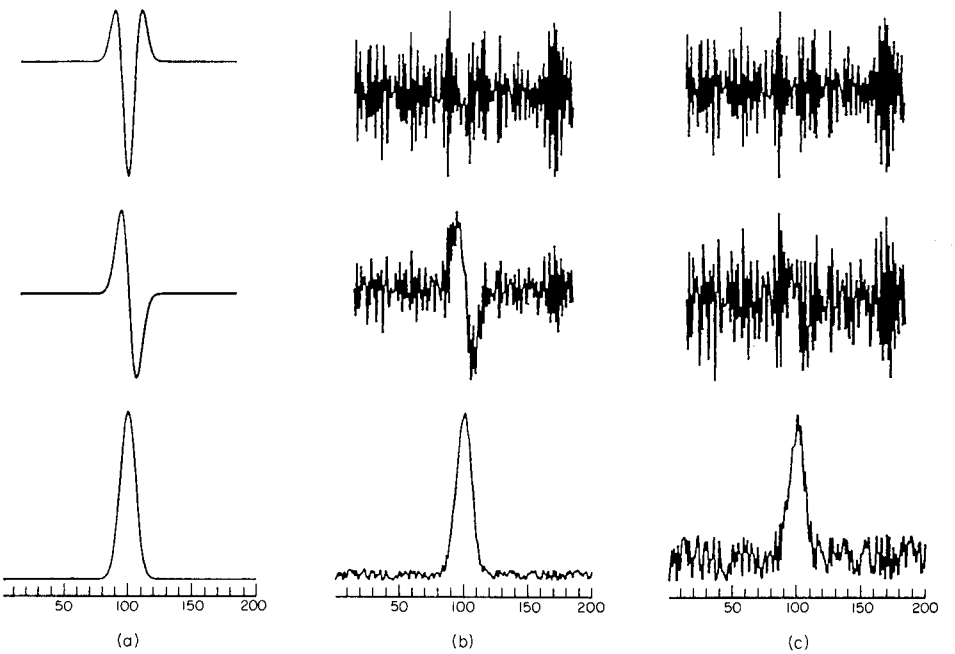

Fig. 1. A Gaussian peak (bottom row) with its first (middle row) and second (top row) derivatives with different noise levels: (a) no noise; (b) $S/N = 50$; (c) $S/N = 10$.

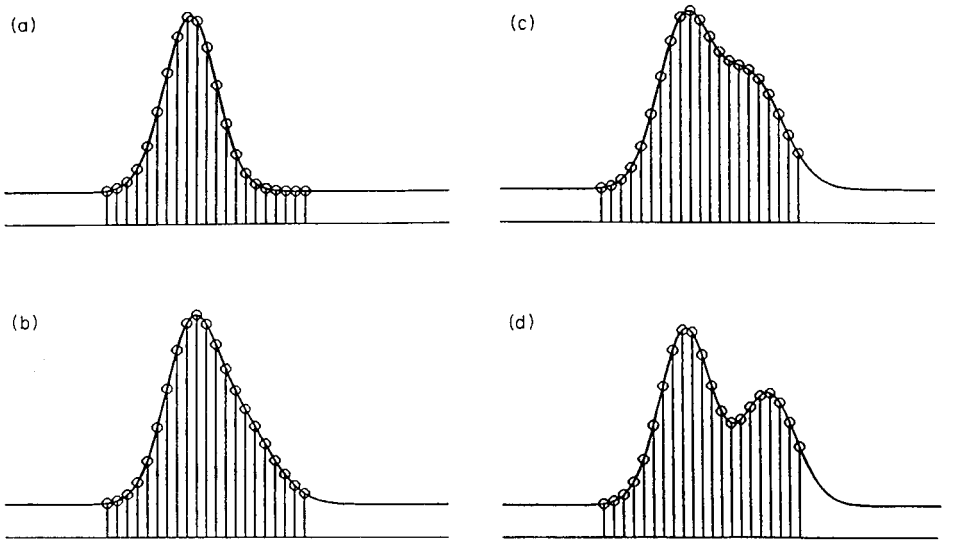

Fig. 2. Definition of the 20 dimensions of a peak for representation in 20-dimensional space: (a) Gaussian peak; (b) asymmetric peak; (c) and (d) two unseparated peaks.

A representation in the pattern space is shown in Fig. 3. The pattern space can be shown only for three dimensions, therefore the Gaussian peak, the asymmetric peak and the two pairs of overlapping Gaussian peaks can be represented only by three amplitudes. This produces little difference for the asymmetric peak and the second overlapping peaks, but it suffices for illustration of the algorithm (and there is no alternative on the printed page).

The processing of the chromatogram is simple. Consecutive digitized values at time t are taken to form a point in the pattern space. The number of values taken corresponds to the number of dimensions of the pattern space. In the above example, twenty consecutive digitized values are used as the coordinates of a single point in the 20-dimensional pattern space. This is termed the "chromatogram point". Comparison of the defined peak profile and a part of the chromatogram is done by calculating the distance between the profile point and the chromatogram point in the pattern space. The more similar the shape of the chromatogram is to the peak profile, the smaller will be the value of the distance. This distance is termed the peak-recognition function (PRF). The distance measure used in this first evaluation is the euclidian distance, which is defined as

$$d_{ij} = [\sum_{k} (x_{ik} - x_{jk})^2]^{1/2}$$

where d_{ij} is the distance, and x_{ik} and x_{jk} are the coordinates of the profile point and the chromatogram point, respectively.

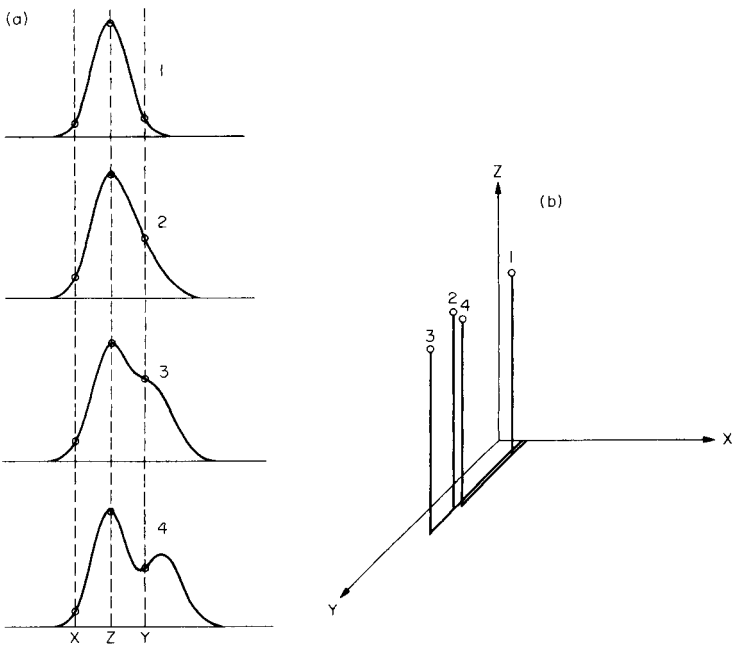

Fig. 3. As in Fig. 2, but in only three dimensions (a) and representation of these peaks in a three-dimensional coordinate system (b).

In the next step, the group of twenty digitized values starting at time $t + 1$ are taken to form the next chromatogram point. This is repeated along the whole chromatogram and with this procedure the group of selected digitized values is scanned across the whole chromatogram. The resulting sequence of distance values give the values of the peak-recognition function (PRF). Figure 4(a) shows the profile (P) and seven positions of the group of digitized values around a peak (points A—G). The corresponding pattern points in the pattern space are shown in Fig. 4(b). The track of the chromatogram point in the three-dimensional pattern space is also shown in Fig. 4(b); the distance of point D from profile point P is indicated. The change of the distance from the chromatogram point to the profile point is indicated in Fig. 4(c). The minimum in the distance, i.e., the peak recognition function (PRF), corresponds with the peak position. If there is no noise and if the profile corresponds exactly with the chromatographic peak, then the peak-recognition function has a value of zero. This is the case shown in Fig. 4(c).

RESULTS AND DISCUSSION

The peak shape in chromatography is not constant and the baseline is rarely a straight horizontal line in practice. The difficulties thus created must be taken into account in testing the performance of this algorithm. The effects

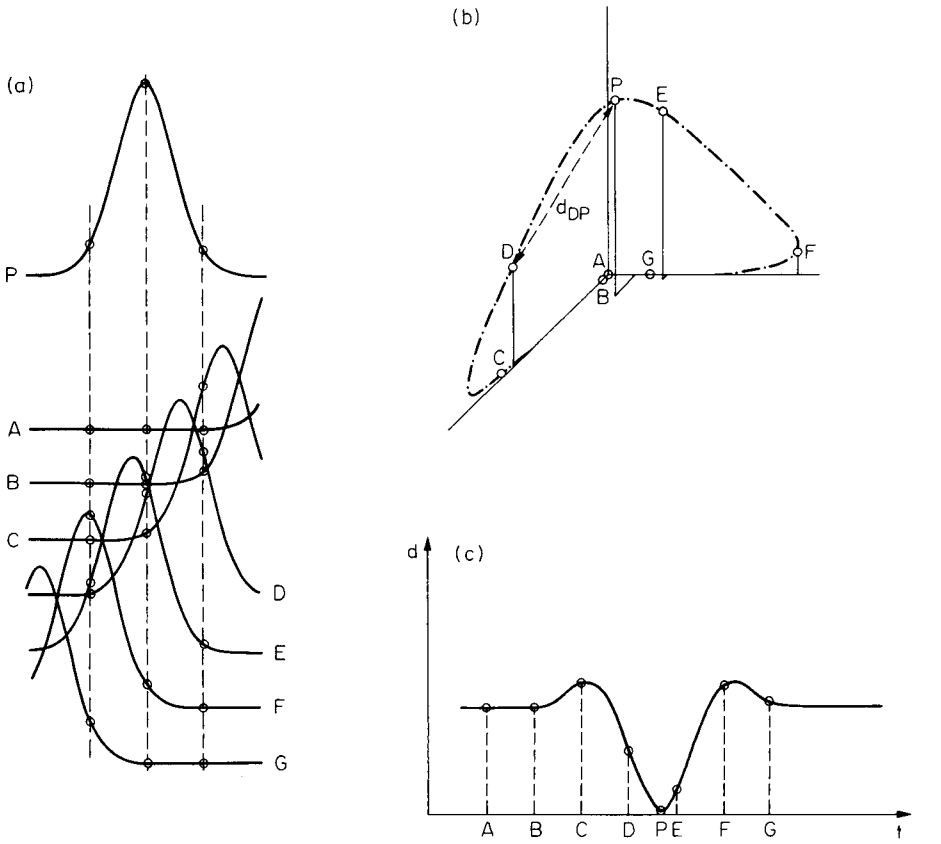

Fig. 4. Representation of the algorithm. (a) Peak profile (P) and seven positions of the chromatogram with indication of the coordinates in three-dimensional space. (b) The profile point (P) and the seven chromatogram points (A—G) in a three-dimensional coordinate system; the broken line shows the track of the chromatogram point as the profile moves over the chromatogram, and the peak-recognition function is given for chromatogram point D (distance from D to P). (c) Distances *d* from each point of the track to point P, i.e., the value of the peak recognition function (PRF).

of the following parameters on the peak-recognition function (PRF) have to be examined: peak width, peak amplitude, peak shape, *S/N* ratio and baseline slope. Checking the minimum of the recognition function was done with an extremely simple algorithm: a minimum is defined as the smallest value after several values with a negative slope or after crossing a certain threshold value. This algorithm was selected to check the properties of the recognition function without the help of a clever minimum-finding algorithm. More powerful algorithms can of course be used in applying this recognition algorithm in real situations.

The sensitivity of the recognition function to a given parameter can be characterized by the value of the minimum of the PRF depending on the

parameter value. The shape of the PRF and the value of the PRF for the baseline of the chromatogram depend on the parameters of the selected profile, especially on the number of points per profile width. This can be seen in Fig. 5. In most cases, there is a maximum before and after the minimum of the PRF. A detailed description of the PRF for a defined set of parameters is given in Table 1. The results for the tables are calculated with a 30-dimensional space.

Influence of the peak width

The sensitivity to the variation of peak width is important, because the use of isocratic and isothermal elution in chromatography produces ever-increasing widths of the eluted peaks. The variation of the value of the PRF with different profile peak widths and different *S/N* ratios is given in Table 1. A complete description of the PRF is listed, i.e., the minimum for the function, the maximum before the minimum and the value of the baseline before the peak; the difference between the minimum and the maximum of the PRF is also given. It can be seen that for all given values of the peak width there is a clearly defined minimum and good recognition of the peak. If the profile and the chromatographic peaks have the same width, the smallest minimum of the PRF will be reached. However, for small *S/N* values the smallest value is found by broader profile functions. The given noise minimum is calculated from a piece of baseline and the straight line calculated by linear regression of these baseline points, which is used as the profile function. Figure 5 shows the PRF for three different width ratios. Because the number of chromatogram points are the same for all three widths, the profile covers different parts of the whole peak. This affects the PRF; the value of the PRF in the baseline region of the chromatogram depends on it. Therefore different numbers of points are also used so that the same part of the profile is covered with these points. The central column in Fig. 5 (b, e, h) contains the profile with the same number of points as the chromatogram peak (40). In the top row (a—c) only half as many points are used (20) for the smaller profile and only the small profile (a) forms a complete peak. In the bottom row (g, h and i) double the number of points is used (80) and only the broad profile (i) has no baseline included. It can be seen that the maximum before and after the minimum of the PRF does not appear when the profile covers only the upper part of the peak and does not come near the baseline. Which form of the PRF is better for the recognition of the peak depends on the algorithm used for finding the minimum of the PRF. Another feature is that with an increasing number of digitized points the remaining noise of the PRF is decreased. This means that a better noise reduction can be achieved by increasing the sampling rate. When the conventional algorithm is used, an increase in the sampling rate leads to a loss of recognition ability. The unscaled values given in Table 1 correspond to Fig. 5(d—f). Table 1 also shows the results with a scaling step included (see below). The noise minimum is always calculated without the scaling step.

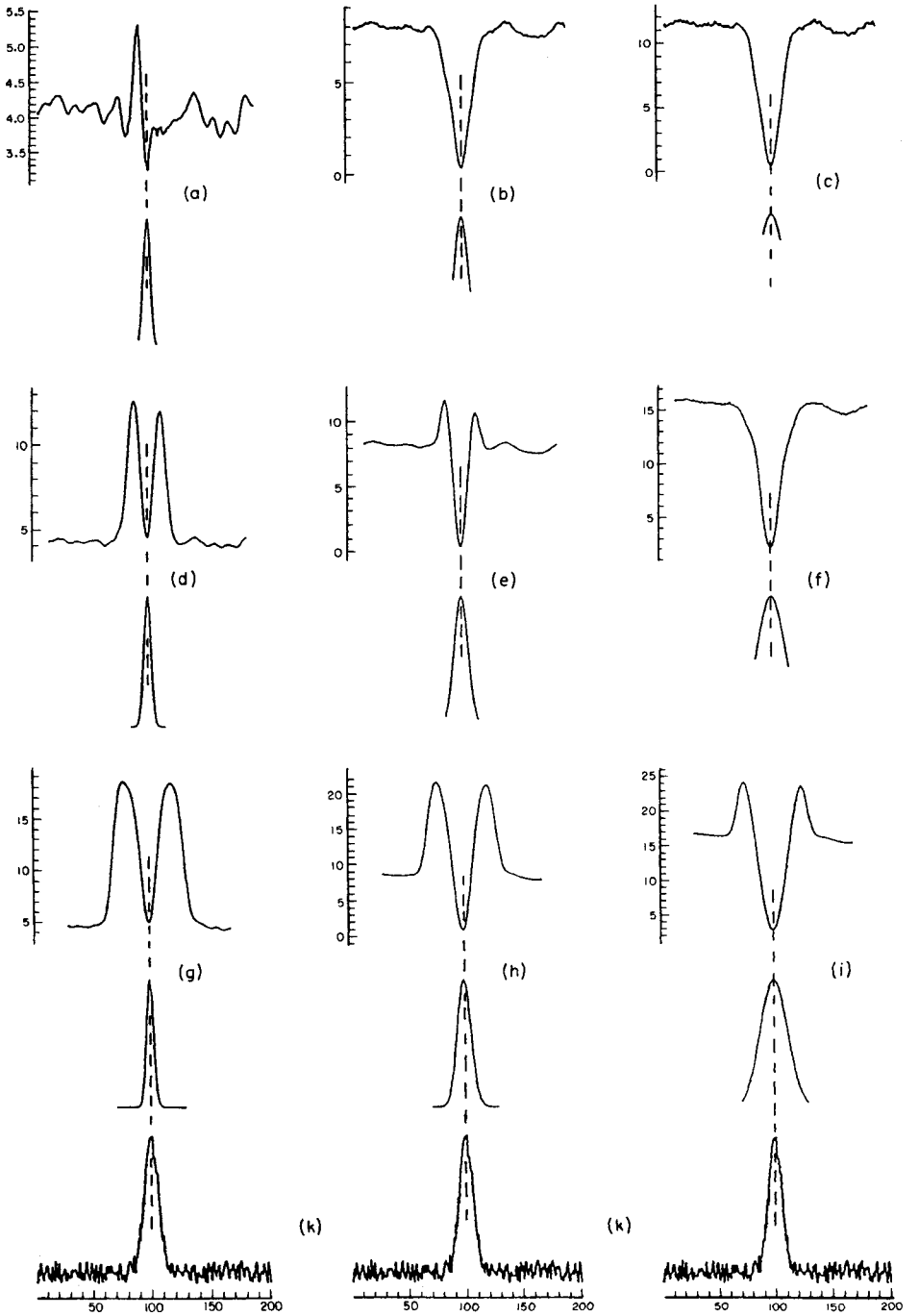
(a)
(b)
(c)
(d)
(e)
(f)
(g)
(h)
(i)
(k)
(k)
50
100
150
200

Influence of the peak amplitude

The value of the peak recognition function is very much influenced by the peak amplitude. This is an obvious characteristic, which can be understood by visualization of the underlying model. If a peak has double the height of another peak, then all the amplitudes of this peak are twice as large, and the distance must be larger. This behaviour is described in Table 2 under the heading Unscaled without noise and with $S/N = 100$; only the minimum of the PRF is given. To eliminate this phenomenon, range scaling is necessary. The scaling is done with

$$x_i' = (x_i - x_{\min})/(x_{\max} - x_{\min})$$

where x_i is the digitized value of the chromatogram in the interval of interest, x_i' is the scaled value, and $x_{\min}$ and $x_{\max}$ are the minimum and maximum value of x_i in the interval. The interval of interest consists of n values, where n is the dimensionality of the pattern space. The values of the distance function for the scaled chromatogram are given in Table 2 under the heading Scaled, without noise and with $S/N = 100$. It will be necessary to look for other distance measures, because the scaling needs computational resources, which may be avoidable. Other characteristics of the algorithm are also influenced by the range scaling, including the noise rejection of the PRF. On the baseline of the chromatogram away from a peak the noise is actually scaled to the full profile height (Fig. 6, d—f). Figure 6 shows the dependence of the PRF on the peak height. The first peak and the profile match exactly. The second peak has the same height as the first (b, e) or is a factor of five larger (c, f) or smaller (a, d). Figure 6(a—c) shows the influence of the peak height; there is no noise in the PRF but otherwise the peak height greatly affects the PRF. When the scaled algorithm is used (Fig. 6, d—f), all peaks are recognized equally well, but noise appears on the PRF at the baseline parts, though not on the parts of the chromatogram where peaks are located. The same result can be seen in Table 2.

Influence of the signal-to-noise-ratio

One of the reasons to adopt this algorithm was the high sensitivity to a low signal-to-noise-ratio of the commonly used algorithm. The KNN algorithm shows much less sensitivity to noise (Table 3). It can be seen that the noise sensitivity depends on the number of dimensions used in the algorithm, which is expected because integration over more points gives better noise reduction. The increase in the value of the PRF with increasing S/N ratio in the unscaled mode corresponds to an increasing noise amplitude, and does not provide

---

Fig. 5 (opposite). Variation of the PRF with variation of the ratio of the width of the profile peak and the chromatographic peak and with a varying number of dimensions of the pattern space. In (b), (e) and (h) both peaks have the same width; in (a), (d) and (g) the profile peak has half the width, and in (c), (f) and (i) double the width, of the chromatographic peak. (a), (b) and (c) represent a 20-dimensional space; (d), (e) and (f) a 40-dimensional space; and (g), (h) and (i) an 80-dimensional space. The profile function and the corresponding PRF are shown. (k) is the chromatogram.

TABLE 1

Value of the minimum of the PRF depending on the ratio of the width of the profile function to the peak width for different *S/N* ratios. A full description of all the values is given in the text

Width ratio	UNSCALED *S/N ratio*									
		∞		100		50		20		10	
0.500	Min.	1.67	>8.14	1.85	>8.18	2.05	>8.10	2.88	>7.75	4.45	>8.85
	Max.	9.81		10.03		10.15		10.63		13.30	
	Bas.[a]	3.54		3.45		3.23		3.01		3.10	
0.625	Min.	0.89	>9.54	1.04	>9.57	1.19	>9.50	3.17	>7.73	3.22	>10.01
	Max.	10.43		10.61		10.69		10.90		13.23	
	Bas.	4.43		4.28		4.02		3.71		3.54	
0.750	Min.	0.38	>10.59	0.48	>10.61	0.59	>10.54	1.14	>10.05	2.29	>11.00
	Max.	10.97		11.09		11.13		11.19		13.29	
	Bas.	5.31		5.09		4.81		4.41		3.97	
0.875	Min.	0.09	>11.42	0.15	>11.41	0.22	>11.34	0.62	>10.77	1.63	>11.66
	Max.	11.51		11.56		11.56		11.39		13.29	
	Bas.	6.20		5.96		5.60		5.12		4.40	
1.000	Min.	0.00	>11.93	0.01	>11.94	0.05	>11.84	0.30	>11.29	1.18	>12.03
	Max.	11.93		11.95		11.89		11.59		13.21	
	Bas.	7.09		6.80		6.40		5.83		4.83	
1.125	Min.	0.08	>12.21	0.04	>12.20	0.04	>12.08	0.15	>11.55	0.90	>12.24
	Max.	12.29		12.24		12.12		11.70		13.14	
	Bas.	7.97		7.67		7.19		6.54		5.27	
1.250	Min.	0.29	>12.36	0.21	>12.34	0.17	>12.20	0.14	>11.61	0.77	>12.20
	Max.	12.65		12.55		12.37		11.75		12.97	
	Bas.	8.86		8.51		7.98		7.26		5.71	
1.375	Min.	0.62	>12.32	0.49	>12.32	0.42	>12.15	0.25	>11.59	0.74	>12.01
	Max.	12.94		12.81		12.57		11.84		12.75	
	Bas.	9.74		9.33		8.78		7.97		6.16	
1.500	Min.	1.04	>12.15	0.87	>12.14	0.76	>11.97	0.45	>11.45	0.82	>11.67
	Max.	13.19		13.01		12.73		11.90		12.49	
	Bas.	10.63		10.18		9.58		8.69		6.62	
1.625	Min.	1.52	>11.98	1.31	>11.90	1.16	>11.78	0.74	>11.20	0.97	>11.27
	Max.	13.50		13.21		12.94		11.94		12.24	
	Bas.	11.51		11.03		10.37		9.42		7.10	
1.750	Min.	2.06	>11.74	1.80	>11.68	1.63	>11.53	1.08	>10.91	1.19	>10.88
	Max.	13.80		13.48		13.16		11.99		12.07	
	Bas.	12.38		11.86		11.17		10.14		7.59	
1.875	Min.	2.63	>11.46	2.34	>11.39	2.13	>11.25	1.48	>10.57	1.46	>10.47
	Max.	14.09		13.73		13.38		12.05		11.93	
	Bas.	13.23		12.68		11.95		10.86		8.09	
2.000	Min.	3.22	>11.21	2.89	>11.10	2.66	>10.94	1.91	>10.28	1.78	>10.03
	Max.	14.43		13.99		13.60		12.19		11.81	
	Bas.	14.06		13.48		12.72		11.57		8.60	
2.125	Min.	3.82	>10.97	3.46	>10.85	3.21	>10.67	2.37	>10.00	2.12	>9.60
	Max.	14.79		14.31		13.88		12.37		11.72	
	Bas.	14.87		14.27		13.47		12.26		9.11	
2.250	Min.	4.42	>10.75	4.03	>10.60	3.76	>9.43	2.84	>9.71	2.48	>9.21
	Max.	15.17		14.63		13.19		12.55		11.69	
	Bas.	15.65		15.03		14.20		12.94		9.61	
Noise Minimum		0.000		0.003		0.012		0.064		0.258	

[a]Baseline.

SCALED *S/N ratio*				
∞	100	50	20	10
1.66 9.81 >8.15	1.65 9.68 >8.03	1.73 9.49 >7.76	1.91 11.72 >9.81	2.58 11.16 >8.58
4.54	—	—	—	—
0.89 10.43 >9.54	0.89 10.26 >9.37	0.97 10.07 >9.10	1.19 11.68 >10.49	1.72 11.16 >9.44
5.43	—	—	—	—
0.37 10.98 >10.61	0.38 10.76 >10.38	0.45 10.56 >10.11	0.67 11.51 >10.84	1.10 10.91 >9.81
6.32	—	—	—	—
0.09 11.51 >11.42	0.10 11.26 >11.16	0.14 11.04 >10.90	0.34 11.22 >10.88	5.95 10.56 >8.51
7.20	—	—	—	—
0.00 11.94 >11.94	0.004 11.67 >11.67	0.02 11.44 >11.42	0.18 10.86 >10.68	0.43 10.16 >9.73
8.08	—	—	—	—
0.07 12.32 >12.25	0.07 12.01 >11.94	0.07 11.76 >11.69	0.17 10.47 >10.30	0.34 9.77 >9.43
8.95	—	—	—	—
0.27 12.71 >12.44	0.25 12.38 >12.13	0.23 12.12 >11.89	0.27 11.14 >10.87	0.35 9.41 >9.06
9.78	—	—	—	—
0.53 13.06 >12.53	0.51 12.72 >12.21	0.46 12.44 >11.98	0.45 11.43 >10.98	0.45 9.11 >8.66
10.56	—	—	—	—
0.83 13.36 >12.53	0.80 13.01 >12.21	0.73 12.71 >11.98	0.67 11.70 >11.03	0.60 8.87 >8.27
11.27	—	—	—	—
1.14 13.64 >12.50	1.10 13.27 >12.17	1.01 12.99 >11.98	0.91 11.99 >11.08	0.78 8.68 >7.90
11.90	—	—	—	—
1.43 13.93 >12.50	1.38 13.55 >12.17	1.28 13.26 >11.98	1.13 12.24 >11.11	0.96 8.53 >7.57
12.45	—	—	—	—
1.71 14.18 >12.47	1.65 13.80 >12.15	1.54 13.50 >11.96	1.34 12.47 >11.13	1.13 8.42 >7.29
12.93	—	—	—	—
1.96 14.40 >12.44	1.90 14.01 >12.11	1.77 13.71 >11.94	1.53 12.67 >11.14	1.30 8.34 >7.04
13.36	—	—	—	—
2.19 14.60 >12.41	2.12 14.20 >12.08	1.99 13.89 >11.90	1.71 12.85 >11.14	1.45 8.28 >6.83
13.72	—	—	—	—
2.39 14.76 >12.37	2.32 14.36 >12.04	2.18 14.04 >11.86	1.86 13.02 >11.16	1.59 8.23 >6.64
14.04	—	—	—	—
0.000	0.003	0.012	0.064	0.258

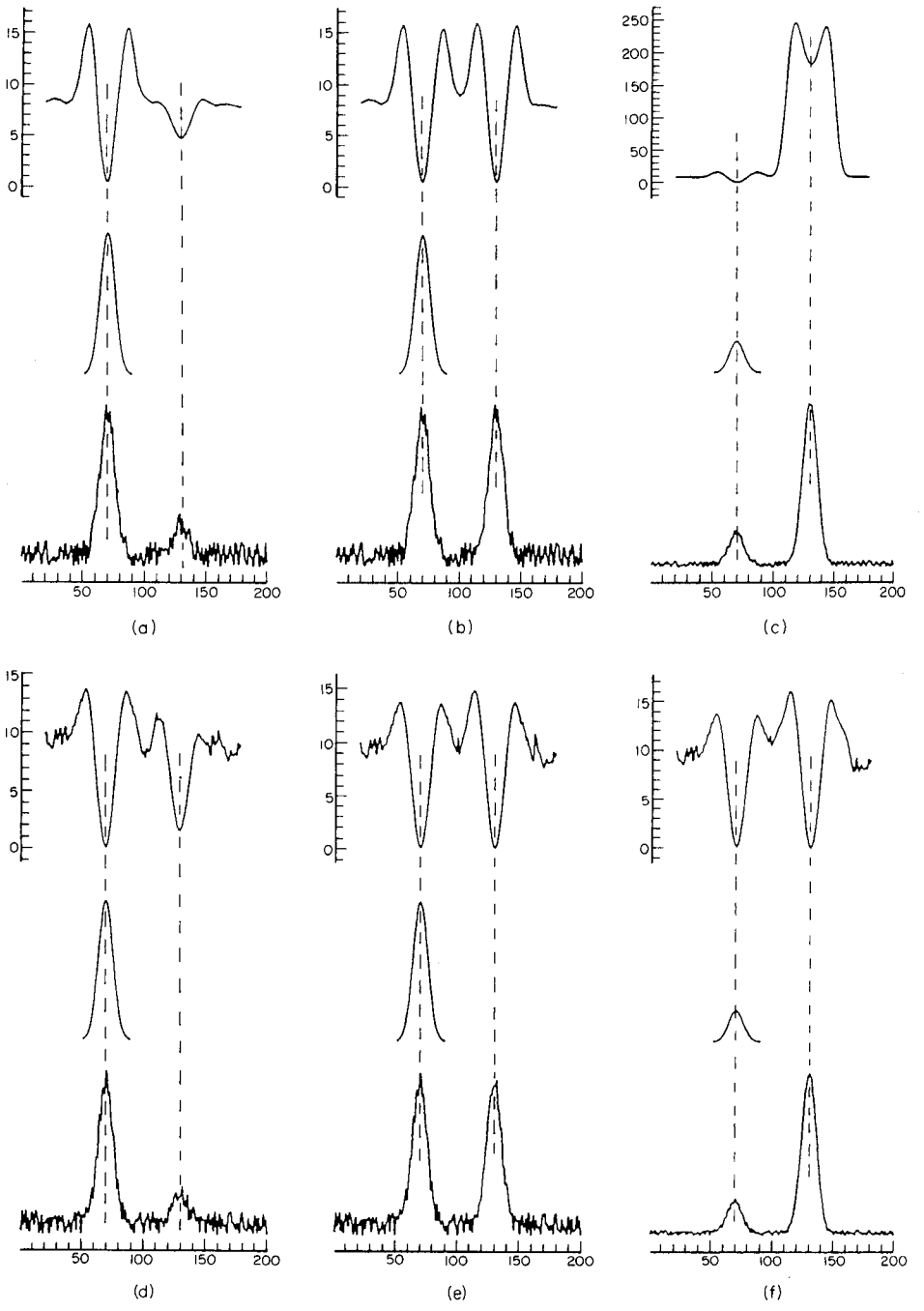
15
10
5
0
250
200
150
100
50
50
100
150
200
(a)
(b)
(c)
(d)
(e)
(f)

TABLE 2

Minimum of the PRF for varying peak heights

Peak height ratio	Minimum of the PRF			
	$S/N = \infty$		$S/N = 100$	
	Unscaled	Scaled	Unscaled	Scaled
0.001	6.87	0.00	—[a]	—[a]
0.01	6.75	0.00	6.42	4.104
0.1	5.74	0.00	5.36	0.272
0.2	4.53	0.00	4.20	0.084
0.3	3.47	0.00	3.18	0.040
0.4	2.55	0.00	2.30	0.023
0.5	1.77	0.00	1.57	0.015
0.6	1.13	0.00	0.97	0.010
0.7	0.64	0.00	0.52	0.007
0.8	0.28	0.00	0.21	0.006
0.9	0.07	0.00	0.04	0.004
1.0	0.00	0.00	0.02	0.004
1.1	0.07	0.00	0.13	0.003
1.2	0.28	0.00	0.39	0.002
1.3	0.64	0.00	0.79	0.002
1.4	1.13	0.00	1.33	0.002
10.0	576.00	0.00	579.00	0.000
100.0	—[b]	0.00	—[b]	0.000
1000.0	—[b]	0.00	—[b]	0.000
Baseline	6.66	6.85	6.36	6.889
Maximum	11.90	11.94	12.00	11.946

[a] Value corresponds to a S/N ratio of 0.1. [b] Value too large and meaningless.

better recognition. This is easily verified by comparison with the scaled approach. Figure 7 shows the recognition of two peaks with and without noise. It can be seen that, even for $S/N = 1$, recognition is possible.

Influence of the peak resolution

The recognition of the smaller peak of a pair offers some problems. Table 4 gives the minimum of the PRF for the smaller peak, depending on the resolution of the two peaks and on the S/N ratio. In the absence of noise, with $R = 6$, the peak is correctly located and the minimum of the PRF has a value corresponding to the peak height. When the resolution is inadequate, the recognized peak location is shifted away from the larger peak, indicating

Fig. 6 (opposite). Variation of the PRF with varying peak height: (a—c) unscaled mode; (d—f) scaled mode. In each part, the bottom row shows the chromatogram, the middle row shows the peak profile and the top row shows the PRF. The first peak of the chromatogram corresponds to the profile peak. The second peak has a peak height of 0.2 in (a) and (d), of 1 in (b) and (e), and 5 in (c) and (f) compared to the first peak. $S/N = 20$ for the first peak, and 4, 20 and 100 for the second peaks in (a—c), respectively.

TABLE 3

Difference between the maximum before the peak and the minimum of the PRF depending on the *S/N* ratio of the peak and on the number (8—40) of points (dimensions) used in the algorithm

S/N	Difference								
	8	12	16	20	24	28	32	36	40
UNSCALED									
∞	5.94	6.83	7.05	7.08	9.95	11.36	12.41	13.12	13.57
100	5.70	6.60	6.63	7.99	10.01	11.14	12.30	13.20	13.51
50	5.66	6.32	5.87	7.79	9.74	11.24	12.33	13.07	13.26
20	4.81	5.36	5.61	7.20	9.45	10.62	11.76	13.08	12.60
10	3.58	4.66	3.92	6.48	8.35	10.72	12.42	12.69	13.37
5	2.32	1.97	4.86	6.72	7.50	11.21	14.23	13.15	11.07
2	—	—	—	—	—	8.66	10.13	16.47	25.09
1	—	—	—	—	—	—	—	—	31.75
SCALED									
∞	4.69	5.59	7.34	8.36	10.00	11.37	12.41	12.47	13.57
100	3.79	5.42	6.73	8.29	9.69	11.13	12.28	12.92	13.12
50	3.59	5.16	6.76	7.99	9.63	10.81	12.05	12.64	13.23
20	3.66	4.54	6.22	7.60	9.09	10.25	11.26	11.65	12.39
10	2.80	4.26	5.36	6.83	8.25	8.82	10.41	10.95	10.56
5	2.03	4.06	4.10	5.83	5.81	7.23	8.12	9.04	9.28
2	—	—	2.41	2.55	4.43	5.23	4.42	7.95	8.12
1	—	—	—	—	2.90	5.83	4.45	2.57	5.37

a greater separation. Increasing the noise intensity increases this effect. With high noise values and low resolution, recognition of the small peak is impossible. Moreover, high noise can shift the position of the recognized peak. Figure 8 shows these effects.

This unsatisfactory characteristic can be substantially improved by changing the mode of action of the algorithm. Recognition can be achieved by changing the shape of the profile function. If this profile is the sum of two overlapped peaks, these overlapped peaks can be found. Because of the large number of possible peak combinations, an appropriate plan for the calculations is needed. This PRF can then be used as the response function for optimization of the profile function. The smallest possible minimum value of the PRF can be calculated from the baseline noise and the difference to the actual value of the PRF gives an indication of the similarity between these two peak shapes. It is thus possible to include peak deconvolution in the recognition algorithm. This will be discussed in more detail in Part 2.

Figure 9 shows an example of a measured chromatogram, compared with a group of peak profiles. This latter group consists of a single Gaussian peak and several combinations of two Gaussian peaks with resolutions of 1.5, 2, 2.5, 3, 3.5, 4, 4.5, 5 and 5.5 and peak-height ratios from 0.1 to 1 in steps of 0.1. The line on top represents the minimum of all recognition functions. The scale of the PRF is given on the right side. In some cases, an asymmetric peak

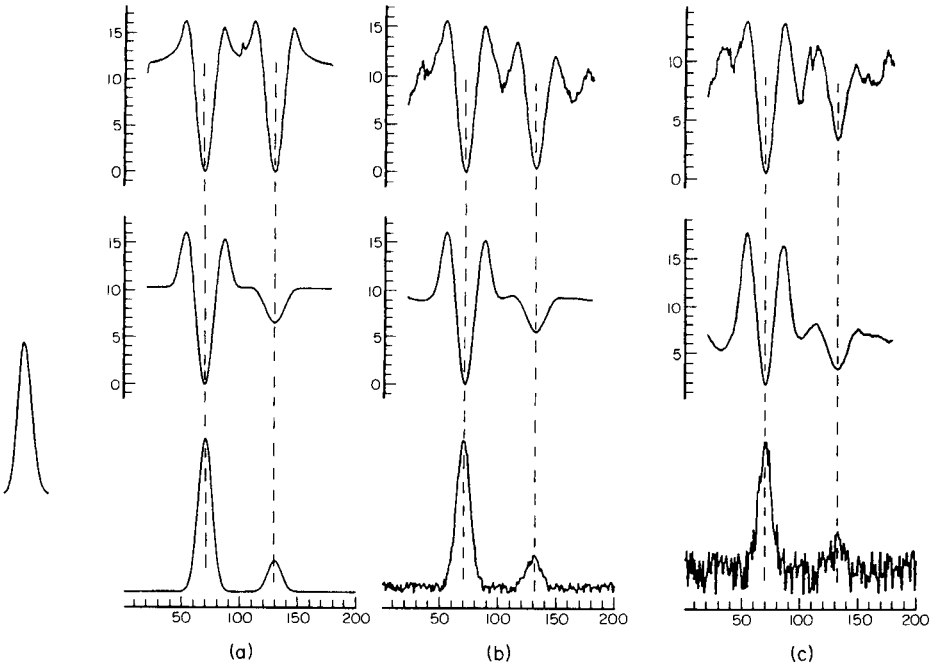

Fig. 7. PRF for different S/N ratios. Far left is the profile function. The bottom row gives the chromatogram, the middle row gives the unscaled PRF and the top row gives the scaled PRF. S/N ratio for the large peak: (a) ∞; (b) 20; (c) 5. The small peak has a fifth of the height of the large peak, thus $S/N = 4$ for (b) and 1 for (c).

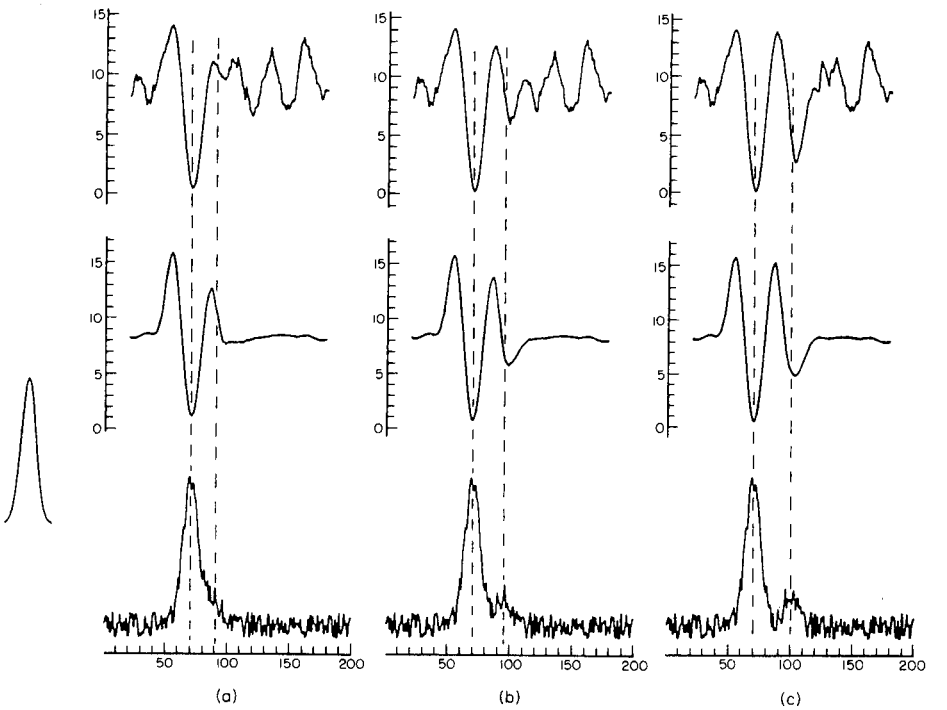

Fig. 8. PRF for different peak resolutions. Layout as in Fig. 7. Resolution (R): (a) 3.5; (b) 4; (c) 5.

TABLE 4

Minimum of the peak recognition function (PRF) and the deviation (number of points) of the peak location, depending on the resolution (R) of two peaks and on the S/N ratio (∞—10). The peak amplitude ratio is 0.2 in all cases.

R[a]	∞		100		50		20		10	
	Dev.	Min.	Dev.	Min.	Dev.	Min.	Dev.	Min.	Dev.	Min.
UNSCALED										
3.0	+9	7.10	+7	6.30		—		—		—
3.5	+5	5.90	+5	5.61	+5	5.52	+5	5.43	+6	4.76
4.0	+3	5.30	+3	5.00	+3	4.91	+3	4.79	+4	4.12
4.5	+2	4.88	+2	4.58	+2	4.45	+2	4.33	+3	3.58
5.0	+1	4.65	+1	4.34	+1	4.18	+1	4.02	+2	3.21
5.5	0	4.56	0	4.25	0	4.07	+1	3.80	+1	3.05
6.0	0	4.54	0	4.24	0	4.02	+1	3.66	+1	2.90
6.5	0	4.54	0	4.26	0	3.99	+1	3.50	+1	2.82
7.0	0	4.54	0	4.27	0	3.97	+1	3.41	−1	2.81
7.5	0	4.54	0	4.27	0	3.97	0	3.31	−1	2.96
8.0	0	4.54	0	4.25	0	3.98	0	3.28	−2	3.15
8.5	0	4.54	0	4.22	0	3.99	0	3.27	−3	3.49
9.0	0	4.54	0	4.20	0	4.01	0	3.27	+1	3.56
Noise minimum		0.000		0.002		0.011		0.054		0.372
SCALED										
3.0		—		—		—		—		—
3.5	+5	6.42	+5	6.15	+5	6.11	+5	5.61		—
4.0	+4	4.94	+4	4.75	+3	4.74	+3	4.64		—
4.5	+2	3.35	+2	3.21	+3	3.36	+4	3.64		—
5.0	+2	1.62	+2	1.51	+2	1.69	+2	2.36		—
5.5	+1	0.46	+1	0.61	+1	0.91	+1	1.53		—
6.0	0	0.065	0	0.24	0	0.54	0	1.38		—
6.5	0	0.004	0	0.22	0	0.40	0	1.38	+1	2.29
7.0	0	0.000	0	0.17	0	0.38	0	1.34	+1	2.31
7.5	0	0.000	0	0.14	0	0.66	0	1.36	0	2.55
8.0	0	0.000	0	0.12	0	0.53	0	1.29	−2	2.87
8.5	0	0.000	0	0.21	0	0.51	0	1.25	−2	3.73
9.0	0	0.000	0	0.16	0	0.40	0	1.59	+1	4.72
Noise minimum		0.000		4.70		5.68		3.542		4.685

[a]Resolution was calculated from the formula $R_{ij} = (t_j - t_i/\sigma_i) = (r_{ji} - 1)(K_i/K_iM)\mu^{1/2}$.

is indicated as a combination of two peaks with small resolution. This is mathematically correct and provides an example of some of the difficulties found in correctly interpreting chromatograms with a computer.

Influence of the remaining factors

A baseline drift has very little effect on the recognition of a peak, although the value of the minimum increases when the baseline is steeper. The peak

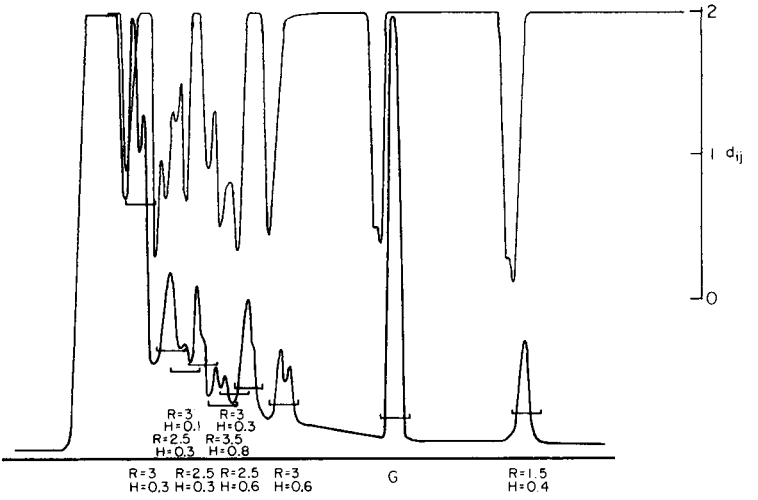

Fig. 9. Example of a chromatogram (bottom). Above is the minimum of several PRF's (see text). The parameters of the profile function for each minimum are given. G, Gaussian peak; R, resolution of two peaks; H, height ratio of the peaks.

shape also affects only the obtainable minimum of the recognition function, similarly to the effect of a drifting baseline. Both effects can be compensated by changing the profile function.

REFERENCES

1 H. W. Johnson, Jr., Anal. Chem., 35 (1963) 521.
2 J. T. Walsh, R. E. Kramer and C. Merritt, Jr., J. Chromatogr. Sci., 7 (1969) 348.
3 H. M. Gladney, B. F. Dowden and J. D. Swalen, Anal. Chem., 41 (1969) 883.
4 A. Fozard, J. J. Franses and A. J. Wyatt, Chromatographia, 5 (1972) 130.
5 B. Weimann, Chromatographia, 9 (1974) 472.
6 M. H. J. van Rijswick, Chromatographia, 9 (1974) 491.
7 L. Koskinen, Trends Anal. Chem., 1 (1982) 324.
8 J. L. Excoffier and G. Guiochon, Chromatographia, 15 (1982) 543.
9 W. J. Taraszewski, D. T. Haworth and B. D. Pollard, Anal. Chim. Acta, 157 (1984) 73.
10 R. E. Synovec and E. S. Yeoung, Anal. Chem., 57 (1985) 2162.
11 H. C. Smit and H. L. Walg, Chromatographia, 8 (1975) 311.
12 J. M. Laeven and H. C. Smit, Anal. Chim. Acta, 176 (1985) 77.
13 R. Annino, J. Chromatogr. Sci., 14 (1976) 265.
14 T. T. Lub, H. C. Smit and H. Poppe, J. Chromatogr., 149 (1978) 721.
15 T. T. Lub and H. C. Smit, Anal. Chim. Acta, 112 (1979) 341.
16 P. J. H. Scheeren, Z. Klous, H. C. Smit and D. A. Doornbos, Anal. Chim. Acta, 171 (1985) 45.
17 D. R. Cooper, J. Chromatogr., 80 (1973) 246.
18 H. J. G. Debets, A. W. Wijnsma, D. A. Doornbos and H. C. Smit, Anal. Chim. Acta, 171 (1985) 33.
19 L. S. Ramos, J. E. Burger and B. R. Kowalski, Anal. Chem., 57 (1985) 2620.
20 W. F. Hargrove, D. Rosenthal and P. C. Cooley, Anal. Chem., 53 (1981) 538.
21 D. R. Mattson and R. L. Julian, J. Chromatogr. Sci., 17 (1979) 416.

22 P. M. Owens, R. B. Lam and T. L. Isenhour, Anal. Chem., 54 (1982) 2344.
23 A. F. Fell, H. P. Scott, R. Gill and A. C. Moffat, J. Chromatogr., 282 (1983) 123.
24 J. K. Strasters, H. A. H. Billiet, L. De Galan, B. G. M. Vandeginste and G. Kateman, J. Chromatogr., 385 (1987) 181.
25 R. P. Singhal and D. B. Smoll, J. Liq. Chromatogr., 9 (1986) 2719.
26 I. G. Giles and M. G. Gore, Anal. Chim. Acta, 151 (1983) 123.
27 P. M. Lyne and K. F. Scott, J. Chromatogr. Sci., 19 (1981) 599.
28 S. R. Lowry, S. Tsuge, J. J. Leary and T. L. Isenhour, J. Chromatogr. Sci., 12 (1974) 124.
29 M. A. Pichler and S. P. Perone, Anal. Chem., 46 (1974) 1790.
30 S. P. Cram, S. N. Chesler and A. C. Brown III, J. Chromatogr., 126 (1976) 279.
31 J. M. Anderson, J. Liq. Chromatogr., 6 (1983) 2809.

Analytica Chimica Acta, 201 (1987) 171—183
Elsevier Science Publishers B.V., Amsterdam — Printed in the Netherlands

RECOGNIZING CHROMATOGRAPHIC PEAKS WITH PATTERN RECOGNITION METHODS
Part 2. Evaluation of Different Distance Measures

GREGOR REICH

Institute for Analytical Chemistry, University of Vienna, Waehringerstr. 38, A-1090 Vienna (Austria)

(Received 21st May 1987)

SUMMARY

The proposed method for the recognition of peaks in a chromatogram is based on the *k*-nearest neighbour (KNN) algorithm, in which the chromatogram is compared with a predefined peak profile. A critical part of the KNN algorithm is the selection of the distance measure used to calculate the similarity between points in the pattern space. Here, five different distance functions are evaluated. In addition to the euclidian distance, which was used in the initial tests of the algorithm, the correlation coefficient, the cross-correlation, and the angle between two vectors and its cosine are tested. All these distance measures show satisfactory behaviour. Their different characteristics are discussed.

A different algorithm for recognition of chromatographic peaks was described in the preceding paper [1]. This algorithm is based on the KNN (*k*-nearest neighbour) method (see, e.g. [2—4]). With the KNN method, the different points in an *n*-dimensional pattern space are classified according to the distance between them. Obviously, the definition of this distance is of great importance to the success of the classification. In using the KNN algorithm for the recognition of chromatographic peaks, some new constraints for the distance measure are needed. One of the more important properties that the distance measure should have is that it should be extremely insensitive to different peak heights such as occur in chromatograms. Other desirable features of the distance measure were discussed in the preceding paper [1].

The proposed algorithm is based on the concept of comparing a piece of a chromatogram with a predefined profile function which has the shape of a chromatographic peak. This function can also be in more generalized form, e.g., for finding a combination of peaks. The profile and the piece of the chromatogram are defined by n values which are the amplitudes of the digitized chromatogram. These n values define a point in a n-dimensional pattern space. A complete description of the algorithm has been given [1]. The newly defined peak-recognition function (PRF) is the distance between the two points in the pattern space. The distance function has a great influence on the recognition of the peak and has to be chosen carefully.

0003-2670/87/$03.50

SELECTION OF DIFFERENT DISTANCE MEASURES

An often-used distance measure is the euclidian distance, which is defined as

$$d_{ij} = \left[\sum_k (x_{ik} - x_{jk})^2 \right]^{1/2} \tag{1}$$

where d_{ij} is the distance and x_{ik} and x_{jk} are the amplitudes for the profile and the chromatogram, respectively. This distance measure was used in the original evaluation of the method [1], where its limitations were discussed. The geometric definition is shown in Fig. 1(a). Another often-used measure is the correlation coefficient, which is defined as

$$r_{ji} = \left[\sum_k (x_{ik} - \bar{x}_i)(x_{jk} - \bar{x}_j) \right] \Big/ \left[\sum_k (x_{ik} - \bar{x}_i)^2 \sum_k (x_{jk} - \bar{x}_j)^2 \right]^{1/2} \tag{2}$$

where $\bar{x}_i$ and $\bar{x}_j$ are the mean values of x_i and x_j in the selected interval.

The cross-correlation function has been used in processing data from other analytical methods [5], and for peak recognition in gas chromatography with mass spectrometry [6] or Fourier-transform infrared spectrometry [7]. In mass spectrometry, the peak shape is rather constant and cross-correlation is fairly straightforward. The cross-correlation function is defined as

$$c_{ji} = \int_{-\infty}^{+\infty} f(t)g(t + \Delta t)\, dt = \sum_k (x_{ik}x_{jk}) \tag{3}$$

where $f(t)$ is the function of the profile which is being sought, $g(t)$ is the chromatogram, and Δt indicates the shift of the profile over the chromatogram. It is a known property of cross-correlation that the magnitude of the cross-correlation function depends on the magnitude of both functions. This can be an advantage [7], but in the present context it is a disadvantage. Extensive discussions of correlation methods are available [5, 8].

A fourth possible measure is the angle between the two vectors which are defined by the origin and the two points in the pattern space. The points represent the profile and a certain piece of the chromatogram as described before [1]. The geometric properties are shown in Fig. 1(b). This angle can

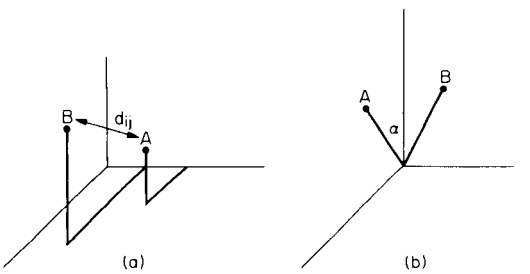

Fig. 1. Definition of different distance measures: (a) the euclidian distance; (b) the vector angle.

be calculated from

$$\cos \alpha = X_i X_j / |X_i| \, |X_j| = \Sigma x_i x_j / [(\Sigma x_i^2)^{1/2} (\Sigma x_j^2)^{1/2}] \quad (4)$$

The promising feature of this distance measure is that the direction of the vector does not change when the distance of the point from the origin changes. This means that if there is a larger peak, then all its points have a greater distance from the baseline, but the direction of the vector from the origin to the point in the pattern space does not change; this property is indicated in Fig. 2. The vector angle can be used in two forms, namely the angle itself and, for simplicity in calculation by avoiding a transcendental function, the cosine of the angle.

To achieve equivalent behaviour for all five measures, the negative values of the distance function are taken for the correlation coefficient, the cross-correlation and the cosine of the vector angle. Then all PRFs have a minimum at the peak position. The algorithm for finding a peak (i.e., the minimum of the PRF) is the same algorithm as before [1]. Another algorithm for the detection of a peak is a simple threshold comparison. It can be seen from all figures that this is a useful method for detection of peaks. Only if there are great differences between the shape of the profile peak and the actual chromatographic peak, or if the *S/N* ratio drops well below one, does it become impossible to use this algorithm.

RESULTS AND DISCUSSION

Effect of the peak height

The first test for all the distance measures is the test for the influence of the peak height. The results obtained with each measure for the unscaled mode and the scaled mode are given in Table 1. The reason for using a scaling step has been discussed [1]. Also two different signal-to-noise ratios (*S/N*) were used. It can be seen that, as expected, the euclidian distance and cross-correlation in the unscaled mode are very dependent on the ratio of the

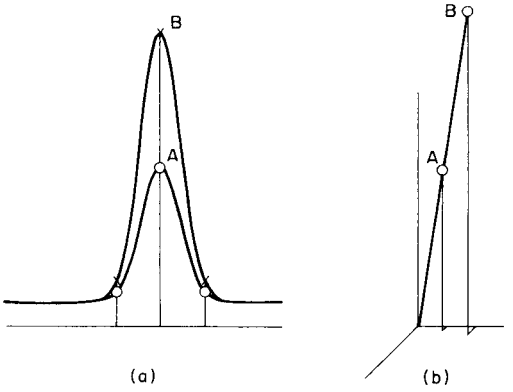

Fig. 2. Position of the peak vector for different peak heights: (a) two peaks with peak B double the height of peak A; (b) the vector for peaks A and B.

TABLE 1

Minimum of the PRF depending on the height of the peak with $S/N = \infty$ and $S/N = 100$

Peak height ratio	Euclid. distance	Correlation coefficient	Cross-correlation	Cosine vector angle	Vector angle	Peak height ratio	Euclid. distance	Correlation coefficient	Cross-correlation	Cosine vector angle	Vector angle
S/N = ∞. UNSCALED						*S/N = 100. UNSCALED*					
0.1	5.74	−1.00	−0.71	−1.00	0.000	0.1	5.36	−0.965	−0.19	−0.970	0.211
0.2	4.53	−1.00	−1.42	−1.00	0.000	0.2	4.20	−0.992	−0.90	−0.991	0.120
0.3	3.47	−1.00	−2.13	−1.00	0.000	0.3	3.18	−0.996	−1.61	−0.995	0.084
0.4	2.55	−1.00	−2.84	−1.00	0.000	0.4	2.30	−0.998	−2.32	−0.997	0.064
0.5	1.77	−1.00	−3.55	−1.00	0.000	0.5	1.57	−0.999	−3.03	−0.998	0.052
0.6	1.13	−1.00	−4.25	−1.00	0.000	0.6	0.97	−0.999	−3.73	−0.999	0.044
0.7	0.64	−1.00	−4.96	−1.00	0.000	0.7	0.52	−0.999	−4.44	−0.999	0.038
0.8	0.28	−1.00	−5.67	−1.00	0.000	0.8	0.21	−0.999	−5.15	−0.999	0.033
0.9	0.07	−1.00	−6.38	−1.00	0.000	0.9	0.04	−1.000	−5.86	−0.999	0.030
1.0	0.00	−1.00	−7.09	−1.00	0.000	1.0	0.02	−1.000	−6.57	−1.000	0.027
1.1	0.07	−1.00	−7.80	−1.00	0.000	1.1	0.13	−1.000	−7.28	−1.000	0.024
1.2	0.28	−1.00	−8.51	−1.00	0.000	1.2	0.39	−1.000	−7.99	−1.000	0.023
1.3	0.64	−1.00	−9.22	−1.00	0.000	1.3	0.79	−1.000	−8.70	−1.000	0.021
1.4	1.13	−1.00	−9.93	−1.00	0.000	1.4	1.33	−1.000	−10.12	−1.000	0.019
Baseline[a]	6.66	0.01	−0.10	−0.66	0.786	Baseline	6.36	0.005	−0.26	−0.623	0.841
Maximum[b]	11.90	0.51	−0.10	−0.05	1.526	Maximum	12.00	0.513	−0.25	−0.072	1.499
S/N = ∞. SCALED						*S/N = 100. SCALED*					
0.1	0.00	−1.00	−7.08	−1.00	0.000	0.1	0.272	−0.960	−7.21	−0.977	0.233
0.2	0.00	−1.00	−7.08	−1.00	0.000	0.2	0.084	−0.990	−7.25	−0.994	0.121
0.3	0.00	−1.00	−7.08	−1.00	0.000	0.3	0.040	−0.995	−7.26	−0.997	0.078
0.4	0.00	−1.00	−7.08	−1.00	0.000	0.4	0.023	−0.997	−7.27	−0.998	0.057
0.5	0.00	−1.00	−7.08	−1.00	0.000	0.5	0.015	−0.998	−7.28	−0.999	0.045
0.6	0.00	−1.00	−7.08	−1.00	0.000	0.6	0.010	−0.999	−7.27	−0.999	0.037
0.7	0.00	−1.00	−7.08	−1.00	0.000	0.7	0.007	−0.999	−7.24	−1.000	0.032
0.8	0.00	−1.00	−7.08	−1.00	0.000	0.8	0.006	−0.999	−7.22	−1.000	0.028
0.9	0.00	−1.00	−7.08	−1.00	0.000	0.9	0.004	−0.999	−7.20	−1.000	0.024
1.0	0.00	−1.00	−7.08	−1.00	0.000	1.0	0.004	−1.000	−7.19	−1.000	0.022
1.1	0.00	−1.00	−7.08	−1.00	0.000	1.1	0.003	−1.000	−7.18	−1.000	0.020
1.2	0.00	1.00	−7.08	−1.00	0.000	1.2	0.002	−1.000	−7.17	−1.000	0.018
1.3	0.00	−1.00	−7.08	−1.00	0.000	1.3	0.002	−1.000	−7.16	−1.000	0.016
1.4	0.00	−1.00	−7.08	−1.00	0.000	1.4	0.002	−1.000	−7.16	−1.000	0.015
Baseline	6.85	0.00	0.00	0.00	0.967	Baseline	6.889	0.005	−4.71	−0.567	0.912
Maximum	11.94	0.51	0.00	0.00	1.571	Maximum	11.946	0.513	−0.20	−0.047	1.524

[a] Value of the PRF on the chromatogram in the baseline region. [b] Value of the maximum before the minimum of the PRF.

TABLE 2

Minimum of the PRF depending on the ratio of the peak widths with $S/N = \infty$ and $S/N = 100$

Peak width ratio	Euclid. distance	Correlation coefficient	Cross-correlation	Cosine vector angle	Vector angle	Peak width ratio	Euclid. distance	Correlation coefficient	Cross-correlation	Cosine vector angle	Vector angle
S/N = ∞. UNSCALED						*S/N = 100. UNSCALED*					
0.500	2.04	−0.88	−0.90	−0.89	0.46	0.500	1.95	−0.88	−0.95	−0.864	0.52
0.625	2.59	−0.94	−1.06	−0.95	0.35	0.625	2.46	−0.94	−1.13	−0.919	0.40
0.750	3.20	−0.98	−1.20	−0.98	0.20	0.750	3.03	−0.97	−1.28	−0.956	0.30
0.825	3.85	−0.99	−1.32	−1.00	0.09	0.825	3.65	−0.99	−1.41	−0.977	0.21
1.000	4.54	−1.00	−1.42	−1.00	0.00	1.000	4.30	−0.99	−1.52	−0.989	0.15
1.125	5.26	−1.00	−1.50	−1.00	0.08	1.125	4.99	−0.99	−1.62	−0.993	0.12
1.250	6.01	−0.99	−1.57	−0.99	0.16	1.250	5.70	−0.98	−1.70	−0.991	0.13
1.375	6.79	−0.98	−1.62	−0.98	0.22	1.375	6.44	−0.96	−1.77	−0.987	0.17
1.500	7.58	−0.97	−1.67	−0.96	0.28	1.500	7.19	−0.95	−1.84	−0.979	0.21
1.625	8.38	−0.95	−1.71	−0.95	0.33	1.625	7.95	−0.94	−1.89	−0.970	0.25
1.750	9.18	−0.94	−1.74	−0.93	0.38	1.750	8.72	−0.93	−1.94	−0.960	0.29
1.875	9.98	−0.93	−1.77	−0.91	0.42	1.875	9.48	−0.92	−1.99	−0.949	0.32
2.000	10.76	−0.92	−1.79	−0.90	0.46	2.000	10.24	−0.91	−2.03	−0.939	0.35
2.125	11.53	−0.92	−1.81	−0.88	0.49	2.125	10.98	−0.90	−2.06	−0.928	0.38
2.250	12.27	−0.91	−1.83	−0.87	0.52	2.250	11.70	−0.89	−2.09	−0.918	0.41
S/N = ∞. SCALED						*S/N = 100. SCALED*					
0.500	1.66	−0.88	−4.48	−0.850	0.46	0.500	1.92	−0.879	−4.27	−0.868	0.50
0.625	0.89	−0.94	−5.31	−0.948	0.32	0.625	1.13	−0.939	−5.07	−0.926	0.38
0.750	0.37	−0.98	−6.02	−0.980	0.20	0.750	0.58	−0.974	−5.75	−0.962	0.27
0.825	0.09	−1.00	−6.60	−0.996	0.09	0.825	0.24	−0.989	−6.33	−0.983	0.19
1.000	0.00	−1.00	−1.09	−1.000	0.00	1.000	0.10	−0.992	−6.81	−0.991	0.13
1.125	0.07	−1.00	−7.48	−0.997	0.08	1.125	0.11	−0.986	−7.22	−0.992	0.12
1.250	0.27	−0.99	−7.80	−0.989	0.15	1.250	0.24	−0.975	−7.57	−0.989	0.14
1.375	0.53	−0.98	−8.06	−0.979	0.21	1.375	0.44	−0.962	−7.85	−0.982	0.17
1.500	0.83	−0.97	−8.26	−0.969	0.25	1.500	0.68	−0.949	−8.10	−0.975	0.21
1.625	1.14	−0.95	−8.42	−0.959	0.29	1.625	0.94	−0.935	−8.28	−0.968	0.23
1.750	1.43	−0.94	−8.55	−0.949	0.32	1.750	1.20	−0.923	−8.43	−0.961	0.26
1.875	1.71	−0.93	−8.66	−0.941	0.34	1.875	1.43	−0.912	−8.56	−0.954	0.28
2.000	1.96	−0.92	−8.74	−0.934	0.37	2.000	1.65	−0.901	−8.66	−0.949	0.30
2.125	2.19	−0.92	−8.81	−0.928	0.38	2.125	1.85	−0.892	−8.74	−0.944	0.31
2.250	2.39	−0.91	−8.87	−0.923	0.40	2.250	2.03	−0.884	−8.81	−0.940	0.33
Baseline[a]	6.85	0.00	0.00	0.00	0.967	Baseline	6.89	0.005	−4.71	−0.567	0.91
Maximum[b]	11.94	0.51	0.00	0.00	1.571	Maximum	11.95	0.513	−0.20	−0.047	1.52

[a, b] See Table 1.

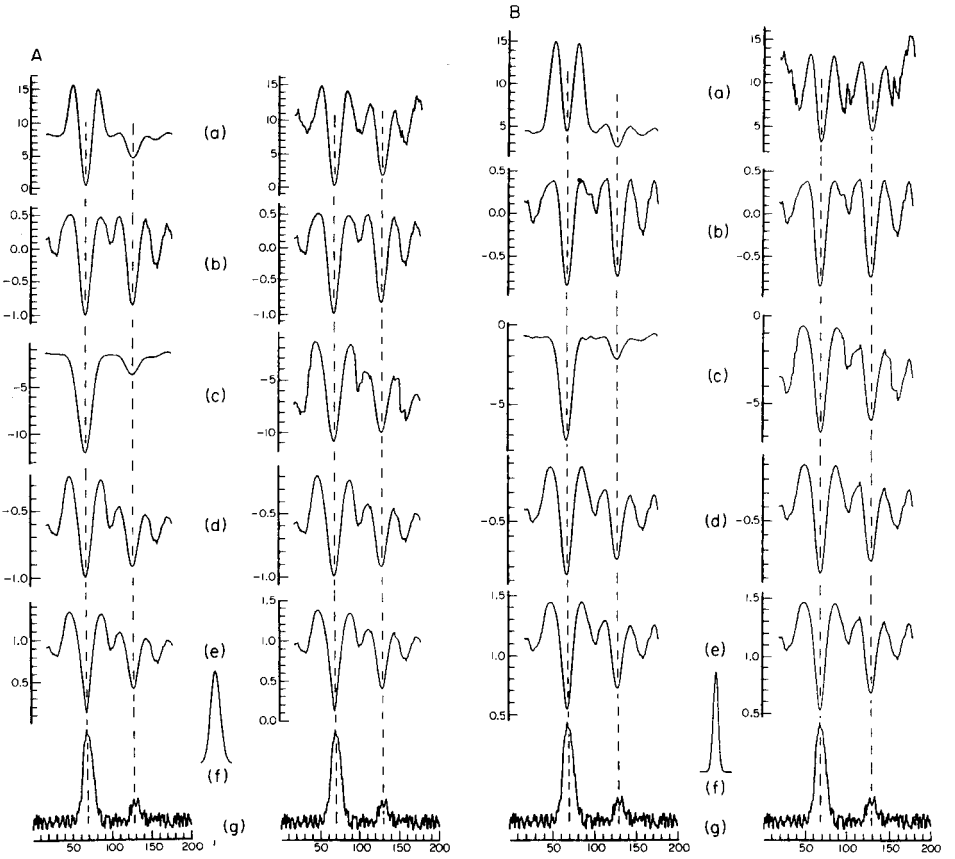

Fig. 3. Recognition of different peak heights with all distance measures in unscaled mode (left side) and scaled mode (right side). (a) Euclidean distance; (b) correlation coefficient; (c) cross-correlation; (d) cosine of the Vector angle; (e) vector angle; (f) peak profile; (g) chromatogram. 40-dimensional space is used; S/N = 20 for the large peak and S/N = 4 for the small peak. (A) The right-hand peak has the same width as the larger peak but a fifth of its height; recognition with a profile peak of the same width as the chromatographic peak. (B) As for (A), but the profile peak is half the width of the chromatographic peak.

height of the profile and the height of the peak. This is not the case for the three other measures and when the scaling step is included.

The minimum of the PRF is given in all tables; in most tables, additional information is given on the value of the PRF on the chromatogram in the baseline region, and the value of the maximum before the minimum of the PRF (see [1]). For some parameters, the baseline value and the value of the maximum change with the parameter value and are then not given in the table.

Figure 3A shows the results for all five distance measures in the unscaled mode (left side) and the scaled mode (right side). The vector angle has a distinct feature if the profile and the chromatographic peak become very similar; it shows a very sharp tip. The arc cosine is a nonlinear transformation

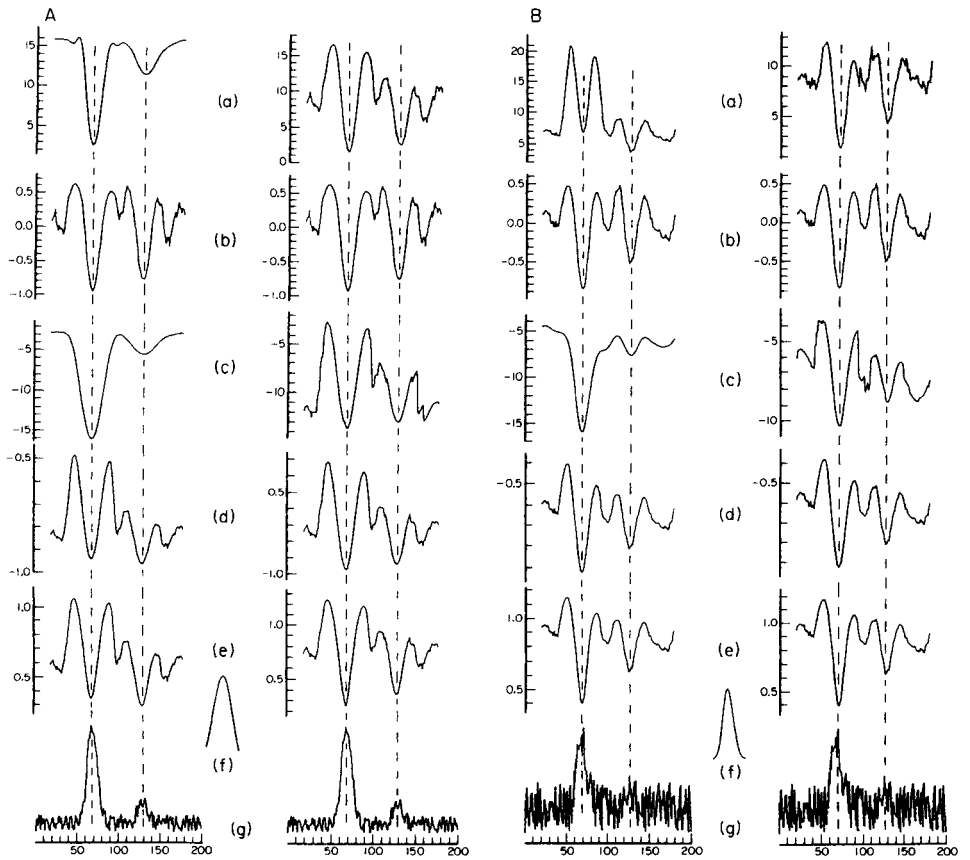

Fig. 4. (A) Recognition with a profile with double the width of the chromatographic peak. (B) Recognition with S/N = 5 for the large peak and S/N = 1 for the small peak. Parameters other than those specified are the same as in Fig. 3A.

and when the cosine of an angle approaches unity then there is a large change in the angle for a small change in the cosine. In all figures, the simulated chromatogram consists of two peaks where the second peak is one fifth of the height of the first peak (i.e., peak amplitude ratio is 0.2). The S/N ratio is 20 and the profile peak corresponds to the first peak unless indicated otherwise.

Effect of profile peak width

The influence of a change in the width of the profile peak compared with the chromatographic peak was then tested. In Fig. 3A, the profile and the chromatographic peak have the same width. In Fig. 3B, the profile has half the width, and in Fig. 4A double the width, of the chromatographic peak. It can be seen that the behaviour of all distance functions, when the ratio of the peak widths change, shows the same peculiarity as discussed in Part 1 [1]. Only for cross-correlation in the unscaled mode is there no increase in

TABLE 3

Minimum of the PRF depending on the signal-to-noise ratio

Signal/ noise	Euclid. distance	Correlation coefficient	Cross correlation	Cosine vector angle	Vector angle
UNSCALED					
∞	0.000	−1.000	−7.10	−1.000	0.00
70	0.017	−0.999	−7.38	−0.999	0.05
65	0.020	−0.999	−7.40	−0.999	0.06
60	0.024	−0.999	−7.42	−0.998	0.06
55	0.028	−0.999	−7.46	−0.998	0.07
50	0.034	−0.999	−7.50	−0.998	0.07
45	0.042	−0.998	−7.54	−0.997	0.08
40	0.053	−0.998	−7.60	−0.996	0.09
35	0.069	−0.997	−7.67	−0.996	0.10
30	0.095	−0.996	−7.77	−0.994	0.12
25	0.136	−0.994	−7.90	−0.992	0.14
20	0.213	−0.991	−8.10	−0.988	0.17
15	0.378	−0.984	−8.44	−0.980	0.21
10	0.851	−0.964	−9.12	−0.961	0.30
7.0	2.651	−0.939	−9.35	−0.939	0.32
6.5	3.075	−0.930	−9.53	−0.933	0.34
6.0	3.609	−0.920	−9.73	−0.926	0.36
5.5	4.291	−0.907	−9.9	−0.917	0.38
5.0	5.176	−0.891	−10.26	−0.908	0.40
4.5	6.376	−0.870	−10.61	−0.897	0.42
4.0	8.058	−0.845	−11.05	−0.883	0.45
3.5	10.47	−0.815	−11.62	−0.868	0.48
3.0	—	−0.776	−12.37	−0.849	0.52
2.5	—	−0.723	−13.43	−0.828	0.56
2.0	—	−0.653	−15.05	−0.803	0.60
1.5	—	−0.559	−17.73	−0.776	0.63
1.0	—	−0.448	−23.17	−0.716	0.67
0.5	—	−0.341	—	−0.701	0.72
SCALED					
∞	0.000	−1.000	−7.085	−1.000	0.00
70	0.015	−0.999	−7.027	−0.999	0.04
65	0.017	−0.999	−7.023	−0.999	0.05
60	0.020	−0.999	−7.019	−0.999	0.05
55	0.024	−0.999	−7.015	−0.999	0.05
50	0.029	−0.998	−7.009	−0.998	0.06
45	0.036	−0.998	−7.002	−0.998	0.07
40	0.045	−0.997	−6.994	−0.998	0.07
35	0.058	−0.996	−6.984	−0.997	0.08
30	0.078	−0.995	−6.970	−0.996	0.10
25	0.109	−0.993	−6.965	−0.994	0.11
20	0.164	−0.989	−6.968	−0.991	0.14
15	0.275	−0.981	−6.972	−0.986	0.18
10	0.548	−0.958	−6.979	−0.972	0.25
7.0	0.670	−0.923	−6.381	−0.955	0.34
6.5	0.746	−0.912	−6.343	−0.950	0.36
6.0	0.837	−0.899	−6.300	−0.945	0.38
5.5	0.944	−0.882	−6.252	−0.939	0.40
5.0	1.059	−0.862	−6.199	−0.931	0.43
4.5	1.198	−0.360	−6.138	−0.922	0.46
4.0	1.371	−0.803	−6.088	−0.912	0.50
3.5	1.587	−0.761	−6.029	−0.899	0.53
3.0	1.854	−0.707	−5.962	−0.884	0.58
2.5	2.141	−0.635	−5.882	−0.865	0.63
2.0	2.531	−0.544	−5.787	−0.842	0.70
1.5	3.077	−0.427	−5.672	−0.814	0.76
1.0	3.596	—	−5.405	−0.777	—
0.5	3.860	—	−5.656	−0.731	—

TABLE 4

Minimum of the PRF depending on the baseline slope with $S/N = \infty$ and $S/N = 100$

Baseline slope (%)	Euclid. distance	Correlation coefficient	Cross-correlation	Cosine vector angle	Vector angle	Baseline slope (%)	Euclid. distance	Correlation coefficient	Cross-correlation	Cosine vector angle	Vector angle
S/N = ∞. UNSCALED						*S/N = 100. UNSCALED*					
0	0.00	−1.000	−7.09	−1.000	0.00	0	0.01	−1.000	−7.26	−0.999	0.03
5	0.01	−1.000	−7.30	−1.000	0.03	5	0.04	−1.000	−7.48	−0.998	0.06
10	0.05	−0.998	−7.51	−0.998	0.06	10	0.11	−1.000	−7.69	−0.996	0.09
15	0.12	−0.996	−7.72	−0.996	0.09	15	0.20	−1.000	−7.90	−0.993	0.11
20	0.22	−0.992	−7.93	−0.994	0.11	20	0.31	−0.999	−8.11	−0.990	0.14
25	0.34	−0.988	−8.14	−0.990	0.14	25	0.46	−0.999	−8.31	−0.987	0.16
30	0.49	−0.983	−8.35	−0.987	0.16	30	0.63	−0.999	−8.52	−0.983	0.18
35	0.66	−0.977	−8.56	−0.983	0.18	35	0.82	−0.999	−8.74	−0.979	0.20
40	0.87	−0.971	−8.77	−0.979	0.20	40	1.05	−0.999	−8.95	−0.975	0.22
45	1.10	−0.963	−8.98	−0.975	0.22	45	1.30	−0.998	−9.16	−0.971	0.24
50	1.35	−0.957	−9.20	−0.971	0.24	50	1.58	−0.998	−9.37	−0.966	0.26
55	1.64	−0.951	−9.41	−0.966	0.26	55	1.88	−0.998	−9.58	−0.962	0.27
60	1.95	−0.944	−9.62	−0.962	0.28	60	2.21	−0.997	−9.79	−0.957	0.29
65	2.29	−0.936	−9.83	−0.958	0.29	65	2.57	−0.997	−10.00	−0.953	0.31
70	2.65	−0.927	−10.04	−0.953	0.31	70	2.96	−0.996	−10.21	−0.949	0.32
Baseline[a]	6.66	0.006	−0.10	−0.662	0.79	Baseline	6.36	0.005	−0.26	−0.623	0.841
Maximum[b]	11.90	0.514	−0.10	−0.053	1.53	Maximum	12.00	0.513	−0.25	−0.072	1.499
S/N = ∞. SCALED						*S/N = 100. SCALED*					
0	0.000	−1.000	−7.085	−1.000	0.000	0	0.005	−1.000	−7.120	−1.000	0.029
5	0.000	−1.000	−7.091	−1.000	0.013	5	0.005	−1.000	−7.117	−1.000	0.024
10	0.001	−1.000	−7.101	−1.000	0.013	10	0.007	−1.000	−7.107	−1.000	0.022
15	0.003	−1.000	−7.111	−1.000	0.020	15	0.009	−1.000	−7.117	−1.000	0.021
20	0.005	−1.000	−7.121	−1.000	0.027	20	0.012	−0.999	−7.127	−1.000	0.023
25	0.008	−1.000	−7.131	−0.999	0.030	25	0.015	−0.999	−7.137	−0.999	0.027
30	0.012	−0.999	−7.141	−0.999	0.040	30	0.019	−0.999	−7.147	−0.999	0.032
35	0.017	−0.999	−7.151	−0.999	0.047	35	0.024	−0.999	−7.156	−0.999	0.038
40	0.022	−0.998	−7.161	−0.999	0.054	40	0.029	−0.998	−7.166	−0.999	0.044
45	0.027	−0.998	−7.170	−0.998	0.060	45	0.035	−0.998	−7.185	−0.998	0.050
50	0.034	−0.998	−7.180	−0.998	0.067	50	0.042	−0.998	−7.195	−0.998	0.056
55	0.041	−0.998	−7.190	−0.997	0.073	55	0.049	−0.997	−7.204	−0.998	0.062
60	0.048	−0.997	−7.199	−0.997	0.080	60	0.057	−0.997	−7.214	−0.997	0.068
65	0.056	−0.997	−7.208	−0.996	0.086	65	0.065	−0.996	−7.223	−0.997	0.074
70	0.065	−0.996	−7.218	−0.996	0.092	70	0.074	−0.996	−7.232	−0.996	0.080
Baseline	6.847	0.000	0.000	0.000	0.967	Baseline	6.889	0.005	−4.712	−0.567	0.912
Maximum	11.939	0.513	0.000	0.000	1.571	Maximum	11.946	0.513	−0.204	−0.047	1.524

[a, b] See Table 1.

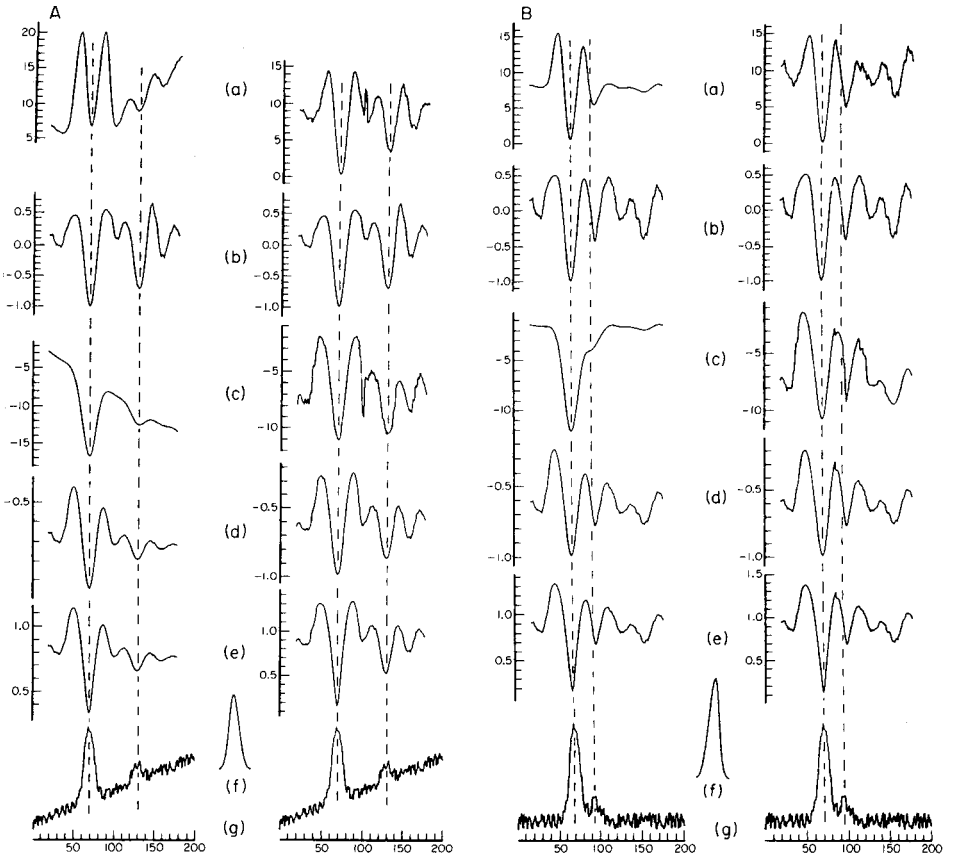

Fig. 5. (A) Recognition with a drifting baseline. (B) Recognition of poorly separated peaks (R = 3.5). Parameters other than those specified are the same as in Fig. 3A.

the PRF before and after the minimum which indicates the peak position. But this effect does not affect the ability to recognize a peak. The results are given in Table 2. For all measures, it can be seen that the value of the minimum is lowest when the profile peak and the chromatographic peak have the same width. The unscaled cross-correlation has no minimum when the two widths are equal, but the steepness of the change for a given variation in the width ratio changes at a ratio of one. All other measures have a minimum by equal peak width. It is evident that a changing peak width has little effect on the recognition of a peak. For a large change of peak width, the profile function has to be adjusted.

Effect of signal-to-noise ratio and sloping baselines

The results obtained with different S/N ratios are given in Table 3. There is no great difference between the performance of the measures. This is not surprising because all the distance functions involve integration, which means

TABLE 5

Minimum of the PRF and deviation of the recognized peak location from the real value depending on the peak resolution, R (the peak amplitude ratio is 0.2 in all cases)

R[a]	Euclid. distance		Correlation coefficient		Cross-correlation		Cosine vector angle		Vector angle	
	Dev.	Min.	Dev.	Min.	Dev.	Min.	Dev.	Min.	Dev.	Min.
S/N = ∞. UNSCALED										
3.0		—		—		—		—		—
3.5	+5	5.90	+5	0.09		—		—		—
4.0	+3	5.30	+4	−0.17		—	+4	−0.59	+4	0.94
4.5	+2	5.30	+3	−0.51		—	+3	−0.79	+3	0.70
5.0	+1	5.88	+2	−0.79		—	+2	−0.89	+2	0.47
5.5	0	4.65	+1	−0.94	0	−1.42	+1	−0.97	+1	0.25
6.0	0	4.56	0	−0.99	0	−1.42	0	−1.00	0	0.10
6.5	0	4.53	0	−1.00	0	−1.42	0	−1.00	0	0.02
7.0	0	4.53	0	−1.00	0	−1.42	0	−1.00	0	0.01
7.5	0	4.53	0	−1.00	0	−1.42	0	−1.00	0	0.00
8.0	0	4.53	0	−1.00	0	−1.42	0	−1.00	0	0.00
8.5	0	4.53	0	−1.00	0	−1.42	0	−1.00	0	0.00
9.0	0	4.53	0	−1.00	0	−1.42	0	−1.00	0	0.00
9.5	0	4.53	0	−1.00	0	−1.42	0	−1.00	0	0.00
10.0	0	4.53	0	−1.00	0	−1.42	0	−1.00	0	0.00
Baseline[b]		6.66		0.01		−0.10		−0.66		0.79
Maximum[c]		11.90		0.51		−0.10		−0.05		1.53
S/N = ∞. SCALED										
3.0		—		—		—		—		—
3.5	+5	6.42	+5	0.092		—		—		—
4.0	+4	4.94	+4	−0.18		—	+4	−0.59	+4	0.94
4.5	+2	3.35	+3	−0.51	+3	−5.60	+3	−0.76	+3	0.70
5.0	+2	1.62	+2	−0.79	+2	−6.67	+2	−0.89	+2	0.47
5.5	+1	0.46	+1	−0.94	0	−7.10	+1	−0.97	+1	0.25
6.0	0	0.07	0	−0.99	0	−7.09	0	−0.995	0	0.10
6.5	0	0.004	0	−1.00	0	−7.09	0	−1.00	0	0.02
7.0	0	0.00	0	−1.00	0	−7.09	0	−1.00	0	0.004
7.5	0	0.00	0	−1.00	0	−7.09	0	−1.00	0	0.00
8.0	0	0.00	0	−1.00	0	−7.09	0	−1.00	0	0.00
8.5	0	0.00	0	−1.00	0	−7.09	0	−1.00	0	0.00
9.0	0	0.00	0	−1.00	0	−7.09	0	−1.00	0	0.00
9.5	0	0.00	0	−1.00	0	−7.09	0	−1.00	0	0.00
10.0	0	0.00	0	−1.00	0	−7.09	0	−1.00	0	0.00
Baseline		6.85		0.00		0.00		0.00		0.96
Maximum		11.94		0.51		0.00		0.00		1.57
S/N = 100. UNSCALED										
3.0	+7	6.30		—		—		—		—
3.5	+5	5.61	+5	0.11		—		—		—
4.0	+3	5.00	+4	−0.16		—	+5	−0.62	+4	0.90
4.5	+2	4.58	+3	−0.48		—	+3	−0.78	+3	0.67
5.0	+1	4.34	+2	−0.77		—	+2	−0.90	+2	0.46
5.5	0	4.25	+1	−0.937	0	−1.58	+1	−0.96	+1	0.29
6.0	0	4.24	0	−0.98	0	−1.58	0	−0.98	0	0.18
6.5	0	4.26	0	−0.99	0	−1.58	0	−0.99	0	0.15
7.0	0	4.27	0	−0.99	0	−1.59	0	−0.99	0	0.14
7.5	0	4.27	0	−0.99	0	−1.60	0	−0.99	0	0.15
8.0	0	4.25	0	−0.99	0	−1.61	0	−0.99	0	0.15
8.5	0	4.22	0	−0.99	0	−1.61	0	−0.99	0	0.14
9.0	0	4.20	0	−0.99	0	−1.61	0	−0.99	0	0.14
9.5	0	4.20	0	−0.99	0	−1.61	0	−0.99	0	0.14
10.0	0	4.23	0	−0.99	0	−1.59	0	−0.99	0	0.14
Baseline		6.66		0.01		−0.10		−0.66		0.786
Maximum		11.90		0.51		−0.10		−0.05		1.526

TABLE 5 (continued)

R^a	Euclid. distance		Correlation coefficient		Cross-correlation		Cosine vector angle		Vector angle	
	Dev.	Min.	Dev.	Min.	Dev.	Min.	Dev.	Min.	Dev.	Min.
S/N = 100. SCALED										
3.0		—		—		—		—		—
3.5	+5	6.15	+5	0.07		—		—		—
4.0	+4	4.75	+4	−0.20	+6	−4.34	+4	−0.60	+4	0.92
4.5	+2	3.21	+3	−0.52	+4	−5.97	+3	−0.77	+3	0.69
5.0	+2	1.51	+2	−0.77	+2	−6.97	+2	−0.90	+2	0.48
5.5	+1	0.61	+1	−0.92	0	−6.81	+1	−0.97	+1	0.29
6.0	0	0.24	0	−0.99	0	−7.04	0	−0.99	0	0.17
6.5	0	0.22	0	−0.99	0	−7.11	0	−0.99	0	0.12
7.0	0	0.17	0	−0.99	0	−7.32	0	−0.99	0	0.11
7.5	0	0.14	0	−0.99	0	−7.00	0	−0.99	0	0.12
8.0	0	0.12	0	−0.99	0	−7.00	0	−0.99	0	0.09
8.5	0	0.21	0	−0.99	0	−6.67	0	−0.99	0	0.11
9.0	0	0.16	0	−0.99	0	−6.89	0	−0.99	0	0.12
9.5	0	0.13	0	−0.99	0	−6.99	0	−0.99	0	0.11
10.0	0	0.14	0	−0.99	0	−6.93	0	−0.99	0	0.14
Baseline		6.89		0.01		−4.71		−0.57		0.91
Maximum		11.95		0.51		−0.20		−0.05		1.52

[a]For definition, see [1]. [b,c]See footnotes a and b in Table 1.

that the *S/N* ratio is improved for all of them. Fig. 4B shows the results for *S/N* = 5 for the large peak and *S/N* = 1 for the small peak. A minimum can be seen, regardless of the distance measure, but the maxima before and after the peak make it sometimes difficult to distinguish between this artefact and the real peak minimum, when the *S/N* ratio is low. The threshold approach may give better results in this case.

The results obtained for different baseline slopes are listed in Table 4. The baseline slope is given as the difference between the baseline at the beginning and at the end of the given chromatogram as a percentage of the peak height. The behaviour is very similar for all distance measures. The minimum obtained depends on the baseline slope but recognition is not hindered in any case. The influence of the baseline slope (Fig. 5A) is similar to the effect of different peak heights (Fig. 3A). The euclidian distance and the cross-correlation produce a slope in the PRF in the unscaled mode; the slope shown is 70%.

Effect of incompletely resolved peaks

The behaviour of all the distance measures with incompletely resolved peaks is shown in Table 5. The earlier discussion [1] is relevant to all the measures. The worst results are given by cross-correlation if scaling is not used. The best results are produced by using the euclidian distance and the correlation coefficient in the scaled mode. Comparison of the minima with the dashed line, which shows the actual positions of the peaks, indicates the shift in the recognized peak location for the second peak.

Conclusions

To summarize, each of the distance measures tested has its own characteristics. The best overall characteristics are shown by the correlation coefficient, which also needs the greatest computation time. The cross-correlation and the euclidian distance are very sensitive to peak-height variations, and for peak recognition the scaling step is essential. However, if curve fitting is to be included in the peak processing, then either of these distance measures can be used for optimization of the peak profile. The vector angle and its cosine have good properties for every tested parameter and the computational overhead is relatively small, especially for the cosine of the angle.

REFERENCES

1 G. Reich, Anal. Chim. Acta, 201 (1987) 153.
2 B. R. Kowalski and C. F. Bender, Anal. Chem., 44 (1972) 1405.
3 M. A. Pichler and S. P. Perone, Anal. Chem., 46 (1974) 1790.
4 N. W. Bell, Computer Detection of MS Peaks by Real-Time Cross-Correlation, Technical Paper No. MS-2, Hewlett Packard, Palo Alto, CA, 1973.
5 G. Horlick and G. M. Hieftje, in D. M. Hercules, G. M. Hieftje, L. R. Snyder and M. A. Evanson (Eds.), Contemporary Topics in Analytical and Clinical Chemistry, Plenum, New York, 1978.
6 W. F. Bryant, M. Trivedi, B. Hinchman, IV, S. Sofranko and P. Mitacek, Jr., Anal. Chem., 52 (1980) 38.
7 R. B. Lam, D. T. Sparks and T. L. Isenhour, Anal. Chem., 54 (1982) 1927.
8 Y. W. Lee, Statistical Theory of Communication, Wiley, New York, 1960.

Analytica Chimica Acta, 201 (1987) 185—191
Elsevier Science Publishers B.V., Amsterdam — Printed in The Netherlands

RESOLUTION OF OVERLAPPED CHROMATOGRAMS BY MEANS OF THE KALMAN FILTER
Dimensional Reduction of Error Covariance Matrices and State Estimate Vectors

YUZURU HAYASHI*, TOSHIO SHIBAZAKI and MITSURU UCHIYAMA
National Institute of Hygienic Sciences, 1-18-1, Kamiyoga, Setagaya-ku, Tokyo (Japan)
(Received 23rd January 1987)

SUMMARY

If many samples are successively injected into a high-performance liquid chromatograph at short intervals, then overlapped chromatograms will be obtained. A simplified version of the Kalman-filter algorithm is described for rapid resolution of several such overlapped peaks on small laboratory computers; the dimensionalities of the error covariance matrix P_k and state estimate vector $\bar{X}_k$ are reduced to far less than the total number of the peaks. Computer simulation shows that at least twenty partially overlapped Gaussian peaks, used as a model of the successive injections can be successfully resolved, with the 4×4 matrix P_k and 4-vector $\bar{X}_k$. This version is independent of the number of injections and is effective for the resolution of a finite number of peaks in that injection mode. The algorithm of small dimensions is applicable to a wide variety of peak resolution procedures.

The Kalman filter is a linear digital filter with a recursive least-squares algorithm and is mathematically expressed as a projection in a linear probability space (Gaussian space). Recently, data processing by Kalman filters has been evaluated for use in many areas of analytical chemistry [1]. The commonest use of the filter has been for resolution of overlapped peaks in ultraviolet-visible spectra [2—5] and voltammograms [6—8].

Overlapped chromatograms will result from injections of many samples at short intervals in high-performance liquid chromatography (HPLC). A rapid, precise method for peak resolution of these overlapped chromatograms would save much time for assays of a large number of samples. For example, the kinetics of a sample which contains some "known" components with "unknown" concentrations often needs a series of measurements of the components. However, a fast reaction will not be satisfactorily monitored by a single apparatus for HPLC, because of the long observation times usually involved. Rapidly repeated injections would make it possible to determine fast time-variations in the component concentrations more easily by HPLC.

The Kalman filter is a strong candidate for such a method because of the rapidity of the calculation, if important quantities such as height, position and width of the component peaks are not altered by the rapidly repeated

0003-2670/87/$03.50

injections in an unexpected way. Most sufficiently dilute samples loaded into a liquid or gas chromatograph will meet this condition. The former, equipped with loop injector and photometric detector, will be suitable for the rapid-injection method because of the superior reproducibility of the peak parameters and fairly small solvent peaks. However, for a gas chromatograph equipped with a flame ionization detector, large solvent peaks will hamper the precise determination of the other components. In any case, peak resolution with the Kalman filter holds good for samples having known components but not for those with unknown components.

The most critical problem of the rapidly-repeated injection method based on the Kalman filter is the large dimensionality of the matrices involved in the algorithm for the resolution of many peaks; the dimensionality is important in governing the calculation speed and the number of estimates. It is difficult to calculate large matrices rapidly on small laboratory computers. Furthermore, their dimensionality is usually specified to be equal to, or more than, the number of component peaks in the total chromatogram or the number of estimates, and should be augmented as additional samples are injected. Consequently, a more useful version of the Kalman filter algorithm would be of small dimensions and be independent of the number of estimates.

The aim of this paper is to derive and justify a simplified Kalman filter algorithm of small dimensions for the resolution of a large number of overlapped peaks in overlapped chromatograms. An application of this algorithm to data processing of HPLC signals will be discussed in a later paper.

EXPERIMENTAL

All programs used here were written in BASIC with a computer (PC-9801 VMII, NEC) equipped with an Intel-8086-compatible CPU (10 MHz), 640 kB of RAM memory and two 5-in. floppy disk drives (2 MB). The Kalman filter algorithm was prepared as described by Kunita [9]; Gaussian white noise was constructed from uniform random numbers according to the central limit theorem [10].

THEORY

The Kalman filter algorithm is reviewed briefly to facilitate understanding of the proposed simplified version. The detailed formulation of the filter has been discussed for chemical [1], engineering [11, 12] and mathematical [9] purposes.

The Kalman filter is used to estimate unknown quantities represented by a model state vector X. For a chromatogram consisting of n components, the vector X denotes the peak heights (or concentrations) of the components. It is assumed that an observed value Y_k (scalar) of X at a data point k is described by the linear combination (measurement model)

$$Y_k = \mathbf{F}_k\mathbf{X} + W_k \tag{1}$$

where W_k denotes white noise in the measurement process of $\mathbf{X}$; $\mathbf{F}_k$ is the measurement matrix ($1 \times n$). If the noise W_k can be neglected or the raw data Y_k successfully smoothed, every element of $\mathbf{F}_k$ can be measured experimentally from the noise-free or smoothed data at the point k and the "known" true values $\mathbf{X}$ ($Y_k = \mathbf{F}_k\mathbf{X}$). The mean of W_k is assumed to be zero and its variance $\hat{W}_k$ at every point k should be known from prior experiments.

The estimated values of $\mathbf{X}$ at the point k are described by the state estimate vector $\tilde{\mathbf{X}}_k$

$$\tilde{\mathbf{X}}_k = \tilde{\mathbf{X}}_{k-1} + \mathbf{L}(k)\,(Y_k - \mathbf{F}_k\tilde{\mathbf{X}}_{k-1}) \tag{2}$$

where $\mathbf{L}(k)$ is called the Kalman gain ($n \times 1$ matrix). Given an initial condition $\tilde{\mathbf{X}}_0$ and the matrix $\mathbf{L}(k)$ at every point k, the update estimate $\tilde{\mathbf{X}}_k$ can be recursively given by the update measurement Y_k and the previous estimate $\tilde{\mathbf{X}}_{k-1}$. Before $\mathbf{X}$ is measured, $\mathbf{L}(k)$ can be calculated from the simultaneous equations

$$\mathbf{L}(k) = \mathbf{P}_{k-1}\mathbf{F}_k^*(\hat{W}_k + \mathbf{F}_k\mathbf{P}_{k-1}\mathbf{F}_k^*)^{-1} \tag{3a}$$

$$\mathbf{P}_k = \mathbf{P}_{k-1} - \mathbf{L}(k)\mathbf{F}_k\mathbf{P}_{k-1} \tag{3b}$$

where $\mathbf{P}_k$ denotes the error covariance matrix ($n \times n$) of the state estimate vector $\tilde{\mathbf{X}}_k$ at point k, and $\mathbf{F}_k^*$ is the transpose of $\mathbf{F}_k$; the term $\hat{W}_k + \mathbf{F}_k\mathbf{P}_{k-1}\mathbf{F}_k^*$ in Eqn. 3(a) is scalar. Given an initial condition $\mathbf{P}_0$ (diagonal matrix), the Kalman gain $\mathbf{L}(k)$ and error covariance matrix $\mathbf{P}_k$ can be calculated beforehand at every point k.

Of importance is that although the Kalman gain $\mathbf{L}(k)$ crucially affects the estimate $\tilde{\mathbf{X}}_k$ of $\mathbf{X}$ (see Eqn. 2), $\mathbf{L}(k)$ depends mainly on the error covariance matrix $\mathbf{P}_{k-1}$ and the measurement matrix $\mathbf{F}_k$. Figure 1 shows a schematic diagram of the calculation of $\mathbf{L}(k)$ and $\mathbf{P}_k$; the sequence of the calculation results is $\mathbf{P}_0 \rightarrow \mathbf{L}(1) \rightarrow \mathbf{P}_1 \rightarrow \mathbf{L}(2)\cdots$. In order to reduce the dimension of the Kalman filter algorithm, therefore, $\mathbf{P}_{k-1}$ or $\mathbf{F}_k$ should be manipulated rather than $\mathbf{L}(k)$. Obviously, if $\mathbf{P}_{k-1} = 0$ and $\mathbf{F}_k = 0$, then $\mathbf{L}(k) = 0$ (see Eqn. 3a), but the reverse is not always true. It should be noted that $\mathbf{L}(k)$ represents the "activity" of the Kalman filter; if $\mathbf{L}(k) = 0$, then the estimate $\tilde{\mathbf{X}}_{k-1}$ is not altered by the new information Y_k concerning $\mathbf{X}$ (Eqn. 2 can be reduced to $\tilde{\mathbf{X}}_k = \tilde{\mathbf{X}}_{k-1}$). However, over the region where $\mathbf{L}(k)$ takes large values, the

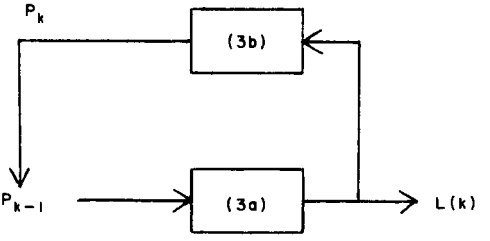

Fig. 1. The main part of the Kalman filter algorithm.

estimation process is "active" and then the recursive estimate $\tilde{\mathbf{X}}_{k-1}$ is improved increasingly as the new information Y_k is included.

RESULTS AND DISCUSSION

Figure 2 shows the close relationships between the diagonal elements of the error covariance matrix $\mathbf{P}_k$ (4 × 4) and the Kalman gain $\mathbf{L}(k)$ (4 × 1) for four overlapped Gaussian peaks. It is usually favorable to choose a large value of $\mathbf{P}_0$ (diagonal matrix) as an initial condition [2]. If $[O]_{ij}$ is defined as an element of matrix $\mathbf{O}$ and $[V]_i$ as an element of vector $\mathbf{V}$, then the Kalman gain element $[L(k)]_{11}$ for peak *a* (Fig. 2c) takes large values only in the region A (Fig. 2), where the signal $[F_k]_{11}[X]_1$ of peak *a* begins to appear, and the diagonal element $[P_k]_{11}$ for peak *a*, which represents the mean square difference $[\tilde{X}_k]_1 - [X]_1$, decreases abruptly. After this active region A, the estimate $\tilde{\mathbf{X}}_{k-1}$ is no longer improved by the new information Y_k. At a point of this inactive region (indicated by B in Fig. 2), the elements $[P_k]_{1i}$ and $[P_k]_{i1}$ ($i = 1,\cdots,4$) are almost zero (data not shown). Therefore, the 4 × 4 error covariance matrix $\mathbf{P}_k$ may be regarded as a 3 × 3 matrix at point B, i.e., the estimation of the single peak *a* is already complete.

It should be noted that relatively large values of both $[P_{k-1}]_{11}$ and $[F_k]_{11}$ are necessary for active estimation of peak *a* (see Eqn. 3a); at the points slightly after region A where the signal $[F_k]_{11}[X]_1$ of peak *a* is large enough but $[P_{k-1}]_{11}$ is very small, the Kalman gain $[L(k)]_{11}$ for peak *a* is almost zero and then the estimation of peak *a* becomes inactive. However, not all the off-diagonal elements $[P_{k-1}]_{1i}$ and $[P_{k-1}]_{i1}$ are near zero in this region.

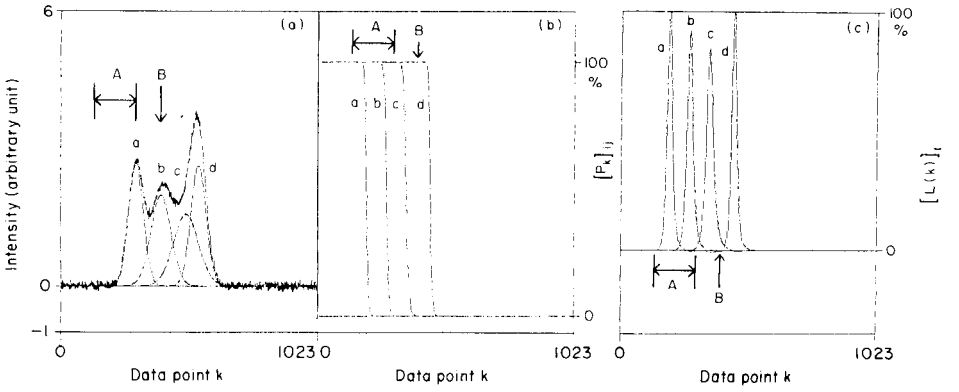

Fig. 2. Simulation of a chromatogram comprised of four Gaussian peaks (a) and changes in the diagonal elements of the error covariance matrix $\mathbf{P}_k$ (b) and the Kalman gain $\mathbf{L}(k)$ (c). (a) The component peaks are labeled (*a*—*d*); the variance $\hat{W}_k$ of the white noise W_k which accompanies the chromatogram is 2.5×10^{-3}. (b) All the diagonal elements of $\mathbf{P}_0$ (initial condition) are 10^6; the ordinate is normalized by $\mathbf{P}_0$. (c) The ordinate is normalized by the maximum (ca. 4700) of the $\mathbf{L}(k)$ elements for peak *a*. For meanings of A and B, see text.

It can be concluded that when the estimation of the single peak *a* is complete (point B), the dimensionality of the error covariance matrix $\mathbf{P}_k$ can be reduced by one. Furthermore, in the region before point B, peak *d* can be neglected, because its Kalman gain $[L(k)]_{41}$ still does not increase. It is quite satisfactory to start the estimate of peak *d* at point B by re-use of the already meaningless element $[P_k]_{11}$ of peak *a*.

Figure 3 shows the four component peaks in a chromatogram, and the superimposed diagram obtained by five successive injections. The period of the single chromatogram is 1023 points; the intervals of the successive injections are 511 points. The Gaussian peaks *b*, *c* and *d* partially overlap, but their resolution by means of the Kalman filter is known to be successful [1, 2]. The overlapped chromatograms were simulated with the normally-distributed component peak heights as well as white noise W_k (see Fig. 4). This simulation is a model for situations in which HPLC data are obtained for numerous samples which involve some known components with unknown concentrations, e.g., examinations of kinetics of a sample or assay of a series of samples. The simplified algorithm for the Kalman filter which can resolve these twenty partially overlapped peaks in the total chromatogram, can be described by the 4 × 4 matrix $\mathbf{P}_k$ and the 4-vector $\bar{\mathbf{X}}_k$: at the intermediate, inactive points between peaks 1*a*—5*a* (indicated by arrows B_1—B_4 in Fig. 3), the element $[P_k]_{11}$ was forced to be the large value of the initial condition $[P_0]_{11}$ for the subsequent estimation; the off-diagonal elements $[P_k]_{1i}$ and $[P_k]_{i1}$ (i = 2, 3, 4) were forced to zero (only this process can be omitted); and the measurement model of the peaks 2*a*—5*a* was also involved in $[F_k]_{11}$.

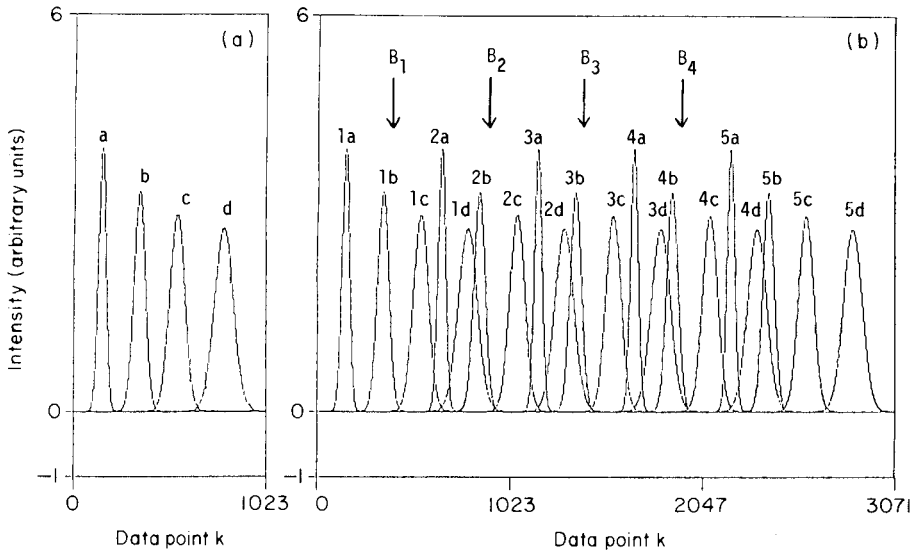

Fig. 3. Component peaks in a chromatogram (a) and the diagram derived from superimposing five successive injections (b). Arrows B_1—B_4 denote the initiation points for the subsequent estimation (see text).

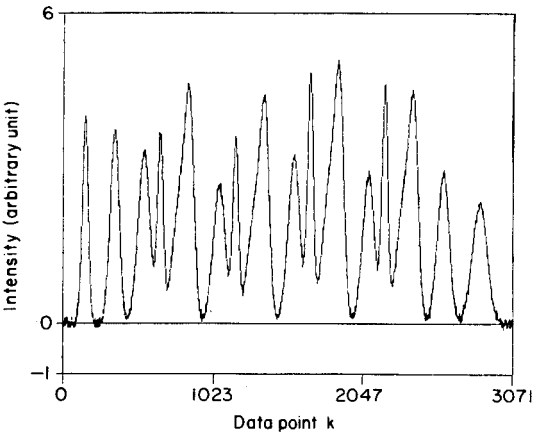

Fig. 4. Simulation of the total chromatogram obtained by the five successive injections. All the diagonal elements of $\mathbf{P}_0$ are 10^5; $\hat{W}_k$ is 2.5×10^{-3}.

The value $[\tilde{X}_{B_i-1}]_1$ was adopted as the final estimate of peak *ia* ($i = 1,\cdots,4$); the last $[\tilde{X}_{3071}]_1$ was taken as the final estimate of peak 5*a*. The other peaks *b*, *c* and *d* were manipulated in the same way.

This simplified algorithm with the 4×4 matrix $\mathbf{P}_k$ and the 4-vector $\tilde{\mathbf{X}}_k$ provides satisfactory estimates of twenty peaks in overlapped chromatograms. Peak *d* strongly overlaps with the peak *b* in the subsequent chromatogram (see Fig. 3b). Figure 5 shows that the final estimates of peaks 1*d*—4*d* (indicated by B_1—B_4) and 5*d* (the last $[\tilde{X}_{3071}]_4$) correspond to their true values satisfactorily; the relative standard deviation of the error was less than 0.24% in the presence of the white noise W_k ($\hat{W}_k = 2.5 \times 10^{-3}$) on twenty runs (100 estimates for each component).

If another two injections are added in the same intervals to the total chromatogram shown in Fig. 4, the total region increases to 4096 points. However, the 4×4 Kalman gain $\mathbf{L}(k)$ and the 1×4 measurement matrix $\mathbf{F}_k$ in the region of 1023—2046 points are available in the same form for the newly added region of 2047—3070 points where the peaks originating from the fourth to sixth injections participate. This procedure makes the dimensionality of the algorithm independent of the number of injections or peaks. Consequently, any finite number of overlapped peaks derived from the same injection mode can be rapidly resolved by the simplified four-dimensional Kalman filter, because the Kalman filter is a real-time means of data processing and so there is no need to store all the past raw data (see Eqn. 2).

The simplified Kalman filter algorithm with small dimensions, as described above, makes it possible to resolve a large number of peaks in HPLC rapidly on small laboratory computers. This algorithm should be applicable to a wide variety of peak-resolution procedures and may lead to novel designs for experimental procedures.

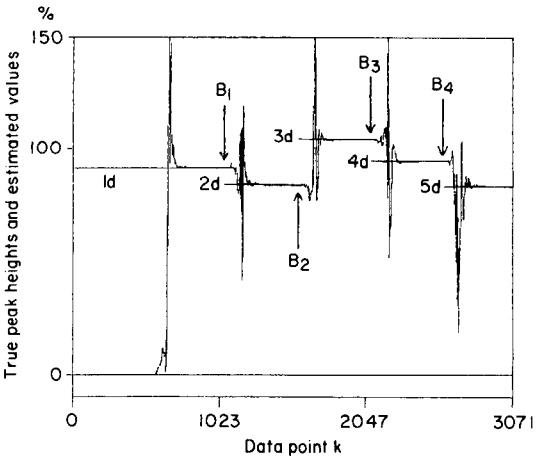

Fig. 5. Estimates (continuous line) and true values (horizontal lines indicated by 1*d*—5*d*) of peaks 1*d*—5*d*. The ordinate is normalized by the mean M of the normally distributed peaks d (M = 350). The initial condition $\tilde{\mathbf{X}}_0$ is zero. Arrows B_1—B_4 represent the final estimates of peaks 1*d*– 4*d*; the final estimate of 5*d* is the last $[\tilde{X}_{3071}]_4$.

REFERENCES

1 S. D. Brown, Anal. Chim. Acta, 181 (1986) 1 (and references therein).
2 H. N. J. Poulisse, Anal. Chim. Acta, 112 (1979) 361.
3 C. B. M. Didden and H. N. J. Poulisse, Anal. Lett., Part A, 13 (1980) 921.
4 A. van Loosbroek, H. J. G. Debets and D. A. Doornbos, Anal. Lett., Part A, 17 (1984) 677.
5 A. van Loosbroek, H. J. G. Debets and P. M. J. Coenegracht, Anal. Lett., Part B, 17 (1984) 779.
6 T. F. Brown and S. D. Brown, Anal. Chem., 53 (1981) 1410.
7 C. A. Scolari and S. D. Brown, Anal. Chim. Acta, 166 (1984) 253; 178 (1985) 239.
8 S. C. Rutan and S. D. Brown, Anal. Chem., 55 (1983) 1707.
9 H. Kunita, Estimations of Random Processes, Sangyo Tosho, Japan, 1976.
10 W. Feller, An Introduction to Probability Theory and Its Applications, Vol. 2, Wiley, New York, 1971.
11 S. Arimoto, Kalman Filter, Sangyo Tosho, Japan, 1977.
12 A. H. Jazwinski, Stochastic Processes and Filtering Theory, Academic, New York, 1970.

Analytica Chimica Acta, 201 (1987) 193—205
Elsevier Science Publishers, B.V., Amsterdam — Printed in The Netherlands

AN EXPERIMENTAL STUDY OF THE EFFICIENCY OF DIFFERENT STATISTICAL FUNCTIONS FOR THE RESOLUTION OF CHROMATOGRAMS WITH OVERLAPPING PEAKS

JOAN GRIMALT*

Department of Environmental Chemistry (C.I.D./C.S.I.C.), Jorge Girona Salgado 18-26, E-08034 Barcelona (Spain)

HORTENSIA ITURRIAGA and JOAQUIM OLIVE[a]

Department of Analytical Chemistry, Science Faculty, Universitat Autònoma de Barcelona, Bellaterra, Barcelona (Spain)

(Received 13th October 1986)

SUMMARY

The effectiveness of different functions of statistical distribution (Gaussian, log-normal, gamma and Weibull) is examined for the deconvolution of chromatograms with overlapped peaks. A modified Gaussian function is also considered for comparison. The results obtained in the curve fitting of individual peaks, corresponding to diverse solutes run in polar, semi-polar and apolar columns, show that the log-normal function is generally the best for description of the chromatographic shapes. This function proved to be the most useful in the resolution of a test set of 32 overlapped chromatographic profiles prepared from mixtures of standards of known quantitative composition.

Chemometric studies for the resolution of signals derived from analytical instrumentation (spectroscopy, chromatography, etc.) are of great current interest [1]. Obviously, this is a consequence of the increasing automation of routine analytical work. The use of calculation techniques allows the range of application of analytical methods to be enlarged considerably in cases where there is peak overlapping. This can be a more convenient approach to automated laboratory work than the utilization of a large number of special procedures, each relevant only to small groups of samples or particular problems. Hardware problems related to setting up each new method (change of instrumental conditions, recalibration, etc.) can thus be avoided. However, the possibilities of these generalized procedures are not unlimited, because of the intrinsic characteristics of the analytical techniques. In addition, the use of numerical systems raises problems of calculation that in many cases have not been successfully solved. The numerical resolution of chromatograms with overlapped peaks is one such case.

Curve-resolution methods for overlapping of chromatographic peaks have two main aspects: (1) the type of function (mathematical or empirical)

[a]Present address: Escola Universitària Politècnica, Avgda. Víctor Balaguer, Vilanova i la Geltrú, E-08800 Barcelona, Spain.

0003-2670/87/$03.50

used to describe the components present in the mixture; (2) the method selected for obtaining the best match between the experimental profile and a sum of a convenient number of these individual functions. The present paper is devoted to the first aspect.

In chromatography, it is well known that Gaussian functions describe the elution front of an ideal compound in an ideal system, but it is also well known that Gaussian peaks are rare in real chromatograms [2, 3]. Among other variables, peak shapes depend on the functional groups of the solutes [4]. Several types of modified Gaussian functions have therefore been used in curve-resolution procedures for chromatography, as outlined earlier [5]. In contrast to that approach, Grimalt et al. [5] considered the utility of various distribution functions currently in use in statistics (Gauss, log-normal, gamma and Weibull). Because the statistical probability functions correspond to given types of phenomena, their utilization in fitting of chromatographic peaks is of interest, for it may help in characterizing some factors of the chromatographic process. In this sense, non-Gaussian statistical functions have already proved useful in spectroscopic analysis [6].

Recently, much attention has been devoted to numerical techniques that do not involve assumptions on peak shapes [7, 8]. These use factor analysis for studying the multiparametric data available with hyphenated instrumentation. From such information, the chromatographic bands corresponding to the solutes present in the mixture can be discerned. Successful applications of this technique have been reported in gas chromatography/mass spectrometry [7, 9], liquid chromatography coupled with diode-array u.v.-visible spectrophotometry [10, 11] and gas chromatography/Fourier-transform infrared spectroscopy [8]. However, most gas or liquid chromatographs are not coupled to sophisticated detectors but to simple devices monitoring a single property of the eluting mixture. Thus, the increasing computing facilities of most laboratories are still faced with the problem of deconvolution of mere overlapped chromatograms. This problem is not so well resolved. With simple instrumentation, the lack of assumptions on the form of the chromatographic profiles involves several drawbacks like the need for calibration methods [12, 13] or comparison with shapes of reference peaks [14]. These features considerably complicate and limit the resolution of overlapping profiles by numerical techniques. In fact, a major question related to functions for profile prediction lies in evaluating the extent of application of the assumed shapes. Very few papers dealing with curve-resolution problems provide many examples of calculation for real cases, so that the breadth of application of the proposed functions can rarely be estimated.

In this paper, an extensive evaluation is presented of the various statistical functions (Gauss, log-normal, gamma and Weibull) as well as a modified Gaussian function proposed by Littlewood et al. [15] which was chosen for comparison. A mathematical description of these functions has already been given [5]. Thirty-nine compounds, including aliphatic, olefinic and aromatic hydrocarbons, alcohols, ketones, esters, carboxylic acids, phenols,

anilines and nitrate and halogenated compounds, were grouped in suitable mixtures and analyzed by gas chromatography. Three columns packed with stationary phases covering a wide range of polarity (SE-30, OV-17 and Carbowax 20M) were used. As result, thirty-two overlapped chromatograms were studied for resolution with these functions, covering a wide span of types of profiles and degrees of overlapping. Extreme cases like high column overloading or nonlinear or saturated detector response factors are not considered because they can readily be avoided in quantitative chromatography, especially in routine analysis.

Curve fitting was done by means of a least-squares generalized method. Details of the method and program used have been given [5]. The residual sum of squares function, $R(\bar{x})$, was used to define the criterion of convergence and to evaluate the quality of the fittings:

$$R(\bar{x}) = \sum_{k=1}^{m} [\mathbf{F}^k_{\text{diff}}(\bar{x})]^2 \tag{1}$$

where $\mathbf{F}^k_{\text{diff}}(\bar{x}) = \mathbf{F}^k_{\text{predicted}}(\bar{x}) - \mathbf{F}^k_{\text{observed}}$, $\bar{x}$ is the vector of the parameters defining the adjusted functions (a sum of individual shapes), and k refers to a particular point (abscissa) of the chromatogram. After deconvolution, the areas (A) corresponding to the resulting component peaks were measured and used for evaluation. Thus, the errors of the estimated quantitative peak composition were calculated, and their absolute values were averaged and compared:

$$E = (\sum_{L=1}^{n} |A^L_{\text{diff}}|)/n \tag{2}$$

where $A^L_{\text{diff}} = (A^L_{\text{predicted}} - A^L_{\text{real}})/A^L_{\text{real}}$, and L refers to a particular component of the mixture.

EXPERIMENTAL

Thirty-nine compounds covering a wide span of polarity were selected for testing. They include aliphatic hydrocarbons (cyclohexane, heptane and heptadecane), olefins (cyclohexene) and aromatics (1,3-, 1,5- and 1,6-dimethylnaphthalenes, bromobenzene and 1,4-dichlorobenzene), alcohols (n-butan-1-ol, n-butan-2-ol, n-pentan-1-ol, n-hexan-1-ol, n-hexan-3-ol, 2-methylpropan-1-ol, 2-methylbutan-1-ol, 4-methylpentan-1-ol and 2-butoxyethanol), ketones (n-hexan-2-one, 4-methylpentan-2-one, cyclohexanone and acetophenone), esters (ethyl n-hexanoate, ethyl n-heptanoate and isobutyl ethanoate), carboxylic acids (acetic acid, n-propanoic acid and n-butanoic acid), phenols (3-bromophenol, 2-bromo-4-chlorophenol and 2,6-dibromophenol), naphthols (1-hydroxynaphthalene), amines (aniline, *N*,*N*-dimethylaniline and 1-aminonaphthalene) and nitrated hydrocarbons (nitromethane, nitroethane and nitrobenzene).

A Varian Aerograph 90-P instrument equipped with a thermal conductivity detector was used. Three stainless-steel columns packed with stationary

phases of different polarity were used: (a) the apolar phase was 3% SE-30 on Varaport 30 (100/120 mesh, 2 m, 0.25-in. i.d.); (b) the semi-polar phase was 5% OV-17 on Chromosorb W.AW (80/100 mesh, 1 m, 0.25-in. i.d.); and (c) the polar phase was 10% Carbowax-20M on Chromosorb W.AW (100/120 mesh, 1 m, 0.25-in. i.d.). Helium was the carrier gas. The flow rates were: (a) and (b) 12.5 ml min^{-1}; (c) 10.2 ml min^{-1}. Injector temperature 255°C; detector temperature 260°C.

Suitable mixtures of the above-mentioned compounds were prepared and submitted to gas chromatography on the three columns indicated. Those presenting peak overlapping were selected. The thirty-two chromatograms studied are listed in Table 1. The quantitative composition of the mixtures and the particular chromatographic conditions are also indicated. The relative response factors of the detector for the compounds present in each mixture were evaluated by comparison of the areas corresponding to the individual components. These were obtained either by instrumental resolution under other chromatographic conditions (e.g., changing oven temperature) or by individual injection of the compounds. A listing of these response factors is also given in Table 1.

RESULTS AND DISCUSSION

The chromatographic profiles selected for numerical analysis include variable degrees of overlapping. These can be assessed by the relation between the retention time (t_R) and the sum of half-widths at half-height (H).

$$D = 2(t_{R,a} - t_{R,b})/(H_a + H_b) \quad (3)$$

where $t_{R,a}$ and $t_{R,b}$ are the retention times for peaks a and b, respectively, and H_a and H_b are the respective widths at half-height of the band. This D ratio was calculated and is given in Table 1 for each of the thirty-two chromatograms considered. It ranges between 0.75 and 2.0; the first value corresponds to a high degree of overlapping (no minimum in the unresolved profile) and the second to a situation of almost full resolution.

A preliminary step to the deconvolution of overlapped profiles was to fit the individual chromatographic peaks with the functions considered in the present study. Accordingly, a group of compounds including extreme cases of polarity like n-heptane and n-propionic acid was selected for injection in the three columns described above. The compounds were subjected separately to gas chromatography and, after curve calculation, their chromatograms were compared with the best fitting curve obtained with each function. The accuracy of the adjustments was evaluated from the resulting residual sum of squares (Eqn. 1).

The results corresponding to thirty-two profiles are presented in Table 2. Their main characteristic is the good performance of the log-normal function which always gives the best fit, regardless of the solute and column used. In contrast, it is also noticeable that, with two exceptions (n-propionic acid

TABLE 1

List of chromatograms studied by means of several statistical functions

Chromatogram no.	Column	Temp. (°C)	Composition of the mixture[a]		Relative response factor[b]	Degree of overlapping
S-1	SE-30	175	2-Bromo-4-chlorophenol/2,6-dibromophenol	(44.8:55.2)	1.18	1.7
S-2	SE-30	140	1,5-Dimethylnaphthalene/1,3-dimethylnaphthalene	(42.7:57.3)	0.92	0.75
S-3	SE-30	80	n-Hexan-2-one/4-methylpentan-2-one	(47.9:52.1)	1.00	1.5
S-4	SE-30	105	n-Butan-1-ol/n-pentan-1-ol	(41.6:58.7)	1.25	1.4
S-5	SE-30	105	*N,N*-dimethylaniline/acetophenone	(44.4:55.6)	0.80	0.8
S-6	SE-30	168	1-Hydroxynaphthalene/1-aminonaphthalene	(47.8:52.2)	0.73	0.75
S-7	SE-30	80	Cyclohexanone/bromobenzene	(49.4:50.6)	0.86	1.15
S-8	SE-30	90	Cyclohexanone/bromobenzene	(49.4:50.6)	0.86	1.6
S-9	SE-30	110	n-Butan-2-ol/4-methylpentan-2-one	(48.8:51.2)	1.23	1.1
S-10	SE-30	82	n-Hexan-3-ol/2-methylbutan-1-ol	(33.2:66.8)	0.83	1.6
S-11	SE-30	95	n-Hexan-3-ol/2-methylbutan-1-ol	(33.2:66.8)	0.83	1.3
O-12	OV-17	90	n-Hexan-1-ol/4-methylpentan-1-ol	(48.3:51.7)	0.91	1.5
O-13	OV-17	60	n-Butan-2-ol/2-methylpropan-1-ol/n-butan-1-ol	(31.4:34.0:34.6)	1.17 and 1.14	0.95 and 1.8
O-14	OV-17	65	n-Butan-2-ol/2-methylpropan-1-ol/n-butan-1-ol	(31.4:34.0:34.6)	1.17 and 1.14	0.90 and 1.6
O-15	OV-17	90	n-Heptane/cyclohexane/cyclohexene	(25.2:33.7:41.1)	0.70 and 0.96	1.65 and 0.9
O-16	OV-17	80	n-Heptane/cyclohexane/cyclohexene	(25.2:33.7:41.1)	0.70 and 0.96	2.0 and 1.0
O-17	OV-17	100	Isobutyl acetate/n-propionic acid	(40.0:60.0)	1.81	1.45
O-18	OV-17	100	n-Hexan-2-one/4-methylpentan-2-one	(47.9:52.1)	1.09	1.9
O-19	OV-17	245	2-Bromo-4-chlorophenol/2,6-dibromophenol	(44.8:55.2)	1.18	2.0
O-20	OV-17	190	1,5-Dimethylnaphthalene/1,3-dimethylnaphthalene	(42.7:57.3)	0.92	0.8
O-21	OV-17	90	n-Propionic acid/1,4-dichlorobenzene	(40.4:59.6)	0.49	1.8
O-22	OV-17	185	Nitrobenzene/aniline	(49.0:51.0)	0.75	1.9
O-23	OV-17	200	Nitrobenzene/aniline	(49.0:51.0)	0.75	1.6
O-24	OV-17	125	Nitromethane/nitroethane	(33.6:66.4)	1.37	1.0
O-25	OV-17	135	n-Butan-2-ol/4-methylpentan-2-one	(48.8:51.2)	1.20	1.6
O-26	OV-17	205	1-Hydroxynaphthalene/1-aminonaphthalene	(47.8:52.2)	0.88	1.6
C-27	Carb.20M	100	Ethyl n-hexanoate/acetic acid	(38.2:61.8)	0.76	1.25
C-28	Carb.20M	120	2-Methylpropan-1-ol/n-butan-2-ol	(44.4:55.6)	0.85	1.5
C-29	Carb.20M	170	n-Butanoic acid/*N,N*-dimethylaniline	(45.3:54.7)	0.95	1.2
C-30	Carb.20M	175	n-Propionic acid/1,4-dichlorobenzene	(40.4:59.6)	0.78	1.2
C-31	Carb.20M	70	Cyclohexene/cyclohexane	(46.2:53.8)	1.38	1.5
C-32	Carb.20M	85	Cyclohexene/cyclohexane	(46.2:53.8)	1.38	1.2

[a]The percentage (w/w) of the components in the mixture is given in parentheses. [b]The detector relative response factors (*w/w*) are referred to the last compound of every mixture.

TABLE 2

Curve fitting of chromatographic profiles corresponding to a single compound. The usefulness of the selected functions is evaluated by comparison of the residual sum of squares (Eqn. 1) obtained for every fit

Column	Compound	Residual sum of squares				
		Gauss	Log-normal	Gamma	Weibull	Littlewood
SE-30	n-Propionic acid	16	1.6	9.0	—	11
	Ethyl n-heptanoate	25	3.3	11	9.1	14
	Aniline	13	0.80	5.4	3.9	7.1
	n-Hexan-1-ol	26	0.27	17	3.9	19
	n-Hexan-2-one	14	0.20	1.1	3.2	3.1
	n-Heptane	1.9	0.098	0.15	0.80	0.31
	n-Heptadecane	6.2	0.93	1.5	3.7	2.3
	1,4-Dichlorobenzene	4.9	1.1	1.2	3.1	1.5
	3-Bromophenol	1.8	0.054	0.70	0.46	0.94
	1,6-Dimethylnaphthalene	3.0	0.18	0.77	1.1	1.2
	Nitromethane	7.7	0.08	3.5	1.1	4.5
OV-17	n-Propionic acid	16	1.7	26	2.5	23
	Ethyl n-heptanoate	15	2.1	11	—	12
	Aniline	13	2.4	6.0	5.6	7.6
	2-Butoxyethanol	29	6.9	18	15	20
	n-Hexan-1-ol	2.9	0.068	0.52	0.79	—
	n-Hexan-2-one	1.9	0.10	0.16	0.79	0.36
	n-Heptane	2.1	1.2	1.7	2.0	1.8
	n-Heptadecane	0.20	0.065	0.16	0.20	0.085
	1,4-Dichlorobenzene	15	5.2	9.1	17	10
	3-Bromophenol	3.7	0.39	0.61	1.8	1.0
	1,6-Dimethylnaphthalene	1.1	0.15	0.16	0.40	0.24
	Nitromethane	3.3	0.073	0.11	1.5	0.38
Carbowax 20M	n-Propionic acid	17	0.31	7.6	2.3	9.6
	Ethyl n-heptanoate	3.7	0.30	1.3	1.4	1.8
	Aniline	4.2	0.48	2.3	1.7	2.7
	2-Butoxyethanol	13	2.5	10	5.7	11
	n-Hexan-1-ol	18	3.2	11	8.9	13
	n-Hexan-2-one	2.9	0.45	1.0	1.9	1.3
	n-Heptane	11	0.81	6.0	3.2	7.0
	1,4-Dichlorobenzene	1.3	0.038	0.18	0.51	0.36
	Nitromethane	2.5	0.16	0.18	1.2	0.33

and 1,4-dichlorobenzene run in the OV-17 column), the Gaussian function always gives the highest residual sum of squares. As indicated above, this function is hypothesized for elution profiles in ideal chromatographic processes, notwithstanding the fact that the highest fitting errors are found in its application. This is observed even in the cases of apolar compounds (n-heptane and n-heptadecane) tested in an apolar column (SE-30), which represent the situation closest to ideal conditions of elution. A large number of references is available in the literature (see, e.g., [2—4]), in which many

distortion effects which force real chromatographic peaks to deviate from the ideal profiles are studied.

The behaviour of the gamma, Weibull and Littlewood functions depends on the polarity of the solutes. Thus, in cases of compounds of low polarity (i.e., n-heptane, n-hexan-2-one or 1,4-dichlorobenzene), the gamma function gives the smaller fitting errors and the Weibull function yields worse fits. In contrast, for products of high polarity (i.e., n-hexan-1-ol, 2-butoxyethanol or n-propionic acid), the Weibull function gives the best results. These trends are essentially independent of the type of column used (SE-30, OV-17 or Carbowax 20M).

An important aspect for consideration is the number of parameters needed for the description of every function. The log-normal and Weibull functions are described by four parameters and the Gaussian, gamma and Littlewood are described by only three. In principle, a higher number of parameters involves more flexibility for adapting to any shape, independently of the process originating the profiles. However, at least for the curves considered in the present paper (chromatographic bands), this is not a general rule. The log-normal function gives better fits in all cases but the Weibull function is rating second only for peaks of compounds of high polarity. If the solutes are not very polar, the gamma and Littlewood functions perform better than the Weibull.

These results are especially significant with regard to a paper by Vaidya and Hester [16] where a generalized exponential function was proposed for the adjustment of chromatographic peaks. That function, in fact, can be described as an extension, using five parameters, of the Weibull function. Better fits were reported [16], although they may be a mere consequence of the increased bending possibilities coming from the added parameter. In contrast to this approach, the results of Table 2 show that other functions with four parameters, like the log-normal, are defined in such a way that they give a better fit to the chromatographic profiles. In this sense, the parameters of the log-normal function (maximum height (h), abscissa reading (t_0) at h, width at half-height (w) and coefficient of asymmetry (p) [5]) are correlated more directly with the characteristics of a chromatographic peak than the parameters corresponding to the Weibull function. The latter function is defined by h and t_0, and by the starting point of the function (a) as well as a complex parameter (c) defining w and p for a given value of t_0 [5].

The profiles resulting from the curve fitting of several chromatographic shapes with the Gaussian, log-normal, gamma and Weibull functions are presented in Figs. 1 and 2. These selected examples include polar (n-propanoic acid) and apolar (n-heptane) solutes run in polar (Carbowax 20M) and apolar (SE-30) columns. The good performance of the log-normal function in all cases is significant.

The results obtained in the deconvolution of the fused chromatograms of Table 1 are reported in Table 3. In agreement with the fitting of individual chromatographic peaks, the log-normal function gives the best results in

almost all cases. Only in two chromatograms, S-6 and O-17, does the Weibull function give a slightly smaller error than the log-normal function. Furthermore, according to the size of the residual sum of squares, after the log-normal function, the gamma function generally gives the best fits but, in cases of very polar compounds, the Weibull function performs better. The Gaussian function gives the worst fits for most of the profiles, which is again in agreement with the results in Table 2. The deconvolution of chromatogram O-15

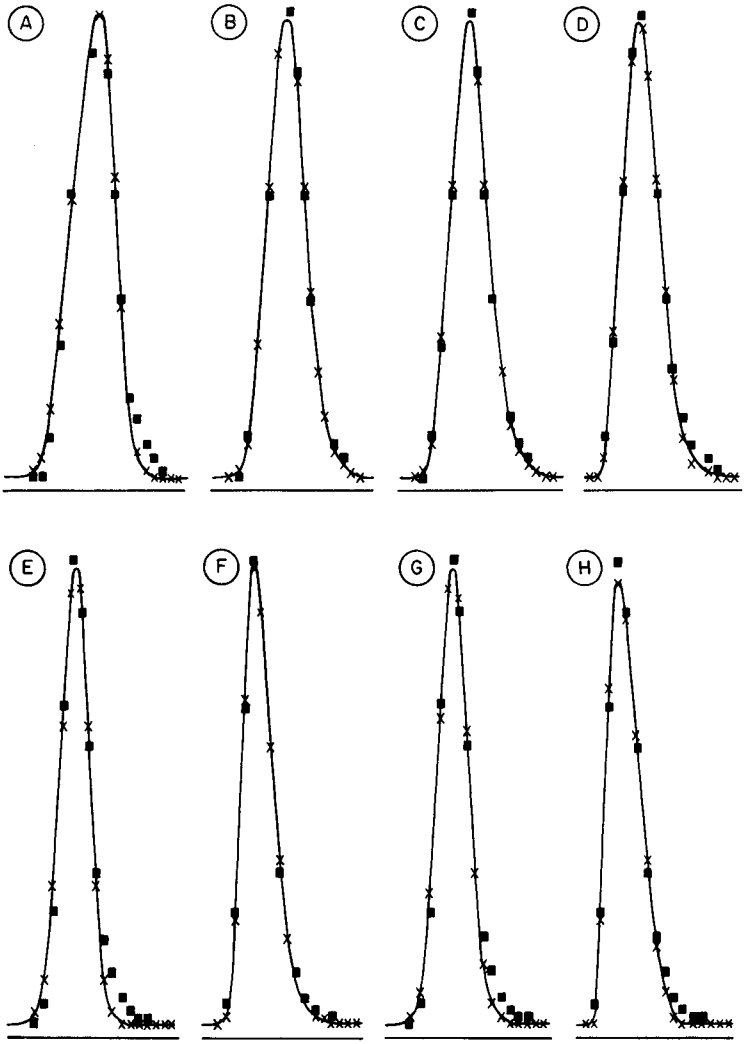

Fig. 1. Curve-fitting profiles of n-heptane run in SE-30 (A—D) and Carbowax 20M (E—H) columns. Examples with Gaussian (A, C), log-normal (B, F), gamma (C, G) and Weibull (D, H) functions are presented. The total fitting profile is indicated by the continuous line. (■) Real points; (×) fitted points in the chromatogram. Priority pointing rule: × over ■; real points are not shown where they coincide with fitted points.

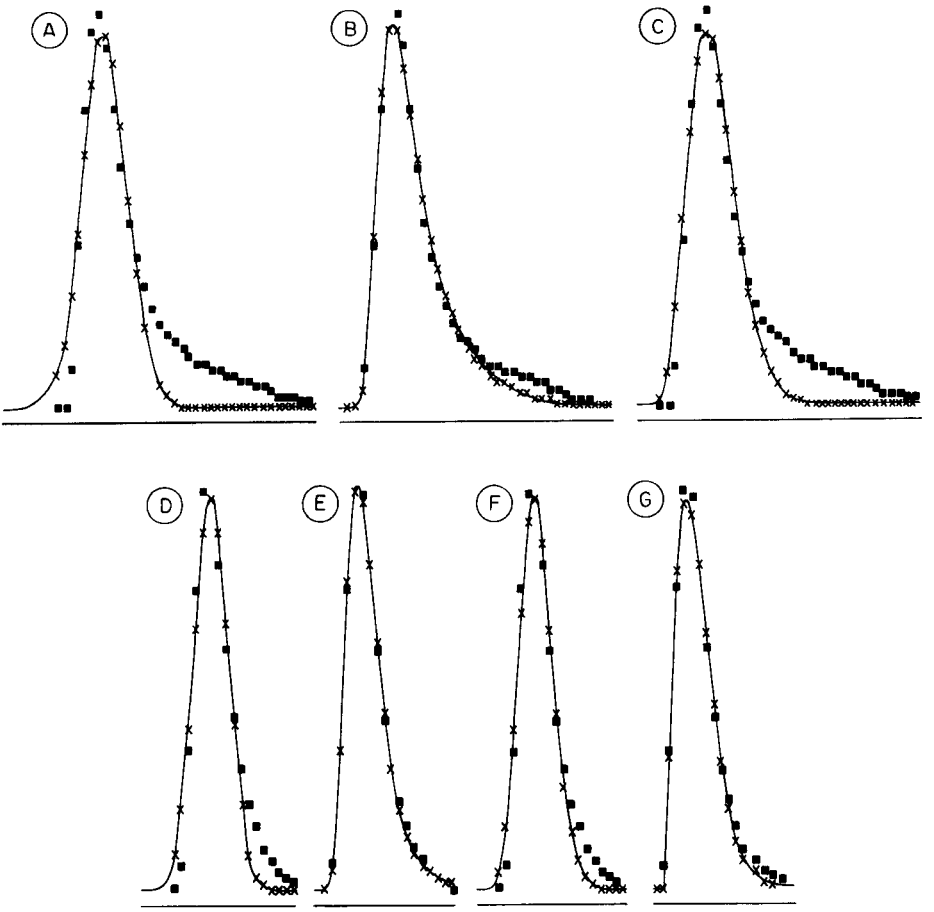

Fig. 2. Curve-fitting profiles of n-propionic acid run in SE-30 (A—C) and Carbowax 20M (D—G) columns. Examples with Gaussian (A, D), log-normal (B, E), gamma (C, F) and Weibull (G) functions are presented. Symbols as in Fig. 1.

with all the functions studied in this paper is illustrated in Fig. 3. Nevertheless, if the error in the prediction of the quantitative composition of the mixtures is considered, significant discrepancies can be obtained in some cases with the log-normal function. The origin of this problem is illustrated in Fig. 4, where the resolution of chromatogram C-27 is shown. Where asymmetric peaks are concerned, if the tailing side of one of these peaks is masked within the unresolved area, the deconvolution with log-normal functions may give rise to very asymmetric bands which do not correspond with the real shape of the elution profiles. Thus in these cases, the mathematical point of convergence of the fitting (that giving the smallest residual sum of squares) may not be in agreement with the real chromatographic process.

TABLE 3

Resolution of chromatograms with overlapping peaks. For each function, the results are compared by considering the residual sums of squares of the fittings (R; Eqn. 1) and the average error produced in the determination of the quantitative composition of the mixtures (E; Eqn. 2)

Chrom. no.	Gaussian		Log-normal		Gamma		Weibull		Littlewood	
	R	E	R	E	R	E	R	E	R	E
S-1	14	2.0	4.1	0.3	10	2.9	11	3.5	11	3.0
S-2	1.0	11	0.39	48	—	—	0.51	35	1.7	49
S-3	6.5	4.4	0.15	0.7	3.1	1.2	3.6	3.4	3.7	0.8
S-4	6.2	8.2	0.44	2.5	3.6	3.8	4.5	1.0	4.1	4.5
S-5	—	—	0.42	51	—	—	—	—	—	—
S-6	0.78	26	0.30	4.1	0.44	14	0.23	25	0.49	1.7
S-7	14	7.6	1.1	6.1	8.0	4.6	7.8	6.4	9.2	4.2
S-8	0.87	23	0.07	2.1	0.55	14	—	—	0.60	16
S-9	2.1	18	0.71	7.8	1.9	0.7	2.2	22	2.0	5.2
S-10	12	11	0.087	1.2	8.3	9.4	4.5	2.0	9.2	9.8
S-11	3.0	17	0.058	0.3	0.73	7.2	0.61	9.0	1.1	9.8
O-12	0.64	1.0	0.22	6.4	0.24	5.1	0.32	3.4	0.27	3.4
O-13	2.6	8.3	0.51	28	1.5	2.3	2.4	7.0	1.7	3.9
O-14	1.1	12	0.21	18	0.41	5.8	—	—	0.54	2.1
O-15	0.38	16	0.27	11	0.33	18	0.38	18	0.34	8.8
O-16	0.99	16	0.11	9.9	0.81	25	0.32	16	0.86	14
O-17	21	24	2.8	2.5	30	29	2.8	—	27	28
O-18	5.9	0.2	0.50	1.3	0.73	3.0	7.1	2.7	1.0	2.3
O-19	2.8	1.3	0.15	1.1	1.3	0.9	2.3	0.8	1.6	0.5
O-20	0.27	41	0.16	19	0.30	2.3	0.27	51	0.29	10
O-21	0.98	1.8	0.38	2.7	2.0	7.4	0.94	7.3	0.92	6.0
O-22	5.2	0.6	0.92	2.6	2.9	0.1	5.0	6.6	3.4	0.5
O-23	4.4	1.5	2.0	1.6	2.9	1.0	4.3	0.3	3.2	0.6
O-24	0.65	17	0.15	3.2	0.63	4.0	0.40	23	0.63	2.4
O-25	3.9	2.9	0.52	0.2	1.0	1.2	3.6	0.2	1.5	0.6
O-26	0.25	4.2	0.10	0.4	0.17	3.3	0.11	1.1	0.18	4.0
C-27	12	15	1.6	31	9.9	12	9.6	0.9	10	14
C-28	2.0	3.7	0.16	5.8	0.32	7.7	1.5	5.3	0.54	6.1
C-29	8.1	1.0	0.93	1.0	7.0	1.5	—	—	7.3	1.5
C-30	1.5	0.6	0.39	4.4	0.98	7.7	0.84	2.1	0.93	5.8
C-31	0.33	1.1	0.017	5.4	0.025	4.1	0.29	3.9	0.058	3.2
C-32	0.13	4.8	0.017	7.6	0.032	2.1	0.097	5.6	0.046	0.1

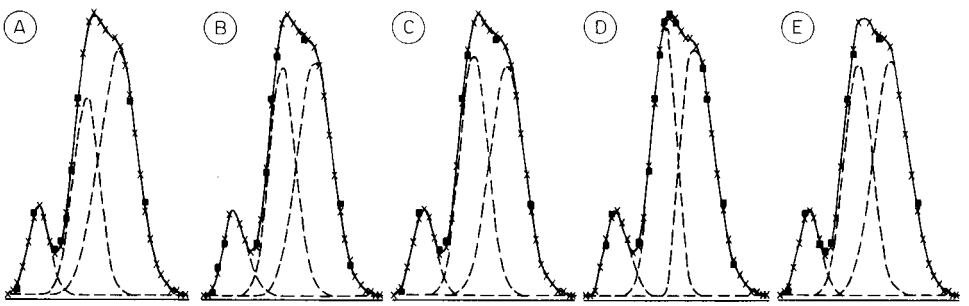

Fig. 3. Curve-fitting profiles of chromatogram O-15. Fits with Gaussian (A), log-normal (B), gamma (C), Weibull (D) and Littlewood (E) functions are shown. The total adjustment profile (——) and the contour of each component peak (- - - - -) are indicated. Symbols as in Fig. 1.

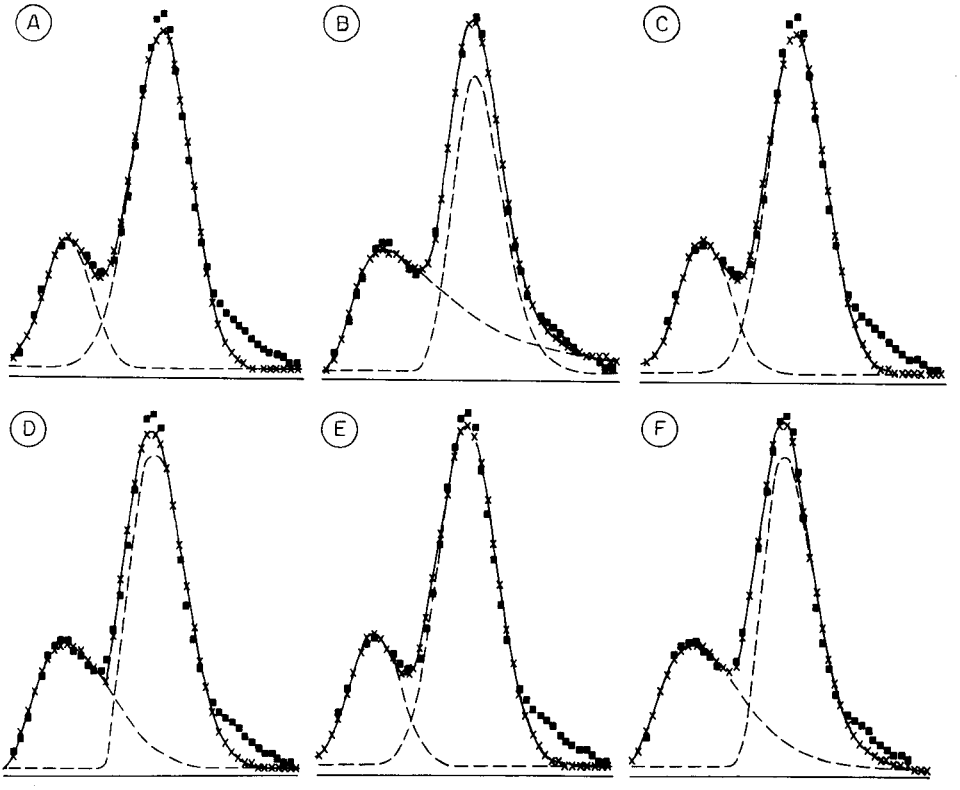

Fig. 4. Curve-fitting profiles of chromatogram C-27. Fits with Gaussian (A), log-normal (B), gamma (C), Weibull (D) and Littlewood (E) functions, and with a log-normal function (F) with a fixed coefficient of asymmetry (see Table 4) are shown. Symbols as in Fig. 3.

This problem can easily be solved by the introduction of some restriction in the parameters of the functions used in the deconvolution process, e.g., in the case of log-normal functions, by setting a maximum value for the coefficient of asymmetry. An example of this approach is also illustrated in Fig. 4. The values of the coefficient of asymmetry used in this example as well as the resulting residual sum of squares and average quantitative error are given in Table 4. It can be observed that the error of the areas is now minimized and that the residual sum of squares is still smaller than that corresponding to the other functions (although it is higher than that initially obtained).

In Table 4, besides chromatogram C-27, other examples of resolution with log-normal functions with a fixed coefficient of asymmetry are presented. In all cases, the problems of unreal points of convergence are successfully resolved and, compared with the data in Table 3, better estimates of the quantitative composition are again obtained with the log-normal function. Consequently, it is concluded that these types of anomaly, mainly observed

TABLE 4

Elucidation of unresolved chromatograms with log-normal functions with fixed coefficient of asymmetry. The residual sum of squares of the fittings (R; Eqn. 1) and the average error produced in the determination of the quantitative composition of the mixtures (E; Eqn. 2) are considered for comparison

Chromatogram no.	Coefficients of asymmetry			R	E
	Peak 1	Peak 2	Peak 3		
S-6	1.2	1.06		0.44	1.7
S-9	1.2	1.3		0.88	1.4
	1.18	1.3		1.1	0.90
O-13	1.08	1.20	1.169	0.74	5.3
	1.05	1.22	1.169	0.81	4.3
O-14	1.08	1.20	1.169	0.26	1.7
O-20	1.1	1.2		0.18	7.4
	1.1	1.1		0.26	4.6
	1.1	1.15		0.22	2.0
O-24	1.05	1.15		0.39	0.60
C-27	1.5	1.3		4.4	3.1
	1.6	1.35		3.7	0.60
C-31	1.02	1.13		0.34	3.2
	1.02	1.17		0.55	2.9
C-32	1.10	1.13		0.045	3.4
	1.02	1.13		0.16	1.3
	1.06	1.13		0.088	3.4

in some cases of application of the log-normal function, are related to the method selected for curve fitting or with the criterion of convergence and not with the numerical characteristics of the function. The selection of other criteria of convergence than the minimization of the residual sum of squares may allow the problem to be avoided, but this is outside the scope of the present paper.

Conclusions

A broad variety of chromatographic profiles was prepared by injection of a set of compounds of very different polarity (from n-alkanes to carboxylic acids) in apolar (SE-30), semi-polar (OV-17) and polar (Carbowax 20M) columns. Curve fitting of the resulting thirty-two peaks with different functions has shown that the log-normal function is the more useful for describing all types of chromatographic bands. In the second level of effectiveness, the gamma function gives the best results for the solutes of low polarity (hydrocarbons, ketones, etc.), but the Weibull function performs better in the case of profiles corresponding to carboxylic acid, phenols and other highly polar compounds. The Gaussian function gives the worst fitting errors in almost all cases. These results were essentially confirmed when the same functions were used for the deconvolution of thirty-two overlapped chromatograms. Again, the performance of the log-normal function was excellent.

REFERENCES

1 L. S. Ramos, K. R. Beebe, W. P. Carey, E. Sánchez M., B. C. Erikson, B. E. Wilson, L. E. Wangen and B. R. Kowalski, Anal. Chem., 58 (1986) 294R.
2 A. H. Anderson, T. C. Gibb and A. B. Littlewood, J. Chromatogr. Sci., 8 (1970) 640.
3 S. N. Chesler and S. P. Cram, Anal. Chem., 45 (1973) 1354.
4 S. D. Mott and E. Grushka, J. Chromatogr., 126 (1976) 191.
5 J. Grimalt, H. Iturriaga and X. Tomas, Anal. Chim. Acta, 139 (1982) 155.
6 D. B. Siano and D. E. Metzler, J. Chem. Phys., 51 (1969) 1856.
7 A. M. Sharaf and B. R. Kowalski, Anal. Chem., 54 (1982) 1291.
8 R. F. Lacey, Anal. Chem., 58 (1986) 1404.
9 M. D. King and G. S. King, Anal. Chem., 57 (1985) 1049.
10 B. Vandeginste, R. Essers, T. Bosman, J. Reynen and G. Kateman, Anal. Chem., 57 (1985) 971.
11 S. D. Frans, M. L. McConnell and J. M. Harris, Anal. Chem., 57 (1985) 1552.
12 N. J. D'Allura and R. S. Juvet, Jr., J. Chromatogr., 239 (1982) 439.
13 M. Otto, W. Wegscheider and E. P. Lankmayr, Anal. Chim. Acta, 171 (1985) 13.
14 A. H. Anderson, T. C. Gibb and A. B. Littlewood, Anal. Chem., 42 (1970) 434.
15 A. B. Littlewood, A. H. Anderson and T. C. Gibb, in C. L. A. Harbourn (Ed.), Gas Chromatography, Proc. Seventh Int. Symp., 1968, Institute of Petroleum, London, 1969, p. 297.
16 R. A. Vaidya and R. D. Hester, J. Chromatogr., 287 (1984) 231.

Analytica Chimica Acta, 201 (1987) 207—216
Elsevier Science Publishers B.V., Amsterdam — Printed in The Netherlands

PRECALCULATION OF THE OPTIMUM COLUMN TEMPERATURE FOR GAS CHROMATOGRAPHIC SEPARATION OF PETROLEUM FRACTIONS

E. STOYANOV*

Higher Institute of Chemical Engineering "Prof. Dr. Assen Zlatarov", 8010 Bourgas (Bulgaria)

N. DIMOV

Chemical Pharmaceutical Institute, 1156 Sofia (Bulgaria)

(Received 21st July 1986)

SUMMARY

Determination of the optimum column temperature is very time-consuming when a new gas chromatographic method is set up. An algorithm is proposed for precalculation of the optimum temperature. It is based on two concepts, the so-called unified retention index and a mathematical description of dependence of peak widths on the retention indices and on column temperature. By means of a defined object function and a scanning optimization strategy, a program is written in BASIC. Several different problems are considered, including the optimum temperature for calculation of the composition of n- and iso-alkanes, cycloalkanes, alkenes and arenes in a petroleum fraction, determination of individual contents and of key components, and separation at any given temperature. The possibilities of the program are illustrated by three examples.

There are several reasons for a qualitative and quantitative analysis of hydrocarbon mixtures. It may be necessary to determine the PONA content (determination of the total contents of normal and isoparaffins, olefins, naphthenes and aromatic compounds), or determine individual hydrocarbons in general or only a few which are of particular interest, or calculate some specific properties of the mixture such as vapour pressure, simulated distillation curve, etc., or simply to distinguish one mixture from another. For such purposes, two approaches can be used: either to design special methods and/or instrumentation to meet the defined need, or to use methods based on full separation followed by specified manipulation of the obtained data. The methods described by various authors [1—3] and made commercially available by Hewlett-Packard involve the first approach. However, the second approach seems to be more promising, particularly when the availability of highly efficient columns is considered.

This paper presents a solution to a general problem by offering a preliminary, computer-aided temperature optimization as a first approximation followed by gas chromatographic analysis on a specified column. The algorithm given is valid for any stationary phase or column, but the more

0003-2670/87/$03.50

preliminary information is available about the retention properties and efficiency of the column, the more complete will be the results. The solution presented here was obtained by using retention data for hydrocarbons separated on squalane, because this is the only system for which enough retention indices could be found in the literature. The concept of the unified retention index UI_T, proposed recently [4], includes statistical treatment of all available experimental (literature) data, which leads to the equation

$$UI_T = UI_0 + (\mathrm{d}UI/\mathrm{d}T)T \qquad (1)$$

where UI_0 is the statistical retention at 0°C, $\mathrm{d}UI/\mathrm{d}T$ is the statistical temperature increment, and T is the column temperature.

METHODS

The experimental determination of the optimum column temperature for a given analysis is time-consuming. That is why one generally uses those temperatures for which retention index data are known. Therefore, it is often uncertain that the separation obtained is the optimum one. It is well established that the retention indices change with temperature [5, 6]. Thus, at any temperature, the peaks are arranged in a definite manner. There should be at least one temperature (the optimum temperature) at which this arrangement is optimum for the purpose of the analysis. Considering the temperature-programmed gas chromatographic (GC) separation introduced in 1963 [7], it could be said that numerous practical and theoretical problems were involved in connection either with the corresponding retention-index calculation or with identification. In spite of the very good repeatability of the relative retentions obtained in temperature-programmed GC [8, 9] and some success in recalculation of retention indices for one column temperature to temperature-programmed conditions [10], the interlaboratory reproducibility remains unsatisfactory. Identification based on retention indices in routine temperature-programmed GC remains questionable. Besides, the time needed to find a suitable temperature programme could be longer than the time for two isothermal separations at precalculated optimum temperatures.

The resolution R is considered to be the most suitable magnitude for optimization. The conventional expression of R is dimensionless and the necessary data are given in seconds or in mm. Here, expression of the distance between the peaks and the $W_{1/2}$ in retention index units is preferred to seconds (or mm) for the precalculation of optimum temperature, because the data bank contains retention data given in such units. While the distance between peaks is easily calculated from their UI_T values, peak width is an individual property for each column and should be calculated for any column used separately. To do this, a known mixture of C_5—C_{10} hydrocarbons was analyzed at four different temperatures. By calculating the I_T^{exp} values and comparing them with UI_T, the column could be classified as standard or not. If it was a standard one, the data bank could be used for a computer-assisted identification.

The experimental data for I_T^{exp} and T were used to evaluate $W_{1/2}$ for every peak in seconds. Two additional indices, I_1 and I_2, which correspond to the retention times $t_R - 0.5\,W_{1/2}$ and $t_R + 0.5\,W_{1/2}$ were calculated. The difference $\Delta = I_2 - I_1$ gave the value of $W_{1/2}$ in retention index units.

With the experimentally obtained values for I, T and $W_{1/2}$, the modelling of the dependence of $W_{1/2}$ on I and T became possible. The following regression equation with a satisfactory correlation coefficient (0.99) and standard deviation, s, of 0.2 was obtained:

$$W_{1/2} = b_0 + b_1\,T + b_2\,UI + b_3\,T^2 + b_4\,UI^2 + b_5\,UI\,T + b_6\,T/UI \qquad (2)$$

The $W_{1/2}$ dependence on I and T has to be established for the particular column for which the optimum temperatures have to be calculated. The constants b_0 to b_6 are characteristic for the particular column used.

By using Eqn. 2 and the data bank for UI_T, the value of $R_{I,I+1}$ for any two adjacent peaks can be calculated at any realistic column temperature. The separation depends, however, also on the mass ratio of the compounds in the adjacent peaks, which is obviously unknown before the analysis. That is why a probability function, estimating the probable separation according to the resolution $R_{I,I+1}$ must also be defined. It is well known that below R = 0.5 there is no separation while raising R above 1.5 is meaningless. On this basis, investigation of the problem leads to the following probability, P, of separation:

$$P = [s(2\pi)^{1/2}]^{-1} \int_0^R \{\exp[-(R - R_m)^2/2s^2]\}dR$$

The maximum R_m and the standard deviation s can be chosen according to the separation required. The values of $R_m = 0.9$ and $s = 0.2$ are used in these studies. For example, when $R \leqslant 0.5$, $P \approx 0$; at $R = 0.7$, $P = 0.159$; at $R = 0.9$, $P = 0.5$; at $R = 1.1$, $P = 0.841$; at $R = 1.3$, $P = 0.977$; and at $R \geqslant 1.5$, $P \approx 1$. This function allows optimization of the separation on two bases, either on equalization of $R_{I-1,I}$ and $R_{I,I+1}$ if both of them are greater than R_m, or on overlapping two of three adjacent peaks in order to obtain a better separation of one of them. For example, if at a given column temperature the separation looks like the chromatograms from Fig. 1A and 1C, then at the optimized temperature it should look like Fig. 1B and 1D. The separation of 3-ethylpentane is quite clear in Fig. 1B. The temperature for separation of the second group of three compounds is such that cyclopentane and 2-methylpentane overlap, while 2,3-dimethylpentane emerges as a separate peak.

The next step is to make assumptions about the first and last compounds present in the fraction, and about the type of hydrocarbons present in the mixture. A raffinate fraction, for example, contains only n-, iso- and cycloalkanes, whereas a petroleum fraction also contains arenes, and a cracking gasolene may include all types of hydrocarbon. Sometimes, when the temperature has been optimized for all hydrocarbons, overlapping peaks appear for certain components of special interest or of different types. In

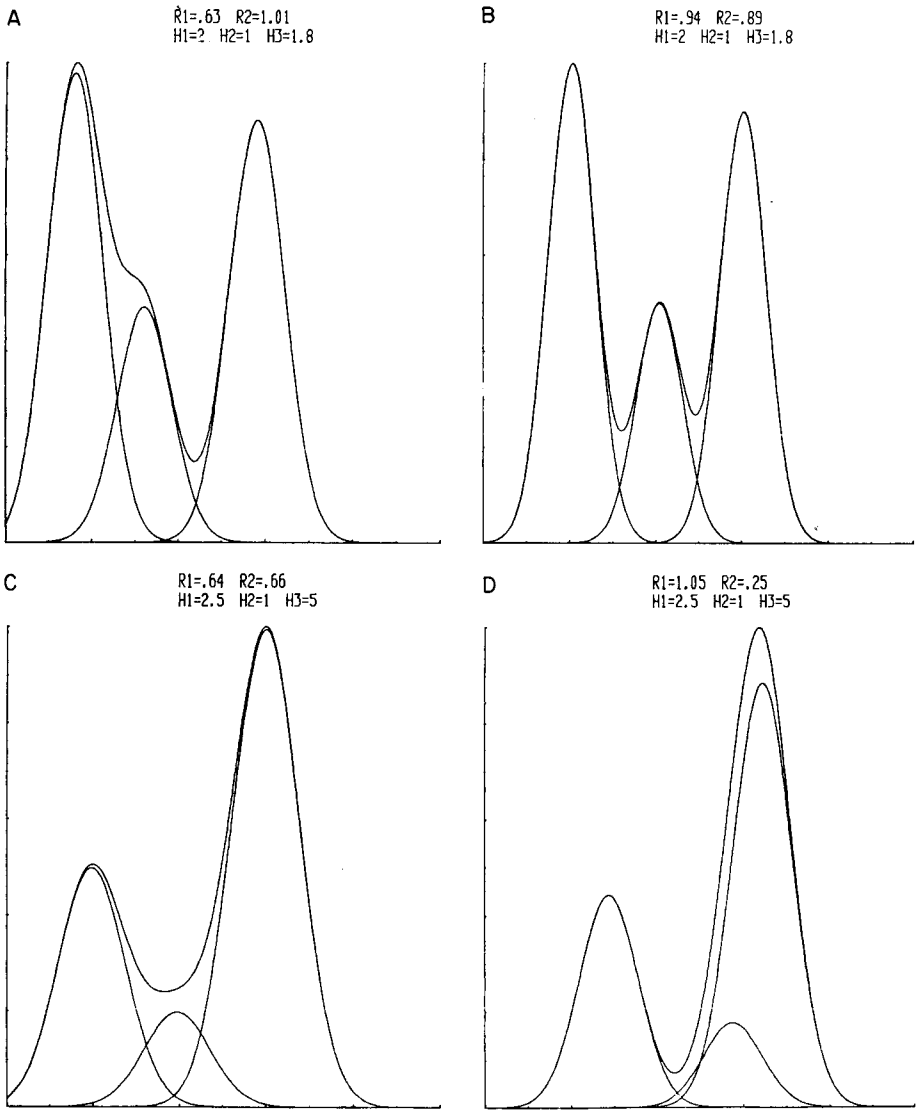

Fig. 1. Computer-calculated curves: (A) unresolved peak of 1-*trans*-3-dimethylcyclopentane and 3-ethylpentane at 65°C with resolved peak of 1-*cis*-3-dimethylcyclopentane (cf. Table 2); (B) separation at 60°C of the mixture in A; (C) unresolved group of peaks consisting of 2,3-dimethylpentane, cyclopentane and 2-methylpentane; (D) the separation at optimum temperature.

such cases, it should be possible to ask the computer for another temperature which is optimum for the required separation. These hydrocarbons are here termed the "key components". Some hydrocarbons which are not expected in the sample, but which have their unified retention index values in the data

bank, would also be listed in the computer report. Therefore, the possibility of excluding any hydrocarbon from the computer report should also be provided.

The algorithm proposed for the precalculation of the optimum temperature is shown in Fig. 2. This algorithm permits the solution of several different problems. If a PONA analysis is the problem, route 1 should be followed. The computer report gives the optimum temperature for separation of n-, iso- and cyclo-alkanes and arenes (NICALAR), as well as a list of all mixed peaks corresponding to components of different types. If individual components

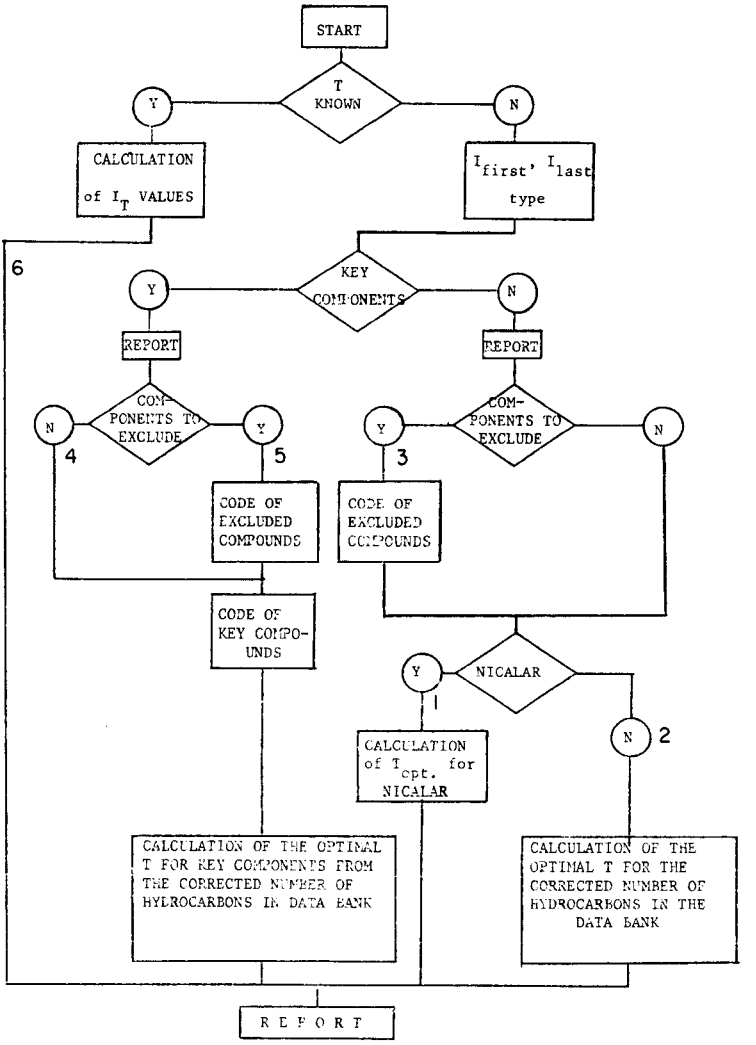

Fig. 2. Block diagram of the routes for calculation of the optimum column temperature.

TABLE 1

Computer report for the separation at the optimum column temperature for NICALAR analysis of a given fraction (n-C_7H_{16} to n-C_8H_{18}) and the separation at two additional temperatures

Index interval	700—800
How many classes to be excluded	0
Number of hydrocarbons	43
Temperature (°C)	Probability (average value)
45	0.544
50	0.741
55	0.66
50.5	0.743 (optimum temperature)
51	0.703

	Optimum temperature;	50.5°C			60°C			70°C	
No.	Hydrocarbon	Type[a]	R_{calc}	No.	Type[a]	R_{calc}	No.	Type[a]	R
1	n-Heptene	N		1	N		1	N	
			1.537			1.527			1.
2	*cis*-2-heptane	O		2	O		2	O	
3	2,3-Dimethyl-2-pentene	O		3	O		3	O	
4	2,4,4-Trimethyl-2-pentene	O		4	O		4	O	
5	2,2-Dimethyl-*cis*-3-hexene	O		5	O		5	O	
			1.874			1.44			0.
6	2,2-Dimethylhexane	I		6	I		6	I	
			1.277						
7	1-*cis*-2-dimethylcyclopentane	C		7	C		7	C	
8	1,1,3-Trimethylcyclopentane	C		8	C		8	C	
									0.6
9	Methylcyclohexane	C		9	C		10	I	
			1.687			0.435[b]			0.6
10	2,5-Dimethylhexane	I		10	I		9	C	
									1.4
11	2,4-Dimethylhexane	I		11	I		11	I	
			1.303			2.012			2.3
12	Ethylcyclopentane	C		12	C		12	C	
			2.187			1.9			1.4
13	2,2,3-Trimethylpentane	I		13	I		13	I	
			2.683			2.507			2.0
14	1-*trans*-2-*cis*-4-trimethylcyclopentane	C		14	C		14	C	
			1.344			1.073			0.7
15	3,3-Dimethylhexane	I		15	I		15	I	
			1.331			1.95			2.2
16	Toluene	A		16	A		16	A	
			1.884			1.251			0.5
17	1-*trans*-2-*cis*-3-trimethylcyclopentane	C		17	C		17	C	
			2.955			2.811			2.3
18	2,3,4-Trimethylpentane	I		18	I		18	I	
19	2,3,3-Trimethylpentane	I		20	I		20	I	
20	2,3-Dimethylhexane	I		19	I		19	I	
21	2-Methyl-3-ethylpentane	I		21	I		21	I	
			0.097[b]			0.593[b]			
22	1,1,2-Trimethylcyclopentane	C		22	C		23	I	
			2.277			0.891			0.4
23	2-Methylheptane	I		23	I		22	C	
									1.0
24	4-Methylheptane	I		24	I		24	I	
25	3,4-Dimethylhexane	I		25	I		26	I	
26	3-Methylheptane	I		26	I		25	I	
27	3-Ethylhexane	I		27	I		27	I	
28	3-Methyl-3-ethylpentane	I		28	I		30	I	

TABLE 1 (continued)

	Optimum temperature:	50.5°C			60°C			70°C	
No.	Hydrocarbon	Type[a]	R_{calc}	No.	Type[a]	R_{calc}	No.	Type[a]	R_{calc}
			0.382[b]						
29	1-*cis*-2-*trans*-4-trimethylcyclopentane	C		30	I		28	I	
			1.262			0.095[b]			1.229
30	2,2,5-Trimethylhexane	I		29	C		29	C	
			3.221			2.936			1.056
31	1-Octene	O		31	O		31	O	
32	*trans*-4-octene	O		32	O		32	O	
			1.583						
33	1-*cis*-3-dimethylcyclohexane	C		36	O		36	O	
						0.306[b]			
34	1-*trans*-4-dimethylcyclohexane	C		33	C		38	O	
						0.399[b]			
35	1,1-Dimethylcyclohexane	C		37	O		37	O	
			0.079[b]						1.0
36	*cis*-4-octene	O		38	O		33	C	
						0.23[b]			
37	*cis*-3-octene	O		34	C		34	C	
									0.26[b]
38	*trans*-3-octene	O		35	C		39	I	
			0.446[b]			0.475[b]			0.615[b]
39	2,2,4-Trimethylhexane	I		39	I		35	C	
			1.429			2.117			
40	1-Ethyl-*trans*-2-methylcyclopentane	C		40	C		40	C	
									1.552
41	1-Methyl-1-ethylcyclopentane	C		41	C		42	O	
			2.329			0.546[b]			1.326
42	*trans*-2-octene	O		42	O		41	C	
			1.328			1.511			0.107[b]
43	n-Octane	N		43	N		43	N	

[a]Type: N, n-alkane; I, isoalkane; O, alkene; A, arene. [b]Hydrocarbons with peaks that are not expected to be separated.

are to be determined, route 2 should be used. The report also gives a list of the composite peaks, specifying the hydrocarbons expected in them. In the case of samples of simpler composition, separation is easier and route 3 is recommended, while route 4 should be used when compounds of special interest are expected in the sample. Route 5 can also be reserved for simple compositions. Finally, if it is considered useful to know what the separation will look like at any required temperature, route 6 should be followed. In such a way, using only the computer, one can study in advance all the possibilities offered by the system (phase, column, data bank). After consideration of all the computer reports, the most efficient decision on the appropriate temperature can be taken before the start of the analysis.

RESULTS AND DISCUSSION

The possibilities given by the algorithm and the performance of the BASIC software will be demonstrated by several examples. Route 1 is the first example. The interval of retention indices was assumed to be from 700 to 800. The computer was asked to set the column temperature which would

TABLE 2

Computer report for the separation at the optimum column temperature of an oil fraction in which the components of interest are 3-ethylpentane and 1,3-dimethylcyclopentanes, as well as the separation at two additional temperatures

Index interval	670—700
How many classes to be excluded	1
Code	2 ALKENES
Number of hydrocarbons	9
Number of key components	3
Temperature (°C)	Probability (average value)
55	0.425
60	0.504 (optimum temperature)
65	0.306
60.5	0.503

No.	Hydrocarbon	60°C		55°C		65°C	
		I	R_{calc}	I	R_{calc}	I	R_{calc}
1	2,3-Dimethylpentane	672.7		672.3		673.1	
			1.27		1.16		1.32
2	1,1-Dimethylcyclopentane	675.62		674.71		676.54	
			0.362		0.76		0.03
3	3-Methylhexane	676.44		676.27		676.62	
			3.64		3.77		3.5
4[a]	1-*cis*-3-dimethylcyclopentane	684.67		683.88		685.45	
			0.94		1.29		0.63[b]
5[a]	3-Ethylpentane	686.68		686.39		686.97	
			0.89		0.69[b]		1.01
6[a]	1-*trans*-3-dimethylcyclopentane	688.54		687.72		689.36	
			1.24		1.36		1.11
7	1-*trans*-2-dimethylcyclopentane	691.13		690.32		691.95	
			0.11		0.25		0
8	2,2,4-Trimethylpentane	691.37		690.78		691.95	
			4.2		4.9		3.5
9	n-Heptane	700		700		700	

[a]Key component. [b]Key components with peaks that are not expected to be separated.

be optimal for the NICALAR analysis. This means the temperature at which compounds from the same class may appear together in composite peaks, but separated from compounds of other classes. The computer output is given in Table 1. No compound is excluded and the computer reports that, according to the inputs, there are 43 hydrocarbons in the data bank. As an additional output, the computer is asked to indicate the separation at 60°C and 70°C. It is evident from the output that at arbitrary selected column temperatures there are eight unresolved compounds, while at the proposed optimum column temperature there are only four overlapping peaks.

TABLE 3

Computer report for the separation at the optimum column temperature for individual contents of crude oil fraction boiled from 98°C to 110°C and the separation at two additional temperatures

Index interval	690—750
How many classes to be excluded	1
Code	2 ALKENES
Number of hydrocarbons	14
Temperature	Probability (average value)
45	0.69
50	0.977
55	
52.5	0.9914
53	0.991

No.	Hydrocarbon	52.5°C		45°C		60°C	
		I	R_{calc}	I	R_{calc}	I	R_{calc}
1	2,2,4-Trimethylpentane	690.49		689.62		691.37	
			5.25		6.1		4.2
2	n-Heptane	700		700		700	
			11.4		11.7		10.3
3	2,2-Dimethylhexane	719.73		719.34		720.12	
			1.44		0.77[a]		1.94
4	1-*cis*-2-dimethylcyclopentane	722.03		720.55		723.5	
			1.44		1.43		1.32
5	1,1,3-Trimethylcyclopentane	724.29		722.82		725.77	
			1.27		1.1		1.32
6	Methylcyclohexane	726.28		724.55		728.01	
			1.42		2.35		0.44[a]
7	2,5-Dimethylhexane	728.48		728.23		728.74	
			2.5		2.38		2.4
8	2,4-Dimethylhexane	732.34		731.93		732.75	
			1.48		0.78[a]		2
9	Ethylcyclopentane	734.58		733.13		736.04	
			2.15		2.22		1.9
10	2,2,3-Trimethylpentane	737.82		736.55		739.1	
			2.67		2.61		2.5
11	1-*trans*-2-*cis*-trimethylcyclopentane	741.82		740.56		743.08	
			1.3		1.41		1.07
12	3,3-Dimethylhexane	743.74		742.73		744.75	
			1.48		0.88		1.95
13	Toluene	745.92		744.07		747.77	
			1.76		2.13		1.25
14	1-*trans*-2-*cis*-3-trimethylcyclopentane	748.49		747.3		749.67	

[a]Hydrocarbons whose peaks are not expected to be separated.

The results in Table 2 demonstrate the well-known difficulties encountered in the gas chromatography of hydrocarbons, i.e., the separation of 3-ethylpentane from both 1-*cis*-3-dimethylcyclopentane and 1-*trans*-3-dimethylcyclopentane. The best column temperature found experimentally was 60°C and these compounds could be separated only at this temperature. By using route 4, the optimum temperature for separation of these compounds, which are considered as key components, was indeed calculated to be 60°C. Another advantage is that the computer report provided the information that at this temperature 2,2,4-trimethylpentane and 1-*trans*-2-dimethylcyclopentane, as well as 1,1-dimethylcyclopentane and 3-methylhexane, would be present in composite peaks. It is useful to be aware of this fact in advance, before the actual analysis is started. The experimental results confirmed this prediction.

Route 2 was checked with a crude oil fraction boiling from 98°C to 110°C. The results are given in Table 3. It is evident that the separation at the optimum temperature is not only the best one but is also complete. The lowest R_{calc} is 1.27. At 45°C, there are two unresolved peaks and one has R_{calc} = 1.1, which means that a baseline separation cannot be expected.

The examples presented show that the time-consuming experiments usually needed to establish the optimum column temperature can be avoided. By using repeatable experimental data for the retention index or the values of the unified retention indices given earlier [4], the optimum column temperature for a selected separation can easily be calculated.

REFERENCES

1 G. B. Ury, Anal. Chem., 53 (1981) 481.
2 H. Boer and P. van Arkel, Chromatographia, 4 (1971) 300.
3 V. Kvasova, S. Leontieva and N. Lulova, Zh. Anal. Khim. 38 (1983) 1834.
4 N. Dimov, J. Chromatogr., 347 (1985) 366.
5 L. S. Ettre and K. Billeb, J. Chromatogr., 30 (1967) 1.
6 D. A. Tourres, J. Chromatogr., 30 (1967) 357.
7 H. van den Dool and P. D. Kratz, J. Chromatogr., 11 (1963) 463.
8 P. C. Hayes and E. W. Pitzer, J. Chromatogr., 253 (1982) 179.
9 N. G. Johansson and L. S. Ettre, J. Chromatogr., 256 (1982) 393.
10 J. Curvens, K. Knauss, P. Larson and C. Cramers, in P. Sandra (Ed.), Proc. 6th Int. Symp. Capillary Chromatography, Riva del Garda, Italy, Huething, University of Gent, Belgium, 1985, p. 744.

Analytica Chimica Acta, 201 (1987) 217—224
Elsevier Science Publishers B.V., Amsterdam — Printed in The Netherlands

GENERAL MODEL FOR PRECALCULATION OF THE RETENTION INDICES OF ISOALKANES SEPARATED BY GAS OR LIQUID CHROMATOGRAPHY

N. DIMOV

Chemical Pharmaceutical Institute, 1156 Sofia (Bulgaria)

(Received 3rd June 1986)

SUMMARY

A general model consisting of two terms is proposed for precalculation of retention indices of isoalkanes separated by gas chromatography (GC) on a squalane column and by high-performance liquid chromatography (HPLC) on a column containing a bonded octadecyl phase. The first term (referred to as extensive) includes parameters which have the greatest correlation with the experimental value of the index; the second term (referred to as intensive) includes parameters which can modify the value of the roughly calculated index in the direction of the experimental value. The equations derived have correlation coefficients better than 0.99. The maximum discrepancy between the experimental and calculated retention index for twenty C_6—C_8 isoalcanes was less than ±1 index unit in gas chromatography and less than 4 index units in HPLC. The retention indices of 23 other C_7—C_9 isoalkanes, calculated in the extrapolation region of the equations, were sufficiently accurate.

The presentation of relative retention by means of the Kovats retention index, I, is well established in gas chromatography (GC). Attempts to apply similar indices in high-performance liquid chromatography (HPLC) have been reported [1, 2] but the capacity factor (k') is more widely used to express retention.

Many studies have been published concerning the precalculation of retention characteristics both in GC [3—5] and in HPLC [6—12]. These studies were intended to provide: (1) information about the identity of a given peak or even its identification from the chromatographic data only; (2) better prior selection of separation conditions; and (3) better knowledge about solute/solvent interactions and structure/retention relationships. The better the mathematical model that is used, the more reliable the results obtained from the derived equations.

The validity of the equations used to model chromatographic retention can be characterized either by the correlation coefficient or by the standard deviation or variance. From the physicochemical point of view, the value of the correlation coefficient seems to be sufficient, while the standard deviation is more informative for chromatographic purposes.

The aim of this paper is to present a general model for the derivation of

0003-2670/87/$03.50

suitable equations for precalculation of relative retention of isoalkanes separated both by GC and HPLC, expressed in the form of the Kovats retention index. The basic concept is that the retention depends mostly on limited physicochemical properties and is less affected by structural and geometrical features of the solute.

METHOD OF CALCULATION

A unified retention index, UI_T, is used here instead of the usual retention index values. The unified retention index [13] represents the linear regression of the retention index data published by various authors at different temperatures. The values of UI_T can be calculated for any temperature of interest and here they are given for squalane at 50°C.

The capacity factor values, k', of isoalkanes reported by Burda et al. [12] were utilized for the calculation of I in HPLC, by using the equation

$$I_{\mathrm{HPLC}} = 100\,n + 100\,(\log k'_{\mathrm{x}} - \log k'_n)/(\log k'_{n+1} - \log k'_n)$$

where k'_{x} is the capacity factor of the corresponding hydrocarbon; the retention of the n-alkanes is represented by k'_n and k'_{n+1}. The data were obtained on a LiChrosorb RP-18 column at 20°C, with 8:2 methanol/water as the mobile phase.

Deviations of ±1 in the retention index are accepted as attainable for interlaboratory reproducibility in GC. As few data are available in the literature about the reproducibility of HPLC retention data, it is assumed here that their repeatability is about 1% [1] and for the C_5—C_6 isoalkanes the repeatability of the retention index is taken as ±5.

The general model proposed here is based on the models given previously [14, 15]. The idea is to separate the magnitude of a relative retention into two parts. The first part includes one or more parameters that are the most important for retention, which have the greatest correlation with the experimental retention indices and which therefore give a calculated value of I which is 80% to 120% of the experimental retention value, I^{exp}. The second part includes parameters which may have low correlation with I^{exp}, but modify the calculated value of I in a direction towards the I^{exp} value. In the case of separation of nonpolar compounds, this can be achieved if physicochemical properties of the solute are correlated with the chromatographic retention. Structural and geometrical parameters can then be included in the regression, playing a modifying role. These are referred to as intensive parameters, Σ(IP). The first term is connected with more extensive properties of the solute, Σ(EP). The second term includes different molecular fragments, which are considered to be responsible for the intensive properties of the solute. Thus,

$$I^{\mathrm{calc}} = b_0 + \sum_{i=1}^{n} b_i\,(\mathrm{EP}) + \sum_{j=n+1}^{n+k} b_j\,(\mathrm{IP}) \qquad (1)$$

where the various b values are constants, depending mainly on the stationary phase used for the separation. The subscript i refers to the linear regression between I and the extensive properties (EP) of the solute, while j refers to the linear regression between I and the intensive properties (IP) of the same solute.

The following modification of model 1 was also studied:

$$I^{calc} = I\,(EP) + SN \tag{2}$$

where SN, the structural number [14], is calculated from a regression equation obtained from the differences between I_{exp} or UI_T and the value of the calculated I only, according to the accepted extensive property:

$$I^{exp} - I\,(EP) = b_0 + b_j\,(IP) \tag{3}$$

Molecular mass, number of methylene groups of C atoms (n_0), different type of topological indices [16] and the physicochemical index (PCI) [17] were tested as elements of the first term, Σ (EP). Different types of structural fragments, such as quaternary or tertiary carbon atoms on the structure of an isoalkane, the distance between alkyl substituents, etc. [18] were used to produce the correct value of the second term, Σ (IP). The calculation of the different topological indices was as given elsewhere (see, e.g. [16]). The calculation of PCI needs only the values of the vapour pressure (p_0) and the molecular volume (V_{mol}) of the corresponding solutes:

$$PCI = 100\,n + 100\,[\log(p^0_n\ V_{mol,n}) - \log(p^0_x\ V_{mol,x})]\,/$$
$$[\log(p^0_n\ V_{mol,n}) - \log(p^0_{n+1}\ V_{mol,n+1})] \tag{4}$$

Data on the vapour pressure and the density of the hydrocarbons (see, e.g. [19]) can be used as a data bank for computerized calculation of PCI at any desirable temperature.

The structural fragments considered as responsible for the extensive properties of a given solute are: n_0, the number of carbon atoms in the isoalkane; n_L, the number of carbon atoms in the straight chain (e.g., 3-ethylpentane (3-EP) has $n_0 = 7$ and $n_L = 5$); n_{CH_3}, the number of methyl groups in the molecule; and n_B, the number of butane chains in the whole molecule. For example, 2,3,4-trimethylpentane (2,3,4-TMP) has $n_{CH_3} = 5$ and $n_B = 8$. The term n_B is a topological index introduced in GC by Altenburg [20] and used in chemical graph theory [21]. It cannot be considered as an extensive property only, because it is an indication of possible confirmation based on the carbon-chain. The latter can also be expressed by the number of Gosh conformers, n_G [22]. It was found here that the intercorrelation between n_B and n_G is reasonable ($r = 0.866$). It was also found that n_G can be calculated more easily from the following equation:

$$n_G = n_{CH_3} + n_i + n_{qt} - 2 \tag{5}$$

n_i and n_{qt} are explained below.

The structural fragments considered as responsible for the intensive proper-

ties of the solute (parts of a given molecule responsible for some specific properties, especially when n_o, n_L, etc. are equal) are as follows: n_i, the number of carbon atoms in the alkyl substituents in an internal position, located after the second carbon atom from both ends of the straight chain (e.g., 2,3-dimethylbutane has $n_i = 0$, 2,3-dimethylpentane has $n_i = 1$ and 3-ethylpentane has $n_i = 2$); n_d, the number of carbon atoms between neighbouring substituents (e.g., 3,4-dimethylhexane has $n_d = 0$ and 2,6-dimethylheptane has $n_d = 3$); n_q, the number of quaternary carbon atoms in the isoalkane; n_t, the number of tertiary carbon atoms; n_{qt}, the number of adjacent quaternary and tertiary carbon atoms; and n_{tt}, the number of adjacent tertiary carbon atoms.

The most significant parameters which can be used for the characterization of isoparaffins and all the necessary input data for a calculation are summarized in Table 1. The abbreviations used are listed in Table 2.

RESULTS AND DISCUSSION

During the search for the most suitable parameters for the first term of the model, the highest correlation was found to exist between I^{exp} and *PCI*:

$$I_{GC}^{calc} = 2.79 + 1.00218\,PCI \qquad (6)$$

TABLE 1

Values of UI_{50}, I_{HPLC}, *PCI* and significant structural fragments of the C_6—C_8 isoalkanes studied

No.	Isoalkane[a]	UI_{50}	I_{HPLC}	*PCI*	n_o	n_{CH_3}	n_L	n_d	n_q	n_{qt}	n_i	n_{tt}	n_t
1	2,2-DMB	536.9	536.5	531.7	6	4	4	0	1	0	0	0	0
2	2,3-DMB	567.6	553.2	561.6	6	4	4	0	0	0	0	1	2
3	2-MP	569.7	574.1	568.6	6	3	5	0	0	0	0	0	1
4	3-MP	584.4	569.6	580.8	6	3	5	0	0	0	1	0	1
5	2,3-DMP	671.9	647.6	665.2	7	4	5	0	0	0	1	1	2
6	2,4-DMP	629.9	636.7	627.8	7	4	5	1	0	0	0	0	2
7	3-EP	686.1	656.4	680.9	7	3	5	0	0	0	2	0	1
8	2-MH	666.6	667.0	665.7	7	3	6	0	0	0	0	0	1
9	3-MH	676.1	663.4	673.3	7	3	6	0	0	0	1	0	1
10	2,3-DMH	760.3	734.3	754.8	8	4	6	0	0	0	1	1	2
11	2,4-DMH	732.2	722.7	728.4	8	4	6	1	0	0	1	0	2
12	2,5-DMH	728.4	727.0	726.8	8	4	6	2	0	0	0	0	2
13	3-EH	772.6	745.4	768.8	8	3	6	0	0	0	2	0	1
14	2,2,3-TMP	737.4	708.4	727.8	8	5	5	0	1	1	1	0	1
15	2,2,4-TMP	690.2	701.3	683.5	8	5	5	1	1	0	0	0	1
16	2,3,4-TMP	752.4	717.8	743.9	8	5	5	0	0	0	1	2	3
17	2-M-3-EP	761.5	723.1	754.6	8	4	5	0	0	0	2	1	2
18	2-MHp	764.9	765.8	763.7	8	3	7	0	0	0	0	0	1
19	3-MHp	772.4	759.6	769.6	8	3	7	0	0	0	1	0	1
20	4-MHp	767.2	759.2	765.0	8	3	7	0	0	0	1	0	1

[a]See Table 2.

TABLE 2

Examples of abbreviations

Abbreviation	Hydrocarbon	Abbreviation	Hydrocarbon
2,2-DMB	2,2-Dimethylbutane	2-MHp	2-Methylheptane
2,3-DMP	2,3-Dimethylpentane	2,6-DMHp	2,6-Dimethylheptane
2,2,4-TMP	2,2,4-Trimethylpentane	3-EHp	3-Ethylheptane
3-EH	3-Ethylhexane	2-M-3-EP	2-Methyl-3-ethylpentane
2-M-3-EH	2-Methyl-3-ethylhexane	2,3,5-TMH	2,3,5-Trimethylhexane
3,3-DMH	3,3-Dimethylhexane	3-MO	3-Methyloctane

The correlation coefficient was very high (r = 0.99945) but the standard deviation, s, was 2.6, and the maximum discrepancy between I^{exp} and I^{calc}, Δ_{max}, was 5.2. Thus the equation was inadequate. The following equation was obtained for the correlation of I_{HPLC} with PCI:

$$I_{HPLC}^{calc} = 41.09 + 0.92756\, PCI \tag{7}$$

with r = 0.9861, s = 12.4 and Δ_{max} = 26. In both cases, the I^{calc} values were more than 95% of the magnitude of I_{exp}. Thus the selected characteristic of the solute is suitable for inclusion in the first term in Eqns. 1 and 2.

In the search for the best parameters for the modifier, Σ (IP), it was found that different structural fragments could be used. The final derived equations for the precalculation of values of I_{GC} and I_{HPLC} that gave the best statistics were:

$$I_{GC}^{calc} = -24.49 + 1.18496\, PCI - 16.751\, n_0 + 9.327\, n_{CH_3} - 1.357\, n_L - \\ - 1.770\, n_d - 5.90\, n_{qt} - 5.01\, n_{tt} \tag{8}$$

with correlation coefficient r = 0.999979, variance s^2 = 0.30, standard deviation s = 0.55 and maximum deviation Δ_{max} = 0.94

$$I_{HPLC}^{calc} = 42.17 + 0.33448\, PCI + 58.336\, n_0 - 11.629\, n_{CH_3} + \\ + 5.056\, n_L - 3.729\, n_d - 3.44\, n_q - 7.55\, n_i \tag{9}$$

with r = 0.99959, s^2 = 6.74, s = 2.59 and Δ_{max} = 3.8.

Model 2 gave the following equations for the SN calculation:

$$SN_{GC} = -4.308 - 0.526\, n_0 + 3.195\, n_{CH_3} - 1.10\, n_d + 0.50\, n_q + \\ + 1.69\, n_i + 0.53\, n_{tt} - 0.42\, n_t \tag{10}$$

with r = 0.9824, s = 0.60 and Δ_{max} = 0.99.

$$SN_{HPLC} = 10.26 - 6.539\, n_{CH_3} + 2.10\, n_L + 6.22\, n_d - 17.90\, n_q - \\ - 12.65\, n_i - 12.70\, n_{qt} \tag{11}$$

with r = 0.9420, s = 5.45 and Δ_{max} = 9.5.

TABLE 3

Values of I_{GC}^{calc}, I_{HPLC}^{calc}, SN and corresponding errors[a]

No	Isoalkane	I_{GC}^{calc}	Error	I_{HPLC}^{calc}	Error	SN_{GC}	Error
1	2,2-DMB	536.88	0.02	540.3	−3.8	5.76	0.56
2	2,3-DMB	567.40	0.19	553.7	−0.5	5.06	0.94
3	2-MP	570.00	0.30	572.8	1.3	1.75	0.65
4	3-MP	584.42	0.02	569.3	0.3	3.43	0.17
5	2,3-DMP	672.01	−0.11	644.3	3.3	6.19	0.51
6	2,4-DMP	630.87	−0.98	635.5	1.1	2.67	0.57
7	3-EP	686.24	−0.14	653.6	2.8	4.55	0.65
8	2-MH	666.95	−0.35	668.6	−1.6	1.20	0.30
9	3-MH	675.97	0.13	663.6	−0.2	2.88	0.08
10	2,3-DMH	760.06	0.24	737.6	−3.3	5.64	0.14
11	2,4-DMH	732.00	0.18	725.0	−2.3	3.80	0.00
12	2,5-DMH	728.40	0.00	728.3	−1.3	1.60	0.00
13	3-EH	772.40	0.20	746.4	1.0	4.00	0.20
14	2,2,3-TMP	737.82	−0.42	708.4	0.0	9.60	0.00
15	2,2,4-TMP	689.46	0.73	697.5	3.8	6.13	0.57
16	2,3,4-TMP	752.82	−0.42	717.5	0.5	8.95	0.45
17	2-M-3-EP	761.16	0.34	724.9	−1.8	7.32	0.42
18	2-MHp	764.90	0.00	764.8	1.0	0.65	0.55
19	3-MHp	772.30	0.10	759.3	0.3	2.33	0.17
20	4-MHp	766.50	0.70	757.7	1.5	2.33	0.13

[a]Errors are expressed in the retention index units.

The values of the calculated indices are given in Table 3. Estimation of the adequacy of the models by applying Fisher criterion (F) to the variances showed that Eqns. 8—10 are satisfactory. They permit interpolation calculations with errors less than ±1 in retention index for gas chromatography and less than 4 for HPLC, which is the best result so far for precalculation methods [23]. Especially for gas chromatography, Eqns. 8 and 10 permit extrapolation calculations of I^{calc} of isoalkanes separated on squalane at any column temperature within the interval 30—70°C with the same error, because the extensive factor *PCI* is temperature-dependent.

The extrapolation power of Eqns. 8—10 was tested in precalculation of the I_{GC}^{calc} values of further C_7—C_9 isoalkanes. The results are given in Table 4. The discrepancies are greater, but the results were obtained in the extrapolation region of the equations and the discrepancies between I^{exp} and I^{calc} are still similar to those given for the interpolation region of other calculation methods for the same compounds [3, 23, 24].

The results obtained show that the mathematical models 1 and 2 proposed here are suitable for deriving equations for precalculation of isoalkane retention indices on squalane, as well as for their retention in HPLC on the RP-18 column. The most significant structural elements that should be included in the equations may differ according to the stationary phase or for other reasons, but the model remains the same. The essential thing is to find the best

TABLE 4

Comparison of the values of I^{calc} of 23 isoalkanes calculated in the extrapolation region with the corresponding UI_T and I_{HPLC} values

No.	Isoalkane	I_{GC}^{calc}	Error[a]	I_{HPLC}^{calc}	Error[a]
1	2,2-DMP	626.25	−0.35	—	—
2	3,3-DMP	657.93	1.07	—	—
3	2,2,3-TMB	639.06	0.94	—	—
4	2,2-DMH	720.16	0.56	—	—
5	2,5-DMH	728.37	0.03	—	—
6	3,3-DMH	743.87	−0.47	—	—
7	3,4-DMH	770.72	0.18	—	—
8	2,3,3-TMP	760.11	−0.51	—	—
9	3-M-3-EP	774.50	−0.40	—	—
10	2,4-DMHp	820.34	−1.12	813.8	−4.7
11	2,5-DMHp	833.06	0.61	816.3	−2.6
12	2,6-DMHp	828.10	1.03	829.9	8.1
13	3,4-DMHp	851.66	−6.63	823.9	4.0
14	3-EHp	862.96	−4.02	835.9	−4.6
15	4-EHp	852.96	−4.59	831.2	−6.4
16	2-M-4-EH	824.55	0.35	802.6	−4.1
17	3-M-3-EH	854.30	0.84	813.5	6.2
18	2,2,5-TMH	777.56	1.09	775.9	−11.7
19	2,3,5-TMH	814.47	2.23	792.7	−9.6
20	3,3-DEP	877.71	0.24	805.0	4.0
21	2-MO	865.94	1.44	865.3	3.5
22	3-MO	869.45	−0.92	853.7	−1.6
23	4-MO	859.38	−3.39	849.2	−3.2

[a]See footnote to Table 3.

combinations of parameters that should be included in the two terms of the models. The results show that, at least for C_6—C_8 isoalkanes, an adequate mathematical equation for precalculation of I on squalane is now available and that the error limit of ±1 for a correct precalculation method is attainable.

REFERENCES

1 J. K. Baker, J. Liq. Chromatogr., 5 (1982) 829.
2 P. L. Grizzle and J. S. Thomson, Anal. Chem., 54 (1982) 1071.
3 M. Randić, J. Chromatogr., 161 (1978) 1.
4 A. N. Korol, Usp. Khim., 54 (1982) 1225.
5 M. V. Budahegyi, J. Chromatogr., 271 (1983) 213.
6 T. Hanai, Chromatographia, 12 (1979) 77.
7 J. Hubert, J. High Res. Chromatogr., 4 (1981) 454.
8 M. J. Wells, C. R. Clark and R. M. Patterson, J. Chromatogr., 235 (1982) 61.
9 N. R. Ayyangar and K. V. Srinivasan, J. Chromatogr., 267 (1983) 399.
10 P. Lehtonen, J. Chromatogr., 267 (1983) 277.
11 P. Jandare, J. Chromatogr., 314 (1984) 15.
12 J. Burda, M. Kuraš, J. Kriź and L. Vodićka, Fresenius' Z. Anal. Chem., 321 (1985) 549.

13 N. Dimov, J. Chromatogr., 347 (1985) 366.
14 N. Dimov, J. Chromatogr., 119 (1976) 109.
15 D. Papazova, N. Dimov and D. Bonchev, J. Chromatogr., 188 (1980) 297.
16 D. Bonchev, Information Theory Indices for Characterization of Chemical Structures, Horwood, Chichester, 1983, p. 198.
17 N. Dimov and D. Shopov, J. Chromatogr., 44 (1969) 170.
18 N. Dimov and D. Papazova, Chromatographia, 12 (1979) 720.
19 Selected Values of Properties of Hydrocarbons, API Research Project 44, Texas University, College Station, TX, 1966.
20 K. Altenburg in H. Struppe (Ed.), Gas Chromatographie 1968, Akademie, Berlin, G.D.R., 1968 p. 1.
21 N. Trinajstić, Chemical Graph Theory, Vol. 2, CRC Press., Boca Raton, FL, 1983, p. 105.
22 G. Mann, Tetrahedron, 23 (1967) 3375, 3393.
23 N. Dimov, J. Chromatogr., 360 (1986) 25.
24 J. Dubois and J. Chretien, J. Chromatogr., Sci., 12 (1974) 811.
25 G. H. Spivakovskii, A. I. Tishchenko, I. I. Zaslavskii and N. S. Wulfson, J. Chromatogr., 144 (1977) 1.

Analytica Chimica Acta, 201 (1987) 225—239
Elsevier Science Publishers B.V., Amsterdam — Printed in The Netherlands

SYMMETRIC DISTANCE MEASURES FOR MASS SPECTRA

FINN DRABLØS
Department of Chemistry, University of Bergen, Allégt. 41, N-5007 Bergen (Norway)
(Received 8th April 1987)

SUMMARY

Several symmetric distance measures are tested on complete mass spectra by four different test methods, based on linear and hierarchical library search. The euclidean distance measure is tested with several normalization procedures by the same methods. The results show that no single distance measure is optimal in all situations. In particular, different types of noise in the spectrum may require different distance measures for optimal identification. Normalization of the spectrum to unit vector length or standard measure can improve the results.

Many methods for evaluating and identifying mass spectra make use of symmetric distance measures, where the distance between objects is independent of the direction of the distance computation. But different distance measures may give different results. Several papers [1—4] have appeared in which distance measures and normalizations have been examined, but the research has concentrated mainly on compressed mass spectra, especially binary-coded spectra. This has been the consequence of low-capacity external storage media, slow arithmetics, and search methods based on a linear search of the complete library file, which has favoured short data vectors and simple distance measures.

New and improved media for external storage, as for example optical discs, have made it simple to store complete spectra. Besides, fast mini- and micro-computers with large central memories and dedicated arithmetic processors, together with efficient presearch algorithms limiting the main search to a small subset of the total library, have made the use of complete mass spectra more interesting. Data compression will, in most cases, lead to a loss of information and one should thus expect a more reliable identification when complete spectra are used.

In this investigation, one accepted and three new test methods, CYCLE, TREE, NOISE and MIX, are applied to a well-defined set of data for testing several different distance measures and normalization procedures.

0003-2670/87/$03.50

TABLE 1

The test data sets A—C

Group number	Group name	Number of spectra		
		A	B	C
1	Alkanes	106	53	22
2	Cycloalkanes	90	45	19
3	Alkenes	146	73	31
4	Ketones	56	28	12
5	Amines	67	33	15
6	Alcohols	115	58	24
7	Amides	36	18	8
8	Esters	76	38	16
9	Ethers	55	27	12
	Total	747	373	159

EXPERIMENTAL

The data set

From a collection of 40 000 mass spectra from the National Bureau of Standards (U.S.A.), a subset of 747 spectra of monofunctional compounds with $M < 150$ were chosen, separated into nine different groups on the basis of functionality, and sorted into ascending order of molecular weight within each group (Table 1). This data set (data set A) was used with the test programs CYCLE, NOISE and MIX. A subset of 373 spectra from A (dataset B) was used by the TREE program. Another subset of 159 spectra from A (dataset C) was used for some preliminary tests. All spectra were initially normalized against the base peak.

The small data set makes it possible to use all spectra in the set as test spectra. This will eliminate the objection that the subset for testing may not be representative of the total data set, although the objection will still be valid when comparing the data set to the complete library of spectra (or all possible mass spectra, for that matter). This may be circumvented to some degree by selecting a random data set from the library, but that would make it difficult to separate the data set into clearly defined groups. The main advantage of a simple data set with well-defined groups is that statistically useful information will be returned even when the search method fails to return the correct spectrum.

Using the same spectra as reference and test spectra makes it possible to treat the concept of noise in the spectra as a separate problem, and the test method in CYCLE in fact assumes that test spectra are drawn from the reference library.

Distance measures

A structure S_i with molecular weight M_i is considered. This structure will give a mass spectrum which may be represented by the vector $\mathbf{x}_i$ with

TABLE 2

Distance measures [2, 4—8]

Number	Definition	Name
1	$d_{ij} = \left[\sum_{k=1}^{n} (x_{ik} - x_{jk})^2 \right]^{1/2}$	euclidean
2	$d_{ij} = \left[\sum_{k=1}^{n} \lvert x_{ik} - x_{jk} \rvert^3 \right]^{1/3}$	Minkowski
3	$d_{ij} = \sum_{k=1}^{n} \lvert x_{ik} - x_{jk} \rvert$	city-block
4	$d_{ij} = \sum_{k=1}^{n} (\lvert x_{ik} - x_{jk} \rvert / \lvert x_{ik} + x_{jk} \rvert)$	Canberra
5	$d_{ij} = \max_{k} \lvert x_{ik} - x_{jk} \rvert$	Chebychev
6	$d_{ij} = \left\{ \sum_{k=1}^{n} [x_{ik} - x_{jk} - n^{-1} \sum_{l=1}^{n} (x_{il} - x_{jl})] \right\}^{2}{}^{1/2}$	variance
7	$d_{ij} = 1 - \left\lvert \sum_{k=1}^{n} (x_{ik} - \bar{x}_i)(x_{jk} - \bar{x}_j) \right\rvert \Big/ \left[\sum_{k=1}^{n} (x_{ik} - \bar{x}_i)^2 \sum_{k=1}^{n} (x_{jk} - \bar{x}_j)^2 \right]^{1/2}$	correlation
8	$d_{ij} = \cos^{-1} \left[\left\lvert \sum_{k=1}^{n} x_{ik} x_{jk} \right\rvert \Big/ \left(\sum_{k=1}^{n} x_{ik}^2 \sum_{k=1}^{n} x_{jk}^2 \right)^{1/2} \right]$	angular separation
9	$d_{ij} = \left[\sum_{k=1}^{n} x_{ik}^2 \sum_{k=1}^{n} x_{jk}^2 - \left(\sum_{k=1}^{n} x_{ik} x_{jk} \right)^2 \right] \Big/ \left[\sum_{k=1}^{n} (x_{ik} + x_{jk})^2 \right]$	
10	$d_{ij} = \left[\sum_{k=1}^{n} x_{ik}^2 \left(\sum_{k=1}^{n} x_{jk}^2 \right)^{1/2} - \sum_{k=1}^{n} x_{ik} x_{jk} \left(\sum_{k=1}^{n} x_{ik}^2 \right)^{1/2} \right] \Big/ \left[\sum_{k=1}^{n} x_{ik}^2 \left(\sum_{k=1}^{n} x_{jk}^2 \right)^{1/2} + \sum_{k=1}^{n} x_{ik} x_{jk} \left(\sum_{k=1}^{n} x_{ik}^2 \right)^{1/2} \right]$	

elements x_{ik} where $k = 1, 2, \ldots, n$. The distance d_{ij} between spectra of structure S_i and S_j can then be defined by using different distance measures (Table 2).

Distance measures 9 and 10 are made by minimizing Eqn. 1 subject to constraint 2 (for 9) or constraint 3 (for 10):

$$d_{ij} = a \sum_{k=1}^{n} (x_{ik} - bx_{jk})^2 \tag{1}$$

$$a(1 + b) = 1 \tag{2}$$

$$a \sum_{k=1}^{n} (x_{ik} + bx_{jk})^2 = 1 \tag{3}$$

They may be regarded as symmetric versions of the scaled distance measures used by Dromey [9] and Atwater et al. [10].

Distance measure 6 is made by computing the variance of $(x_{ik} - x_{jk})$ over all k.

Normalizations

Normalization is used to convert each set of original scores to some standard scale [11]. Because of the experimental methods in mass spectrometry, no common scale exists for comparing different mass spectra. This makes the choice of normalization method difficult, but even more necessary. Some distance measures perform an implicit normalization, but in most cases an explicit normalization is necessary prior to the distance computation. Of the tested normalization methods (Table 3) method 5 is not really a normalization, but is included because it is a part of method 6.

Test methods

Four different test methods are used, based on identification of spectra by library search. All spectra in the library are used as test spectra. The result of

TABLE 3

Normalizations [2, 4, 11]

Number	Definition	Number	Definition
1	$\sum_{k=1}^{n} kx_{ik} = M_i$	6	$\sum_{k=1}^{n} x_{ik} = 0$ and $\left[(n-1)^{-1} \sum_{k=1}^{n} x_{ik}^2\right]^{1/2} = 1$
2	$\max_k (x_{ik}) = 1$		
3	$\sum_{k=1}^{n} x_{ik} = 1$	7	$\sum_{k=m}^{m+13} x_{ik} = 1,$ $m = 6, 20, 34, 48, \ldots$
4	$\left[(n-1)^{-1} \sum_{k=1}^{n} (x_{ik} - \bar{x}_i)^2\right]^{1/2} = 1$		
5	$\sum_{k=1}^{n} x_{ik} = 0$	8	$\left(\sum_{k=1}^{n} x_{ik}^2\right)^{1/2} = 1$

each search will be a spectrum, and the group to which the spectrum belongs. A notation related to Pascal [12] is used for an algorithmic description of each test method.

Each of the m spectra in the library are stored as a vector of length n together with a unique spectrum identification and a group identification, as indicated in the first part of Table 4.

The TREE procedure. This hierarchical method (Table 4) tests the ability to identify spectra by using prototypes representing groups of spectra. Hierarchical cluster analysis [13] is used to organize the spectra into a tree [14] (Fig. 1), and this tree is used as a search tree for identifying spectra by comparing test spectra with nodes in the tree. By using leaf nodes from the tree as test spectra, all spectra should be correctly identified in an optimal search tree.

Different methods of hierarchical cluster analysis [15] may be tested for global fit to the data set by comparing object distance d and amalgamation distance d' by the cophenetic correlation coefficient r_c [16]:

TABLE 4

Storage of spectra and the algorithmic description of the TREE procedure

```
var Lib: array[1..m] of record
                          Spec: array[1..n] of real;
                          Id, Group: integer
                        end;

procedure TREE(Lib);
var Tree: array of record
                    Spec: array[1..n] of real;
                    case Leaf: boolean of
                      false: Left, Right: pointer;
                      true: Id, Group: integer
                    end
                  end;
begin
  normal (Lib,Spec) {Normalize all spectra in library.};
  make tree(Lib,Tree) {Make search tree.};
  mS:=mG:=0;
  for i:=1 to m do begin
    Test:=Lib[i].Spec; p:=Root;
    repeat {Compute distance to spectrum in each child.}
      if dist(Test,Tree[Tree[p].Left].Spec) <
        dist(Test,Tree[Tree[p].Right].Spec) then p:=Tree[p].Left
                                            else p:=Tree[p].Right
    until Tree[p].Leaf;
    if Tree[p].Id=Lib[i].Id then mS:=mS+1;
    if Tree[p].Group=Lib[i].Group then mG:=mG+1
  end;
  pS:=100*mS/m; pG:=100*mG/m
end;
```

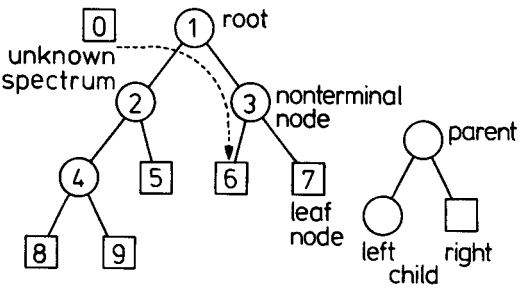

Fig. 1. A binary hierarchical search tree with nine nodes. Node 1 is the root node, (2—4) are non-terminal nodes, and (5—9) are leaf nodes. All leaf nodes are spectra. Each non-terminal or parent node may be viewed as a prototype representing all leaf nodes connected to this node (via its left or right child). This tree has skewness ($|1-1|+|2-1|+|1-1|+|3-2|$) = 2, or 100% × 2 × 2((5 − 2)(5 − 1)) = 33.3%. The identification of S_0 is shown, and assuming that $d_{03} < d_{02}$ and $d_{06} < d_{07}$, S_6 is used as a candidate for S_0.

$$r_c = \left[\sum_{j<i}(d_{ij}-\bar{d})(d'_{ij}-\bar{d}')\right] \Big/ \left[\sum_{j<i}(d_{ij}-\bar{d})^2 \sum_{j<i}(d'_{ij}-\bar{d}')^2\right]^{1/2} \tag{4}$$

and by Jardine and Sibson's $\hat{\Delta}_1$ [17]:

$$\hat{\Delta}_1 = \left(\sum_{j<i}|d_{ij}-d'_{ij}|\right) \Big/ \sum_{j<i} d_{ij} \tag{5}$$

Here d_{ij} is the distance between object i and j, d'_{ij} is the amalgamation distance for the step where object i and j appear together in the same cluster for the first time, and $\bar{d}$ and $\bar{d}'$ are the means of d_{ij} and d'_{ij} over i and j for $j < i$.

The global-fit measures only test how well the clustering method preserves the structure of the original data set, not how well this structure description may serve as a search tree. But it seems reasonable to assume that a good representation of the structure of the data set is a favourable quality of a search tree.

A search tree should have a short mean search length; the tree should be balanced. Therefore, a measure of skewness is computed. For each non-terminal node p, the absolute difference between the number of leaf nodes in left and right subtree, $|m_{L(p)} - m_{R(p)}|$, is computed and added up over all non-terminal nodes. For a completely balanced tree with $m = 2^k$ leaves, the total will be zero; the left and right subtrees are always of the same size. In the worst case, the total difference will be $(m-2)(m-1)/2$, where m is the number of leaf nodes (spectra) in the tree. The relative skewness s is then computed as

$$s = 2 \times \sum_p |m_{L(p)} - m_{R(p)}| / [(m-2)(m-1)] \tag{6}$$

The CYCLE procedure. The CYCLE method (Table 5) tests the propagation of a linear library search, i.e., the ability to find related compounds

TABLE 5

Algorithmic description of the CYCLE procedure

```
procedure CYCLE(Lib);
var New, Test: stack;
   Included: array[1..m] of boolean;
begin
   normal(Lib.Spec); mT:=mG:=0;
   for i:=1 to m do begin
      Included[1..m]:=false; empty(New); empty(Test) {Reset stack.};
      push(i,New) {Place pointer to current record on stack.};
      Included[i]:=true;
      for j:=1 to q do begin
         Test:=New; empty(New);
         while length(Test)>0 {Number of items on stack.} do begin
            nn[2..mN+1]:=neigh(Lib[pop(Test)].Spec,Lib.Spec)
               {Find mN nearest neighbours to test spectrum.};
            for k:=2 to mN+1 do if not Included[nn[k]] then begin
               Included[nn[k]]:=true; push(nn[k],New); mT:=mT+1;
               if Lib[nn[k]].Group=Lib[i].Group then mG:=mG+1
            end
         end
      end
   end;
   pC:=100*(1—(mT—m*mN)/(q*m*mN—m*mN)); pG:=100*mG/mT
end;
```

when the spectrum of the unknown is not represented in the library. It is a slightly modified version of a test method described by Rasmussen and Isenhour [4]. If a linear library search is conducted with a test spectrum from the library, a sorted list of candidates will be made with the test spectrum as the first candidate on the list. The other candidates will be spectra with characteristics in common with this spectrum. New searches with spectra from this list will generate new lists of candidates. These candidates may be new spectra or spectra already found in the first list. New spectra can be used for new searches, and this operation can be repeated to any required depth, or until no new spectra are included. The process should converge and only a limited number of spectra from similar compounds should be included before the process stops, as this indicates that the search method is able to identify common characteristics in a satisfactory way. Figure 2 shows the propagation of a single search step, corresponding to one iteration of the outermost loop in CYCLE.

In the optimal case, m_N new spectra will be included for each test spectrum, where $m_N + 1$ is the total number of candidates in the sorted list. New searches from these candidates will include no new spectra. In the most divergent case, m_N new spectra will be included in each search, and the total number of spectra will be

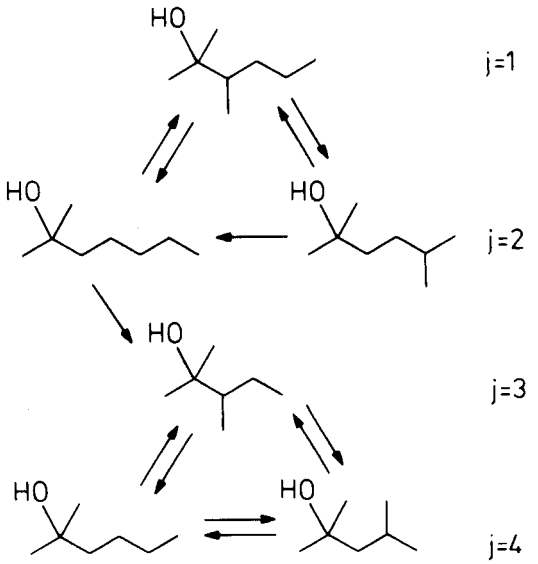

Fig. 2. The propagation of a single search step in CYCLE, starting from 2,3-dimethyl-2-hexanol. Arrows from each structure point to the two nearest neighbours of this structure in the library file.

$$s_T = m \sum_{k=1}^{q} m_N^k \tag{7}$$

where q is the maximum depth of the search. However, in most cases, the result will be closer to the optimal situation, and an empirical lower limit of convergence is therefore defined:

$$s'_T = m \sum_{k=1}^{q} m_N \quad \text{or} \quad s'_T = qmm_N \tag{8}$$

If a total of m_T new spectra is included when the library is searched to depth q, the degree of convergence will be

$$p_C = 100 \times [1 - (m_T - mm_N)/(qmm_N - mm_N)] \tag{9}$$

The NOISE procedure. This method (Table 6) tests the ability to identify noise-distorted spectra, i.e., for noise sensitivity. Spectra recorded under different conditions will show some degree of variation, and in connection with a library search this variation can be regarded as noise. Noise is simulated in this test method by contaminating spectra with random noise before they are used as test spectra in a linear library search. Two kinds of noise are added; background noise b in per cent of the total intensity of the spectrum, and fluctuation f as per cent of the intensity of the current peak. Peak number k of spectrum i, x_{ik}, is transformed by

$$x'_{ik} = x_{ik} + \left(\sum_{l=1}^{n} x_{il} \right) f(\mathrm{r}) b/100 + x_{ik}[2f(\mathrm{r}) - 1] f/100 \tag{10}$$

TABLE 6

Algorithmic description of the NOISE and MIX procedures

```
procedure NOISE(Lib);
begin
   normal(Lib.Spec); mS:=mG:=0;
   for i:=1 to m do begin
      Test:=normal(noise(Lib[i].Spec)) {Add noise to test spectrum.};
      nn:=neigh(Test,Lib.Spec);
      if Lib[nn].Id=Lib[i].Id then mS:=mS+1;
      if Lib[nn].Group=Lib[i].Group then mG:=mG+1
   end;
   pS:=100*mS/m; pG:=100*mG/m
end;

procedure MIX(Lib);
begin
   if DoShuffle then shuffle(Lib) {Make random permutation of library.};
   normal (Lib.Spec); mSS:=mS0:=m0S:=0; mGG:=mG0:=m0G:=0;
   for i:=1 to m—1 do begin
      Test:=normal(sum(Lib[i].Spec,Lib[i+1].Spec,Weight))
         {Make a weighted sum of a spectrum and its neighbour.};
      nn[1..2]:=neigh(Test,Lib.Spec);
      case [Lib[nn[1]].Id,Lib[nn[2]].Id]—[Lib[i].Id,Lib[i+1].Id] of
         []: mSS:=mSS+2;
         [Lib[nn[2]].Id]: mS0:=mS0+1;
         [Lib[nn[1]].Id]: m0S:=m0S+1
      end;
      {Count group identifications the same way.};
   end;
   pS:=100*(mSS+mS0+m0S)/m; p'S:=100*(mSS+mS0)/m;
   pG:=100*(mGG+mG0+m0G)/m; p'G:=100*(mGG+mG0)/m
end;
```

where $f(r)$ is a random number generator with uniform distribution between 0.0 and 1.0.

The MIX procedure. This method (Table 6) tests the ability to identify compounds in a mixture, as spectra will be contaminated when the sample under investigation is a mixture of several compounds; the spectrum is then a combination of spectra from each of the components. Ideally, it should be possible to identify all compounds in the mixture.

Spectra are combined in pairs in a given proportion, and the combined spectrum is used as a test spectrum in a linear library search, so that both components can be identified. Each search can give four different results, depending on whether both (SS), the first (S0), the second (0S) or none of the candidates are correct. This is used to compute both the total number of correct candidates and the number of correct candidates returned as the first (or first and second) alternative. Each spectrum is mixed with its successor in the library. Either the sorted library or a random permutation of it

can be used. The random permutation is made by the shuffling algorithm of Moses and Oakford [18, 19].

All test methods were programmed in ASCII FORTRAN (essentially FORTRAN 77 with some extensions) and run on a Unisys (Sperry) 1100/82 under OS1100.

RESULTS AND DISCUSSION

A principal components plot [13] (Fig. 3) of data set C shows a large degree of overlap between different groups; although this can be explained in part by the reduction in variance, only 47.48% of the total variance is explained in the plot. A stepwise discriminant analysis of data set A, using the program P7M from the BMDP package [21], shows a total correct classification of 79.7%. This demonstrates that the data set is difficult to classify on the basis of functionality, which is reasonable from a spectroscopic point of view. But the classification may be of potential interest for an end user. This data set is thus suitable for testing because it contains interesting information which is difficult to extract. Further research on the classification of this data set is in progress.

Testing the global fit for different methods of hierarchical clustering shows (Table 7) that the group average algorithm gives the best results, followed by the simple average and furthest neighbour. This result is in agreement with the results of Cunningham and Ogilvie [22]. Group average means that, when two groups are joined, the new group centre is computed as the mean of the original group centres weighted by the number of objects in each group. As most of the groups combined during the clustering process are of comparable size, this produces a reasonably balanced tree (Fig. 4).

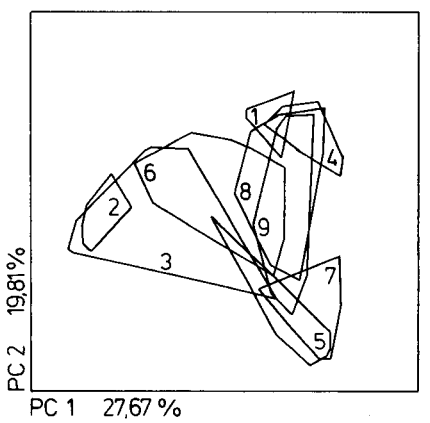

Fig. 3. Data set C plotted against its two first principal components. Each group in the data set is described by its convex hull [20].

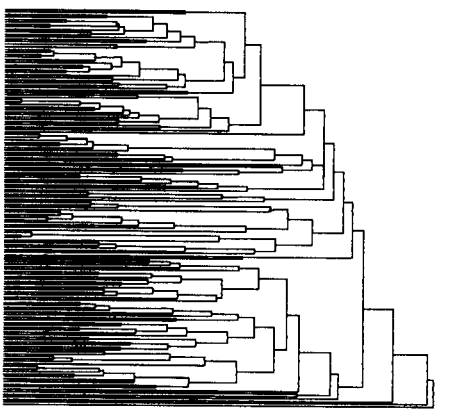

Fig. 4. The result of hierarchical clustering of data set C using the group average algorithm. The horizontal scale is proportional to the amalgamation distance d'.

TABLE 7

Goodness of fit for different hierarchical clustering algorithms with the euclidean distance measure and data set C

Method	r_c	$\hat{\Delta}_1$
Nearest neighbour	0.64	0.41
Furthest neighbour	0.76	0.42
Centroid	0.59	0.51
Median	0.59	0.46
Group average	0.83	0.11
Simple average	0.80	0.16

On the basis of this result, the group average algorithm was used for building the search tree in TREE. CYCLE was used with depth $q = 10$ and $m_N = 2$. NOISE results were the average of three different runs for each test, with different initial seeds for the random number generator, and with 10% background noise and 100% fluctuation. The differences between individual runs were small; the mean standard deviation for p_S over all distance measures was 1.5. The deviation was also quite systematic, so that each run gave the same relative order of the distance measures. In MIX, each spectrum was contaminated to an extent of 50% (of the combined spectrum) by its successor in the sorted file. The effect of combining spectra at random was also tested (Table 8), and the results were similar to those for the sorted file, although a lower number of correct identifications was found. The mixing of spectra from compounds that are closely related is a common situation in analytical problems (for example g.c./m.s.), therefore in all tests neighbours in the sorted file were combined. Vector length $n = 150$ was used in all tests.

The test results (Table 9) show that for each test method the distance measures can be divided into groups with high and low scores. For TREE, the distance measures (1, 2, 6, 7, 8, 9, 10) produce mainly high p_S scores, and distance measures (3, 4, 5) mainly low p_S scores. The same grouping seems natural for the results from CYCLE. This seems reasonable, as both the clustering and search step in TREE and the search step in CYCLE

TABLE 8

Test scores from MIX by using a random permutation of data set A and normalization 2

MIX	Distance measure									
	1	2	3	4	5	6	7	8	9	10
p_S	27	15	49	53	4	27	28	28	23	28
p'_S	19	10	45	62	3	20	21	20	17	20
p_G	57	49	67	67	41	56	56	56	56	56
p'_G	51	43	66	69	34	51	51	51	50	51

TABLE 9

Test scores from TREE, CYCLE, NOISE and MIX for all distance measures, with normalization 2

		Distance measure									
		1	2	3	4	5	6	7	8	9	10
TREE	s	6.5	5.7	8.1	9.9	5.9	6.2	4.9	4.8	5.5	4.6
	p_S	83	84	68	0	72	87	85	86	81	85
	p_G	92	92	80	13	82	94	93	94	88	93
CYCLE	p_C	65	67	54	48	56	65	66	65	66	65
	p_G	52	53	53	59	49	53	54	54	52	54
NOISE	p_S	28	31	22	0	33	26	37	29	12	29
	p_G	64	68	55	16	74	66	73	64	48	64
MIX	p_S	39	30	57	73	20	39	42	42	40	42
	p'_S	32	23	50	71	15	32	35	35	33	35
	p_G	86	81	93	96	74	86	88	87	86	87
	p'_G	83	77	92	96	68	83	85	85	83	85

depend on the identification of a limited number of closely related spectra. For the results from NOISE, a natural grouping may be (1, 2, 5, 6, 7, 8, 10) with high p_S scores and (3, 4, 9) with low p_S scores. This is quite similar to the results from TREE and CYCLE, except for distance measures 5 and 9. The high score for distance measure 5 in the NOISE test may be due to the fact that most noise distortions are small, and the maximum distance between the original spectrum and the noise-distorted spectrum will thus remain small. Mixing spectra, as in TREE and MIX, may introduce new peaks, with large maximum differences (and distances) as a result. For the results from MIX, a grouping into three groups seems natural, with distance measures (3, 4) with high p_S scores (1, 6, 7, 8, 9, 10) with medium scores and (2, 5) with low p_S scores. This is very different from the other results, and the difference is most pronounced in distance measures 3 and 4. This is probably due to different methods for weighting the differences between vectors. Distance measure 1 will square each difference, thereby increasing the importance of large differences. Distance measure 3, in contrast, uses absolute values for differences, which means that many small differences may outweigh a few larger ones. This is still more marked in distance measure 4, for which the importance of variation in large data values is reduced by dividing the difference by the sum of the values.

The noise added to each spectrum introduces many small shifts, especially as background noise. This has little influence on distance measure 1, but can lead to a large distance between the reference spectrum and the noise-distorted spectrum when distance measure 3 is used. Distance measure 4 will cause even larger distances between the spectra because data values different from zero (caused by background noise) will contribute maximally to the total distance.

Compared to noise distortion, mixing of two spectra will give more large differences, especially when the main fragments of the compounds are different in the combined spectra. This will lead to relatively large distances when distance measure 1 is used whereas distance measures 3 and 4 will give better results.

As the proportions of the mixed spectra vary (Fig. 5a), the degree of correct identification decreases with increasing contamination for distance measure 1, but increases for distance measure 4. Distance measure 1 is seriously affected by the increasing intensity of the foreign peaks, whereas for distance measure 4 this increased intensity leads mainly to better identification of the minor component in the mixture. If noise is added as 80% fluctuation to the mixed spectra (Fig. 5b), the degree of correct identification when distance measure 1 is used, is reduced by about 20 units, whereas the results for distance measure 4 show little difference. This is reasonable, as fluctuation creates few and relatively large differences (most spectra in the library have data values in only a few positions). If 5% background noise is also added, the additional shift in the results for distance measure 1 is small, whereas the results for distance measure 4 approach a level corresponding to random assignment of spectra.

However, the noise used in these tests was artificial, and more knowledge about the exact nature of noise in mass spectra would be useful for additional tests.

The p_G scores in Table 9 are mainly similar to the p_S scores. But the p_G scores from CYCLE show an important difference for distance measures 3 and 4. Whereas the p_C scores are low, the corresponding p_G scores are high. This indicates that although these distance measures allow for the inclusion of more spectra, the new spectra are mainly from the same group

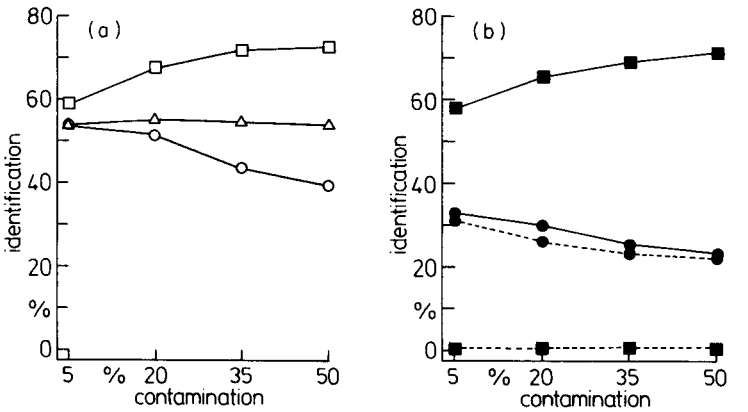

Fig. 5. Test scores from MIX (identification of spectra) for distance measures 1 (○, ●), 3 (△) and 4 (□, ■). (a) With different levels of contamination; (b) for distance measures 1 and 4 with 80% fluctuation noise (——) and 5% background noise (- - -) added to the combined spectra.

as the first spectrum, probably because these distance measures, by reducing the importance of large differences, allow a shift in the base peak position, as long as the general pattern of the mass spectrum remains the same.

The distance measures 3 and 4, both with low p_S scores, give skewed search trees compared to the other distance measures (Table 9).

The effect of using different normalization procedures was tested by using the same test methods and distance measure 1. The results (Table 10) obtained with normalization 6 seems to be best, especially from the NOISE score. But the method ignores the absolute zero of mass spectra, and zeros in the raw spectrum will be nonzero in the normalized spectrum. This makes compact storage of spectra difficult. Normalization 8 may therefore be an interesting alternative.

Conclusions

The tests show that although the differences in most cases are small, no single distance measure seems to be optimal in all situations. Most of the distance measures tested in this paper can be grouped into two different groups. Distance measures of type 1 (1, 2, 6, 7, 8, 10) tend to emphasize large differences between spectra. Distance measures of type 2 (3, 4) tend to reduce the importance of large differences between spectra. Distance measures 5 and 9 seem to be different from the other distance measures with respect to this grouping.

In a presearch of a library of mass spectra, based on prototypes for groups of spectra, the distance measure should be of type 1. In a search of a library for spectra of related compounds, distance measures of type 1 will limit the number of retrievals, but distance measures of type 2 may return additional useful information.

TABLE 10

Test scores from TREE, CYCLE, NOISE and MIX for normalization procedures, using distance measure 1 (for test scores for normalization 2, see Table 9)

		Normalization						
		1	3	4	5	6	7	8
TREE	s	6.7	7.9	4.8	6.2	4.9	8.7	4.8
	p_S	77	77	87	87	86	84	88
	p_G	85	88	96	94	95	94	95
CYCLE	p_C	59	63	65	65	66	47	65
	p_G	50	55	54	53	54	40	54
NOISE	p_S	29	28	29	28	37	0	29
	p_G	64	63	64	67	73	19	64
MIX	p_S	38	39	42	39	42	31	42
	p'_S	31	33	35	32	35	24	35
	p_G	87	87	88	86	88	74	87
	p'_G	85	85	85	83	85	69	85

If noise is a problem in the spectra, the choice of distance measure depends on the nature of the noise. If the samples are pure, but background noise and instrumental differences introduce variation in the spectra, the distance measure should be of type 1. However, if instrumental and experimental conditions are stable, both for reference and query spectra, but the query spectra are contaminated by other compounds, the distance measure should be of type 2.

The effect of choosing different normalization procedures seems to be small, but normalization procedures 6 and 8 may give some improvement over the basepeak normalization often encountered in mass spectrometry.

The author is indebted to the Norwegian Council for Scientific and Industrial Research (NTNF) for financial support.

REFERENCES

1 R. J. Mathews and J. D. Morrison, Aust. J. Chem., 27 (1974) 2167; 29 (1976) 689.
2 K. Varmuza, Fresenius' Z. Anal. Chem., 282 (1976) 129.
3 H. Rotter and K. Varmuza, Anal. Chim. Acta, 103 (1978) 61.
4 G. T. Rasmussen and T. L. Isenhour, J. Chem. Inf. Comput. Sci., 19 (1979) 179.
5 R. M. Cormack, J. R. Stat. Soc., Part A, 134 (1971) 321.
6 E. Diday and J. C. Simon, in K. S. Fu (Ed.), Digital Pattern Recognition, Springer, Berlin, 1976, p. 47.
7 L. Domokos and D. Henneberg, Abstr. Pap. Am. Chem. Soc., 188 (1984) 59.
8 D. D. Saperstein, Appl. Spectrosc., 40 (1986) 344.
9 R. G. Dromey, Anal. Chim. Acta, 112 (1979) 133.
10 B. L. Atwater, D. B. Stauffer, F. W. McLafferty and D. W. Peterson, Anal. Chem., 57 (1985) 899.
11 M. G. Kendall and W. R. Buckland, A Dictionary of Statistical Terms, 4th edn., Longman, London, 1982, p. 138.
12 K. Jensen and N. Wirth, Pascal User Manual and Report, 3rd edn., Springer, New York, 1985.
13 B. S. Everitt and G. Dunn, Advanced Methods of Data Exploration and Modelling, Heinemann, London, 1983, pp. 39, 87.
14 E. Horowitz and S. Sahni, Fundamentals of Data Structures, Pitman, London, 1976, p. 218.
15 G. N. Lance and W. T. Williams, Comput. J., 9 (1967) 373.
16 R. R. Sokal and F. J. Rohlf, Taxon, 11 (1962) 33.
17 N. Jardine and R. Sibson, Comput. J., 11 (1968) 177.
18 L. E. Moses and R. V. Oakford, Tables of Random Permutations, Stanford University Press, Stanford, CA, 1963.
19 D. E. Knuth, The Art of Computer Programming, Vol. 2: Seminumerical Algorithms, 2nd edn., Addison-Wesley, Reading, MA, 1981, p. 139.
20 R. Sedgewick, Algorithms, Addison-Wesley, Reading, MA, 1984, p. 321.
21 W. J. Dixon (Ed.), BMPD Statistical Software, 1983 printing with additions, University of California Press, Berkeley, CA, 1983, p. 519.
22 K. M. Cunningham and J. C. Ogilvie, Comput. J., 15 (1972) 209.

Analytica Chimica Acta, 201 (1987) 241—252
Elsevier Science Publishers B.V., Amsterdam — Printed in The Netherlands

THEORETICAL ASPECTS OF QUANTITATIVE MASS SPECTROMETRY OF GAS MIXTURES

FILIP V. BABALIEVSKI

Institute of General and Inorganic Chemistry, Bulgarian Academy of Sciences, 1040 Sofia (Bulgaria)

(Received 3rd October 1985)

SUMMARY

The problem of calibration of mass spectrometers with standard gas mixtures is studied theoretically. The results obtained can be used in deciding the number and optimum composition of standard mixtures. An analogy is drawn between this calibration problem and the mathematical theory of experimental design when mixtures are considered. It is shown that calibration based on a number of standard mixtures is more accurate than calibration with pure gases. A procedure for correction of calibration coefficients is described; it can be applied during measurements on the composition of gas mixtures or gas flows. Application to gas mixtures containing CO, N_2 and CO_2 is discussed.

Data interpretation in quantitative mass spectrometry can be somewhat difficult. When gas mixtures with known components are analysed, there are two main obstacles: (1) the sensitivity of mass spectrometers varies with different gases and also changes with time and varying conditions; (2) many compounds give spectra containing several peaks, and peaks from different molecular species may overlap in the mixture spectrum. Increasing the resolution would be expensive and does not solve the problem entirely, because of the presence of isobaric compounds, e.g., compositional and/or structural isomers as well as different types of fragment ions. For instance, when mixtures of carbon monoxide, nitrogen and carbon dioxide are analysed, all the molecules give peaks at mass 28 where the CO_2 peak is due to a CO^+ fragment and cannot be resolved from the CO molecular peak.

These problems have generally been solved without paying attention to the advantages which calibration of the spectrometer by means of several standard mixtures instead of pure gases would provide. It has not been taken into account that the accuracy of calibration depends strongly on the way that the composition of calibration mixtures is selected. The purpose of the present paper is to propose a possibility of improving the accuracy of quantitative mass spectrometry of gas mixtures by calibration with a set of standard mixtures (calibration mixtures) and by correction of calibration coefficients during measurements.

0003-2670/87/$03.50

THEORY

General procedures of quantitative mass spectrometry of gas mixtures have been described [1—3] and mixtures containing CO, N_2 and CO_2 have been studied [4]. In these papers, the analysis of gas mixtures with known components is reduced to the solution of a set of simultaneous linear equations:

$$\begin{aligned} g_1 &= a_{11}P_1 + a_{12}P_2 + \ldots + a_{1n}P_n \\ &\vdots \\ g_i &= \ldots + a_{ij}P_j + \ldots \\ &\vdots \\ g_m &= a_{m1}P_1 + a_{m2}P_2 + \ldots + a_{mn}P_n \end{aligned} \qquad (1)$$

where g_i is the intensity (height or area) of mass peak i; $P_1, P_2, \ldots, P_n$ are the partial pressures of the components, and a_{ij} are coefficients obtained after preliminary measurements (calibration of the mass spectrometer), which determine the contribution to the ith peak height of unit pressure of component j.

The above system can be written in matrix notation

$$\mathbf{G} = \mathbf{AR} \qquad (2)$$

where $\mathbf{R} = (P_1, P_2 \ldots P_j \ldots P_n)^T$. When $m = n$, the unknown concentrations are obtained from the expression

$$\mathbf{R} = \mathbf{A}^{-1}\mathbf{G} \qquad (3)$$

When $m > n$, Eqns. 1 are usually solved by the least-squares method (LSM) [1, 5]. Irrespective of the method used for solution of Eqns. 1, the accuracy of the P_j determination depends mainly on the accuracy of estimating the elements of matrix **A**. It is here that extension of the theory is badly needed. The determination of a_{ij} on the introduction of a sequence of pure gases into the spectrometer can be described as follows. When a certain gas with a known pressure P_j is admitted to the spectrometer, Eqns. 1 can be represented as follows: $g_i = a_{ij}P_j$ with $i = 1, \ldots, m$ and $j = 1, \ldots, n$, hence $a_{ij} = g_i/P_j$. Obviously, each a_{ij} value is obtained from a single measurement and its error coincides with the error of measurement. In addition to the set of successively introduced pure gases, a mixture of all gases was used by Ruth [2] and the error in measurement of the pure gas pressures was avoided by additional mathematical treatment of the data. In this case, each a_{ij} value was the result of two measurements based on the spectrum of the corresponding gas and the spectrum of the mixture.

Here, the use of several mixtures with known compositions (calibration mixtures) instead of pure gases is proposed for the calibration of the mass spectrometer. In this case, a_{ij} is obtained by processing the data from all

measurements (Eqns. 5, see below). It can be shown [6] that with suitable compositions of the mixtures, the variance of the estimate of a_{ij} is about l times lower than the variance of a separate measurement (l is the number of mixtures used). Thus, by an appropriate choice of l calibration gas mixtures (against the same number of pure gases), it should be possible to obtain more accurate calibration.

If it is assumed that l calibration mixtures with different compositions have been successively introduced into the mass spectrometer, the data obtained can be used in writing the following system of equations (matrix notation is given to the right):

$$g_1^1 = a_{11}P_1^1 + a_{12}P_2^1 + \ldots + a_{1n}P_n^1$$

$$g_m^1 = a_{m1}P_1^1 + a_{m2}P_2^1 + \ldots + a_{mn}P_n^1; \mathbf{G}^1 = \mathbf{A}\mathbf{R}^1$$

$$\vdots$$

$$g_1^l = a_{11}P_1^l + a_{12}P_2^l + \ldots + a_{1n}P_n^l$$

$$\vdots$$

$$g_m^l = a_{m1}P_1^l + a_{m2}P_2^l + \ldots + a_{mn}P_n^l; \mathbf{G}^l = \mathbf{A}\mathbf{R}^l \qquad (4)$$

where P_j^k ($k = 1,\ldots, l; j = 1,\ldots, n$) is the partial pressure of component j in the calibration mixture k; P_j^r and P_j^f ($r, f = 1,\ldots, l; r \neq f$) are the partial pressures of the same gases in different calibration mixtures; g_i^k is the measured peak height at mass i for calibration mixture k. Moreover, it is assumed that the coefficient of pressure reduction of the inlet system (CPRIS) for the same gas does not change with the different calibration mixtures. Then, system 4 can be presented as m independent systems of the type

$$g_i^1 = a_{i1}P_1^1 + a_{i2}P_2^1 + \ldots + a_{in}P_n^1$$

$$g_i^2 = a_{i1}P_1^2 + a_{i2}P_2^2 + \ldots + a_{in}P_n^2$$

$$\vdots$$

$$g_i^l = a_{i1}P_1^l + a_{i2}P_2^l + \ldots + a_{in}P_n^l \qquad (5)$$

where $i = 1, 2,\ldots, m$. In matrix notation:

$$\Gamma_i = \mathbf{P}\Lambda_i$$

where

$$\mathbf{P} = \begin{Bmatrix} P_1^1, P_2^1, \ldots, P_n^1 \\ \vdots \\ P_1^l, P_2^l, \ldots, P_n^l \end{Bmatrix} \qquad \begin{aligned} \Gamma_i &= (g_i^1, g_i^2 \ldots)^{\mathrm{T}} \\ \Lambda_i &= (a_{i1}, a_{i2}, \ldots)^{\mathrm{T}} \end{aligned}$$

The solution of each of these systems by the least-squares method is given [7] by

$$\Lambda_i = (\mathbf{P}^{\mathrm{T}}\mathbf{P})^{-1}\mathbf{P}^{\mathrm{T}}\Gamma_i \qquad (6)$$

The error in each a_{ij} element is given [7] by

$$D(a_{ij}) = C_{jj}s^2$$

Here, C_{jj} is a diagonal element of the matrix $(\mathbf{P}^T\mathbf{P})^{-1}$. It is assumed that the error of the peak-height determination is a normally distributed random variable having mean zero and variance s^2. $D(a_{ij})$ depends only on this error and on the elements of the $\mathbf{P}^T\mathbf{P}$ matrix (the so-called information matrix). This matrix depends only on the composition of the set of calibration mixtures. Hence, the calibration can be improved not only by reducing the measurement error but also by varying the composition of the calibration mixtures. For that purpose, a criterion is needed for optimization of the calibration, as well as methods for achieving this optimal condition.

The methods of finding suitable criteria of optimization and the ways of achieving the optimal state are based on the mathematical theory of experimental design [6—8]. One aim of this paper is to establish analogies between the problem of mass spectrometric calibration and optimum experimental design.

The second problem related to the accuracy of measurement is the presence of drifting calibration coefficients (the elements of matrix **Y**, see below). Thus, in the proposed approach, these coefficients are corrected without interruption of measurement. The procedure for this correction (as described in the section on Measurement Protocol) is based on Dalton's gas law, i.e., the sum of partial pressures of definite pure gases is equal to the pressure of the mixture of these gases. Hence, when the changes of the sum of partial pressures (measured by the spectrometer) are not proportional to the changes in total pressure (measured by a manometer), it can be concluded that there is a drift in the values of the calibration coefficients.

The problems of discovering which calibration coefficients have changed and of estimating their new values are similar to those dealt with in some sections of cybernetics, especially system identification [9]. In the present paper, the stochastic approximation method is used [10, 11] (see below). As already indicated, the construction and functioning of a given spectrometer is not considered here. The aim is to obtain results which are valid for all kinds of mass spectrometers. The spectrometer is regarded as an abstract system with known inputs and outputs but unknown structure and parameters of the system model. The two working protocols, calibration and measurement, will be considered separately.

Calibration protocol

The purpose of this regime is to estimate the elements of the matrix **A** by means of a number of calibration mixtures and mathematical processing of the data obtained. As can be seen in Fig. 1, the problem can be presented as follows: the object under investigation is an abstract system with observable n inputs and m outputs; the available data comprise l sets of inputs and outputs (l calibration mixtures and the corresponding m multiple peak

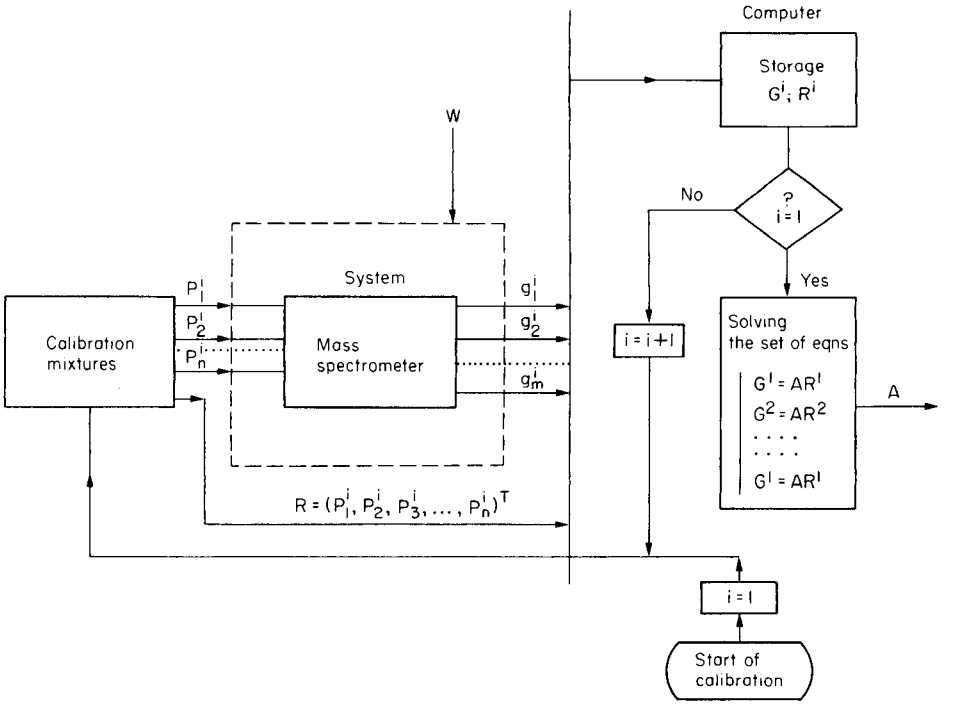

Fig. 1. Calibration protocol. **R**, **G** and **W** are matrix columns; **R** contains the partial pressures P_j^i of the components of calibration mixture i. The corresponding peak intensities g_j^i form $\mathbf{G}^i$ while the measurement errors are given by **W**; n is the number of components in all calibration mixtures; m, number of monitored masses; l, number of calibration mixtures.

heights). It is necessary to find a connection between the input and the output of the system:

$$\mathbf{G} = \mathbf{AR} + \mathbf{W} \tag{7}$$

(**W** is a matrix column containing the errors of measurement of the peak heights).

Equation 7 will be correct if some conditions are fulfilled, which are usually assumed by default. However, if some of these conditions are not fulfilled, the solution must be sought in another class of systems. The three conditions are as follows. First, the input/output connection is linear without an intercept. This means that a correction for the background is needed, i.e., the signals caused by the residual gas in the spectrometer are taken into account. It is assumed that possible nonlinearity of the spectrometer response has been corrected by an expression of the kind

$$g_i^{\text{new}} = g_i + rg_i^2 \tag{8}$$

where r is a coefficient obtained by introducing mixtures with a constant

composition but different pressures, and is chosen so as to ensure that g_j^{new} is directly proportional to the pressure. Secondly, the matrix A must be constant during the calibration time. (Even if there is some drift in the A elements, it is negligibly small.) Thirdly, G and W must be independent of the prior history of the spectrometer, i.e., calibration mixtures must be introduced into the spectrometer at time intervals which are sufficiently large to eliminate traces of the preceding mixture. Of course these intervals should not be too large because the second condition must also be fulfilled.

As was already pointed out, the accuracy of the solution to the problem thus defined strongly depends on the choice of the composition of the calibration mixture (the inputs of the system).

The experimental design for multiple input/output systems has been described [12]. Irrespective of the different approaches used, most of them reduce the problem to the single-output system design; this is also done here. The sum of the peak heights obtained by introducing a definite calibration mixture will be considered as the only output of the system. Then, instead of the set of equations (Eqns. 1), an equation is obtained by summing the left- and right-hand sides of the equations separately;

$$\sum_{i=1}^{m} g_i = \sum_{j=1}^{n} \left(\sum_{i=1}^{m} a_{ij}\right) P_j \tag{9}$$

If the more general case of weighted sums is considered, then given the definitions $q = \Sigma_{i=1}^{m} V_i g_i$ and $b_j = \Sigma_{i=1}^{m} V_i a_{ij}$ for $j = 1 \ldots n$, the "reduced" Eqn. 9 can be written as

$$q = b_1 P_1 + b_2 P_2 + \ldots + b_n P_n \tag{10}$$

The minimization of errors in the b_j values could lead to smaller errors in the a_{ij} values; this is true when the covariances between the different $D(a_{ij})$ are not negative, i.e., $\mathrm{cov}[D(a_{ij}), D(a_{ik})] \geqslant 0$. This condition does not impose essential restrictions because in most cases the covariance in question is close to zero.

An important consideration is the presence of connections between the different P_j values: $P = \Sigma_{j=1}^{n} P_j$, where P denotes the pressure of the calibration mixture. In many cases, the mixture concentrations are determined instead of the partial pressures. Thus, without loss of generality, it is possible to write $\Sigma_{j=1}^{n} P_j = 1$. By introducing this condition, the calibration problem can be presented in a form (Eqn. 10) which is mathematically equivalent to the general problem of experimental design for mixtures [13, 14].

Tables of optimum experimental designs have been published [14, 15]. In principle, these tables can be used for designs based on preset values of n (number of factors) and l (number of experiments). Some difficulty arises in this respect because the published designs have usually $l \geqslant 4$. It is awkward to use more than 3—4 calibration mixtures for routine measurements. A design for three mixtures is therefore preferred (see below).

Measurement protocol

After calibration, the composition of the mixtures to be analysed can be found by the formula

$$\mathbf{R} = \mathbf{YG} \tag{11}$$

When $m = n$, $\mathbf{Y} = \mathbf{A}^{-1}$. When $m > n$, the solution of Eqns. 1 and 5 with respect to **R** can have a form similar to Eqn. 11, and, with the least-squares method,

$$\mathbf{Y} = (\mathbf{A}^{\mathrm{T}}\mathbf{A})^{-1}\mathbf{A}^{\mathrm{T}}$$

Here again, an abstract system including the spectrometer is considered, but part of the gas volume to be analysed is also involved. The system so defined (Fig. 2) has only one input signal, i.e., the pressure of the analysed gas flow. The system parameters to be estimated are the partial pressures of the gas-flow components.

In the measurement protocol, the changes with time in the composition of the gas flow being analysed are monitored. It is assumed that the above-mentioned first and third conditions are valid and that the elements of **Y** may change slowly with time as a result of unpredictable changes in working of the spectrometer. Ensuring the fulfilment of the third condition is not a trivial matter, but the approach proposed below allows extension to cases in which the condition is not strictly observed.

Methods for tracing the model parameter drift have been developed in system identification theory. These methods will work if the estimate of **R** from Eqn. 11 is periodically compared with the "real" value of **R**. This can

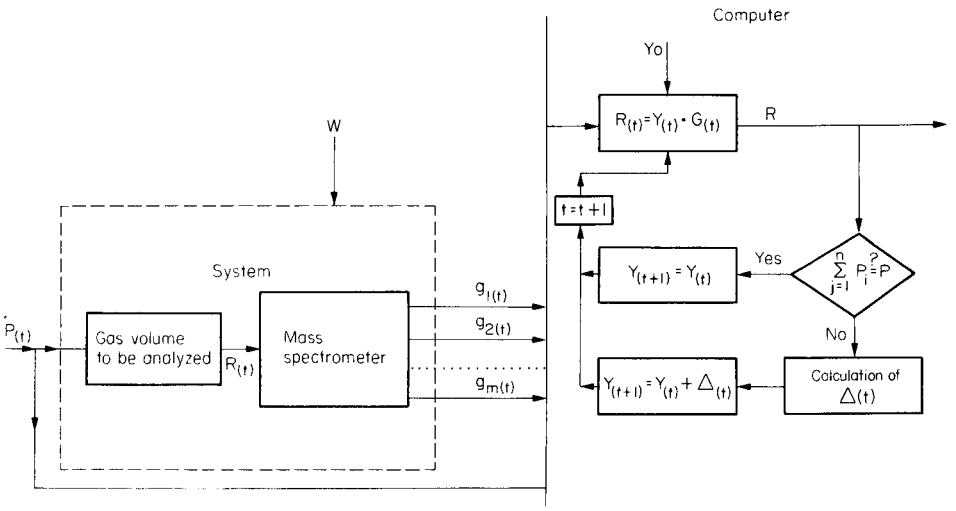

Fig. 2. Measurement protocol, P, pressure of analysed gas flow (or sequence of mixtures) measured by another monitor; t, time (measured in sampling intervals); $\Delta_{(t)}$, on-line correction of matrix **Y** calculated from Eqns. 15—18; $Y_0 = f(A)$, the connection between Y and A is discussed in the text.

be achieved if the measurement is stopped and the calibration mixture is again introduced into the spectrometer, i.e., the calibration is repeated. It has been shown [16], albeit for another area of analytical chemistry, that this is not simply a re-formulation of known things in different words.

In the proposed approach, periodic calibrations are not necessary and the calibration coefficients can be corrected without interruption of measurement. It is assumed that the pressure and the temperature of the mixture being analysed can be measured with sufficient accuracy and that their values allow application of the ideal gas equation. The pressure of the analysed mixture can be estimated from the responses of the spectrometer by using the expression

$$\hat{P} = k \sum_{j=1}^{n} P_j \tag{12}$$

where k is the ratio between CPRIS during the calibration and CPRIS at the beginning of measurement. For convenience, $k = 1$ here.

If P is the "real" value of the pressure measured very precisely by a monitor (some kind of manometer), then comparison between P and $\hat{P}$ would give the necessary feed-back for correction of the elements of Y. If $Y_i^* = \Sigma_{j=1}^{n} Y_{ij}$, then Eqn. 12 can be written as $P = \Sigma_{i=1}^{m} Y_i^* g_i$. The initial Y_i^* values can be obtained from the definition of Y_i^* after the end of calibration and after the determination of Y. The mathematical problem in this case is how to estimate this drift, if Y_i^* changes slowly with time, when $P_{(t-i)}$, $G_{(t-i)}$ ($i = 0, 1, 2, \ldots, t$) are known (t being measured in a number of sampling intervals).

In most cases this problem is reduced to the measurement of Y_i^* values for which a function of the type

$$\sum_{i=0}^{t} w_i [P_{(t-i)} - \hat{P}(Y_i^*, g_i)_{(t-i)}]^2 \tag{13}$$

is minimized (w_i denotes coefficients, the value of which depends on the method chosen for estimating the drift of Y_i^*). The most used method is the Kalman filter [9, 17]. Hence, the stochastic approximation method is used because it is simpler and more appropriate for parameter drift tracing than the Kalman filter. The procedure for the correction of Y_i^* can be presented as follows:

$$Y_{i(t)}^* = Y_{i(t-1)}^* + \gamma_{i(t)} [P_{(t-1)} - \sum_{j=1}^{m} Y_{j(t-1)}^* g_{j(t-1)}] g_{i(t-1)} \tag{14}$$

(for $i = 1, 2 \ldots, m$); $\gamma_{i(t)}$ represents a suitable series of numbers which tend to constants with increasing t.

In general, the idea used in Eqn. 14 can be explained as follows: With each step of the algorithm ($t = 1, 2, 3 \ldots$), a definite part of the difference $P - \hat{P}$ is "distributed" between all the Y_i^* values, the contribution to a given i value being directly proportional to the corresponding intensity g_i. It can be

shown that the expression $(P - \Sigma_{j=1}^{m} Y_j^* g_j)g_i$ is proportional to the mathematical expectation for the ith component of the gradient of a function similar to expression 13. Therefore, Eqn. 14 is a recursive version of the method of steepest descent [18] for minimization of functions. Of course, the above method can only be applied to Y_i^* changes which are very slow in comparison with the sampling cycle.

Once Y_i^* has been obtained, it is impossible to calculate Y_{ij} directly and unambiguously. An additional hypothesis about the change in Y_{ij} with Y_i^* is needed. For real mass-spectrometric systems, this hypothesis can be based on a study of the physical reasons for the drift in calibration coefficients. In the general case, an assumption about direct proportionality of the type

$$Y_{ij(t)} = (1 + C_i)Y_{ij(t-1)}$$

is used, whence

$$Y_{i(t)}^* - Y_{i(t-1)}^* = C_i \sum_{j=1}^{n} Y_{ij(t-1)} \tag{15}$$

where C_i is the coefficient to be evaluated. Replacing $Y_{i(t)}^* - Y_{i(t-1)}^*$ by rearrangement of Eqn. 14 yields

$$C_i = [\gamma_i(P_{(t-1)} - \sum_{j=1}^{m} Y_j^* g_j)g_i] / \sum_{j=1}^{n} Y_{ij(t-1)}$$

Then, the final formula for the correction of the calibration coefficients will be

$$Y_{ij(t)} = \{1 + [\gamma_i(P_{(t-1)} - \sum_{j=1}^{m} Y_j^* g_j)g_i / \sum_{j=1}^{n} Y_{ij(t-1)}]\} Y_{ij(t-1)} \tag{16}$$

In matrix form, this becomes

$$\mathbf{Y}_{(t)} = \mathbf{Y}_{(t-1)} + \Delta_{(t)} \tag{17}$$

The elements of Δ can be defined as

$$\Delta_{ij(t)} = C_i(t)Y_{ij(t-1)} \tag{18}$$

The above algorithm can be changed if k from Eqn. 12 is not a constant and has a certain drift; k can be updated in several intervals of the above algorithm by means of

$$k_{(t)} = P_{(t)} / \sum_{j=1}^{n} P_{j(t)}$$

ANALYSIS OF CO, N_2 AND CO_2-CONTAINING MIXTURES IN THE CASE OF LOW RESOLUTION

The spectrum of a mixture of CO, N_2 and CO_2 reported by Chapman [3] is taken as an example. It is assumed that the remaining components of the mixture produce peaks which do not coincide with those of the above gases

or with one another. In fact, CO and CO_2 give peaks not only at *m/z* 12, 14, 28, 44 but also at 16, 22 and 32. In the spectrum there are also peaks related to carbon-13 and oxygen-18, but their inclusion would complicate matters without causing essential changes in the solution to the problem. On the basis of the foregoing, Eqns. 5 can be written as

$$
\begin{aligned}
g_1^i &= a_{11}P_1^i + a_{12}P_2^i \\
g_2^i &= a_{22}P_2^i + a_{23}P_3^i \\
g_3^i &= a_{31}P_1^i + a_{32}P_2^i + a_{33}P_3^i \\
g_4^i &= a_{41}P_1^i \\
&\vdots \\
g_m &= \qquad\qquad\qquad\qquad\qquad\qquad a_{mn}P_n
\end{aligned}
\tag{19}
$$

($i = 1, 2 \ldots l$) where P_1, P_2 and P_3 are the partial pressures of CO_2, CO and N_2, respectively, in the ith calibration mixture; g_1^i, g_2^i, g_3^i and g_4^i denote the *m/z* 12, 14, 28 and 44 peak heights, respectively, for the ith mixture; n is the number of components to be quantified in the mixture and is equal to the number of gases used for the calibration mixture preparation; l is the number of calibration mixtures. For the system to have a solution, $l \geqslant 3$ suffices.

In the above theoretical section, it has been shown that an optimum experimental design developed for the investigation of mixtures can be applied to determination of the composition of the calibration mixtures. Here, a formula is proposed for determination of the composition of calibration mixtures used in the analysis of mixtures containing CO, N_2 and CO_2. This formula may not be the optimum one according to the criteria of optimum experimental design (optimum states of factors D, A, E, etc. [19]), but it appears to represent correctly the basic concepts of mathematical experimental design.

It is assumed that there is preliminary information on the mean value and variance of the partial pressures of the components in the gas mixtures or flows to be analysed. If necessary, preliminary measurements of the composition of a gas flow during the relevant technical process will indicate how these quantities vary during the process. The estimates of the mean and the variance of the partial pressures for the jth component during the rth phase of the process will be denoted by $E^r(P_j)$ and $D^r(P_j)$, respectively.

The equation to be considered is

$$
P_j^i = \sum_r h_{jr}[E^r(P_j) + (-1)^{i+j}\theta(3-i)d_{jr}D^r(P_j)]\,; i = 1, 2, 3 \tag{20}
$$

where $\theta(X) = 0$ when $X \leqslant 0$, and $\theta(X) = 1$ when $X > 0$; $X = 3 - i$; P_j^i is the partial pressures of the jth component of the ith calibration mixture, and h_{jr} and d_{jr} are weighting coefficients ($\Sigma_r h_{jr} = 1$, $d_{jr} \sim 1$—2). Equation 20 was not obtained mathematically but on the basis of general considerations which will now be described.

Experimental designs usually have the form of tables, the factors (here the partial pressures) being presented in coded form: $\underline{1}$ corresponds to the preset upper level of a particular factor, and $\underline{0}$ to the lower level (when linear dependences are involved). The experimental design is represented here as a formula because the number of experiments is small ($l = 3$); by using a formula, application of some of the principles of such experimental designs is shown more clearly.

Selection of levels of factor variation. The purpose is to include, between the upper and lower levels, the prevailing number of values of the factor being investigated without making the difference between the levels too large. By using the weighting coefficients, the points of the design (its spectrum) can be shifted to those stages of the technical (or other) process where very good accuracy is needed. The widespread opinion that the variation range of the factors should include all its possible values obviously cannot be accepted in this case.

Optimum use of the factorial space. In the formula proposed, all factors are varied simultaneously. The element arrangement in **R** (see Eqn. 2). which is not according to atomic weight but in the sequence CO_2, CO, N_2, permits alternative changes of the factor levels in the separate equations of system 19. In Eqn. 20, the condition $\Sigma_{j=1}^{n} P_j = 1$ has been taken into account. However, its strict observance requires additional correction of the coefficients h_{jr} and d_{jr}.

Randomization is not essential because of the small number of points in the design. However, if possible, the calibration mixtures should be introduced into the spectrometer several times, their arrangement in time being random.

The solution of the systems corresponding to Eqns. 5 and Eqn. 2 will not be discussed. It should be noted that for the usual gas mixtures of CO, N_2, CO_2 and Ar, in which nitrogen and argon come from air only, the accuracy of analysis can be improved significantly by adding, to Eqn. 3, the equation $P_{N_2} = \sigma P_{Ar}$, where σ is the ratio between the concentrations of nitrogen and argon in air.

The measurement protocol was found to coincide completely with the general formulation of the problem.

Conclusions

The assumption that the pressures of the calibration and analysed mixtures are measured outside the spectrometer with sufficient accuracy, CPRIS being constant, was used repeatedly in the above descriptions. The results obtained might also be applied to cases when the above assumptions are not valid. In the measurement protocol, this could be done by correcting coefficient k in Eqn. 12 as proposed after Eqn. 18. The errors caused by changes in CPRIS for different mixtures in the calibration protocol can be reduced by using, in the calculations, the concentrations of the mixture components and not their partial pressures. A method for that purpose has been described [2].

The errors in concentration measurements are also not always negligible. Here, such errors were amalgamated with the errors in the peak heights. A more precise discussion is available [20, 21].

REFERENCES

1 G. P. Barnard, Modern Mass Spectrometry, Institute of Physics, London, 1953, pp. 214, 225.
2 J. M. Ruth, Anal. Chem., 40 (1968) 747.
3 I. R. Chapman, Computers in Mass Spectrometry, Academic, London, 1978, p. 220.
4 U.S. Patent, No. 4251269, 1981.
5 I. Seppa and R. Multala, Kem. Teollisuus, 30 (1973) 457.
6 V. V. Nalimov and T. I. Golikova, Logicheskie osnovania planirovanie eksperimenta (in Russian), Metallurgia, Moscow, 1981, pp. 12, 17.
7 C. R. Rao, Lineare Statistische Methoden und ihre Anwendungen, Akademie, Berlin, 1973, pp. 180, 183.
8 R. A. Fisher, The Design of Experiments, Oliver and Boyd, Edinburgh, 1935.
9 P. Eykhoff (Ed.), Trends and Progress in System Identification, Pergamon, Oxford, 1981.
10 J. R. Blum, Ann. Math. Stat., 25 (1954) 737.
11 M. T. Wasan, Stochastic Approximation, Cambridge University Press, Cambridge, 1969.
12 R. K. Mehra, in R. K. Mehra and D. G. Lainiotis (Eds.), System Identification, Advances and Case Studies, Academic, New York, 1976, p. 211, and references therein.
13 I. A. Cornell, Technometrics, 15 (1973) 47.
14 N. R. Draper and W. E. Lawrence, J. R. Stat. Soc., 27 (1965) 450.
15 N. R. Draper and W. E. Lawrence, J. R. Stat. Soc., 27 (1965) 473.
16 P. Thijssen, S. M. Wolfrum, G. Kateman and H. C. Smit, Anal. Chim. Acta, 156 (1984) 87.
17 H. N. J. Poulisse, Anal. Chim. Acta, 112 (1979) 361.
18 G. E. Forsythe, M. A. Malcolm and C. B. Maler, Computer Methods for Mathematical Computations, Prentice Hall, Englewood Cliffs, NJ, 1977, p. 190.
19 D. A. Harville, in I. N. Srivastava (Ed.), Statistical Design and Linear Models, North Holland, New York, 1975.
20 J. Berkson, J. Am. Stat. Assoc., 45 (1950) 164.
21 V. V. Fedorov, Biometrica, 61 (1974) 49.

Analytica Chimica Acta, 201 (1987) 253—262
Elsevier Science Publishers B.V., Amsterdam — Printed in The Netherlands

PRINCIPAL COMPONENTS ANALYSIS FOR THE ESTIMATION OF INTERDEPENDENCES AMONG TRACE METALS IN COW MILK

L. FAVRETTO, G. PERTOLDI MARLETTA, L. GABRIELLI FAVRETTO and D. VOJNOVIĆ

Istituto di Merceologia, Università di Trieste, 34100 Trieste (Italy)

(Received 14th April 1986)

SUMMARY

Seven trace metals (Cr, Mn, Fe, Ni, Cu, Cd, Pb) were determined in the dissolved ash of pasteurized milk by electrothermal atomic absorption spectrometry. The distribution of the concentration (c) of the metals in milk and of $x = \log_{10} c$ for each metal was investigated by means of the Lin-Mudholkar test for normality. Logarithmically transformed variables were first considered for further processing, as their distribution passed the normality test at a 0.05 significance level for a sample size of 48. The correlation matrix around the mean was used as a starting matrix for principal components analysis; the principal components were obtained from the FACTOR program of the SPSS package. Dimensions were reduced to four principal components, accounting for 78% of the total variance. Various orthogonal rotations indicated associations with Cd- Pb, Cr- Ni, and Mn- Cu. The correlation matrix was also estimated from the c matrix after row-normalization for each sample. The first eigenvalue estimated from this matrix accounted for 50% of the total variance, but three eigenvalues were needed to reach 80% of explained variance. Cadmium and lead formed a cluster of variables, indicating a common origin. Features concerned with natural metal contents and contamination during transport and processing are discussed.

Traces of heavy metals in cow milk have been investigated extensively and particularly in milk products intended for nutrition of infants [1, 2]. Trace metals in milk and factors controlling their variability in animal feeds have been discussed [3]. Contaminating elements in mineral supplements were reviewed by Ammermann et al. [4]. The aim of this paper is to consider the concentration of some trace metals (Cr, Mn, Fe, Ni, Cu, Cd, Pb) in whole pasteurized milk from a single origin and to establish any associations existing among these metals, by means of principal component analysis (PCA) [5—8].

Forina et al. [9] applied PCA to the classification of olive oils; Silva [10] classified Italian wines. Discriminant techniques with PCA have been applied for the latter purpose [11, 12]. Favretto et al. [13] applied PCA to cluster variables (minor and trace metals) according to their origin in Parmesan cheese [13]. The method has also been used to study mineral constituents in mussels in relation to pollution levels [14], and to define clusters of variables in relation to source [15].

0003-2670/87/$03.50

EXPERIMENTAL

Apparatus, reagents and samples

A Perkin-Elmer HGA-500 graphite furnace mounted on a Perkin-Elmer 372 atomic absorption spectrometer was used with a Hitachi model 56 recorder and a Perkin-Elmer AS-40 autosampler. Pyrolytically-coated graphite tubes were used with background correction (deuterium lamp). Working standard solutions were prepared by diluting standard solutions for atomic absorption spectrometry (1 mg ml^{-1}) with 0.1 M nitric acid (AristaR, BDH Chemicals). All water used was twice-distilled in pure silica apparatus.

Samples (48) of pasteurized whole milk from Latterie Carsiche (Duino, Trieste) were taken in the period December 1981—October 1984. Each metal was determined independently twice on each milk sample, and the mean values were taken for statistical processing.

Procedures

Sample preparation. The milk sample (10.00 g) was first charred under an i.r. lamp and then ashed at 470°C for 1 h in a platinum dish. The ash was heated with 1.00 ml of 2.0 M nitric acid at 95°C for 5 min and then mixed with 2.00 ml of 0.1 M nitric acid. The solution was filtered through a 5-cm diameter filter paper (Schleicher and Schüll 589[1]) into a 10-ml calibrated flask and the filter was washed with 0.1 M nitric acid up to the mark.

Electrothermal atomic absorption spectrometry (a.a.s.). Table 1 shows the instrumental conditions used. The calibration graphs of $A - A_0$ (i.e., absorbance corrected for reagent blank A_0, both measured as peak height, mm) versus q (mass of metal ion injected, ng) for Cr, Mn, Fe, Ni, Cu, Cd and Pb deviated from linearity. The use of a simple function, $A - A_0 = aq/(1 + bq)$, where $q > 0$, $A - A_0 > 0$, has been recommended for fitting the points of the calibration graph near the origin [16]. When extra-pure analytical reagents are used, $A_0 = 0$ or is just significant for these metals ($A_0 < 2$ mm). Therefore, $A - A_0 = A$ and the function can be written $A = aq/(1 + bq)$. Although the equation is intrinsically linear, a and b were estimated by a Marquardt program [17, 18] for nonlinear least-squares regression, in order to check the adequacy of the fit. The program was started with parameters previously evaluated by linear regression of $1/A$ on $1/q$, using the F ratio from the analysis of variance for the linearized function as an approximate index of adequacy. Linearized calibration lines have been utilized for multiple standard additions [19, 20].

The effect of decreasing sensitivity was considered in detail. Sensitivity is defined here as $dA/dq = a/(1 + bq)^2$; it reaches a maximum at $q = 0$ where $(dA/dq)_{q=0} = a$ and would reach the asymptotic null value for $q \to \infty$ ($A \to a/b$). In order to define a q range of acceptable sensitivity for a given metal, the graph is checked from $q = 0$ (maximum sensitivity) to $q = q_L$ at which the sensitivity is half of the maximum, that is $a/2 = a/(1 + bq_L)^2$,

TABLE 1

Experimental conditions for the atomic absorption spectrometric determinations of metals with electrothermal atomization[a]

Element	Wavelength (nm)	Slit width (nm)	Charring[b]	Atomization[c]
Cr	357.9	0.7	1000°C/20 s/20 s	2500°C/1 s/5 s
Mn[d]	279.5	0.2	1000°C/20 s/30 s	2600°C/1 s/5 s
Fe[d]	248.3	0.2	1000°C/20 s/30 s	2500°C/1 s/5 s
Ni[d]	232.0	0.2	1000°C/20 s/20 s	2600°C/1 s/5 s
Cu	324.7	0.7	900°C/20 s/30 s	2600°C/1 s/5 s
Cd[d]	228.8	0.7	250°C/15 s/20 s	2100°C/1 s/5 s
Pb[d]	283.3	0.7	500°C/15 s/20 s	2100°C/1 s/5 s

[a]For all metals, the drying step was the same: 120°C with 20-s ramp, 30-s hold and a nitrogen flow of 250 ml min^{-1}. Charring and atomization conditions are given as temperature/ramp/hold. [b]200 ml min^{-1} nitrogen. [c]20 ml min^{-1} nitrogen. [d]With background correction.

whence $q_L = (b^2 + 1)^{1/2} - b$. To estimate the adequacy of the fitting function, the test of Lin and Mudholkar [21] for normality was used for analysis of residuals. The test is particularly sensitive to asymmetry of the distribution of residuals and was used in the simple form given by Nelson [22]. The observed Lin-Mudholkar r value (r_{obs}) was computed on an Olivetti M20ST computer with a BASIC program. Table 2 shows the r_{obs} value for the calibration line of each metal; r_{obs} is to be compared with r_{crit}, the critical value indicated by Nelson's table [22] for the given n and for $\alpha = 0.05$ confidence level. The test is passed if $|r_{obs}| < r_{crit}$ (n, $\alpha = 0.05$). Adequacy of the fitting function was also tested by examining the runs of the sign of deviations [23]; applied to the sequence of residuals, this showed that the arrangement of signs was random therefore substantiating the model.

Table 2 summarizes the parameters of the calibration curves. The mass q of a given metal in an injected solution was evaluated from the observed from $q = A/(a - bA)$. The absorbance A was measured within the interval ΔA = 60—80 mm (0.25—0.28 absorbance) by suitable dilution of the sample solutions with 0.1 M nitric acid. The corresponding blank was run in parallel.

Statistical data processing. The descriptive statistics of the concentration, c, (or $x = \log_{10} c$) vector for each metal were evaluated with a standard program on an Olivetti P6040 desk computer. The normality of the monovariate distributions was examined by the Lin-Mudholkar test.

The data matrix consisted of 7 variables (Cr, Mn, Fe, Ni, Cu, Cd, Pb) which were measured on 48 samples. The correlation matrices were examined by means of the FACTOR program of the SPSS [24]. Factors of unrotated and orthogonally rotated matrices were obtained. The program was run on a CDC Cyber 170-730D computer (Computing Centre, University of Trieste).

TABLE 2

Parameters of the calibration lines $A = aq/(1 + bq)$ under the analytical conditions given Table 1[a]

Metal	n	q range (ng)	$a \pm s_a$	$b \pm s_b$	$\lvert\pm s_{res}\rvert$ (mm)	q_L (ng)	Lin-Mudholkar test	
							r_{obs}	r_{crit} (n, α 0.05)
Cr	13	0.1—1.2	196.6 ± 4.7	0.319 ± 0.035	2.21	0.731	—0.259	—0.708
Mn	12	0.05—1.25	255.0 ± 7.7	0.722 ± 0.025	1.21	0.511	—0.163	0.726
Fe	12	0.1—1.5	117.0 ± 2.2	0.307 ± 0.023	1.23	0.739	0.216	0.726
Ni	10	0.2—2.0	40.13 ± 0.66	0.0804 ± 0.0096	0.56	0.922	—0.554	0.767
Cu	17	0.5—1.2	161.6 ± 3.2	0.253 ± 0.028	0.25	0.78	—0.455	0.650
Cd	12	0.01—0.3	1328 ± 44	3.04 ± 0.26	3.53	0.16	0.371	0.726
Pb	11	0.25—4.0	48.3 ± 1.3	0.164 ± 0.018	2.14	0.85	0.540	0.746

[a] n, number of observations; a, b, parameters; s_a, s_b, standard error of parameters; $\lvert\pm s_{res}\rvert$ absolute value of residual standard error; q_L, limiting value of the calibration graph; r_{obs} r_{crit}, observed and critical values of test on residuals. Recorder 10 mV (50 mm - 0.2 absor bance).

RESULTS AND DISCUSSION

Determination of trace metals in milk

The direct utilization of the calibration line is allowed only if there is no uncompensated matrix effect at the wavelength used. Metals quantified at <350 nm exhibited a slight matrix effect in presence of the mineral components of the milk ash solution, but background compensation with the deuterium lamp was effective at the required dilution. Calibration lines of the pure metal did not differ from those obtained by multiple standard additions of metal to the ash solution under the conditions reported in Table 1. These conditions are in accordance with those reported earlier for the analysis of milk.

For lead, Koops and Westerbeek [25] adopted a maximum temperature of 480°C in the charring step for a diluted milk sample, but they observed no appreciable losses up to 500°C with this matrix. The latter charring temperature was adopted (see Table 1), as earlier observations [19] showed no losses when a similar amount of lead was added to a fresh milk sample before ashing at 500°C for 6 h in a platinum dish. Koops and Westerbeek [26] used 350°C as the charring temperature for cadmium in a digested milk sample; a temperature of 250°C was used here because the injected liquid was a solution of an already ashed milk sample. Losses of metal (about 15%) were observed in ashing milk at 480°C for 6 h [20], but under milder conditions the loss decreased, tending to be masked by the instrumental errors. Koops et al. [27] determined nickel in both diluted and digested samples of milk, under the same

conditions as given in Table 1. However, the nickel content found by electrothermal a.a.s. was higher than that obtained by a spectrophotometric method. The difference was attributed to the spectral interference from the calcium phosphate matrix at 232.0 nm. In order to confirm the amount of metal found by electrothermal a.a.s., a solution of ashed milk sample (10.00 ml) was extracted 3 times with ammonium pyrrolidinecarbodithioate in heptan-2-one (3.00 ml) at pH 2.0; both phases were tested by electrothermal a.a.s. The organic extracts were ashed and the ash was dissolved in 10 ml of 0.1 M nitric acid, a corresponding blank was prepared. Testing of this solution gave a nickel recovery of 98% in a sample of milk containing 19 $\mu g\ kg^{-1}$ nickel.

The repeatabilities, estimated from two samples analyzed in parallel and expressed as standard deviation were: Cr 2.1, Mn 1.9, Fe 18, Ni 2.3, Cu 12, Cd 0.44, Pb given as 2.8 $\mu g\ kg^{-1}$ of milk.

Examination of monovariate distributions

The distribution of concentration, c, for each variable in the samples was examined by means of the Lin-Mudholkar test for normality. This test is sensitive to asymmetry of distribution, i.e., to anomalous high values, which sometimes appear in polluted food. The descriptive statistics and the results of the test are summarized in Table 3. The sample distribution of c does not pass the test for normality for all the considered metals except copper. For all the metals, the skewness and r_{obs} indicate positively tailed distributions. The skewness in the distribution decreases for the logarithmically transformed variable $x = \log_{10} c$. The distribution of all metals, except manganese, is then normal (see r_{obs} values, Table 3). A plot of x_i as a function of sample i in a time-ordered sequence shows that x_i oscillates around the sample mean $\bar{x}$ without visual appearance of extended autocorrelated patterns.

Table 3 indicates the modal value c_M calculated from x for the metals passing the test for normality. The c_M values appear to be in the lower ranges of concentrations quoted by Tiscornia [3], Koops and Westerbeek [26] and Muzzarelli et al. [28]. Among trace metals of toxic interest, the c distribution of chromium is in a higher range (5.8—18.2 $\mu g\ kg^{-1}$) than that reported by various authors (e.g., 0.2—3.6 $\mu g\ l^{-1}$ [28] in some commercial Italian milk). The c range for nickel (12.4—39.2 $\mu g\ kg^{-1}$) is also higher than literature values (2—4 $\mu g\ l^{-1}$ [27]).

Principal components of the correlation matrix from the x *data matrix*

Table 4 reports the correlation matrix obtained from logarithmically transformed elements of the data matrix. The correlation matrix was used as a starting matrix in PCA. Eigenvalues and the unrotated factor matrix are shown in Table 4. The number of principal components was first defined by the ordinary rule of choosing >1 eigenvalues only. However, under this condition, three principal components were extracted, which accounted for only 66% of the total variance. When a further nearest-to-one eigenvalue was con-

TABLE 3

Descriptive statistics and results of the test for normality of the frequency distribution of c ($\mu g\ kg^{-1}$) or of $x = \log_{10} c$ of some trace metals in milk[a]

Metal	c distribution			x distribution			
	c range	a	r_{obs}	a	r_{obs}	$\bar{x} \pm s$	$c_M = 10^{\bar{x}}$
Cr	5.80—18.2	1.183	0.693	0.396	0.327	1.02 ± 0.16	0.5
Mn	15.9—31.7	0.778	0.643	0.488	0.453	—	—
Fe	128—564	1.018	0.656	0.370	0.309	2.37 ± 0.02	234
Ni	12.4—39.2	1.265	0.671	0.477	0.413	1.32 ± 0.13	20.9
Cu	71.0—160	0.573	0.407	0.018	0.034	2.019 ± 0.106	104
Cd	0.508—3.85	0.482	0.472	−0.122	−0.149	0.204 ± 0.257	1.60
Pb	11.2—39.7	1.081	0.699	0.475	0.405	1.340 ± 0.153	21.9

[a] a, skewness. r_{obs}, observed value in the Lin-Mudholkar test for normality; if $|r_{obs}| > r_{crit}$ (n = 48, α = 0.05) = 0.443, the sample distribution does not pass the test (underlined values). $\bar{x} \pm s$, mean and standard error (n = 48 observations). c_M, modal value of c.

TABLE 4

Correlation matrix between trace metals ($x = \log_{10} c$ with c expressed in $\mu g\ kg^{-1}$) in whole milk

	Cr	Mn	Fe	Ni	Cu	Cd	Pb
Cr	1.	0.287	0.075	0.296	−0.134	0.131	0.021
Mn		1.	0.249	0.057	0.442	−0.229	−0.201
Fe			1.	−0.033	0.198	−0.041	−0.033
Ni				1.	−0.102	0.161	−0.062
Cu					1.	−0.103	−0.053
Cd						1.	0.517
Pb							1.

sidered, the four principal components accounted for about 78% of the total variance (Table 5). The communality (proportion of variance of a variable involved in a 4-dimensional factor space) was >0.7, except for nickel (h^2 = 0.63). In this space of orthogonal vectors, Mn is positively associated and Cd and Pb are negatively associated with the first principal component (PC 1); Cr and Ni are positively associated with PC 2; Cu is positively associated with PC 3; Fe is negatively associated with PC 4.

Table 6 summarizes the values of factors after a VARIMAX rotation (other available orthogonal rotations essentially produced similar results). The factors shown indicate that PC 1 is positively associated with both Cd and Pb, PC 2 with Cr and Ni and PC 3 with Mn and Cu but PC 4 with Fe only. The degree of association, expressed by the factors, varies from 0.75 (Mn) to 0.94 (Fe). On axis 1, the toxic metals Cd and Pb form a definite cluster, which indicates a possible common origin. On the axis 2, Cr and Ni are apparently associated, but not with the other metals. However, no

TABLE 5

Eigenvalues and variance (V%) accounted for by the principal components, and communality (h^2)

Eigenvalues	1.867	1.481	1.260	0.837	
V (%)	26.7	21.2	18.0	12.0	
Variables	Principal components				h^2
	PC 1	PC 2	PC 3	PC 4	
Cr	0.041	0.792	−0.255	−0.120	0.708
Mn	0.738	0.420	0.140	0.197	0.779
Fe	0.408	0.258	0.399	−0.721	0.911
Ni	−0.100	0.627	−0.425	0.219	0.632
Cu	0.589	0.026	0.559	0.454	0.866
Cd	−0.657	0.419	0.400	0.091	0.775
Pb	−0.605	0.206	0.603	0.054	0.776

TABLE 6

VARIMAX rotated factor matrix

Metals	PC 1	PC 2	PC 3	PC 4
Cr	0.058	0.809	0.012	0.229
Mn	−0.244	0.317	0.751	0.232
Fe	−0.010	−0.006	0.138	0.945
Ni	0.025	0.766	−0.020	−0.211
Cu	0.025	−0.208	0.907	0.019
Cd	0.852	0.190	−0.102	−0.044
Pb	0.876	−0.094	−0.035	0.023

significative correlation appears in the correlation matrix. The presence of nickel in milk was already observed [3] and was attributed to metal release from industrial equipment. Within the European Community, milk is transported and processed in various stainless-steel materials. Corrosion of such materials by washing and disinfectant solutions has been reported [29]. Treatment with diluted nitric acid is common for removal of milk deposits from heated surfaces during pasteurization, UHT treatments, etc. [30]. The release of nickel from stainless steel by 0.16 M nitric acid has been reported [27]. The high levels of nickel can be explained by metal release during milk transport and processing. The absence of association of iron with nickel can be explained by the fact that iron is a normal macro-constituent of the milk ash. The most probable concentration of iron in the milk under examination is given by the modal value c_M = 234 μg kg^{-1} (Table 3).

Principal components of correlation matrix from row-normalized data

To confirm the associations of trace metals observed with logarithmically transformed data, the c data were also considered. The rows of c to unit length in the data matrix were first normalized, to compensate for the differences in the mean values of c. The resulting correlation matrix is reported in Table 7. Some previously indicated correlations are confirmed and enhanced (Cd—Pb, Cr—Mn) but the picture is substantially changed. This also appears from Table 8 which shows eigenvalues and the unrotated factor matrix. Although the first eigenvalue explains nearly 50% of the total variance, a cumulative explanation of variance near 80% is obtained only by considering three principal components. Comparison with the factor matrix of Table 5 shows that principal components can be reduced to three only.

In the unrotated factor matrix, Cd and Pb are positively and strongly associated with PC 1, whereas Cr, Mn and Cu are only slightly associated with PC 1; iron shows a mildly positive association with PC 2 and nickel is

TABLE 7

Correlation matrix between trace metals in whole milk (row-normalized c)

	Cr	Mn	Fe	Ni	Cu	Cd	Pb
Cr	1.	0.582	−0.168	0.218	0.192	0.516	0.460
Mn		1.	−0.123	0.262	0.342	0.555	0.488
Fe			1.	−0.560	−0.615	−0.546	−0.377
Ni				1.	0.344	0.352	0.362
Cu					1.	0.569	0.494
Cd						1.	0.705
Pb							1.

TABLE 8

Eigenvalues and variance (V%) accounted for by principal components, and communality (h^2)

Eigenvalues	3.417	1.295	0.853	
V (%)	48.8	18.5	12.2	
Variables	Principal components			h^2
	PC 1	PC 2	PC 3	
Cr	0.653	0.424	0.401	0.766
Mn	0.704	0.388	0.345	0.764
Fe	−0.598	0.646	0.136	0.794
Ni	0.414	0.494	−0.731	0.950
Cu	0.620	−0.546	0.047	0.777
Cd	0.900	−0.045	−0.059	0.815
Pb	0.825	0.610	0.121	0.699

negatively associated with PC 3 only. The picture of the associations obtained after an orthogonal rotation is shown in Table 9 and Fig. 1; PC 2 is now associated with the cluster Cr—Mn, whereas PC 1 is positively associated with Cu and Cd but negatively with iron; nickel is positively associated with PC 3. The association between Cd and Pb, which is clear from the factors of the unrotated factor matrix, becomes weaker after an orthogonal rotation. By definition, variables lying on orthogonal axes are uncorrelated. Different physical origins can perhaps be suggested as an explanation of the observed associations. The strong association of nickel on an axis orthogonal to that of Cr—Mn—Fe tentatively suggests that nickel comes from an external source.

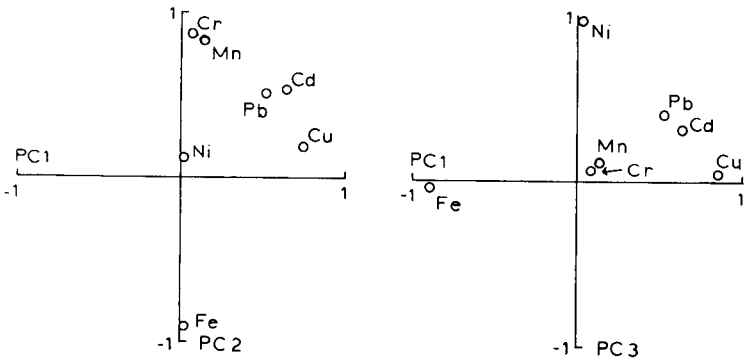

Fig. 1. Projections on principal components (PC) of the factors and associations between trace metals (row-normalized c) after a VARIMAX transformation.

TABLE 9

VARIMAX rotated factor matrix

Metals	Principal components		
	PC 1	PC 2	PC 3
Cr	0.076	0.869	0.072
Mn	0.143	0.853	0.120
Fe	−0.891	0.008	−0.028
Ni	0.002	0.133	0.965
Cu	0.856	0.203	0.049
Cd	0.641	0.543	0.331
Pb	0.521	0.515	0.404

The authors are grateful to Professor Sharon Neol, Chemistry Dept., University of Indiana, Bloomington, IN 47401, U.S.A., for help in the review of the paper.

This paper was presented at the Third International Conference on Chemometries in Analytical Chemistry, Lerici, Italy, May 25—30, 1986.

REFERENCES

1 E. J. Underwood, Trace Elements in Human and Animal Nutrition, 3rd edn. Academic Press, New York, 1971.
2 F. Amore, M. Bergomi, P. Borella, G. Fantuzzi, G. Vivoli, P. Lauriola and C. A. Goldoni, Latte, 8 (1983) 528.
3 E. Tiscornia, Riv. Soc. Ital. Sci. Alim., 6 (1977) 423.
4 C. B. Ammerman, S. M. Miller, K. R. Fick and S. L. Hansard II, J. Anim. Sci., 44 (1977) 485.
5 T. W. Anderson, An Introduction to Multivariate Statistical Analysis, Wiley, New York, 1958.
6 R. Gnanadesikan, Methods for Statistical Data Analysis of Multivariate Observations, Wiley, New York, 1977.
7 E. R. Malinowski and D. G. Howery, Factor Analysis in Chemistry, Wiley, New York, 1980.
8 M. Kendall, A. Stuart and K. J. Ord, The Advanced Theory of Statistics, 4th edn., Vol. 3, Griffin, London, 1983.
9 M. Forina, C. Armanino, S. Lanteri, C. Calcagno and E. Tiscornia, Riv. Ital. Sost. Grasse, 60 (1983) 607.
10 A. Silva, Ind. Bevande., 9 (1980) 55.
11 G. Scarponi, I. Moret, G. Capodaglio and P. Cescon, J. Agric. Food Chem., 30 (1982) 1135.
12 M. Baldi, V. Riganti and M. Specchiarello, Ind. Bevande, 13 (1984) 1.
13 L. Favretto, C. Calzolari and L. Gabrielli Favretto, Proc. 3rd Eur. Conf. Food Chem., Antwerp, March 1985, Vol. I, 1166.
14 J. D. Popham and J. M. D'Auria, Environ. Sci. Technol., 17 (1983) 576.
15 L. Favretto and L. Gabrielli Favretto, Z. Lebensm. Unters. Forsch., 179 (1984) 201, 377.
16 L. Favretto, G. Pertoldi Marletta and L. Gabrielli Favretto, Mikrochim. Acta, Part II, (1981) 387.
17 D. W. Marquardt, J. Soc. Ind. Appl. Math., 2 (1963) 431.
18 Y. Bard, Nonlinear Parameter Estimation, Academic Press, New York, 1974.
19 G. Pertoldi Marletta, L. Gabrielli Favretto and C. Calzolari, in W. Baltes, P. B. Czedik-Eysenberg, W. Pfannhauser (Eds.), Proc. Euro Food Chem. 1 on Recent Developments in Food Analysis (Vienna, Austria, 17—20 February 1981), Verlag Chemie, Basel, 1982, p. 377.
20 G. Pertoldi Marletta and L. Gabrielli Favretto, Z. Lebensm. Unters. Forsch., 176 (1983) 32; in Proc. Euro Food Chem. II (Rome, March 1983), SCI, Rome, 1983, p. 305; Riv. Soc. Ital. Sci. Alim. 13 (1984) 237.
21 C. C. Lin and G. S. Mudholkar, Biometrika, 67 (1980) 455.
22 L. S. Nelson, J. Qual. Technol., 13 (1981) 76.
23 N. R. Draper and H. Smith, Applied Regression Analysis, Wiley, New York, 1966, p. 85.
24 H. H. Nie, C. H. Hull, J. G. Jenkins, K. Steinbrenner and D. H. Bent, Statistical Package for Social Sciences, 2nd edn. McGraw-Hill, New York, 1970, p. 468.
25 J. Koops and D. Westerbeek, Neth. Milk Dairy J., 34 (1980) 31.
26 J. Koops and D. Westerbeek, Neth. Milk Dairy J., 32 (1978) 149.
27 J. Koops, H. Klomp and D. Westerbeek, Netherl. Milk Dairy J., 36 (1982) 333.
28 R. A. D. Muzzarelli, C. E. Eugeni, F. Tanfani, G. Caramia and D. Pezzola, Milchwissenschaft, 38 (1983) 453.
29 L. Kerherve, G. Daufin and F. Michel, Lait, 63 (1983) 129; Ind. Aliment. Agric., 101 (1984) 779.
30 K. R. Swartzel, J. Food Sci., 48 (1983) 1507.

Analytica Chimica Acta, 201 (1987) 263—268
Elsevier Science Publishers B.V., Amsterdam — Printed in The Netherlands

Short Communication

AUTOMATED DETERMINATION OF TOTAL ARSENIC IN SEA WATER BY FLOW CONSTANT-CURRENT STRIPPING ANALYSIS WITH GOLD FIBRE ELECTRODES

CHI HUA, DANIEL JAGNER* and LARS RENMAN

Department of Technical Analytical Chemistry, Chemical Center, University of Lund, P.O. Box 124, S-221 00 Lund (Sweden)

(Received 5th November 1986)

Summary. Total arsenic in sea water is determined in a fully automated flow system, by means of potentiostatic deposition for 4 min at a 25-μm gold fibre electrode and subsequent constant-current stripping in 5 M hydrochloric acid. Previously the sample is acidified with hydrochloric and arsenic(V) is reduced to arsenic(III) with iodide. During stripping, the potential vs. time transient is recorded with a real-time measurement rate of 26.5 kHz and a potential resolution of 1 mV. Cleaning and regeneration of the gold electrode are fully automated. The total arsenic concentrations in two reference sea waters (NASS-1 and CASS-1) were evaluated by single-point standard addition and found to be 1.58 and 1.14 $\mu g\ l^{-1}$ with standard deviations of 0.39 and 0.28 $\mu g\ l^{-1}$, respectively; certified values are 1.65 ± 0.19 and 1.04 ± 0.07 $\mu g\ l^{-1}$. The arsenic(III) content in these samples was below the detection limit (0.15 $\mu g\ l^{-1}$).

Arsenic in the low $\mu g\ l^{-1}$ concentration range is normally determined by hydride-generation atomic absorption spectrometry or by neutron activation analysis. Both these techniques are somewhat elaborate and not well suited to automated determinations or to field work. For this reason, several attempts have been made to determine arsenic electrochemically by means of various stripping techniques [1—4]. Various problems are, however, encountered, the main one being that arsenic is normally in the non-electroactive arsenic(V) state and must be reduced to arsenic(III). In batch analysis, the reducing agent often gives rise to overlapping stripping peaks when the arsenic which has been reduced onto the working electrode is reoxidized in the stripping phase. Another problem is that gold is the only electrode material which can be used for low arsenic(III) concentrations and the surface of the electrode is readily poisoned by elemental arsenic. In order to obtain reproducible readings between consecutive electrolysis/stripping cycles, extensive and frequent cleaning of the electrode surface is therefore necessary. A third problem is that copper present in the sample interferes with the arsenic stripping peak.

In this communication, an automated method for the determination of arsenic in sea water is described. The method is based on computerized flow potentiometric and constant-current stripping analysis [5], the flow approach

0003-2670/87/$03.50

making it possible to pre-condition the electrode in one solution and clean it in another between consecutive runs. Moreover, stripping can be done in a medium containing no reducing agents and where the arsenic stripping peak is well separated from that of copper.

Experimental

Instrumentation and electrodes. A computerized flow potentiometric and constant-current stripping analyzer described elsewhere [6] was used. In this analyzer, six different solutions can be sucked into the flow cell by a peristaltic pump, the flow rate, the inlet magnetic valves, the electrolysis potential and the constant-current generation all being under computer control.

A saturated calomel electrode and a platinum tube were used as reference and counter electrodes, respectively. A gold fibre with a diameter of 25 μm (Goodfellow, Cambridge, Gt. Britain), inserted in a polyvinyl tube as shown in Fig. 1, was used as working electrode (cf. [7]). All potentials given below are vs. SCE.

Reagents. All reagents were of analytical grade. Stock solutions of arsenic(V) were prepared by diluting standard solutions (Titrisol, Merck) with Millipore-Q water. Sea-water reference samples from Southeast Bermuda (NASS-1) and off Halifax harbour (CASS-1) were purchased from the National Research Council of Canada.

Procedure for the determination of arsenic in sea water. A portion (10 ml) of concentrated hydrochloric acid containing 0.02 M potassium iodide is added to 10 ml of the sea-water sample, and 10 ml of concentrated hydrochloric acid containing 0.02 M potassium iodide and 6.0 μg l^{-1} arsenic(V) is added to another 10 ml of the sample. The samples are placed in two inlets of the analyzer. The other inlets contain an electrode pre-treatment solution consisting of 50 mg l^{-1} gold(III) in 1 M hydrochloric acid, an electrochemical cleaning solution consisting of 6 M nitric acid and 2 M sulfuric acid, a

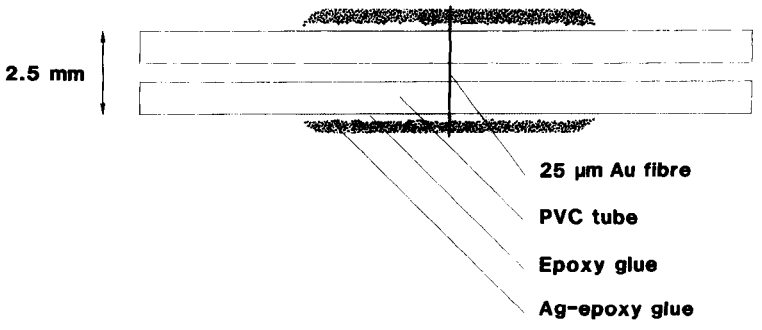

Fig. 1. Schematic drawing of the gold fibre flow electrode.

cleaning solution of 99% (v/v) ethanol, and a stripping solution containing 5 M hydrochloric acid.

In the initial step, the electrode pre-treatment solution is allowed into the cell at a flow rate of 0.7 ml min^{-1} and a potential of —0.1 V is applied for 1 s, after which the potential is increased to 0.10 V for 20 s and to 0.40 V for 1 s. Finally, a potential of 0.10 V is applied for 30 s, after which the unspiked sample is allowed into the cell for 4 min at a flow rate of 1 ml min^{-1} and a potential of —0.30 V. The stripping solution is then allowed into the cell for 30 s at a flow rate of 2.2 ml min^{-1} and a potential of —0.05 V. One second before stripping, the potential is decreased to —0.40 V, an oxidizing current of 2.5 μA is applied, and the stripping curve is recorded in the potential range from —0.20 to 0.50 V with a real-time sampling rate of 25.6 kHz and a potential resolution of 1 mV. After 1 s at this potential, a potential of —0.05 V is applied for 20 s and then —0.40 V for 1 s and the background is recorded. Finally, the electrode is washed with the ethanol solution for 10 s at —0.05 V, with the electrochemical cleaning solution for 10 s at 2.0 V, and with 5 M hydrochloric acid for 2 s at + 0.90 V. The same cycle is then repeated with the spiked sample.

After derivation, subtraction of the background and digital filtration, the program locates the arsenic stripping peak, searching the region from 0.15 to 0.25 V, and integrates the peak in the region ±0.080 V around the maximum. Finally, the program calculates the concentration of arsenic in the sample, using the normal equations for standard addition. The stripping curves are displayed on the strip-chart recorder and printer/plotter using an averaging filter of 30 mV and a Savitsky-Golay filter of 15 mV.

Results and discussion

Sample composition and reducing agent. The dominant oxidation state of arsenic in sea water is arsenic(V). Consequently, in order to determine the total concentration of arsenic, arsenic(V) must be reduced to arsenic(III). Although this reduction is possible in various media, hydrochloric acid would seem to be the only such medium which can be obtained commercially in acceptable purity. The arsenic concentration in analytical-grade hydrochloric acid is negligible as are the concentrations of metal ions which can interfere with the arsenic stripping peak.

Iodide is the most suitable reducing agent in hydrochloric acid. By varying the hydrochloric acid concentration in the range 0.1—10 M and the iodide concentration in the range 0.001—0.50 M, it was found that ca. 6 M hydrochloric acid and 0.01M idoide gave optimum results with respect to efficient reduction and minimum sample dilution.

Composition of stripping solution. The stripping solution must provide a medium in which elemental arsenic deposited on the working electrode can be re-oxidized reversibly, and stripping-peak overlap from other elements (e.g., copper) is avoided. As copper is oxidized to copper(I) in media with high chloride concentrations, it is possible to separate the stripping peaks of

arsenic and copper. By varying the hydrochloric acid concentration in the range 0.1—10 M, it was found that neither the shape nor the potential of the arsenic stripping peak altered significantly on increasing the concentration of acid from 3 to 10 M. A stripping solution of 5 M hydrochloric acid was thus regarded as being optimal.

Stripping mode. Elemental arsenic deposited onto the gold fibre electrode can be reoxidized in the stripping medium, either chemically or by means of constant current. In both modes, the potential vs. time transient is recorded during stripping and exactly the same computer program is used to process the data. In order to oxidize arsenic chemically, a rather strong oxidant is required. Manganese(VII) and chromium(VI) are not stable on storage in hydrochloric acid owing to the formation of chlorine. The only strong oxidant found to be compatible with the 5 M hydrochloric acid medium was gold(III). It was shown that the stripping rate increased linearly with the gold(III) concentration in the concentration range investigated, viz. 5—500 mg l^{-1}. A gold(III) concentration of 100 mg l^{-1} was found to be optimal with respect to reproducibility and detection limit.

The chemical and constant-current methods of stripping were compared by means of consecutive electrolysis/stripping cycles in unspiked reference sea water NASS-1. The procedure described above was used with the exception that during chemical re-oxidation the constant-current generator was not activated. No significant differences were found with respect to reproducibility, the relative standard deviation for ten consecutive electrolysis/stripping cycles in the same sample being 8—10% for both stripping modes.

Interferences. The commonest interferents in the determination of arsenic with a gold working electrode are mercury(II) and copper(I). In the 5 M hydrochloric acid used as stripping medium, mercury is stripped at a potential almost 0.35 V positive to that of the arsenic peak at + 0.16 V, with which it does not interfere. In the high chloride concentration, copper yields a very broad and unsymmetrical stripping peak commencing at approximately —0.1 V. This is illustrated in Fig. 2(a) where a solution containing 6 M hydrochloric acid, 0.01 M potassium iodide and 50 $\mu g\ l^{-1}$ copper(II) was analyzed as described above, with the exceptions that the sample electrolysis time was 90 s and that the potential was held at —0.30 V in the stripping medium. The corresponding stripping curve if the potential is increased to —0.07 V for 40 s prior to stripping is shown in Fig. 2(b). Obviously, copper is completely re-oxidized at this potential and separate experiments showed that no arsenic is lost.

Linear range. The linear range was investigated by analyzing sea water reference NASS-1, spiked with 1—10 $\mu g\ l^{-1}$ arsenic(V), by the procedure described above. A linear relationship between peak area and sample concentration was obtained up to 5 $\mu g\ l^{-1}$, after which the peak area increased less rapidly than the concentration. This rather limited linear range implies that elemental arsenic is not dissolved in the gold electrode but deposited on the surface. The low conductivity of elemental arsenic makes this depos-

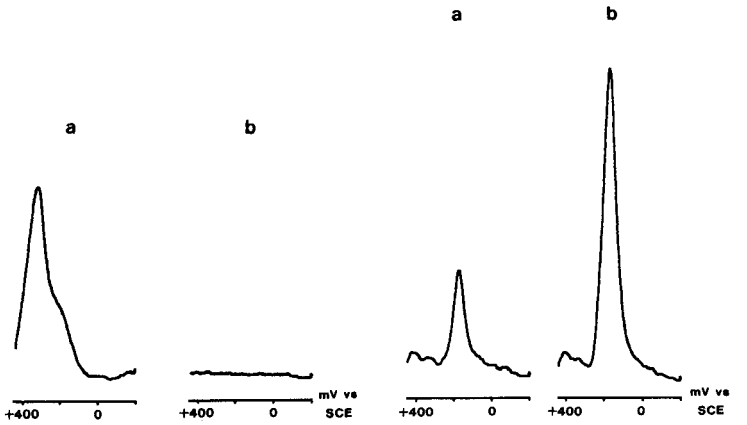

Fig. 2. Copper interference. Electrolysis for 90 s at −0.30 V vs. SCE in a solution containing 6 M hydrochloric acid, 0.01 M potassium iodide and 50 $\mu g\ l^{-1}$ copper(II), and subsequent stripping in 5 M hydrochloric acid: (a) at a potential of −0.30 V vs. SCE in the stripping medium, and (b) after increasing the potential to −0.07 V vs. SCE for 40 s prior to stripping.

Fig. 3. Stripping curves obtained in sea water reference sample NASS-1 before (a) and after (b) the standard addition of 3 $\mu g\ l^{-1}$ arsenic(V).

ition less effective with increasing surface coverage. The limited linear range also indicates that if concentrations of arsenic higher than those in sea water are to be determined, the electrolysis time must be decreased accordingly, and that spiked samples should be electrolyzed for shorter periods of time than unspiked samples.

Arsenic(III) and total arsenic in sea water. In order to investigate if the NASS-1 and CASS-1 standards contained arsenic(III), these samples were analyzed as in the procedure above except that no iodide was added to the samples. No arsenic stripping signals could be detected, which suggests that the arsenic(III) concentrations in the two samples were below the estimated detection level of the technique, i.e., 0.15 $\mu g\ l^{-1}$.

The stripping curve obtained on the strip-chart recorder in the analysis of the NASS-1 standard is shown in Fig. 3(a) and the corresponding curve after the addition of 3 $\mu g\ l^{-1}$ arsenic(V) in Fig. 3(b). Analysis of eight different subsamples of NASS-1 and CASS-1 yielded average values for total arsenic equal to 1.58 and 1.14 $\mu g\ l^{-1}$ with standard deviations of 0.39 and 0.28 $\mu g\ l^{-1}$, respectively; the certified values are 1.65 ± 0.19 and 1.04 ± 0.07 $\mu g\ l^{-1}$. Clearly, the results agree well with the reference values. The rather high values for the standard deviations can be decreased by including more experimental points in the standard addition evaluation. This will, of course, increase the time required for analysis proportionally.

This work was supported by the Swedish Natural Science Research Council and by the Carl Trygger Research Foundation.

REFERENCES

1 F. G. Bodewig, P. Valenta and H. W. Nürnberg, Fresenius' Z. Anal. Chem., 311 (1982) 187.
2 J. W. Hamilton, J. Ellis and T. M. Florence, Anal. Chim. Acta, 119 (1980) 225.
3 G. Forsberg, J. W. O'Laughlin, R. G. Megargle and S. R. Koirtyohann, Anal. Chem., 47 (1975) 1586.
4 P. H. Davies, G. R. Dulude, R. M. Griffin, W. R. Matson and E. W. Zink, Anal. Chem., 50 (1978) 137.
5 D. Jagner, M. Josefson and S. Westerlund, Anal. Chem., 53 (1981) 2144.
6 L. Renman, D. Jagner and R. Berglund, Anal. Chim. Acta, 188 (1986) 137.
7 H. Huiliang, C. Hua, D. Jagner and L. Renman, Anal. Chim. Acta, 193 (1987) 61.

Analytica Chimica Acta, 201 (1987) 269—273
Elsevier Science Publishers B.V., Amsterdam — Printed in The Netherlands

Short Communication

DETERMINATION OF MERCURY IN AIR BY MEANS OF COMPUTERIZED FLOW CONSTANT-CURRENT STRIPPING ANALYSIS WITH A GOLD FIBRE ELECTRODE

HUANG HUILIANG[a], DANIEL JAGNER* and LARS RENMAN

Department of Technical Analytical Chemistry, Chemical Center, University of Lund, P.O. Box 124, S-221 00 Lund (Sweden)

(Received 6th April 1987)

Summary. Mercury in air was determined after collection in potassium permanganate or sodium carbonate solution. The mercury concentration in these solutions was determined in a computerized flow potentiometric stripping analyzer with a 10-μm gold fibre working electrode, a glassy carbon reference electrode and a platinum counter electrode. After sample electrolysis for 1—10 min, stripping was done in a 1 mg l^{-1} gold(III) solution in 0.01 M nitric acid/0.01 M sodium nitrate with a constant stripping current of 0.50 μA. Results obtained for flue gas samples were in good agreement with results from cold-vapor atomic absorption spectrometry.

Mercury in air is normally determined spectrometrically after collection either in a permanganate trap or on gold pellets. These two enrichment procedures obviously yield different results, the permanganate trap giving total mercury and the gold trap only mercury in elemental form. An alternative way of determining total mercury is by electrochemical methods after permanganate trapping. Because the concentrations involved are usually very low, only electrochemical stripping techniques can be exploited for mercury determinations. Several procedures based on anodic stripping voltammetry, usually with gold disc or gold rod electrodes, have been proposed [1—8]. A problem frequently encountered when gold disc electrodes are used is the high background caused by the continuous oxidation of copper impurities in the gold matrix. Moreover, at very long potentiostatic deposition times, mercury atoms diffuse into the gold electrode so that the re-oxidation must be done very slowly in order to oxidize all the mercury.

Gold fibres in a flow cell arrangement have been proposed as sensor electrodes for the determination of mercury [9]. Such electrodes have better diffusional characteristics than gold disc electrodes and their small dimension (10 μm diameter) simplifies their purification from copper impurities either chemically or electrochemically. The small fibre dimension means also that

[a]Permanent address: Scientific Instrumentation Department, Xiamen (Amoy) University, Fujian Province, China.

0003-2670/87/$03.50

the maximum diffusion distance in the electrode is very small so that re-oxidation can be achieved rapidly. For this reason, one is not limited to slow potential-ramp differential-pulse stripping and faster techniques such as potentiometric or constant-current stripping [10] can be exploited; the latter techniques often offer improved reproducibility and reliability.

This communication describes a method for the determination of total mercury in air by constant-current stripping potentiometry. In order to test the usefulness of this technique, it was also applied in the analysis of carbonate and permanganate traps used in the determination of water-soluble and metallic mercury in flue gases.

Experimental

Instrumentation. The computerized flow potentiometric and constant-current stripping analyzer used has been described in detail [10].

Flow electrodes. The 10-μm diameter gold fibre electrode was mounted perpendicular to the flow direction of a Viton tube (inner diameter 0.8 mm). A 1-mm diameter glassy carbon rod inserted perpendicularly to the flow direction in a PVC tube (2-mm inner diameter) and mounted downstream from the working electrode was used as reference electrode (GCE). A 5-mm long platinum tube (inner diameter 0.7 mm) mounted downstream from the reference electrode served as the counter electrode.

Sampling equipment. In laboratory tests, air samples were collected in glass impinger bottles. To check for sample breakthrough, up to three impingers could be connected in series through ground-glass fittings. Air was drawn through the impingers at rates of 0.5—2.1 min^{-1} with constant-flow personal sampling pumps (Airchek VI; SKC., Eighty Four, PA 15330).

Reagents. All chemicals were of analytical-reagent grade except the mineral acids which were of Suprapur grade. Potassium permanganate with low mercury content (Merck) was used throughout.

The mercury-trapping solution for laboratory tests contained 50 mg of potassium permanganate in 1 l of 0.50 M nitric acid. The gold-plating solution was 100 mg gold(III) chloride in 1 l of 0.10 M hydrochloric acid. The electrode rinsing solution was 0.10 M hydrochloric acid in 50% (v/v) ethanol. The stripping solution contained 1 mg of gold(III) chloride in 1 l of 0.01 M nitric acid/0.01 M sodium nitrate.

Constant-current stripping procedure. The procedure consisted of four steps: plating of a fresh gold film onto the gold fibre surface, electrolysis in the permanganate trap solution (and in the next run the mercury(II)-spiked trap solution), constant-current stripping in the stripping solution, and finally rinsing of the electrodes. The flow rate was 1 ml min^{-1} throughout. Gold plating was done in the plating solution for 20 s at a potential of —0.50 V. The potential was then increased to 0.20 V for 2 s in order to re-oxidize traces of mercury in the plating solution. Electrolysis was then done in the sample solution at —0.50 V for 1—10 min depending on the mercury concentration. A constant current of 0.50 μA was then applied and the

potential vs. time transient was recorded in the potential range —0.50 to 0.20 V. Finally, the rinsing solution was sucked through the cell for 10 s at a potential of —0.20 V. The same cycle was repeated on the mercury(II)-spiked sample.

Sampling procedure for mercury in air. The serially coupled impinger flasks were each filled with 10 ml of mercury-trapping solution and air was sucked through the flasks at a controlled rate of 0.5—2 l min^{-1} for 1—60 min, depending on the mercury concentration expected in the air sample. The contents of the flasks were transferred to a 50-ml volumetric flask and the two impingers were cleaned with the mercury-trapping solution to yield a final volume of 50 ml. From that, two 15-ml samples were taken and one was spiked with an appropriate amount of mercury(II).

Flue gas samples. Mercury samples collected from flue gases were obtained from Miljökonsulterna, Studsvik, Sweden. In all cases, these samples had been collected with three samplers in series. The first of these contained either 10% (w/v) sodium carbonate or 10% (w/v) sodium carbonate in saturated sodium chloride. The second and third bottles in all cases contained 10% (w/v) potassium permanganate and diluted (1 + 9) sulphuric acid. Before injection, samples containing sodium carbonate were acidified with hydrochloric acid. Samples with high mercury concentration were also diluted with hydrochloric acid.

Results and discussion

Accuracy and reproducibility of the constant-current stripping procedure. In order to test the reproducibility of the stripping procedure, the mercury trap solution was spiked with 2 $\mu g\ l^{-1}$ mercury and processed twenty times as described above with an electrolysis time of 2 min. Figure 1 shows the dif-

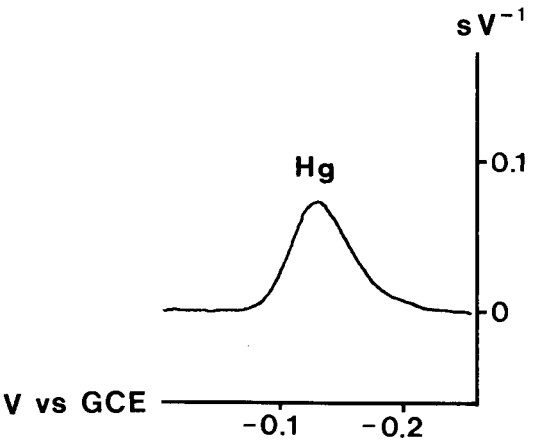

Fig. 1. Differentiated background-corrected constant-current stripping curve for mercury. Electrolysis at —0.50 V vs. glassy carbon reference electrode (GCE) for 1 min in a 2.1 $\mu g\ l^{-1}$ solution prior to stripping in 1 mg l^{-1} Au(III) in 0.01 M nitric acid/0.01 M sodium nitrate with a constant current of 0.50 μA.

ferentiated stripping curve (dt/dE vs. E) obtained from one of these runs. The twenty runs yielded a relative standard deviation of 1.7%. The accuracy of the stripping procedure was tested by processing portions of permanganate trap solutions spiked with 2 or 5 $\mu g\ l^{-1}$ mercury and with a 10 $\mu g\ l^{-1}$ standard addition. The samples were processed ten times at each concentration level with an electrolysis time of 2 min. In the trap solutions containing 2 or 5 $\mu g\ l^{-1}$ of mercury(II), the results obtained were 2.1 or 5.3 $\mu g\ l^{-1}$ with standard deviations of 0.08 and 0.61 $\mu g\ l^{-1}$, respectively. No mercury was detected in the unspiked trap solution and it was concluded that the blank value was below the estimated detection limit of 0.1 $\mu g\ l^{-1}$ mercury(II). This was confirmed by increasing the electrolysis time to 10 min, whereby a mercury concentration of 0.1 $\mu g\ l^{-1}$ with a standard deviation of 0.02 $\mu g\ l^{-1}$ was obtained.

Efficiency of the mercury trapping procedure. Trapping of mercury in permanganate solutions is very well established. In order to test the efficiency of the particular design used, three serial impingers containing the laboratory-test trapping solution were used and an outdoor air sample was drawn through an empty impinger flask (40-ml capacity) containing about 0.1 ml of mercury. The contents of the three impingers were processed separately. Even after two hours of sampling at a flow rate of 0.5 $l\ min^{-1}$, no mercury could be detected in the third permanganate trap. From the mercury concentrations in the two first traps, the mean value for mercury in air was 30 $\mu g\ m^{-3}$, which is close to the Swedish threshold limiting value of 50 $\mu g\ m^{-3}$.

Determination of mercury in flue gas samples. The mercury(II) concentrations in flue gas samples were determined by the proposed procedure. The results are summarized in Table 1, where they are compared with the results obtained by cold-vapor atomic absorption spectrometry (AAS). The results agree satisfactorily except for sample 3/3; the reason for this difference is not known but is probably due to contamination. Sodium carbonate was used in the first sampler in order to collect water-soluble mercury species while the metallic mercury was trapped in the permanganate solution in the second and third samplers.

Conclusions

Constant-current stripping potentiometry can be used for the determination of mercury in air samples containing more than 0.2 $\mu g\ m^{-3}$. This is about 100 times higher than atmospheric background values but it suffices for the analysis of indoor air and flue gases. In such samples, sampling times of 1—10 min are generally sufficient. Compared to the AAS techniques, flow constant-current stripping has the advantage of highly automated compact instrumentation. The possibility of continual monitoring with computer control of replenishment and transference of the trapping solutions as well as the gas sampling pump is attractive. The long-term stability of the gold fibre sensor would permit several hundreds of electrolysis/stripping cycles without the need for changing the fibre. Currently under investigation is the possibility of direct sampling of elemental mercury in air on the gold

TABLE 1

Comparison between the results obtained by cold-vapor atomic absorption spectrometry (AAS) and automated constant-current stripping analysis (CCSA) for different trapping solutions used for sampling mercury species in flue gases

Sample	Bottle no.	Trap soln.[a]	Mercury content (μg/test)		Sample	Bottle no.	Trap soln.[a]	Mercury content (μg/test)	
			AAS	CCSA[b]				AAS	CCSA[b]
1	1	A	21.0	26.4 ± 5.5	5	1	B	20.0	26.1 ± 2.7
	2	C	3.4	3.8 ± 0.2		2	C	3.6	5.5 ± 0.6
	3	C	0.1	0.21 ± 0.02		3	C	0.1	0.18 ± 0.03
2	1	A	7.6	9.6 ± 1.3	6	1	B	8.7	8.6 ± 1.5
	2	C	1.7	1.8 ± 0.2		2	C	2.9	2.8 ± 0.5
	3	C	<0.1	0.26 ± 0.02		3	C	0.1	0.09 ± 0.01
3	1	A	20.3	20.0 ± 2.4	7	1	B	19.3	22.0 ± 2.0
	2	C	2.6	2.3 ± 0.06		2	C	3.3	3.8 ± 0.3
	3	C	<0.1	4.1 ± 0.4		3	C	<0.1	0.15 ± 0.01
4	1	A	6.3	7.5 ± 0.4	8	1	B	10.8	14.4 ± 2.3
	2	C	1.3	1.8 ± 0.2		2	C	1.7	2.1 ± 0.3
	3	C	<0.1	0.31 ± 0.03		3	C	<0.1	0.16 ± 0.01

[a](A) 10% sodium carbonate; (B) 10% sodium carbonate in saturated sodium chloride; (C) 10% potassium permanganate in (1 + 9) sulphuric acid. [b]Mean and standard deviation for $n = 5$.

fibre sensor with subsequent determination by constant-current stripping potentiometry.

REFERENCES

1 F. Vydra, M. Stulikova and P. Peták, J. Electroanal. Chem., 40 (1972) 99.
2 L. Luong and F. Vydra, J. Electroanal. Chem., 50 (1974) 379.
3 L. Ulrich and P. Z. Ruegsegger, Anal. Chem., 277 (1975) 277.
4 R. Fukai and L. Herynh-Ngoc, Anal. Chim. Acta, 83 (1976) 375.
5 M. Taddia, Microchem. J., 23 (1978) 64.
6 J. Golimowski and I. Gustavsson, Z. Anal. Chem., 317 (1984) 481.
7 D. Jagner and K. Årén, Anal. Chim. Acta, 117 (1980) 165.
8 D. Jagner, M. Josefsson and K. Årén, Anal. Chim. Acta, 141 (1982) 147.
9 H. Huiliang, D. Jagner and L. Renman, Anal. Chim. Acta, 201 (1987) 1.
10 L. Renman, D. Jagner and R. Berglund, Anal. Chim. Acta, 188 (1986) 137.

Analytica Chimica Acta, 201 (1987) 275—280
Elsevier Science Publishers, B.V., Amsterdam — Printed in The Netherlands

Short Communication

ADSORPTIVE STRIPPING VOLTAMMETRY OF CHLORDIAZEPOXIDE AT THE HANGING MERCURY DROP ELECTRODE

E. LORENZO and L. HERNANDEZ*

Department of Analytical Chemistry, Faculty of Sciences, Autonoma University, Madrid (Spain)

(Received 2nd February 1987)

Summary. Controlled adsorptive accumulation at the hanging mercury drop electrode enables 0.8—11 × 10^{-8} M chlordiazepoxide to be quantified by differential-pulse stripping voltammetry with accumulation times of 1—3 min. With 3-min accumulation, the peak current is enhanced 12-fold for 1.0 × 10^{-7} M chlordiazepoxide compared to the current from differential pulse polarography. The detection limit is 0.9 × 10^{-9} M for 4-min accumulation. The procedure is applied to spiked human serum after preseparation of the drug on a Sep-Pak C_{18} cartridge.

Chlordiazepoxide (7-chloro-2-methylamino-5-phenyl-3*H*-1,4-benzodiazepine-4-oxide), marketed as Librium, is widely used as a psychotherapeutic drug. Methods reported for the determination of this compound include spectrophotometric [1] and spectrofluorimetric [2, 3] procedures. The polarographic behaviour of chlordiazepoxide was described by Oelschlager [4], who reported three reduction waves for the compound in Britton—Robinson buffer. Below pH 4.0, only the first two waves were observed; the height of these waves was proportional to concentration in the range 0.1—1 mM. The polarographic reduction mechanism has been studied [5—8]; the first step is a 2-electron reduction of the N-oxide group and the second step a 2-electron reduction of the C=N group. Two hydrogen ions are consumed in each step. Polarographic methods have been used for the determination of chlordiazepoxide in pharmaceutical formulations [9], toxicological samples [10] and horse serum [7]. None is sufficiently sensitive for convenient application to biological fluids.

An extremely sensitive procedure for traces of chlordiazepoxide based on adsorptive stripping is described below. This technique has been applied for a wide range of electroactive compounds adsorbing onto the electrode [11—13]. The determination of chlordiazepoxide by this method is very sensitive and simple. The adsorption is sufficiently pronounced that immersion of the hanging mercury drop electrode (HMDE) in the sample solution for a few minutes allows convenient quantitation of the drug at nanomolar levels.

Experimental

Apparatus and reagents. Stripping voltammograms were obtained with a Metrohm compact analyzer for voltammetry and polarography, consisting of

0003-2670/87/$03.50

a 646-VA processor and a 647-VA stand with an Ag/AgCl (3 M KCl) reference electrode, a glassy carbon auxiliary electrode, a mercury multimode electrode and a stirring bar that provided convective transport during the preconcentration.

Stock solutions (1.0×10^{-4} M) of chlordiazepoxide (Roche Laboratorios, Madrid) were prepared by dissolving the drug in ethanol and diluting daily the necessary amounts with water. The solutions were stored in the dark at 4°C. All water used was twice-distilled. Analytical-reagent grade reagents were used throughout. The serum sample was obtained from a pool of serum from the Ramon y Cajal Hospital. The artificial serum was prepared as suggested by Duncal [14].

General procedure. A known volume (10 ml) of the supporting electrolyte (usually Britton—Robinson buffer pH 6.8) was made up to 25 ml, added to the cell and degassed by nitrogen purging for 10 min (and for 10 s before each adsorptive stripping cycle). The accumulation potential (usually —660 mV) was applied to the electrode for a selected time, while the solution was stirred at 1920 rpm. The stirring was then stopped, and after a 10 s rest period, a negative-going differential-pulse scan was initiated, with simultaneous recording of the resulting voltammogram. The operational parameters for the scan were: rate, 15 mV s^{-1}; pulse amplitude, —50 mV; pulse repetition, 0.4 s. The scan was terminated at —1.100 mV, and the adsorptive stripping cycle was repeated with a new drop. After background stripping voltammograms had been obtained, aliquots of chlordiazepoxide standards were introduced. All data were obtained at ambient temperature.

Preseparation procedure. Human serum (1.0 ml) doped with chlordiazepoxide (0.7—3.0 μg) and 10 ml of pH 6.8 Britton—Robinson buffer were mixed. This mixture was applied slowly to a Sep-Pak C_{18} cartridge (Millipore) from a 20-ml syringe. After washing with 10 ml of water, the drug was eluted with 1.0 ml of diethyl ether. The eluate was evaporated to dryness under a stream of nitrogen. The residue was dissolved in 10 ml of pH 6.8 Britton—Robinson buffer. The solution was made up to 25 ml with water, transferred to the polarographic cell and then treated as described above.

Results and discussion

Effect of operational parameters. Figure 1A shows a differential pulse voltammogram with a HMDE that had been immersed in a stirred 1.0×10^{-7} M chlordiazepoxide solution for 3 min and the corresponding response with no accumulation. A well-defined stripping peak is observed, with a peak potential of —925 mV and a half-width of 50 mV. A 12-fold peak-current enhancement is observed even after the short accumulation period used. Obviously, longer accumulation periods will result in further enhancements (see below). The choice of the electrolyte and its concentration are critical to the adsorptive stripping behaviour. The response was examined in the presence of various supporting electrolytes, viz., acetate buffer (0.05, 0.1 and 0.5 M) 5, 10 and 25 ml of Britton—Robinson buffer (acetic acid,

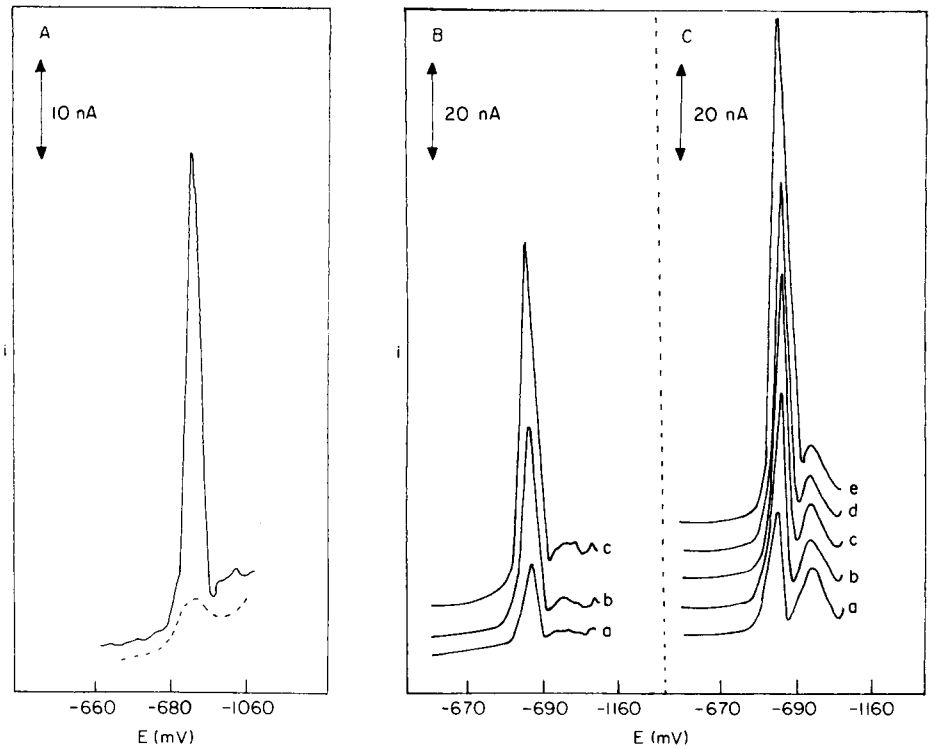

Fig. 1. Differential-pulse voltammograms for 1.0×10^{-7} M chlordiazepoxide in pH 6.8 Britton—Robinson buffer. (A) With accumulation for 3 min at —660 mV and 1920 rpm; (- - -) without accumulation. (B) Effect of drop size: (a) 0.16 mm^2, (b) 0.33 mm^2, (c) 0.48 mm^2; scan rate 15 mV s^{-1}. (C) Effect of scan rate: (a) 5, (b) 10, (c) 15, (d) 20, (e) 30 mV s^{-1}; drop size 0.48 mm^2.

boric acid and phosphoric acid, all 0.04 M) pH 2.0—12.0; borate buffer (0.1 M, pH 9.0); sodium hydroxide (0.01 and 0.1 M) and 0.1 M sulphuric acid. The best results, with respect to peak enhancement, shape and reproducibility, were obtained with Britton—Robinson buffers pH 6.0—9.0 (10 ml).

Figure 1 also shows the effects of the drop size (B) and differential-pulse scan rate (C) on the stripping peak. A four-fold increase in the peak current was observed on changing the drop area from 0.16 mm^2 to 0.48 mm^2. As the background current remains essentially the same, the larger drop size is recommended when maximum sensitivity is required. Scan rates of 10 and 20 mV s^{-1} offer two- and three-fold peak current enhancements, respectively, compared with 5 mV s^{-1}. However, this gain in sensitivity is accompanied by peak broadening. Overall, a scan rate of 15 mV s^{-1} is the best compromise with regard to sensitivity, resolution and speed requirements.

Figure 2 shows the dependence of the peak current on the preconcentration time for two concentration levels of chlordiazepoxide in different

electrolytes. The peak height increases linearly with time at shorter times but levels off at longer times in both electrolytes; for the higher concentration of electrolyte, the current levels off at a shorter period. At low concentration (1.0×10^{-7} M), full surface coverage is approached for preconcentration times longer than 3 min; at a higher concentration (1.0×10^{-6} M), it is approached at times exceeding 1 min. The dependence of the stripping peak currents on the preconcentration potential was also investigated. A gradual 30% increase in current was observed as the preconcentration potential was changed from —540 to —680 mV. A potential of —660 mV is recommended, and was used during the remainder of the study. Mass transport during preconcentration affects the amount of analyte adsorbed and thus the sensitivity. The effect of stirring rate was studied in the range 1220—2620 rpm (for 1.0×10^{-7} M chlordiazepoxide, accumulation for 3 min). The best results were obtained at 1920 rpm.

Quantitative utility. For convenience it is desirable that the response be a linear function of concentration. Figure 3 shows the dependence of the peak current on the chlordiazepoxide concentration for different accumulation periods. At 2 and 3 min, the response is linear over the entire concentration range examined (8.0×10^{-9}—1.1×10^{-7} M) with slopes of 5.5 and 6.5 nA per 10^{-8} M, respectively (correlation coefficients 0.998 and 0.988, respectively). For a 4-min accumulation, the response is linear up to $1.1 \times$

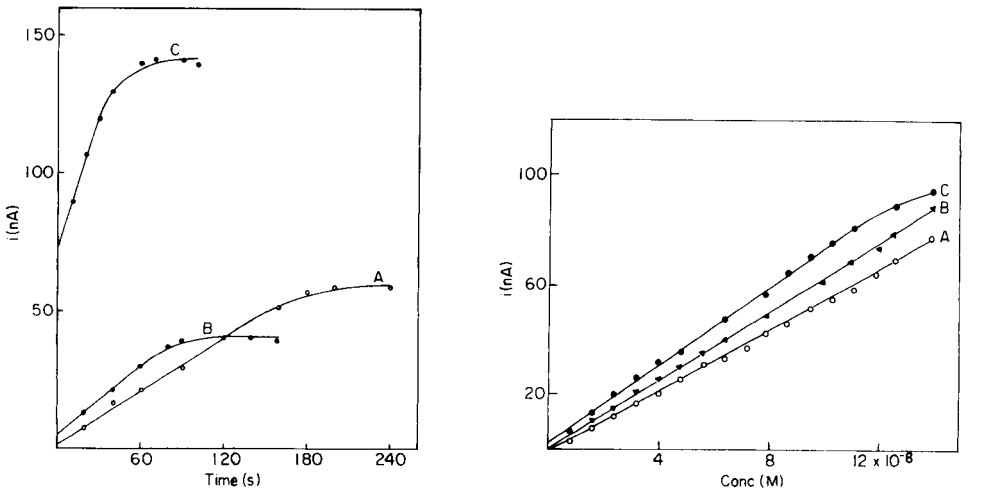

Fig. 2. Dependence of the stripping peak current (i) on the accumulation time at different concentrations and in different electrolytes. (A, B) 1.0×10^{-7} M chlordiazepoxide with accumulation at —660 mV: (A) 5 or 10 ml; (B) 25 ml of pH 6.8 Britton—Robinson buffer. (C) 1.0×10^{-6} M drug in 0.1 M acetate buffer with accumulation at —400 mV. Other conditions as in Fig. 1A.

Fig. 3. Dependence of the stripping peak current (i) on chlordiazepoxide concentration at different accumulation times: (A) 2; (B) 3; (C) 4 min. Other conditions as in Fig. 1A.

10^{-7} M (slope 7.2 nA per 10^{-8} M; correlation coefficient 0.999). Deviations from linearity occur at higher concentrations and/or for longer accumulation periods, as full surface coverage is approached. The adsorptive accumulation results in extremely low detection (3σ) and determination limits [15], 9.0×10^{-10} and 6.3×10^{-9} M, respectively (accumulation for 4 min); in the 25 ml of solution used, 6.8 ng can be detected. The sensitivity is significantly enhanced over that obtained by conventional differential-pulse voltammetry.

The precision was estimated by ten repeated measurements of 5.0×10^{-8} M chlordiazepoxide. The mean peak current found was 27.5 nA with a relative standard deviation (r.s.d.) of 4.0% (accumulation for 2 min). Similar studies with accumulation for 4 min yielded 39.8 nA for the mean peak current with r.s.d. of 3.8%.

The method was applied to the determination of chlordiazepoxide in an artificial serum. With 15 ml of serum, well defined peaks were observed with detection and determination limits of 1.0×10^{-9} and 6.6×10^{-9} M, respectively (accumulation for 4 min). The sensitivity of the method was found to be 6.9 nA per 10^{-8} M for concentrations ranging from 8.0×10^{-9} to 9.5×10^{-8} M; the r.s.d. for 8 determinations of 5.0×10^{-8} M drug was 4.9%.

Stripping measurements in biological fluids would require separation of potential interferences, mainly proteins, that compete for the surface sites; in authentic serum no peak was obtained at concentrations of 1.0×10^{-7}—5.0×10^{-7} M. Oelschlager and Sengun [16] have combined the Extrelut column preseparation method with polarographic methods for the deter-

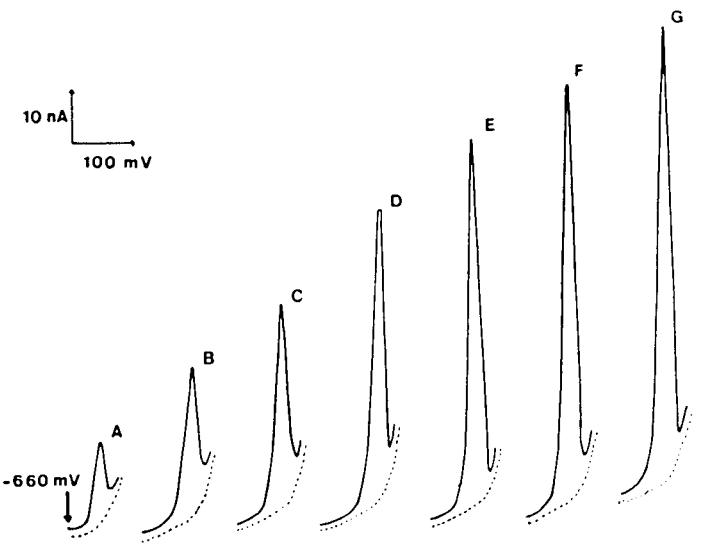

Fig. 4. Stripping voltammograms of chlordiazepoxide after extraction from human serum with a Sep-Pak C_{18} cartridge: (A) 1.0×10^{-7}; (B) 1.6×10^{-7}; (C) 2.0×10^{-7}; (D) 2.4×10^{-7}; (E) 3.0×10^{-7}; (F) 3.6×10^{-7}; (G) 4.0×10^{-7} M. Accumulation for 1 min. Other conditions as Fig. 1A. The dotted lines represent the background stripping voltammograms.

mination of Triazolam. In the present study, preseparation of chlordiazepoxide on a Sep-Pak C_{18} reverse-phase cartridge was examined for spiked human serum samples. Figure 4 shows the adsorptive stripping voltammograms after accumulation for 1 min. These data yield a linear calibration graph with a slope of 2.4 nA per 10^{-8} M and a correlation coefficient of 0.996. The detection limit was 6.9×10^{-8} M and the determination limit 8.1×10^{-8} M. At 1.0×10^{-7} M the r.s.d. was 5.0% (n = 6).

REFERENCES

1 P. Jatlow, Clin. Chem., 18 (1972) 516.
2 B. A. Koechlin and L. D'Arconte, Anal. Biochem., 5 (1963) 195.
3 B. A. Koechlin, M. A. Schwatrz, G. Krol and W. Oberhansli, J. Pharmacol. Exp. Ther., 148 (1965) 399.
4 H. Oelschlager, Arch. Pharm. (Weinheim, Ger.), 296 (1963) 396.
5 H. Oelschlager and H. Hoffmann, Arch. Pharm. (Weinheim, Ger.), 300 (1967) 817.
6 H. Oelschlager, J. Volke, H. Hoffmann and E. Kurek, Arch. Pharm (Weinheim, Ger.), 300 (1967) 250.
7 E. Jacobsen and T. V. Jacobsen, Anal. Chim. Acta, 55 (1971) 293.
8 J. M. Clifford and W. F. Smyth, Fresenius' Z. Anal. Chem., 264 (1973) 149.
9 G. Caille, J. Braun and J. A. Mockle, Can. J. Pharm. Sci., 5 (1970) 78.
10 G. Cimbura and R. C. Gupta, J. Forensic. Sci., 10 (1965) 282.
11 J. Wang, Stripping Analysis: Principles, Instrumentation and Applications, Verlag Chemie, Deerfield Beach, FL, 1985.
12 R. Kalvoda, Anal. Chim. Acta, 162 (1984) 197.
13 L. Hernandez, A. Zapardiel, J. A. Perez and V. Rodriguez, in M. R. Smyth and J. G. Vos (Eds.), Electrochemistry, Sensors and Analysis, Elsevier, Amsterdam, 1986, pp. 385—390.
14 L. Duncal, Clinical Analysis by AAS, Varian Techtron, Springvale, Australia, 1976.
15 J. H. Mamson, Anal. Chem., 52 (1980) 2241.
16 H. Oelschlager and F. I. Sengun, Arch. Pharm. (Weinheim, Ger.), in press.

Analytica Chimica Acta, 201 (1987) 281—287
Elsevier Science Publishers B.V., Amsterdam — Printed in The Netherlands

Short Communication

COMPARISON OF AMPEROMETRIC MEASURING PRINCIPLES FOR DETERMINATIONS OF GLUCOSE WITH ELECTRODES BASED ON GLUCOSE OXIDASE

L. ASPERGER*, G. GEPPERT and CH. KRABISCH

Institute of Biotechnology, Academy of Science of the GDR, Permoserstrasse 15, Leipzig 705 (German Democratic Republic)

(Received 22nd January 1987)

Summary. The three measuring principles for glucose determination (H_2O_2 formation, O_2 consumption, or enzymatically reduced acceptor) were studied with an apparatus that was the same for all measurements, with virtually identical electrode design. The methods were compared with regard to measurement range, sensitivity, time behaviour, operational lifetime, precision and accuracy. Essential differences were found with respect to measurement range as well as to time. Measurements under anaerobic conditions have advantages over those done aerobically.

Glucose determinations with amperometric enzyme sensors are well established. The well-known principles differ in their application mainly in the type of electrode used. The theory of enzyme electrodes has been described by several authors [1, 2]. In the commercially available devices containing sensors based on glucose oxidase, the oxygen partial pressure [3, 4], the hydrogen peroxide concentration [5, 6] or the amount of reduced hydrogen acceptor formed during the detection reaction [7, 8] can be recorded. Such analysers have been developed for the assay of glucose in blood [9, 10] and in fermentation medium [11]. Though the electrodes have been widely investigated with regard to performance in commerical devices, they have not been compared on the basis of the three operating principles mentioned above. In this communication, the individual methods are compared by using the same apparatus and general construction but with different enzyme electrodes.

Experimental

Chemicals. A commercial glucose oxidase from *Penicillium notatum* (46 U mg^{-1}; VEB Arzneimittelwerk, Dresden) was bound to Sepharose CL-6B (Pharmacia, Sweden) as described elsewhere [12] and suspended in phosphate buffer, pH 7.5, containing 0.02% (w/w) sodium azide. A portion (5 μl) of the suspension was deposited on the electrode surface of the corresponding probe, and the buffer was removed with filter paper. Dialysis membrane

0003-2670/87/$03.50

(Nephrophan; VEB Chemiekombinat, Bitterfeld) was attached to the tip of the electrode in order to fix the enzyme. The reaction layer contained about 0.01 mg of glucose oxidase. For anaerobic measurements, *p*-benzoquinone (VEB Jenapharm-Laborchemie, Apolda) was chosen as the most satisfactory hydrogen acceptor; being rather unstable, the acceptor solution was prepared at short intervals during the measurement cycle. *p*-Benzoquinone concentrations in the range 1.0—5.0 mM were found to provide very precise glucose measurements.

Apparatus and procedure. A block diagram of the measuring device is shown in Fig. 1. In anaerobic glucose determinations based on oxygen consumption or H_2O_2 production, air is introduced into the measuring cell containing 0.01 M phosphate buffer, pH 7.0, in order to achieve aerobic conditions. Amperometric current/time curves are recorded after injection of the sample into the buffer. Each step of the analytical cycle (e.g., rinsing, emptying and dosing, sample dilution, time control) is done by corresponding parts controlled by an electrical system. Except for evaluation of the amperometric current/time curves, the whole quasi-continuous cycle proceeds automatically.

For glucose measurements under anaerobic conditions, changes in the apparatus were limited to the addition of a convenient hydrogen acceptor, with use of an inert gas instead of air and installation of the corresponding

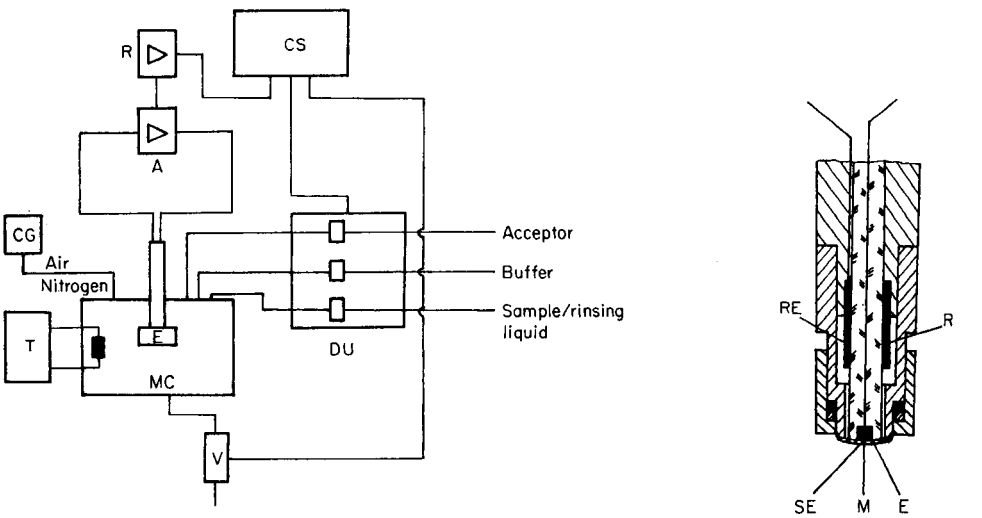

Fig. 1. Block diagram of measuring apparatus: MC, measuring cell; T, thermostat; DU, dosing unit; CG, compressed gas cylinder; CS, control system; A, amplifier; R, recorder; V, valve; E, enzyme electrode.

Fig. 2. Basic configuration of enzyme electrode: SE, sensitive element; R, reference electrode; RE, reference electrolyte; M, semipermeable membrane; E, enzyme preparation.

enzyme electrode. All measurements were made at 25°C. With the mechanized system, samples were diluted by a factor of 4 and the measuring frequency was 15 samples per hour. The current/time curves were monitored by using a polarograph (GWP 563, ADW der DDR) coupled with an X,Y recorder (endim 620.01, VEB Meßapparatewerk, Schlotheim). The indicator electrode was polarized at a constant potential of −600 mV vs. the saturated calomel electrode (SCE) for indication of the oxygen consumption, and at +800 mV for detection of hydrogen peroxide or the reduced hydrogen acceptor.

Electrodes. Depending on the substance to be quantified, the enzyme electrodes were modified, although the general design was the same. The principal construction is presented in Fig. 2, and the modifications are listed in Table 1. All electrodes were produced by means of special resin-casting technology.

Results and discussion

Concentration range. With regard to their wide concentration range, glucose sensors owe their success to the fairly high Michaelis constants of glucose oxidases compared with many other enzymes. Figure 3 depicts the amperometric current/concentration curves for the different methods investigated. Measurements of oxygen consumption and peroxide production allow the indication of only relatively small concentrations. The dependence of the enzymatic reaction rate on glucose concentration could not be represented successfully by Lineweaver–Burke plots. Hence, it seems reasonable to assume that the enzymatic reaction rate is restricted by lack of oxygen inside the enzyme layer because of the enzymatic reaction itself as well as the electrochemical reduction of dissolved oxygen. In contrast to these results, the amperometric current is proportional to the glucose content over a wide range up to 0.1 mol l^{-1} when the acceptor principle is used (Fig. 3A). Beyond the linear range, glucose can be measured to still higher concentrations. As the Lineweaver–Burke relation is valid, the enzymatic reaction rate is influenced only by Michaelis–Menten kinetics.

TABLE 1

Different parameters for the glucose oxidase/dialysis membrane system depending on the components to be quantified

Electrode number	Measured variable	Indicator electrode	Electrode diameter (mm)	Reference electrode	Reference electrolyte
1[a]	O_2	C/MoS_2	2	Pb	CH_3COONa
2	H_2O_2	Pt	1	C	$K_3[Fe(CN)_6]$
3	Acceptor[b]	C	1	C	$K_3[Fe(CN)_6]$
4	Acceptor[b]	C	3	C	$K_3[Fe(CN)_6]$

[a]In this case, a polyethylene membrane was placed between the indicator electrode and the enzyme layer. [b]Reduced hydrogen acceptor.

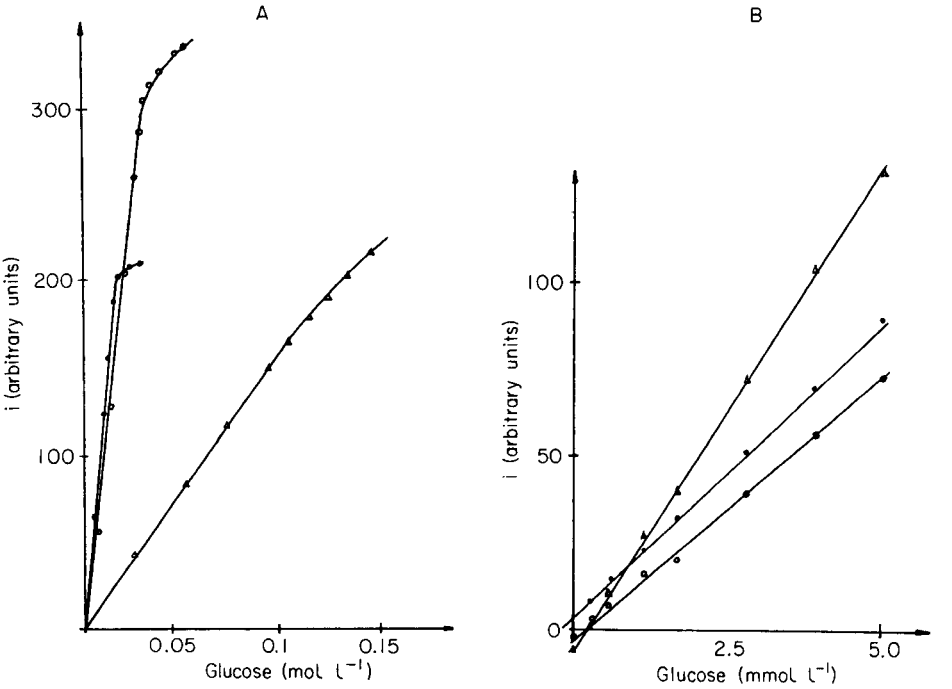

Fig. 3. Amperometric current i (arbitrary units) depending on glucose concentration in two ranges: (A) up to 0.15 mol l^{-1}; (B) up to 5 mmol l^{-1}. Measurement: (○) H_2O_2 production; (●) O_2 consumption; (△) reduced acceptor formation.

Both calculations described by Kaiser and Specker [13], and calibration curves obtained from electrodes 1—3 (Table 1) corresponding to Fig. 3B, showed that glucose cannot be measured below 0.28 mmol l^{-1}. It proved impossible to obtain a more sensitive response even when the pure reactants hydrogen peroxide and hydroquinone were added to the buffer. Therefore, reduced acceptor measurements were tested with an indicator electrode having a larger active area (number 4, Table 1); even less than 5×10^{-2} mmol l^{-1} glucose could then be detected. The signal-to-noise ratio of the apparatus did not permit scanning of the very small (nA range) currents produced at low concentrations when indicator electrodes with small active areas were used. It is known that under diffusion-controlled conditions the anodic current density is proportional to hydrogen peroxide concentration without restrictions [14]. It seems likely, therefore, that more sensitive glucose determinations than presented in Fig. 3B can also be attained by measuring enzymatically formed hydrogen peroxide.

In general, the relative error of oxygen electrodes based on gas-diffusion membranes is assumed to be about 2%. The present investigations showed that as little as 18 mmol l^{-1} glucose decreases the oxygen partial pressure within the enzymatic layer by two orders of magnitude. Accordingly,

0.18 mmol l^{-1} glucose lowers the oxygen partial pressure by 1%, and so the oxygen electrode is already working at the limit of inaccuracy. Glucose measurements by oxygen consumption are expected to be less sensitive than those of hydrogen peroxide or reduced acceptor. Finally, it should be pointed out that a larger signal is obtained by the acceptor principle than with hydrogen peroxide formation for the same glucose concentration and for the same geometric surface area of the indicator electrode. This is due to the faster back-diffusion of the smaller hydrogen peroxide molecules, compared to the hydroquinone molecules, from the enzymatic reaction layer to the bulk solution.

Time behaviour. The time behaviour of the electrodes is illustrated in Fig. 4. The dead time t_d and the time constants t_c were identical for the hydrogen peroxide and hydroquinone sensors. They were much lower than the values for oxygen electrodes equipped with an additional gas-diffusion membrane. There was also a difference in the electrode response times between the acceptor and the hydrogen peroxide sensors. The response times (t_{95}) for the hydroquinone, hydrogen peroxide and oxygen sensors were 40, 10 and 60 s, respectively. Obviously, in the hydrogen peroxide measurements, steady-state conditions are reached more rapidly because of the small size of peroxide molecules. The hydroquinone molecules diffuse more slowly towards the indicator electrode, and attainment of steady-state conditions can be retarded if the hydroquinone is adsorbed on the Sepharose particles within the reaction layer.

Operation lifetime. The electrodes tested were kept under aerobic or anaerobic conditions in the presence of 0.1 mol l^{-1} glucose at 25°C when not in use. In the anaerobic measurements, 0.5 g l^{-1} *p*-quinone was added. The daily-established calibration curves based on the acceptor principle were essentially

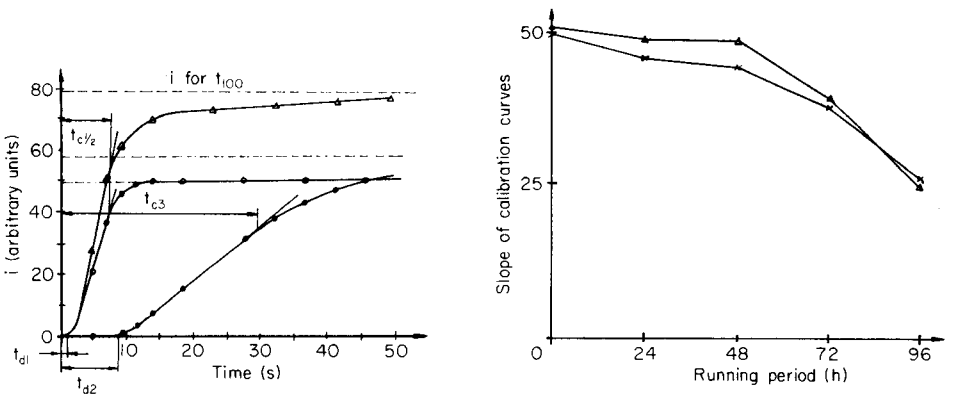

Fig. 4. Time response of electrodes based on: (○) H_2O_2 production; (●) O_2 consumption; (△) reduced acceptor formation. t_d, Dead time; t_c, time constant.

Fig. 5. Operation lifetime of electrodes under aerobic (△) and anaerobic (×) conditions. Slope is given as scale divisions/10^{-2} mol l^{-1}.

the same as those obtained on the first day for a 48-h period. As shown in Fig. 5, the slopes decreased to 50% of the initial values after four days. A similar decrease was found for electrodes kept under aerobic conditions.

Assessment of experimental results. Every measuring principle was proved by five calibration plots extending up to 20 mmol l^{-1} glucose, and by five measurements per calibration curve of samples containing 10 mmol l^{-1} glucose. The results are summarized in Table 2. The slopes of the calibration curves are nearly identical for the acceptor principle. The instability of *p*-quinone leads to alteration of the intercepts of the linear plots without greatly affecting the accuracy and precision. Repetitive measurements showed that the slope of the calibration graphs changes depending on measurement of samples with increasing or decreasing glucose concentrations. This causes a systematic error, which is reflected by higher values compared to the actual ones.

Obviously, for hydrogen peroxide measurements, factor *b* diminishes in the course of time without changing the correlation coefficient. The results are compatible with the fact that decrease of the electrocatalytic surface properties is generally found for anodic processes on noble metals. For the measurements of oxygen consumption, the difference between the excellent relative standard deviations and the greater errors of the mean values should be mentioned. For these measurements, the slope of the calibration graphs tended to increase in the range above 10^{-2} mol l^{-1} glucose. It is probably

TABLE 2

Characteristics of measurement methods with respect to accuracy and precision

Measured variable	No. of graphs	Mean value[a] $\bar{x}$	Error[b] (%)	RSD[c] (%)	Linear regression equation[d]	Corr. coeff.
Reduced hydrogen acceptor	1	2.011	+0.55	0.83	$x = 45.978u + 3.723$	0.99976
	2	2.028	+0.41	1.92	$x = 46.351u + 1.427$	0.99979
	3	2.072	+3.60	1.81	$x = 46.307u - 0.126$	0.99985
	4	2.029	+1.45	1.38	$x = 46.159u - 1.244$	0.99990
	5	2.017	+0.85	1.42	$x = 46.674u - 1.241$	0.99975
H_2O_2	1	2.077	+3.85	2.22	$x = 49.671u - 6.151$	0.99970
	2	2.087	+4.35	1.77	$x = 48.537u - 3.721$	0.99943
	3	2.026	+1.30	2.35	$x = 48.711u - 3.035$	0.99972
	4	2.032	+1.60	1.39	$x = 48.690u - 4.784$	0.99902
	5	2.126	+6.30	3.16	$x = 46.526u + 1.641$	0.99976
O_2	1	1.989	−0.55	1.23	$x = 61.314u - 7.800$	0.99915
	2	1.959	−2.03	1.04	$x = 63.468u - 5.600$	0.99937
	3	1.936	−3.20	0.55	$x = 65.429u - 9.667$	0.99782
	4	1.888	−5.61	1.67	$x = 65.829u - 8.867$	0.99694
	5	1.970	−1.50	1.30	$x = 66.171u - 8.133$	0.99920

[a]Mean reading for measurements of 10 mmol l^{-1} glucose. [b]Difference of mean from true value. [c]Relative standard deviation. [d]$x = bu \pm a$, where x is in nA and u in mmol l^{-1}

better not to use gas-diffusion electrodes unless the sample can be stirred as well as aerated.

Conclusion

The proposed apparatus with a suitable enzyme electrode allows mechanized glucose determinations under aerobic as well as anaerobic conditions. The resin-casting technique is useful in manufacturing the electrodes for detecting, regardless of whether a reduced hydrogen acceptor, hydrogen peroxide or oxygen consumption is measured. With respect to concentration range and sensitivity, measurements under anaerobic conditions are superior to aerobic assays. For quick measurements, gas-diffusion electrodes are less suitable. The systems tested show no essential differences regarding operational lifetime, accuracy and precision.

The authors thank Dr. M. Gomoll for providing the enzyme preparation.

REFERENCES

1 F. Scheller and D. Pfeiffer, Z. Chem., 18 (1978) 50.
2 P. W. Carr and L. D. Bowers, Immobilized Enzymes in Analytical and Clinical Chemistry, Wiley, New York, 1980.
3 S. D. Updike and G. P. Hicks, Nature (London), 214 (1967) 986.
4 G. G. Guilbault and G. J. Lubrano, Anal. Chim. Acta, 64 (1973) 439.
5 G. G. Guilbault and G. J. Lubrano, Anal. Chim. Acta, 60 (1972) 254.
6 D. R. Thevenot, P. R. Coulet, R. Sternberg and D. C. Gautheron, Bioelectrochem. Bioeng., 5 (1978) 548.
7 D. L. Williams, A. R. Doig and A. Korosi, Anal. Chem., 42 (1970) 118.
8 P. Schläpfer, W. Mindt and P. Racine, Clin. Chim. Acta, 57 (1974) 283.
9 F. Scheller, D. Pfeiffer, M. Kühn, J. Hundertmark, A. Quade, M. Jänchen, G. Lange, H. Holesch and D. Dittmer, Acta Biol. Med. Ger., 39 (1980) 671.
10 F. Scheller, 1st Heiligenstäder Kolloquium, Heiligenstadt, 1—4 November, 1982, p. 189.
11 J.-R. Mor and R. Guarnaccia, Anal. Biochem., 79 (1977) 319.
12 S. J. Gutcho, Immobilized Enzymes, Noyes Data Corporation, Park Ridge NJ, 1974, p. 25.
13 H. Kaiser and H. Specker, Z. Anal. Chem., 149 (1977) 319.
14 K. J. Vetter, Elektrochemische Kinetik, Springer, Berlin, 1970, p. 516.

Analytica Chimica Acta, 201 (1987) 289—294
Elsevier Science Publishers B.V., Amsterdam — Printed in The Netherlands

Short Communication

INVESTIGATION OF THE ORIGIN OF ARCHAEOLOGICAL GLASS ARTEFACTS BY MEANS OF PATTERN RECOGNITION

K. DANZER*, K. FLÓRIÁN[a] and R. SINGER

Department of Chemistry, Steiger 3, Friedrich Schiller University, DDR-6900 Jena (German Democratic Republic)

F. MÄURER

Computing Centre, Humboldstr. 2, Friedrich Schiller University, DDR-6900, Jena (German Democratic Republic)

ABO-BAKR M. EL-NADY[b] and K. ZIMMER

Department of Inorganic and Analytical Chemistry, L Eötvös University, P.O.B. 123, H-1443 Budapest (Hungary)

(Received 14th October 1986)

Summary. The origin of medieval glass artefacts is studied by using a supervised learning technique, which is shown to be helpful when samples cannot be identified by typical design and appearance. A set of seventy pieces of glass was analyzed for ten trace elements by optical emission spectrography. The data matrix of 33 known objects from five origins was evaluated by multivariate variance and discriminant analysis in a training step. The extracted non-elementary discriminant functions were used to classify the 37 unidentified samples. The classification result is discussed in terms of its cultural/historical information content.

The age and origin of archeological artefacts are usually estimated from the appearance, e.g., colour and shape, of the objects. Evidence about the site and depth where the object was found and about any accompanying objects from the same era is also valuable. But most such artefacts remain unidentified if no such external evidence exists or if they are only fragments. In such cases, it has proved to be useful to investigate internal properties of the artefacts, e.g., chemical structure and composition. Typical combinations of constituent elements, the "finger-print" of the raw material source, or typical structures produced by a certain technology, are useful aids in estimating the age and origin of medieval objects.

During excavations in the Budapest area, several types of historical glass were found. Some of them were identified, but others remained unknown. To obtain information about the unknown glassware, seventy pieces of glass, thirty-three of them already identified, were analyzed by optical emission

[a]Permanent address: Technical University Košice, Department of Chemistry, Svermova 9, CS-04385 Košice, Czechoslovakia.
[b]Permanent address: University of Assiut, Department of Chemistry, Assiut, Egypt.

0003-2670/87/$03.50

spectrography. The contents of iron, manganese, lead, tin, chromium, vanadium, titanium, copper, silver and zinc were determined.

The known objects were divided into five classes according to their origin. Class B consisted of Byzantine glassware, made in the Levant in the 13th century; these were the earliest samples, and similar objects have been found in Greece. Class V comprised Venetial glassware, products of the glass-making centre at Murano in the 14—16th century. Class G was German glassware (potash glass) from the end of the 15th century and the beginning of the 16th century. Class HV included products moulded in Hungary after receipt of glass from Venice. Class H comprised products of Hungarian glassworks.

Spectrographic analysis

Nine calibration samples were prepared by using a model matrix containing 66% SiO_2, 11% CaO, 5% MgO, 7% Na_2O and 11% K_2O with different ratios of minor and trace elements [1]. Both standards and glass samples were pulverized and mixed with lithium carbonate as the spectrochemical buffer, carbon powder and salts of palladium and gallium added as reference elements in the ratio 1:1:2:0.001 in a ball mill.

The emission source was a d.c. arc (8 A current) from a UBI-1 (universal arc impulse generator; VEB Carl Zeiss Jena). The carrier electrode SW380 was polarized as anode against a counter electrode SW202 (Elektrocarbon, Topolcany); both were water-cooled. The optical arrangement led the emitted light through an intermediate collimator with 3.2-mm aperture to a PGS-2 grating spectrograph (VEB Carl Zeiss Jena). The experimental conditions were as follows: spectral order 1; grating constant 1302 mm^{-1}; dispersion 3.63 A mm^{-1}; wavelength range 250—380 nm; slit 20 μm; sample weight 19.5 mg ± 2%; exposure time total burning (80—120 s); photographic emulsion Agfa Gevaert Scientia 34-B-50; developer Agfa 1; development 5 min, 20°C; densitometer G-II (VEB Carl Zeiss Jena).

Calibration curves were constructed from data for four portions of each standard sample. Blackening values were measured with a modified G-II microphotometer; calibration curves were established by using L-transformation [2].

Pattern recognition

When connections between properties of objects and measured analytical values are studied, it is usual to observe modifications caused by varying one parameter while all others are kept constant. This univariate method has the disadvantage that interactions between the parameters in multivariate systems cannot be identified. For complex systems, the application of multivariate data analysis has proved valuable. From the many methods for pattern recognition [3], a supervised learning technique was chosen because weighting of the parameters according to their information content for the intended classification is possible with this technique.

In the first training step, the data matrix of thirty-three pieces of glass of known origin was analyzed by using multidimensional variance and discriminant analysis (MVDA) [4]. Table 1 shows the age and origin of these pieces, as well as the result of arranging the unknown objects into the five classes. The relatively low statistical reliability of class G, which contained only two objects supposed to be German-made, suggested the use of a second training procedure neglecting class G. The classification results obtained by using the non-elementary discriminant functions extracted in this way are shown in the last column of Table 1. The reclassification yields an error rate of 10: 33 = 0.303, whereas repetition of the procedure neglecting class G has a misclassification rate of only 7:31 = 0.226. The improved reclassification rate is the result of the higher statistical reliability in the latter case (Table 2).

Although the question of the statistical adequacy of training sets for pattern recognition algorithms is not generally clear and can depend on the real structure of the data matrix, an empirical rule has proved to be advantageous for practical purposes. According to this rule, a classification becomes meaningful if the number of training objects per class is at least three times greater than the number of features [5]. Because some classes in the present ten-dimensional training set had only 2—5 objects, the statistical risk of the results is obvious. Figure 1 shows the position of the four classes B, H, HV and V, the two-dimensional display of the first two most discriminating non-elementary discriminant functions and the distribution radii of two-dimensional Fisher distribution at the 95% level. Class B which was poorly separated when class G was considered, is now relatively well separated, whereas classes H, HV and V overlap extensively in both cases.

Evaluation of the classification from the archaeological point of view

The results of the classification can be divided into four groups concerning its information content for the identification of the objects. First, in twenty-three cases, the classification result was in accordance with archaeological opinion. In the second group, the results helped in the identification of some objects which could not be identified by archaeological methods. Thus samples 10, 22, 38 and 66 are window glasses, the form of which remained unchanged for a long interval. With the help of MVDA, they were exactly classified. Sample 11 was unidentifiable by its shape, and only the place where it was found indicated its dating from the 13th century. Classification supported this hypothesis. Samples 12, 29 and 41 were accompanied at the site by objects from various periods; MVDA clarified the chronology. The origin of sample 12 remains uncertain; according to the 5-class model, it was found to be from Venice but in the 4-class model from Byzantium. For samples 24 and 32, an alternative provenance was possible on the basis of their shape and material; the data analysis decided the correct source.

In the third group, the result of classification of sample 18 rectified a mistaken identification. This piece is not a Venetian one but was made in Hungary after a Venetian model. Finally, in two cases, the results of pattern

TABLE 1

Age and origin of the glass artefacts and their reclassification by MVDA

Obj. No.	Age (century)	Origin	Object	Discrimination result	
				With class G	Without class G
1	15/16	V	Dish	HV	HV
2	15/16	G	Glass	G	(HV)[a]
3	?	?	Bottle	HV	HV
4	15/16	H	Cup	HV	HV
5	13	B	Bottle	B	B
6	14/15	H	Window glass	H	H
7	14/15	?	Glass	HV	HV
8	14/15	?	Glass	HV	HV
9	13/14	?	Window glass	HV	HV
10	14/15	?	Window glass	B	B
11	13/14	?	?	B	B
12	13	?	Bottle	V	B
13	16/17	H?	Beer goblet	H	H
14	15/16	H?	Bottle	HV	H
15	17/18	H?	Bottle	H	H
16	14/15	HV?	Bottle	HV	HV
17	18	H	Bottle	H	H
18	15/16	G	Glass	HV	HV
19	15/16	V	Cup	V	V
20	16	H?	Cup lid	H	H
21	?	H?	?	B	B
22	?	?	Window glass	HV	HV
23	14	V	Glass wall	V	V
24	15	V	Glass bottom	HV	HV
25	15	HV?	Cup	H	HV
26	15/16	V	Cup lid	H	HV
27	14/15	?	Wall/Melting pot	H	H
28	14	V	Glass	V	V
29	?	?	Bottle	V	V
30	15/16	V?	Glass bottom	V	V
31	15/16	HV?	Cup	H	H
32	15/16	G?, H?	Bottle	H	H
33	16	V?	Bracelet	V	V
34	16	V?	Bracelet	V	V
35	16	V?	Bracelet	V	V
36	?	?	Window glass	V	V
37	?	?	Window glass	H	H
38	13	?	Mosaic window	B	V
39	13	B	Glass wall	B	B
40	13	B	Bottle	B	B
41	?	?	Lamp	B	B
42	13	?	Bottle	V	V
43	13	B	Glass	B	B
44	13	B	Bottle	V	V
45	14	V	Glass	V	V

TABLE 1 (continued)

Obj. No.	Age (century)	Origin	Object	Discrimination result	
				With class G	Without class G
46	16/17	H	Oil lamp	H	H
47	?	?	Window glass	H	H
48	15	H?	Distillation app.	HV	HV
49	16	H	Bottle	H	H
50	16	H	Bottom to 49?	H	H
51	?	?	?	V	V
52	?	?	?	H	H
53	?	?	?	H	H
54	?	?	Melting-pot	H	B
55	?	?	?	B	B
56	?	?	?	HV	HV
57	?	?	?	HV	HV
58	?	?	?	HV	HV
59	?	?	?	HV	HV
60	?	?	?	B	B
61	?	?	Window glass	V	V
62	?	?	?	V	V
63	?	?	?	HV	HV
64	?	?	?	HV	HV
65	?	?	?	HV	HV
66	?	?	?	B	B
67	?	?	?	HV	HV
68	?	?	?	HV	HV
69	?	?	?	HV	HV
70	?	?	?	HV	HV

[a]Outlier (beyond the dispersion circle).

TABLE 2

Reclassification matrix of the MVDA results for five and four classes

Prior knowledge	Discriminant result					Prior knowledge	Discriminant result			
	H	HV	V	B	G		H	HV	V	B
H(11)	8	2	0	1	0	H(11)	9	1	0	1
HV(4)	2	2	0	0	0	HV(4)	1	3	0	0
V(11)	1	2	8	0	0	V(11)	0	3	8	0
B(5)	0	0	1	4	0	B(5)	0	0	1	4
G(2)	0	1	0	0	1					
						?(39)	6	18	7	8
?(37)	7	16	7	7	0					

recognition were not acceptable for archaeological reasons. Sample 8 is a 14th century Venetian product on the basis of its shape and place of finding. The erroneous classification results from the closeness of classes V and HV

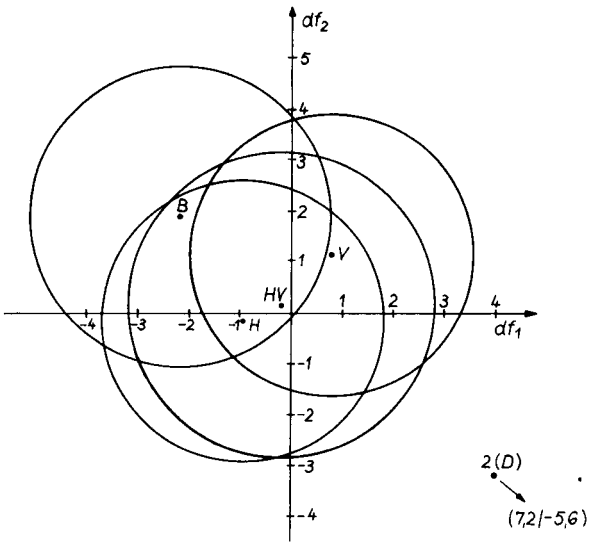

Fig. 1. Mean values and distribution radii at the 95% reliability level: two-dimensional display of the first two most discriminating non-elementary discriminant functions for the four-class model.

and the large overlapping range of the deviation circles. Sample 21 is an exception among the other artefacts; the other objects investigated were windows, cups, bottles, etc. but sample 21 is a piece of a cover knob and therefore probably not from one of the five origins considered.

Conclusions

Multidimensional variance and discriminant analysis is useful for the classification of medieval glasses into groups from different origins according to their content of minor and trace elements. Glasses with similar microcomposition can be presumed to originate from the same epoch, when the method of fabrication is unlikely to have changed significantly, and also from the same manufacturing area. In the case of imitation of a certain style, like the Venetian, in another country, chemical investigation connected with multivariate data exploration yields good results in the differentiation of originals and imitations.

REFERENCES

1 Abo-Bakr M. El Nady, Dissertation, L. Eötvös University, Budapest, 1985.
2 K. Zimmer, G. Heltai and K. Florian, Prog. Anal. At. Spectrosc., 5 (1982) 341.
3 M. P. Derde and D. L. Massart, Fresenius' Z. Anal. Chem., 313 (1982) 484.
4 J. Läuter and J. Hampicke, MVD (Programmpaket Mehrdimensionale Varianz- und Diskriminanzanalyse), AdW der DDR, Berlin-Buch, 1975.
5 C. F. Bender, H. D. Shepherd and B. R. Kowalski, Anal. Chem., 45 (1973) 617.

Analytica Chimica Acta, 201 (1987) 295—299
Elsevier Science Publishers B.V., Amsterdam — Printed in The Netherlands

Short Communication

THEORETICAL ANALYSIS OF THE RESPONSE OF AN ELECTRODE TO WHITE NOISE AND EVALUATION OF SOME PARAMETERS

M. S. LORENZO, P. CAÑAS, R. DUO* and A. ALDAZ

Departamento de Electroquimica, Facultad de Ciencias, Universidad Autónoma de Madrid, Cantoblanco, Madrid 28049 (Spain)

(Received 18th December 1986)

Summary. Random electrochemical systems are studied by using digital simulation and probability theory. The simulated data are used with experimental data in order to evaluate the heterogeneous rate constant and symmetry factor for the electrochemical systems Cd(II)/Cd(Hg) in 1 M sodium sulphate and $Cr(CN)_6^{3-}/Cr(CN)_6^{4-}$ in 1 M potassium cyanide.

Studies of electrode systems with the aid of random signals, generally white noise, have increased recently [1]. Among the various advantages offered by this method, the most notable is that the entire spectrum of the response frequencies of the system can be observed with only one measurement. The theoretical study of an electrode system excited by random signals presents considerable difficulty because the differential equations that characterize it are differential stochastic equations [2] with their inherent difficulties.

In the present work, electrode stochastic systems are studied by using digital simulation [3] and probability theory [4]. It should be pointed out that the computer time required to reach convergent solutions is very large even for simple electrode systems. Once digital simulation of this type of system is achieved, it can be used together with experimental data to establish some of the parameters that characterize the electrode system.

Theory

The simple electrode system considered is $O + ne^- \rightleftharpoons R$, to which is applied a random potential, i.e., white noise, $W(t)$. White noise is a stochastic process, which in its most elementary form can be characterized by its autocorrelation function, $R(\tau)$, which can be described [5] by $R(\tau) = K\delta(\tau)$, where K is a constant and $\delta(\tau)$ is the Dirac delta.

The power spectrum of an electrode process can be defined by

$$S(w) = \int_{-\infty}^{\infty} \exp(-jw\tau) R(\tau)\, d\tau \qquad (1)$$

where ω is the angular frequency. When this definition is applied to white noise, the following equation is obtained:

0003-2670/87/$03.50

$$S_W(w) = \int_{-\infty}^{\infty} \exp(-jw\tau)\, K\delta(\tau)\, d\tau = K \tag{2}$$

Thus, white noise can also be defined as a stochastic process having a constant power spectrum.

Considering semi-infinite plane geometry, the differential equations that describe the above situation are

$$\partial C_O(x, t)/\partial_t = D_O\ [\partial^2 C_O(x, t)/\partial x^2] \tag{3}$$

$$\partial C_R(x, t)/\partial t = D_R\ [\partial^2 C_R(x, t)/\partial x^2] \tag{4}$$

$$i(t) = nFk^0\ \{C_O(0, t)\exp[-\alpha\phi(t)] - C_R(0, t)\exp[(1-\alpha)\phi(t)]\} + [(C_{dl}/nF) \times RT\, d\phi(t)/dt] \tag{5}$$

where $\phi(t)$ is the stochastic normalized potential and C_{dl} is the double layer capacity:

$$\phi(t) = nF[W(t) - E^0]/RT \tag{6}$$

and $W(t)$ is the random applied potential:

$$W(t) = \Delta E\, \xi(t) + E_{dc} \tag{7}$$

In Eqn. 7, $\xi(t)$ is a stochastic white-noise process having values in the interval $(-1,1)$, ΔE is the perturbation amplitude, and E_{dc} is the direct current level; other symbols have their usual meanings.

The boundary conditions of the above system of differential equations are as follows:

$$C_O(x, 0) = C_O^0;\ C_R(x, 0) = C_R^0;\ C_O(\infty, t) = C_O^0;\ C_R(\infty, t) = C_R^0$$

$$\text{and } D_O\ [\partial C_O(x, t)/\partial x]_{x=0} = -D_R\ [\partial C_R(x, t)/\partial x]_{x=0}$$

The problem that arises in solving the above system of equations is that it is a system of differential stochastic equations [6]. Both the input potential, $W(t)$, and the output current density, $i(t)$, are stochastic processes: $W(t)$ is known, but deducing $i(t)$ even at the level of second-order statistics is very complicated. The concentrations $C_O(x, t)$ and $C_R(x, t)$ are simultaneously stochastic processes and random functions. Their study is also full of difficulties. In order to solve this system, probability theory [4] is used along with the techniques of digital simulation.

Simulation

In order to simulate the stochastic process $\xi(t)$, $\eta(t)$ was created from the white noise provided by the IBM subroutine standard GGL. This subroutine gives random numbers that come from a uniform distribution in the interval $(0, 1)$. $\xi(t)$ was obtained as a linear transformation based on $\eta(t)$:

$$\xi(t) = 2\,[\eta(t) - 0.5] \tag{8}$$

Thus, the process $\xi(t)$ will be included in the interval $(-1, 1)$.

The solution to the system comprising Eqns. 3–6 was done with the ex-

plicit method used by Feldberg [7, 8]. The result of this simulation is the stochastic numerical current density $i(t)$. In order to be able to compare the results of the simulation with the existing experimental data, it is necessary to obtain the Fourier transform of the numerical current density, $I(w)$:

$$I(w) = \int_{-\infty}^{\infty} i(t) \exp(-jwt)\, dt \tag{9}$$

The Fourier transform $I(w)$ was obtained in numerical form by using the standard algorithm FFT, considering 2048 time-steps.

If the process studied were deterministic, the application of the FFT algorithm to the series of obtained values of $i(t)$ would permit $I(w)$ to be found. But $i(t)$ is a stochastic process, so that only the Fourier transform of one outcome of the stochastic process is obtained. By taking advantage of probability theory, an estimator of the authentic $I(w)$ could be constructed by using a considerable number of values of $i(t)$. Thus, the number of volume elements to be considered in the solution of Eqns. 3—6 is related to the number of time-steps considered, by means of the formula [7]:

$$N = 6\,(D_{max}\,T)^{1/2} + 10 \tag{10}$$

where N is the number of volume elements, D_{max} is the greater of the dimensionless diffusion coefficients and T is the number of time-steps considered. Thus, a very high value of T implies a high value of N and makes digital simulation practically impossible even for high-capacity computers.

An alternative algorithm [9] which uses probability theory without the need for such a high number is

$$\hat{I}(w) = \sum^{n} \hat{I}^{K}_{2048}(w)/n \tag{11}$$

where $\hat{I}^{K}_{2048}(w)$ is a Fourier transform taken over 2048 time-steps and n is a number that should be evaluated in such a way that the estimates of $I(w)$ do not vary when n is increased. According to the studies done, after n = 500, the estimates do not differ significantly.

Results

The digital simulation was effected for the system Cd(II)/Cd(Hg) in 1 M sodium sulphate. Creason and Smith [10] experimentally analyzed this system, using white noise and showing the relationship $I(w)$ vs. $w^{1/2}$. By comparing the experimental data obtained by these authors to the data obtained with digital simulation, the values of some of the parameters that define the electrode system could be deduced.

The process Cd(II)/Cd(Hg) in 1 M sodium sulphate was analyzed in the frequency interval $w^{1/2}$ = 7.5 (rad s^{-1})$^{1/2}$ to $w^{1/2}$ = 65 (rad s^{-1})$^{1/2}$. Figures 1 and 2 show the experimental responses, as well as a series of simulated responses which correspond to different values of the heterogeneous standard rate constant, k^0, and symmetry factor, α. The other parameters that define

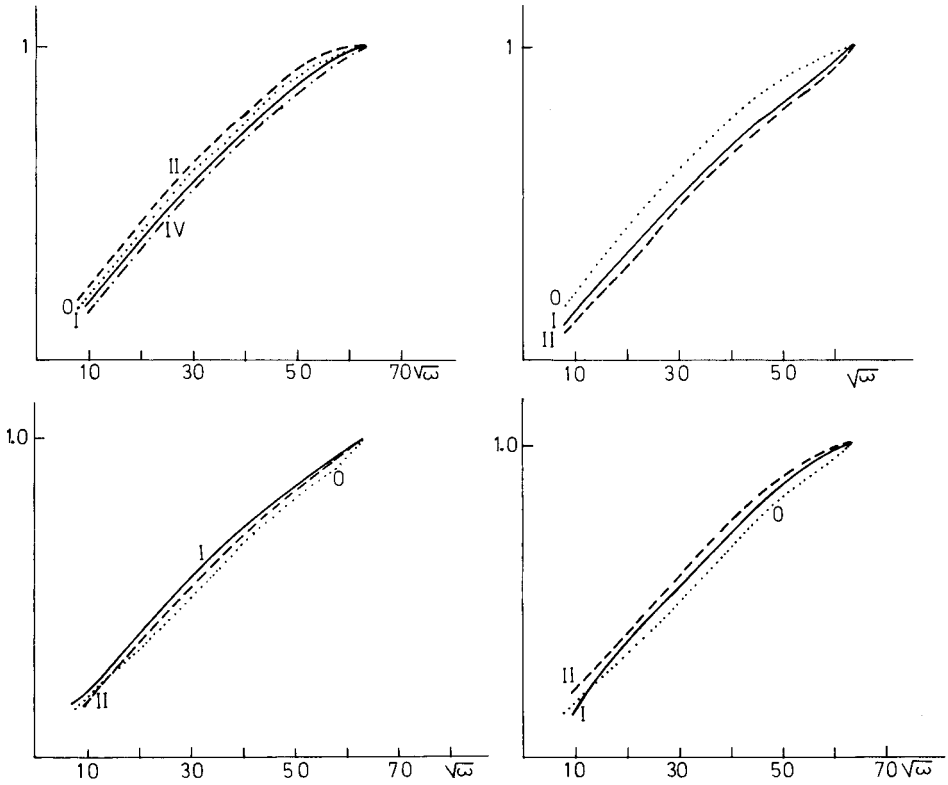

Fig. 1. (top left) $I(w)$ versus $w^{1/2}$ for the systems: (O) k^0 = 0.14 cm s^{-1}, α = 0.30 and experimental data; (I) k^0 = 0.15 cm s^{-1}; (II) k^0 = 0.10 cm s^{-1}; (IV) k^0 = 0.18 cm s^{-1}. In all cases, α = 0.30.

Fig. 2. (top right) $I(w)$ versus $w^{1/2}$ for the systems: (O) α = 0.45 and experimental data; (I) α = 0.40; (II) α = 0.30. In all cases, k^0 = 0.15 cm s^{-1}.

Fig. 3. (bottom left) $I(w)$ versus $w^{1/2}$ for the systems: (O) k^0 = 0.22 cm s^{-1}, α = 0.59 and experimental data; (I) k^0 = 0.16 cm s^{-1}; (II) k^0 = 0.30 cm s^{-1}. In all cases, α = 0.59.

Fig. 4. (bottom right) $I(w)$ versus $w^{1/2}$ for the systems: (O) experimental data; (I) k^0 = 0.24 cm s^{-1}, α = 0.50; (II) k^0 = 0.24 cm s^{-1}, α = 0.56.

this electrode system were taken from Brown et al. [11]. In order to allow the comparison, $I(w)$ was normalized by dividing by its largest value. As can be observed, plots O in Figs. 1 and 2 fit the experimental data, i.e., through digital simulation of the electrode process considered, two pairs of values are obtained: α = 0.30 and k^0 = 0.14 cm s^{-1} and α = 0.45 and k^0 = 0.15 cm s^{-1}, which fit the experimental data. By comparison with the experimental data [11] i.e., k^0 = 0.15 cm s^{-1} and α = 0.30, shows that the data obtained by digital simulation (especially the first pair) are in fairly good agreement.

Digital simulation of the electrode process $Cr(CN)_6^{3-}/Cr(CN)_6^{4-}$ in 1 M potas-

sium cyanide with a mercury electrode was also tested. This system was studied experimentally by Creason and Smith [10]. The procedures followed were the same as for the Cd(II)/Cd(Hg) process. Figures 3 and 4 show the experimental responses [10] and the responses obtained by digital simulation with various values for k^0 and α. As before, the other parameters that characterize this process were taken from Brown et al. [11]. It is clear from these figures that the electrode system that best fits the experimental data is the one characterized by the values $k^0 = 0.22$ cm s^{-1} and $\alpha = 0.59$, although the fit is less good than in the case of the Cd(II)/Cd(Hg) system. The literature values of these parameters [11] are $k^0 = 0.24$ cm s^{-1} and $\alpha = 0.59$.

Conclusions

Digital simulation can be used in studies of electrode systems to which random signals are applied. The above-described techniques can be used with the experimental data to evaluate electrode parameters. The application of this method to the Cd(II)/Cd(Hg) system in 1 M sodium sulphate produced two pairs of values. Additional information would be necessary to decide which of these pairs is better.

For the $Cr(CN)_6^{3-}/Cr(CN)_6^{4-}$ system in 1 M potassium cyanide at a mercury electrode. The values obtained ($k^0 = 0.22$ cm s^{-1} and $\alpha = 0.59$) were in agreement with literature values.

REFERENCES

1 M. Seralathan and S. K. Rangarajan, J. Electroanal. Chem., 208 (1986) 13, 29. M. Seralathan and S. K. Rangarajan, J. Electroanal. Chem., 208 (1986) 29.
2 A. Papoulis, Probability, Random Variables and Stochastic Processes, McGraw-Hill, Tokyo, 1965.
3 D. Britz, Digital Simulation in Electrochemistry, Springer, Berlin, 1981.
4 I. Guikhman, Introduction to the Theory of Random Processes, Mir, Moscow, 1980 (in French).
5 L. E. Franks, Signal Theory, Prentice-Hall, Englewood Cliffs, New York, NY, 1969.
6 D. Vasilescu, M. Teboul, H. Kranck and F. Gutmann, Electrochim. Acta, 19 (1974) 184.
7 S. W. Feldberg, in A. J. Bard (Ed.), Electroanalytical Chemistry, Vol. 3, M. Dekker, New York, 1969.
8 S. Gottesfeld and S. W. Feldberg, J. Electroanal. Chem., 194 (1985) 1.
9 M. Schwartz, Signal Processing, McGraw-Hill, New York, 1975.
10 S. C. Creason and D. E. Smith, J. Electroanal. Chem., 36 (1972) App. 1; 40 (1972) App. 1.
11 E. R. Brown, H. L. Hung, T. G. McCord, D. E. Smith and G. L. Booman, Anal. Chem., 40 (1968) 1424.

Analytica Chimica Acta, 201 (1987) 301—304
Elsevier Science Publishers B.V., Amsterdam — Printed in The Netherlands

Short Communication

EFFECT OF SAVITZKY—GOLAY SMOOTHING ON SECOND-DERIVATIVE SPECTRA

KEISUKE KITAMURA* and KEIICHIRO HOZUMI

Laboratory of Analytical Chemistry, Kyoto Pharmaceutical University, 5 Nakauchi-cho Misasagi, Yamashina-ku, Kyoto 607 (Japan)

(Received 25th March 1987)

Summary. The rounding error arising from analog/digital conversion (12-bit) of a spectrum introduces small shoulders on the zero-order spectrum, which are enhanced in the second-derivative spectrum. To reduce this noise, Savitzky—Golay smoothing of the zero-order spectrum was examined by simulation. This smoothing procedure brings the second-derivative spectrum closer to the true spectrum. The effects of smoothing on the ultraviolet spectrum of salicylic acid in ethanolic solution are reported.

To obtain a derivative spectrum by the Savitzky—Golay method [1] on a personal computer, the spectral analog output from the spectrophotometer has to be digitized by an analog-to-digital (A/D) converter and stored in the computer memory. Because the resolution of an A/D converter is not infinite, an increment in the analog output smaller than that which can be represented by the least significant bit of the A/D converter will be rounded during the conversion. Previously [2], it was shown, by simulations, that this rounding error forms small shoulders on the digitally reproduced absorption spectrum; noise was then considerable when the second-derivative spectrum was calculated. In this communication the effect of smoothing the digitally reproduced absorption spectrum by the Savitzky—Golay method is investigated for suppression of these shoulders and consequently for decreasing the noise in the resulting second-derivative spectrum.

Simulation and calculation

Simulation of the absorption spectrum and A/D conversion was as described previously [2], i.e., an absorption spectrum was simulated by a Gaussian curve and the digital data were assumed to be acquired as 800 points at 0.25-nm intervals on an absorbance scale of 0—1. As it had been found [2] that the noise generated on the second-derivative spectrum is more intense in the quintic polynomial convolution (QPC) than in the cubic convolution (CPC) in the Savitzky—Golay method, both smoothing and differentiation were performed by CPC of 17 points.

The integer data were first smoothed and then differentiated. The effect of smoothing was evaluated by two parameters as previously [2]. One was the ratio (R) of the trough lengths of the second-derivative spectrum, obtained from smoothed or unsmoothed data to the mathematically obtained true

0003-2670/87/$03.50

value. The other was the mean deviation (s) of the amplitude of the second-derivative spectrum obtained from smoothed or unsmoothed data relative to that of the corresponding true derivative spectrum over the range of $L_0 \pm W$ where L_0 is the center of the absorption peak and W is the width at half height. The computer program (BASIC) was executed on a personal computer, NEC PC-9801F2.

Results and discussion

The trough ratio R for sharp peaks having widths of 10—15 nm did not show any particular difference with and without the smoothing procedure. As previously reported [2], the rounding error for such peaks did not affect their second-derivative spectra. In real spectra, there will also be noise from various sources, so that it is important that the smoothing does not induce an attenuation of the signal intensity of the sharp peaks [3, 4] under the conditions used.

The variation of R with peak height A_0 is plotted in Fig. 1A for peaks having widths of 20, 30 and 50 nm. The results show that the R values obtained with smoothing are usually closer to unity than those obtained without smoothing at all peak heights and widths studied. Since $R = 1$ means that the trough length is equal to the true value obtained mathematically, the results indicate that the smoothing recovers the true trough lengths which had been degraded by the noise. The relative mean deviation s and the trough

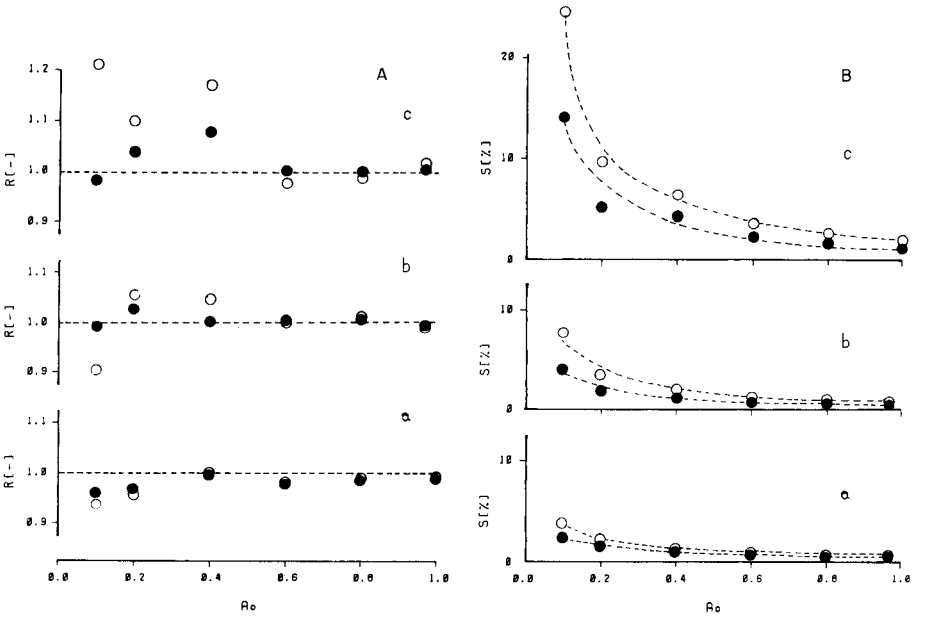

Fig. 1. Effect of smoothing at different peak heights, A_0, on the trough length ratio, R (A) and on the relative mean deviation, s (B). Peak width: (a) 20; (b) 30; (c) 50 nm. (○) Unsmoothed data; (●) smoothed data.

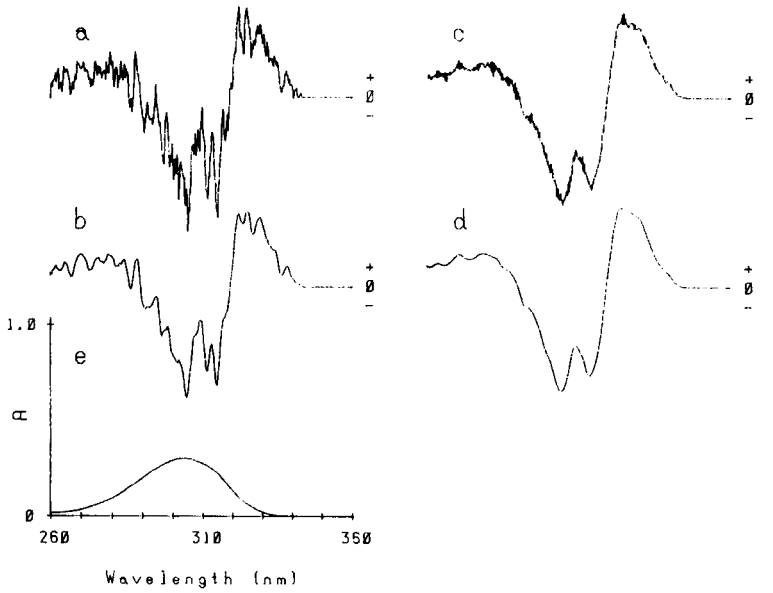

Fig. 2. Second-derivative ultraviolet spectra of 10.6 μg ml^{-1} salicylic acid in ethanol. Smoothing and differentiation were done with a 17-point cubic convolution (Savitzky—Golay method); $\Delta\lambda$ (smoothing) = 0.25 nm. Spectra: (a) from unsmoothed data; (b) from smoothed data; (c) from unsmoothed data; (d) from smoothed data; (e) zero-order spectrum. $\Delta\lambda$ (differentiation): (a, b) 0.25 nm; (b, c) 0.5 nm.

ratio provided similar results. The value of s did not show much improvement on smoothing for peaks of 10 or 15 nm width. But for wider peaks, the smoothing procedure had a beneficial effect on the s value (Fig. 1B). The second-derivative spectrum of the smoothed data was closer to the true spectrum than that of the unsmoothed data. These results show that smoothing of the A/D-converted spectral data before differentiation brings the second-derivative spectrum closer to the true spectrum by decreasing the noise caused by the rounding error in the A/D conversion, without degrading peak sharpness.

The effect of smoothing the zero-order spectrum before differentiation was examined on real data. Because a real spectrum includes noise from several sources, the results show the overall effect of smoothing. The ultraviolet absorption spectrum of an ethanolic salicylic acid solution was acquired at 0.25-nm intervals through a 12-bit A/D converter into a personal computer. The details of the data-acquisition system have been reported [5]. The second-derivative spectra obtained from the raw and smoothed data are depicted in Fig. 2. Comparison of spectrum (a) with (b) and of (c) with (d) shows an appreciable decrease in noise by use of the smoothing procedure before differentiation.

REFERENCES

1 A. Savitzky and M. J. E. Golay, Anal. Chem., 36 (1964) 1627.
2 K. Kitamura and K. Hozumi, Anal. Chim. Acta, 172 (1985) 111.
3 C. G. Enke and T. A. Nieman, Anal. Chem., 48 (1976) 705A.
4 T. C. O'Haver, Anal. Proc., 19 (1982) 22.
5 K. Kitamura, E. Morita and K. Hozumi, Yakugaku Zasshi, 105 (1985) 161.

Analytica Chimica Acta, 201 (1987) 305—310
Elsevier Science Publishers B.V., Amsterdam — Printed in The Netherlands

Short Communication

MATHEMATICAL TREATMENT OF CONCENTRATION PROFILES AND ANODIC CURRENT OF AMPEROMETRIC ENZYME ELECTRODES WITH CHEMICALLY-AMPLIFIED RESPONSE

THOMAS SCHULMEISTER

Central Institute for Molecular Biology, Academy of Sciences of the German Democratic Republic, Robert-Rössle-Str. 10, 1115 Berlin-Buch (German Democratic Republic)

(Received 15th January 1987)

Summary. Formulae are presented for explicit solutions of partial differential equations describing the transient and stationary behaviour of concentration profiles and the anodic current in amperometric chemically-amplified enzyme electrodes. The mathematical treatment is based on reaction/diffusion models with irreversible first-order catalytic reactions. Numerical results for an L-lactate-sensing electrode are used to demonstrate the application of the derived formulae.

There are three types of amperometric two-enzyme sensors, the enzyme sequence electrode [1], the enzyme competition electrode [2] and the chemically-amplified electrode [3–7]. Recently, formulae were derived for explicit solutions of reaction/diffusion models describing the transient behaviour of concentration profiles and the anodic current in the enzyme sequence and the enzyme competition electrodes [8]. The present communication deals with a mathematical model for the electrode with chemically-amplified response.

Theory

An amperometric one-layer enzyme electrode with two co-immobilized enzymes homogeneously distributed in the layer is assumed. The irreversible enzyme reactions are assumed to depend linearly on the corresponding substrate concentration. The basic principle of cycling sensors is the use of an enzyme pair which cycles the substrate, S, and therefore causes a relatively large concentration change of some measurable substance:

$$S + H_1 \xrightarrow{k_1} P + H_2; \quad P + H_3 \xrightarrow{k_2} S + H_4$$

where H_i ($i = 1 \ldots 4$) denotes substances that have no influence on the reaction rates, $k_1 S$ and $k_2 P$; one of these reactants is a substance measurable with the considered sensor. Corresponding to recently developed enzyme electrodes [6, 7], H_1 is regarded here as the monitored substance. Then, the use of two counteracting enzymes generates a continous consumption/regeneration cycle for S and P, and this results in an increased consumption of H_1 and

0003-2670/87/$03.50

H_3 and production of H_2 and H_4 beyond the usual stoichiometric limitations. This cycling method leads to a substrate measurement with high sensitivity [3—7, 9].

If a one-dimensional diffusion model is used, the transient behaviour of the cycling enzyme electrode can be described by a system of three reaction/diffusion equations [6, 8]:

$$\partial S/\partial t = D_S \partial^2 S/\partial r^2 - k_1 S + k_2 P \quad (1)$$

$$\partial P/\partial t = D_P \partial^2 P/\partial r^2 + k_1 S - k_2 P \quad (2)$$

$$\partial H_1/\partial t = D_{H_1} \partial^2 H_1/\partial r^2 - k_1 S \quad (3)$$

where $D = D_S = D_P$, the substrate diffusion coefficient, is assumed to be the same for S and P, and k_1 and k_2 are the first-order rate constants of the counteracting enzymes. The functions $S(r, t)$, $P(r, t)$ and $H_1(r, t)$ denote the concentrations of substrate, product and the electrode active reactant at point r ($0 \leqslant r \leqslant d$) and time t ($t \geqslant 0$), respectively; d is the thickness of the enzyme layer.

At the start of the measurement ($t = 0$), substrate and product are assumed to be absent in the enzyme membrane. For the monitored substance, the initial conditions are stationary. Perfect stirring is assumed. Therefore, the boundary and initial conditions of the model can be written [6, 8] as follows:

$S(d, t) = S^0$; $\partial S/\partial r(0, t) = 0$ for $t > 0$; $S(r, 0) = 0$ for $0 \leqslant r \leqslant d$

$P(d, t) = 0$; $\partial P/\partial r(0, t) = 0$ for $t > 0$; $P(r, 0) = 0$ for $0 \leqslant r \leqslant d$

$H_1(d, t) = H_1^0$; $H_1(0, t) = 0$ for $t > 0$; $H_1(r, 0) = H_1^0 r/d$ for $0 \leqslant r \leqslant d$

where S^0 and H_1^0 denote the bulk concentrations of S and H_1, respectively, the sensor side of the membrane corresponds to $r = 0$.

If $C(r, t) = S(r, t) + P(r, t)$ is defined, then Eqns. 1 and 2 lead to the simple diffusion system $\partial C/\partial t = D\partial^2 C/\partial r^2$, with $C(d, t) = S^0$ $\partial C/\partial r(0, t) = 0$ for $t > 0$ and $C(r, 0) = 0$ for $0 \leqslant r \leqslant d$. The solution of this equation is well known [10]:

$$C(r, t) = S^0 - S^0 \, (4/\pi) \sum_{n=0}^{\infty} \frac{\sin[(2n + 1)\, \pi \, (d - r)/(2d)]}{2n + 1} \exp(-vt) \quad (4)$$

with $v = D \, (2n + 1)^2 \, \pi^2/(4d^2)$.

Inserting $P(r, t) = C(r, t) - S(r, t)$ into Eqn. 1 gives an inhomogeneous reaction/diffusion system:

$$\partial S/\partial t = D \, \partial^2 S/\partial r^2 - kS + k_2 C(r, t) \quad (5)$$

with $k = k_1 + k_2$. This equation can be solved by using the integral-transform technique [10]:

$$S(r, t) = S^0 \, (4/\pi) \sum_{n=0}^{\infty} \frac{\sin[(2n + 1)\, \pi \, (d - r)/(2d)]}{2n + 1} \{(k_2 + v)/(k + v)$$

$$(1 - \exp[-(k + v)t]) - (k_2/k) \, (\exp(-vt) - \exp[-(k + v)t])\} \quad (6)$$

From the definition of $C(r, t)$, $P(r, t) = C(r, t) - S(r, t)$. Insertion of the expression for S into Eqn. 3 again gives a linear parabolic differential equation that can be solved with the same formulae:

$$H_1(r, t) = H_1^0 \frac{r}{d} - 8k_1 S^0 \pi^{-2} \sum_{m=1}^{\infty} \left\{ \sin(m\pi r/d) \sum_{n=0}^{\infty} \frac{(-1)^n}{2n+1} \right.$$
$$\frac{m}{m^2 - (2n+1)^2/4} \left[\frac{k_2 + v}{k+v} \left\{ \frac{1 - \exp(-wt)}{w} \right.\right.$$
$$\left. - \frac{\exp[-(k+v)t] - \exp(-wt)}{w - k - v} \right\} - \frac{k_2}{k} \left\{ \frac{\exp(-vt) - \exp(-wt)}{w - v} \right.$$
$$\left.\left. \left. - \frac{\exp[-(k+v)t] - \exp(-wt)}{w - k - v} \right\} \right] \right\} \qquad (7)$$

with $w = D_{H_1} m^2 \pi^2 / d^2$.

The infinite series converges rapidly for all values of t unless they are very close to zero [10]. The stationary solutions ($t \to \infty$) may be derived in the same order by using the formulae for undamped inhomogeneous oscillations [4, 8] even for different values of D_S and D_P:

$$S(r) = S^0 Q^{-2} \{Q_1^2 [\cosh(Qr)/(\cosh(Qd)] + Q_2^2\}$$

$$P(r) = (D_S/D_P)[S^0 - S(r)]$$

$$H_1(r) = S^0 \frac{k_1}{D_{H_1} Q^2} \left\{ \frac{Q_1^2}{Q^2} \frac{\cosh(Qr) - 1 + r/d}{\cosh(Qd)} + \frac{Q_2^2}{2} r(r-d) - \frac{Q_1^2 r}{Q^2 d} \right\} + H_1^0 r/d \qquad (8)$$

where $Q_1 = (k_1/D_S)^{1/2}$, $Q_2 = (k_2/D_P)^{1/2}$ and $Q = (Q_1^2 + Q_2^2)^{1/2}$.

The anodic current can be obtained explicitly from Faraday's Law and Fick's Law with the flux of H_1 at the electrode surface:

$$i(t) = nFAD_{H_1} (\partial H_1/\partial r)(0, t)$$

where n, F and A denote the number of electrons involved in the electrochemical reaction of substance H_1, the Faraday constant and the electrode surface area, respectively. In the arrangement considered, the change of the anodic current from the initial current, i_0 ($i_0 = nFAD_{H_1} H_1^0/d$) is actually measured.

Results and discussion

If only the first enzyme is working ($k_2 = 0$), the situation is that of the single-enzyme electrode [11]. In the cycling enzyme electrode, the ratio of the current decrease measured with the cycling electrode ($k_2 > 0$) to the current measured with the conventional one ($k_2 = 0$) represents the gain in sensitivity, $G(t)$, for the substrate. In the stationary case ($t \to \infty$),

$$G = \left\{\left(\frac{Q_1}{Q}\right)^4 \left[\frac{1}{\cosh(Qd)} - 1\right] - \frac{k_1 k_2 d^2}{2D_B Q^2}\right\}\left[\frac{1}{\cosh(Q_1 d)} - 1\right] \quad (9)$$

which for $D_S = D_P = D$ and high enzyme loading of the membrane [4] can be approximated by

$$G \approx k_1 k_2 d^2 / 2(k_1 + k_2) D$$

The gain increases with the thickness, d, and decreases for larger values of the diffusion coefficient. For very high values of k_1 or k_2, the gain approaches the maximum values $G_{\max,k_1} = k_2 d^2/2D$ and $G_{\max,k_2} = k_1 d^2/2D$, respectively. The gain is independent of the bulk concentration values of the substrate and the monitoring substance, S^0 and H_1^0.

To demonstrate the practical use of the derived formulae, they were applied to the L-lactate cycling electrode [6]:

$$\text{L-lactate} + O_2 \xrightarrow[\text{lactate oxidase}]{k_1} \text{pyruvate} + H_2O_2$$

$$\text{pyruvate} + \text{NADH} + H^+ \xrightarrow[\text{lactate dehydrogenase}]{k_2} \text{L-lactate} + \text{NAD}^+$$

The consumption of oxygen by the lactate oxidase reaction was monitored amperometrically in the usual way (i.e., $n = 4$). The following values of the electrode parameters were used [6]: $k_1 = 1.0\ s^{-1}$, $k_2 = 1.1\ s^{-1}$, $D = 9.0 \times 10^{-7}\ cm^2\ s^{-1}$, $d = 0.1$ mm and $n = 4$. The chemical gain in the stationary case was about 29.3. Concentration profiles and the current decrease are shown in Figs. 1 and 2. The dependence of G on the thickness of the enzyme layer, d, is shown in Fig. 3.

Theoretical investigations and the practical use of models of chemically-amplified electrodes usually require tedious numerical procedures. Explicit expressions for the concentration profiles and the anodic current were

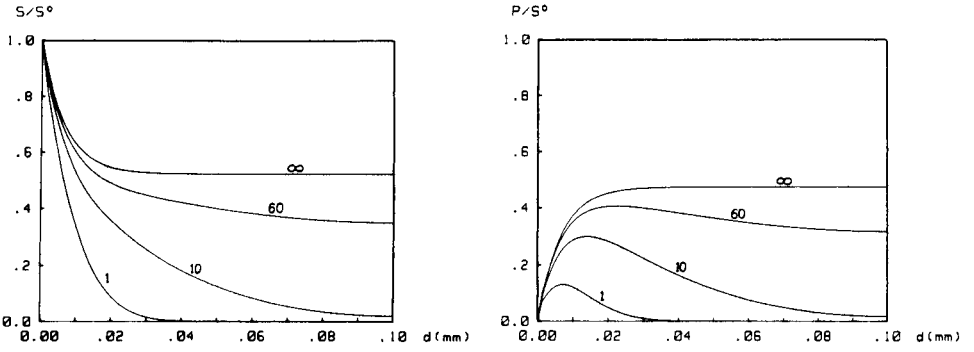

Fig. 1. Concentration profiles of the L-lactate-sensing enzyme electrode. Profiles of L-lactate (left) and pyruvate (right) are given for t = 1, 10, 60 s and the stationary case. Values of the parameters are given in the text. Lactate and pyruvate are rendered dimensionless with S^0.

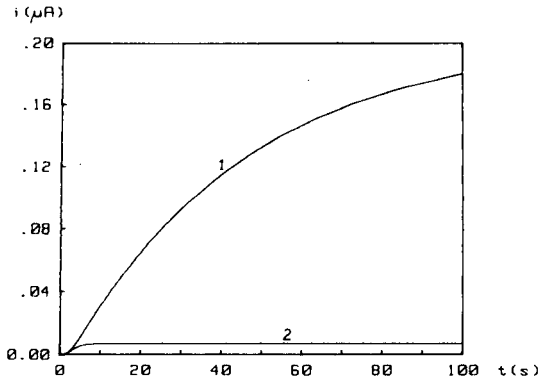

Fig. 2. Current/time behaviour of the L-lactate electrode. The current decrease is shown for S^0 = 10 μM: (1) with NADH ($k_2 > 0$); (2) without NADH ($k_2 = 0$). Electrode surface area 0.2 mm²; values of other parameters are given in the text.

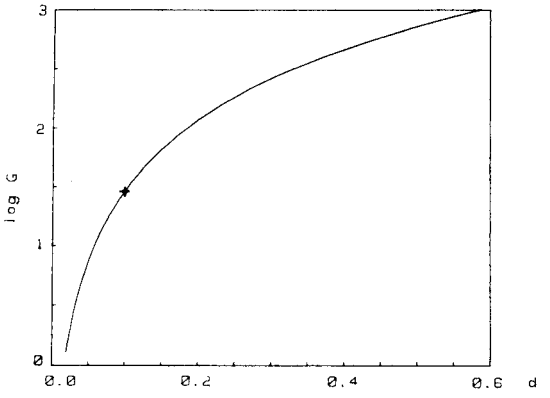

Fig. 3. Chemical gain, G, as a function of the thickness, d, obtained by using Eqn. 9. The gain obtained for d = 0.1 is marked by the plus sign.

therefore derived. In the case of first-order reaction rates, the presented formulae allow application of this approach. The chosen approach is based on a reaction/diffusion model which includes a differential equation for oxygen. This seems to be a more precise approach than the use of the oxygen consumption rate of Mizutani et al. [6]. In the development described above, the boundary layer effects and the influence of dialysis membranes were ignored. These features have to be investigated with more complex models. There are further types of amperometric chemically-amplified electrodes which could be investigated similarly, e.g., "double cycling" [12] and the combination with an enzyme sequence electrode [13]. The derived formulae could also be used to model enzymatic substrate amplification [14, 15]. A formula for the anodic current in arrangements with cyclic conversion and non-stationary initial conditions has already been given [16].

REFERENCES

1 M. A. Jensen and G. A. Rechnitz, J. Membr. Sci., 5 (1979) 117.
2 F. Scheller and D. Pfeiffer, Anal. Chim. Acta, 117 (1980) 383.
3 D. Pfeiffer, F. Scheller, M. Jänchen and K. Bertermann, Biochimie, 62 (1980) 587.
4 J. J. Kulys, Enzyme Microbiol. Technol., 3 (1981) 344.
5 F. Mizutani, Y. Shimura and K. Tsuda, Chem. Lett., 2 (1984) 199.
6 F. Mizutani, T. Yamanaka, Y. Tanabe and K. Tsuda, Anal. Chim. Acta, 177 (1985) 153.
7 F. Schubert, D. Kirstein, K. L. Schröder and F. W. Scheller, Anal. Chim. Acta, 169 (1985) 391.
8 Th. Schulmeister and F. Scheller, Anal. Chim. Acta, 171 (1985) 111.
9 F. Scheller, F. Schubert, R. Renneberg and H. G. Müller, Biosensors, 1 (1985) 135.
10 M. N. Özisik, Heat Conduction, Wiley, New York, 1980, Chap. 6.
11 Th. Schulmeister and F. Scheller, Anal. Chim. Acta, 170 (1985) 279.
12 G. H. Lowry, Acc. Chem. Res., 6 (1973) 289.
13 F. Scheller, N. Siegbahn, B. Danielsson and K. Mosbach, Anal. Chem., 57 (1985) 1740.
14 R. Renneberg, F. Schubert and F. Scheller, Trends Biochem. Sci., 11 (1986) 216.
15 F. Schubert, D. Kirstein, F. Scheller, R. Appelqvist, L. Gorton and G. Johansson, Anal. Lett., 19 (1986) 1273.
16 J. J. Kulys, V. V. Sorochinskii and R. A. Vidziunaite, Biosensors, 2 (1986) 135.

Analytica Chimica Acta, 201 (1987) 311—315
Elsevier Science Publishers B.V., Amsterdam — Printed in The Netherlands

Short Communication

DETERMINATION OF ANTIMONY DOPANT AND SOME ULTRA-TRACE ELEMENTS IN SEMICONDUCTOR SILICON BY ATOMIC ABSORPTION SPECTROMETRY WITH INTRODUCTION OF SOLID SAMPLES INTO THE FURNACE

J. B. HEADRIDGE* and D. JOHNSON
Department of Chemistry, The University, Sheffield S3 7HF (Great Britain)
K. W. JACKSON[a]
Department of Chemistry, Sheffield City Polytechnic, Sheffield S1 1WB (Great Britain)
J. A. ROBERTS
Philips Research Laboratories, Redhill, Surrey RH1 5HA (Great Britain)
(Received 5th December 1986)

Summary. Antimony as a dopant at a level of ca. 35 atom/10^6 atoms (ppm, atomic) and ultra-trace concentrations of lead and manganese (<0.02 ppm, atomic) are determined in semiconductor silicon by atomic absorption spectrometry after introduction of milligram samples of silicon to a pyrolytically-coated graphite furnace. Calibration was done with standard aqueous solutions. Iron, silver, zinc and cadmium were sought but were at concentrations below the limits of detection. The graphite microboats used for sample introduction were useful for only 3—10 samples because of silicon carbide formation.

Trace elements have profound effects on the electrical properties of silicon and other semiconductors. Frequently, a trace element within the concentration range 10^{-2}—10^2 ppm (atomic) (i.e., atoms/10^6 atoms of base element) is deliberately added as a dopant, but trace elements in the undoped semiconductor often need to be determined at concentrations ideally as low as 10^{-4} ppm (atomic). Among the few analytical techniques that have the required sensitivity to determine trace concentrations below 0.1 ppm (atomic) in semiconductor silicon are spark-source mass spectrometry (SSMS), neutron activation analysis and graphite-furnace atomic absorption spectrometry (AAS) [1—3]. Normally, graphite-furnace AAS with solutions is not sufficiently sensitive to allow determinations of trace elements below the stated level but, with silicon as base element, the method is applicable down to about 2×10^{-3} ppm (atomic) because silicon can readily be volatilized from

[a]Present address: State of New York Department of Health, Corning Tower, The Governor Nelson A. Rockefeller Empire State Plaza, Albany, NY 12201, U.S.A.

0003-2670/87/$03.50

dissolved samples as its tetrafluoride and the trace elements concentrated into a small volume of solution. However, the sample must be dissolved and, even with the most stringent precautions, there is the possibility of introducing contaminating trace elements from the reagents used.

A wider range of analytical techniques can be used for the determination of dopants in silicon and other semiconductors [1] but many of these methods also involve dissolution of samples, which takes time. Graphite-furnace AAS with the introduction of solid samples was used successfully for the determination of trace elements in metals [4], glasses [5] and semiconductor-grade gallium arsenide [6, 7]. The possibility of using this technique was therefore investigated for the determination of antimony dopant and some ultra-trace elements in semiconductor silicon; the results are reported here.

Experimental

Materials and standard solutions. Degreased silicon slices, provided by Philips Research Laboratories, were rinsed thoroughly in 1.5 M nitric acid to remove any particulate surface material and etched as follows. A slice was immersed in concentrated nitric acid for 2 min and in hydrofluoric acid for a further 2 min. It was replaced in the nitric acid, to which hydrofluoric acid was added slowly until effervescence occurred, and left for 30 s in this etching mixture. The etching was stopped by adding deionized water and the slice was washed ten times in water. It was left to dry between filter papers. A slice was shattered, as described previously [7], until the tiny fragments obtained were suitable for solid-sample insertion. The samples were stored in clean sample tubes to prevent contamination.

Deionized water was used throughout. Stock standard solutions (1 mg ml^{-1}) of antimony(III), lead, manganese(II), iron(III), silver, zinc and cadmium were prepared from potassium antimony tartrate hemihydrate and hydrated cadmium chloride in water, iron sponge and manganese flake dissolved in the minimum volume of 8 M nitric acid, lead and silver nitrates dissolved in 1% (v/v) nitric acid, and zinc shot dissolved in the minimum volume of 6 M hydrochloric acid. These solutions were diluted to volume with water (Sb, Cd, Fe), 1% nitric acid (Pb, Mn, Ag) or 1% hydrochloric acid (Zn). More dilute standard solutions were produced daily by appropriate dilution. The concentrations used for preparing the calibration graphs were (in μg ml^{-1}): lead, 0.01; manganese, 0.01; iron, 0.05—0.2; silver, 0.1; zinc, 0.01; cadmium, 0.01; antimony, 2—7 (for solid samples), and 0.2—0.75 (for dissolved samples). In all cases, these solutions were 1% (v/v) in nitric acid.

Apparatus. A Varian Techtron AA6 atomic absorption spectrometer was used with an Instrumentation Laboratory controlled-temperature furnace atomizer, and the sample was inserted in a pyrolytically-coated graphite microboat, exactly as described previously [7].

Determination of trace elements in solid silicon samples. Set up the atomic absorption spectrometer and furnace as in the instruction manual, using the

most sensitive resonance line for each element being determined except for antimony where a less sensitive line at 231.2 nm is preferable. Set the heating programme for the element under study to the conditions given in Table 1. Subject an empty microboat to the heating programme repeatedly until there is no element blank or until the blank is reasonably small and constant. Add a small sample of silicon (see Table 1), weighed to the nearest 0.01 mg, to the microboat and run the heating programme. Repeat this operation a further six times. If the quality of the absorbance peaks deteriorates, replace the microboat. Obtain the mass of element producing each peak area, corrected for any blank, from the appropriate calibration graph and calculate the concentration of trace element in the sample in $\mu g\ g^{-1}$. Average the seven concentrations and calculate their standard deviation. Convert the concentration to ppm (atomic) from ppm (atomic) = $(\mu g\ g^{-1}) \times (M/m)$, where M and m are the relative atomic masses for silicon and the trace element, respectively.

Construction of calibration graphs. Heat an empty microboat repeatedly (see Table 2) until there is no element blank or until the blank is reasonably small and constant. Pipette a suitable volume of a standard solution of the element into the microboat (see Table 1) and obtain the absorbance peak by initiating the heating programme, which is usually identical to that for solids except that a drying stage is added. Repeat the operation a further six times with various masses of the element. Measure each peak area, correct for any blank, and plot peak area vs. mass of element.

Determination of antimony in silicon after dissolution. Weigh accurately ca. 50 mg of antimony-doped silicon pieces into the PTFE liner of a stainless-steel decomposition vessel with screw-on cap. Add 3 ml of concentrated hydrofluoric acid, 5 ml of concentrated nitric acid and 2 ml of deionized water. Heat the sealed vessel at 120°C for 2 h. Rinse the digest into a PTFE volumetric flask and dilute to 25 ml with water. Prepare a blank solution in a similar way without added silicon. Process ten 10-μl aliquots of the silicon solution in the IL-555 furnace using the following heating programme and the more sensitive resonance line at 217.6 nm: ramp to 70°C over 15 s, to 120°C over 15 s and to 300°C over 10 s; hold for 10 s; step to 2250°C; hold for 10 s. Measure the mean peak area and correct it for the mean peak area for the blank.

For calibration, introduce aliquots of standard antimony solution and acid blank into the furnace, and proceed as described above. From the plot of corrected peak area vs. mass of antimony, obtain the mass of antimony in 10 μl of silicon solution and hence calculate the concentration of antimony in the silicon.

Results and discussion

Calibration graphs for antimony, lead, manganese, iron, silver and zinc were straight lines through the origin. That for cadmium was slightly curved towards the mass axis. The characteristic masses producing 1% absorption,

TABLE 1

Sample sizes and heating programmes for the IL 555 furnace

Element	Sample size	Heating programme[a]
Antimony	0.2—1.2 mg[b]	R70(15), R120(15), R1600(15), H(5), S(2250), H(10)
	10 μl[c]	R70(15), R120(15), R900(15), H(5), S(2250), H(10)
Lead	1—2.5 mg[b]	R500(10), H(5), S(2500), H(10)
	2—8 μl[c]	R75(15), R120(15), then as for solids
Manganese	1—2.5 mg[b]	R500(10), H(5), S(2700), H(10)
	1—4 μl[c]	R75(15), R120(15), then as for solids
Iron	1.5—3 mg[b]	R750(10), H(5), S(2900), H(10)
	10 μl[c]	R75(15), R120(15), then as for solids
Silver	1—2.5 mg[b]	R750(10), H(5), R2400(10), H(5)
	1—6 μl[c]	R75(15), R120(15), then as for solids
Zinc	0.5—4 mg[b]	R250(5), H(5), R1900(10), H(5)
	0.5—2.5 μl[c]	R75(15), R120(15), then as for solids
Cadmium	1—5 mg[b]	R250(10), H(5), R1750(5), H(5)
	0.5—3.5 μl[c]	R75(15) R120(15), then as for solids

[a]For example, R70(15) means ramp to 70°C over 15 s; H(5) means hold for 5 s; S(2250) means step to 2250°C. [b]With solid silicon. [c]With standard solution(s) used for calibration.

TABLE 2

Results for the determination of ultra-trace elements in silicon obtained by different methods

Sample no.	Element	Conc. found (ppm, atomic)		Element	Conc. found (ppm, atom	
		AAS on solid	SSMS		AAS on solid	SSI
3	Lead	0.0031 ± 0.0006[a]	<0.02	Silver	<0.002	<0.0
4	Manganese	0.014 ± 0.003[a]	0.04	Zinc	<0.00006	<0.0
4	Iron	<0.02	<0.2	Cadmium	<0.00004	<0.1

[a]Standard deviation on 7 measurements.

were 53 pg antimony (217.6 nm), 11 pg lead, 1.5 pg manganese, 17 pg iron, 4 pg silver, 0.14 pg zinc and 0.20 pg cadmium.

Results for the determination of antimony (mean ± SD for 7 measurements) in one sample were 31 ± 5 ppm (atomic) for analysis of the solid sample compared with 33 ± 2 after dissolution; for another solid sample, the result was 35 ± 5 compared to 30 obtained by SSMS. The results for antimony in both samples determined without dissolution by graphite-furnace AAS were in good agreement with the results obtained by the independent methods and are considered to be accurate. Therefore calibration with aqueous standards is permissible. However the method with solid samples, although faster than the similar method involving dissolution, is less precise. This probably

arises because the antimony in the silicon slices is not distributed homogeneously. The masses analysed by solid and solution graphite-furnace AAS were 0.2—1.2 mg and 46 mg, respectively. Above 1600°C, molten silicon reacts with the graphite microboats to produce silicon carbide, which erodes the graphite surface. The reaction does not affect the determination of antimony and other elements by AAS but it limits the lifetime of the microboat, because it can only accommodate 10—15 mg of silicon in total before a gross deterioration in performance is noticed. This amounts to 3—10 determinations. The estimated limit of detection for antimony is 0.03 ppm (atomic).

Only lead and manganese were found to be present at concentrations above their limits of detection. The accuracy of the results for these elements (Table 2) should be quite good but conclusive proof is impossible in the absence of results obtained by a reliable independent method. The SSMS result for manganese is only semiquantitative; the results reported for iron, silver, zinc and cadmium are less than their limits of detection. The limits of detection ($\mu g\ g^{-1}$) for silver, zinc and cadmium were estimated from the formula [8] (characteristic mass × 0.2 × average RSD)/sample mass. The average RSD values for lead and manganese (Table 2) were 20%; detection limits thus calculated were converted to ppm (atomic). For iron, absorbance peaks obtained from silicon pieces had similar areas to those obtained from the microboats themselves. The limit of detection for iron was calculated from twice the standard deviation of these peak areas; the blank iron signals could not be removed by repeated firings of the furnace. If furnace materials free from traces of iron were used, the limit of detection for iron would be lower.

Graphite-furnace AAS with solid samples of semiconductor silicon has excellent limits of detection for some elements, those for lead, manganese, silver, zinc and cadmium being below 10^{-2} ppm (atomic). It can be recommended as a rapid method for establishing the purity of undoped silicon. However, dissolution and removal of silicon as its volatile tetrafluoride is preferred if results of higher accuracy are required, particularly for doped material. A drawback to graphite-furnace AAS with solid silicon samples is the short lifetime of the graphite microboats.

We thank the Science and Engineering Research Council and Philips Research Laboratories for the award of a studentship (to D. J.).

REFERENCES

1 Y. A. Zolotov and M. Grasserbauer, Pure Appl. Chem., 57 (1985) 1133.
2 D. A. Stewart and D. C. Newton, Analyst, 108 (1983) 1450.
3 V. J. Phelan and R. J. W. Powell, Analyst, 109 (1984) 1269.
4 J. B. Headridge, Spectrochim. Acta, Part B, 35 (1980) 785.
5 J. B. Headridge and I. M. Riddington, Analyst, 109 (1984) 113.
6 D. Johnson, J. B. Headridge, C. W. McLeod, K. W. Jackson and J. A. Roberts, Anal. Proc., 23 (1986) 8.
7 I. S. Busheina, J. B. Headridge, D. Johnson, K. W. Jackson, C. W. McLeod and J. A. Roberts, Anal. Chim. Acta, 197 (1987) 87.
8 J. B. Headridge and R. A. Nicholson, Analyst, 107 (1982) 1200.

Analytica Chimica Acta, 201 (1987) 317—323
Elsevier Science Publishers B.V., Amsterdam — Printed in The Netherlands

Short Communication

EXCITATION OF MOLECULES IN THE AFTERGLOW OF AN ELECTRIC DISCHARGE

T. YU, K. TANABE[a] and J. D. WINEFORDNER*
Department of Chemistry, University of Florida, Gainesville, FL 32611 (U.S.A.)
(Received 2nd February 1987)

Summary. The afterglow of an electrical discharge under reduced pressures (1—10 torr) of nitrogen, argon, helium or a mixture of two of these is used to examine the excitation process for atomic and molecular species. Emissions of benzene and anthracene are not observed in any of the systems. The metastable species, $N_2(A)$, is shown to be responsible for excitation of mercury and nitric oxide.

In the afterglow of a dielectric discharge produced with flowing nitrogen gas, polynuclear aromatic hydrocarbons (PAHs) were excited and the luminescence signals were observed [1]. The mechanism for the excitation process was proposed to be metastable energy transfer to the sample molecules from "active nitrogen", the properties of which have been described [2]. Chemically reactive nitrogen can be created with a discharge at reduced pressure (1–10 torr) and is a result of the following processes:

$$N_2 \xrightarrow[\text{discharge}]{\text{electrical}} N_2^*(M) + N_2^*(E); N_2^*(M) + A \rightarrow A^* + N_2; A^* \rightarrow A + h\nu$$

where A is an analyte molecule and A* is a metastable state of the molecule. Metastable nitrogen molecules $N_2^*(M)$ and other excited states $N_2^*(E)$ are formed in the dielectric discharge. Only $N_2^*(M)$ survives in the downstream in the flow system to transfer energy to analyte molecules through collisions. The analytes are then excited and later relaxed by luminescence (fluorescence or phosphorescence); $N_2(A\,^3\Sigma_u^+)$ is believed to be the metastable state involved in the excitation.

The discharge cell was constructed with two concentric glass tubes. A high voltage (2000—7000 V) was applied between the inner tube which was filled with saturated salt solution and the outer surface of the outer concentric tube which was wrapped with conducting tape and grounded. Benzene and various PAHs were introduced into the afterglow downstream of the discharge cell with two light traps inserted between the cell and the sample port. Molecular emission spectra of parent molecules were obtained [1] rather than

[a]Present address: Department of Community Environmental Sciences, National Institute of Public Health, 4-6-1, Shirokanedai, Minato-ku, Tokyo 108, Japan.

emission spectra of fragments like CN, C_2, CH, etc. Therefore, $N_2(A)$ seemed to be a potential excitation source for PAHs. However, two unexplained phenomena were observed after a close look at new experimental results. The nitrogen afterglow generated by the concentric glass-tube electrodes could be deflected by a magnetic bar (also reported by Kishman et al. [3]). Metal parts such as metal fittings always attracted the afterglow and discharge sparks were sometimes observed at metal parts. Charged particles should not be found downstream if only $N_2(A)$ molecules were present. The second question arose from the dominant background of the nitrogen second-positive emission in the afterglow [4]. The formation of $N_2(A)$ was believed to result from the consecutive decay of excited nitrogen from higher excited states [5]. The following two steps were responsible for the second-positive and first-positive radiation, respectively:

$$N_2(C^3\Pi_u) \rightarrow N_2(B^3\Pi_g) + h\nu_2;\ N_2(B^3\Pi_g) \rightarrow N_2(A^3\Sigma_u^+) + h\nu_1$$

The partial energy diagram [6] for nitrogen is shown in Fig. 1. N_2(C) can be formed either by electron impact or by recombination of N_2(A):

$$N_2(A^3\Sigma_u^+) + N_2(A^3\Sigma_u^+) \rightarrow N_2(X^1\Sigma_g^+) + N_2(C^3\Pi_u)$$

where $N_2(X^1\Sigma_g^+)$ is the nitrogen ground state. It was very unlikely that the above quantum-mechanically forbidden reaction [7] was responsible for the very intense, second-positive emission. With the existence of many other excited-state species in the reaction cell of the dielectric system, a question remained whether $N_2(A)$ molecules were the only species involved in PAH excitation. The present study was conducted to reevaluate the previously proposed mechanism. A technique developed by Stedman, Setser and co-workers [7—10] was adopted to separate nitrogen metastables from other

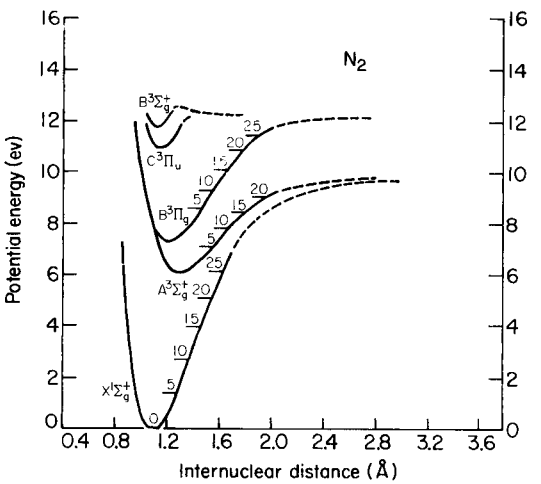

Fig. 1. Energy diagram of N_2 showing selected energy levels of interest, taken from [6].

species in a flowing system where metastable $N_2(A)$ molecules were generated by interaction of metastable argon atoms with molecular nitrogen. Through energy transfer, nitrogen molecules were excited to form $N_2(C)$ which later de-excited by the above two steps to produce $N_2(A)$. With this source of $N_2(A)$, it was possible to examine the reaction between pure $N_2(A)$ and the analytes of interest.

Experimental

The technique to obtain an essentially pure $N_2(A)$ source with minimal nitrogen atoms has been described in detail by Stedman, Setser and co-workers [7—10]. Some modifications were needed for the present experiments. The reaction cell is shown in Fig. 2. An electric discharge was produced between two hollow copper electrodes. The argon metastables formed in the discharge cell then passed a light trap and intersected with nitrogen gas at the mixing chamber where energy-transfer generated $N_2(C)$. A sample port was placed in the mixing zone and an observation quartz window (first window in Fig. 2) was inserted to monitor reactions by means of emitting species. Any metastable nitrogen $N_2(A)$ traveled downstream to reach a second sample port near another light trap and emitted radiation was detected through the second quartz window.

The system was evacuated by a vacuum pump (Stokes Microvac, Model 900-149-11) with a capacity of 2265 l min^{-1} which gave pressures of ca. 2 torr with a flow rate of ca. 20 ml s^{-1}. The electrodes were made of copper sheet (0.1 mm thick) and were operated at a voltage of 450 V DC. The DC voltage was supplied by a hollow-cathode lamp power supply (Heath, Model EU-703-62).

Argon and nitrogen were purified by passing the gases over heated copper turnings and then through two traps packed with glass wool cooled by liquid

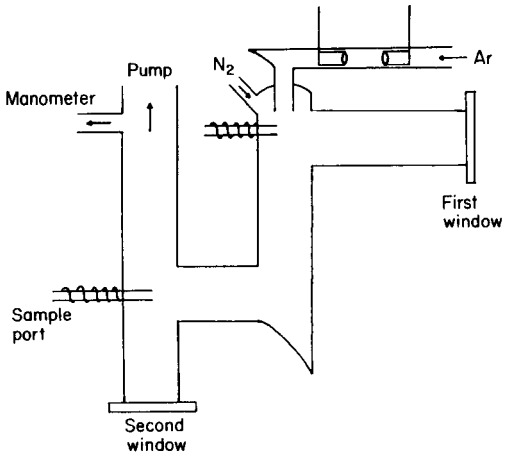

Fig. 2. Reaction cell of the apparatus.

nitrogen to remove moisture and other organic material. A trap cooled with dry ice was placed between the vacuum pump and the detection cell to minimize contamination of the sample vapor and the detection cell by pump oil. The sample port was connected directly to the gas cylinder when nitric oxide was needed. Otherwise, it was connected to a 10-ml round flask containing the analyte of interest. For example, to introduce anthracene, the sample flask was heated to ca. 150°C with a heating mantle. In addition, heating tape was required to heat the sample tube to keep the sample in the gas phase. Swagelok fittings were used at the high-pressure side of the system, while ultratorr Cajon fittings were used at the low-pressure side.

All measurements were made with a 0.35-m Heath scanning spectrometer equipped with an RCA 1P28A photomultiplier tube (PMT). The signal current from the PMT was converted to voltage and then plotted on a strip-chart recorder. The monochromator was placed directly in front of the quartz window without an entrance lens. The pressure in the cell was monitored by a Baratron 321A pressure gauge (MKS Instruments).

The reagents used were as follows: helium (Matheson, high-purity grade, >99.995%), argon (Matheson, ultra-high-pure grade, >99.999%), nitrogen (Matheson, ultra-high-pure grade, >99.999%), nitric oxide (Matheson, C.P. grade, >99.0%), benzene (Fisher Scientific, certified ACS), and anthracene (Aldrich Chemical Company, 99.9%). The flowing discharge gases were purified as described above; other chemicals were used directly as received.

Results and discussion

In the initial studies, only one observation window was used to investigate the reaction between $N_2(A)$ and the analyte vapor. Because negative results were obtained for the excitation of benzene and anthracene by $N_2(A)$ (described below in the argon/nitrogen experiment), another window (first observation window in Fig. 2) was introduced to examine the possible reactions caused by other excited states such as $N_2(C)$ and $N_2(B)$.

By using helium or argon in the concentric glass-tubing dielectric discharge system, molecular emissions of benzene and anthracene were also observed, and so the evaluation of helium and argon metastables was required. Pure helium and argon gases were evaluated with the same apparatus and under similar conditions as the argon/nitrogen system described below.

Argon/nitrogen system. The Vegard-Kaplan band, i.e., radiational decay of $N_2(A)$ [5], which was barely detected by Stedman, Setser and co-workers was not detected in this system. The reason was probably a result of the small radiational probability compared with the collisional decay probability, with the presence of quenchers such as oxygen in the system. However, the existence of $N_2(A)$ has been indirectly determined by the reaction of $N_2(A)$ with nitric oxide producing a fairly intense γ-band; the pertinent reaction is $N_2(A) + NO(X) \rightarrow N_2(X) + NO(A)$, and the γ-band is produced by the radiational decay of $NO(A)$. Therefore, the system in Fig. 2 was optimized by monitoring the NO band at the second observation zone. A total pressure of

2.5—3.0 torr was found to be optimal. The intense nitrogen second-positive band was detected as expected at the first observation window. To obtain pure $N_2(A)$, a large fraction of nitrogen was admitted to quench argon metastables.

As mentioned earlier, other excited-state nitrogen molecules were also of interest. Because of the short lifetimes of $N_2(C)$ and $N_2(B)$, samples were introduced at the location where these excited species had maximum concentrations. Because a flame-like nitrogen second-positive emission was observed even under full room light, it facilitated finding the right location to introduce samples.

Attempts were made to measure spectral lines/bands of 253.7 nm for mercury, 247.1 nm for nitric oxide, 274.1 nm for benzene and 399 nm for anthracene at both windows (see Fig. 2) in the argon/nitrogen system as well as other gas systems. Both mercury and nitric oxide always gave detectable emission while benzene and anthracene emission could not be detected, as shown in Table 1.

The excitation process producing the NO γ-band and mercury emission at the second window involved collisions with only $N_2(A)$ molecules. This provided the opportunity to investigate the reaction between the analyte molecules and pure $N_2(A)$ molecules that mixed with other excited species in an electric discharge. At the first observation site, a mixture of $N_2(C^3\Pi_g)$, $N_2(B^3\Pi_g)$ and other possible minor excited states co-existed. The contribution to excitation from these states could not be evaluated separately. However, negative results were obtained at both windows for benzene and anthracene under all experimental conditions. Therefore, neither $N_2(A)$, nor $N_2(C)$ and $N_2(B)$, excited benzene and anthracene.

Nitrogen system. Stedman, Setser and co-workers [7—10] used the argon/nitrogen system to generate pure $N_2(A)$ because argon metastable states, $^3P_0$ and $^3P_2$, carried energies sufficient to excite $N_2(C)$ but low enough not to excite higher nitrogen metastable states such as $N_2(E^3\Sigma_g^+)$ (see energy diagram in Fig. 1). In the study described above, pure $N_2(A)$ was shown not

TABLE 1

Responses of nitric oxide, mercury, benzene, and anthracene to Ar/N_2, N_2, Ar and He systems

	Ar^*/N_2		N_2		Ar		He
	1[a]	2[a]	1	2	1	2	1
Nitric oxide	++[b]	++	+++	+++	+	+	–
Mercury	++	++	+++	+++	+	+	–
Benzene	–[b]	–	–	–	–	–	–
Anthracene	–	–	–	–	–	–	–

[a]Observation windows, first and second. [b](+) positive response; (++, +++) higher intensities; (—) no response.

to be involved in the excitation of benzene and anthracene. In order to obtain higher concentrations of $N_2(A)$, nitrogen gas was excited directly in the discharge. In this case, $N_2(A)$ as well as other possible higher energy metastables co-existed in the afterglow.

Considerable intensity of the NO γ-bands were detected as radiational background. The NO emission band was formed because of the presence of oxygen as impurity in the active nitrogen; a weak second-positive emission of nitrogen resulted from energy pooling of $N_2(A)$. With the introduction of nitric oxide, the NO γ-band was 10-fold higher than the background radiation and almost 100-fold higher than that observed in the argon + nitrogen system. Large mercury signals were further indicative of the high concentration of $N_2(A)$ in the system. It was not surprising to see higher signals of nitric oxide and mercury at both windows than those with the argon/nitrogen system. Even though higher concentrations of $N_2(A)$ existed in this system, negative results for benzene and anthracene were still obtained.

Argon system. With pure argon gas, a weak second-positive band of nitrogen appeared in the background radiation. The nitrogen impurity could have come from either the argon gas cylinder or air leaks in the system. It was impossible to separate argon metastables from nitrogen molecules. At the first window, nitric oxide and mercury emissions were detected, while there was no emission from benzene and anthracene. At the second window, the same results were obtained. According to the study of Prince et al. [11], there was no emission from nitric oxide in the presence of argon metastables. The present positive results could have occurred because of the presence of the excited nitrogen which transferred energy to nitric oxide and mercury. At any rate, benzene and anthracene did not emit in the presence of argon metastables.

Helium system. Helium gas was introduced into the discharge tube without mixing with other gases. No emission for any of the four species was observed at the first window. Collins and Robertson [12] detected weak β- and γ-bands when nitric oxide was directed into the helium afterglow of a microwave discharge. The reason for the negative results of these studies is not clear. It could have been a result of the low-power electric discharge which did not generate a high enough number density of helium metastables for excitation of nitric oxide.

Conclusions

The major aim of this work was to examine the role of $N_2(A)$ in the excitation of benzene and its derivatives. From the results on the four model analytes (mercury, nitric oxide, benzene, and anthracene), it was concluded that $N_2(A)$ was involved in the excitation of mercury and nitric oxide but not in the excitation of anthracene and benzene. However, in a dielectric discharge with nitrogen, argon or helium as medium gases, benzene and anthracene were excited and emitted radiationally. Therefore the excitation of these species in the dielectric discharge was assumed to result from collisions with electrons, a common energetic species in all these systems.

In the dielectric glass electrode system [1], electrons and other charged particles were not confined between the two electrodes. When a high voltage was applied to the inner glass tube, an electric current flowed through different routes to ground, such as to the outer grounded glass tube, metal fittings and the vacuum gauge, etc. Therefore, a sufficient electron number density existed in the "afterglow" to excite the nitrogen second-positive emission as well as the PAHs [1].

This research was supplied by grant no. DOE-DE-A505-780 R06002.

REFERENCES

1 H. A. Jurgensen, T. Yu and J. D. Winefordner, Can. J. Spectrosc., 29 (1984) 113.
2 A. N. Wright and C. A. Winkler, Active Nitrogen, Academic, New York, 1968.
3 J. Kishman, E. Barish and R. O. Allen, Appl. Spectrosc., 37 (1983) 545.
4 W. B. Dodge and R. O. Allen, Anal. Chem., 53 (1981) 1279.
5 D. H. Stedman and D. W. Setser, Chem. Phys. Lett., 2 (1968) 542.
6 F. R. Gilmore, J. Quant. Spectrosc. Radiat. Transfer, 5 (1965) 369.
7 D. H. Stedman and D. W. Setser, J. Chem. Phys., 50 (1969) 2256.
8 D. H. Stedman, J. A. Meyer and D. W. Setser, J. Am. Chem. Soc., 90 (1968) 6856.
9 D. W. Setser, J. A. Coxon and D. H. Stedman, J. Chem. Phys., 53 (1970) 1004.
10 J. A. Meyer, D. H. Klosterboer and D. W. Setser, J. Chem. Phys., 55 (1971) 2084.
11 J. F. Prince, C. B. Collins and W. W. Robertson, J. Chem. Phys., 40 (1964) 2619.
12 C. B. Collins and W. W. Robertson, J. Chem. Phys., 40 (1964) 701.

Analytica Chimica Acta, 201 (1987) 325—329
Elsevier Science Publishers B.V., Amsterdam — Printed in The Netherlands

Short Communication

CONTINUOUS FLOW EXTRACTION OF INDIUM WITH BIS(2-ETHYLHEXYL)PHOSPHORIC ACID IN 4-METHYLPENTANE-2-ONE COUPLED ON-LINE WITH FLAME ATOMIC ABSORPTION SPECTROMETRY

JORDI COELLO

Departament de Quimica, Diviso Quimica Analitica, Universitat Autonoma de Barcelona, 08193 Bellaterra (Spain)

LARS-GÖRAN DANIELSSON and SANTIAGO HERNANDEZ-CASSOU[a]

Department of Analytical Chemistry, Royal Institute of Technology, S-100 44 Stockholm (Sweden)

(Received 30th April 1987)

Summary. Extraction in liquid-liquid segmented flow is used for preconcentration of indium from dilute nitric acid solutions into bis(2-ethylhexyl)phosphoric acid dissolved in 4-methylpentane-2-one. The extraction setup is coupled on-line with flame spectrometry to give a fully mechanized system. The detection limit of the method is 0.03 mg l^{-1}, the calibration plot is linear up to 1.75 mg l^{-1}. Repeatability is 1.5% RSD measured at 1 mg l^{-1}. Sample throughput is 60 h^{-1}.

Indium found its main technical use as a corrosion inhibitor until its more recent applications in microelectronics, nuclear technology and metallurgy. In most cases, indium is present in trace amounts so that very sensitive methods, often involving a preconcentration step, are needed for its determination. For metals, such demands are often met by a combination of liquid-liquid extraction and atomic absorption spectrometry (a.a.s.) [1]. This approach has been chosen in several papers concerning the determination of indium [2—7]. Extractions done manually are, however, generally considered to be very tedious and for trace determinations, they can suffer from contamination. Extraction in liquid-liquid segmented flow coupled on-line with flame a.a.s. is, because of its simplicity, versatility and modest cost, an interesting alternative to the manual methods [8—13].

Bis(2-ethylhexyl)phosphoric acid (HDEHP) is a well-known reagent forming extractable complexes with many trivalent metals. A special advantage of HDEHP is that extractions can be done from solutions of low pH, simplifying the work-up of samples brought into solution with concentrated acid. This reagent has been used for the extraction of indium [7, 14, 15] and here the earlier methods are adapted to a liquid-liquid segmented flow system coupled on-line with flame a.a.s.

[a]Permanent address: Department of Analytical Chemistry, University of Barcelona, 08028 Barcelona, Spain.

0003-2670/87/$03.50

Experimental

Reagents. The stock indium solution was prepared by dissolving the metal (99.99% pure) in a little 7 M nitric acid, evaporating to dryness and dissolving the residue in 0.1 M nitric acid. The solution was standardized by titration with EDTA and 1-(1-pyridylazo)-2-naphthol indicator [16]. Working solutions were prepared by suitable dilution with 0.1 M HNO_3. Bis(2-ethylhexyl)phosphoric acid (HDEHP; general-purpose reagent, BDH Chemicals GPR, and 4-methylpentane-2-one, (MIBK; analytical grade, Merck) were used as received. All other chemicals were of analytical grade.

Apparatus. A Varian 1475 atomic absorption spectrometer was used in the single-beam mode. The instrument was equipped with an adjustable nebulizer; an indium hollow-cathode lamp was used as light source. Instrumental settings were as recommended by the manufacturer except for the fuel flow. This flow was reduced as much as possible in order to avoid too fuel-rich conditions upon introduction of the extract into the flame.

Flow-system. The flow system (Fig. 1) comprised two peristaltic pumps (FIA-08, Bifok, Sweden) and a variable-volume injector (FIA-05, Bifok). Standard tygon pump tubes were used and the organic solvent was delivered from a displacement bottle (Tecator, Sweden).

The sample is pumped into the system and merges with an organic phase containing the extractant in a T-piece segmentor (SG). Extraction takes place during passage through 3 m of 0.7-mm i.d. teflon tubing (E). The two phases are separated with the aid of a 0.2-μm teflon membrane (Fluoropore; Millipore) placed on a rigid support in a phase separator (SE) of the type previously described [17]. In this case, the volumes of the two cylindrical cavities were 42 μl and 8.5 μl for the segmented and unsegmented sides, respectively. The organic phase is fed to the injector (I). When enough time

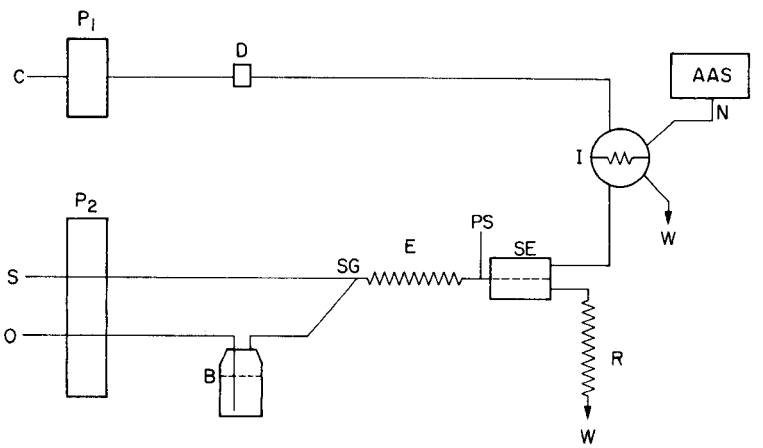

Fig. 1. Flow system: P_1 and P_2 peristaltic pumps; C, water carrier to nebulizer; D, pulse damper; S, sample; O, water feed to displacement bottle (B); SG, segmentor; E, extraction coil; PS, pressure sensor; SE, phase separator; R, restrictor; I, injection valve; N, nebulizer; W, waste.

has passed to wash out the previous sample, the injector drive is triggered and the amount of extract collected in the injector loop is transferred to the flame at the rate of the carrier stream (Q_C). For all connections 0.7-mm i.d. teflon tubing was used, save the length between the separator and the injector which was of 0.35 mm i.d. Details about the use of the pressure sensor (PS) and about the restrictor (R) can be found in a previous paper [17].

Results and discussion

Preliminary studies. The parameters affecting the performance of the interface between the flow system and the a.a.s. instrument were first studied. The extraction manifold was kept unchanged and the following parameters were varied; nebulizer aspiration rate Q_N, carrier flow rate Q_C, and the volume of extract injected V_I. The results showed that the response is strongly dependent on Q_C. This must be greater than 4 ml min^{-1} to provide adequate sensitivity and should preferably slightly exceed Q_N in order to give good repeatability. The response increased with increasing volume of extract injected for volumes smaller than about 90 μl. These results were all in agreement with those found earlier for similar systems [18—20]. Consequently, the following values were chosen and used throughout this work: Q_C = 6.6 ml min^{-1}, Q_N = 5.5 ml min^{-1}, V_I = 86 μl.

The preconcentration factor can be defined as the phase flow ratio Q_{aq}/Q_{org} provided that the extraction constant for the system used is high enough. Higher preconcentration factors yield lower detection limits as long as the stability of the system and thus the precision are not affected, but a low organic-phase flow rate gives slow sample turnover because of the time needed to fill the injector loop with an extract of the new sample. Previous experience has shown that a flow rate of organic extract of 0.3 ml min^{-1} is a good compromise between stability of the flow system and acceptable sampling frequency. A sample flow rate Q_S of 3 ml min^{-1} provides a theoretical preconcentration factor of 10. In reality, the factor will be slightly greater, owing to the solubility of MIBK in water. These flows are well within the range found suitable for the separator used [17, 21].

Extraction-coil length and reagent concentration. The effect of varying the length of the extraction coil for two reagent concentrations is shown in Fig. 2. With 0.4 M HDEHP and 1 mg l^{-1} indium, the response did not improve when the extraction-coil length was increased beyond 2 m. When a lower reagent concentration (0.1 M HDEHP) with a higher indium concentration (2 mg l^{-1}) was tested, a somewhat longer coil was needed to obtain full response.

When a 3-m extraction coil was used for extraction of solutions containing 1 and 2 mg l^{-1} indium with MIBK containing various concentrations of HDEHP, maximum response was given by the 0.1 M reagent (Fig. 3).

Characteristics of the method. A linear calibration curve was obtained for indium in the range 0—1.75 mg l^{-1} under the following conditions: Q_S = 3 ml min^{-1}, Q_{MIBK} = 0.3 ml min^{-1}, Q_N = 5.5 ml min^{-1}, Q_C = 6.6 ml min^{-1}, V_I = 86 μl

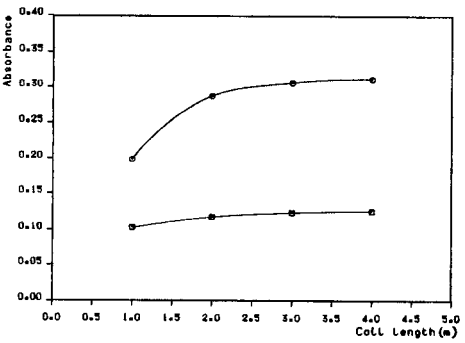

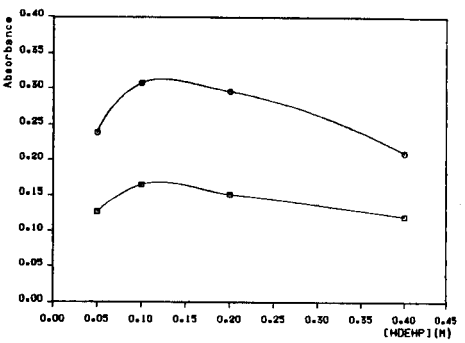

Fig. 2. Absorbance versus length of the extraction coil. Q_N = 5.5 ml min^{-1}, Q_C = 6.6 ml min^{-1}, Q_S = 3.0 ml min^{-1}, Q_{MIBK} = 0.3 ml min^{-1}, V_I = 86 μl. Indium concentration: (□) 1 mg l^{-1}, 0.4 M HDEHP; (○) 2 mg l^{-1}, 0.1 M HDEHP.

Fig. 3. Absorbance versus HDEHP concentration. For conditions see Fig. 2; coil length 3 m. Indium concentration: (□) 1 mg l^{-1}; (○) 2 mg l^{-1}.

and 0.1 M HDEHP. The equation for the straight line was $A = 0.1533\ C_{In} + 2.27 \times 10^{-3}$ (n = 12). The standard deviations for slope and intercept were 5.93×10^{-4} and 5.98×10^{-4}, respectively. The sensitivity of the method was thus 6.5 mg l^{-1} or, given as the concentration corresponding to 1% absorption, 0.03 mg l^{-1}. The detection limit, calculated as the concentration giving a signal three times the standard deviation of 31 measurements on a standard 1 mg l^{-1} indium solution was 0.03 mg l^{-1}. A relative standard deviation of 1.49% was found when 10 solutions containing 1 mg l^{-1} indium were injected. The sampling frequency was 60 h^{-1}.

Effect of foreign ions. The influence of foreign ions was tested at an indium concentration of 1 mg ml^{-1}. The cations, Ag, Al, Cd, Co, Cu, Cr(III), Fe(III), Hg(II), La, Mn(II), Ni, Pb, Zn and Bi were added as their nitrate salts while Tl(I) was added as its carbonate. The concentration used was 1 g l^{-1} in all cases except for bismuth which was tested only at the 100 mg l^{-1} level. Anions were added as their sodium salts and the concentrations tested were 0.1—0.001 M. All solutions were made 0.1 M in nitric acid. The influence of foreign cations was in all cases less than 3%. Fluoride and iodide did not affect the results in concentrations up to 0.1 M. Perchlorate and thiocyanate gave a slight positive interference in concentrations above 0.01 M. Chloride, bromide and sulphate gave severe negative interference in concentrations above 0.001 M.

Determination of indium in a synthetic sample. A synthetic sample was prepared with an indium concentration of 1 mg l^{-1} (8.71×10^{-6} M) in 0.1 M nitric acid. The sample was also made 0.005 M in the nitrate salts of the following cations: Ag(I), Al(III), Cd(II), Cu(II), Ni(II) and Pb(II), which are commonly present in indium alloys. The determinations were done under the conditions recommended above. The indium content was found to be 0.99 ± 0.01 mg l^{-1} (n = 10).

S. H-C. thanks the Swedish Institute for providing financial support for his visit to Stockholm, and also Prof. Folke Ingman and colleagues for their pleasant cooperation.

REFERENCES

1 M. S. Cresser, Solvent Extraction in Flame Spectroscopic Analysis, Butterworths, London, 1978.
2 O. M. Talapova and I. S. Levin, Izv. Sib. Otd. Akad. Nauk SSSR, Ser. Khim. Nauk, 2 (1981) 60.
3 E. Sekiguchi, K. Yamamoto, K. Takano, M. Tutumi, K. Uehara, T. Ohno and S. Tasaka, Sangyo Igaku, 25 (1983) 415; Chem. Abstr., 100: 48039 m.
4 W. H. Evans, P. J. Brooke and B. E. Lucas, Anal. Chim. Acta, 148 (1983) 203.
5 Shan Xiao-Quan, Ni Zhe-Ming and Yuan Zhi-Neng, Anal. Chim. Acta, 171 (1985) 269.
6 A. E. Hubert and H. H. Chao, Talanta, 32 (1985) 568.
7 J. Coello, J. Genè and H. Iturriaga, Mikrochim. Acta, Part I, (1986) 221.
8 L. Nord and B. Karlberg, Anal. Chim. Acta, 145 (1983) 151.
9 K. Ogata, S. Tanabe and T. Imari, Chem. Pharm. Bull., 31 (1983) 1419.
10 K. Bäckström, L.-G. Danielsson and L. Nord, Analyst, 109 (1984) 323.
11 M. Bengtsson and G. Johansson, Anal. Chim. Acta, 158 (1984) 147.
12 M. Gallego, M. Silva and M. Valcárcel, Anal. Chem., 58 (1986) 2285.
13 M. Gallego, M. Silva and M. Valcárcel, Fresenius' Z. Anal. Chem., 323 (1986) 50.
14 J. Coello and H. Iturriaga, Analusis, in press.
15 T. Sato, J. Inorg. Nucl. Chem., 37 (1975) 1485.
16 A. I. Busev, V. G. Tiptsova and V. M. Ivanov, Handbook of the Analytical Chemistry of Rare Elements, Ann Arbor-Humphrey Science Publishers, London, 1970, p. 262.
17 K. Bäckström, L.-G. Danielsson and L. Nord, Anal. Chim. Acta, 169 (1985) 43.
18 S. Olsen, L. C. R. Pessenda, J. Růžička and E. H. Hansen, Analyst, 108 (1983) 905.
19 M. W. Brown and J. Růžička, Analyst, 109 (1984) 1091.
20 A. S. Attiyat and G. D. Christian, Anal. Chem., 56 (1984) 439.
21 K. Bäckström, L.-G. Danielsson and L. Nord, Anal. Chim. Acta, 187 (1986) 255.

Analytica Chimica Acta, 201 (1987) 331—334
Elsevier Science Publishers B.V., Amsterdam — Printed in The Netherlands

Short Communication

ACCURATE DETERMINATION OF SELENIUM IN BIOLOGICAL MATERIALS WITHOUT PERCHLORIC ACID FOR DIGESTION

VALDA W. BUNKER and H. TREVOR DELVES*

Department of Chemical Pathology and Human Metabolism, Level D, South Laboratory Block, Southampton General Hospital, Tremona Road, Southampton S09 4XY (Great Britain)

(Received 13th May 1987)

Summary. Selenium (10—80 $\mu g\ kg^{-1}$) is determined by hydride-generation atomic absorption spectrometry in mixed diet, faecal and urine samples and in standard reference materials (bovine liver, rice flour, wheat flour and horse kidney) after two digestion procedures. No difference was found in digestion efficiency between a nitric/sulphuric acid mixture and a nitric/sulphuric/perchloric acid mixture. The results suggest that the digestion of most biological materials for the determination of selenium does not require the use of perchloric acid.

Accurate determination of selenium in biological materials by use of hydride-generation atomic absorption spectrometry (AAS) requires complete decomposition of the organic matrix and conversion of organoselenium to selenium(IV). It is claimed that some compounds, particularly the trimethylselenonium cation, which may be a major urinary metabolite of selenium, are resistant to acid digestion unless perchloric acid is included in the mixture [1, 2]. It is not surprising, therefore, that most digestion procedures for the determination of selenium in biological materials involve the use of perchloric acid despite the attendant potential hazards and the need for special venting facilities.

Recent work has shown that alternative digestion mixtures such as nitric acid/phosphoric acid/hydrogen peroxide are suitable for the digestion of food samples, [3], urine [4] and blood plasma [5] prior to selenium determination by hydride-generation AAS. Work done in this laboratory has shown a nitric/sulphuric acid mixture to be effective for the determination of selenium in plasma and whole blood [6]. In view of these observations, the efficiency of two acid mixtures (with and without perchloric acid) are compared here for the digestion of biological samples prior to hydride-generation AAS. It is shown that perchloric acid is not essential for complete oxidation of many biological samples.

Experimental

Reagents and apparatus. All chemicals (unless stated otherwise) were of BDH AnalaR grade. Selenous acid standard solution (1 mg ml^{-1}) was diluted to give a range of working standards (0, 50, 100, 150, 200, 250 ng ml^{-1}).

0003-2670/87/$03.50

Standard reference materials Bovine Liver (No. 1577a), Rice Flour (No. 1568) and Wheat Flour (No. 1567) were obtained from the National Bureau of Standards (Washington, DC). Horse kidney (No. H-8) was obtained from International Atomic Energy Agency (Vienna).

Sample digestion was done in standard laboratory borosilicate test tubes and Kjeldahl digestion tubes (Tecator) which were heated in a Techne Dri-block heater (FSA, Loughborough) and a Tecator Kjeldahl 1007 digestor, respectively. A Perkin-Elmer Model 2380 atomic absorption spectrometer and MHS-20 hydride-generation system were used as previously described [6].

Procedures. Six different samples of homogenates of diet and faecal samples and 12 different 24-h urine samples were analysed by hydride-generation AAS following one of two different ashing procedures. For nitric/sulphuric acid digestion, the modified techniques of Lloyd et al. [6] and Fairhurst et al. [7] were used. Samples (5 g of diet or faecal homogenate, and 7.5 g of urine) or standard reference materials were accurately weighed into 25-ml glass cylinders and ca. 15 ml of a (1 + 1) nitric acid (16 M)/ sulphuric acid (18 M) mixture was added. When the initial reaction had subsided, samples were gently mixed and left for a minimum of 16 h to predigest. Samples were diluted to 25 ml, warmed slightly to dissolve the fat, transferred to a beaker and mixed. Three 1-ml aliquots of this homogenate were transferred to borosilicate glass tubes and 2 ml of the acid mixture was added. The tubes were heated in a block at 140—150°C for 3 h and cooled, and 2 ml of 6 M hydrochloric acid was added. The tubes were heated at 95°C for 30 min and cooled. The contents were transferred to reaction vessels, diluted to 20 ml, and mixed with 200 μl of a 1% (v/v) antifoam emulsion DB-110A (Dow Corning). Selenium was quantified in this solution as described previously [6].

A calibration graph was prepared by transferring 100 μl of standards to test tubes and adding 3 ml of the nitric/sulphuric acid mixture. Thereafter the tubes were treated as in the sample digestion procedure.

For perchloric acid digestion, essentially the recommended scheme for wet oxidation of urine proposed by Janghorbani et al. [1] was followed. Samples of urine (7.5 g), faecal (5 g) or diet homogenate (5 g) or standard reference material were accurately weighed into Kjeldahl digestion tubes and 5 ml of 16 M nitric acid was added. The tubes were placed in a digestion block fitted with an exhaust system. The temperature was slowly (20 min) raised to 140°C and maintained for 20 min. The tubes were cooled and 2.5 ml of 18 M sulphuric acid and 1 ml of 11.6 M perchloric acid were added. The temperature was slowly (15 min) raised to 140°C, maintained for 15 min, slowly (15 min) increased to 205°C and kept at this level until the contents of the tubes had decreased in volume to ca. 3.5 ml and white fumes of perchloric acid were evident. The tubes were cooled, 100 ml of 5 M hydrochloric acid was added and the mixture was heated at 95°C for 30 min. After cooling, the tube contents were diluted to 200 ml and 20-ml aliquots taken for selenium measurements (in triplicate).

TABLE 1

Comparison of acid digestion mixtures for the determination of selenium in standard reference materials

Sample	Selenium concentration ($\mu g\ g^{-1}$ dry weight)		
	Assigned value[a]	Values obtained[b]	
		HNO_3/H_2SO_4 digestion	$HNO_3/H_2SO_4/HClO_4$ digestion
Bovine liver (1577a)	0.71 ± 0.07	0.721 ± 0.017(10)	0.718 ± 0.025(10)
Wheat flour (1567)	1.1 ± 0.2	1.00 ± 0(2)	0.94 ± 0.02(2)
Rice flour (1568)	0.4 ± 0.1	0.36 ± 0.01(2)	0.39 ± 0(2)
AEA horse kidney (H-8)	4.67 ± 0.3	4.70 ± 0.14(2)	4.72 ± 0.18(2)

[a]Mean ± estimated uncertainty. [b]Mean ± standard deviation with number of determinations in parentheses.

A calibration graph was prepared by adding 1-ml portions of each standard to the digestion tubes and proceeding as above.

Results and discussion

Table 1 shows that the agreement between the certified value of the reference material and the results found was excellent for both digestion procedures. Good precision of both methods was demonstrated by the replicate analysis of 10 samples of bovine liver. The within-batch precision was 2.4% for the nitric/sulphuric acid digestion and 3.5% for that with

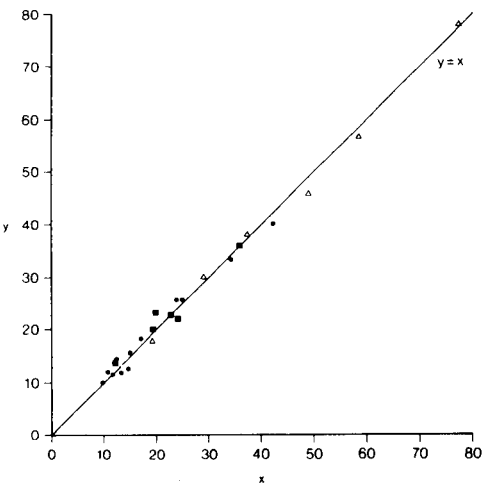

Fig. 1. Comparison of selenium concentrations ($\mu g\ kg^{-1}$) found by hydride-generation AAS after digestion with $HNO_3/H_2SO_4/HClO_4(x)$ and $HNO_3/H_2SO_4(y)$. Samples: (■) diet; (△) faeces; (●) urine. The line of equality ($y = x$) is shown.

perchloric acid added. Figure 1 shows the results obtained by the two digestion methods for diet, faecal and urine samples. The regression equation is $y = 0.966x + 1.093$, where y corresponds to the nitric/sulphuric acid digestion and x to the nitric/sulphuric/perchloric acid digestion. The correlation coefficient was 0.996.

This study has shown that a mixture of nitric and sulphuric acids is suitable for the digestion of composite diet, faecal and urine samples and the specified standard reference materials. Earlier work from this laboratory has also shown nitric/sulphuric acid digestion to be acceptable for blood, plasma [6] and heart tissue [7]. This list, although not exhaustive, is sufficiently comprehensive to indicate that digestion of most biological matrices does not require the use of perchloric acid.

REFERENCES

1 M. Janghorbani, B. T. G. Ting, A. Nahapetian and V. R. Young, Anal. Chem., 54 (1982) 1188.
2 J. Neve, M. Hanocq, L. Molle and G. Lefebvre, Analyst, 107 (1982) 934.
3 D. C. Reamer and C. Veillon, Anal. Chem., 53 (1981) 1192.
4 D. C. Reamer and C. Veillon, J. Nutr., 113 (1983) 786.
5 D. C. Reamer and C. Veillon, Anal. Chem., 55 (1983) 1605.
6 B. Lloyd, P. Holt and H. T. Delves, Analyst, 107 (1982) 786.
7 J. Fairhurst, B. Lloyd and H. T. Delves, Anal. Chim. Acta, 197 (1987) 97.

Analytica Chimica Acta, 201 (1987) 335—338
Elsevier Science Publishers, B.V., Amsterdam — Printed in The Netherlands

Short Communication

RAPID SPECTROFLUORIMETRIC DETERMINATION OF PLASMA SALICYLATE WITH EDTA AND TERBIUM

M. P. BAILEY and B. F. ROCKS*

Biochemistry Department, Royal Sussex County Hospital, Eastern Road, Brighton BN2 5BE (Great Britain)

C. RILEY

Centre for Medical Research, University of Sussex, Falmer, Sussex BN1 9RF (Great Britain)

(Received 19th February 1987)

Summary. A rapid single-reagent spectrofluorimetric assay for salicylate in human blood plasma is reported. The method is based on ternary complex formation with terbium and EDTA in alkaline solution; it requires only 10 μl of plasma, and protein precipitation is not necessary. Within-assay relative standard deviations were better than 2.5%, and correlation with the Trinder method was excellent. The procedure is particularly suited for emergency use in cases of suspected aspirin poisoning.

A simple rapid method for the determination of salicylate in blood plasma is required in cases of accidental or suicidal overdose with aspirin. Determination of salicylate is also useful in monitoring blood concentrations in patients on long-term aspirin therapy. Therapeutic concentrations are usually below 200 mg l^{-1} while, above 300 mg l^{-1}, symptoms of toxicity appear. Concentrations of salicylate in plasma exceeding 600 mg l^{-1} are usually lethal.

Techniques described for the assay of salicylate include fluorimetry of plasma extracts [1], liquid chromatography [2], enzymatic methods [3], and immunoassay [4]. By far the most commonly used method, however, is the colorimetric procedure of Trinder [5], which is based on the use of a reagent containing iron(III) nitrate, mercury(II) chloride and hydrochloric acid, which precipitates the proteins and simultaneously reacts with salicylate to produce a purple solution. After centrifugation, the absorbance of the supernatant liquid, which contains the soluble iron(III)/salicylate complex, is measured at 540 nm. Unfortunately, this simple method suffers from interference by a number of drugs and metabolites which give colour reactions similar to that for salicylate [6, 7].

A fluorescent ternary complex of terbium with ethylenediaminetetraacetic acid (EDTA) and sulphosalicylic acid was reported by Charles and Riedel [8] in 1966. A similar fluorescent complex is formed from terbium, EDTA and salicylic acid in alkaline solution. This complex absorbs radiation at 320 nm and transfers the energy to the terbium ion, which emits a narrow-line spectrum with maxima at 488, 547 and 596 nm (see Fig. 1). In this

0003-2670/87/$03.50

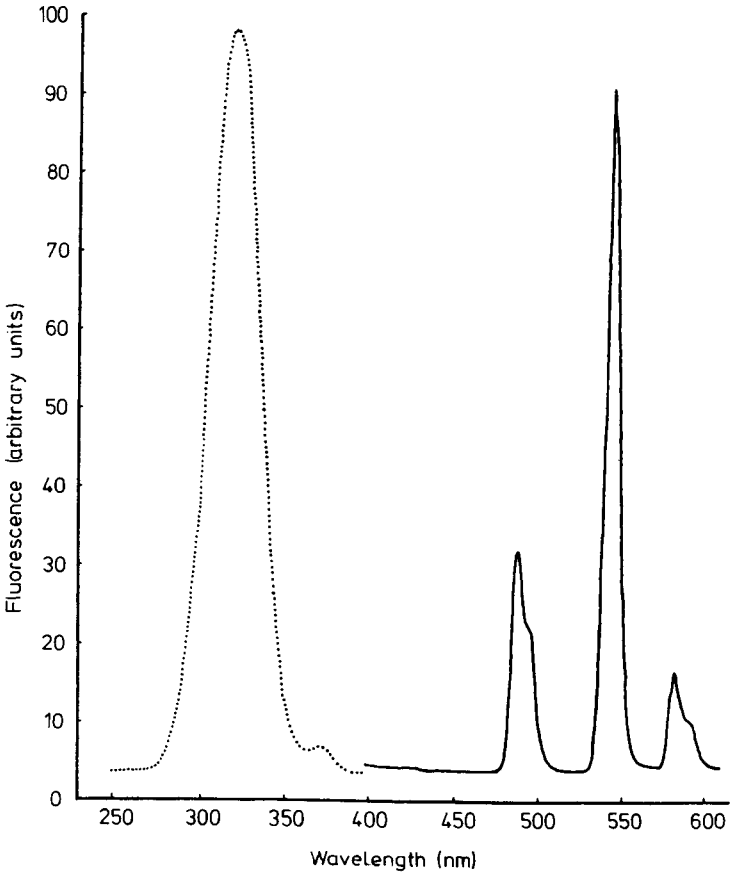

Fig. 1. Excitation (···) and emission (—) spectra of the terbium/EDTA/salicylate complex.

communication, a reagent containing terbium and EDTA at pH 12 is used to determine salicylate spectrofluorimetrically, with greater selectivity than the Trinder method.

Experimental

Reagents. Demineralized water was used throughout. Sodium salicylate and EDTA, tetrasodium salt, were laboratory reagents and sodium hydroxide was AnalaR grade (BDH). Terbium chloride was obtained from Aldrich. A stock 10 g l^{-1} salicylate standard was prepared by dissolving 292 mg of sodium salicylate in 25 ml of water. Working standards were prepared by dilution of this solution with 0.05 mol l^{-1} sodium hydroxide to give concentrations of 200, 400, 600, 800 and 1000 mg l^{-1} salicylic acid.

Alkaline terbium/EDTA reagent was prepared by dissolving 1.86 g of terbium chloride hexahydrate and 4.1 g of EDTA (tetrasodium salt) in water, adding 20 ml of 1 mol l^{-1} sodium hydroxide, and diluting to 500 ml with water. The terbium chloride and EDTA should be completely dissolved

before the sodium hydroxide is added, otherwise terbium hydroxide is precipitated and is extremely slow to redissolve. The pH of the reagent should be ca. 12.

Procedure. A 10-μl portion of standard or sample was mixed with 3.0 ml of reagent and the fluorescent intensity was measured in a 1 × 1 cm quartz cuvette with a Perkin-Elmer MPF-3L spectrofluorimeter. The instrument settings were: excitation wavelength 320 nm; excitation slitwidth 10 nm; emission wavelength 547 nm; emission slitwidth 16 nm; instrument sensitivity 1.0. The emission peak is very narrow, and is best located initially by manual scanning in the region around 545 nm.

Results and discussion

The fluorescence intensity increased linearly with salicylate concentration up to at least 1000 mg l^{-1}. The reagent blank reading was less than 0.5% of the reading given by the 1000 mg l^{-1} standard. Table 1 shows the recovery of added salicylate from 10 plasma specimens. The mean recovery, in specimens with salicylate concentrations corresponding to the upper limit of the therapeutic range, was 100.3% with a range from 98 to 103%. The within-assay relative standard deviation for 20 replicate samples from each of two pools of spiked plasma was 2.4% at 50 mg l^{-1} and 1.4% at 500 mg l^{-1}. The between-assay r.s.d. (n = 8) was 7.2% at 50 mg l^{-1} and 2.3% at 500 mg l^{-1}. The limit of detection (3σ) was 0.4 mg l^{-1}.

Comparison between the present method (X) and the Trinder colorimetric method [7] (our routine assay, Y) for 16 plasma samples received in the emergency laboratory from patients with possible salicylate poisoning, gave a linear correlation equation of $X = 1.06Y - 21$ (in mg l^{-1}) with a correlation coefficient of 0.997 (n = 16). In addition, 6 plasma samples which were reported as "not detected" by the colorimetric method showed salicylate concentrations of less than 2 mg l^{-1} by the fluorimetric method.

Several compounds tested which showed substantial interference in the Trinder method [7] showed no fluorescence with terbium and EDTA. The following concentrations (mg l^{-1}) gave less fluorescence intensity than 2 mg l^{-1}

TABLE 1

Recovery of salicylate added to plasma samples

Salicylate concentration (mg l^{-1})		Recovery (%)	Salicylate concentration (mg l^{-1})		Recovery (%)
Expected	Measured		Expected	Measured	
189	188	99.5	202	205	101.5
213	209	98.1	185	188	101.6
232	230	99.1	217	216	99.5
222	223	100.5	253	260	102.8
247	245	99.2	211	213	100.9

salicylate: acetoacetate (10 300), *p*-acetaminophenol (200), 3-hydroxytyramine (500), 3,4-dihydroxybenzylamine (1300), 3,4-dihydroxycinnamic acid (1400), 5-hydroxyindoleacetic acid (600), *p*-hydroxybenzoic acid (750), salicyluric acid (200) and gentisic acid (240). Enhancement of terbium fluorescence by catechol derivatives has been observed under conditions when the catechol is in excess, but the complete absence of interference by such compounds in the present method probably reflects their extreme instability in dilute oxygenated alkaline solution.

Moderate amounts of lipaemia, icterus or haemolysis did not interfere with the estimation of salicylate in plasma. The use of a whole blood specimen yields a solution which rapidly becomes clear, but is strongly coloured and gives a measured concentration about 30% of the true concentration. The reaction mixture in this instance had an absorbance of 0.59 at 320 nm, indicating that the underestimate was a result of absorption of the exciting radiation. By using a shorter excitation pathlength, or by measuring front-surface emission, it should be possible to use the present method to measure salicylate in whole blood.

It is worth noting that Trinder's reagent is a highly corrosive and toxic solution.

Salicylate estimation is frequently requested as an emergency out-of-hours procedure: the assay should therefore be rapid and simple. The method presented here uses a single stable reagent and requires no sample extraction, protein precipitation or blank correction. The test can be read immediately after reagent addition, and the calibration is sufficiently stable that a single graph could be used for determinations over several days. The small sample volume ensures that even paediatric specimens should present no problem.

We thank the South-East Thames Regional Health Authority for financial support under a Locally Organized Research Scheme. We also thank the staff of the emergency laboratory, and the on-call staff, for their assistance in collecting blood samples from patients with suspected aspirin overdose.

REFERENCES

1 D. O'Brien, F. A. Ibbott and D. O. Rodgerson, Laboratory Manual of Paediatric Microbiochemical Techniques, Harper and Row, New York, 1968.
2 P. J. Twitchett, A. E. P. Gorvin, A. C. Moffat, P. L. Williams and A. T. Sullivan, in P. F. Dixon, C. H. Gray, C. K. Lim and M. S. Stoll (Eds.), High Pressure Liquid Chromatography in Clinical Chemistry, Academic, London, 1976.
3 K. You and J. A. Bittikofer, Clin. Chem., 30 (1984) 1549.
4 C. L. Keegan, F. Ungemach, J. Simpson and M. Aden, Clin. Chem., 31 (1985) 942.
5 P. Trinder, Biochem. J., 57 (1954) 301.
6 K. D. Mutchie, G. H. Saunders, A. S. Hanissan and T. E. Poe, J. Rheumatol., 7 (1980) 737.
7 E. S. Kang, T. A. Todd, M. T. Capaci, K. Schwenzer and J. T. Jabbour, Clin. Chem., 29 (1983) 1012.
8 R. G. Charles and E. P. Riedel, J. Inorg. Nucl. Chem., 28 (1966) 527.

Analytica Chimica Acta, 201 (1987) 339—343
Elsevier Science Publishers B.V., Amsterdam — Printed in The Netherlands

Short Communication

FLOW-INJECTION DETERMINATION OF EUROPIUM AFTER ON-LINE REDUCTION

KAMAIL H. AL-SOWDANI[a] and ALAN TOWNSHEND*
Chemistry Department, University of Hull, Hull HU6 7RX (Great Britain)
(Received 3rd March 1987)

Summary. A zinc reductor minicolumn is used in a flow-injection system for reduction of europium(III) to europium(II). Europium(II) is indirectly determined either spectrophotometrically by oxidation with iron(III) and reaction of the iron(II) formed with 1,10-phenanthroline, or spectrofluorimetrically by reaction with cerium(IV) and measurement of the cerium(III) produced. The reductor functions efficiently at flow rates up to 1 ml min^{-1}, which allows sample injection rates up to 100 h^{-1}. Linear calibration is achieved for 10—200 and 0.5—4 $\mu g\ ml^{-1}$ with detection limits of 2.5 and 0.25 $\mu g\ ml^{-1}$, by spectrophotometry and spectrofluorimetry, respectively.

Only three lanthanide elements can exist as dipositive ions in aqueous solution. These are samarium, europium and ytterbium. Europium(III) ions are more easily reduced than samarium(III) and ytterbium(III). Reduction is possible by several methods, the commonest of which are electrolytic reduction [1] and treatment with amalgamated zinc (Jones reductor) [2, 3]. The Jones reductor offers a very selective method for determination of europium(III) in the presence of all other lanthanides because samarium, ytterbium or any other lanthanides are not reduced.

Europium(III) can be determined by iodimetric titration after treatment in a Jones reductor [4], or by collecting the solution from a Jones reductor in an excess of iron(III) chloride solution and titrating the resulting iron(II) with permanganate [5] or dichromate [3]. Europium(II) is a very strong reductant and its solution obtained from a Jones reductor is usually collected under an atmosphere of carbon dioxide to prevent oxidation by oxygen. In flow injection analysis (f.i.a.), detection occurs in a flow-through cell. A great advantage of this method is that an unstable oxidation state of a metal ion, produced after on-line reduction or oxidation, only needs to be sufficiently stable during its residence time in the flow system, which may be less than 1 min [6]. Because of the closed flow-injection system, reductants are

[a]Present address: Chemistry Department, Education College, University of Basrah, Basrah, Iraq.

0003-2670/87/$03.50

protected from external oxidants; inert gases to prevent oxidation of unstable species are unnecessary.

The use of a zinc reductor minicolumn in a flow-injection system for reduction of europium(III) to europium(II) is described in this communication. The europium(II) is indirectly detected either spectrophotometrically, by reaction with iron(III), and determination with 1,10-phenanthroline of the iron(II) formed [7], or spectrofluorimetrically, by reaction with cerium(IV) and measurement of the fluorescence of the cerium(III) produced [8].

Experimental

Reagents. All chemicals were of analytical-grade except for europium(III) nitrate pentahydrate (99.9%; Koch-Light Laboratories) and ammonium cerium(IV) nitrate (99.9%; Sigma Chemical Co.). Distilled/deionized water was used throughout. A 1000 μg ml^{-1} europium(III) solution was prepared by dissolving 0.3095 g of europium(III) nitrate pentahydrate in water. Calibration solutions were prepared by serial dilution. A 100 μg ml^{-1} cerium(IV) solution was prepared as described previously [7]. A 1,10-phenanthroline solution (1.5% w/v) was prepared by dissolving 1.5 g of 1,10-phenanthroline hydrochloride (BDH) in 100 ml of 0.1 M hydrochloric acid. Citrate buffers were prepared by mixing appropriate volumes of 0.1 M citric acid and 0.1 M sodium citrate to give the desired pH values between 3.0 and 6.2 [9]. A 0.5 M iron(III) solution was prepared by dissolving iron(III) chloride in 0.1 M hydrochloric acid.

Apparatus. The absorbance was measured at 512 nm with a Cecil CE-737 linear readout spectrophotometer in an 18-μl flow cell. The detector used for spectrofluorimetric measurements was a Perkin-Elmer model 3000 fluorescence spectrometer with a flow cell comprising a silica tube (0.8 mm i.d., 40 mm long) held vertically in the sample compartment in a rigid mount [8]. The fluorescence intensity was measured at 350 nm with excitation at 260 nm; excitation and emission slits were set at 10. The spectrometers were connected to a Tekman Labwriter TE-200 chart recorder.

The flow system for the spectrophotometric determination is shown in Fig. 1A. A 4-channel peristaltic pump (Gilson Minipuls 2) was used, and europium(III) solutions were introduced via a Rheodyne RH5020 injection valve (Anachem) with a sample loop of 100 μl. Teflon tubing (0.5 mm i.d.) was used for the manifold. The flow system for the spectrofluorimetric determination is shown in Fig. 1B. The same pump and injection valve (80-μl loop) were used. The zinc reductor minicolumns were prepared as described previously [7].

Results and discussion

Spectrophotometric determination. A 0.1 M hydrochloric acid carrier solution is used for sample reduction, but a change in pH is required subsequently for the spectrophotometric reaction. Citrate buffers have been recommended for this purpose [7] because they do not produce coloured

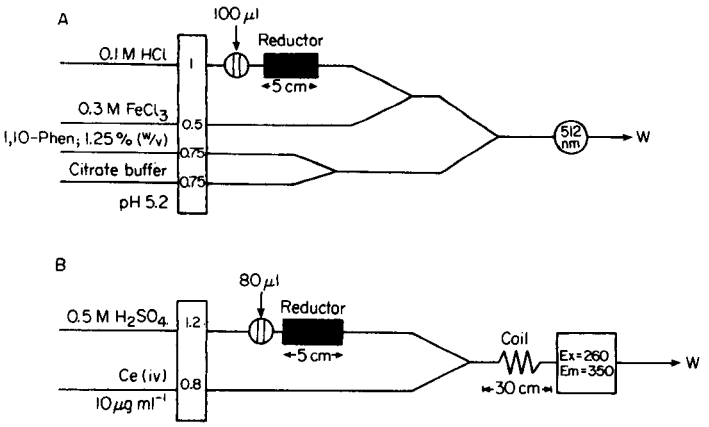

Fig. 1. Manifolds used for the indirect determination of europium: (A) spectrophotometric determination; (B) spectrofluorimetric determination (flow rates in ml min^{-1}; W = waste).

complexes with iron(II) and citrate can also mask certain potential interferences [9, 10]. The effect of citrate buffers in the pH range 3.0—6.2 [11] was therefore studied for use in the flow line as shown in Fig. 1. The europium(III) responses were the same throughout this range, therefore pH 5.2 was selected for further work.

At this pH the effect of the flow in the sample line on the europium response was studied. The results are shown in Fig. 2. Increasing the flow rate through the reductor column up to 1 ml min^{-1} was accompanied by increasing peak height. As the flow rate was increased further, the peak height decreased gradually probably indicating incomplete reduction of europium(III). Therefore 1 ml min^{-1} was used in subsequent experiments. The effects of iron(III) and 1,10-phenanthroline concentrations were also studied. Maximum response (peak height) was obtained with a 0.3 M iron(III) solution and a 1.25% 1,10-phenanthroline solution was satisfactory, as was found previously [8], so these concentrations are recommended.

A linear calibration graph was obtained for 0—200 $\mu g\ ml^{-1}$ europium under the recommended conditions (given in Fig. 1A). Typical calibration peaks are shown in Fig. 3. The resulting calibration graph has a regression coefficient of 0.999 (5 points). The detection limit (2 × noise) was 2.5 $\mu g\ ml^{-1}$ and the relative standard deviation (r.s.d.) for 11 replicate determinations of 50 $\mu g\ ml^{-1}$ europium(III) was 1.56%. The residence time was 15 s and the sample throughput could be up to 100 h^{-1}.

Many metals (e.g., copper(II), cobalt(II) and nickel [12, 13]) are known to affect the iron(II) absorbance by competing with iron(II) for 1,10-phenanthroline. Faizullah and Townshend [7] reported that the interferences of such metals can be eliminated by using citrate buffer as masking agent; they also reported that molybdate and vanadium interfered seriously. In this work, only the effects of the possibly reducible samarium(III) and

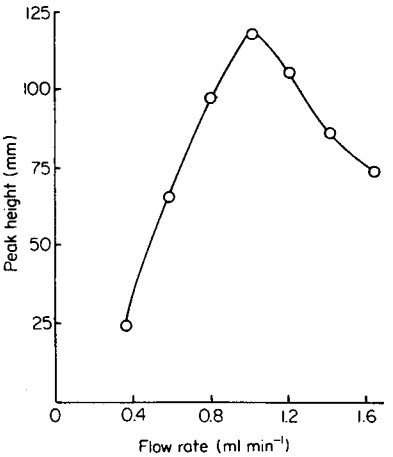

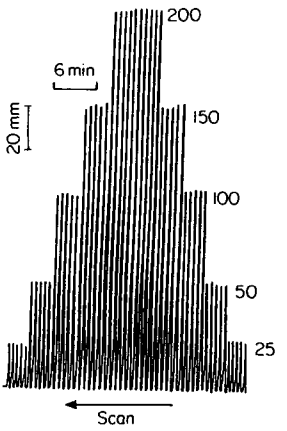

Fig. 2. Effect of flow rate on peak height for 100 μg ml^{-1} europium.

Fig. 3. Absorbance peaks for europium standards of the concentrations (μg ml^{-1}) shown.

ytterbium(III) ions were studied (Fig. 4). Both ions caused a decrease in the response to europium which is also thought to be due to competition of these ions with iron(II) for 1,10-phenanthroline, rather than to any reduction of these ions, which would result in increased responses.

Indirect spectrofluorimetric determination. In an earlier paper [8], cerium(III) fluorescence was shown to have equal sensitivity in several inorganic acids of concentrations in the range 0.05—1 M, including sulphuric acid, when studied in a flow system. Because the cerium(IV) solution was prepared in sulphuric acid and because an acidic solution had to be used as carrier stream through the Jones reductor, 0.5 M sulphuric acid was selected for this purpose. The effect of cerium(IV) concentration on the response of europium(II) was studied. A 10 μg ml^{-1} cerium(IV) solution gave the greatest peak height sensitivity. Again, 1 ml min^{-1} was found to be a satisfactory flow rate.

Under these recommended conditions (shown in Fig. 1B) a linear calibration graph for europium(III) was obtained in the range 0—4 μg ml^{-1}; the regression coefficient was 0.999 (5 points). Typical calibration peaks are shown in Fig. 5. The detection limit (2 × noise) was 0.2 μg ml^{-1} and the r.s.d. for 11 replicate determinations of 2 μg ml^{-1} was 1.1%. The residence time was 18 s and the sample throughput could be up to 90 h^{-1}.

The effects of many ions (copper, nickel, lead, iron(II), nitrate and lanthanides) on cerium(III) fluorescence were described previously [8]. Only iron(III) and nitrate interfered seriously. However, in the present system, passage through the reductor column would reduce iron(III) to iron(II), which does not interfere. Therefore, only the effects of samarium(III) and ytterbium(III) were studied here. It was found that samarium slightly enhanced

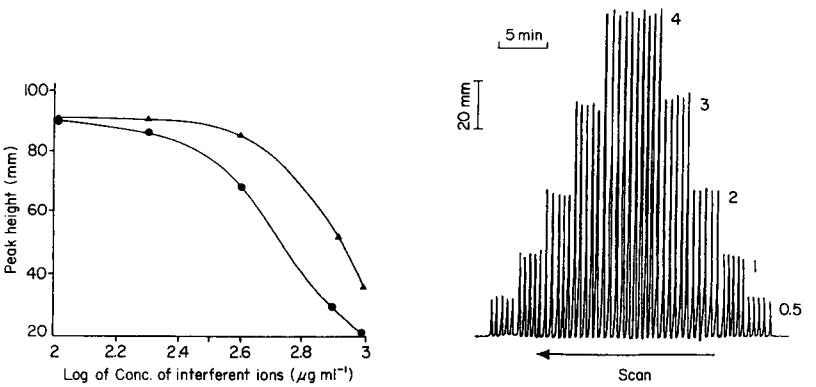

Fig. 4. Effects of samarium(III) (▲) and ytterbium(III) (●) on the absorbance peak height for 100 μg ml^{-1} europium.

Fig. 5. Fluorescence peaks for europium standards of the concentrations (μg ml^{-1}) shown.

the peak height, and ytterbium slightly depressed it, at concentrations 20 and 25 times more than the europium(III) concentration (2 μg ml^{-1}), respectively.

Conclusions

The incorporation of a reductor minicolumn into a flow-injection system provides simple and highly selective procedures for the determination for europium(III). The indirect spectrofluorimetric method is particularly attractive because of its simpler manifold and greater sensitivity than the spectrophotometric procedure. The flow system provides a rapid and reproducible method of generating europium(II) without the need for elaborate precautions to prevent its re-oxidation. Such a reduction system could also be used to study the chemistry of europium(II) under relatively simple conditions.

REFERENCES

1 H. N. McCoy, J. Am. Chem. Soc., 63 (1941) 3432.
2 H. N. McCoy, J. Am. Chem. Soc., 57 (1935) 1756; 59 (1937) 1131.
3 D. C. Foster and H. E. Kermers, Anal. Chem., 25 (1953) 1921.
4 H. N. McCoy, J. Am. Chem. Soc., 58 (1936) 1577.
5 H. N. McCoy, J. Am. Chem. Soc., 61 (1939) 2455.
6 G. den Boef and R. C. Schothorst, Anal. Chim. Acta, 180 (1986) 1.
7 A. T. Faizullah and A. Townshend, Anal. Chim. Acta, 167 (1985) 225.
8 K. H. Al-Sowdani and A. Townshend, Anal. Chim. Acta, 179 (1986) 469.
9 Z. Marczenko, Crit. Rev. Anal. Chem., 10 (1981) 246.
10 Analytical Methods Committee, Analyst, 103 (1978) 391.
11 D. D. Perrin and B. Dempsey, Buffers for pH and Metal Ion Control, Chapman and Hall, London, 1974, p. 132, Table 10.14.
12 B. P. Bubnis, M. R. Straka and G. E. Pacey, Talanta, 30 (1983) 841.
13 P. W. Alexander, R. J. Finlayson, L. E. Smythe and A. Thalib, Analyst, 107 (1982) 1335.

Analytica Chimica Acta, 201 (1987) 345—350
Elsevier Science Publishers B.V., Amsterdam — Printed in The Netherlands

Short Communication

USE OF MICROEMULSIONS IN FLOW INJECTION ANALYSIS: SPECTROPHOTOMETRIC DETERMINATION OF COPPER

M. HANIF MEMON and PAUL J. WORSFOLD*
School of Chemistry, University of Hull, Hull HU6 7RX (Great Britain)
(Received 13th March 1987)

Summary. The use of microemulsions as media for liquid/liquid extraction is considered, with particular reference to the copper(II)/2,9-dimethyl-1,10-phenanthroline complex. Aqueous copper(II) standards covering the range 2.5×10^{-5}—7.5×10^{-3} M were determined by a batch extraction procedure and by three flow-injection extraction procedures, one based on a pre-made water in oil microemulsion, one on a water in oil microemulsion formed on-line and one on an oil in water microemulsion.

Microemulsions are stable, optically transparent, monodisperse droplets of oil in water (o/w) or water in oil (w/o); the droplets have diameters in the range 5—100 nm [1]. Water in oil microemulsions are formed by dispersing water in a hydrophobic solvent, such as heptane, with the help of a suitable surfactant, such as 1,2-bis(2-ethylhexyloxycarbonyl)-1-ethane sulphonate (dioctyl sulphosuccinate, (Aerosol OT, AOT). The mean size of the water droplets in a w/o microemulsion is a function of the water/surfactant mole ratio (R). Oil in water microemulsions are similarly formed by dispersing oil in water with the help of a suitable surfactant, e.g., sodium dodecyl sulphate (SDS) and cosurfactant, e.g., butan-1-ol or pentan-1-ol.

An attractive feature of microemulsions from an analytical standpoint is their ability to solubilize an aqueous component and a non-aqueous component within a homogeneous environment and thus allow, for example, the determination of C_6—C_{10} primary amines in a non-aqueous medium by fluorescence derivatization with *o*-phthalaldehyde and 2-mercaptoethanol in aqueous solution [2], and the determination of lipase activity (aqueous) by reaction with 4-methylumbelliferyl heptanoate (non-aqueous) [3]. Such reactions can be done in a discrete manner or within a flow-injection manifold.

It should therefore be possible to use microemulsions where a heterogeneous interfacial reaction is normally used, e.g., in liquid/liquid extraction [4—6]. By judicious selection of experimental conditions, it may also be possible to improve the rate of reaction, the position of equilibrium and the selectivity. This communication describes the use of microemulsions for the extraction and complexation of copper(II) ions from an aqueous environment into an organic environment containing neocuproine (2,9-dimethyl-1,10-phenanthroline).

0003-2670/87/$03.50

Experimental

Reagents. Distilled, deionized water was used for all aqueous solutions. A stock 0.01 M copper(II) sulphate pentahydrate solution was prepared by dissolving 2.495 g of the compound (BDH AnalaR) in 1 l of water; working standards were prepared by serial dilution. A stock 0.5 M AOT solution was prepared by dissolving 55.58 g of dioctyl sulphosuccinate, sodium salt (Sigma) in 250 cm^3 of h.p.l.c.-grade heptane (Fisons), and a stock 0.15 M SDS solution was prepared by dissolving 4.326 g of sodium dodecyl sulphate (BDH AnalaR) in 100 cm^3 of water. Solutions of ascorbic acid (BDH AnalaR) in water (0.1 g cm^{-3}), sodium acetate (BDH AnalaR) in water (0.4 g cm^{-3}) and neocuproine (Sigma) in absolute ethanol (20 mg cm^{-3}) were prepared as required.

Instrumentation. A single-beam spectrophotometer (LKB Ultrospec II) fitted with a 1-cm path length cell (for batch measurements) or an 8-μl flow cell (for flow-injection measurements) was used to monitor the absorbance of the copper/neocuproine complex at 460 nm. For the flow-injection experiments, the appropriate solution (20 μl) was introduced into the carrier stream via a teflon rotary valve (Rheodyne 5020). A peristaltic pump (Gilson Minipuls 2) equipped with solvent-resistant isoversinic pump tubing (Anachem) was used to propel the carrier streams through teflon tubing (0.5 mm i.d.). All flow rates and mixing coil lengths are given in Fig. 1. The glass bead reactor (GBR) was a glass tube (2 mm i.d., 15 mm long) filled with glass beads (0.1-mm diameter).

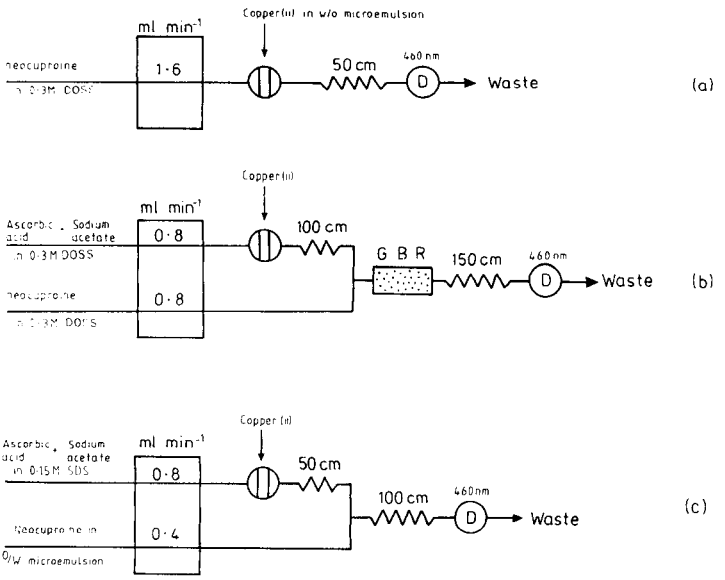

Fig. 1. Flow-injection manifolds for the complexation of aqueous copper(II) standards with neocuproine: (a) with pre-made w/o microemulsions; (b) with on-line w/o microemulsions; (c) with o/w microemulsions.

Batch extraction procedure. A series of nine aqueous copper(II) standards covering the range 5×10^{-5}—7.5×10^{-3} M was used. Ascorbic acid (0.5 cm^3) and sodium acetate (0.05 cm^3) were added to 0.5-cm^3 aliquots of each standard and the mixtures shaken; 0.5 M AOT (13.3 cm^3), butan-1-ol (1.25 cm^3) and neocuproine (0.5 cm^3) were added sequentially to each solution, and the mixtures were diluted to 25.0 cm^3 with heptane to give a final AOT concentration of 0.30 M in the non-aqueous phase. The R value for the w/o microemulsions formed by the above procedure was 7.7.

Flow-injection extraction with pre-made w/o microemulsions. A manifold with a sample dispersion of 5.0 was used (Fig. 1a). The w/o microemulsions containing copper(II) standards were prepared as in the batch procedure except that neocuproine was omitted. Each of the w/o microemulsions was injected into a carrier stream of neocuproine (0.4 cm^3) diluted to 100.0 cm^3 with 0.3 M AOT.

Flow-injection extraction with on-line w/o microemulsions. A manifold with a sample dispersion of 13 was used (Fig. 1b). The carrier stream was prepared by sequentially mixing ascorbic acid (2.0 cm^3), sodium acetate (0.2 cm^3), 0.5 M AOT (54.5 cm^3), butan-1-ol (5.0 cm^3) and absolute ethanol (2.0 cm^3) and diluting to 100.0 cm^3 with heptane. Five aqueous copper(II) standards covering the range 5×10^{-5}—1×10^{-3} M were injected into the carrier stream and merged with a reagent stream containing neocuproine (0.4 cm^3) diluted to 100.0 cm^3 with 0.3 M AOT.

Flow-injection manifold with o/w microemulsions. A manifold with a sample dispersion of 6.2 was used (Fig. 1c). The carrier stream was prepared by mixing ascorbic acid (2.0 cm^3) and sodium acetate (0.2 cm^3) and diluting to 100.0 cm^3 with 0.15 M SDS. Six aqueous copper(II) standards covering the range 2.5×10^{-5}—1×10^{-3} M were injected into the carrier stream and merged with a reagent stream containing 0.15 M SDS (91.0 cm^3), pentan-1-ol (5.0 cm^3), neocuproine (1.0 cm^3) and heptane (3.0 cm^3).

Results and discussion

Batch extraction procedure. In previous applications [2, 3] AOT w/o microemulsions were used without the incorporation of a cosurfactant. For this work, butan-1-ol was added as a cosurfactant in order to decrease the interfacial tension [7, 8] and therefore enhance the solubilization of electrolytes within the microemulsion core.

The results for batch extraction of copper(II) (5×10^{-5}—7.5×10^{-3} M) from water droplets into the bulk organic phase of w/o microemulsions (R = 7.7) are given in Table 1. The correlation coefficient (r) for a linear fit of the data was 0.9999. The results are in good agreement with those obtained by a conventional two-phase extraction into chloroform with the same bulk volume (25 cm^3) as the w/o microemulsion. Therefore, in this particular case, the rates of complexation and extraction and the equilibrium position when a w/o microemulsion is used are similar to those achieved with chloroform. The attraction of the microemulsion system in this particular case is

TABLE 1

Calibration data for the determination of copper(II) standards

Concentration (mM)	Batch extraction Absorbance	Pre-made w/o microemulsion		On-line w/o microemulsion		Oil/water microemulsion	
		Absorbance	R.s.d.[a] (%)	Absorbance	R.s.d.[a] (%)	Absorbance	R.s.d.[a] (%)
0	0.005	0.000	0.0	0.062	0.0	0.012	0.0
0.025	—	—	—	—	—	0.027	1.9
0.050	0.010	—	—	0.080	2.5	0.040	1.3
0.075	0.015	—	—	0.093	2.6	0.068	0.8
0.10	0.020	—	—	0.106	2.3	0.084	0.9
0.50	0.085	0.012	5.0	0.255	1.4	0.337	0.6
1.0	0.153	0.022	7.4	0.442	0.6	0.700	0.3
2.5	0.385	0.068	1.9	—	—	—	—
5.0	0.765	0.150	1.1	—	—	—	—
7.5	1.143	0.232	0.5	—	—	—	—

[a] $n = 10$.

the simplicity of the experimental procedure, but the disadvantage is the lack of sensitivity owing to the dilution of the sample. Future work will focus on the use of microemulsions to increase the rate of extraction of complexes, e.g., zinc(II) dithizonate, relative to the rates obtained when conventional two-phase liquid/liquid extraction procedures are used.

Flow-injection extraction with pre-made w/o microemulsions. To simplify the experimental procedure, the batch-extraction method was adapted to flow-injection. Water/oil microemulsions containing aqueous copper(II) standards (5×10^{-4}—7.5×10^{-3} M) were prepared off-line as in the batch procedure, and neocuproine in AOT, at one fifth of the batch concentration to compensate for a sample dispersion of 5.0, was pumped continuously as the carrier stream. The results, given in Table 1, show an acceptable relative standard deviation of 0.5—7.4% (r.s.d., $n = 10$) and an excellent extraction efficiency (>75%, allowing for a dispersion of 5.0), as compared with the batch procedure. The sample throughput was 120 h^{-1} and the correlation coefficient over the quoted range was 0.9990.

Flow-injection extraction with on-line w/o microemulsions. To minimize sample treatment procedures, aqueous copper(II) standards (5×10^{-5}—1×10^{-3} M) were injected directly into the manifold shown in Fig. 1(b) and incorporated into a w/o microemulsion on-line. Mixing efficiency was enhanced by using a glass bead reactor, and neocuproine was added downstream. The results, given in Table 1, show good precision (0.6—2.6% r.s.d., $n = 10$) and an extraction efficiency of ca. 70% (allowing for a dispersion of 13 in this procedure and a sample dilution of 50 in the batch procedure) of that of the batch procedure. It is not surprising that there is a relatively high blank signal because aqueous samples are being mixed on-line with an

AOT/heptane phase. However, the sensitivity of the on-line method is much better than that of the off-line method because there is less sample dilution. The sample throughput was 60 h^{-1} and the correlation coefficient over the quoted range was 0.9998.

The manifold shown in Fig. 1(b) is very simple and no sample pretreatment is required because the masking and reducing agents are present in the carrier stream. The results suggest that this method could be used routinely and applied to a wide range of metal/ligand interactions.

Flow-injection extraction with o/w microemulsions. In order to demonstrate the versatility of microemulsions for analytical use, extractions were also performed on-line with a sodium dodecyl sulphate (SDS) o/w microemulsion. Aqueous copper(II) standards (2.5×10^{-5}—1×10^{-3} M) were injected directly into an SDS carrier stream and neocuproine in an o/w microemulsion was added downstream. The results (Table 1) show excellent precision, (0.3—1.9% r.s.d., $n = 10$), and an extraction efficiency of ca. 60% (allowing for a dispersion of 6.2 and a batch sample dilution of 50) of that of the batch procedure. The sample throughput was 60 h^{-1} and the correlation coefficient over the quoted range was 0.9995.

The SDS was preferred to AOT for the preparation of o/w microemulsions because of its better solubility in water (0.15 M was used) compared with AOT (0.02 M maximum). There are two advantages of using an o/w microemulsion compared to a w/o microemulsion. First, aqueous samples are more easily mixed with o/w microemulsions, resulting in better sensitivity because of the lower blank signal and the possibility of using a manifold with lower dispersion. Secondly, it is possible to incorporate higher concentrations of water-soluble additives, e.g., reducing agents, masking agents and buffers in the aqueous phase.

Conclusions

Microemulsions provide an interesting medium for the complexation and extraction of copper(II) from aqueous solution. A batch extraction into a w/o microemulsion requires less sample manipulation than a conventional extraction, but sensitivity is decreased because of sample dilution. The procedure can be adapted for flow-injection analysis, by using either pre-made, or on-line formation of w/o microemulsions, or an o/w microemulsion.

One of us (M.H.M.) thanks the Ministry of Education, Government of Pakistan, for a Research Grant and the University of Sind for study leave.

REFERENCES

1 J. H. Fendler, Membrane Mimetic Chemistry, Wiley, New York, 1982, p. 69.
2 M. H. Memon and P. J. Worsfold, Anal. Chim. Acta, 183 (1986) 179.
3 M. H. Memon and P. J. Worsfold, Anal. Proc., 23 (1986) 418.
4 W. Chin-Kwang, K. Hung-Cheng, C. Tien, L. Seng-Chung, K. Tien-Chu and H. Kwang-Hsien, Proc. Int. Solv. Extr. Conf., Vol. 1, Liege, 1980, Paper 80-23.

5 P. Fourre, D. Bauer and J. Lemerie, Anal. Chem., 55 (1983) 662.
6 P. Fourre and D. Bauer, Solvent Extr. Ion Exchange, 1 (1983) 465.
7 M. Baviere, R. Schechter and W. Wade, J. Colloid Interface Sci., 81 (1981) 266.
8 J. T. G. Overbeek, P. L. de Bruyn and Fr. Verhoeckx, in T. F. Tadros (Ed.), Surfactants, Academic, London, 1984, pp. 111—132.

Analytica Chimica Acta, 201 (1987) 351—355
Elsevier Science Publishers B.V., Amsterdam — Printed in The Netherlands

Short Communication

SENSITIVE FLOW-INJECTION DETERMINATION OF L-LACTATE IN HUMAN BLOOD WITH IMMOBILIZED ENZYME COLUMNS AND FLUORIMETRIC DETECTION

KIYOSHI ZAITSU, MASAO NAKAYAMA and YOSUKE OHKURA*

Faculty of Pharmaceutical Sciences, Kyushu University 62, Maidashi, Higashi-ku, Fukuoka 812 (Japan)

(Received 18th March 1987)

Summary. Enzyme columns prepared by packing L-lactate oxidase and horseradish peroxidase immobilized chemically on controlled-pore glass beads are connected in series. Hydrogen peroxide formed in the enzymatic conversion of L-lactate in the first column is mixed with 3-(*p*-hydroxyphenyl)propionic acid before passage through the peroxidase column and fluorimetric measurement. Linear calibration was obtained for 0.5—500 pmol of L-lactate in 20 μl of 1000-fold diluted, deproteinated whole blood. A rapid sampling rate (60 h^{-1}) was possible.

The determination of L-lactate in blood and cerebrospinal fluid is important for the diagnosis of hypoxemic or hypoperfusion states [1] and severe head injury [2]. L-Lactate monitoring in blood is also significant for checking for lactic acidosis in diabetic patients who have been given biguanides as antidiabetic agents [3]. Several methods have been reported for the determination of L-lactate in human blood or other biological materials. Enzymatic methods using a L(+)-lactate dehydrogenase (LDH) [4, 5] have been used. A recently developed spectrophotometric method using L-lactate oxidase (from *Pediococcus* species; no EC number) is based on the measurement of hydrogen peroxide, formed enzymatically from L-lactate, by reaction with 4-aminoantipyrine and *N*-ethyl-*N*-(2-hydroxy-3-sulfopropyl)-*m*-toluidine in the presence of horseradish peroxidase (HRP) [6]. Enzyme electrodes with lactate oxidase [7, 8] or L-lactate 2-monooxygenase (decarboxylating; EC 1.13.12.4) [9] and a flow-injection system based on immobilized LDH [10] are simple to use, but the sensitivities are not always adequate for low concentrations of L-lactate in blood.

This communication describes a flow-injection method for the sensitive and rapid determination of blood L-lactate with immobilized lactate oxidase. The hydrogen peroxide formed is quantified by an immobilized HRP-catalyzed reaction with 3-(*p*-hydroxyphenyl)propionic acid as the fluorogenic substrate [11—14].

Experimental

Reagents. Double-deionized water was filtered through a Milli-Q-II system (Japan Millipore, Tokyo) just before use. *N*-Ethyl-*N*-(2-hydroxy-3-sulfo-

0003-2670/87/$03.50

propyl)-*m*-toluidine (EHSPT) and 3-(*p*-hydroxyphenyl)propionic acid (HPPA) were obtained from Dojindo Laboratories (Kumamoto) or Otsuka Chemical Co. (Osaka). L-Lactate oxidase (10–30 U mg^{-1}), HRP (285 purpurogallin U mg^{-1}, type VI) and lithium L-lactate were all from Sigma Chemical Company. Unless otherwise noted, all other chemicals were of reagent grade.

Preparation of immobilized enzyme column. Immobilized HRP on glass beads was prepared as described previously [13]. L-Lactate oxidase was immobilized on amino-derivatized controlled-pore glass beads (120–200 mesh, AMP-CPG 1400; Electro-Nucleonics, Fairfield, NJ, U.S.A.) by the glutaraldehyde technique [14–16]. Both immobilized enzymes were stored at 4°C in 100 mM sodium phosphate/potassium phosphate buffer containing 150 mM sodium chloride (pH 7.0, PBS).

The activity of the immobilized HRP was measured as described previously [13]. The activity of the immobilized L-lactate oxidase was measured as follows: the immobilized enzyme on glass beads (ca. 4 mg, dry weight) was dispersed in 30 ml of 50 mM sodium phosphate/potassium phosphate buffer (pH 6.6) containing 370 μM 4-aminoantipyrine (Wako, Osaka), 420 μM EHSPT and 13 U ml^{-1} HRP. To the suspension, 6 ml of 2.5 mM L-lactate was added and the mixture was stirred continuously at 25°C. At 1.5-min intervals, portions (ca. 3 ml) of the reaction mixture were filtered through a polyamide net, the absorbances were measured at 550 nm at 25°C, and the solutions were returned to the mixture. Thereafter, the immobilized L-lactate oxidase was collected on a sintered glass filter and dried in a vacuum. The glass beads were weighed. The molar absorptivity of the chromophore at 550 nm (16 800 l mol^{-1} cm^{-1}) was used for calculation of the activity. The enzyme activities (U g^{-1} glass beads) were 14.4 for HRP and 46.7 for L-lactate oxidase.

Columns of the enzyme glass beads were prepared by packing the beads in polytetrafluoroethylene (PTFE) tubes (40 × 0.86 mm i.d., 1.46 mm o.d.; Sanko Plastic Co., Osaka) as described previously [17].

Preparation of deproteinated blood sample. Venous or earlap blood (1.0 μl) was taken with a disposable capillary pipette and the blood was mixed immediately with 250 μl of cold 30 mM zinc sulfate. To the turbid mixture were added successively 250 μl of cold 30 mM barium hydroxide and 500 μl of cold 20 mM imidazole/hydrochloric acid buffer (pH 7.0). The resulting mixture corresponds to a 1000-times dilution of the blood. The mixture was centrifuged for 5 min at ca. 1000 g. A portion (20 μl) of the supernatant liquid was used for the flow-injection procedure.

Flow-injection apparatus and assay procedure. A schematic diagram of the flow-injection system is shown in Fig. 1. PTFE tubing (0.25 mm i.d., 1.5 mm o.d., Gasukuro Kogyo, Tokyo) was used for the tubing and back-pressure coil (10 m). The carrier solution (10 mM imidazole/hydrochloric acid buffer, pH 7.0), and the reagent solution (10 mM HPPA in 75 mM Tris/hydrochloric acid buffer, pH 8.5), were pumped with a Hitachi 655 pump and a Shimadzu LC-3A pump equipped with the back-pressure coil, respectively; the flow

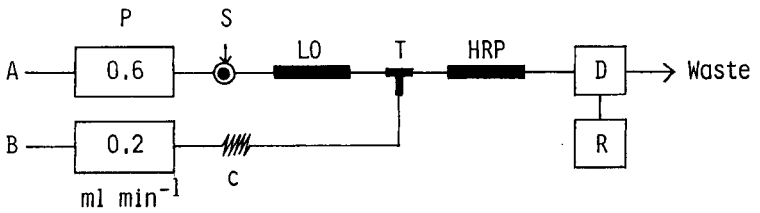

Fig. 1. Schematic diagram of the flow-injection system: (A) carrier solution; (B) reagent solution; (P) pump; (S) sample injector; (C) back-pressure coil; (T) T-piece; (D) detector; (R) recorder; (LO) L-lactate oxidase column.

rates were 0.6 and 0.2 ml min^{-1}. The sample solution was injected through a Rheodyne 7125 syringe-loading sample injector valve (20-μl loop) into the carrier stream. A T-connector was installed in the flow line between the two immobilized enzyme columns. The sample solution was passed through both the columns, but the reagent solution only through the HRP column. The fluorescence intensity was measured at an excitation wavelength of 320 nm and an emission wavelength of 415 nm with a Hitachi F1000 fluorescence spectrophotometer equipped with a 12-μl flow cell and a Hitachi 561 chart recorder. The flow system was operated at fixed room temperature (20–28°C) in any one run.

For calibration, L-lactate standard solutions in the carrier solution (0.25–5.0 μM, corresponding to 0.25–5 mM L-lactate in blood) were taken through the procedure. Peak heights were used for quantitative evaluation.

Results and discussion

The L-lactate concentration in whole blood is rapidly increased by the action of endogeneous catabolic enzymes once blood has been withdrawn from a living body [1, 5]. In addition, when diluted blood was introduced repeatedly without deproteination into the flow system, the inner pressure in the system increased and the flow line became damaged. Therefore blood should be rapidly deproteinated, to deactivate the catabolic enzymes, by a modified Somogyi method, where zinc sulfate is added followed by barium hydroxide. The order of addition of reagents given above was effective in obtaining a clear supernatant solution after centrifugation [6]. The addition of 20 mM imidazole/hydrochloric acid buffer (pH 7.0) to the deproteination mixture served to eliminate erroneous peak heights caused by the difference in composition between the sample and carrier solutions. Deproteination also served to remove reducing substances other than glucose, such as uric acid and ascorbic acid [18], which inhibit the HRP-catalyzed reaction [14, 19]. HPPA inhibits L-lactate oxidase irreversibly, and thus HPPA solution was introduced through a T-piece installed between the two enzyme columns.

A lactate sensor prepared with L-lactate oxidase works most effectively at ca. pH 7 [7, 20], thus 10 mM imidazole/hydrochloric acid buffer of pH 7.0 was used for the enzymatic reaction. The buffer could be replaced by 10 mM

sodium phosphate/potassium phosphate buffer of pH 7.0. The L-lactate oxidase activity decreases as a function of temperature [8]. A great deterioration in the activity was observed even at as low a temperature as 40°C in this study. The present flow-injection system should be operated at a fixed room temperature between 20 and 28°C.

When 10 mM HPPA was used, the highest peak was achieved at carrier and reagent solution flow rates of 0.6 and 0.2 ml min^{-1}, respectively. The HPPA concentration in the mixture of the carrier and reagent solutions was 2.5 mM and the pH was 7.8, which were optimum for the HRP-mediated reaction in the flow system [13].

Typical calibration results obtained with 3—100 pmol of L-lactic acid (in 20 μl) and blood samples are shown in Fig. 2. This concentration range corresponds to 0.16—5.0 mM L-lactate in whole blood. The calibration graph was linear up to at least 500 pmol and passed through the origin. A parallel test between an enzymatic spectrophotometric method [6] and the present method was carried out on 21 blood samples. The linear regression equation (for 0.6—4.7 mM lactate) was y (present method) = 0.964 x (spectrophotometric method) + 0.053; the correlation coefficient (n = 21) was 0.973.

The mean L-lactate concentration in venous blood from normal subjects who had fasted (21—39 years of age, n = 12) was 0.921 ± 0.214 mM (mean ± SD). This value is similar to those obtained by other workers [1, 4].

Recoveries of L-lactate added to blood at concentrations of 1.0, 5.0 and 10 mM were ca. 100%. Interfering effects of compounds such as reducing substances were examined by adding the compounds to the zinc sulfate solu-

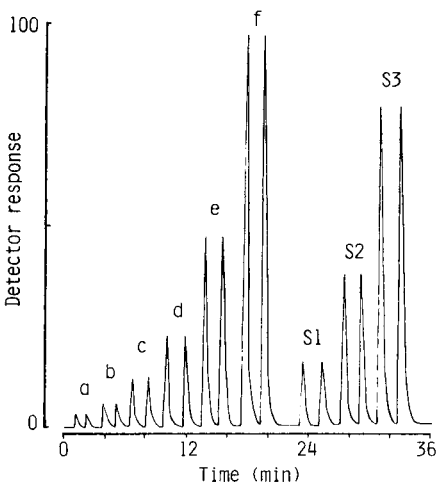

Fig. 2. Flow-injection peaks for standard L-lactate solutions and blood samples: (a—f) standard solutions; (S_1—S_3) blood samples. Values for L-lactate are given as pmol in 20-μl injection volume (and as mM in standard solutions and blood samples in parentheses): (a) 3.13 (0.156); (b) 6.25 (0.313); (c) 12.5 (0.625); (d) 25.0 (1.25); (e) 50.0 (2.50); (f) 100 (5.00); (S1) 17.0 (0.850); (S2) 38.5 (1.93); (S3) 82.5 (4.13).

tion used in the preparation of proteinated blood samples. Uric acid (590 μM), ascorbic acid (280 μM), bilirubin (130 μM) or glucose (11.1 mM) added to blood at the abnormally high concentrations shown in parentheses had no effect on the L-lactate recovery. The lower determinable limit (signal-to-noise ratio = 5) for L-lactate was 0.5 pmol in a 20-μl injection volume. The sensitivity is higher than that of any other method. A rapid sampling rate (60 h^{-1}) was possible. The relative standard deviations in repeated determinations (n = 10) of blood samples with mean L-lactate concentrations of 0.83 and 3.9 mM were 1.4 and 0.97%, respectively.

To check the stability of the immobilized enzyme columns, various deproteinated blood samples and L-lactate standard solutions were processed 200—300 times a week. The columns were stored at 4°C after filling with PBS when they were not required for use. The HRP column was usable for at least 4 months; the L-lactate oxidase column could be used for 2 months but a 50% decrease in peak height was detected after the period when 500 pmol of L-lactate had been introduced to the flow system. The immobilized enzymes retained more than 95% of the initial activities for at least 6 months when stored in PBS at 4°C.

We wish to thank Misses Sayuri Tsuno and Ikuko Hanayama for their valuable technical assistance.

REFERENCES

1 J. O. Westgard, B. L. Lahmeyer and M. L. Birnbaum, Clin. Chem., 18 (1972) 1334.
2 A. A. F. DeSalles, H. A. Kontos, D. P. Becker, M. S. Yang, J. D. Ward, R. Moulton, H. D. Gruemer, H. Lutz, A. L. Maset, L. Jenkins, A. Marmarou and P. Muizelaar, J. Neurosurg., 65 (1986) 615.
3 M. Haslbeck, P. Wittmann, W. Bachmann and H. Mehnert, Infusionsther. Klin. Ernahr., 5 (1978) 8.
4 E. P. Marbach and M. H. Weil, Clin. Chem., 13 (1967) 314.
5 R. B. Rutkowski and L. DeBaare, Am. J. Clin. Pathol., 46 (1966) 405.
6 K. Fujikawa, I. Komatsuda, M. Inoue, E. Maruoka, K. Imataka and T. Nishina, Jpn. J. Clin. Chem., 14 (1985) 198.
7 I. Karube, T. Matsunaga, N. Teraoka and S. Suzuki, Anal. Chim. Acta, 119 (1980) 271.
8 L. C. Clark, Jr., L. K. Noyes, T. A. Grooms and M. S. Moore, Crit. Care Med., 12 (1984) 461.
9 M. Mascini, D. Moscone and G. Palleschi, Anal. Chim. Acta, 157 (1984) 45.
10 T. Yao, Y. Kobayashi and S. Musha, Anal. Chim. Acta, 138 (1982) 81.
11 K. Zaitsu and Y. Ohkura, Anal. Biochem., 109 (1980) 109.
12 C. Hamada, M. Iwasaki, K. Zaitsu and Y. Ohkura, Chem. Pharm. Bull., 33 (1984) 1277.
13 Y. Hayashi, K. Zaitsu and Y. Ohkura, Anal. Sci., 1 (1985) 65.
14 Y. Hayashi, K. Zaitsu and Y. Ohkura, Anal. Chim. Acta, 186 (1986) 131.
15 H. H. Weetall, in K. Mosbach (Ed.), Methods in Enzymology, Vol. 44, Academic, New York, 1976, p. 134.
16 R. Tawa, M. Kitoh, S. Hirose and K. Adachi, Chem. Pharm. Bull., 30 (1982) 615.
17 K. Zaitsu, Y. Hayashi and Y. Ohkura, J. Flow Injection Analysis, 2 (1985) 50.
18 D. C. Williams, G. F. Huff and W. R. Seitz, Clin. Chem., 22 (1976) 372.
19 H. Nagai, K. Zaitsu, C. Hamada and Y. Ohkura, Chem. Pharm. Bull., 27 (1979) 2245.
20 F. Mizutani, K. Sasaki and Y. Shimura, Anal. Chem., 55 (1983) 35.

Analytica Chimica Acta, 201 (1987) 357—361
Elsevier Science Publishers B.V., Amsterdam — Printed in The Netherlands

Short Communication

DETERMINATION OF ISONIAZID IN TABLETS BY SECOND-DERIVATIVE ULTRAVIOLET SPECTROPHOTOMETRY OF SCRAPED-SPOT SOLUTIONS FROM THIN-LAYER CHROMATOGRAPHY

KEISUKE KITAMURA*, MAYUMI HATTA, SEIKO FUKUYAMA and KEIICHIRO HOZUMI

Kyoto Pharmaceutical University, 5 Nakauchi-cho, Misasagi, Yamashina-ku, Kyoto 607 (Japan)

(Received 19th May 1987)

Summary. Isoniazid in solutions of tablets was separated by thin-layer chromatography (TLC). The portion of the precoated plate carrying the isoniazid spot was cut out and the coating was scraped off into water. The isoniazid was quantified in the solution, without separation of suspended adsorbent, by second-derivative spectrophotometry, which eliminated the background in the zero-order spectra. Relative standard deviations ($n = 5$) were <1%. Results obtained for commercial tablets were in good agreement with those given by a liquid-chromatographic method.

Isoniazid is an important drug in the treatment of tuberculosis, and is generally formulated as tablets. It has been reported that isoniazid forms 1-isonicotinoyl-2-lactosylhydrazone by the interaction with lactose used as an excipient in tablets at high humidity and/or elevated temperatures [1]. Pharmacokinetic studies have shown that 6 h after administration the hydrazone was neither absorbed nor converted into free isoniazid in the stomach or gut [2]. Titration methods such as bromometric, nitrous acid, iodometric and non-aqueous titration with perchloric acid were incapable of distinguishing between isoniazid and the hydrazone [3—6]. Furthermore, the absorption spectra of isoniazid and the hydrazone closely resemble each other.

Thin-layer chromatography (TLC) [3—6], spectrophotometry with chemical derivatization of isoniazid [4, 6] and high-performance liquid chromatography (HPLC) [3, 5, 6] have been discussed for the determination of isoniazid in the presence of the hydrazone. Among these, TLC is simple, cheap and rapid [6] but has not been used in quantifying isoniazid. For quantitation of a substance in a spot separated on a TLC plate, it is usual to scrape off the spot, extract the substance and quantify it in the extract by spectrophotometry. The extraction should be quantitative and the TLC adsorbent must be entirely removed from the extract because even a trace of the adsorbent in the sample solution can cause excessive background in the absorption spectrum. However, if derivative spectrometry is applied to

0003-2670/87/$03.50

quantify the solute in the extract, any adsorbent in the extract need not be removed because the derivative procedure can eliminate background effects [7, 8]. Therefore, quantitation in a TLC spot will be more simply achieved.

In this communication, therefore, the application of second-derivative ultraviolet (UV) spectrometry to quantify isoniazid in scraped TLC-spot solutions is described for a simple and rapid assay of isoniazid in tablets.

Experimental

Reagents and chemicals. Isoniazid (Kanto Chemical Co., Tokyo) was recrystallized from ethanol. 1-Isonicotinoyl-2-lactosylhydrazone was synthesized [5]. All other reagents were laboratory grade. Water was deionized and distilled. TLC plates (5 × 10 cm) were provided by cutting a precoated plate (Merck DC-Alufolien Kieselgel 60 F_{254}, 20 × 20 cm, aluminum sheet). The plates were prewashed (predeveloped) with chloroform and dried before use.

Four standard isoniazid solutions (7.5—30 mg ml^{-1}) were prepared by dissolving accurately weighed amounts of isoniazid in (1 + 4) water/methanol.

TLC method. A 15-μl aliquot of a standard or assay solution was applied by a microsyringe (Hamilton 705-SNR) on a plate as a narrow band (ca. 3 cm long) and developed for 8 cm with a mobile phase of methanol/chloroform (60:65, v/v) [1]. The location of the isoniazid spot was detected by irradiation at 254 nm.

Preparation of scraped spot solutions. The portion of the TLC plate carrying the isoniazid spot (R_f = 0.47) was cut out with scissors, and the cut piece was transferred to a 50-ml beaker containing ca. 15 ml of water and immersed for 5 min. The adsorbent was entirely removed from the sheet into the water with a spatula. The sheet was rinsed into the beaker with ca. 3 ml of water and removed. The material in the beaker was entirely transferred to a 50-ml volumetric flask with the aid of ca. 5 ml of water, and 15 ml of aqueous 0.2 M hydrochloric acid was added to the flask to increase the absorbance of isoniazid. The solution was diluted to volume with water and shaken vigorously. The second-derivative spectrum was then measured. For calibration, spots of the four standard isoniazid solutions were taken through the above procedure.

Second-derivative ultraviolet spectrophotometry. The second-derivative spectra were obtained by a microcomputer-controlled scanning spectrophotometer (Shimazu MPS-2000), equipped with a graphic printer (PR-3), in 1-cm cells, at a slit width of 5 nm and a FAST scan speed. The digital differentiation was executed by the installed computer at the PROGRAM SELECT mode of 724 which meant real-time differentiation and a second-derivative spectrum at a wavelength increment of 4 nm.

Assay of isoniazid tablets. Ten tablets were weighed and finely powdered. A portion of the powder equivalent to ca. 200 mg of isoniazid was weighed accurately and transferred to a 15-ml centrifuge tube. A 10-ml portion of the (1 + 4) water/methanol mixture was pipetted into the tube and the tube was stoppered and shaken by a Labo-mixer (Iwaki PC-351) for 5 min. After

centrifuging at 3000 rpm for 5 min, the supernatant solution was used for TLC.

HPLC method. The assay results by the proposed method were compared with those obtained by a HPLC method [5]. The system used was a Shimazu LC-3A chromatograph with a SPD-2A monitor operated at 254 nm. The 250 × 4-mm pre-packed Lichrosorb CN 5 μm column (Merck) was operated at a flow rate of 1 ml min^{-1} (130 kg cm^{-2}). The mobile phase and the procedure were as described by Butterfield et al. [5].

Results and discussion

Figure 1 shows the zero-order and second-derivative spectra of a solution of isoniazid from a scraped spot. It is apparent that the large background signal in the zero-order spectrum caused by the suspended adsorbent from the plate is entirely eliminated by differentiation.

The recovery of isoniazid from the TLC plate was examined. A 15-μl aliquot of an isoniazid standard solution was chromatographed and the second-derivative spectrum of its solution from the scraped spot was obtained. Another 15-μl aliquot of the same isoniazid solution was diluted to 50 ml with 0.1 M hydrochloric acid and its second-derivative spectrum was also obtained. The derivative amplitudes (denoted by D in Fig. 1b) of both solutions were compared. The amplitude for the former solution was 95.4% of

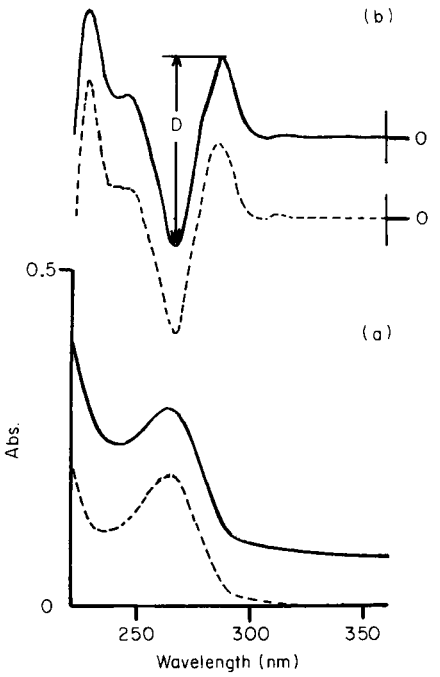

Fig. 1. Zero-order (a) and second-derivative (b) spectra of a 0.1 M HCl solution of isoniazid from a TLC spot. Dotted lines are spectra of isoniazid prepared directly in 0.1 M HCl.

TABLE 1

Effect of 1-isonicotinoyl-2-lactosylhydrazone on the assay of 10.0 mg ml^{-1} isoniazid in synthetic mixtures

Hydrazone added (mg ml^{-1})	3.0	1.6	0.6
Isoniazid found (mg ml^{-1})	10.0	9.9	10.1

TABLE 2

Assay results for commercial isoniazid tablets

Tablet	Nominal content (mg/tablet)	Found (mg/tablet)	
		Proposed method	HPLC
A	100	96.6 ± 0.4[a] 96.6 ± 1.0[a] 96.9 ± 0.3[a] 96.9 ± 0.9[a] 96.4 ± 0.8[a] 96.7 ± 0.2[b]	97.2 ± 0.7[c]
B	100	99.8 ± 0.5[a] 99.5 ± 1.4[a] 99.5 ± 0.6[a] 99.1 ± 0.4[a] 99.9 ± 0.7[a] 99.6 ± 0.3[b]	99.7 ± 0.5[c]
C	50	49.0 ± 0.4[a] 49.3 ± 0.2[a] 49.0 ± 0.4[a] 49.7 ± 0.3[a] 48.7 ± 0.4[a] 49.1 ± 0.4[b]	49.4 ± 0.2[c]

[a]Mean ± standard deviation (SD) for 5 determinations on one sample. [b]Mean ± SD for the above 5 samples. [c]Mean value ± SD for 3 samples.

that for the latter solution for 16.7 mg ml^{-1} isoniazid and 97.2% for 30.1 mg ml^{-1}. These results show that most of the isoniazid in a spot can be extracted.

Calibration. Five replicate measurements on each of the standard isoniazid solutions were used for calibration. A plot of the derivative amplitude (y) against the isoniazid concentration (x) was linear for the range 7.5—30 mg l^{-1} with a correlation coefficient of 0.99992. The equation of the regression line was $y = 9.74 \times 10^{-4} x - 2.02 \times 10^{-4}$. As the amplitude was of the order of 10^{-2} (ca. 0.0071—0.0292), the intercept of -2.02×10^{-4} was negligible. The differences between the observed and calculated amplitudes in this experiment were within 1%.

Effect of the hydrazone. Because the R_f value of isoniazid was 0.47 and that of the hydrazone was 0.13 under the conditions used, it was not likely that the hydrazone would affect the determination of isoniazid. This was confirmed by an experiment in which a synthetic mixture of known amounts of isoniazid and the hydrazone was chromatographed and the amount of isoniazid was determined according to the proposed method. As the results in Table 1 show, the hydrazone present in the mixture was completely separated by TLC and did not affect the isoniazid determination.

Assay of commercial isoniazid tablets. Three kinds of commercially available isoniazid tablets were assayed. The results are summarized in Table 2. The samples were also assayed by the reported HPLC method [5] for comparison; the results showed good agreement, as seen in Table 2. The standard deviations listed in Table 2 indicate the good reproducibility of the new method.

It has been demonstrated, therefore, that the combination of TLC separation and second-derivative spectrophotometry of the scraped-spot solutions is a convenient and accurate method for determining isoniazid in tablets. Second-derivative spectrophotometry of such solutions may be generally applicable for quantifying substances in TLC spots.

REFERENCES

1 W. Wu, T. Chin and J. L. Lach, J. Pharm. Sci., 59 (1970) 1234.
2 K. V. N. Rao, S. Kailasam, N. K. Menon and S. Radhakrishna, Indian J. Med. Res., 59 (1971) 1343.
3 L. C. Bailey and H. Abdou, J. Pharm. Sci., 66 (1977) 564.
4 M. B. Devani, C. J. Shishoo, M. A. Patel and D. D. Bhalara, J. Pharm. Sci., 67 (1978) 661.
5 A. G. Butterfield, E. G. Lovering and R. W. Sears, J. Pharm. Sci., 69 (1980) 222.
6 G. P. R. Carr and B. J. Fish, Anal. Proc., 20 (1983) 181.
7 G. Talsky, L. Mayring and H. Kreuzer, Angew. Chem. Int. Ed. Engl., 17 (1978) 785.
8 K. Kitamura, M. Takagi and K. Hozumi, Chem. Pharm. Bull., 32 (1984) 1484.

Analytica Chimica Acta, 201 (1987) 363—376
Elsevier Science Publishers B.V., Amsterdam — Printed in The Netherlands

Book Reviews

P. J. Potts, *A Handbook of Silicate Rock Analysis.* Blackie, Glasgow, 1987 (ISBN 0-216-91794-8). xi + 622 pp. Price £128.00.

To prepare a text on silicate rock analysis which covers both classical and instrumental methods, without resorting to gross oversimplification, is a formidable task. Dr. Potts is to be congratulated for apparently maintaining a high standard throughout his text. By making extensive use of Tables and very high quality Figures, he has packed a vast amount of information into 622 pages, and yet he has managed to produce a very readable text. The book may be highly recommended not just to practitioners of geochemical analysis requiring a bench handbook and/or an update in the very latest instrumental methods, but also to aspiring analytical chemists in many other disciplines. The instrumental techniques which are covered in depth include atomic absorption, arc, spark source- and inductively coupled plasma-emission spectrometry, ion-selective electrodes, X-ray fluorescence, electron microprobe and related techniques, neutron activation and other nuclear techniques, and thermal ionization-, gas source-, spark source- and inductively coupled plasma-mass spectrometry. The book contains many references to the original literature up to 1984, with a few for 1985. This lag is acceptable for a volume of this size. At £128 the book costs a good deal, but, in the reviewer's opinion, it is good value for money, combining as it does quality and comprehensiveness.

Malcolm Cresser

A. P. F. Turner, I. Karube and G. S. Wilson (Eds.), *Biosensors: Fundamentals and Applications.* OUP, Oxford, 1987 (ISBN 0-19-854724-2). xvi + 770 pp. Price £60.00.

There has been a sustained interest in biosensors since the advent of potentiometric immobilized enzyme electrodes 25 years ago, and this interest has mushroomed in recent years to include biosensors incorporating a variety of biological elements, e.g., organisms, tissues, membranes, enzymes, receptors and antibodies, and a range of transducers, e.g., potentiometric, amperometric, optical, acoustic and mechanical. The impetus for biosensor development has come primarily from the medical field, but there is considerable potential for their use in areas such as veterinary science, biotechnology and pollution monitoring.

This particular monograph stands out from other contributions on biosensors because of the clear and concise style of the contributions and the generally realistic appraisal of the subject. There are 37 contributions from

acknowledged experts in their fields and these are contained within seven subject areas, namely, the biological component, bioelectrochemistry (potentiometric and amperometric sensors), mechanical and acoustic impedance, calorimetry, photometry, applications of microprocessors, and commercialization and future prospects. The section on amperometric sensors is by far the largest and includes several papers on chemically modified amperometric biosensors and in vivo biosensors. The final chapter adds the finishing touch to the preceding papers by discussing the clinician's requirements and the economic realities of biosensor exploitation.

This book is well written and well produced, with a comprehensive index, and I would strongly recommend it as the best available text on the subject of biosensors.

P. J. Worsfold

E. A. M. F. Dahmen, *Electroanalysis.* Elsevier, Amsterdam, 1986 (ISBN 0-444-42534-9). xv + 383 pp. Price US$ 139 (Dfl. 375).

This book is the 7th in a series on "Techniques and Instrumentation in Analytical Chemistry", and is subtitled "Theory and applications in aqueous and nonaqueous media and in automated chemical control". The author is Emeritus Professor at Twente University (The Netherlands), well known for his work with non-aqueous solvents. Electroanalysis is defined as "chemical-analytical techniques in which an essential or at least an indispensable role is played by electrochemistry". There are three sections: one subdivided into three chapters: a systematic treatment of electroanalysis, non-Faradaic methods, and Faradaic methods; and two of single chapters each, on non-aqueous media and automatic chemical control.

The first section is a review of basic electrochemical principles, which could with benefit have been further subdivided, for we find, for example, Debye-Hückel theory (in cgs units!) sandwiched within a discussion of pH standards which strangely concludes by directing the reader to the CRC Handbook for details. Here as elsewhere some obvious, key references are missing. Potentiometry includes discussion of ion-selective electrodes, and also ISFETs appropriately since the concept originated with Bergveld in Twente. There are signs of late updating by way of footnotes. Photographs of instruments are included, a sure way of dating a book. The most useful sections are those where the author reaches his own specialities.

Overall, the book is clearly written and presented with good diagrams. Some discussions are overly concise and tend to stop short of providing really useful information for researchers, presumably the intended readership. Such readers might do better with some of the edited, specialist multi-authored texts available.

A. K. Covington

P. W. J. M. Boumans (Ed.), *Inductively Coupled Plasma Emission Spectroscopy, Part 1: Methodology, Instrumentation and Performance.* Horwood, Chichester, 1987 (ISBN 0-471-09686-5). xi + 584 pp. Price £71.75.

Although this book is edited by Dr. Boumans his actual contribution to the text is very significant as he authors or co-authors seven of the nine chapters. The style of the text is tutorial with respect to the theory and concepts of ICP/AES. However a good deal of relevant literature has been critically reviewed also. All nine chapters are easy to read and each of the topics discussed is essential for a complete and detailed coverage of the subject. The first three chapters provide a sound introduction which includes the theory of atomic emission spectroscopy (AES), qualitative and quantitative analysis using AES, sample introduction, a literature guide, alternative plasmas, historical development, performance of ICP/AES, plus the utilization of the ICP for atomic fluorescence and mass spectrometry. Throughout the book the reader is directed to the extensive bibliography at the end of each chapter in order to obtain a more in-depth discussion on a particular point. The literature guide in Chapter 1 and the review of reviews in Chapter 3 are especially useful for those embarking on ICP/AES for the first time.

In Chapter 4, "Basic Concepts and Characteristics", Dr. Boumans tackles those areas of ICP/AES which are most fervently argued about, i.e., the figures of merit. An introductory section on line selection and spectral interference is also given and this provides the basis for the detailed discussion in Chapter 7. An excellent theoretical and practical treatment of the much debated area of detection limits is presented which is well supported by tabulated ICP/AES detection limits obtained by various workers under different instrumental parameters. Chapters 5, 6, 8 and 9 are concerned with torches, sample introduction, spectrometers and detection systems.

The book does have some weak points. Some topics such as internal standardization and the use of slurry nebulization are out of date. The major drawback is the expense. As just the first part, it is far too expensive for the average research student or scientist.

Neil W. Barnett

William Kemp, *Qualitative Organic Analysis, Spectrochemical Techniques, 2nd edn.* McGraw-Hill, London, 1986 (ISBN 0-07-084158-6). xv + 197 pp. Price £8.95.

In the first edition (1970) of this popular undergraduate text, Dr. Kemp undertook the extraordinarily difficult task of producing a laboratory manual for the systematic identification of organic compounds of varying degrees of complexity, in which the classical chemical methods were used side-by-side with modern spectroscopic techniques. In the new edition the essential format of the book is unchanged. Minor changes have been made to the

chapter on the separation of mixtures and to the tables of data. The major modification is the inclusion of a new half-chapter on the uses of ^{13}C n.m.r. spectroscopy. As in the first edition, i.r. spectroscopy has been incorporated throughout the text, and the reader is referred to later chapters for relevant u.v., n.m.r., and mass spectral data. In this day and age it seems a pity that ^{1}H n.m.r. techniques are not used routinely, but it is appreciated that such a change would necessarily produce a more cluttered and less readable text.

The author stresses that "black box" techniques cannot entirely replace classical chemical tests, though one wonders whether the "smoky flame" test or soda lime fusions have any real place in modern analysis! In a similar vein, bromine and chlorine are detected by the sodium fusion test, with no cross reference to the mass spectrometry chapter. Despite these minor criticisms, the author has done a good job; his easy-to-read book will be appreciated by both student and teacher alike.

R. M. Scrowston

Glenn I. Ouchi, *Personal Computers for Scientists.* American Chemical Society, Washington, DC, 1986 (ISBN 0-8412-1000-4 clothbound or -1000-2 paperbound). x + 250 pp. Price $41.95 (clothbound), $27.95 (paperbound).

This book gives an introduction to the use of the personal computer (PC) for scientists who have little or no previous experience with computers. The first section, comprising about 30% of the total text, is concerned with the basic concepts of the PC. It gives a short description of various hardware components and operating systems. The topics are not treated in depth, but enough information is given to allow the reader to understand which parts and modules are used when application software is run. Furthermore, this first part serves as an excellent introduction to the relevant terminology. The second section (about 50%) is devoted to application software. The main topics are word processing, spread-sheets, graphics, and data base management. Well chosen and extensively commented examples from the field of chemistry are used to demonstrate the possibilities and limitations of the respective application programs. The last section deals with remote communication and interfacing.

The author uses an uncomplicated language, which helps to make the book easy to read and understand for readers not so fluent in English. Lengthy discussions of technical details are avoided. Emphasis is placed rather on topics relevant to those users who want to use their PC as a tool without bothering too much on what is going on inside the "black box". Thus, the reader should not expect to become an expert on the PC. However, he gets all the information required to become an efficient and well informed user of standard application programs.

J. T. Clerc

Neil A. B. Gray, *Computer Assisted Structure Elucidation.* Wiley, New York, 1986 (ISBN 0-471-89824-4). 536 pp.

The last twenty years have seen major developments in structure elucidation and representation using computational techniques. This book gives a historical view of the development of some of the programs used and illustrates, in an applied manner, several of these. It gives a comprehensive review of all related work in computer-assisted structural chemistry and introduces the most important algorithms used in this area. The book is not aimed at undergraduates, but is essential reading for those chemists and spectroscopists involved in the application or development of computational methods in infrared spectroscopy, mass spectroscopy or NMR. The development of microcomputers incorporating transputers makes the application of such techniques more accessible to a wider spectrum of scientists who do not have main-frame capabilities.

Albert Platt

L. Šafařík and Z. Stránský, in G. Svehla (Ed.), *Titrimetric Analysis in Organic Solvents (Comprehensive Analytical Chemistry, Vol. XXII).* Elsevier, Amsterdam, 1986 (ISBN 0-444-98984-6). 532 pp. Price US$ 186.75 (Dfl. 420.00).

This volume provides a well balanced account of the theory and applications of titrimetric analysis in organic solvents. The first three chapters deal with theoretical aspects including acid-base theories and equilibria in all types of solvent, classification of solvents, and the expression of acidity. The chapter "Choice and Purification of Solvents" also most usefully discusses storage and health and safety aspects of organic solvents. This is followed by treatment of the detailed procedures provided for the preparation and standardization of volumetric solutions and the range of available primary standards. Considerable attention is paid to the various instrumental modes for detection of titration end points in addition to the theory and practice of visual indicators and methodology of titrations, including applications to pharmaceutical preparations. The text concludes with three chapters dealing with acid-base and redox titrations and the determination of molecular mass. Appendices detail physical constants for nonaqueous solvents, and official drugs and their dosage forms assayed by nonaqueous titration. This volume provides a theoretical guide and practical manual for working analysts in many areas, particularly in the pharmaceutical, food, petro- and agro-chemical industries. It is a well referenced scholarly volume written, or edited, in a pleasing coherent style based on the wealth of the authors' practical experience.

D. Thorburn Burns

T. Chard, *An Introduction to Radioimmunoassay and Related Techniques, 3rd edn.* Elsevier, Amsterdam, 1987 (ISBN 0-444-80792-6). xvi + 274 pp. Price Dfl. 245.00 (hardback), Dfl. 79.00 (softback).

The third edition of this book is one of a series on laboratory techniques in biochemistry and molecular biology. It is indicative of the rapid advances that have been made in immunoassay techniques since the first edition appeared in 1978. This edition is aimed particularly at the staff of clinical and research laboratories who conduct or intend to conduct immunoassays and at the clinicians who make use of such services.

The three major developments in immunoassays in the recent past, namely the growth of non-isotopic labels, the increased availability of monoclonal antibodies and the switch from labelled-antigen to labelled-antibody assays are all considered. Requirements for binding assays, e.g., purified ligands, radioisotopic and non-isotopic labels, antibodies, separation techniques, sensitivity, specificity and precision, are logically and clearly presented in separate chapters, each of which also contains detailed practical instructions. A brief discussion of automation and the organisation of assay services and a list of manufacturers/suppliers are also included.

This book is therefore a useful contribution to the field of immunoassay techniques, and is particularly recommended to readers wishing to develop practical expertise in the subject.

P. J. Worsfold

Sergio Caroli (Ed.), *Improved Hollow Cathode Lamps for Atomic Spectroscopy.* Horwood, Chichester, 1985 (ISBN 0-853-12707-7). 232 pp. Price £35.00.

This is an authoritative text covering most aspects of hollow cathode lamp technology as applied in atomic spectrometry. The editor, Dr. Caroli, and several guest authors give a comprehensive appraisal of the progress achieved over the past decade in the development of various types of improved hollow cathode discharge (HCD) sources.

The eight chapter text begins with a discussion of the characteristics of microwave-coupled HCDs, which includes comments on method fundamentals, modes of operation and analytical applications. This is followed by a chapter on hot and cold microcavity HCDs which also cites examples of analytical applications. Chapter 3 describes pulsed HCDs for use in AAS and AFS, as well as AES and this section acts as an introduction to a later chapter on radio-frequency boosted pulsed hollow cathode lamps. There is a major chapter on the combination of an HCD with electrothermal vaporisation which has resulted in the evolution of a new technique known as furnace atomic non-thermal excitation spectrometry (FANES). This development has still to be fully evaluated, but the principle is attractive in that it combines

many of the advantages of electrothermal atomic absorption spectrometry and plasma emission spectrometry. The final chapters give details of methods used to alter the nature of the HCD by for example interaction with a magnetic field, addition of a secondary discharge, and modification of the cathode geometry to give a conical bottom HCD.

Most of the chapters achieve an admirable balance between a discussion of plasma physics and a description of HCD applications in chemical analysis. The clarity of the text is augmented by a considerable number of illustrations, graphs and tables of data, and a full reference list is provided at the end of each chapter. The only minor criticism is that the order of the chapters could have been more systematic. It seems to me that recent developments in HCD techniques can be categorised as procedures that improve spectral output by modification of the cathode design, alteration of the operating procedure, or interaction of the HCD with electric and magnetic fields. Perhaps it would have been more logical to arrange the text in accordance with this classification. Otherwise, it can be thoroughly recommended to those active in all areas of atomic spectroscopy.

David Littlejohn

Douglas T. Gjerde and James S. Fritz, *Ion Chromatography, 2nd edn.* Hüthig, Heidelberg, 1987 (ISBN 3-7785-1207-2). xi + 283 pp. Price DM 86 (US$ 45).

For many years chromatographers have sought to separate simple inorganic ions with the ease and effectiveness with which organic species are separated by g.c. and h.p.l.c. In 1975 Hamish Small led the way by demonstrating good, fast resolution of inorganic ions on small lightly functionalised ion exchange beads, and since then developments and interest in the technique have increased enormously. This second edition of Fritz, Gjerde and Pohlandt's, "Ion Chromatography" surveys in crisp style the early developments and takes us up to the very latest advances. A wealth of knowledge and experience has been enshrined in classical ion exchange studies since 1935 and the authors show clearly how this has been translated into modern high performance methods. Though these authors are concerned with non-suppressed ion chromatography, they nevertheless give full attention to the suppression techniques espoused by Dionex. In the course of this well presented and produced book the authors cover in appropriate detail all the relevant points concerning anion and cation column chromatography. The final chapter is novel in that it consists of a list of papers with full titles, grouped under various application areas such as natural waters, clinical and pharmaceutical analysis. There are some minor errors but overall it was an enjoyable read and may be recommended as a means of acquainting any chemist with the essentials of this exciting technique.

M. A. Leonard

C. H. Bamford and R. G. Compton (Eds.), *Electrode Kinetics: Principles and Methodology (Comprehensive Chemical Kinetics, Vol. 26).* Elsevier, Amsterdam, 1986 (ISBN 0-444-42550-0). xviii + 450 pp. Price US$ 172.00 (Dfl. 430.00).

This is not a book for the practising analyst. Indeed, it might not even appeal to a research electroanalytical chemist. It is certainly not one that they are likely to purchase. Nevertheless, it is one that they might ponder over in the university library. The book is the first of two to be devoted to reactions occurring at electrodes arising from the passage of current, and this one is concerned with the basic ideas and experimental methodology, while the next (Vol. 27) will deal with reactions at particular types of electrodes. This is a multi-authored work, with the first chapter (by Calvo) covering the fundamentals of electrode reactions and thus serving as an introduction to both volumes. It stresses that important technologies are based on or related to electrode reactions, e.g., the aluminium and chloralkali industries, energy conversion in batteries and fuel cells, electrodeposition, electrorefining, organic electrosynthesis, corrosion and corrosion protection, and industrial and biomedical sensors. Thus, "analysis" is tied to electrodeposition and sensors, and, of course, each is based on electrodes and events thereat.

Chapter 2 deals with mass transport to electrodes (Oldham and Zoski), Chapter 3 with linear sweep and cyclic voltammetry (Parker), Chapter 4 with a.c. and pulse methods (Sluyters-Rehbach and Sluyters), and Chapter 5 with hydrodynamic electrodes (Brett and Brett). This list serves to indicate that electroanalytical chemists might be attracted by the theory of at least Chapters 3 and 6, and it is interesting to be reminded of the fundamentals of the Ilkovič equation, the dynamic nature of the dropping mercury electrode and the background to the new generation solid-state micro-electrodes. Yes, this is a book to ponder over, not only as a recap, but also to reflect on the statement (p. 273) "It is a lack of knowledge about theoretical backgrounds of (particular) electrode reactions that hampers the reliable application of electroanalytical techniques, especially in more involved practical systems."

J. D. R. Thomas

A. Vértes and I. Kiss, *Nuclear Chemistry.* Elsevier, Amsterdam, 1987 (ISBN 963-05-4063-0). 619 pp. Price US$ 122.25 (Dfl. 275.00).

This is monograph 22 in a series on Topics in Inorganic and General Chemistry edited by R. J. H. Clark. The original manuscript was published in Hungarian and has now been translated into English. The standard of the translation is poor and the quaint, misconstructed, and sometimes incorrect expressions used markedly detract from the readability of this large volume. The twelve chapters touch upon fundamental topics such as the structure of the nucleus, nuclear reactions and radioactive decay, the interaction of radiation with matter, and then move on to methodology for chemical structure

determination, radioactive tracing, hot atom chemistry and isotope effects. The book concludes with a consideration of a wide range of nuclear reactors and of isotope enrichment techniques. It is well illustrated and contains some 400 references but, whereas one chapter covers almost half of these, others get by with a mere handful of literature references. Many of these sources of further information are rather elderly and only a few are more recent than the late 1970s.

The chapters cover all the important information necessary for a research student or other research worker in this field and it is pleasing to see that references are given to useful monographs, many published in languages other than English. It is also very helpful to find constructive exercises at the end of each paragraph which enable readers to revise their understanding of the work. In summary, this is a good volume although somewhat outdated in terms of its content, spoiled by the language difficulties but, nevertheless, recommended as back-up material for anyone having sufficient funds to purchase a second textbook in this area.

David R. Williams

I. B. Bersuker, *The Jahn—Teller Effect and Vibronic Interactions in Modern Chemistry*. Plenum, New York, 1984 (ISBN 0-306-41319-1). xiv + 319 pp. Price US$ 45.00.

Probably most chemists think of the Jahn—Teller effect as an obscure phenomenon, of interest mainly to spectroscopists studying transition-metal complexes. In recent years, however, much attention has been given to the interaction between electronic and nuclear motions. Professor Bersuker, who is probably the foremost authority on the effect, argues convincingly that "vibronic effects influence all significant areas of modern chemistry" and are also "of indispensable practical importance". The book begins with three chapters in which the basic ideas are developed, and the dynamic instabilities that result from vibronic coupling in various situations are analysed in some detail. The two longest chapters discuss the application of these ideas to spectroscopy (e.s.r., Mössbauer, infrared, Raman, and electronic) and to crystal chemistry (including ferroelectrics and structural phase transitions). The final chapter describes their relatively recent application to problems of chemical reactivity and catalysis. Inevitably, the majority, but by no means all, of the examples are in transition-metal chemistry. Throughout, the ideas are carefully and systematically explained, with mathematics that most physical or inorganic chemists will find manageable. There are over five hundred references.

A. B. Blake

I. B. Bersuker, *The Jahn—Teller Effect: A Bibliographic Review.* IFI/Plenum, New York, 1984 (ISBN 0-306-65206-4). ix + 589 pp. Price US$ 85.00.

This is a list of over 3000 publications (including titles in English as well as authors and locations), carefully classified into five sections and thirty-four subsections. The latter include, e.g., optical band shapes, luminescence, photoelectron and x-ray spectroscopy, e.s.r., n.m.r., and double resonance. Each subsection is preceded by a brief outline of the main developments contained in the work cited. Although mainly for the specialist in vibronic interactions, it also represents an important source of background information for a researcher in any field in which such effects may need to be considered. There is a formula index.

A. B. Blake

C. Kuo, A. J. Thunem and N. P. Sundby (Eds.), *Automation for Safety in Shipping and Offshore Petroleum Operations.* North-Holland, Amsterdam, 1986 (ISBN 0-444-70101-X). xix + 513 pp. Price US$ 80.00 (Dfl. 200.00).

This collection of papers represents the proceedings of the conference of the same name held in June 1985 in Norway. The shipping and offshore industries are unusual in that they belong almost to a different world to land-based operations. Each ship, platform or submersible is a self-contained unit which must support life and carry out tasks in extremes of weather, movement, vibration and spray, 24 h a day without ceasing. Often the manpower is multi-national with occasional language difficulties, yet operating equipment at the forefront of engineering and systems technology. To operate the ships and platforms efficiently the procedures must be safe. The study of safety in all aspects of the maritime industries is carried on continuously and possibly at a higher level than most industries, with the likely exception of aviation. The conflict between commercial pressures, safe operations, cost and human frailty makes the enacting of these procedures a fascinating technical and sociological task.

Anyone interested in the detail of ship and platform operations will be taken by these papers. Over 100 pp. are devoted to risk analysis and management, and human reliability safety systems. Training and operation in hostile environments, with two papers on rescue methods, occupy a section of similar length. This is a book which would appeal to any measurement scientist who likes to think about the practice of his profession. The means of monitoring hazards, both physical and chemical are discussed, with greater emphasis on the physical side. There are two papers which have an analytical content: in one a new hydrogen sulphide detector christened the "Sulphistor" is introduced which it is hoped will permit monitoring of hydrogen sulphide near the TLV of 10 ppm. Details are sketchy, but it works much like the pellistor. The paper on laser gas detection says nothing new, and not very well. Analytical chemists, however, will be fascinated to dream about the "marinising" of

analytical procedures for toxic and flammable gases, air purity monitoring, cargo contamination etc. and how they can fit into and contribute to the complex marine operations.

J. F. Alder

C. Paquot and A. Hautfenne, *Standard Methods for the Analysis of Oils, Fats and Derivatives, 7th edn.* Blackwell, Oxford, 1987 (ISBN 0632-015861). xvii + 347 pp. Price £41.25.

This is a revised and expanded version of the 6th edition (1979) of the compendium of methods provided by the Commission on Oils, Fats and Derivatives of IUPAC. The detailed methods are arranged into the following four sections: oleaginous seeds and fruits, oils and fats, glycerines, and alkaline soaps, and are assembled in a loose-leaf ring binder. It is intended to produce a supplement of ca. 80 loose pages every two years, which can be inserted as appropriate into the binder. The detail provided is sufficient for an analyst to carry out the complete analytical procedure, without the need to refer elsewhere. The IUPAC recommendation will give confidence in the results.

David A. Kurtz (Ed.), *Trace Residue Analysis: Chemometric Estimations of Sampling, Amount, and Error (ACS Symposium Series, No. 284).* American Chemical Society, Washington, DC, 1985 (ISBN 0-8412-0925-1). x + 284 pp. Price $59.95 (U.S.A. and Canada), $71.95 (elsewhere).

All aspects of the analytical process are amenable to mathematical treatment to achieve optimal performance. Trace analysis is no exception, the apparently less demanding requirements for precision and accuracy being offset by the greater impact of perturbing factors at the trace level. This book is a collection, in camera-ready copy, of 13 papers presented at an ACS symposium, and includes sampling, outliers, detection limits, correlation chromatography, calibration (including cubic spine functions), SIMCA and the scientific method of enquiry. A summary (15 pp.) of the ensuing panel discussion is also included, together with a substantial subject index. The presentation is generally satisfactory and the subject matter varied and interesting.

Joseph D. Rosen (Ed.), *Applications of New Mass Spectrometry Techniques in Pesticide Chemistry.* Wiley, New York, 1987 (ISBN 0-471-83280-4). xi + 264 pp. Price £50.45.

Analytical mass spectrometry is developing very rapidly. In consequence, its value in a wide range of fields is growing commensurately, and nowhere

more so than in the determination of pesticides and herbicides and their metabolites. This book sets out to demonstrate how these developments (chemical ionization, fast atom bombardment, selected ion monitoring, tandem mass spectrometry, combination with HPLC, etc.) have been useful in this area. After the introduction, it contains sixteen chapters, by a wide range of (mostly) U.S. scientists, giving detailed and often personal accounts of particular topics, based on techniques or applications to certain compounds. Mass spectra and fragmentation patterns abound! The material is referenced up to 1985, and experimental detail is usually included. Nowhere is the power of modern analytical chemistry more clearly demonstrated than in applications of this type, and, as such, the book is highly recommended.

Satinder Ahuja (Ed.), *Chromatography and Separation Chemistry: Advances and Developments (ACS Symposium Series, No. 297).* American Chemical Society, Washington, DC, 1986 (ISBN 0-8412-0953-7). viii + 304 pp. Price $54.95 (U.S.A. and Canada), $65.95 (elsewhere).

This collection of 15 articles developed from a symposium at the ACS meeting in Philadelphia in August 1984. Most of the articles, produced in camera-ready copy, deal with a variety of aspects of HPLC (enantiomer separation, new detectors, optical detector noise, column packings, laser fluorimetry detection, retention calculation and prediction, cyclodextrins). The first chapter, however, by Laub proposes a unified theory of sorption for gas, liquid and ion-exchange chromatography, and the last two describe gel electrophoresis of proteins and supercritical fluid chromatography and its combination with mass spectrometry. Interestingly the new detectors are also considered in connection with flow injection analysis. The book is useful in that it provides timely descriptions of areas of analytical science that are developing rapidly, and is therefore essential reading for all chromatographers.

A. H. El-Shaarawi and R. E. Kwiatkowski (Eds.), *Statistical Aspects of Water Quality Monitoring (Developments in Water Science, Vol. 27).* Elsevier, Amsterdam, 1986 (ISBN 0-444-42698-1). ix + 502 pp. Price US$ 112.00 (Dfl. 280.00).

This monograph contains the proceedings of a workshop held at the Canada Centre for Inland Waters, Burlington, Ontario on 7—10 October 1985. The aim of the workshop was to bring together scientists and statisticians working in various areas of water management, e.g., limnology, water quality regulation and control, monitoring network design, and modelling of aquatic environments. There are 37 contributions produced in camera-ready form, most of which are concerned with the statistical evaluation of chemical information derived from various water systems in North America.

The contents of the book are therefore highly specialized but nonetheless demonstrate effectively the benefits of statistical methods for the interpretation of large and/or complex data sets. This book is therefore of interest to readers with a sound knowledge of statistics rather than those with a general interest in analytical chemistry.

J. Hollo, K. J. Kaffka and J. L. Gonczy (Eds.), *Near Infrared Diffuse Reflectance/Transmittance Spectroscopy*. Akadémiai Kaidó, Budapest, 1987 (ISBN 963-05-4625-6). xiv + 319 pp. Price US$ 38.00.

This is the proceedings of the conference on the above subjects held in Budapest in May 1986. It contains in camera-ready copy thirty-two papers covering theory, methodology, instrumentation and applications (in agriculture and food analysis). As might be expected from the current state of knowledge of the subject, just two papers are included, somewhat optimistically, under "Theory" and only three are validly instrumentation. The vast majority deal with how to use the technique, and what to apply it to. Practitioners will find many of these papers useful in helping to apply near infrared spectroscopy to their particular analytical problems.

Verein Deutscher Ingenieur — Kommission Reinhaltigung der Luft. The following final versions of reports have recently been published, in German/English, and are available from Beuth Verlag, P.O. Box 1145, D-1000 Berlin-30, F.R.G.

VDI 2452 Part 3
Gaseous air pollution measurement. Measurement of fluoride ion concentration. Sorption measurement with prepared silver balls and heated membrane filter.
July 1987 Price DM 41.50.

VDI 3863 Part 1
Measurement of gaseous emission. Determination of acrylonitrile. Gas chromatographic method. Grab sampling.
April 1987 Price DM 36.70.

VDI 2267 Part 4
Chemical analysis of particulates in ambient air. Determination of lead, cadmium and their inorganic compounds as part of the dust precipitation by atomic absorption spectrometry.
March 1987 Price DM 36.70.

VDI 2267 Part 6
Chemical analysis of suspended particulates in ambient air. Measurement of the mass concentration of cadmium by atomic absorption spectrometry.
March 1987 Price DM 36.70.

VDI 2268 Part 1
Chemical analysis of particulate matter. Determination of Ba, Be, Cd, Co, Cr, Cu, Ni, Pb, Sr, V, Zn in particulate emissions by atomic spectroscopic methods.
April 1987 Price DM 41.50.

VDI 2463 Part 9
Particulate matter measurement. Measurement of mass concentration in ambient air. Filter method. LIS/P filter device.
February 1987 Price DM 41.50.

Analytica Chimica Acta, 201 (1987) 377
Elsevier Science Publishers B.V., Amsterdam — Printed in The Netherlands

Erratum

M. Veber, S. Gomišček and V. Streško, Electrothermal Atomic Absorption Spectrometry of Elements after Electrochemical Deposition on Graphite Electrodes.

Anal. Chim. Acta, 193 (1987) 157—167.

The equations on p. 165 of this paper should read:

$$M^{n+} + mL^{-} \rightleftharpoons ML_m^{(n-m)+} ; K = [ML_m^{(n-m)+}]/[M^{n+}][L^{-}]^m$$

$$E_c = E^0_{M^{n+}/M} - (0.059/n) \log K - (0.059/n) \log ([L^{-}]^m/[ML_m^{(n-m)+}]$$

ANALYTICA CHIMICA ACTA, VOL. 201 (1987)

AUTHOR INDEX

ACA announcements

AWARD

1988 PITTSBURGH CONFERENCE MEMORIAL NATIONAL COLLEGE GRANTS AWARD PROGRAM

The Pittsburgh Conference on Analytical Chemistry and Applied Spectroscopy, Inc., and its co-sponsoring technical societies, the Spectroscopy Society of Pittsburgh and The Society for Analytical Chemists of Pittsburgh, are happy to announce the 15th year of funding for The Pittsburgh Conference Memorial National College Grants Award Program. At least eight colleges will be selected to receive awards (U.S.$2500 maximum), based on their submitted proposals, for the purchase of scientific equipment, audio-visual and other teaching aids, and/or library materials for use in the teaching of science at the undergraduate level.

To be eligible for an award, the school must meet these criteria:

(1) A school must have an enrollment of not more than 2500 students.

(2) Receive no more than 25% of its operating budget from national or state governments. Two-year community colleges sponsored by political subdivisions of a state are not bound by these requirements.

(3) Requests for materials to be used only for research purposes shall not be funded.

(4) Previous awardee schools are not eligible for an award for a three-year period following their award. (For example, the 1985, 1986, and 1987 awardee schools are not eligible for the 1988 program.)

(5) This award may be used a part of a "Matching Grant" program for undergraduate studies as described above. In fact, generating "Matching Funds" is recommended.

Any interested faculty member is urged to participate by completing an application form and submitting it with a proposal (original and 3 copies of each), by April 1, 1988, to Richard S. Danchik, The Pittsburgh Conference, Inc., 12 Federal Drive, Suite 322, Pittsburgh, PA 15235, U.S.A. For application/proposal information write to the same address. Award-winning schools will be announced by May 1, 1988.

ANNOUNCEMENTS OF MEETINGS

4th SYMPOSIUM ON HANDLING OF ENVIRONMENTAL AND BIOLOGICAL SAMPLES IN CHROMATOGRAPHY, BASEL, SWITZERLAND, APRIL 27–29, 1988

For this 4th Symposium on "Handling of Environmental and Biological Samples", it is the intention to bring together specialists in this field who can give good accounts of the state-of-art in different areas of matrix handling and chromatographic techniques and present first-hand experience in their specialty. Robotics, continuous-flow extraction techniques, solid-surface sample handling with pre-column technology (on-line and off-line), pre-chromatographic use of derivatization techniques and column-switching methodology of complex samples are some of the topics that will be treated and extensively discussed. Special emphasis will be placed on techniques with automation potential and actual automated procedures suitable for routine handling of large series of samples. Much of

this methodology and 'philosophy' can be applied to different types of matrices and problem solving but it is the intention to concentrate on applications to biological (urine, blood, tissue, plant material) and environmental (water, waste-water, air) samples with drugs (pharmaceuticals) and priority pollutants as the analytes.

The proceedings of the symposium will be published in a special issue of *Journal of Chromatography*. The deadline for receipt of abstracts is March 1, 1988. There will also be a short course on Sample Handling in Liquid Chromatography including Robotics on April 25–26, 1988.

For further information contact: Workshop Office IAEAC, M. Frei-Hausler, Postfach 46, CH-4123 Allschwil 2, Switzerland.

2nd INTENSIVE SEMINAR ON ANALYTICAL BIOTECHNOLOGY, BALTIMORE, MD, U.S.A., MAY 17–20, 1988

Selection of analytical methods in biotechnology for monitoring genetically engineered product composition and purity will be critically examined at the 2nd Intensive Seminar on Analytical Biotechnology, at the Sheraton Inner Harbor Hotel in Baltimore, MD, U.S.A. on May 17–20, 1988.

The latest advances in analytical techniques and their application to polypeptide purity and structure analysis will be a major focus of the meeting. The broad objectives are to provide a clearer understanding of the critical issues, a broader perspective on alternative methods, practical approaches to production and quality control problems, and a look into the future of analytical methodology. The seminar will also contain a scientific poster session. Efforts will be made to incorporate appropriate scientific posters into the programme and discussions.

This seminar is designed for senior scientists in biotechnology research, product development, manufacturing, process development, quality assurance, technical applications, marketing, and management.

Programme, poster and registration information may be obtained from the Seminar Coordinator, Mrs. Janet Cunningham, of Barr Enterprises, P.O. Box 279, Walkersville, 21793, U.S.A. Tel.: (301) 898-3772.

CAC 88, 4th INTERNATIONAL CONFERENCE ON CHEMOMETRICS IN ANALYTICAL CHEMISTRY, AMSTERDAM, THE NETHERLANDS, MAY 18–20, 1988

The theme of this 4th CAC conference will be "chemometrics in analytical chemistry, with emphasis on practical applications, theoretical developments, and chemometric software".

The following topics will be covered: chemometrics, automation and optimization, including a.o. multivariate data analysis, formal techniques for optimization, signal-, image-, and data processing, expert systems, artificial intelligence, robotics, library searching, laboratory management systems.

The scientific programme will include invited plenary lectures, keynote lectures, and submitted research papers. Papers presented at the conference will be refereed for publication in a special issue of *Analytica Chimica Acta*.

For further information and registration contact: Secretariat CAC 88, Laboratory for Analytical Chemistry, University of Amsterdam, Nieuwe Achtergracht 166, 1018 WV Amsterdam, The Netherlands.

7th INTERNATIONAL SYMPOSIUM ON MASS SPECTROMETRY IN LIFE SCIENCES, GHENT, BELGIUM, AUGUST 23–26, 1988

The above-mentioned symposium is being sponsored by the Faculty of Pharmaceutical Sciences of the State University of Ghent, the National Foundation of Scientific Research (N.F.W.O.-F.N.R.S.) and the Ministry of National Education of Belgium. Contributed papers and posters will cover the following topics: fundamental aspects and applications of mass spectrometry in biological, environmental and health sciences; new developments in instrumentation and techniques of analysis; qualitative and quantitative applications in drug analysis, pharmacokinetics, clinical chemistry, biochemistry, toxicology, environmental and ecological research.

All papers must be presented in English and no simultaneous translation will be provided. The deadline for receipt of abstracts is May 15, 1988.

Further information may be obtained from: Professor Dr. A. De Leenheer, Laboratoria voor Medische Biochemie en voor Klinische Analyse, Harelbekestraat 72, B-9000 Ghent, Belgium. Tel.: (091) 218951, ext. 324.

4th SEPARATION SCIENCE AND BIOTECHNOLOGY SYMPOSIUM, GARGNANO DEL GARDA, ITALY, AUGUST 31–SEPTEMBER 3, 1988

Scientific and economic aspects of the role played by separation principles in biotechnology will be examined by recognized experts and discussed with participants at the 4th Separation Science and Biotechnology Symposium, presented by the Department of Biomedical Sciences and Technologies of the University of Milano, on August 31–September 3, 1988; at the Palazzo Feltrinelli, Gargnano del Garda, Italy.

In addition to analytical and preparative chromatographic techniques, other state-of-the-art approaches such as sedimentation field flow fractionation, gel electrophoresis and other biomacromolecular and particle separation techniques will be reviewed. Recent advances in applying separation science and engineering to biotechnological processes will be highlighted.

The economics of bioprocessing with regard to obtaining funding, to the development of cost-efficient systems with enhanced yields, and to ensuring regulatory compliance, will also be treated by leading authorities.

For further information, contact: Pier Giorgio Righetti, Professor of Biochemistry and Symposium Chairman, Euro Business Center, P.O. Box 10552, 1001 EN Amsterdam, The Netherlands.

INTERNATIONAL CONGRESS ON APPLIED CRIMINOLOGY, GHENT, BELGIUM, SEPTEMBER 1–3, 1988

The International Congress on Applied Criminology will be held at the State University of Ghent on the occasion of the 50th Anniversary of the School of Criminology in Ghent, Belgium, from September 1–3, 1988.

The subjects covered will be: organized crime; drugs; mass disasters; civil protection; toxicological evaluation; terrorism, detection of explosives and gases.

For the Secretariat contact: Professor Dr. R. Dierkens, Apotheekstraat 5, B-9000 Ghent, Belgium. Tel.: (32) 91-25316. For further information contact: Professor Dr. A. Heyndrickx, Department of Toxicology and Criminalistics, Hospitaalstraat 13, B-9000 Ghent, Belgium, tel: (32) 91-251021, telex: 11.558 A.Z. Ghent – mention "Toxicology".

5th INTERNATIONAL SYMPOSIUM ON BIOLUMINESCENCE AND CHEMILUMINESCENCE, FLORENCE, ITALY, SEPTEMBER 25–29, 1988

The symposium in Florence will cover the fundamental aspects and the most recent applications of Bioluminescence and Chemiluminescence in clinical sciences, biotechnology, genetics, microbiology, phagocytosis, immunoassay, environmental monitoring. The symposium will consist of Invited Lectures, Short Communications, Poster Sessions and Workshops. The deadline for abstracts is 15th March 1988.

The meeting will include a special Symposium "*Alma Mater Studiorum Saecularia Nona*" on 27th September 1988 in Bologna as part of the celebration to mark the foundation of the University of Bologna in the XIth Century.

Further information is available from: Professor Mario Pazzagli, Endocrinology Unit, University of Florence, Viale Morgagni 85, 50134 Florence (Italy).

ISAME, INTERNATIONAL SEMINAR ON ANALYTICAL TECHNIQUES IN MONITORING THE ENVIRONMENT, TIRUPATI, INDIA, JANUARY 10–12, 1989

The international seminar will be focussed on state-of-the-art discussions and progress in developing analytical methods for monitoring the environment. Scientific sessions will include electroanalytical, spectral, radioanalytical and chromatographic methods. About 15 overseas speakers have agreed to attend. Invited and contributed papers, as well as posters, will be presented.

The seminar will be held at the Sri Venkateswarlu University, Tirupati, India. Tirupati is a famous place of pilgrimage with many important temples in and around the city. January weather is dry with temperatures in the 17–25°C range.

For further information contact: Professor S. Jayarama Reddy, Director, ISAME, Department of Chemistry, Sri Venkateswarlu University, College of Engineering, Tirupati 517 502, India.

13th INTERNATIONAL SYMPOSIUM ON COLUMN LIQUID CHROMATOGRAPHY, STOCKHOLM, SWEDEN, JUNE 25–30, 1989

The above-mentioned symposium will be held at the Folkets Hus, a congress centre in the heart of Stockholm. These symposia have become the most important series of meetings on column liquid chromatography, and a high scientific standard has characterized previous meetings.

The scientific programme will cover a variety of aspects of liquid chromatography that are of current interest. Expert scientists will be invited to give lectures on topics of special interest such as capillary columns, retention mechanisms, detector characteristics and bioanalytical applications. Numerous papers will be presented on the latest achievements in chromatographic theory, instrumentation and methodology. Poster sessions will play an important part in the symposium since they offer unique opportunities for stimulating informal discussions. Seminars and talk sessions in different organizational forms will cover topics of immediate interest, such as enantiomer separations, column switching, macromolecular separations, post-column reactors and equipment design. The latest versions of instrumentation, packing materials and accessories will be exhibited by all major suppliers, and special sessions will be reserved for manufacturers.

A lively social programme will be arranged.

For further information contact: 13th International Symposium on Column Liquid Chromatography, The Swedish Academy of Pharmaceutical Sciences, P.O. Box 1136, S-111 81 Stockholm, Sweden. Tel.: (468) 24 50 85.

SAC 89, AN INTERNATIONAL CONFERENCE ON ANALYTICAL CHEMISTRY, CAMBRIDGE, U.K., JULY 30–AUGUST 5, 1989

The Analytical Division of the Royal Society of Chemistry is to hold SAC 89 at the University of Cambridge. This is the next in the series of triennial conferences originally started by the Society for Analytical Chemistry (hence SAC). The conference will be held from Sunday, July 30th, to Saturday, August 5th, 1989. Sponsorship by the Federation of European Chemical Societies and the International Union of Pure and Applied Chemistry has been granted.

The scientific programme will be organised around plenary, invited and contributed papers and posters covering the whole field of analytical chemistry. As at previous conferences, special symposia on particular analytical themes will be organised by RSC Groups and the Region of the Analytical Division. The programme will include workshops, where research workers can demonstrate new apparatus and techniques. Update courses are also planned, to provide all-day tutorial and practical demonstration sessions.

A wide ranging social programme is planned. This will include a Banquet in the historic Dining Hall of King's College.

Further information may be obtained from: The Secretary, Analytical Division, Royal Society of Chemistry, Burlington House, London, W1V 0BN, U.K.

CALENDAR OF FORTHCOMING MEETINGS

'eb. 10–12, 1988
)rlando, FL, U.S.A.

1st International Symposium on the Impact of Pesticides, Industrial and Consumer Chemicals in the Near Environment
Contact: Dr. T.A. Perenich, University of Georgia, Dawson Hall 305, Athens, GA 30602, U.S.A. Tel.: (404) 542-4888.

'eb. 22–26, 1988
lew Orleans, LA,
J.S.A.

39th Pittsburgh Conference and Exposition on Analytical Chemistry and Applied Spectroscopy
Contact: Mrs. Alma Johnson, Program Secretary, 12 Federal Drive, Suite 322, Pittsburgh, PA 15235, U.S.A. (Further details published in Vol. 197.)

'eb. 22–26, 1988
iraz, Austria

Methoden der Datenauswertung in der Atomspektroskopie
Kontaktadresse: Dr. W. Wegscheider, Institut für Analytische Chemie, Makro- und Radiochemie, Technische Universität Graz, Technikerstrasse 4, A-8010 Graz, Austria. Tel.: (0316) 7061-8303, telex: 31121.

larch 15–18, 1988
voriaz, France

Selenium in Medicine and Biology, 2nd Congress on Trace Elements in Medicine and Biology
Contact: Congrès Oligoéléments: Sélénium, Laboratore de Biochimie C, C.H.R.U.G., BP 217 X, 38043 Grenoble Cedex, France.

larch 29–31, 1988
loordwijkerhout,
he Netherlands

ANABIOTEC '88, 2nd International Symposium on Analytical Methods and Problems in Biotechnology
Contact: Symposium Secretariat ANABIOTEC '88, c/o QLT Convention Services, Keizersgracht 792, 1017 EC Amsterdam, The Netherlands. Tel.: (20) 261372, telex 31578 INTER NL attn. QLT. (Further details published in Vol. 190, No. 2.)

pril 15–18, 1988
leuherberg, F.R.G.

5th International Workshop on Trace Element Analytical Chemistry in Medicine and Biology
Contact: Gesellschaft für Strahlen- und Umweltforschung mbH, Institut für Ökologische Chemie, AG "Spurenelementanalytik", Dr. P. Schramel, Ingolstädter Landstrasse 1, D-8042 Neuherberg, F.R.G. (Further details published in Vol. 190, No. 2.)

pril 18–21, 1988
as Vegas, NV, U.S.A.

Flow Analysis IV, An International Conference on Flow Analysis
Contact: Dr. Gilbert E. Pacey, Department of Chemistry, Miami University, Oxford, OH 45056, U.S.A. (Further details published in Vol. 181.)

pril 19–22, 1988
lunich, F.R.G.

Biochemische Analytik 88, 11th International Conference on Biochemical Analysis
Contact: Biochemische Analytik 88, Nymphenburger Strasse 70, D-8000 Munich, F.R.G. (Further details published in Vol. 197.)

pril 27–29, 1988
asle, Switzerland

4th Symposium on Handling of Environmental and Biological Samples in Chromatography
Contact: Professor R.W. Frei, Department of Analytical Chemistry, Free University, De Boelelaan 1083, 1081 HV Amsterdam, The Netherlands. Tel.: (020) 5485379. (Further details published in Vol. 190, No. 2.)

May 4–6, 1988
Stockholm, Sweden

International Symposium on Biomolecules — Analytical Options
Contact: The Swedish Academy of Pharmaceutical Sciences, P.O. Box 1136, S-111 81 Stockholm, Sweden.

May 17–20, 1988
Baltimore, MD, U.S.A.

2nd Intensive Seminar on Analytical Biotechnology
Contact: Mrs. Janet Cunningham, Seminar Coordinator, Barr Enterprises, P.O. Box 279, Walkersville, MD 21793, U.S.A. Tel.: (301) 898-3772.

May 18–20, 1988
Amsterdam, The Netherlands

CAC–88, 4th International Conference on Chemometrics in Analytical Chemistry
Contact: CAC–88, Laboratory for Analytical Chemistry, University of Amsterdam, Nieuwe Achtergracht 166, 1018 WV Amsterdam, The Netherlands. Tel.: (020)-5223541 (Dr. Smit). (Further details published in Vol. 190, No. 2.)

June 5–11, 1988
Toronto, Canada

3rd Chemical Congress of North America
Contact: Anne Alper, The Chemical Institute of Canada, 300-1785 Alta Vista Drive, Ottawa, Ontario, K1G 3Y6 Canada. Tel.: (613) 526-4652.

June 5–11, 1988
Frankfurt am Main, F.R.G.

ACHEMA 88, International Meeting on Chemical Engineering and Biotechnology, 22nd Exhibition-Congress
Contact: DECHEMA, Organisation ACHEMA, Postfach 97 01 46, D-6000 Frankfurt am Main 97, F.R.G.

June 6–9, 1988
Turku, Finland

ElectroFinn Analysis, An International Conference on Analytical Chemistry
Contact: ElectroFinnAnalysis, Dr. Ari Ivaska, Laboratory of Analytical Chemistry, Abo Akademi, SF-20500 Turku (Åbo), Finland. (Further details published in Vol. 197.)

June 19–24, 1988
Washington, DC, U.S.A.

HPLC '88, 12th International Symposium on Column Liquid Chromatography
Contact: Symposium Manager, Barr Enterprises, P.O. Box 279, Walkersville, MD 21793, U.S.A. Tel.: (301) 898 3772.

June 19–26, 1988
Trieste, Italy

EUCHEM Conference on Chemometrics in Organic and Bioorganic Chemistry
Contact: Professor Paolo Linda, EUCHEM Conference on Chemometrics, c/o Istituto di Chimica Farmaceutica, Università degli Studi, Piazzale Europa 1, 34128 Trieste, Italy. Tel.: (040) 574181, telex: 460865 univts i.

June 20–23, 1988
Gaithersburg, MD, U.S.A.

10th Symposium on Thermophysical Properties
Contact: A. Cezairliyan, Room 124, Hazards Building, National Bureau of Standards, Gaithersburg, MD 20899, U.S.A., tel.: (301) 975-5931, or J.V. Sengers, Institute for Physical Science and Technology, University of Maryland, College Park, MD 20742, U.S.A., tel.: (301) 454-4117.

June 27–July 2, 1988
Moscow, U.S.S.R.

ISEC '88, International Solvent Extraction Conference
Contact: Dr. B. Spivakov, Vernadsky Institute of Geochemistry and Analytical Chemistry of the U.S.S.R., Academy of Sciences, 117975 GSP-1, Kosygin Str. 19, Moscow V-334, U.S.S.R. (Further details published in Vol. 190, No. 2.)

July 24–29, 1988 Compiegne, France	**1st International Conference on Modern Aspects of Protein Dye Interaction — Role in Downstream Processing** Contact: Secrétariat, C. Lacroix, Université de Technologie de Compiegne, BP 233, 60206 Compiegne Cédex, France
Aug. 23–26, 1988 Ghent, Belgium	**7th International Symposium on Mass Spectrometry in Life Sciences** Contact: Professor Dr. A. De Leenheer, Laboratoria voor Medische Biochemie en voor Klinische Analyse, Harelbekestraat 72, B-9000 Ghent, Belgium. Tel.: (091) 218951, ext. 324.
Aug. 29–Sept. 2, 1988 Bordeaux, France	**11th International Mass Spectrometry Conference** Contact: The Conference Secretary, 11th International Mass Spectrometry Conference, École Polytechnique, F-91128 Palaiseau, France.
Aug. 31–Sept. 3, 1988 Gargnano del Garda, Italy	**4th Separation Science and Biotechnology Symposium** Contact: Professor P.G. Righetti, Symposium Chairman, Euro Business Center, P.O. Box 10552, 1001 EN Amsterdam, The Netherlands
Sept. 1–3, 1988 Ghent, Belgium	**International Congress on Applied Criminology** Contact: Professor Dr. A. Heyndrickx, Department of Toxicology and Criminalistics, Hospitaalstraat 13, B-9000 Ghent, Belgium. Tel.: (32) 91-251021, telex 11.558 A.Z. Ghent – mention "Toxicology".
Sept. 5–8, 1988 Okayama, Japan	**1st International Conference on Computational Methods in Flow Analysis** Contact: Okayama University of Science, 1-1 Ridaicho, Okayama 700, Japan.
Sept. 5–8, 1988 Jena, G.D.R.	**COMPANA '88, 4th Conference on Computer Application in Analytical Chemistry** Contact: Professor Dr. K. Danzer, c/o Friedrich Schiller University Jena, Department of Chemistry, Steiger 3, 6900 Jena, G.D.R. Tel.: Jena 82 25028, telex: 05886134 uni dd. (Further details published in Vol. 190, No. 2.)
Sept. 19–24, 1988 Graz, Austria	**Probenvorbereitung für die Bestimmung von Spurenelementen** Kontaktadresse: Dr. W. Wegscheider, Institut für Analytische Chemie, Makro- und Radiochemie, Technische Universität Graz, Technikerstrasse 4, A-8010 Graz, Austria. Tel.: (0316) 7061-8303, telex: 311221.
Sept. 21–23, 1988 Gothenburg, Sweden	**Biological Determinants of Drug Response in Man** Contact: The Swedish Academy of Pharmaceutical Sciences, P.O. Box 1136, S-111 81 Stockholm, Sweden.
Sept. 25–29, 1988 Florence, Italy	**5th International Symposium on Bioluminescence and Chemiluminescence** Contact: Organizing Secretariat, O.I.C., Via G. Modena 19, 50121 Florence, Italy. Tel.: (055) 578273/577822.
Oct. 10–12, 1988 Wetzlar, F.R.G.	**3rd International Colloquium on Solid Sampling with Optical Atomic Spectroscopy** Contact: Dr. M. Stoeppler, KFA Jülich, ICH-4, Postfach 1913, D-5170 Jülich, F.R.G.

Oct. 17–19, 1988 Nice, France	**International Symposium on Supercritical Fluids: Properties and Applications** Contact: M. Perut, E.N.S.I.C., 1 rue Grandville, F-54042 Nancy Cédex, France.
Nov. 2–4, 1988 Freiburg, F.R.G.	**5th (Montreux) Symposium on Liquid Chromatography–Mass Spectroscopy** Contact: Professor R.W. Frei, Department of Analytical Chemistry, De Boelelaan 1083, Vrije Universiteit, 1081 HV Amsterdam, The Netherlands. (Further details published in Vol. 190, No. 2.)
Jan. 10–12, 1989 Tirupati, India	**ISAME, International Seminar on Analytical Techniques in Monitoring the Environment** Contact: Professor S. Jayarama Reddy, Director, ISAME, Department of Chemistry, Sri Venkataswarlu University, College of Engineering, Tirupati 517 502, India.
May 23–26, 1989 Ghent, Belgium	**3rd International Symposium on Quantitative Luminescence Spectrometry in Biomedical Sciences** Contact: Dr. Willy R.G. Baeyens, Symposium Chairman, State University of Ghent, Pharmaceutical Institute, Laboratory of Pharmaceutical Chemistry and Drug Quality Control, Harelbekestraat 72, B-9000 Ghent, Belgium.
June 25–30, 1989 Stockholm, Sweden	**13th International Symposium on Column Liquid Chromatography** Contact: 13th International Symposium on Column Liquid Chromatography, The Swedish Academy of Pharmaceutical Sciences, P.O. Box 1136, S-111 81 Stockholm, Sweden. Tel.: (468) 24 50 85.
July 30–August 5, 1989 Cambridge, U.K.	**SAC 89, International Conference on Analytical Chemistry** Contact: SAC 89, Royal Society of Chemistry, Analytical Division, Burlington House, London W1V 0BN, U.K. Tel.: (01) 437-8656.
Aug. 28–Sept. 1, 1989 Wiesbaden, F.R.G.	**11th International Symposium on Microchemical Techniques** Contact: Gesellschaft Deutscher Chemiker, Abt. Tagungen, P.O. Box 900440, D-6000 Frankfurt/Main 90, F.R.G. Tel.: (069) 79 17-366/360, telex: 4170497 gdch d.
Aug. 20–25, 1990 Prague, Czechoslovakia	**J. Heyrovský Centennial Congress on Polarography** Contact: Secretariat, J. Heyrovský Centennial Congress on Polarography, J. Heyrovský Institute of Physical Chemistry and Electrochemistry, Czechoslovak Academy of Sciences, Vlašská 9, 118 40 Prague 1, Czechoslovakia. (Further details published in Vol. 197.)

ANNOUNCEMENT

PERSPECTIVES IN ANALYTICAL CHEMISTRY

An International Symposium in honour of Dr. A.M.G. Macdonald on the occasion of her retirement from the Editorship of *Analytica Chimica Acta*, Beatenberg, Switzerland, July 6–8, 1988

Alison Macdonald has decided to retire as editor of *Analytica Chimica Acta* at the end of 1988. She has been associated with the journal since 1961 when, with Phil West, she took over the editorship from those who had fulfilled the function since it was set up in 1947.

To mark this milestone, Elsevier Science Publishers is organizing a meeting on **Perspectives in Analytical Chemistry** to recognize not only Dr. Macdonald's contributions to the field but also her signal achievements in the establishing of *Analytica Chimica Acta* as a leading analytical journal.

The meeting will bring together a select group of leading researchers who will review the current status of their particular topics and present their views on trends and possible future developments.

The scientific programme of the meeting will comprise invited review lectures covering a wide range of analytical techniques. In addition, there is room for a limited number of submitted contributions within the scope of the meeting. Those wishing to present a paper should submit a short abstract (*ca.* 100 words) in English, as soon as possible and in any case before February 29, 1988 to:

Klaas E. Bij, Symposium Secretary, Elsevier Science Publishers, P.O. Box 330, 1000 AH Amsterdam, The Netherlands

Beatenberg is attractively located in the mountains near Bern above the lake of Thun and opposite the peaks of Eiger, Mönch and Jungfrau.

For further information and registration information, please contact Klaas E. Bij, at the address given above.

As only a limited number of participants can be accepted, early registration is recommended.

INFORMATION FOR AUTHORS

etailed "Information for Authors" was published in Vol. 190, No. 2, pp. 375–378. A free reprint is available from the litors or from:

sevier Editorial Services Ltd., Mayfield House, 256 Banbury Road, Oxford OX2 7DH (Great Britain)

rpes of contribution. The journal welcomes original research papers, short communications and reviews. eviews are written by invitation of the editors, who welcome suggestions for subjects. Short communications are ually complete descriptions of limited investigations, and should generally not exceed six printed pages. Preliminary mmunications of important urgent work can be printed within four months of submission, if the authors are epared to forgo proofs.

anuscripts. The preferred language of the journal is English, but French and German manuscripts are also ceptable. For authors whose first language is not English, French or German, linguistic improvement is provided as rt of the normal editorial processing. Authors should submit three copies of the manuscript in double-spaced typing one side of the paper only, with a margin of 4 cm, on pages of uniform size. If any variety of machine copying is ed (e.g. xerox), authors should ensure that all copies are easily legible and that the paper used can be written on th both ink and pencil. Authors are advised to retain at least one copy of the manuscript. Manuscripts should be eceded by a sheet of paper carrying (a) the title of the paper, (b) the name and full postal address of the person to nom proofs are to be sent, (c) the number of pages, tables and figures.

formation on the *submission of papers* is given on the inside front cover.

ummary. Research papers and reviews begin with a Summary (50–250 words) which should comprise a brief ctual account of the contents of the paper, with emphasis on new information. Short communications and eliminary communications require summaries, which should not exceed 50 words. Uncommon abbreviations, gon and reference numbers must not be used. The Summary should be suitable for use by abstracting services thout rewriting. Papers in French or German require a Résumé or Zusammenfassung preceded by a Title and mmary in English; authors are encouraged to provide translations where necessary.

troduction. The first paragraphs of the paper should contain an account of the reasons for the work, any essential storical background (as briefly as possible and with key references only) and preliminary experimental work.

gures. Figures should be prepared in black waterproof drawing ink on drawing or tracing paper of the same size as at on which the manuscript is typed. One original (or sharp glossy print) and two photostat (or other) copies are quired. Attention should be given to line thickness, lettering (which should be kept to a minimum) and spacing on es of graphs, to ensure suitability for reduction during printing. Axes of a graph should be clearly labelled, along the es, and outside the graph itself.

l figures should be numbered with Arabic numerals, and require descriptive legends. Explanatory information should placed not in the figure, but in the legend, which should be typed on a separate sheet of paper. Simple straight-line aphs are not acceptable, because they can readily be described in the text by means of an equation or a sentence. aims of linearity should be supported by regression data that include slope, intercept, standard deviations of the pe and intercept, standard error, and the number of data points; correlation coefficients are optional.

notographs should be glossy prints and be as rich in contrast as possible; colour photographs cannot be accepted. In neral, line diagrams are more informative and less liable to dating than photographs of equipment, which are erefore not usually acceptable.

mputer outputs for reproduction as figures must be good quality on blank paper, and should preferably be bmitted as glossy prints.

omenclature, abbreviations and symbols. In general, the recommendations of the International Union of Pure d Applied Chemistry (IUPAC) should be followed, and attention should be given to the recommendations of the alytical Chemistry Division in the journal *Pure and Applied Chemistry* (see also *IUPAC Compendium of Analytical omenclature*, 1978).

ferences. The references should be collected at the end of the paper, numbered in the order of their appearance in e text (*not* arranged alphabetically), and typed on a separate sheet.

the list of references, the following forms should be adopted.

urnals

W. Lund and M. Salberg, Anal. Chim. Acta, 76 (1975) 131.

M. McDaniel, A. D. Shendrikar, K. D. Reizneir and P. W. West, Anal. Chem., 48 (1976) 2240.

e title of the journal must be abbreviated as in the Bibliographic Guide for Editors and Authors.

oks

D. D. Perrin, Masking and Demasking of Chemical Reactions, Interscience–Wiley, New York, 1970, p. 188.

S. Hofmann, in G. Svehla (Ed.), Wilson and Wilson's Comprehensive Analytical Chemistry, Vol. 9, Elsevier, Amsterdam, 1979, p. 89.

les of papers are unnecessary. Citations of reports which are not widely available (e.g., reports from government earch centres) should be avoided if possible. Authors' initials should not be used in the text, unless real confusion uld be caused by their omission. If the reference cited contains three or more names, only the first author's name lowed by et al. (e.g., McDaniel et al.) should be used in the text; but the reference list must contain the initials and mes of *all* authors.

Experimental Design: A Chemometric Approach

by **S. N. Deming,** *University of Houston, Houston TX, and* **S. L. Morgan,** *University of South Carolina, Columbia, SC, USA*

(Data Handling in Science and Technology, 3)

One of the greatest needs in all areas of competitive research and development is an efficient approach to experimentation. To be effective scientists, engineers or managers, individuals today require a clear understanding of the principles of experimental design. This book – unlike most current textbooks – approaches experimental design from the point of view of the experimenter, rather than that of the statistician. It provides a *practical* approach to experimental design and allows the reader to obtain the required information in the minimum number of experiments.

The book introduces the reader to the fundamentals of experimental design. Systems theory, response surface concepts, and basic statistics serve as a basis for the further development of matrix least squares and hypothesis testing. The effects of different experimental designs and different models on the variance-covariance matrix and on the analysis of variance (ANOVA) are extensively discussed. Applications and advanced topics (such as confidence bands, rotatability, and confounding) complete the text. Numerous worked examples are presented.

The clear and practical approach adopted by the authors makes the book applicable to a wide audience. It will appeal particularly to those with a practical need (scientists, engineers, managers, research workers) who have completed their formal education but who still need to know efficient ways of carrying out experiments. It will also be an ideal text for advanced undergraduate and graduate students following courses in chemometrics, data acquisition and treatment, and design of experiments.

Contents: 1. System Theory. 2. Response Surfaces. 3. Basic Statistics. 4. One Experiment. 5. Two Experiments. 6. Hypothesis Testing. 7. The Variance-Covariance Matrix. 8. Three Experiments. 9. Analysis of Variance (ANOVA) for Linear Models. 10. A Ten-Experiment Example. 11. Approximating a Region of a Multifactor Response Surface. 12. Additional Multifactor Concepts and Experimental Designs. Appendices: Matrix Algebra. Critical Values of t. Critical Values of F, $\{a\} = 0.05$.

1987 about 294 pages; US $ 109.75 / Dfl. 225.00;
ISBN 0-444-42734-1

ELSEVIER THE SCIENCE PUBLISHER
P O BOX 211 • 1000 AE AMSTERDAM • THE NETHERLANDS
P O BOX 1663 • GRAND CENTRAL STATION • NEW YORK • NY 10163